buildings

Special Issue Reprint

Recent Advances in Intelligent Applications of Well-Being Spaces Design and Engineering

Edited by
Guodan Liu, Hongbing Chen and Sheng Miao

mdpi.com/journal/buildings

MDPI

Recent Advances in Intelligent Applications of Well-Being Spaces Design and Engineering

Recent Advances in Intelligent Applications of Well-Being Spaces Design and Engineering

Guest Editors

Guodan Liu
Hongbing Chen
Sheng Miao

MDPI

Basel • Beijing • Wuhan • Barcelona • Belgrade • Novi Sad • Cluj • Manchester

Guest Editors

Guodan Liu
School of Environmental and Municipal Engineering
Qingdao University of Technology
Qingdao
China

Hongbing Chen
School of Environment and Energy Engineering
Beijing University of Civil Engineering and Architecture
Beijing
China

Sheng Miao
School of Information and Control Engineering
Qingdao University of Technology
Qingdao
China

Editorial Office
MDPI AG
Grosspeteranlage 5
4052 Basel, Switzerland

This is a reprint of the Special Issue, published open access by the journal *Buildings* (ISSN 2075-5309), freely accessible at: https://www.mdpi.com/journal/buildings/special_issues/10RS8S12C3.

For citation purposes, cite each article independently as indicated on the article page online and as indicated below:

Lastname, A.A.; Lastname, B.B. Article Title. *Journal Name* **Year**, *Volume Number*, Page Range.

ISBN 978-3-7258-8873-3 (Hbk)
ISBN 978-3-7258-8874-0 (PDF)
https://doi.org/10.3390/books978-3-7258-8874-0

© 2026 by the authors. Articles in this reprint are Open Access and distributed under the Creative Commons Attribution (CC BY) license. The reprint as a whole is distributed by MDPI under the terms and conditions of the Creative Commons Attribution-NonCommercial-NoDerivs (CC BY-NC-ND) license (https://creativecommons.org/licenses/by-nc-nd/4.0/).

Contents

About the Editors . . . . . **vii**

Preface . . . . . **ix**

Shuhan Zhu, Xingtian Wang, Dongmiao Zhao, Yeliang Song, Xu Li and Shaofei Wang
Evolutionary Game Theory in Architectural Design: Optimizing Usable Area Coefficient for Qingdao Primary Schools
Reprinted from: *Buildings* **2026**, *16*, 244, https://doi.org/10.3390/buildings16020244 . . . . . **1**

Sheng Miao, Sudong Li, Xixin Yang, Hongyu Guan and Xiang Shen
Indoor Light Environment Comfort Evaluation Method Based on Deep Learning and Evoked Potentials
Reprinted from: *Buildings* **2025**, *15*, 4571, https://doi.org/10.3390/buildings15244571 . . . . . **23**

Jianzhen Qiu, Weimei Cai, Jinyu Song, Honghu Zhang and Yating Li
A Study on the Evolution of Lightscapes in the Beijing Road Historic and Cultural Zone, Guangzhou, China
Reprinted from: *Buildings* **2025**, *15*, 3636, https://doi.org/10.3390/buildings15203636 . . . . . **42**

Huiying Zhang, Hui Feng, Xiaolin Zang and Ang Sha
Research on the Optimization of Healthy Living Environments in Liyuan Block Empowered by CFD Technology: A Case Study of the Liyuan Block in Dabaodao, Qingdao
Reprinted from: *Buildings* **2025**, *15*, 3223, https://doi.org/10.3390/buildings15173223 . . . . . **82**

Yanxia Li, Tingkai Yan, Gang Yao, Wenjing Zhang, Chuwen Lai, Yuwei Wu, et al.
Urban Form and Urban Energy Consumption at the Macro Scale in China
Reprinted from: *Buildings* **2025**, *15*, 2909, https://doi.org/10.3390/buildings15162909 . . . . . **100**

Lujin Hu, Yu Liu and Bing Yu
Evolution Method of Built Environment Spatial Quality in Historic Districts Based on Spatiotemporal Street View: A Case Study of Tianjin Wudadao
Reprinted from: *Buildings* **2025**, *15*, 1953, https://doi.org/10.3390/buildings15111953 . . . . . **128**

Congcong Wang, Yu Li, Pengchao Ding, Hongbing Chen, Yan Zhang and Yongjie Xing
Analysis of Airflow Dynamics and Instability in Closed Spaces Ventilated by Opposed Jets Using Large Eddy Simulations
Reprinted from: *Buildings* **2025**, *15*, 1707, https://doi.org/10.3390/buildings15101707 . . . . . **155**

Xu Lu, Qingyu Li, Xiang Ji, Dong Sun, Yumeng Meng, Yiqing Yu and Mei Lyu
Impact of Streetscape Built Environment Characteristics on Human Perceptions Using Street View Imagery and Deep Learning: A Case Study of Changbai Island, Shenyang
Reprinted from: *Buildings* **2025**, *15*, 1524, https://doi.org/10.3390/buildings15091524 . . . . . **180**

Yumeng Meng, Mei Lyu, Dong Sun, Jiaxuan Shi and Hiroatsu Fukuda
Evaluating and Diagnosing Urban Function and Perceived Quality Based on Multi-Source Data and Deep Learning Using Dalian as an Example
Reprinted from: *Buildings* **2025**, *15*, 998, https://doi.org/10.3390/buildings15070998 . . . . . **215**

Gonghu Huang, Yiqing Yu, Mei Lyu, Dong Sun, Bart Dewancker and Weijun Gao
Impact of Physical Features on Visual Walkability Perception in Urban Commercial Streets by Using Street-View Images and Deep Learning
Reprinted from: *Buildings* **2025**, *15*, 113, https://doi.org/10.3390/buildings15010113 . . . . . **243**

Qinfeng Zhao, Zhirui Wu, Yi Yu, Tian Wang and Shan Huang
Exploring Carbon Emissions in the Construction Industry: A Review of Accounting Scales, Boundaries, Trends, and Gaps
Reprinted from: *Buildings* **2025**, *15*, 1900, https://doi.org/10.3390/buildings15111900 . . . . . **267**

About the Editors

Guodan Liu

Guodan Liu, Prof, Dr., School of Environmental and Municipal Engineering, Qingdao University of Technology. Research interests include building energy efficiency, renewable energy utilization, thermal environments, and indoor human thermal comfort. Leadership encompasses two General Programs of the National Natural Science Foundation of China as principal investigator, participation in a National 973 Program sub-project, and involvement in a National Key Technology R&D Program sub-project. Additional research direction includes several provincial and municipal projects, notably a key initiative on new energy integration for subway systems. Scholarly output includes over thirty peer-reviewed papers as first author in journals such as *Building and Environment* and *Renewable Energy*, along with four authorized invention patents. Teaching leadership includes the Shandong Provincial first-class course "Ventilation and Air Conditioning Engineering." Research achievements have been recognized with three Shandong Provincial Science and Technology Progress Awards.

Hongbing Chen

Hongbing Chen, Prof, Dr., School of Environment and Energy Engineering, Beijing University of Civil Engineering and Architecture. Research interests include comprehensive utilization of solar energy, nano phase change fluids, heat and mass transfer in porous media, and green buildings and building energy efficiency. Academic experience includes a postdoctoral visiting research position at the University of Nottingham from 2009 to 2011. Professional recognition includes designation as an EU Marie Curie Fellow and Beijing Municipal Science and Technology Rising Star. Research leadership comprises over forty funded projects, including national and provincial initiatives. Scholarly output includes over 120 peer-reviewed publications, among which 28 are indexed in SCI and 27 in EI, alongside 20 Chinese core journal papers. Also authored two academic monographs and contributed to seven additional volumes. Holds more than ten authorized invention patents. Research achievements have been recognized with three first prizes and two second prizes in provincial and ministerial-level science and technology awards.

Sheng Miao

Sheng Miao, Assoc Prof, Dr., School of Information and Control Engineering, Qingdao University of Technology. Research interests include industrial IoT, multimodal data fusion, data mining, deep learning, and digital twins. Educational background includes a B.E. in Communication Engineering from Qingdao University, an M.S. in Applied Information Technology from Towson University, and a Ph.D. in Information Technology from Towson University. Professional experience includes research assistant positions at the U.S. Army Research Laboratory and faculty roles at Towson University and Qingdao University. Leadership includes directing the Industrial IoT and Digital Twin Technology Innovation Team, with total research funding exceeding one million RMB through projects on smart water management systems, ecological data processing, and groundwater resource analysis. Participated in a U.S. Army intelligent intelligence fusion initiative and a Shandong Provincial Key R&D Program on predictive maintenance for industrial manufacturing equipment. In collaboration with the School of Environmental and Municipal Engineering, established the joint Environmental System Analysis research team, which has secured over four million RMB in research funding over the past three years. Scholarly output includes over ten high-level papers, with six SCI-indexed papers as first or corresponding author.

Preface

Rapid urbanization and escalating climate challenges have redefined expectations for the built environment, which must now actively nurture human health, productivity, and overall well-being. The emerging paradigm of "well-being spaces" integrates physical, psychological, and social dimensions into design and engineering, yet realizing this vision demands sophisticated tools to decode the complex interplay between spatial configurations, environmental parameters, and human perceptions. Recent advances in artificial intelligence, machine learning, computational simulation, and neurocognitive sensing have matured to the point where objective, data-driven, human-centric decision-making is not only feasible but increasingly practical across diverse contexts.

This Reprint curates ten original research articles and one comprehensive review that exemplify the state of the art in intelligent applications for well-being spaces. Spanning scales from indoor environments and courtyard neighborhoods to historic districts and entire cities, these contributions tackle challenges such as optimizing spatial efficiency, improving thermal and visual comfort, enhancing walkability and perceived safety, reducing energy consumption, and mitigating carbon emissions. Methodologically, the studies employ deep learning on street-view imagery, large-eddy simulation, evolutionary game theory, and neurophysiological assessments of lighting quality, among other advanced techniques. The accompanying review critically identifies gaps in lifecycle carbon accounting and proposes a forward-looking research agenda.

Our primary aim is to foster cross-disciplinary dialogue and provide a coherent reference for researchers, urban planners, architects, and policymakers committed to creating resilient, equitable, and vibrant environments that genuinely enhance human well-being. We thank all authors and reviewers for their rigorous contributions and trust that readers will find both inspiration and actionable insights within these pages.

Guodan Liu, Hongbing Chen, and Sheng Miao
Guest Editors

buildings

MDPI

Article

Evolutionary Game Theory in Architectural Design: Optimizing Usable Area Coefficient for Qingdao Primary Schools

Shuhan Zhu [1,2], Xingtian Wang [1,3,*], Dongmiao Zhao [1], Yeliang Song [4], Xu Li [4] and Shaofei Wang [1]

[1] College of Architecture and Urban Planning, Qingdao University of Technology, Qingdao 266520, China; shuhanzhu22@gmail.com (S.Z.); zhaodongmiao@qut.edu.cn (D.Z.); wangshaofei@qut.edu.cn (S.W.)
[2] Qingdao Shinan District Construction and Public Works Center, Qingdao 266071, China
[3] Faculty of Environmental Engineering, The University of Kitakyushu, Kitakyushu 808-0135, Japan
[4] Qingdao Tengyuan Design Associates Co., Ltd., Qingdao 266000, China; song.yeliang@tengyuan.com.cn (Y.S.); li.xu@tengyuan.com.cn (X.L.)
* Correspondence: wangxingtian@qut.edu.cn

Abstract

Amidst the surge of high-density urban development and the growing demand for high-quality spaces, the Usable Area Coefficient (UAC) has emerged as a pivotal metric in the architectural planning. The rational calibration of the UAC for primary school buildings is key to balancing intensive land use, educational demands, and the well-being of children. Taking primary schools in a district of Qingdao as the research subject, this research rationally optimizes the range of UAC by constructing an evolutionary game model, based on quantitatively analyzing the divergent perspectives and requirements of three stakeholders: the government, school administrators, and students. After further identifying the key factors that influence the ultimate decision, the study yields the following insights: (1) The incremental comprehensive benefit emerges as the linchpin influencing the UAC. (2) The government's risk compensation to schools and the benefit-sharing coefficient between schools and students exert significant impacts on system evolution. (3) Effective control of construction and land costs, coupled with enhanced availability of open activity spaces, paves the way for consensus on low UAC. This research not only furnishes a theoretical framework and practical guidance for harmonizing land use efficiency with educational excellence but also steers the design of salubrious primary school environments and informs pertinent policy-making.

Keywords: design optimization; usable area coefficient; primary schools; evolutionary game theory

1. Introduction

Under the dual background of the deepening global concept of healthy living environments and the rapid development of high-density cities, "well-being spaces" in educational settings have become the core medium for ensuring the comprehensive development of children in physiology, mentality, and emotion [1,2]. The creation of healthy spaces must be centered on user needs, while employing data science and technology to enhance spatial efficiency and adaptability [3]. With the continuous decline in the number of school-age children in China, the pursuit of spatial quality in basic education buildings is placing greater emphasis on improving overall quality [1]. However, constrained by practical issues

such as limited funding for basic education and the scarcity of land in high-density urban areas, the current determination of the Usable Area Coefficient (the ratio of functional room area to total building area) in the architectural planning stage has already restricted the evolution of educational models [4–8]. Flexible space remains difficult to achieve, hindering the creation of an open and modern environment conducive to talent cultivation [9]. Particularly in developed, intensive cities where land resources are extremely scarce, primary school buildings generally face an inherent contradiction between "land scarcity" and the "need for open spaces". On one hand, limited land availability compels governments to prefer higher UAC values in order to control construction costs. On the other hand, children's healthy growth and the transformation of modern educational models require ample open activity spaces [10–12], which necessitates lowering the UAC to reserve more flexible spatial resources.

The essence of this contradiction lies in the decision-making conflicts among multiple stakeholders: the government focuses on cost control and intensive land use; schools emphasize teaching quality and spatial flexibility, while students and parents prioritize the assurance of a healthy and active environment. The traditional standards for determining the UAC of primary school buildings are outdated—neither incorporating the new requirements for children's healthy spaces nor accounting for the dynamic game relationships among multiple actors. As a result, design outcomes often fall into a dilemma between "high UAC that compress open spaces" and "low UAC that exceed fiscal budgets". Although technologies such as artificial intelligence and machine learning have been gradually applied to the simulation and optimization of healthy spaces, contraposing key design parameters like the UAC, there is still no quantitative decision-making framework for balancing the interests of all stakeholders in primary school buildings.

This research takes public primary schools in a district of Qingdao as the research object and introduces evolutionary game theory to depict the dynamic strategic adjustment processes of governments, schools, students and parents, approaching the actual decision-making logic comprehensively. This paper quantitatively analyzes the interests and interaction mechanisms among the three parties in determining the UAC, by integrating field survey data with MATLAB R2023b simulation modeling. Stable strategic combinations are identified, which can balance cost efficiency with the demand for healthy spaces, thereby providing theoretical support and practical guidance for the scientific design of healthy spaces in primary school buildings.

The principal contributions of this paper are summarized as follows:

- It fills the research gap in the architectural planning field regarding the multi-stakeholder game phenomenon in the determination of the UAC. For the first time, evolutionary game theory is applied to the optimization of the UAC in primary school buildings, thus expanding interdisciplinary methodologies within architectural planning.
- By constructing a government–school–student three-party evolutionary game model, the study identifies stable evolutionary strategy points and clarifies that the increment of overall benefits under low UAC and government risk compensation are key factors influencing the adoption of lower UAC in primary school buildings.
- Based on the stability conditions, the study proposes practical design strategies such as controlling construction and land-use costs and enhancing the usability of open activity spaces. These strategies not only ensure sufficient open activity spaces necessary for children's education and learning but also balance fiscal budget constraints, thereby contributing to the creation of a healthy and comfortable educational environment.

https://doi.org/10.3390/buildings16020244

2. Literature Review

2.1. Architectural Programming

Post-occupancy evaluation serves as an effective strategy for guiding architectural programming. A series of novel studies have been conducted in the field of post-utilization evaluation. For POI post-occupancy evaluation, an integrated AHP-Fuzzy Integrals approach is proposed to estimate factor weights and subfactor importance, enhancing accuracy via AHP's hierarchical rigor and Fuzzy Integrals' uncertainty handling [12]. Post-occupancy evaluations in the thermal-performance domain also deploy combined in situ environmental monitoring with regression analytics—a transferable method that can benchmark primary-school floor-area coefficients [13]. Fine-grained POE of an open-office shows that a Space-Utilization Index fusing spatial scale, occupancy dots and dwell time raises evaluation accuracy, suggesting primary-school stakeholders could likewise adopt this high-resolution metric to quantify and bargain over the use-area coefficient [14]. These cross-disciplinary advances collectively indicate that the application of POE in primary-school building programming is shifting from rough compliance checks to data-rich, stakeholder-negotiated scientific evaluations.

Participatory design also proves to be highly beneficial for architectural programming. By shifting to a user-participatory pre-planning process, Korean school-renovation cases show that pupils, teachers and facility managers can jointly convert "left-over" circulation zones into quantifiable floor-area credits, providing a negotiation template for fine-tuning primary-school use-area coefficients [15]. By embedding online surveys, living-lab VR trials and post-session focus groups into the sensory-square project, the study turns children into data-driven co-planners in the building program [16]. Evidence-Based Design (EBD) is an important source of scientific knowledge that can be applied to the design process, and the pattern language has long led the way in turning that evidence into a reusable, design-method toolkit [17].

In the architectural programming process, the Usable Area Coefficient (UAC), is an important concept, significantly contributing to enhancing the rationality of functional planning and assessing the economy and practicality of architectural spaces. Current research on UAC rarely focuses specifically on educational buildings, concentrating instead on residential and office building types. Several scholars have explored compact designs for school buildings in slums or unplanned urban areas, demonstrating the feasibility of such approaches. Their findings provide useful references for optimizing UAC under conditions of limited land resources [18]. Other researchers have analyzed the influencing factors of UAC through case studies of university teaching buildings, proposing optimization strategies that offer methodological support for quantitative analyses of these factors [19]. Nevertheless, existing standards for determining UAC do not fully reflect contemporary educational demands and changing trends. Although each stakeholder benefits from feedback obtained during the design and construction phases, the concept of "continuous improvement," prevalent in business management, has not yet been widely adopted in architectural planning or UAC determination. Adopting this mindset and summarizing stakeholders' feedback benefits could play a positive role in optimizing UAC methodologies [20]. Additionally, conducting multidisciplinary design reviews, especially incorporating the perspectives of building users, prior to construction helps identify design shortcomings [21]. Unfortunately, many users and organizations find it challenging to visualize a building's functionality and user experience based solely on architectural drawings and renderings; users typically provide accurate feedback only after occupying the building for a certain period [22]. Thus, multidisciplinary design reviews should be integrated during the architectural planning stage to prevent iterative redesigns at their source.

https://doi.org/10.3390/buildings16020244

Although these studies provide a theoretical foundation for understanding UAC, there remains significant research potential in primary educational buildings, particularly regarding multi-stakeholder decision-making interactions and investment costs. This study draws on existing quantitative analytical methods and combines them with the unique characteristics of primary school buildings to comprehensively investigate the rational determination of UAC.

2.2. Evolutionary Game Theory

Evolutionary game theory relaxes the assumption of complete rationality found in classical game theory, allowing agents to make incremental decisions under conditions of incomplete information and cognitive constraints. Through the replicator dynamics mechanism, strategy adjustment is viewed as a continuous and observable process. Furthermore, by introducing the evolutionarily stable strategy (ESS) concept, evolutionary game theory provides verifiable mathematical conditions for analyzing the long-term behavioral stability of groups [23].

Applying evolutionary game theory to this study offers significant advantages. First, it can simulate multi-stakeholder interactions; for instance, by constructing a tripartite game model involving government, schools, and students, the approach analyzes strategic interactions such as government implementation, school requirements, and student (or parental) requests for optimizing the UAC, thus addressing the shortcomings of traditional research that overlooks stakeholder interaction [24,25]. Second, evolutionary game theory does not require extensive data, allowing the analysis of strategy evolution trends through parameter settings and numerical simulations (e.g., MATLAB), which is particularly suitable for primary school buildings lacking systematic UAC data. Cost, benefits, and subsidies parameters can thus be rationally determined [26]. Third, it enables the analysis of equilibrium stability via the Jacobian matrix, identifying stable conditions for stakeholder strategy combinations (e.g., proactive government guidance, school supervision, student applications for lower UAC), thereby providing clear guidance for policy formulation [27]. Fourth, external environmental uncertainties (e.g., policy adjustments, changes in educational requirements) can be incorporated, enhancing the model's adaptability to real-world scenarios [23,28,29].

2.3. Primary School Architecture

Educational research treats the school environment as a "third teacher" that shapes pupils' cognition, affect and behavior, conditions their well-being and learning, and fosters inclusion without segregating. [30]. The classification of school environments is influenced by a variety of factors. Ahmed (2023) implicitly classifies Cairo primary schools into two spatial archetypes: large-plot campuses (>1200 m^2) that accommodate the standard multi-block layout, and small-footprint sites ($\leq$1200 m^2) embedded in informal settlements where a single, five-story compact block with zero-lot-line setbacks is advanced as the only viable typology [18].

Relevant literature on primary school architectural design provides critical references for the construction and analysis of game theory models, addressing dimensions such as spatial demand characteristics, stakeholder requirements, parameter setting criteria, and verification methods. A study on spatial interactions in primary schools in Ho Chi Minh City, Vietnam, observed children's interactions within classroom and playground spaces ("space-social-nature") and found that shading conditions, seating arrangements, and the distribution of natural elements significantly influence spatial usage efficiency [31]. Research on personalized learning in Indian primary schools emphasized the importance of flexible spatial designs to accommodate diverse student learning needs, underscoring

https://doi.org/10.3390/buildings16020244

the principle of aligning spatial configurations with educational demands [32]. A review of natural learning spaces in Maltese primary schools confirmed that natural elements positively affect student learning and identified the proportion of natural space as a core spatial requirement from the school's perspective [33]. Additionally, research on playful learning landscapes in American primary schools highlighted that school spatial design must match users' practical needs, reinforcing the logic of aligning spatial functions with usage requirements [34]. A study examining the impact of the school environment on teachers' commitment to educational quality indicated that teachers' spatial needs affect educational quality, highlighting the correlation between teachers' spatial requirements and educational environment design [35]. These studies collectively reflect the usage demands of schools and students from various perspectives. Research on school renovations in Nalchik, Russia, revealed conflicts between government planning standards and actual school demands, noting cases where existing schools needed expansions due to insufficient functional spaces [36]. A study on multi-grade teaching in Caowo Primary School, Gansu, China, demonstrated how small-scale schools adapt teaching activities through spatial reconfiguration, exemplifying specific scenarios of spatial adaptation under resource constraints [37].

In summary, the above studies provide multidimensional support for the evolutionary game analysis of primary school building usable area coefficient, covering aspects such as quantitative spatial demand, identification of stakeholder interests, parameter-setting references, and verification methods. This body of research helps clarify the core parameters, stakeholder strategies, and constraints within the game model, thereby enhancing the practical relevance and feasibility of the present study.

3. Methodology

Determining the Usable Area Coefficient (UAC) is a crucial step in architectural planning. However, this process often involves strategic conflicts that arise from neglecting the differing objectives among stakeholders. Evolutionary game theory provides a suitable approach to addressing this issue. It is founded on the principle of bounded rationality, acknowledging the decision-making characteristics of stakeholders (government, schools, and students) under information asymmetry. By using replicator dynamics equations to describe the dynamic evolution of strategy proportions and defining conditions for long-term strategic stability through the evolutionarily stable strategy (ESS), evolutionary game theory effectively characterizes stakeholder interactions during the determination of the UAC.

Constructing an evolutionary game model involves four key steps. First, the interest relationships and strategy set must be clearly defined. Second, a payoff matrix is established to quantify the payoffs of different strategy combinations. Third, a replicator dynamic equation is formulated to describe the dynamic changes in the proportions of each party's strategies over time. Fourth, the stability of equilibrium points is analyzed using the Jacobian matrix. If all eigenvalues of the matrix are less than zero, the corresponding strategy combination is considered an evolutionarily stable equilibrium, which can serve as an optimal direction for determining the UAC of primary school buildings.

3.1. Data Collection

In the process of determining the usable area coefficient, each stakeholder has distinct motivations and objectives, which form the basis for constructing the game model. The stakeholders include three main groups. First, governmental departments responsible for policy formulation, resource allocation, and project construction, which have strategies of "active implementation" or "inactive implementation". Second, schools responsible for

https://doi.org/10.3390/buildings16020244

management and operation after project completion, specifically the "teaching" component, which may choose between "request" and "no request". Third, students and their guardians (parents), representing the "learning" component, which may choose between "assert demands" and "not assert demands" (Figure 1). Additionally, the architectural design unit, which is distinct from the direct stakeholders, assists in planning and implementing specific designs. However, considering that the design unit primarily executes planning decisions and has limited influence on the game's outcomes due to its weak ties to the building's strategic decisions, it is excluded from participation in the game analysis.

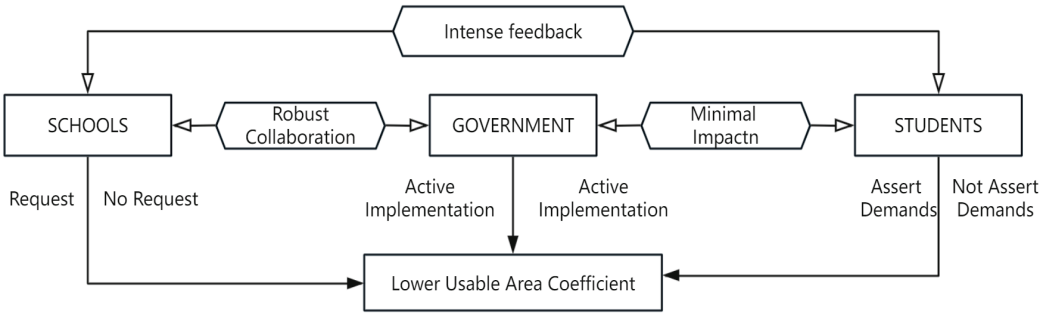


Figure 1. Tripartite game relationship in determining the UAC.

Data collection focused on stakeholders' interests, benefit parameters, and strategic costs related to UAC decisions for primary school buildings. The following two sections detail the methodology used to gather and analyze relevant data.

- **Determination of benefit and cost parameters**
- Benefits and cost parameters for each stakeholder were established through case studies and comparative policy analysis. Nine public primary schools in a district of Qingdao, characterized by floor area ratios of at least 1.9 and land compliance rates of no more than 0.5, were selected as samples. Architectural drawings and construction cost reports were collected, extracting key indicators such as total construction area, functional room areas (teaching, administrative, and logistical spaces), open activity spaces, and auxiliary circulation areas. These data formed a database correlating actual UAC with spatial configurations. Additionally, 11 national, provincial and municipal regulations were collated to extract constraint parameters, such as per-student land area, per-student building area, functional space ratios, and maximum floor area ratios. This process defined the policy-based range of UAC (e.g., provincial recommendation of UAC = 0.6). Cost parameters and investment data from the sample projects were systematically compared with corresponding standards, enabling accurate determination of government benefit parameters and costs.
- **Stakeholder interests and survey data**
- Two types of surveys were conducted to gather data on stakeholder interests. First, interviews were held with government officials, focusing on "UAC requirements" and the "distribution ratio of comprehensive benefits from low UAC between government and schools," These interviews yielded 28 valid records. Second, questionnaires were distributed to schools (principals and academic staff) and students in grades 4–6, addressing "satisfaction with open spaces and spatial utilization issues" and the "distribution ratio of comprehensive benefits from low UAC between schools and students." Out of 200 questionnaires distributed, 163 valid responses were received. Both survey instruments primarily collected quantitative data. Satisfaction and spatial utilization issues were analyzed using Likert scales, while distribution ratios were evaluated using a two-round Delphi method. This approach enabled comprehensive

https://doi.org/10.3390/buildings16020244

insight into stakeholder preferences and cost acceptance, offering robust data support for subsequent analyses and decision-making.

3.2. Data Processing

- **Processing benefit and cost parameters**
  Collected benefit and cost parameters were screened for outliers and standardized. Grubbs' test was employed to exclude anomalous UAC (e.g., K > 0.85 or K < 0.35) arising from special policies (such as renovations of historical buildings), retaining nine valid samples for model parameter calibration. Data from primary schools of varying sizes (24, 36, and 48 classes) were converted to per-student indicators (m^2/student) to eliminate interference from class-size differences. Additionally, various area types from schools of different scales were proportionally converted to eliminate project-scale disparities, using area proportion as a unified comparison dimension. Monetary and quasi-monetary data, including government subsidies, school costs, and parental expenditures, were uniformly adjusted to constant 2024 prices, removing inflationary influences and ensuring data comparability.
- **Validation of stakeholder interest data**
  Survey data consistency was validated using cross-analysis to examine correlations between questionnaire satisfaction ratings and actual proportions of open space, ensuring alignment between survey results and case data. A group-comparison validation strategy was employed, dividing the nine schools into three categories based on actual open space proportions: high (>10%), medium (5–10%), and low (<5%). Mean satisfaction scores across these groups were compared using ANOVA ($p < 0.05$). Significantly higher satisfaction scores among high-proportion schools compared to medium and low groups confirmed the congruence of survey data with case data, ensuring satisfaction ratings reliably reflected differences in spatial indicators related to UAC and preventing survey findings from diverging from actual spatial conditions.

4. Model Construction and Simulation Analysis

4.1. Model Construction

4.1.1. Stakeholder Analysis

This study develops an evolutionary game model involving three stakeholders, the government, schools, and students, to analyze the decision-making process for the usable area coefficient (UAC) during the architectural planning stage of primary schools. Considering information and power asymmetries, the model assumes that stakeholders are bounded-rational individuals who cannot initially identify a globally optimal strategy. Instead, they adjust their strategies through repeated interactions by observing the average payoffs of the group.

Identifying stakeholders' unique motivations and goals provides a foundational basis for constructing the game model. The key stakeholders are classified as follows: First, government departments (construction authorities) aim primarily to ensure compliance with educational policies and standards, enhance educational quality, optimize resource allocation, control budgets, and ensure construction progress and quality. Second, schools are motivated to meet teaching and learning requirements, ensure buildings are safe, comfortable, and efficient, and minimize long-term operating costs. Their feasible strategies include articulating functional requirements, participating in design and planning, supervising construction quality, and providing usage feedback. Third, the actual users, students and their guardians (parents), are motivated primarily by educational needs and promoting healthy development. Their actionable strategies include school selection, providing

https://doi.org/10.3390/buildings16020244

suggestions on functional requirements, offering feedback, and actively disseminating opinions [38–42].

Based on stakeholder analysis, in response to the low UAC, the strategies for the three stakeholders are defined as follows: the government's strategies are "actively implementation" or "passively implementation," schools' strategies are "request" or "not request," and students' strategies are "assert demands" or "not assert demands."

4.1.2. Model Assumptions

Different choices by the stakeholders directly impact the overall decision-making system, influencing the determination of UAC. To simulate these dynamic interactions, the study follows the core evolutionary game theory premises of "bounded rationality" and "incremental learning," proposing the following assumptions:

Assumption 1: Students and Parents' Assertion of Demands

Students and parents, as direct beneficiaries of educational services, choose between "assert demands" and "not assert demands." Asserting demands involves a fixed cost C_3 (e.g., information collection, attending meetings) but provides incremental benefits from increased open activity space, calculated as abΔR, where a and b are benefit-sharing coefficients between schools and students, and government and schools, respectively. Here, ΔR represents the incremental comprehensive benefit resulting from low UAC, including land-use fee savings and net present value of energy consumption savings (unit: 10,000 yuan/class). Specifically, G_4 represents the supportive benefit that school-built space confers on students when the government, the school, and the students themselves are all in their most proactive state. If demands are not expressed, no costs are incurred, but benefits are not shared. The government's general subsidy G_2 is independent of demand expression behavior. This assumption reflects parents' "cost–benefit" considerations under limited information and participation capabilities.

Assumption 2: Schools' Decision-Making on Demands

Schools must choose between "requesting low UAC" and "not requesting low UAC." Requesting low UAC requires a fixed cost C_2, but yields government incentives G_1, and direct incremental benefits from additional open space (1-a)bΔR. If the government passively implements the policy, and students and parents assert demands, schools must also bear a risk compensation cost W_2. If schools do not request a low UAC, they save C_2, but they forfeit all rewards and savings related to the low UAC. This assumption captures schools' trade-offs between teaching quality, operational efficiency, and policy risks.

Assumption 3: Government's Implementation Strategy

As the resource allocator and policymaker, the government chooses between "actively implementing low UAC" and "passively implementing low UAC." Active implementation necessitates additional construction investments C_1, government incentives to schools G_1, government incentives to students G_2, and reputation benefits G_3. Passive implementation saves C_1, G_1 and G_2, gaining construction cost savings D; however, if schools persistently request a low UAC, the government faces communication and compliance pressures quantified as W_1. This assumption reflects the government's balancing act among fiscal constraints, educational equity, and public reputation.

Assumption 4: Information Structure and Evolutionary Mechanism

All stakeholders simultaneously select strategies at each decision point, with binary strategy sets. Game information is public knowledge, but stakeholders exhibit bounded rationality and thus cannot immediately identify optimal solutions. Instead, they gradually adjust their strategies based on replicator dynamics by observing average group payoffs from previous rounds. Each decision round corresponds to an "evaluation-feedback-re-evaluation" cycle during the planning phase, with discrete time steps of 0.5 and a

https://doi.org/10.3390/buildings16020244

total duration of 20, aligning with simulation settings in Section 4.2.2. Initial values and parameter intervals for all exogenous parameters follow specifications in Table 1, and subsequent sensitivity analyses will systematically explore parameter spaces through Monte Carlo simulations.

Table 1. Overview of Model Parameters.

No.	Symbol	Description	Recommended Initial Value	Sensitivity Interval	Data Source/ Calibration Method	Remarks
			Benefits			
1	ΔR	Incremental comprehensive benefit of low UAC	20	[5, 40]	Mean of 9 public school cases	★ Key control variable
2	a	Benefit-sharing coefficient (schools-students)	0.65	[0.45, 0.85]	Two-round Delphi survey	★
3	b	Benefit-sharing coefficient (government-schools)	0.60	[0.50, 0.75]	Same as above	★
4	D	Construction cost savings	5	—	Cost audit reports	Fixed
5	G_1	Government incentives to schools	2	—	Policy documents	Fixed
6	G_2	Government incentives to students	1	—	Same as above	Fixed
7	G_3	Social reputation benefit	2	—	Converted from social benefits	Fixed
8	G_4	Supportive Benefit of Campus Space	7	–	Academic-return valuation	Fixed
			Costs			
9	W_1	Government risk compensation to schools	8	[1, 15]	Provincial financial audits	★ Policy lever
10	W_2	School risk compensation to students	8	—	School internal regulations	Fixed
11	C_1	Government's active implementation cost	4	[2, 10]	Administrative cost surveys	★
12	C_2	Schools' active demand cost	3	[1, 8]	Expert Delphi survey	★
13	C_3	Cost of students expressing demands	1	—	Questionnaire statistics	Fixed
14	S_1	Schools' opportunity loss	4	—	School surveys	Fixed
15	S_2	Students' opportunity loss	3	—	Same as above	Fixed

★: Key control variable.

4.1.3. Parameter Assumptions

This study systematically calibrated all parameters of the evolutionary game model through literature review, field surveys, and expert consultations. The specific steps were as follows:

First, baseline values and variation ranges for economic variables were established. Completion settlement reports, financial audits, and school operation data from nine public primary schools in a District, Qingdao, were selected as samples. Baseline values and reasonable ranges for each economic variable were determined by combining descriptive statistics and two-round Delphi surveys.

https://doi.org/10.3390/buildings16020244

Second, policy-related parameters (such as risk compensation levels and reward amounts) were identified through supplementary semi-structured interviews with representatives from provincial finance departments, construction units, and school principals.

Third, data sources were cross-validated using construction cost audit reports, current educational finance documents, and questionnaire results, ensuring the diversity and reliability of data.

Table 1 summarizes parameter symbols, economic meanings, recommended initial values, sensitivity analysis intervals, and data sources after the above calibration process. Critical variables, including ΔR, W1, a, and b, were identified as "key control variables" for the Monte Carlo sensitivity analysis in Section 4.2.2. Remaining parameters were held constant during simulations to reduce dimensional complexity and highlight the effects of policy levers. All parameters were uniformly measured in "10,000 yuan/class," consistent with benefit measurement assumptions in Section 4.1.2.

4.1.4. Payoff Matrix

Based on the previously defined strategy sets and parameter system, this study quantified the payoffs (U_G, U_S, U_P) for government, schools, and students (including parents) under various strategic combinations, following the cost–benefit assumptions from Section 4.1.2. When a stakeholder chooses a passive strategy, their payoff may include saved construction or management costs; conversely, choosing an active strategy involves subtracting corresponding costs but adding incremental benefits from a low UAC, government rewards, or reputation gains. If stakeholder strategies lack coordination, risk compensation items are triggered, reflecting real-world policy constraints and opportunity losses. Thus, the following payoff matrix (Table 2) was constructed, providing a numerical basis for replicator dynamics equations and equilibrium analyses in subsequent sections.

Table 2. Payoff Triplets (U_G, U_S, U_P) for Eight Pure Strategy Combinations.

Combination (G, S, P)	Government (U_G)	Schools (U_S)	Students (U_P)
(Active, Request, Assert)	$(1-b)\Delta R + G_3 + D - C_1 - G_1 - G_2$	$(1-a)b\Delta R + G_1 - C_2$	$ab\Delta R + G_2 + G_4 - C_3$
(Active, Request, Not Assert)	$(1-b)\Delta R + G_3 + D - C_1 - G_1$	$(1-a)b\Delta R + G_1 - C_2$	$ab\Delta R + G_2$
(Active, Not Request, Assert)	$(1-b)\Delta R - C_1 - G_2$	$-S_1$	$G_2 - C_3$
(Active, Not Request, Not Assert)	$(1-b)\Delta R - C_1$	$-S_1$	G_2
(Passive, Request, Assert)	$D - W_1$	$G_1 - W_2 - C_2$	$ab\Delta R - C_3$
(Passive, Request, Not Assert)	$D - W_1$	$G_1 - C_2$	$ab\Delta R$
(Passive, Not Request, Assert)	0	0	$-C_3$
(Passive, Not Request, Not Assert)	0	0	0

4.2. Model Simulation Analysis

4.2.1. Stability Analysis

To calculate the evolution of strategies over time for the government, schools, and students (including parents), the Taylor & Jonker replicator dynamics framework was adopted. The strategy growth rate is primarily driven by the difference between expected individual payoffs and average group payoffs. Let the probabilities of the government selecting "actively implementing low UAC," schools "requesting low UAC," and students (and parents) "assert demands" be denoted as z, y, and x, respectively. Complementary probabilities are thus $1-z$, $1-y$, and $1-x$.

(1) Fundamental Derivation

The general form of replicator dynamics equations:

$$\frac{dx_i}{dt} = x_i\left[U_i - \overline{U}_i\right], i \in \{\text{ strategies }\}, \quad (1)$$

https://doi.org/10.3390/buildings16020244

U_i represents the expected payoff for selecting strategy i, and $\bar{U}$ is the average payoff of the group. Expected and average payoffs for each stakeholder were obtained by weighting the payoffs of the eight pure-strategy combinations (Table 2) according to their probabilities.

(2) Expected and Average Payoffs for the Government (G)

Let U_{G1} and U_{G0} represent the expected payoffs for the government choosing "active" and "passive" strategies, respectively:

$$\begin{aligned} U_{G1} &= yx[(1-b)\Delta R + G_3 + D - C_1 - G_1 - G_2] \\ &\quad + y(1-x)[(1-b)\Delta R + G_3 + D - C_1 - G_1] \\ &\quad + (1-y)x[(1-b)\Delta R - C_1 - G_2] \\ &\quad + (1-y)(1-x)[(1-b)\Delta R - C_1] = U\_\{G1\} \\ &= (1-b)\Delta R - C_1 + y(G_3 + D - G_1) - x\,G_2 \\ U_{G0} &= yx(D - W_1) + y(1-x)(D - W_1) \\ &= y(D - W_1) \end{aligned} \tag{2}$$

The average payoff for the government group:

$$\overline{U}_G = zU_{G1} + (1-z)U_{G0} \tag{3}$$

Substituting U_{G1} and $\bar{U}_{G0}$ into the replicator dynamics equation yields the evolutionary equation for the government's strategy:

$$\begin{aligned} \tfrac{dz}{dt} &= z(1-z)[U_{G1} - U_{G0}] \\ &= z(1-z)[(1-b)\Delta R - C_1 + y(G_3 - G_1 + W_1) - xG_2] \end{aligned} \tag{4}$$

(3) Expected and Average Payoffs for Schools (S)

Similarly, the expected payoffs for schools selecting "request" U_{S1} and "not request" U_{S0} strategies are:

$$\begin{aligned} U_{S1} &= xz[(1-a)b\Delta R + G_1 - C_2] + x(1-z)(G_1 - W_2 - C_2) \\ &\quad + (1-x)z[(1-a)b\Delta R + G_1 - C_2] + (1-x)(1-z)(G_1 - C_2) \\ &= z(1-a)b\Delta R + G_1 - x(1-z)W_2 - C_2 \\ U_{S0} &= xz(-S_1) + (1-x)z(-S_1) = -zS_1 \end{aligned} \tag{5}$$

The average payoff for the school group is:

$$\overline{U}_S = yU_{S1} + (1-y)U_{S0} \tag{6}$$

Thus, the evolutionary equation for the school's strategy is:

$$\frac{dy}{dt} = y(1-y)[U_{S1} - U_{S0}] = y(1-y)[z(1-a)b\Delta R + G_1 + zS_1 + zxW_2 - C_2 - xW_2] \tag{7}$$

(4) Expected and Average Payoffs for Students and Parents (P)

The expected payoffs for students and parents choosing "assert" U_{P1} and "not assert" U_{P0} strategies:

$$\begin{aligned} U_{P1} &= zy[ab\Delta R + G_2 + G_4 - C_3] + z(1-y)(G_2 - C_3) + (1-z)y(ab\Delta R - C_3) \\ &\quad + (1-z)(1-y)(-C_3) \\ &= ab\Delta Ry + zG_2 + zyG_4 - C_3 \\ U_{P0} &= zy[ab\Delta R + G_2] + z(1-y)(G_2) + (1-z)yab\Delta R = yab\Delta R + zG_2 \end{aligned} \tag{8}$$

https://doi.org/10.3390/buildings16020244

The average payoff for students and parents is

$$\overline{U}_P = xU_{P1} + (1-x)U_{P0} \tag{9}$$

Consequently, their strategy evolution equation is

$$\frac{dx}{dt} = x(1-x)[U_{P1} - U_{P0}] = -x(1-x)(zyG_4 - C_3) \tag{10}$$

Summarizing the above, the system of replicator dynamics equations for government, schools, and students (including parents) is:

$$\begin{array}{l} \frac{dx}{dt} = x(1-x)[-G_3] \\ \frac{dy}{dt} = y(1-y)[z(1-a)b\Delta R + zG_1 + zS_1 + zxW_2 - C_2 - xW_2] \\ \frac{dz}{dt} = z(1-z)[(1-b)\Delta R - C_1 + y(G_3 - G_1 + W_1) - xG_2] \end{array} \tag{11}$$

Setting this system of equations to zero yields eight pure-strategy equilibrium points, $E_1(0,0,0)$~$E_8(1,1,1)$.

The Jacobian matrix is derived as:

$$J = \begin{bmatrix} \frac{\partial f}{\partial x} & \frac{\partial f}{\partial y} & \frac{\partial f}{\partial z} \\ \frac{\partial g}{\partial x} & \frac{\partial g}{\partial y} & \frac{\partial g}{\partial z} \\ \frac{\partial h}{\partial x} & \frac{\partial h}{\partial y} & \frac{\partial h}{\partial z} \end{bmatrix} \tag{12}$$

By substituting each equilibrium point, an ESS is identified when all eigenvalues are negative. The derivation shows that this occurs only when:

$$\begin{array}{l} C_3 - zyG_4 > 0 \\ (1-b)\Delta R + G_3 + W_1 > c_2 + G_1 + G_2 \\ (1-a)b\Delta R + G_1 + S_1 + W_2 > C_2 \end{array} \tag{13}$$

When all conditions are simultaneously satisfied, $E_8(1,1,1)$ represents the unique evolutionarily stable strategy. Under this equilibrium, the government actively implements the low UAC, schools choose to request a low UAC, and students and parents opt to express their demands, thereby ultimately achieving the goal of adopting and maintaining a low UAC.

4.2.2. Scenario Simulation

The parameterized MATLAB simulation was employed to validate the model through a three-step procedure: parameter configuration, simulation execution, and result output. According to research requirements, two scenarios were defined: a positive scenario (high ΔR and W_1, controllable C_1) and a negative scenario (low ΔR and W1, high C_1) (Table 3).

Table 3. Parameters for Positive and Negative Scenarios.

Scenario	ΔR	W_1	C_1	Expected ESS
Positive	20	8	4	(1,1,1)
Negative	5	2	8	(0,0,0)

MATLAB R2023b was utilized as the simulation tool. Initial strategy probabilities x_0, y_0, z_0 were randomly generated within the interval [0.1, 0.9], creating 50 datasets covering diverse initial states. Simulation parameters were configured as follows: step size = 0.5, total duration = 20 steps, and the numerical solver ode45 was used to record, in real-time, the strategy probabilities of the government, schools, and students (including parents) at

https://doi.org/10.3390/buildings16020244

each step (t = 1 to t = 20). The resulting datasets from these two scenarios were plotted to illustrate dynamic evolution trajectories.

Figure 2 (positive scenario) demonstrates that when ΔR and W_1 are high and C_1 is relatively controllable, the probabilities that the government, schools, and students (including parents) select "active/request/express" strategies exhibit monotonic increases. These probabilities surpass 0.8 at approximately t = 6, subsequently converging smoothly toward (1,1,1). This trajectory confirms the unique evolutionarily stable equilibrium of the low-UAC strategy combination, indicating that under conditions of significant incremental benefits, adequate risk compensation, and manageable implementation costs, stakeholders rapidly reach consensus.

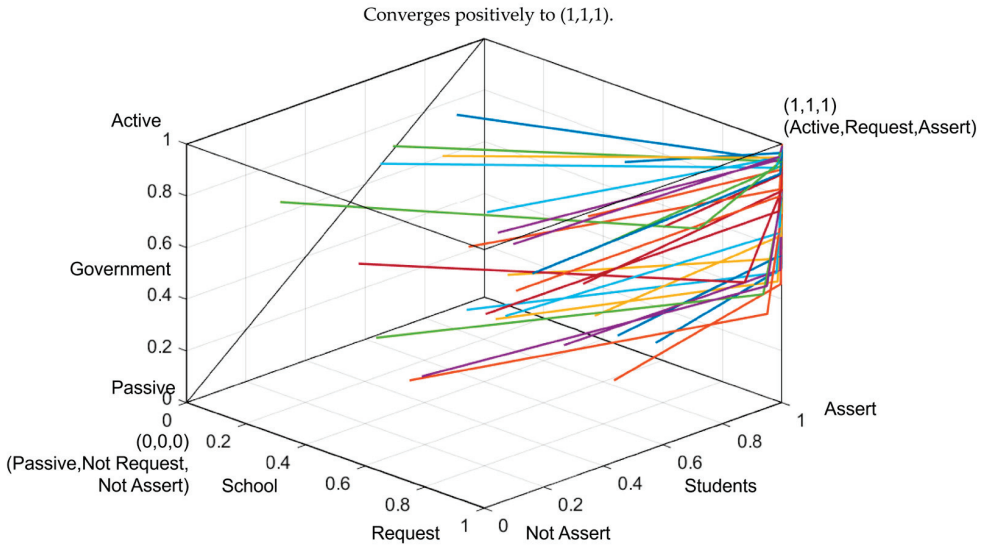


Figure 2. Evolution Trajectories under the Positive Scenario.

In contrast, Figure 3 (negative scenario) illustrates an opposite trend: the three probability curves rapidly decline below 0.2 around t = 4 and eventually stabilize at (0,0,0). This outcome clearly suggests that when incremental benefits are insufficient, risk compensation is inadequate, and implementation costs are excessively high, the high-UAC strategy becomes the stable attractor for the system.

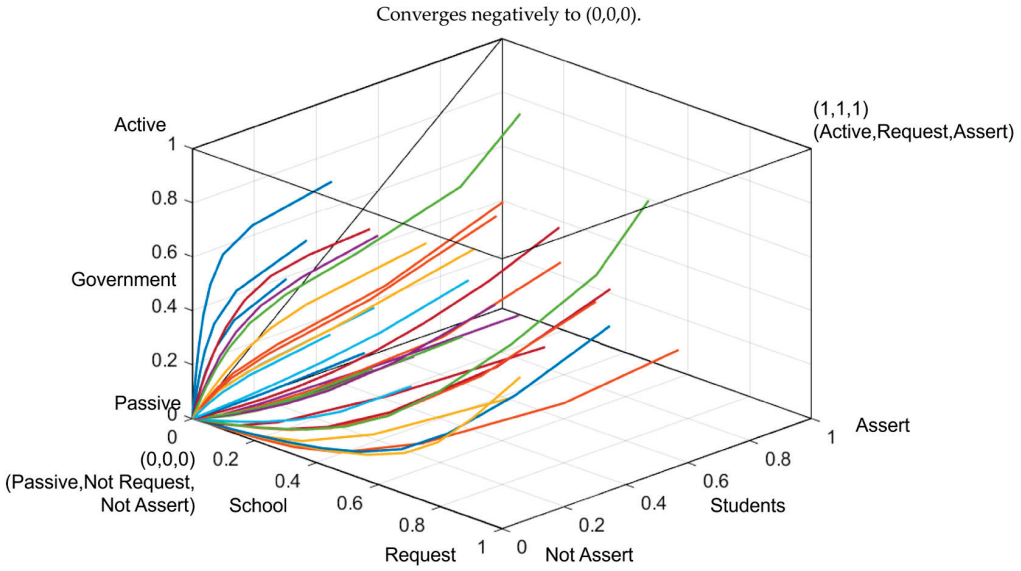


Figure 3. Evolution Trajectories under the Negative Scenario.

https://doi.org/10.3390/buildings16020244

4.2.3. Sensitivity Analysis

This section employed MATLAB-based simulations and single-factor sensitivity analyses to evaluate the model's stability and reliability. By repeatedly executing the simulation process outlined in Section 4.2.2 and comparing the consistency of results across multiple runs, the robustness of the model's outputs was validated. Subsequently, a single-factor sensitivity analysis was conducted by adjusting key parameters individually (ΔR, benefit-sharing coefficients a and b, risk compensation W_1, etc.) while keeping other parameters constant.

For each adjusted parameter, simulations were conducted to record variations in the evolutionary trajectories of stakeholder strategies (Figures 4–6). By comparing the magnitude of fluctuations in these trajectories, the influence of each parameter on the system's evolution was quantified. The sensitivity results allowed the identification of parameters with significant impacts and the determination of critical threshold values (e.g., $W_1 \geq 8$, a within the range 0.6–0.7), providing methodological support for subsequent strategic recommendations.

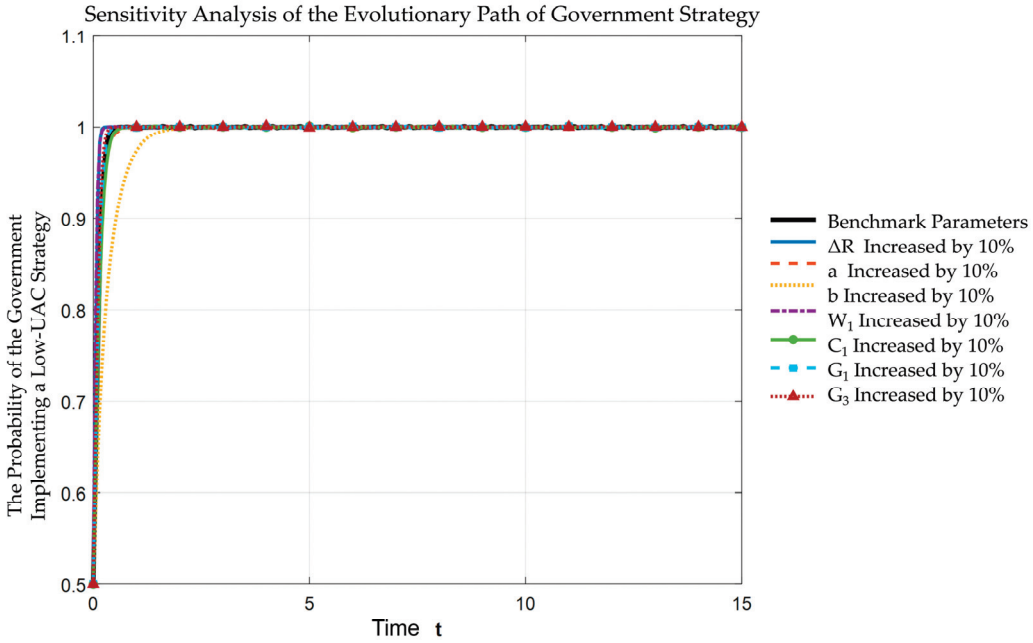


Figure 4. Sensitivity Analysis of Government Strategy Evolution.

The sensitivity analysis of the stakeholders' evolutionary paths indicated notable differences in parameter sensitivity. The incremental comprehensive benefit (ΔR) emerged as the most influential parameter for all stakeholders, with increases in ΔR promoting a simultaneous shift toward proactive strategies. The benefit-sharing coefficient b strongly influenced school behavior by directly determining their cooperative benefits, while the coefficient a primarily impacted student strategies. An optimal range of 0.6–0.7 for a effectively motivated students and parents to express their demands. Government strategy was highly responsive to variations in risk compensation (W_1), with governmental willingness markedly increasing when $W_1 \geq 8$.

https://doi.org/10.3390/buildings16020244

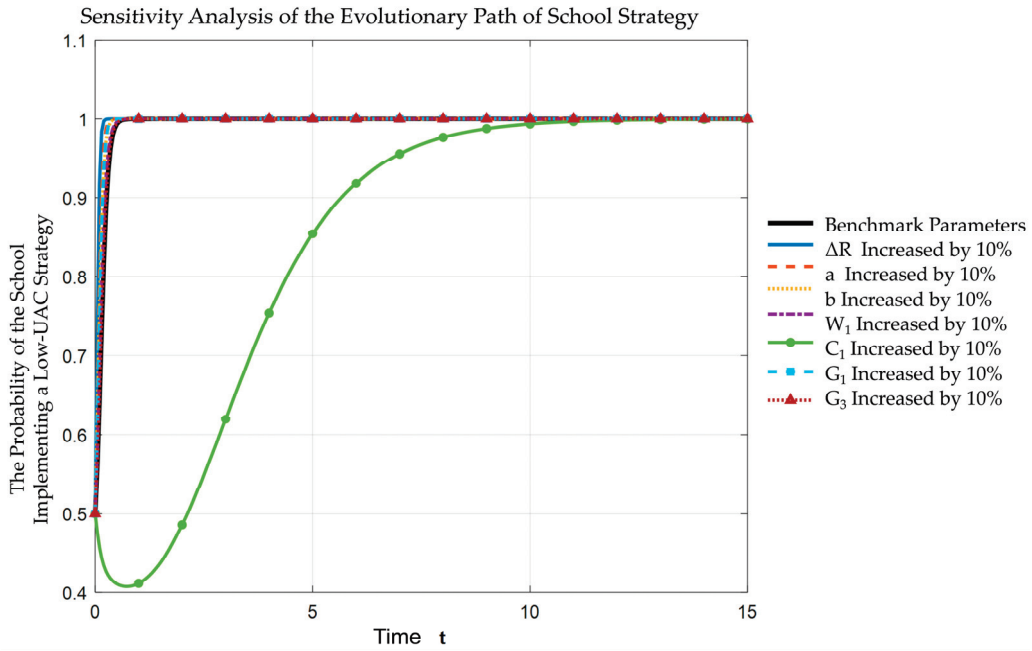


Figure 5. Sensitivity Analysis of School Strategy Evolution.

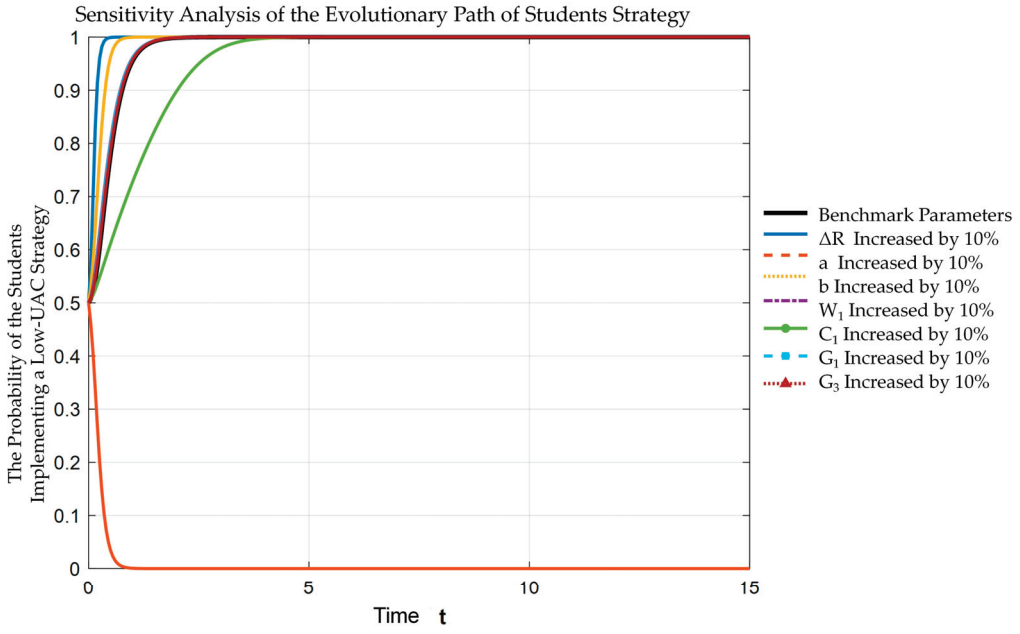


Figure 6. Sensitivity Analysis of Students Strategy Evolution.

Thus, ΔR, as a core economic lever, demonstrated a far greater regulatory effect than other parameters, serving as the most critical driver toward achieving a low UAC.

5. Discussion

5.1. Practical Implications

This study connects the identified game equilibrium directly with primary school architectural design practices. All monetary thresholds are expressed in 10,000-yuan per class (1 unit = CNY 10,000/class) to facilitate direct comparison with Table 1 and the scenario parameters. The core finding "when ΔR > 150,000 yuan/class and W_1 > 80,000 yuan/class, the system converges toward a low usable area coefficient (UAC) (0.48–0.53)" provides a quantitative decision-making basis for primary school designs, thereby overcoming traditional reliance on empirical standards. By examining practical scenarios in a District,

https://doi.org/10.3390/buildings16020244

Qingdao, this conclusion accurately addresses the inherent conflict between "land intensification" and "well-being spaces." When incremental comprehensive benefits of a low UAC (such as land use savings and reduced operational energy consumption) and government risk compensation meet critical thresholds, the demands of the government (cost control), schools (educational space assurance), and students and parents (healthy environment) can be simultaneously met. This aligns strongly with demographic trends and design principles promoting "both spatial efficiency and educational needs."

For instance, given the sensitivity of incremental comprehensive benefits (ΔR), strategies such as "optimizing circulation layouts" and "modular functional design" could be adopted to lower construction costs, thus enhancing the economic feasibility of low UAC. Concerning the threshold effect of government risk compensation (W_1), local governments might introduce targeted subsidies for "low-UAC campuses" to alleviate school concerns about budget overruns. Additionally, the optimal benefit-sharing coefficient (a = 0.6–0.7) suggests integrating "parent-participatory design workshops" and "student space-usage surveys" into decision-making, ensuring that increased open spaces align effectively with children's developmental needs. This deeply resonates with the "user-centered" philosophy inherent in "well-being spaces."

5.2. Theoretical Significance

- **Advancing UAC research within primary school architecture:**

The novelty of this research lies in its focus on the unique context of primary education. Previous UAC studies typically emphasized residential, office [43], or university buildings [44], concentrating primarily on spatial efficiency calculations. In contrast, this study integrates variables specific to primary education, including "children's well-being space needs" and "school operational costs," making parameter settings more aligned with the practical demands of basic educational facilities. For example, incorporating "maintenance costs for open spaces" into cost parameters and "student physical and mental health benefits" into benefit parameters underscores the fundamental differences between primary school buildings and other architectural types.

- **Innovation from a multi-stakeholder dynamic equilibrium perspective:**

The application of evolutionary game theory to primary school UAC decisions breaks from conventional approaches that focus solely on the physical properties of open spaces. It advocates balancing stakeholder interests during architectural planning. The identified equilibrium strategy, "E_8(1,1,1)," demonstrates that a stable increase in open spaces via low UAC requires positive interaction among government, schools, and families. Furthermore, the quantified parameter thresholds provide generalizable evaluation standards for designing healthy school environments. For instance, a threshold of $\Delta R \geq 150{,}000$ yuan/class serves as a baseline criterion for assessing the economic viability of implementing low UAC. In suburban areas with limited financial resources, incremental implementations of low-UAC designs could progressively meet this threshold. Compared to uniform, one-size-fits-all standards, differentiated strategies derived from game-theoretic equilibria offer greater practical adaptability, providing new methodological support for "data-driven applications in healthy built environments."

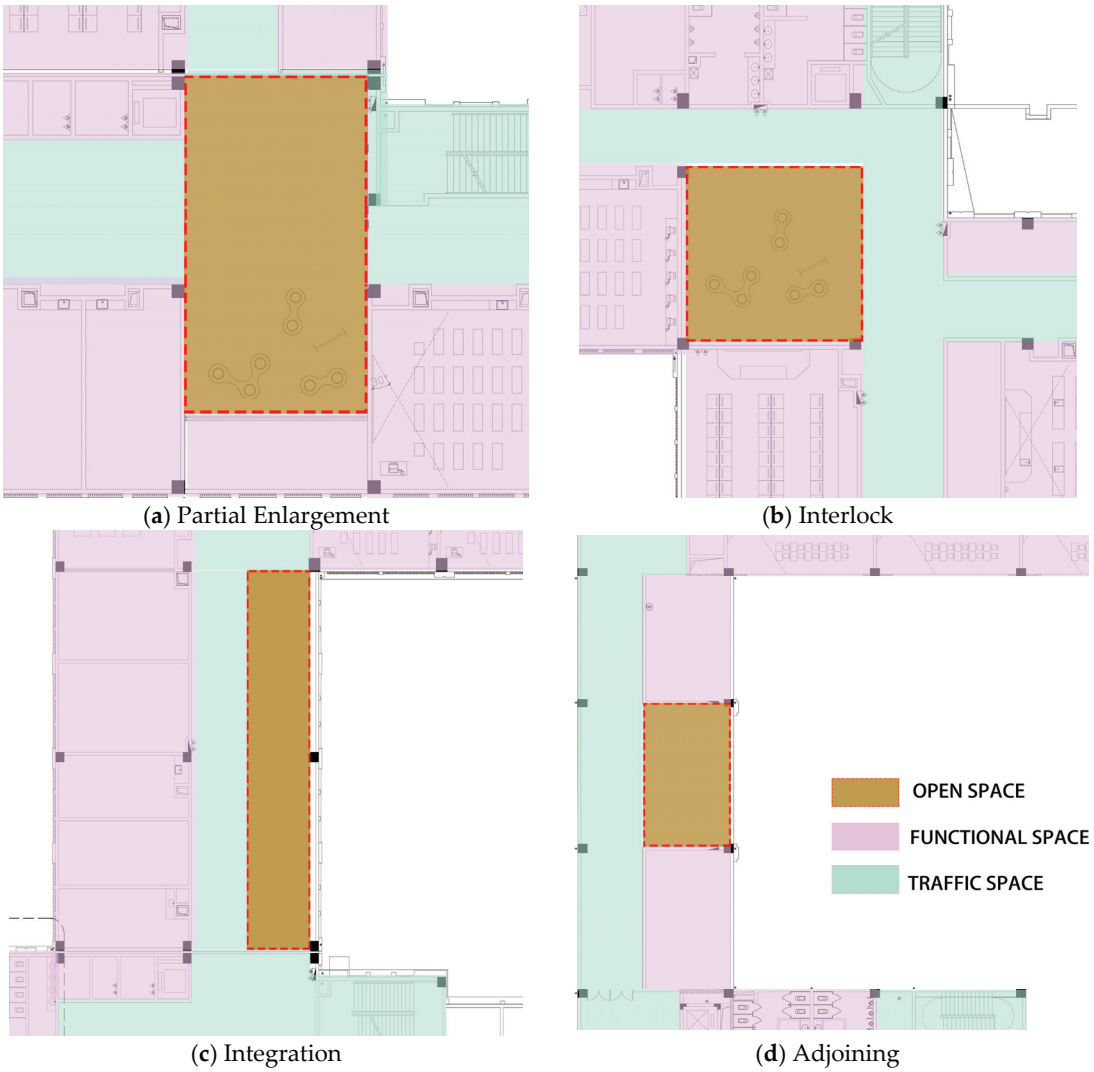
5.3. Primary School Design Suggestions

To translate the simulated ESS into practice, three mutually reinforcing design directives are advanced from an architectural standpoint, each explicitly tied to the key parameters that drive the low-UAC attractor.

https://doi.org/10.3390/buildings16020244

Compact Site Layout: Adopt an intensive, horizontally or vertically consolidated massing that eliminates redundant circulation area and the associated construction-cost waste, thereby enlarging D (construction-cost saving).

Diverse Configuration Approaches for Open Space Planning: Deploy a rich yet code-compliant portfolio of permeable open-space configurations—semi-covered nodes, widened corridors, and locally enlarged bays—that remain classified as ancillary area yet elevate the perceived campus quality(Figure 7), pushing the supportive-benefit coefficient G_4 upward without raising the UAC denominator.



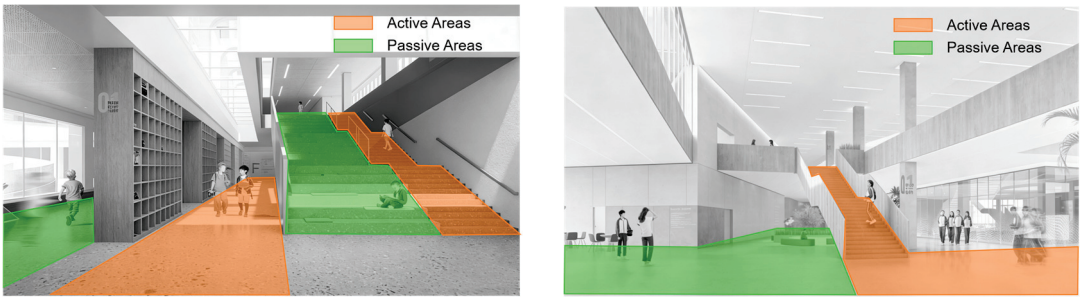
(**a**) Partial Enlargement (**b**) Interlock

(**c**) Integration (**d**) Adjoining

Figure 7. Diagram of the positional relationship of open spaces.

Activity Zones: Dynamic–Static Coupling: Calibrate location, area, and dimensional hierarchies between active and quiet spaces—clustering high-activity zones while embedding scaled-down quiet spaces along circulation spines—so that the resultant dynamic–static gradient delivers an immediately perceived spatial value increment to pupils(Figure 8); this secures the benefit-share coefficient a within the 0.6–0.7 interval that stabilizes the "student-assert" strategy in the replicator dynamics.

https://doi.org/10.3390/buildings16020244



(**a**) horizontal integrating (**b**) vertical integrating

Figure 8. Diagram Illustrating the Separation of Dynamic and Static Zones.

Together, these directives satisfy the fiscal, spatial, and behavioral conditions derived in Sections 3 and 4, guiding land-constrained primary-school projects into the evolutionarily stable low-UAC band (0.48–0.53) while remaining fully aligned with everyday educational and regulatory requirements.

5.4. Policy Optimization Suggestions

Drawing from Williamson's institutional analysis framework and the model's findings, policy recommendations can be proposed at informal institutional, formal institutional, and governance levels to ensure the sustainable implementation of low-UAC campuses:

At the informal institutional level:

A social consensus emphasizing that "low-UAC campuses benefit children's learning and health" should be strengthened. Public dissemination efforts, such as issuing "White Papers on the Benefits of Low-UAC Campuses" and organizing "Healthy Campus Design Exhibitions," would raise awareness of the positive impacts that open space configurations associated with low UAC have on children's learning efficiency and well-being. Additionally, creating a "Parent–School–Government" communication platform to integrate user demands into preliminary design surveys can enhance societal acceptance of low-UAC designs, indirectly reducing the difficulty of realizing incremental comprehensive benefits (ΔR).

At the formal institutional level:

Supporting policies and standards require improvement. Firstly, developing "Technical Guidelines for Low UAC Design in Primary Schools" to specify spatial requirements (e.g., open space ratio $\geq 10\%$) within the recommended UAC range (0.48–0.53) is essential. Secondly, establishing a "Cost-Sharing Mechanism for Low-UAC Campus Construction" to clearly define cost-sharing responsibilities between government and schools would prevent schools from resisting low-UAC schemes due to financial concerns. Thirdly, creating "Incentive Mechanisms for Low-UAC Designs" that reward schools adopting low-UAC schemes and achieving healthy campus certification could enhance schools' motivation for requesting low UAC.

At the governance mechanism level:

Optimizing collaborative decision-making processes is critical. During architectural planning, the government should lead the formation of joint "Design–School–Parent" working groups to concurrently undertake technical assessments and stakeholder negotiations. During implementation, adopting a phased acceptance model that adjusts subsidies according to actual achievement of incremental comprehensive benefits (ΔR) would mitigate budgetary risks. Finally, during the operational phase, introducing "post-occupancy evaluation feedback mechanisms" to integrate satisfaction with open-space utilization into school performance assessments could form a comprehensive "decision–implementation–feedback" management cycle.

https://doi.org/10.3390/buildings16020244

6. Conclusions and Limitations

This study systematically explored the determination of the usable area coefficient (UAC) for primary school buildings by constructing an evolutionary game model involving government, schools, students, and parents in a District, Qingdao. Using MATLAB simulations and sensitivity analysis, the primary conclusions are summarized as follows:

- **Conditions for Evolutionarily Stable Strategies:** When the incremental comprehensive benefit of a low UAC (ΔR) exceeds 150,000 yuan/class and the government's risk compensation to schools (W1) surpasses 80,000 yuan/class, the system converges with a probability of no less than 0.8 to a low UAC range (0.48–0.53). Under these conditions, the stakeholder strategy combination ($E_8(1,1,1)$), namely, "active government implementation–schools requesting low UAC–students and parents expressing demands," emerges as the unique evolutionarily stable strategy, enabling a synergy between intensive land use and well-being spaces.
- **Key Influencing Parameters:** Sensitivity analysis indicates that ΔR serves as the central driver influencing system evolution, with its increase positively aligning stakeholder strategies. The benefit-sharing coefficient a (0.6–0.7) significantly impacts the willingness of students and parents to express their demands. Additionally, when W1 $\geq$ 80,000 yuan/class, governmental willingness for active implementation notably increases, while school strategies demonstrate greater sensitivity to the benefit-sharing coefficient b.
- **Design Strategies:** A combined strategy of centralized compact planning, functionally hybridized circulation, dynamically static zoned activity areas, and modular unit construction enables primary-school projects to achieve simultaneous gains in land efficiency, floor-area utilization, child well-being and construction quality without increasing either site area or overall cost.

This study addresses existing gaps by integrating multi-stakeholder game theory with UAC determination during educational architectural planning, providing an interdisciplinary research perspective. By quantifying critical parameter thresholds for primary school UAC decisions, the study provides explicit guidance for architectural planning. The identified low UAC range (0.48–0.53) and accompanying strategies, such as cost control and risk compensation, can be directly applied to planning new constructions or renovations of primary schools in land-scarce urban areas. This ensures an increase in open space and enhances the educational environment, thereby improving students' overall learning efficiency and promoting children's healthy development.

However, due to limitations in the available literature and data, this study could not comprehensively analyze all potential influencing factors. Moreover, simplifications within the model's assumptions might limit its applicability to complex real-world scenarios. Future research will incorporate additional practical factors into the evolutionary game model and conduct more extensive case studies to provide a more comprehensive analysis.

Supplementary Materials: The following supporting information can be downloaded at: https://www.mdpi.com/article/10.3390/buildings16020244/s1, Semi-structured interviews with representatives from provincial finance departments, construction units, and school principals.

Author Contributions: Conceptualization, S.Z., D.Z. and X.W.; methodology, S.Z., D.Z. and X.W.; software, S.Z. and Y.S.; validation, S.Z., D.Z. and Y.S.; formal analysis, S.Z., D.Z. and Y.S.; investigation, D.Z. and S.W.; resources, Y.S., X.L. and S.W.; data curation, Y.S., X.L. and S.W.; writing—original draft preparation, S.Z. and Y.S.; writing—review and editing, X.W., D.Z.; visualization, Y.S. and X.L.; supervision, D.Z.; project administration, S.Z.; funding acquisition, X.W., S.Z. and X.W. contributed equally to this work. All authors have read and agreed to the published version of the manuscript.

https://doi.org/10.3390/buildings16020244

Funding: This research was funded by SHANDONG PROVINCIAL NATURAL SCIENCE FOUNDATION, grant number ZR2023ME185.

Institutional Review Board Statement: The experimental procedures were in accordance with the Declaration of Helsinki and were approved by the Ethics Committee of Qingdao University of Technology (Approval Number: QUT-HEC-2025012), and informed consent was obtained from all participants.

Informed Consent Statement: Informed consent was obtained from all subjects involved in the study.

Data Availability Statement: The original contributions presented in this study are included in the article/Supplementary Material. Further inquiries can be directed to the corresponding author.

Conflicts of Interest: Authors Yeliang Song and Xu Li are employed by the company Qingdao Tengyuan Design Associates Co., Ltd. The remaining authors declare that the research was conducted in the absence of any commercial or financial relationships that could be construed as a potential conflict of interest.

Abbreviations

The following abbreviations are used in this manuscript:

UAC	Usable Area Coefficient
ESS	Evolutionarily Stable Strategy

References

1. Dumdie, L.B.M.; Mason, B.A.; Hajovsky, D.B.; Ethan, V.F. Student-report measure of school climate: A dimensional review. *Sch. Ment. Heal.* **2020**, *12*, 1–21. [CrossRef]
2. Zorbaz, D.; Akin-Arikan, C.; Terzi, R. Does school climate that includes students' views deliver academic achievement? A multilevel meta-analysis. *Sch. Eff. Sch. Improv.* **2021**, *32*, 543–563. [CrossRef]
3. Duraku, H.Z.; Hoxha, L. Effects of school climate and parent support on academic performance: Implications for school reform. *Int. J. Educ. Reform* **2021**, *30*, 222–236. [CrossRef]
4. Zhu, C.; Liu, Q.; Wu, X. The Environmental Design for Eco Learning Camps for School Children: A Case Study of Changle, Fujian Province, China. In *Towards a Carbon Neutral Future*; Papadikis, K., Zhang, C., Tang, S., Liu, E., Di Sarno, L., Eds.; Springer: Singapore, 2024; Volume 393. [CrossRef]
5. Nemet, B.M.; Velki, T. Some demographic personal and class characteristics as predictors of school climate. *Educ. New Dev.* **2019**, *1*, 17–21.
6. Smul, M.D.; Heirweg, S.; Devos, G.; Keer, H.V. It's not only about the teacher! A qualitative study into the role of school climate in primary schools' implementation of self-regulated learning. *Sch. Eff. Sch. Improv.* **2020**, *31*, 381–404. [CrossRef]
7. Ismail, R.N. Implementation of individual education program (IEP) in curriculum of students with. In Proceedings of the International Conference on Special Education in South East Asia Region 10th Series 2020, Bangi, Malaysia, 29–30 March 2020.
8. Pardamean, B. AI-based learning style prediction in online learning for primary education. *IEEE Access* **2022**, *10*, 35725–35735. [CrossRef]
9. Layang, F.; Mahamod, Z. The level of knowledge, willingness and attitude Malay primary school teachers in teaching and learning map i-Think thoughts. *Malays. J. Educ.* **2019**, *44*, 37–44. [CrossRef]
10. Strand, I.; Nielsen, L.M. Architecture in school practice: Possible tools for supporting spatial literacy. *Int. J. Technol. Des. Educ.* **2025**, *35*, 1597–1618. [CrossRef]
11. Morris, J.E.; Imms, W. Flexible furniture to support inclusive education: Developing learner agency and engagement in primary school. *Learn. Env. Res.* **2025**, *28*, 223–248. [CrossRef]
12. Thakur, I.; Patel, D.A.; Lad, V.H.; Rajesh, M.R. Development of Post Occupancy Index (POI) for High-Rise Residential Buildings. In *Creating Capacity and Capability: Embracing Advanced Technologies and Innovations for Sustainable Future in Building Education and Practice*; Sutrisna, M., Jelodar, M.B., Domingo, N., Le, A., Kahandawa, R., Eds.; Springer: Singapore, 2025; Volume 563. [CrossRef]
13. Mba, E.J.; Okeke, F.O.; Oforji, P.I.; Ozigbo, I.W.; Emmanuel, E.C.; Ozigbo, C.A. Impact of Building Plan Shape on Natural Ventilation Efficiency for Thermal Comfort in Educational Facilities: A Post-occupancy Evaluation. In Proceedings of the 8th International Conference on Civil Engineering, Singapore, 22–24 March 2024; Strauss, E., Ed.; Springer: Singapore, 2025; Volume 539. [CrossRef]

https://doi.org/10.3390/buildings16020244

14. Gao, X.; Osaragi, T.; Ni, J.; Luo, Z.; Geng, Y.; Zhuang, W. A new space utilization assessment paradigm from the perspective of post-occupancy evaluation based on Wi-Fi and Bluetooth positioning systems. *Build. Simul.* **2025**, *18*, 2723–2739. [CrossRef]
15. Yang, J.W.; Yoo, H.Y. Research on the Pre-planning Process for School Space Innovation Project for Operation of High School Credit System. In Proceedings of the 4th International Civil Engineering and Architecture Conference, Seoul, South Korea, 14–17 March 2024; Casini, M., Ed.; Springer: Singapore, 2025; Volume 534. [CrossRef]
16. Deng, L.; Ratavjia, S.; Rattadilok, P. Implementing a Participatory Design Approach to Create a Sensory-Friendly Public Space for Children with Special Needs. In *Innovative Public Participation Practices for Sustainable Urban Regeneration*; Mangi, E., Chen, W., Heath, T., Cheshmehzangi, A., Eds.; Urban Sustainability; Springer: Singapore, 2024. [CrossRef]
17. Kowaltowski, D.C.C.K.; Gonçalves, P.P.; Cleveland, B. Better school architecture through design patterns. *Learn. Environ. Res.* **2024**, *27*, 619–647. [CrossRef]
18. Ahmed, S.H. Compact design concept as an alternative for adapting school buildings to small plots in slums and unplanned urban areas. *Eng. Res. J.* **2023**, *52*, 131–138. [CrossRef]
19. Wang, Y.; Li, Z. Optimal study based on measuring the K value of holistic classroom building group on the college campus. *J. Xi'an Univ. Archit. Technol. Nat. Sci. Ed.* **2011**, *43*, 576–580. [CrossRef]
20. Bordass, B.; Leaman, A. Making feedback and post-occupancy evaluation routine1: A portfolio of feedback techniques. *Build. Res. Inf.* **2005**, *33*, 347–352. [CrossRef]
21. Shen, W.; Shen, Q.; Xiaoling, Z. A user preoccupancy evaluation method for facilitating the designer-client communication. *Facilities* **2012**, *30*, 302. [CrossRef]
22. Daniels, H.; Tse, H.M.; Stables, A.; Cox, S. Design as a social practice: The design of new build schools. *Oxf. Rev. Educ.* **2017**, *43*, 767–787. [CrossRef]
23. Diekmann, A. Evolutionary game theory. In *Evolutionary Social Sciences*; Hammerl, M., Schwarz, S., Willführ, K.P., Eds.; Springer Fachmedien Wiesbaden GmbH: Wiesbaden, Germany, 2025; pp. 152–162.
24. Cai, R.; Loi, E.H.N.; Wang, X.; Zhao, S.; Zhang, T. A stochastic evolutionary game of boosting urban low-carbon development in China. *Sci. Rep.* **2025**, *15*, 33853. [CrossRef]
25. Wang, S.; Zhu, D.; Wang, J. Impact of policy adjustments on low carbon transition strategies in construction using evolutionary game theory. *Sci. Rep.* **2025**, *15*, 3469. [CrossRef]
26. Khan, A.; Qu, X.; Gong, Z. Decision mechanism of farmers' low-carbon agricultural technology adoption: An evolutionary game theory approach. *Empirica* **2025**, *52*, 297–331. [CrossRef]
27. Li, G.; Wu, S.; You, H.; Wang, C. Governments' behavioral strategies in cross-regional reduction of inefficient industrial land: Learned from a tripartite evolutionary game model. *Humanit. Soc. Sci. Commun.* **2025**, *12*, 697. [CrossRef]
28. Li, J.; Zang, Z.; Ji, Q.; Sun, C.; Qiang, W.; Zhang, J.; Zheng, C.; Sun, F.; Xiong, H. Rethinking Generalizability and Discriminability of Self-Supervised Learning from Evolutionary Game Theory Perspective. *Int. J. Comput. Vis.* **2025**, *133*, 3542–3567. [CrossRef]
29. Araujo, G. An evolutionary game theory for event-driven ecological population dynamics. *Theory Biosci.* **2025**, *144*, 95–105. [CrossRef]
30. Hughes, H.; Franz, J.; Willis, J. (Eds.) School Spaces for students wellbeing and learning. In *Insight from Research and Practice*; Springer: Singapore, 2019.
31. AThanh, P.T.; Grierson, D. A Study on Children's Spatial—Social—Natural Interactions Within Primary School: Design Approaches for Case Studies in Ho Chi Minh City, Vietnam. In Proceedings of the 16th Asian Urbanization Conference, Ho Chi Minh City, Vietnam, 11–13 January 2024; Vien, H.T., Pomeroy, G.M., Ngoc Hieu, N., Eds.; AUC 2024. Advances in 21st Century Human Settlements. Springer: Singapore, 2025. [CrossRef]
32. Sreenath, N.; Ranade, P.; Verma, I.K. AI-Powered Personalised Learning in Primary Education: A Design Thinking Perspective. In *Computing and Machine Learning*; Bansal, J.C., Borah, S., Hussain, S., Salhi, S., Eds.; CML 2024. Lecture Notes in Networks and Systems; Springer: Singapore, 2024; Volume 1108. [CrossRef]
33. Falzon, D.; Conrad, E. Designing primary school grounds for Nature-based learning: A review of the evidence. *J. Outdoor Environ. Educ.* **2024**, *27*, 437–468. [CrossRef]
34. Pesch, A.; Hespos, S.; Hirsh-Pasek, K. Playful learning landscapes in the United States: Encouraging intellectual and social risk in everyday spaces. In *Risk and Outdoor Play*; Gray, T., Sturges, M., Barnes, J., Eds.; Springer Nature Singapore Pte Ltd.: Singapore, 2025; pp. 21–36.
35. Al-Zu'bi, M.A.A.; Al-Mseidin, K.I.M.; Yaakob, M.F.M.; Fauzee, M.; Mahmood, M.; Sohri, N.; Al-Mawadieh, R.; Senathirajah, A. The impact of the school educational environment on primary school teachers' commitment to educational quality. *Discov. Sustain.* **2024**, *5*, 449. [CrossRef]
36. Khuranov, V.; Guketlov, K.; Shogenova, F.; Mazloev, A. Analysis of the Space-Planning Solution of the School in Nalchik for Renovation. In Proceedings of the II International Scientific Conference "Recent Advances in Architecture and Construction", Kazan, Russia, 14–15 May 2024; Klyuev, S.V., Vatin, N.I., Nabiullina, K.R., Yumagulova, V.M., Eds.; ICRAAC 2024. Lecture Notes in Civil Engineering. Springer: Cham, Switzerland, 2025; Volume 627. [CrossRef]

https://doi.org/10.3390/buildings16020244

37. Ma, H.; Zhang, W.; Sun, D. Multi-class teaching: The exploration of Caowo Primary School in Gansu. In *New Pathways of Rural Education in China*; Han, J., Ed.; Educational Science Publishing House: Beijing, China, 2024; pp. 115–128.
38. Gomez, R.L.; Suarez, A.M. Do inquiry-based teaching and school climate influence science achievement and critical thinking? Evidence from PISA 2015. *Int. J. STEM Educ.* **2020**, *7*, 43. [CrossRef]
39. Moolman, B.; Essop, R.; Makoae, M.; Swartz, S.; Solomon, J.-P. School climate, an enabling factor in an effective peer education environment: Lessons from schools in South Africa. *S. Afr. J. Educ.* **2020**, *40*, 1–10. [CrossRef]
40. Abdul Latif, N.A.; Mohd Hamzah, M.I.; Mohd Nor, M.Y. Teacher change in practice and holding: The role of collaboration. *World J. Educ.* **2021**, *3*, 279–288.
41. Murphy, M.C. A Bio-Ecological Exploratory Case Study of the Forest School Approach to Learning and Teaching in the Irish Primary School Curriculum. In *Risk and Outdoor Play*; Gray, T., Sturges, M., Barnes, J., Eds.; Springer: Singapore, 2025. [CrossRef]
42. Wang, L. Micro-school Community: The Development and Transformation of Fanjia Primary School in Sichuan. In *New Pathways of Rural Education in China*; Han, J., Ed.; Research in Chinese Education; Springer: Singapore, 2024. [CrossRef]
43. Li, Y. An Empirical Quantitative Analysis of the Plane System of the Office Floor of the Super High-Rise Building. Master's Thesis, Zhejiang University, Hangzhou, China, 2020. Available online: https://kns.cnki.net/kcms2/article/abstract?v=OfZxIIxxsvCrJUgZtw5hQ2zOXzaBsT5nSPKGkZYjNjR0ohyLeQJLxAjz-Ly_Dqz9A0x2KL-hxX6o9dYzZL91DsY0oa9eITznCygUHq9emGPCHbbMgd8SZzhd48t9P1zHqpoeLiYSCzFuisKY7OBYkXdhQRgN-PfjVGMBfjjl5o08ShQevpj5UqSLM5srjIHl&uniplatform=NZKPT&language=CHS (accessed on 10 January 2025).
44. Wang, Y. Study on Optimize Strategy of Holistic Teaching Building Group in University. Ph.D. Thesis, Xi'an University of Architecture and Technology, Xi'an, China, 2012. Available online: https://kns.cnki.net/kcms2/article/abstract?v=OfZxIIxxsvCENSCo9-z0CYDvlaS_TXoRHoW8RyAr3Amk4srnLPSN9NexxR2iEn8C2P86Myb3jo25AwkRUYVaciZI5vpmLIBwCUmVJnXEGV3LXoGuu7BESLwF8vmPVN1-fNe8Mo1ox4a6tNlAmHVcw7HilmKMAmNf-bv_WVyfEV6NIsgaNYqg==&uniplatform=NZKPT&language=CHS (accessed on 10 January 2025).

Disclaimer/Publisher's Note: The statements, opinions and data contained in all publications are solely those of the individual author(s) and contributor(s) and not of MDPI and/or the editor(s). MDPI and/or the editor(s) disclaim responsibility for any injury to people or property resulting from any ideas, methods, instructions or products referred to in the content.

buildings

MDPI

Article

Indoor Light Environment Comfort Evaluation Method Based on Deep Learning and Evoked Potentials

Sheng Miao [1,*], Sudong Li [2], Xixin Yang [2], Hongyu Guan [3] and Xiang Shen [4]

[1] School of Information and Control Engineering, Qingdao University of Technology, Qingdao 266520, China
[2] College of Computer Science and Technology, Qingdao University, Qingdao 266071, China; sudg.lee@gmail.com (S.L.); yangxixin@qdu.edu.cn (X.Y.)
[3] School of Environmental and Municipal Engineering, Qingdao University of Technology, Qingdao 266520, China; guanhongyu@qut.edu.cn
[4] Department of Statistics, The George Washington University, Washington, DC 20052, USA; xiangshen@gwu.edu
* Correspondence: smiao@qut.edu.cn

Abstract: The optimal indoor lighting comfort can enhance physical and mental health and improve work efficiency. The traditional methods for evaluating lighting comfort have problems such as limited data analysis and poor subjectivity. To establish objective criteria, this study proposes a novel method combining deep learning and evoked potentials. This study collected visual evoked potentials across diverse indoor lighting conditions and employed Long Short-Term Memory (LSTM) and Gate Recurrent Unit (GRU) recurrent neural networks to classify temporal evoked electroencephalography data. The experimental results show that both LSTM and GRU achieve higher accuracy than the Feedforward Neural Network. Among them, LSTM performs best, reaching an accuracy of 80.16% while maintaining computational efficiency comparable to GRU. Such effective objective evaluation methods provide a scientific basis for optimizing indoor environments.

Keywords: indoor light comfort; evoked potentials; deep learning; LSTM neural network

1. Introduction

1.1. Background

With the advancement of technology and the acceleration of urbanization, modern people spend more than 90% of their entire day indoors [1]. This trend makes a safe, comfortable and healthy indoor environment not only a fundamental prerequisite for safeguarding human physical and mental health [2], but also a core element for maintaining high productivity and social well-being. Indoor environmental comfort is a complex perception system formed by the coupling of multiple physical factors. It primarily includes sound environment, light environment, and thermal environment [3]. Among many factors, the light environment directly affects the human visual system. And through non-visual imaging effects, it profoundly affects the physiological rhythm, cognitive performance, and emotional state of the human body, and has the most direct and significant impact on work efficiency and physical and mental health [4,5]. Creating a comfortable and healthy indoor lighting environment has evolved from a simple spatial design requirement to an interdisciplinary frontier of shared interest in fields such as architecture, environmental psychology, and ergonomics. However, the development of this field has long been limited

by a core challenge, which is how to establish an objective, accurate, and quantifiable paradigm for evaluating indoor light environment comfort.

1.2. Related Works

With increasing demand for living comfort, researchers have conducted extensive studies on indoor environmental comfort, particularly the indoor lighting environment. Wong et al. studied the acceptable level of noise in office buildings using a mathematical regression model, ultimately evaluating indoor comfort based on the model [6]. Fantozzi summarized the evaluation indicators of indoor environmental comfort in the evaluation of indoor environmental quality, including air quality, sound environment, light environment, and thermal environment [7]. Sugimoto found that human-perceived comfort decreases as illuminance increases within a specific range of illuminance by studying luminance [8]. Guo et al. investigated indoor environmental comfort through subjective questionnaires and established corresponding functional relationships for sound, thermal, and light environmental parameters, ultimately building an indoor overall environmental comfort evaluation model [9]. Yang et al. proposed an evaluation model for indoor environmental comfort using the fuzzy comprehensive evaluation method based on sound, thermal, light, and air quality environmental parameters in university classrooms and found that the indoor thermal environment has a significant impact on indoor environmental comfort [10]. Alshdiefat collected indoor environmental parameter data for twelve months and used response surface analysis to explore the mathematical relationship between indoor environmental factors such as air quality, humidity, illuminance, and indoor environmental comfort, ultimately finding that non-air quality parameteres such as illuminance have a relatively large impact on indoor environmental comfort [11]. Lu et al. researched indoor thermal comfort in buildings and obtained 1400 valid indoor thermal comfort evaluation results through subjective satisfaction questionnaires. Based on the survey results, they studied the thermal comfort in buildings through cluster and linear regression analysis methods [12]. Vieira studied the environmental comfort in the ICUs of hospitals and used the Carnot model as the evaluation model for human comfort [13]. Martinez-Molina et al. assessed indoor thermal comfort using a questionnaire in a historical building in Villar del Arzobispo, Spain, to explore indoor environmental comfort in historical constructions [14]. Nian et al. improved the PMV index proposed by professor Fanger by adding indoor environmental parameters such as CO_2 concentration and established a computational model using a BP neural network, which improved the evaluation effect of the PMV index on indoor environmental comfort [15]. Shamsul's research showed that people have higher comfort levels when living in an indoor lighting environment with an intensity of 4000 K [16]. Wang et al. used a multi-index comprehensive evaluation model including a questionnaire survey method and a weighted scoring method to evaluate the impact of air-source heat pumps on indoor environmental comfort to assess the regulating effect of air-source heat pumps on indoor thermal environments [17]. Liu et al. obtained the weights of different indoor environmental factors using vector similarity and explored the impact of different indoor environments on indoor environmental comfort evaluation by combining subjective questionnaire evaluation methods [18]. Although existing research has laid a certain foundation for the field of lighting design [19–22], the current evaluation methods are essentially based on subjective questionnaires and statistical analysis. The inherent limitations of this approach prevent it from providing objective and reliable assessments of indoor environmental comfort.

Different indoor environments can have an impact on human senses, such as lighting and sound [23]. External environmental stimuli are received by sensory organs and

converted into neural signals, which are then transmitted to the cerebral cortex [24]. The cerebral cortex is the main area for human advanced cognition and information processing, including visual, auditory, and tactile areas [25]. These areas respond differently to different types of stimuli and produce different brainwave activities [26]. These brainwave activities can be transmitted outside the body through the scalp and skull, forming electroencephalography (EEG) signals [27], also known as electrophysiological signals. EEG signals can be recorded and measured using devices such as electrode arrays or EEG amplifiers to study human sensory and cognitive processes. Therefore, EEG activity can be seen as a biological electrical reaction of the human body to external environmental stimuli, reflecting the process of human perception and adaptation to environmental changes [28]. Peng et al. investigated the impact of the train environment on passenger comfort by collecting EEG data from 20 passengers and building a comfort assessment model based on features in the data and the LightGBM algorithm [29]. Küller et al. found that bright light can enhance central nervous system reactivity by studying specific waveforms of brainwaves under different illuminations [30]. These studies suggest that electrical signal activity in the human brain is related to environmental changes. In fact, EEG has been widely used for subjective feeling evaluation and cognitive tasks [31]. Guan et al. studied indoor comfort under the influence of various environmental factors based on subjective evaluation and EEG data. They found that the indoor environment significantly affects cerebral cortex activity [32]. Wu et al. collected EEG signals from 22 volunteers under different indoor thermal environments and used linear discriminant analysis or support vector machines as evaluation models to assess indoor thermal comfort [33]. This indicates that electrical signals generated by the human brain can serve as objective indicators to reflect indoor environmental comfort. However, many studies still have relatively primitive processing of EEG data. For example, Lu et al. estimated the comfort level of people in different environments by observing the latency of the P100 waveform, which is a biological potential signal of visual evoked potential and whose value is related to the reaction speed of the human eye [34]. Individual differences may cause significant differences in P100 latency. Therefore, when analyzing the relationship between EEG and indoor environmental comfort, there is a significant problem with relying on the P100 latency as a physiological parameter for analysis. Simply analyzing a specific waveform in EEG also has a problem of insufficient overall data analysis and inability to fully utilize all the information contained in EEG data. The research methods of analyzing specific EEG waveforms to study indoor environmental comfort have not fully excavated all the information of EEG data, and their processing efficiency is also not high. Therefore, using machine learning methods to process EEG data in different indoor environments and ultimately building a comfort evaluation model for indoor environments based on machine learning algorithms is of great significance.

Over time, traditional methods for analyzing EEG data have shown certain limitations. Consequently, many recent studies have applied machine learning techniques to detect and analyze bioelectrical signals. Researchers have combined machine learning technology with limb rehabilitation movement bioelectrical data to achieve analysis and evaluation of human body rehabilitation movements [35,36]. The application of machine learning technology in EEG analysis has gradually increased. Murtazina used support vector machines and artificial neural network methods to classify brain activity patterns by classifying collected EEG data [37]. EEG data are typical time series data; therefore, using RNN algorithm to analyze EEG data is a better choice. Chowdary et al. used deep learning methods such as LSTM to classify EEG brain wave data according to emotions, with a classification accuracy of over 95%, and achieved good results [38]. EEG signals are a type of bioelectrical signal of human brain activity that has temporal sequence characteristics.

The sampling frequency is generally between tens and hundreds of hertz, and the electrical potential value of brain activity is recorded at each time point, resulting in data with high dimensionality and high spatiotemporal resolution. As a type of neural network that is suitable for processing time series data, RNN is more suitable for processing data with time-dependent relationships. Therefore, using RNN to process EEG data can better explore its time series information and capture the evolution of signals. In addition, using RNN can automatically enable more effective feature representations and improve classification performance. Therefore, it is necessary to use RNN to process EEG data. In this study, different indoor lighting conditions were collected to construct a deep learning-based indoor lighting comfort evaluation model using the RNN algorithm, thus achieving a more objective and accurate evaluation of indoor lighting comfort.

1.3. Research Gap and Contributions

Although progress has been made in the assessment of indoor light environment comfort in existing research, there are still some gaps in the current field. Firstly, in terms of methodology, the evaluation heavily relies on subjective questionnaires, and its results are susceptible to interference from participants' psychological states and individual preferences, lacking a stable and objective physiological evaluation benchmark. Secondly, in terms of data analysis depth, even if physiological signals such as electroencephalography are used, most studies are limited to analyzing specific waveforms or frequency band power. This shallow feature extraction method cannot fully utilize the complete dynamic information contained in EEG as high-dimensional time series data. Thirdly, in terms of matching computational models with data characteristics, traditional machine learning models are difficult to effectively capture the complex temporal dependencies in EEG signals, resulting in limited model performance. Therefore, an automated evaluation framework that can model end-to-end deep temporal sequences based on objective physiological signals and optimize specifically for solving such problems is currently blank.

To find an objective and accurate evaluation method for indoor lighting environment comfort, this study collected EEG data from test subjects under different indoor lighting environments and used deep learning algorithms to process and classify these EEG data. In this way, a more objective and intuitive analysis of the comfort status of the indoor lighting environment is achieved. To overcome the limitations of current methods for evaluating indoor lighting environment comfort, this study constructed a new evaluation method by combining EEG and deep learning technology. This new method uses the mapping relationship between EEG data and environmental comfort level, processes data using recurrent neural network (RNN) models such as LSTM, and achieves classification analysis of EEG data, reducing the incompleteness of manual processing and analysis of data and the subjectivity of traditional questionnaire evaluation. In addition, this study compares the classification results of different RNN methods in terms of time and efficiency and provides a comprehensive discussion of the modeling results. The main contributions of this study are as follows:

(1) A new objective evaluation paradigm for indoor lighting environment comfort has been proposed.
(2) Realized deep end-to-end temporal modeling of EEG signals.

2. Methodology

When the human brain is exposed to different indoor lighting environments, the electrical signal activity in the brain cortex also varies. By capturing the brain electrical activity under different indoor lighting environment comfort levels using an evoked potential

instrument (Haishen NDI-094 (Haishen (Suzhou) Medical Instruments Co., Ltd., Suzhou, China)) and recording the amplitude of these time-varying EEG data, we obtain a dataset of EEG time series data related to indoor lighting comfort levels. Based on LSTM/GRU and EEG, this study constructs a model for evaluating indoor lighting environment comfort to overcome the limitations of traditional subjective evaluation methods, and achieves objective and accurate classification of indoor lighting comfort through end-to-end learning of complete EEG temporal signals.

2.1. Environmental Setup

To simulate the actual indoor environment in daily life more accurately and realistically, the physical and psychological conditions of the participants in the experiment need to meet certain conditions. The specific conditions include the following:participants must have good physical health, normal intelligence, no harmful habits, sound mental health, normal reading and environmental evaluation abilities, normal hearing and vision, and no conditions such as color weakness, color blindness, or amblyopia. The visual acuity of experimental participants should be at least 5.0, or corrected visual acuity should reach 5.0 or higher when wearing glasses.

The psychological and physical conditions of the experimental personnel can cause interference with the experimental results. To ensure the normal operation of the experiment and the objective accuracy of the experimental results, it is necessary to exclude various external factors that may cause interference with the experimental results. Experimental personnel need to maintain a good psychological state for a period of time before the start of the experiment to reduce the impact of psychological fluctuations on human environmental perception. Excessive excitement or negative emotions can have a negative impact on the human body's environmental perception ability. The experiment requires participants to avoid significant emotional fluctuations and ensure that the experimental results are not influenced by emotional factors. Within two days before the start of the experiment, participants are required to ensure that they do not consume alcoholic beverages or beverages containing caffeine or other stimulants, avoid smoking, and do not consume foods or drugs that cause physical stimulation. In addition, the experiment requires the participants to maintain a calm attitude as much as possible within 2 h before the start of the experiment and not participate in sports such as sprinting to ensure that their bodies do not become overly excited and avoid fatigue.

The experiment was conducted in a special double-layer double-room laboratory with a length of 5 m, a width of 3 m, and a height of 2.6 m. The laboratory has environmental control functions and can simulate various indoor environments by adjusting the comfort parameters of indoor temperature, illumination, noise, and humidity. The laboratory is divided into two layers, with a preparation room in the outer layer for test subjects to change into experimental clothes. The inner laboratory is the evoked potential acquisition room, and the temperature and humidity inside the inner laboratory are regulated through a return air vent. The temperature control accuracy inside the laboratory can reach ±0.5 °C, and the humidity control accuracy can reach ±5%. The air conditioning equipment is located in the outer laboratory to avoid the noise generated by the running of the air conditioning equipment to affect the experiment. Sound-absorbing materials are used between the air conditioning equipment and the inner laboratory to reduce noise. The adjustment of color temperature and illumination inside the inner laboratory relies on six intelligent lamps installed in the laboratory, which can adjust brightness and color temperature in real time. By controlling the illumination and color temperature through intelligent lamps, the experiment ensures that the indoor light environment is within the

target value range of the experimental conditions. The interior design of the laboratory is shown in Figure 1.

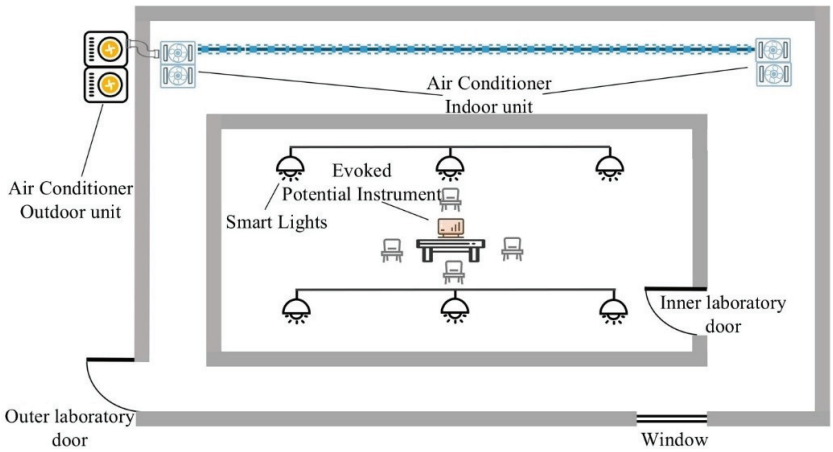


Figure 1. Laboratory internal design.

A long desk is placed in the center of the small room for experimental participants to use, with the desktop 0.75 m above the ground. The brightness measurement point is fixed in the center of the long desktop in the room, making the light environment testing point as close as possible to the experimental participants. The brightness measurement point is approximately 0.80 m from the ground. All experimental lighting and color temperature measurements were conducted at the same measurement point. To simulate the daily work and living environment, the walls of the inner laboratory are painted milky white. The on-site environment of the inner laboratory is shown in Figure 2.



Figure 2. Inner laboratory on-site environment.

2.2. Data Acquisition

A total of 16 volunteers participated in the EEG data collection experiment, with males or females aged between 22 and 26. Among these 16 volunteers, there were a total of 9 male volunteers and 7 female volunteers. The basic information for the 16 experimental participants is shown in Table 1. A total of 13 volunteers had their vision corrected,

including 8 male volunteers and 5 female volunteers. Among the three volunteers with uncorrected vision, there was one male and two females. The study was conducted in accordance with the Declaration of Helsinki, and the protocol was approved by the Ethics Committee, Medical College of Qingdao University (approval No. QDU-HEC-2024172).

Table 1. Basic information of testers.

	Maximum Age (Year)	Minimum Age (Year)	Average Age (Year)
Male	26	22	23.9
Female	25	22	23.3
All Tester	26	22	23.6

Electroencephalogram (EEG) data were collected from participants using the Haishen NDI-094 evoked potential instrument (Haishen NDI-094 (Haishen (Suzhou) Medical Instruments Co., Ltd., Suzhou, China)) in a simulated indoor environment with preset parameters, shown in Figure 3. Following the international 10–20 system, multiple electrodes were placed on the participant's scalp. The recording electrode was positioned at Oz, the reference electrode at Cz, and the ground electrode on the forehead (AFz). Throughout the experiment, electrode impedance was maintained below 15 kΩ. Pattern Reversal Visual Evoked Potential (PRVEP) was employed as the primary stimulation method, shown in Figure 4. An 8 × 6 black-and-white checkerboard pattern was displayed to the subject and reversed at a frequency of 1.5 Hz to elicit visual evoked responses. Participants were instructed to focus binocularly on a red cross at the center of the screen, positioned approximately 0.6 m away. The EEG signals were recorded continuously using a bipolar lead montage at a sampling rate of 2000 Hz (0.5 ms per point), with an online analog band-pass filter of 0.1–100 Hz. Each PRVEP recording spanned 450 ms (900 data points). To enhance the signal-to-noise ratio, 150 trials were averaged. Offline, a 30 Hz low-pass zero-phase digital filter was applied to further reduce high-frequency noise.



Figure 3. Evoked potential instrument.

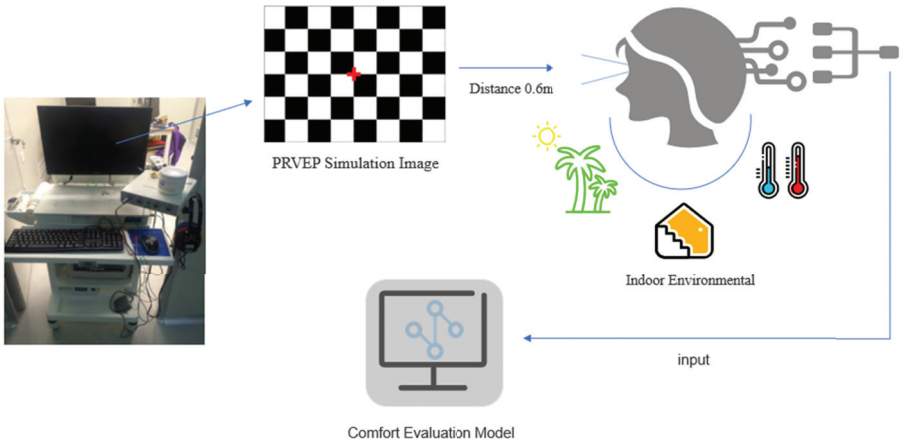


Figure 4. PRVEP collection process.

The process of EEG acquisition experiments is divided into three stages: adaptation, evaluation, and collection. In the adaptation stage, the experimenter adjusts the environmental factors such as illumination, temperature, humidity, and sound pressure level in the laboratory according to the preset working conditions. Meanwhile, the test subjects change into comfortable experimental clothing and familiarize themselves with the evaluation questionnaire and experimental procedure in the preparation room. In the evaluation stage, the test subject enters the inner laboratory where the environmental parameters have been adjusted to the preset values. The test subject must sit quietly in the experimental illumination environment for 10 min to adapt to the laboratory environment, during which the test subject is prohibited from using any electronic devices. After adapting to the laboratory environment, the test subject completed the environmental comfort evaluation questionnaire. The collection stage began after the test subject completed the questionnaire. In this stage, the test subject wears the electrodes of the evoked potential instrument with the assistance of the experimenter, and then the visual evoked potential experiment is conducted. After the data collection for each indoor environmental condition, the test subject rests for 5 min. Under each working condition, each person spends approximately 15 min conducting the experiment. Sixteen test subjects underwent visual evoked potential data collection in the aforementioned stages, with one person per experiment. The experiment includes 27 different indoor environmental conditions, which cover a variety of typical conditions found in daily life and production throughout different seasons. The specific working conditions are presented in Table 2.

Under each experimental condition, every participant provided a subjective evaluation of the indoor comfort level, categorizing it as "uncomfortable", "moderately comfortable", or "relatively comfortable". These responses were converted into discrete labels (0, 1, or 2) corresponding to the perceived comfort level. As a result, each recorded visual evoked potential (VEP) sample was assigned a label specific to both the participant and the experimental condition. The final dataset was constructed by aggregating all participant–condition combinations, with the resulting category distribution reflecting the frequency of individual subjective evaluations across the three comfort categories. In the VEP acquisition experiment, which encompassed 27 distinct working conditions, a total of 279 valid VEP samples were obtained. Each sample was recorded over a duration of 45,000 µs. With a sampling interval of 500 µs, every sample comprises 900 temporal data points, resulting in an evoked potential data length of 900 units. All VEP data were labeled according to the comfort ratings provided by participants under the corresponding experimental

conditions, with the three labels (0/1/2) representing discomfort, moderate comfort, and relative comfort, respectively. Figure 5 illustrates the evoked potential waveforms collected from Tester 001 under working conditions 1 to 11. The vertical axis denotes the amplitude of the evoked potential in nanovolts (nV), while the horizontal axis represents the time in microseconds (μs).

Table 2. Indoor environmental conditions.

Conditions	Temperature (°C)	Illuminance (lx)	Decibel (dB)	Color-Temperature (K)
1	18	100	50	5700
2	18	100	50	4000
3	18	100	50	3000
4	18	300	50	5700
5	18	300	50	3000
6	18	300	50	4000
7	18	500	50	3000
8	18	500	50	4000
9	18	500	50	5700
10	22	300	50	4000
11	22	500	50	3000
12	22	300	50	5700
13	22	500	50	3000
14	22	500	50	4000
15	22	500	50	5700
16	22	100	50	3000
17	22	100	50	5700
18	22	100	50	4000
19	26	500	50	3000
20	26	500	50	5700
21	26	500	50	4000
22	26	300	50	5700
23	26	300	50	4000
24	26	300	50	3000
25	26	100	50	5700
26	26	100	50	3000
27	26	100	50	4000

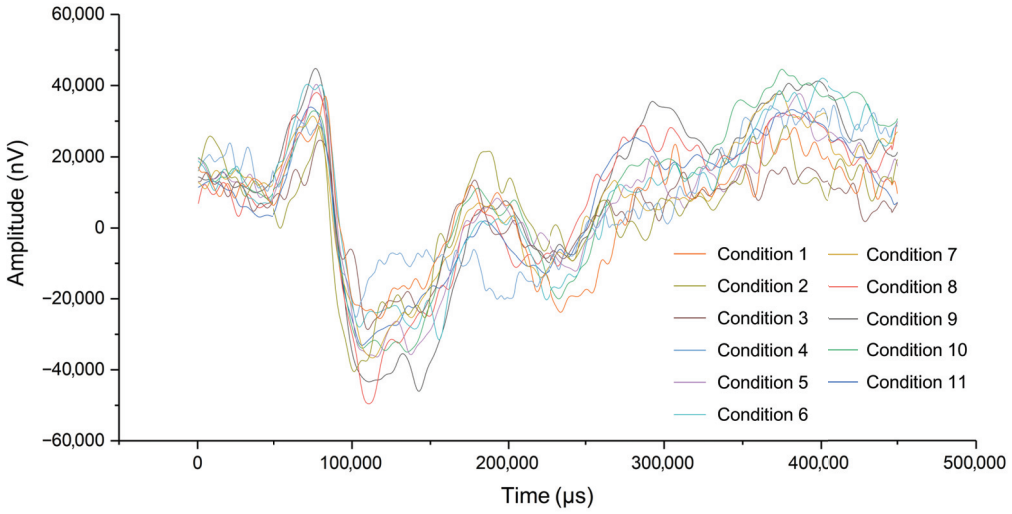


Figure 5. Visual evoked potential data of tester 001.

2.3. Recurrent Neural Network

RNN is a type of neural network that takes sequential data as input, connects all the recurrent units in a chain, and recursively processes the sequence in the forward direction [39]. The internal recurrent structure of RNNs allows them to preserve information from previous time steps and maintain their long-term memory while processing time series data [40]. This structure enables RNNs to learn long-term dependencies from time series data and capture long-term patterns and trends. In time series data classification tasks, RNNs can consider the data at each time step and their relationships to make the final classification decision. Overall, RNNs' internal recurrent structure and long-term dependencies make them particularly suitable for handling long sequential time series data such as EEG data. Figure 6 shows the general structure of an RNN. As shown in Figure 6, the output value at time t is represented by o_t, and x_t represents the input at time t. W and U are the parameter matrices in the network, with U representing the parameter matrix from the output layer to the hidden layer and W representing the parameter matrix from the hidden layer to the output layer. V represents the weight matrix for each time step. The relevant formulae for RNN are shown below [41].

$$o_t = g(V \cdot s_t) \tag{1}$$

$$s_t = f(U \cdot x_t + W \cdot s_{t-1}) \tag{2}$$

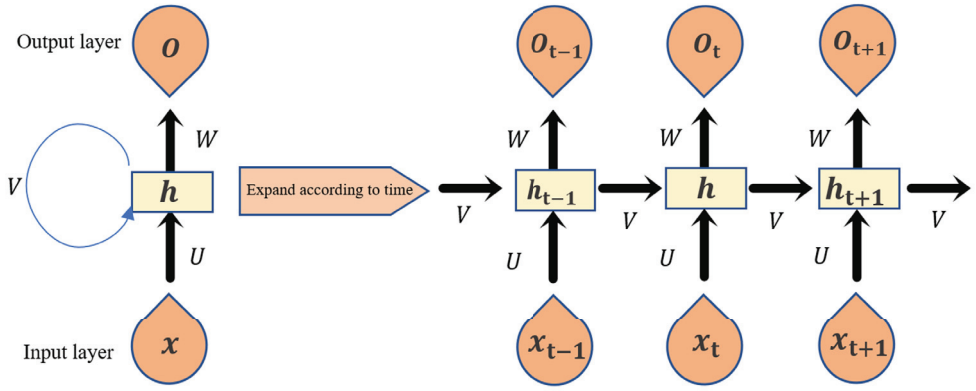


Figure 6. Structure diagram of RNN.

2.4. LSTM and GRU

Due to the problem of vanishing gradients, RNNs have insufficient ability to store long-term information when processing long time series data. LSTM, as a kind of RNN, retains some of the characteristics of RNN while also incorporating the functions of preserving and forgetting information, which effectively solves the problem of short-term memory, and performs well in processing long time series data.

The structure and internal information flow of an LSTM cell are shown in Figure 7a. In an LSTM cell, the input usually consists of two parts: the previous output h_{t-1}, also known as the hidden state, and the current input x_t. After being linearly transformed, these two inputs are fed into three gate controllers: the forget gate, the input gate, and the output gate [42]. The forget gate is used to control how the previous memory C_{t-1} affects the current memory unit, and its calculation formula is shown in (3), where W_f and b_f are the weight and bias of the forget gate, respectively, and σ is the sigmoid function. f_t is the output of the forget gate, which has a value range of $[0, 1]$, and it determines how much information of the cell state should be discarded. When f_t approaches 1, the forget gate

retains all the information of the cell state, while when f_t approaches 0, the forget gate discards all the information of the cell state.

$$f_t = \sigma(W_f[h_{t-1}, x_t] + b_f) \tag{3}$$

GRU and LSTM are two common architectures of recurrent neural networks that can be used for processing time series data. They both use gate mechanisms to control the flow of information, thereby solving the problem of vanishing and exploding gradients in traditional RNNs. Compared to LSTM, the GRU structure is more concise, faster, computationally efficient, and easier to train. In addition, in terms of gate mechanisms, LSTM has three gate controllers: input gate, forget gate, and output gate. The GRU has only two gate controllers: an update gate and a reset gate [43]. It can quickly decide whether to reset the hidden state at the current time step and how much of the information obtained at the current time step should be combined with the hidden state. The internal structure of the GRU is approximately shown in Figure 7b. The gate mechanism of GRU is simplified compared to that of LSTM, and this structure also reduces the number of GRU parameters.

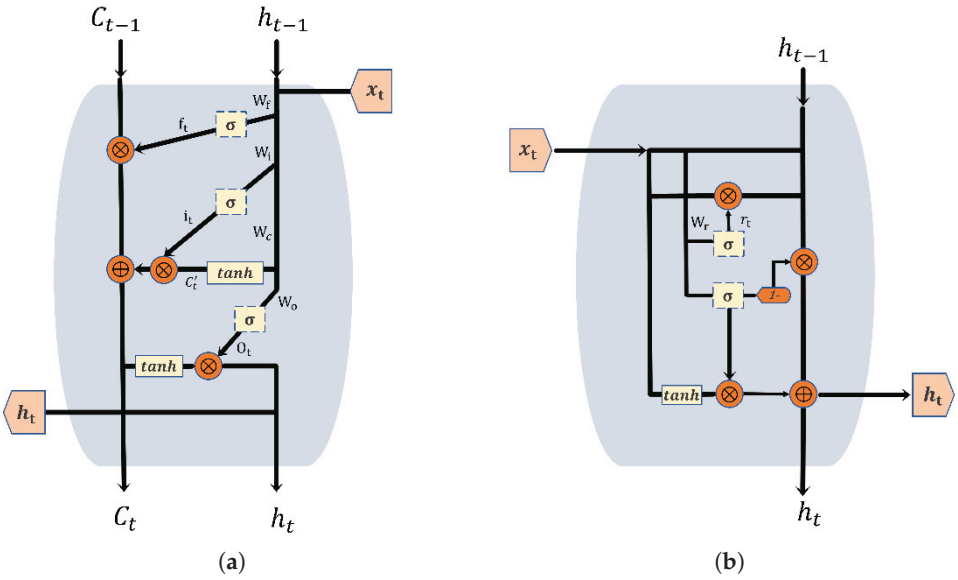


Figure 7. LSTM cell and GRU cell schematic diagram. (**a**) LSTM cell schematic. (**b**) GRU cell schematic.

Compared to GRU, the complex structure of LSTM can usually capture information with more complex time-dependent data, so LSTM may be more effective in processing long-term data such as EEG. The use of GRU or LSTM should depend on the specific situation. Overall, both GRU and LSTM are effective RNN architectures, but LSTM may be better suited for complex problems. GRU can be used for simple problems or time-sensitive scenarios because of its higher computational efficiency. Therefore, the decision to choose between GRU and LSTM should be based on the specific application requirements. In this study, both LSTM and GRU algorithms will be used to process EEG data under different indoor lighting conditions to seek the best results. LSTM and GRU improve the problem of long-term dependencies in RNN. By using a special structure to handle the propagation of information in the network, they allow neural networks to learn long-term dependencies in time series data and can better process temporal data. This study aims to analyze and evaluate indoor comfort by exploring EEG data. The EEG data collected in the experiment have obvious temporal characteristics. Therefore, LSTM and GRU recurrent neural networks will be used in this study to better extract useful information

from EEG data and accurately classify and evaluate EEG data under different indoor lighting conditions. Therefore, this study will analyze and compare the accuracy and classification time of LSTM and GRU to compare their performance in processing long time series data.

2.5. Modeling

This study combines the advantages of using RNNs to process long-term sequential data and the mapping relationship between EEG data and indoor environmental comfort to construct an indoor lighting environment comfort evaluation model. Figure 8 shows the structure of the indoor lighting environment comfort evaluation model. The collected EEG data are combined with data labels and input into the recurrent neural network model for processing. Finally, the network model outputs a classification evaluation result of indoor environmental comfort.

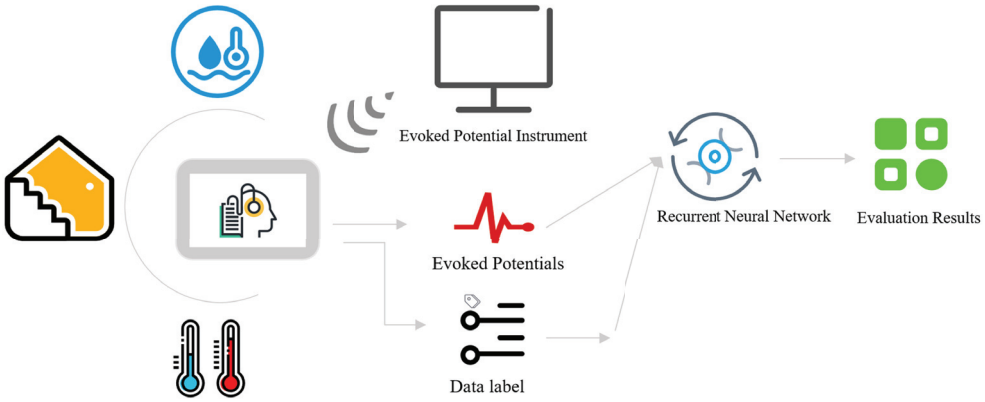


Figure 8. Evaluation model of indoor light environment comfort.

This study constructed an indoor lighting comfort evaluation model based on LSTM/GRU and EEG, as shown in Figure 9. The initial input of the model is the normalized indoor lighting-evoked potential data, which consists of n features. Assuming the input indoor lighting-evoked potential is $x_t = (x_{t1}, x_{t2}, \ldots, x_{tn})$, we integrate these features into a $s \times n$ input matrix according to the time step s. Then, we feed this input matrix into the LSTM or GRU recurrent neural network model. In the recurrent neural network model, the time step s determines the number of times the sample is put in, and at each time step, we input the data sample into the model. The data are then classified based on the EEG data obtained at each time step through the hidden layer. The recurrent neural network model adopts a multilayer neural network model design, and to reduce the impact of data volume on experimental results and prevent overfitting, dropout layers are introduced between layers. Finally, using a fully connected layer as the endpoint, output the categories of indoor light environment comfort, and ultimately form a complete indoor light environment comfort evaluation model.

The system information of the experimental machine used for the research is as follows: the operating system is Windows 10, version number 22H2, the Central Processing Unit (CPU) is an Intel Core i9 12900k @3.9 GHz, and the machine has 64 GB of random access memory (RAM). The graphics card used in the machine is an NVIDIA GeForce RTX 3090 (nVidia Co., Santa Clara, CA, USA). Python version 3.7.2 is used as the primary language for the experiment. The machine learning numerical computing software framework used in the experiment is Google TensorFlow, and the version of TensorFlow used is TensorFlow 2.2.0.

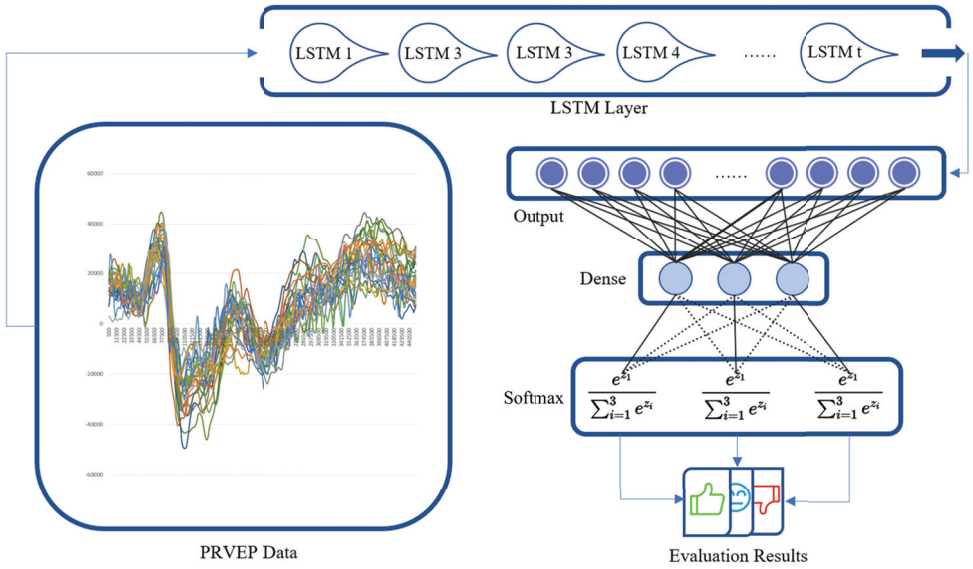


Figure 9. Indoor light environment comfort evaluation model based on LSTM/GRU and EEG.

After multiple experiments and result comparisons, this study adopted a multilayer LSTM structure in the design of the RNN architecture and parameters. The number of hidden layers in the neural network was set to 8, each with 64 units, and dropout layers were added between layers to control the percentage of neurons disconnected during linear transformations. The node retention probability parameter of the dropout layer was set to 0.8. Finally, a fully connected layer was used to form a complete recurrent neural network model. The structures of the GRU and LSTM were the same, both consisting of 8 hidden layers and a fully connected layer in the multilayer design. The models were trained using the Nadam optimizer with a constant learning rate of 0.001 and a batch size of 32. Compared with the Adam optimizer, the Nadam optimizer introduced a Nesterov momentum term, which can better estimate the direction of gradient descent, avoid becoming stuck in local minimum points, and improve the model's generalization ability. Moreover, the Nadam optimizer can perform correction when updating parameters, thereby improving the efficiency and accuracy of training. The loss function used in this experiment was CategoricalCrossentropy. To improve the model performance and alleviate the problem of noise and incorrect labels in the training data, the label smoothing method was used to process the data labels. The label smoothing method smooths the probability distribution of training labels. Label smoothing is a regularization method used for classification problems that can reduce the overfitting degree of the model to noise or incorrect labels in the training data, prevent the model from overfitting during training, and improve the model's generalization ability.

The training process was monitored using a validation set, and we implemented an early stopping routine with a patience of 20 epochs based on the validation loss to halt training if no improvement was observed and to prevent overfitting. The formula for label smoothing is shown in (4), where $\bar{y}_i$ represents the smoothed label, y_i represents the original label, K represents the total number of labels, and ϵ represents the smoothing parameter.

$$\bar{y}_i = (1 - \epsilon) y_i + \frac{\epsilon}{K} \tag{4}$$

3. Results and Discussion

This study collected indoor light environment EEG data based on an evoked potential instrument and a controllable environment laboratory and used GRU and LSTM algorithms to classify and evaluate the collected indoor light environment EEG.

In order to rigorously evaluate the performance and generalization ability of the model, we segmented the dataset, with 75% of the data used as the training set for developing the model and 25% as an independent testing set. After 250 training cycles, the indoor lighting environment comfort evaluation model tends to converge, as shown in Figures 10 and 11. At this point, the accuracy of GRU classification is 75.99%, and the classification time is 32.09 s. The accuracy of the LSTM classification is 80.16%, and the classification time is 36.21 s. To compare the performance and accuracy of recurrent neural network algorithms, this study also used a feedforward neural network (FNN) as a control. In this experiment, the number of hidden layers of the FNN is set to 5, the model optimizer used is the Nadam optimizer, and the loss function used is CategoricalCrossentropy. Figure 12 shows the loss and accuracy of the FNN for indoor lighting environment comfort classification after 100 epochs of training. The accuracy of the FNN classification is 69.74%, and the classification time is 2.31 s. As the number of model iterations increases, the loss and accuracy become stable.

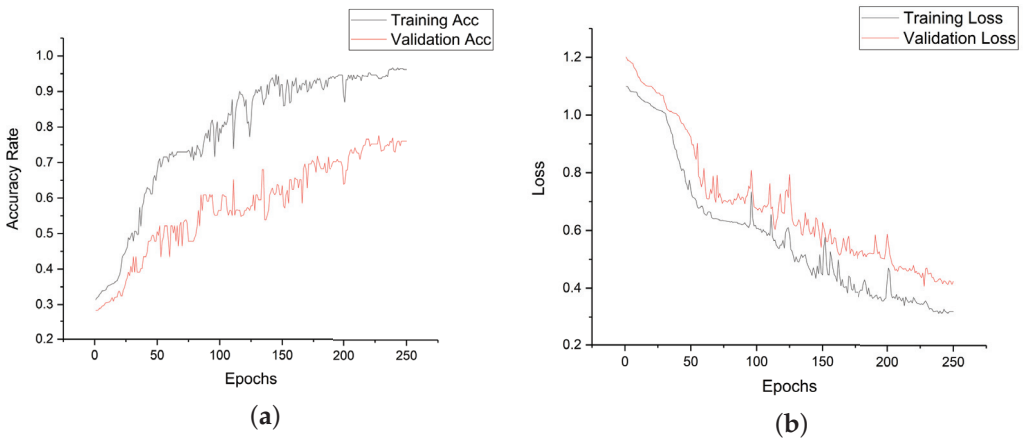


Figure 10. GRU accuracy curve and loss curve. (**a**) GRU accuracy curve. (**b**) GRU loss curve.

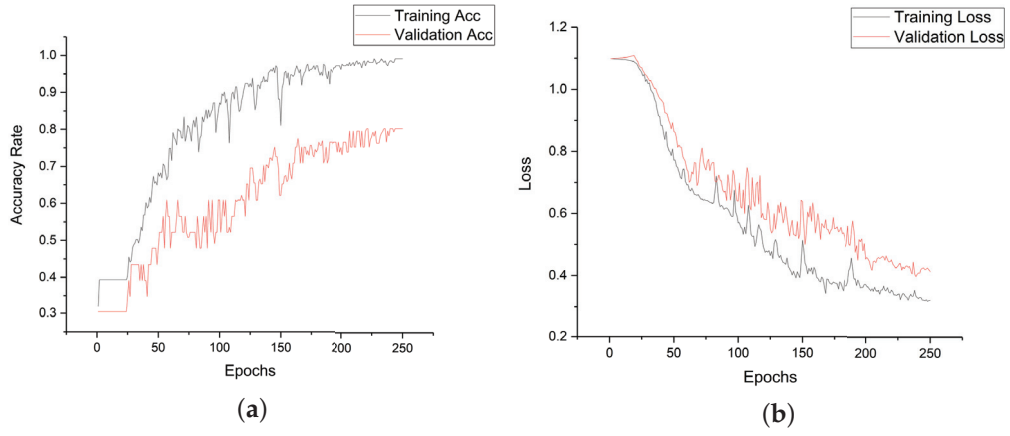


Figure 11. LSTM accuracy curve and loss curve. (**a**) LSTM accuracy curve. (**b**) LSTM loss curve.

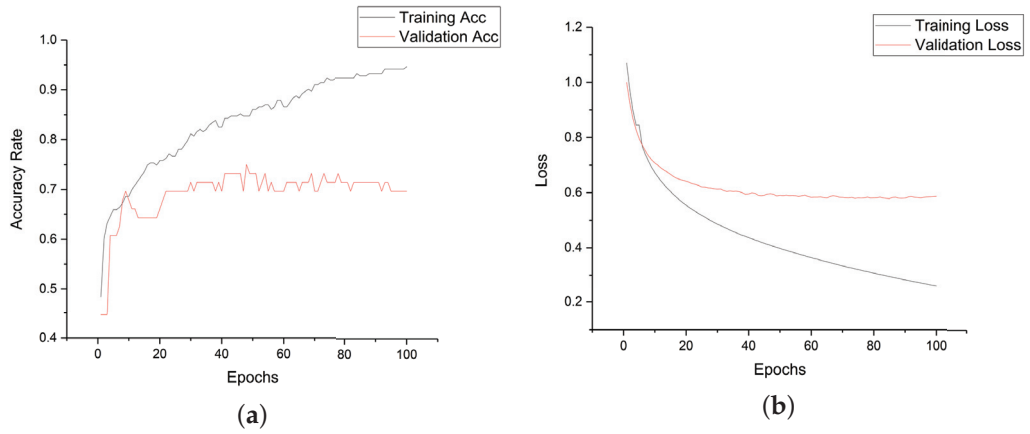


Figure 12. FNN accuracy curve and loss curve. (**a**) FNN accuracy curve. (**b**) FNN loss curve.

In this study, we use four metrics to evaluate the performance of classification models: accuracy, precision, recall, and F1-score. Accuracy reflects the model's performance differences across different categories. Precision measures the accuracy of the model in predicting positive samples, while recall measures the proportion of positive samples detected by the model in the true positive samples. The F1-score is a metric that comprehensively considers precision and recall, and it is the harmonic mean of precision and recall. The comparison of the performance of the FNN, LSTM, and GRU algorithms is shown in Table 3. Through analysis, it is found that LSTM has the best accuracy in the problem of indoor lighting comfort classification, followed by GRU, while FNN performs the worst. LSTM achieved an accuracy of 80.16 % in terms of accuracy, which can complete the task of evaluating indoor lighting comfort. The accuracy of LSTM was improved by 4.17% compared to GRU, but the time overhead was an additional 4.12 s compared to LSTM, which is due to the more complex structure of LSTM, resulting in a lower classification efficiency but an improved classification performance. The accuracy of the FNN in the problem of indoor lighting comfort classification is lower than that of LSTM and GRU, which is 69.64%. Although the time overhead of FNN is much lower than that of LSTM and GRU, its lower accuracy makes FNN not the optimal choice for solving the problem of indoor lighting comfort classification.

Table 3. FNN, LSTM and GRU performance comparison.

Algorithm	Accuracy	Precision	Recall	F1-Score	Time
FNN	69.64%	73.58%	41.96%	53.44%	2.31s
LSTM	80.16%	89.18%	44.54%	59.41%	36.21s
GRU	75.99%	83.96%	42.85%	56.74%	32.09s

The analysis of precision, recall, and F1-score reveals a challenge in our model's performance: while precision is high, the recall rates for the classes are relatively low. This pattern is often indicative of class imbalance within the dataset, where the distribution of samples across the three comfort levels is not uniform. A model trained on such imbalanced data may become biased towards the majority class, leading to a higher number of false negatives for the minority classes, which is reflected in a lower recall. To mitigate the potential negative effects of imbalance and improve generalization, we incorporated the label smoothing regularization technique during training. While this improved overall accuracy by approximately 8% compared to the baseline without label smoothing, it did

not fully resolve the recall imbalance. Future iterations of the model will specifically target this issue.

The observed model bias, particularly the tendency to misclassify 'moderate comfort' samples as 'discomfort', while superficially a performance shortcoming, warrants a more nuanced interpretation from an application perspective. This systematic error can be attributed to the fundamental challenge of defining clear, physiological boundaries between contiguous subjective states. The 'moderate comfort' category, by its nature, represents a transitional zone between clear comfort and clear discomfort. It is plausible that the physiological signatures (VEP patterns) in this transitional state share more characteristics with the 'discomfort' state than with 'relative comfort'. Consequently, the model learns a more conservative decision boundary, erring on the side of caution. Rather than being merely a limitation, this specific misclassification pattern holds significant practical value. In the context of indoor environmental assessment and smart building control, a system that prioritizes sensitivity to potential discomfort is highly desirable. A prediction of 'discomfort' for a state that is on the borderline functions as a valuable early warning. It signals that the current lighting environment is approaching a critical threshold that may lead to occupant unease. This allows a building management system to proactively adjust the lighting conditions preemptively, preventing the environment from degrading into a state of genuine discomfort. Therefore, this bias aligns well with the precautionary principle in human-centric building design, where the cost of a false positive is often far lower than the cost of a false negative.

Although current research prioritizes the end-to-end classification performance of deep learning models, the physiological interpretability of model decisions is a key consideration factor. The excellent accuracy of the LSTM model in classifying comfort indicates that it can automatically identify the most discriminative time periods in VEP signals. From the perspective of visual neurophysiology, a typical VEP waveform is defined by a series of negative and positive peaks, which are known to reflect early visual processing in the striatum and striatum cortex [44]. A large amount of literature has confirmed that the param of visual stimuli, including illuminance and color temperature, systematically adjust the latency and amplitude of these specific components [45]. Given this established knowledge, the discriminative power of our model is likely to stem from its learning sensitivity to these neurophysiological biomarkers. The LSTM architecture has advantages in simulating long-range dependencies and is particularly suitable for capturing temporal relationships and subtle changes in N75-P100-N135 sequences caused by different lighting conditions. Therefore, although attribution graphs were not explicitly visualized in this work, the high performance of our model provides strong indirect evidence that the learned patterns are not arbitrary, but consistent with potential visual neurophysiology influenced by illumination and CCT.

4. Conclusions

A good indoor environment comfort evaluation system is of great significance for improving indoor environment comfort and people's quality of life. However, traditional indoor lighting environment comfort evaluation methods rely too much on subjectivity. Therefore, this study combines techniques such as EEG analysis, indoor environment design, and machine learning to propose a deep learning recursive neural network-based indoor environment comfort evaluation model, providing a new solution for indoor environment comfort evaluation. The experimental results show that compared with GRU and FNN models, the LSTM neural network algorithm achieve higher accuracy and lower time overhead in evaluating indoor lighting comfort, with an accuracy of 80.16%. This

study selected the LSTM recurrent neural network with the best overall performance as the main evaluation model for indoor environmental comfort. This study provides a more objective evaluation method and a new evaluation approach for indoor environmental comfort assessment.

In future work, we will prioritize enhancing the model's robustness and real-world applicability. The most immediate step is to expand the scale and diversity of the validation cohort, encompassing individuals of varying ages, cultural backgrounds, and visual acuity levels, to rigorously assess and improve the model's generalizability. Concurrently, we will address the current limitation of suboptimal recall—an issue likely arising from class imbalance—by implementing and evaluating advanced techniques such as class-weighted loss functions and focal loss, with the aim of achieving more balanced performance across all comfort categories. Furthermore, we plan to explore the integration of consumer-grade wearable EEG devices to reduce operational costs and facilitate the transition of this assessment method from controlled laboratory settings to real-world deployment scenarios. Finally, a comparative analysis with additional baseline models will be incorporated to more comprehensively benchmark the performance of the proposed framework.

Author Contributions: Conceptualization, S.M., H.G. and X.S.; Methodology, S.M., S.L., and H.G.; Validation, S.L., X.Y. and X.S.; Formal analysis, X.Y. and X.S.; Writing—original draft, S.M. and S.L.; Writing—review and editing, X.Y., H.G. and X.S.; Visualization, S.L. and H.G.; Supervision, S.M. and X.S. All authors have read and agreed to the published version of the manuscript.

Funding: This research received no external funding.

Institutional Review Board Statement: The study was conducted in accordance with the Declaration of Helsinki, and approved by the Institutional Review Board of Medical College of Qingdao University (protocol code QDU-HEC-2024172 and date of approval [2 March 2024]).

Informed Consent Statement: Informed consent was obtained from all subjects involved in the study.

Data Availability Statement: The original contributions presented in this study are included in the article. Further inquiries can be directed to the corresponding author.

Conflicts of Interest: The authors declare no conflicts of interest.

References

1. Irga, P.J.; Mullen, G.; Fleck, R.; Matheson, S.; Wilkinson, S.J.; Torpy, F.R. Volatile organic compounds emitted by humans indoors—A review on the measurement, test conditions, and analysis techniques. *Build. Environ.* **2024**, *255*, 111442. [CrossRef]
2. Yang, T.; Zhao, L.; Li, W.; Wu, J.; Zomaya, A.Y. Towards healthy and cost-effective indoor environment management in smart homes: A deep reinforcement learning approach. *Appl. Energy* **2021**, *300*, 117335. [CrossRef]
3. Weerasinghe, A.S.; Rasheed, E.O.; Rotimi, J. Occupants' Decision-Making of Their Energy Behaviours in Office Environments: A Case of New Zealand. *Sustainability* **2023**, *15*, 2305. [CrossRef]
4. Nikookar, N.; Sawyer, A.O.; Goel, M.; Rockcastle, S. Investigating the Impact of Combined Daylight and Electric Light on Human Perception of Indoor Spaces. *Sustainability* **2024**, *16*, 3691. [CrossRef]
5. Chen, P.; Wang, L.; Wu, Y.; Liang, Z.; Yu, J.; Chen, T. Computational design of indoor lighting supported by artificial intelligence: Recent advances and future prospects. *Build. Environ.* **2025**, *285*, 113575. [CrossRef]
6. Wong, L.T.; Mui, K.W.; Hui, P.S. A multivariate-logistic model for acceptance of indoor environmental quality (IEQ) in offices. *Build. Environ.* **2008**, *43*, 1–6. [CrossRef]
7. Fantozzi, F.; Rocca, M. An Extensive Collection of Evaluation Indicators to Assess Occupants' Health and Comfort in Indoor Environment. *Atmosphere* **2020**, *11*, 90. [CrossRef]
8. Sugimoto, S.; Hataoka, H. Physiological effects of illuminance. *J. Light Vis. Environ.* **1986**, *10*, 1_15–1_20. [CrossRef]
9. Guo, T.; Hu, S.; Liu, G. Evaluation Model of Specific Indoor Environment Overall Comfort Based on Effective-Function Method. *Energies* **2017**, *10*, 1634. [CrossRef]

10. Yang, D.; Mak, C.M. Relationships between indoor environmental quality and environmental factors in university classrooms. *Build. Environ.* **2020**, *186*, 107331. [CrossRef]
11. Kaushik, A.K.; Arif, M.; Syal, M.M.G.; Rana, M.Q.; Oladinrin, O.T.; Sharif, A.A.; Alshdiefat, A.A.S. Effect of Indoor Environment on Occupant Air Comfort and Productivity in Office Buildings: A Response Surface Analysis Approach. *Sustainability* **2022**, *14*, 15719. [CrossRef]
12. Lu, S.; Liu, Y.; Sun, Y.; Yin, S.; Jiang, X. Indoor thermal environmental evaluation of Chinese green building based on new index OTCP and subjective satisfaction. *J. Clean. Prod.* **2019**, *240*, 118151. [CrossRef]
13. Vieira, E.M.A.; Neves, A.I.A.; Falcão, C.A.; Sousa, R.V.C.; Carvalho, J.P.; Leite, W.K.S.; Da Silva, L.B. Comfort requirements assessment on indoor environmental quality in hospital's ICU. In Proceedings of the Occupational Safety and Hygiene IV—Selected, Extended and Revised Contributions from the International Symposium Occupational Safety and Hygiene, Guimaraes, Portugal, 23–24 March 2016.
14. Martinez-Molina, A.; Boarin, P.; Tort-Ausina, I.; Vivancos, J.L. Post-occupancy evaluation of a historic primary school in Spain: Comparing PMV, TSV and PD for teachers' and pupils' thermal comfort. *Build. Environ.* **2017**, *117*, 248–259. [CrossRef]
15. Nian, F.; Wang, K. Study on indoor environmental comfort based on improved PMV index. In Proceedings of the 2017 3rd International Conference on Computational Intelligence & Communication Technology (CICT), Ghaziabad, India, 9–10 February 2017; pp. 1–4. [CrossRef]
16. Shamsul, B.M.T.; Sia, C.C.; Ng, Y.G.; Karmegan, K.J.A.J. Effects of Light's Colour Temperatures on Visual Comfort Level, Task Performances, and Alertness among Students. *Am. J. Public Health Res.* **2013**, *1*, 159–165. [CrossRef]
17. Wang, Z.; Wang, F.; Ma, Z.; Bai, M.; Liu, S. Experimental investigation and evaluation of the performance of air-source heat pumps for indoor thermal comfort control. *J. Mech. Sci. Technol.* **2018**, *32*, 1437–1447. [CrossRef]
18. Liu, H.; Shi, H. Evaluating the overall comfort of undergraduates by using the punishment substitution method. *Indoor Built Environ.* **2022**, *31*, 1577–1593. . . [CrossRef]
19. Islam, M.S.; Dangol, R.; Hyvärinen, M.; Bhusal, P.; Puolakka, M.; Halonen, L. User acceptance studies for LED office lighting: Lamp spectrum, spatial brightness and illuminance. *Light. Res. Technol.* **2015**, *47*, 54–79. [CrossRef]
20. Te Kulve, M.; Schlangen, L.; van Marken Lichtenbelt, W. Interactions between the perception of light and temperature. *Indoor Air* **2018**, *28*, 881–891. [CrossRef]
21. Lee, J.; Moon, J.W.; Kim, S. Analysis of Occupants' Visual Perception to Refine Indoor Lighting Environment for Office Tasks. *Energies* **2014**, *7*, 4116–4139. [CrossRef]
22. Shen, E.; Hu, J.; Patel, M. Energy and visual comfort analysis of lighting and daylight control strategies. *Build. Environ.* **2014**, *78*, 155–170. [CrossRef]
23. Tong, L.; Zhang, M.Z.; Hu, S.T.; Zhang, X. Experimental study on thermal sensation and physiological parameter changes under the interaction of environmental temperature and taste. *Energy Build.* **2025**, *345*, 116093. [CrossRef]
24. McKinley, M.J.; Denton, D.A.; Ryan, P.J.; Yao, S.T.; Stefanidis, A.; Oldfield, B.J. From sensory circumventricular organs to cerebral cortex: Neural pathways controlling thirst and hunger. *J. Neuroendocrinol.* **2019**, *31*, e12689. [CrossRef]
25. Saadon-Grosman, N.; Asher, T.; Loewenstein, Y. On the geometry of somatosensory representations in the Cortex. *NeuroImage* **2025**, *317*, 121321. [CrossRef]
26. Godenzini, L.; Alwis, D.; Guzulaitis, R.; Honnuraiah, S.; Stuart, G.J.; Palmer, L.M. Auditory input enhances somatosensory encoding and tactile goal-directed behavior. *Nat. Commun.* **2021**, *12*, 4509. [CrossRef]
27. Noachtar, S.; Remi, J.; Kaufmann, E. Electroencephalography—An Update. *Klin. Neurophysiol.* **2022**, *53*, 243–252. [CrossRef]
28. Teplan, M. Fundamentals of EEG Measurement. *Meas. Sci. Rev.* **2002**, *2*, 1–21.
29. Peng, Y.; Lin, Y.; Fan, C.; Xu, Q.; Xu, D.; Yi, S.; Zhang, H.; Wang, K. Passenger overall comfort in high-speed railway environments based on EEG: Assessment and degradation mechanism. *Build. Environ.* **2022**, *210*, 108711. [CrossRef]
30. Küller, R.; Wetterberg, L. Melatonin, cortisol, EEG, ECG and subjective comfort in healthy humans: Impact of two fluorescent lamp types at two light intensities. *Light. Res. Technol.* **1993**, *25*, 71–80. [CrossRef]
31. Shan, X.; Yang, E.; Zhou, J.; Chang, V.W.C. Human-building interaction under various indoor temperatures through neural-signal electroencephalogram (EEG) methods. *Build. Environ.* **2018**, *129*, 46–53. [CrossRef]
32. Guan, H.; Hu, S.; Lu, M.; He, M.; Zhang, X.; Liu, G. Analysis of human electroencephalogram features in different indoor environments. *Build. Environ.* **2020**, *186*, 107328. [CrossRef]
33. Wu, M.; Li, H.; Qi, H. Using electroencephalogram to continuously discriminate feelings of personal thermal comfort between uncomfortably hot and comfortable environments. *Indoor Air* **2020**, *30*, 534–543. [CrossRef]
34. Lu, M.; Hu, S.; Mao, Z.; Liang, P.; Xin, S.; Guan, H. Research on work efficiency and light comfort based on EEG evaluation method. *Build. Environ.* **2020**, *183*, 107122. [CrossRef]

35. Stinear, C.M.; Byblow, W.D.; Ackerley, S.J.; Smith, M.C.; Borges, V.M.; Barber, P.A. PREP2: A biomarker-based algorithm for predicting upper limb function after stroke. *Ann. Clin. Transl. Neurol.* **2017**, *4*, 811–820. [CrossRef]
36. Bembenek, J.P.; Kurczych, K.; Karliński, M.; Członkowska, A. The prognostic value of motor-evoked potentials in motor recovery and functional outcome after stroke—A systematic review of the literature. *Funct. Neurol.* **2012**, *27*, 79–84. [CrossRef] [PubMed]
37. Murtazina, M.S.; Avdeenko, T.V. Classification of Brain Activity Patterns Using Machine Learning Based on EEG Data. In Proceedings of the 2020 1st International Conference Problems of Informatics, Electronics, and Radio Engineering (PIERE), Novosibirsk, Russia, 10–11 December 2020; pp. 219–224. [CrossRef]
38. Chowdary, M.K.; Anitha, J.; Hemanth, D.J. Emotion Recognition from EEG Signals Using Recurrent Neural Networks. *Electronics* **2022**, *11*, 2387. [CrossRef]
39. Kumar, M.; Kumar, D.R.; Khatti, J.; Samui, P.; Grover, K.S. Prediction of bearing capacity of pile foundation using deep learning approaches. *Front. Struct. Civ. Eng.* **2024**, *18*, 870–886. [CrossRef]
40. Tasneem, S.; Ageeli, A.A.; Alamier, W.M.; Hasan, N.; Safaei, M.R. Organic catalysts for hydrogen production from noodle wastewater: Machine learning and deep learning-based analysis. *Int. J. Hydrogen Energy* **2024**, *52*, 599–616. [CrossRef]
41. Meng, D.; Chen, X.; Wei, Z.; Ji, S. Prediction of flexural and uniaxial compressive strengths of sea ice with optimized recurrent neural network. *Ocean. Eng.* **2023**, *288*, 115921. [CrossRef]
42. Zhang, Y.; Gu, Z.; Thé, J.V.; Yang, S.X.; Gharabaghi, B. The Discharge Forecasting of Multiple Monitoring Station for Humber River by Hybrid LSTM Models. *Water* **2022**, *14*, 1794. [CrossRef]
43. Mahjoub, S.; Chrifi-Alaoui, L.; Marhic, B.; Delahoche, L. Predicting Energy Consumption Using LSTM, Multi-Layer GRU and Drop-GRU Neural Networks. *Sensors* **2022**, *22*, 4062. [CrossRef]
44. Graham, S.L.; Klistorner, A. The Visual Evoked Potential in Humans. In *Stimulation and Inhibition of Neurons*; Pilowsky, P.M., Farnham, M.M.J., Fong, A.Y., Eds.; Humana Press: Totowa, NJ, USA, 2013; pp. 287–299.
45. Bornstein, M.H.; Mash, C.; Arterberry, M.E.; Gandjbakhche, A.; Nguyen, T.; Esposito, G. Visual stimulus structure, visual system neural activity, and visual behavior in young human infants. *PLoS ONE* **2024**, *19*, e0302852. [CrossRef] [PubMed]

Disclaimer/Publisher's Note: The statements, opinions and data contained in all publications are solely those of the individual author(s) and contributor(s) and not of MDPI and/or the editor(s). MDPI and/or the editor(s) disclaim responsibility for any injury to people or property resulting from any ideas, methods, instructions or products referred to in the content.

buildings

MDPI

Article

A Study on the Evolution of Lightscapes in the Beijing Road Historic and Cultural Zone, Guangzhou, China

Jianzhen Qiu [1,2,3,*], Weimei Cai [1], Jinyu Song [1], Honghu Zhang [4] and Yating Li [1]

[1] School of Architecture, South China University of Technology, Guangzhou 510641, China
[2] State Key Laboratory of Subtropical Building and Urban Science, Guangzhou 510641, China
[3] China-Portugal Belt and Road Joint Laboratory on Cultural Heritage Conservation Science, Suzhou 215000, China
[4] Institute of Architectural Technique, Architectural Department, Zhejiang University, Hangzhou 310058, China
* Correspondence: jzqiu@scut.edu.cn

Abstract: With a history spanning over two thousand years, the Beijing Road historic and cultural zone marks the origin of Guangzhou's traditional central axis and serves as one of the earliest commercial centers in the Lingnan region, characterized by a rich historical and cultural heritage and unique Lingnan features. Through a combination of literature collection and review, field observation, and photographic documentation, the research examines the historical natural, artificial, and folk lightscapes of the Beijing Road zone, highlighting the diversity of its lightscape features from past to present. As the city developed and modern technology advanced, the representative lightscapes in the Beijing Road zone have evolved from traditional forms to modern expressions, including 3D projection, multimedia interaction, and LED lighting. These advancements breathe new life into the pedestrian street and enhance its cultural significance within the contemporary commercial environment. By comparing the characteristics and categories of historical and contemporary lightscapes, the paper reveals the transformation of historical lightscapes, the innovation in modern lightscape techniques, and the remnants of vanished lightscapes. It also proposes strategies for the restoration and preservation of historical lightscapes, the innovation and integration of contemporary lightscapes, and the development of sustainable lighting design, while it discusses the direction of work for future research. It underscores the need for further protection and optimization of lightscape resources in the Beijing Road historic and cultural zone, to enhance cultural heritage and commercial appeal, providing valuable insights for the preservation of historic zones and the development of cultural tourism in Guangzhou and the Lingnan region.

Keywords: lightscape; historical and modern lightscape; lightscape construction; evolution of lightscapes; historic and cultural zone

1. Introduction

The concept of "Lightscape" was put forward by Chinese scholar academician Wu Shuoxian, who also advocated for "Lightscape" as a new discipline to parallel the "Soundscape" and "Smellscape" [1]. As a kind of particular visual landscape, lightscape refers to the landscape which is mainly composed of light, shadow, and their changes, which cause a strong visual impression, including two types of natural lightscape and artificial lightscape, as well as the composite lightscape of both [2]. Lightscape pays attention to the role of human sociality, behavior and environmental psychology, and pays attention to human

subjective perception and feelings. At present, insubstantial scenes, including soundscape and smellscape, have gradually played a role in improving the living environment [3–6], Against a background of vigorously advocating the construction of ecological and healthy cities [7], which speeds up the research on another important insubstantial scene in the "Three-scape", the lightscape is of great significance to the construction of a beautiful living environment and the further improvement of people's well-being [8,9].

Guangzhou showcases a variety of lightscapes across different urban spaces. In its urban squares, Flower City Square offers a multi-sensory experience by synchronizing music with light fountains. In its Lingnan public gardens, Liwan Lake Park creates a lightscape rich in local cultural character by combining water features and courtyard vignettes. In media architecture, the dynamic artistic lighting on the building façades along the Pearl River crafts a modern urban night lightscape. While existing research has explored the lightscape characteristics of these spatial types and established a theoretical basis, the studies on historic and cultural zones remain limited and require systematic attention.

The State Council announced Guangzhou as one of the first batch of national famous historical and cultural cities. The city holds the reputation of "millennium commercial capital." Shops first appeared in Guangzhou's urban zone during the Tang Dynasty (618–907). Development throughout the Song and Ming Dynasties (960–1644) resulted in the formation of a commercial center; this center, with Beijing Road at its core, was established in the late Qing Dynasty (1840–1912). The Beijing Road historic and cultural zone (Figure 1) is traversed by both ancient and modern urban axes of Guangzhou. Defining its boundaries, the zone reaches Guangwei Road to the north. To the south, it extends to Wenming Road and Yanjiang Road in the middle. Its eastern limit is West Fuxue Street, while Guangzhou Qiyi Road marks its western extent. Land use in this zone primarily serves commercial, cultural, and entertainment purposes. Currently, this zone remains one of the most prosperous commercial historic and cultural zones in Guangzhou, representing both cultural and economic aspects. As a typical representation of Guangzhou's historic and cultural zones, the numerous waterways on Beijing Road produce a rich natural lightscape. Meanwhile, its vibrant night market culture has given rise to the use of many lamps with local characteristics. Moreover, as a historic public entertainment hub, the Beijing Road area hosts its own folk activities, such as the Spring Festival Flower Market and the Guangfu Temple Fair. This combination of beautiful natural scenery, active commercial culture, and folk activities provides rich resources for its lightscape, making the Beijing Road historic and cultural zone an ideal case for applying lightscape theory.

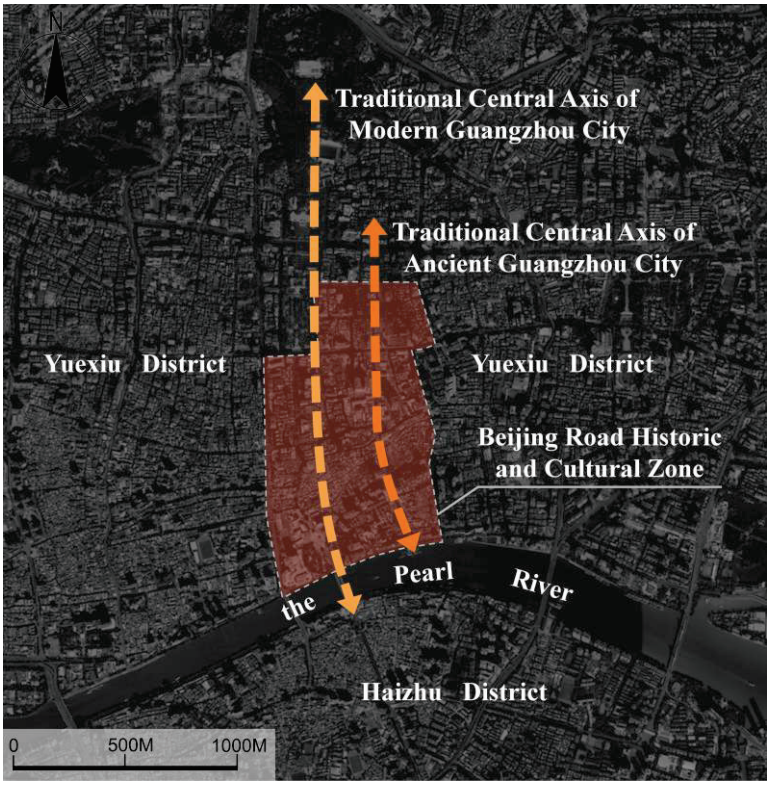


Figure 1. Beijing Road location (author's own work).

2. Historical Lightscape and Construction Characteristics of the Beijing Road Historic and Cultural Zone

For over two millennium, Beijing Road, as the consistent "origin" of urban development in Guangzhou [10], has developed abundant and profound historical and cultural deposits. The unique character of Beijing Road has inspired literati and artists throughout history, from ancient times to the present. This inspiration has resulted in a remarkable collection of themed poems, travel notes, paintings, and photographic works. The term "historical lightscape," as used in this paper, denotes the lightscapes that existed in the past. These lightscapes also reflect particular social and historical importance. An in-depth analysis of ancient documents, classics, and poems forms the basis for classification in this paper. The "historical lightscape" of the Beijing Road historic and cultural zone is categorized into three types: natural, artificial, and folk lightscapes.

2.1. Natural Lightscape

The rich natural lightscape of the Beijing Road historic and cultural zone is a product of its exceptional geographic environment. A natural lightscape is defined as a lightscape primarily created by natural light sources under specific environments or conditions [1]. The geographical location of Beijing Road is unique where Yuexiu Hill, Guangzhou's main mountain range for millennia, lies to the north; the Pearl River, the city's principal water vein, is situated to the south. Historically, extensive water networks defined Guangzhou's landscape. The area's abundant natural environment has, since antiquity, been the source of diverse natural lightscapes. The key historical natural lightscapes observed in this area consist of several phenomena. These include waterscapes, ship shadows, smoke and water vapor, mirages, lightscapes produced by the sun and moon [11,12], and the reflections from buildings (Figure 2).

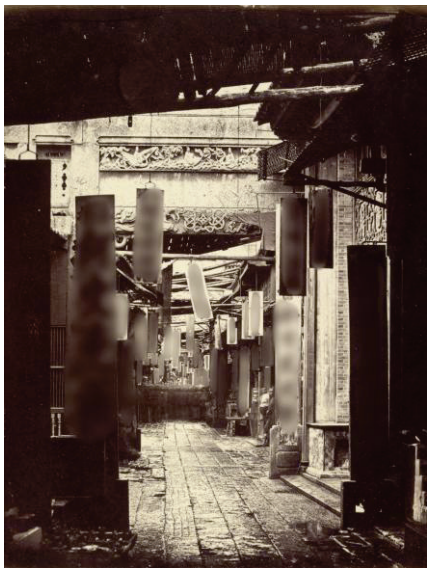
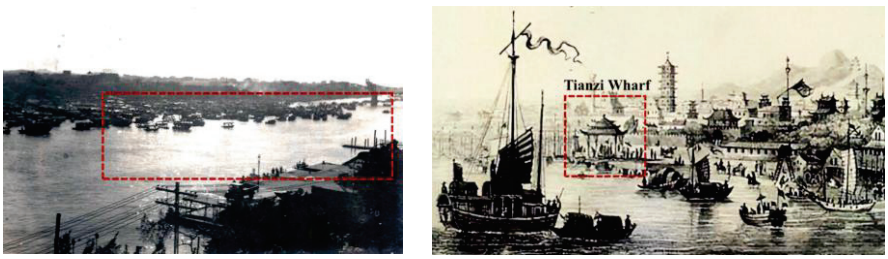


Figure 2. Treasury street (in the Qing Dynasty (1644–1912), it was called Finance Street [13], which is now Beijing Road). (Photography taken in 1860 by Felice Beato, an Italian).

2.1.1. The Pearl River in the Area of Tianzi Wharf

During the Song Dynasty (960–1276), the Pearl River was vast, with its surface swelling to a width of nearly ten li due to the shifting tides. Volume II of *Ping Zhou Ke Tan* records: "the boating Pavilion in Guangzhou stood waterfront at Haishan Tower, facing the five continents, and beneath it lay what was called the little sea." [14]. A westward to eastward course characterizes the Pearl River's flow through Guangzhou's urban area. Picturesque scenery lines both banks of the river. This scenic beauty, enhanced by the glistening wave light visible across different seasons and times of day, has drawn innumerable tourists from antiquity to modern times. The natural lightscape of the Pearl River is depicted in the *Zhuzhi ci Poems of Guangzhou*: "a river encircles both county and city complete, and the Pearl floats in the blue sea and the moon is clear". Constructed in the late Ming Dynasty (1368–1644), Tianzi Wharf connects the Beijing Road area and the Pearl River, while also acting as a popular location for observing the river's lightscape. Numerous old photographs and paintings (Figure 3) depict the sparkling surface of the Pearl River. These images also exhibit sails leisurely navigating around Tianzi Wharf. This combination, along with the surrounding landscape, creates a harmonious "Water–Lightscape," which aligns with the symbolism in Guangdong folk customs (Guangdong folk customs symbolize "Water means fortune").



(**a**) (**b**)

Figure 3. Tianzi Wharf: (**a**) the surface of the Pearl River in the area of Tianzi Wharf is sparkling (redrawn from [15]); (**b**) Tianzi Wharf (Redrawn from [16]).

2.1.2. Haishan Tower

Haishan Tower, a celebrated landmark of old Beijing Road, was built by the Pearl River during the Jiayou era (1056–1063) of Song Dynasty, standing outside Zhennan Gate (at the modern intersection of Beijing Road and Danan Road) [17]. From Haishan Tower, observers could also appreciate the natural lightscape of the Pearl River. In *Yu Di Ji Sheng*, Xiangzhi Wang of the Southern Song Dynasty (1127–1279) recorded the following: "the Haishan Tower stands in the south of Guangzhou city, commanding vistas of thousands of li, a renowned spot for ascending to view the scenery" [18]. Haishan Tower exhibited a mirage-like beauty when spring fog diffused. During thunderstorms, its appearance resembled Penglai Pavilion from a tumultuous sea [19]."Xiao Ji (morning clarity)" particularly accentuated the beauty of Haishan Tower. The expansive water surface of the Pearl River, a brilliant sky, and the natural lightscape created by the relationship of water, gas, and fog were exceptionally beautiful at dawn or following rain [20]. This spectacle constituted one of the renowned Eight Ancient Scenic Spots of Yangcheng (Guangzhou) during the Song Dynasty (960–1276), known as "Hai Shan Xiao Ji (morning clarity in Haishan Tower)" (Figure 4) [21,22]. The Northern Song Dynasty (960–1127) poet Qufei Chen, in his work *climbing the mountain tower* described the scene: "ten thousand sails such as owls take wing, waters void as emptiness. Earthly paths stretch boundlessly wide, and spring seas spread in misty haze. Immortals would speak with mortals here, and mountains lush at twilight hour. Clear seas show no phantom towers, mountains stand firm as Penglai's halls." Then, he composed the poem *Ode to the Haishan tower in the rain*: "A railing of hundred-foot stands by the seaside shore, lifelong aspirations tower high as mountain peaks. The reflection of the sky on the shore came in with the tide, and the view of spring upstairs came with the rain".

Building pavilions near the sea to observe the tide and the moon was a common practice for merchants and literati in ancient times. A prime illustration of this practice is Haishan Tower [23]. Beyond viewing "Hai Shan Xiao Ji," Haishan Tower frequently served another purpose. Literati and optimized scholars utilized it as a venue for watching the tide, admiring the moon, reciting poems, composing essays, and hosting banquets and gatherings on ordinary days. Activities such as ascending the tower to watch the tide, holding banquets to listen to waves, or enjoying the moon with wine resulted in a unique sensory experience. The sound of the tide, combined with moonlight and water light, created a natural beauty integrating soundscape and lightscape.



Figure 4. "Hai Shan Xiao Ji" (morning clarity in Haishan Tower) (source: [24]).

The military commissioner and pacification commissioner conducted naval inspections from Haishan Tower on the fifth day of the fifth lunar month. Song Dynasty (960–1276) military ships sailed on the Pearl River's vast expanse. Their flags fluttered and swords reflected the sun [19]. Meanwhile, background sunlight cast a golden glow upon the river. The relationship of the waves with the ship shadows created a multi-level natural lightscape. This formation offered a grand and magnificent spectacle for the inspection.

Haishan Tower was destroyed by war in the Yuan Dynasty (1271–1368) and no longer exists today.

2.1.3. Taiping Yanhu (A Scenic Beauty)

Five interconnected mounds of sandbanks (today's Taipingsha) were situated along the route from Tianzi Wharf to Haishan Tower between the Ming and Qing Dynasties (1368–1912). The scenic beauty of cooking smoke rising from both sides of the Pearl River amid the sunset glow near the sandbank area captivated Gongyin Chen, a Qing Dynasty (1644–1912) scholar.He titled this scene "Taiping Yanhu".

Taipingsha (sandbars) formerly featured various structures, including pavilions, terraces, and open halls. Examples of these include Liu Hall, Xiuhai Tower, Lubo Tower, Zheyue Tower, Shuiming Tower, Yanzhu Tower, Yanhu Tower, and Yuexue Mansion [25]. The majority of these pavilions and towers were constructed admcent to the water. This placement, in conjunction with the surrounding environment, generated a natural lightscape with unique humanistic charm. Such lightscapes are featured in the poems and essays of preceding dynasties.

Zihu Li's *Manxing liushou* describes the environs of Liu Hall: "after rain the pond waters turn cool, red lotus scents the white lotus blooms. The pond is surrounded by lotus leaves, and a sand gull dances against the setting sun, breaking the tranquility of the pond water. Pond waters illuminate the dawn-lit trees, and flower vendors stand in the rain. Moon rises from deep forest groves at dusk, watching blossoms, and sitting on fishing rocks all day". This passage illustrates an integration of lightscape, soundscape, and smellscape.

The creation of scenery at Xiuhai Tower, Lubo Tower, and Zhuyue Tower involved the use of mirror image methods. A Qing Dynasty (1644–1912) *poem* of *Xiuhai Tower* by Zhang Weiping states: "the tower in the painting gets the moon first, and the curtain in the mirror skillfully hides flowers" [26]. Mirrors reflecting the river sail were a feature of the Lubo Tower. Double mirrors were installed in the Zhuyue Tower, designed to reflect the external scenery. These three structures effectively utilized mirrors; they achieved this by capturing the river scene beyond the building in their reflections.

Taipingsha was integrated with the land on the Pearl River's north bank towards the close of the Qing Dynasty (1644–1912). A street bearing the name "Taipingsha" continues to exist in that location.

2.1.4. West Lake and Yaozhou (An Islet)

The excavation of West Lake occurred in the Southern Han Dynasty (917–971), when it was established as the Southern Palace Garden. At that time, this constituted a large artificial garden project. Extending in a long north–south configuration, the lake area followed today's Jiaoyu Road. Its northern limit was the western section of Yuehua Road, while Xianhu Street marked its southern boundary. Anciently, West Lake presented an open surface where water and sky merged without distinction. The presence of an islet in the lake, cultivated with Hongyao (the red peony flower), resulted in its designation as "Yaozhou." Historical records indicate the abundance of orioles at Huangli Harbor (today's Huangni Lane) situated along the lakeshore [26]. Willows adorned both banks, complemented by the fragrance of flowers and the shadows of lotuses. In this setting, the melodious songs of orioles contributed to a multisensory experience. This experience represented a perfect harmony of lightscape, soundscape, and smellscape.

During the Northern Song Dynasty (960–1127), the beautiful scenery of West Lake and Yaozhou became an attraction for numerous literati and scholars. Therefore, they left behind many poems and inscriptions that described the natural lightscape. An example is Fu Mi, who was a calligrapher, painter, and poet of the Northern Song Dynasty (960–1127). He inscribed the title *Jiuyao Stone* on the Xianzhang stone with the words: "Mirage appears in the blue sea, and summer clouds rise in the blue sky." This inscription depicts the mirage

lightscape observed on Yaozhou's water surface. Another instance is from Yanxian Xu of the Song Dynasty (960–1276), who composed a poem on the Jiuyao Stone in *Yaozhou*. The poem reads: "the anthers suffuse the sea island, cloud shadows in the water flow with the current of sand." The poem describes the diffuse smoke on Yaozhou's water surface. This smoke, in combination with cloud shadows, wave light, and quicksand in the water, formed a hazy and dynamic natural lightscape. In his work *Duyou Yaozhou Huai Yingshu Xiuzhuan*, Xiangzheng Guo of the Song Dynasty (960–1276) recorded the observation: "The domineering spirit of the lake dissipated, and the solitary smoke floated in the sunset." This description portrays the natural lightscape of Yaozhou at sunset. The tranquility associated with the rising solitary smoke also carried a somewhat sad quality.

"The Spring Sunrise of Yaozhou" was recognized as one of the Eight Ancient Scenic Spots of Yangcheng (Guangzhou) during the Ming Dynasty (1368–1644) (Figure 5) [20]. Afterwards, West Lake gradually disappeared. Currently, only remnants such as the names West Lake Road and Xianhu Street, along with the ruins of Nine Star Garden, offer clues to its existence.



Figure 5. The Spring Sunrise of Yaozhou (Source: [27]).

2.1.5. Summary of Natural Lightscape

The diverse natural lightscapes along Beijing Road have undergone changes in types and distributions over different dynasties (Table 1, Figure 6). Among them, there are natural lightscapes that incorporate multi-dimensional perceptual elements such as soundscapes and smellscapes, with a developmental trajectory spanning from the Southern Han Dynasty (917–971) to the Ming (1368–1644) and Qing Dynasties (1644–1912). Although some lightscapes like "Hai Shan Xiao Ji," "Taiping Yanhu," and "The Spring Sunrise of Yaozhou" have now faded away, their lightscape imagery still survives through literature, poetry, and place names, providing historical evidence for interpreting the natural lightscapes of Beijing Road.

Table 1. Natural lightscape dynasty and location.

Dynasty	Natural Lightscape	Location
Southern Han Dynasty (917–971)	The water and sky merged without distinction, floral fragrance and lotus shadow	West Lake, Yaozhou (an islet)
Song Dynasty (960–1276)	"Mirage appears in the blue sea, and summer clouds rise in the blue sky" "The anthers suffuse the sea island, cloud shadows in the water flow with the current of sand" "The solitary smoke floated in the sunset"	West Lake, Yaozhou (an islet)
	"Hai Shan Xiao Ji (morning clarity in Haishan Tower)" "Spring seas spread in misty haze" "The reflection of the sky on the shore came in with the tide"	Haishan Tower
Ming Dynasty (1368–1644)	"The Spring Sunrise of Yaozhou"	Yaozhou (an islet)
	The sparkling surface of the Pearl River	Tianzi Wharf

Table 1. *Cont.*

Dynasty	Natural Lightscape	Location
Qing Dynasty (1644–1912)	Water vapor permeates the sandbars Liu Hall: "Pond waters illuminate the dawn-lit trees" Xiuhai Tower: "The tower in the painting gets the moon first" Lubo Tower has mirrors reflecting the river sail	Taiping Yanhu area (Sandbar)

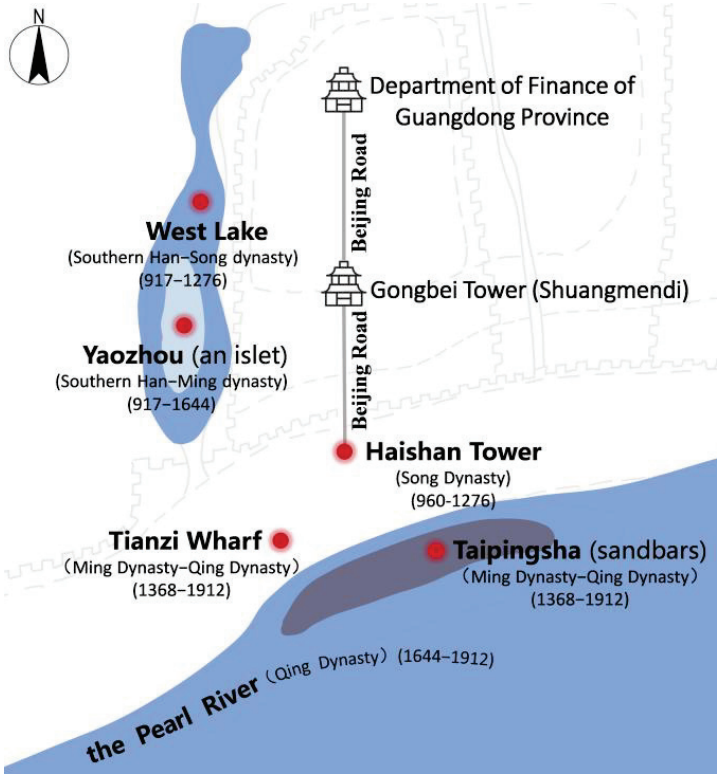


Figure 6. Location of natural lightscape (author's own work).

2.2. Artificial Lightscape

The term artificial lightscape denotes lightscapes primarily created by artificial light sources (candles, torches, lamps, fireworks, etc.) and the changes these sources produce [1]. The historical artificial lightscape on Beijing Road comprised several components. They included the lightscapes produced by lanterns, lamps, and general lighting associated with the commercial market. Additional sources were academy buildings, their related activities, and official activities.

2.2.1. Jasmine Lantern

Jasmine flower (Figure 7), a traditional flower that once flourished throughout Guangzhou, is a small white blossom celebrated for its springtime fragrance and also referred to as "Jade Hibiscus" [28]. These flowers thrive in southern climates. Guangzhou Henan (now the Haizhu District on the South Bank of the Pearl River) gained fame for its jasmine cultivation during the late Ming and early Qing Dynasties (1628–1700). Every morning, florists picked jasmine flowers. These flowers were then transported from the Pearl River's south bank to seven northern city gates for commercial sale [29]. The tradition of stringing freshly picked jasmine flower quilts into fragrant ornaments dates back to the Southern Han Dynasty (917–971). This practice established a dressing fashion in ancient

southern Guangdong, which is known as "colorful thread wearing flowers" and "flower comb hairpin wearing." Reports from the late Ming Dynasty (1573–1644) in Guangzhou indicate the presence of "hundreds of people making lanterns, flower strings, and ornaments." This activity centered on the flower market near South Gate (now the junction of Beijing Road and Danan Road) [30].

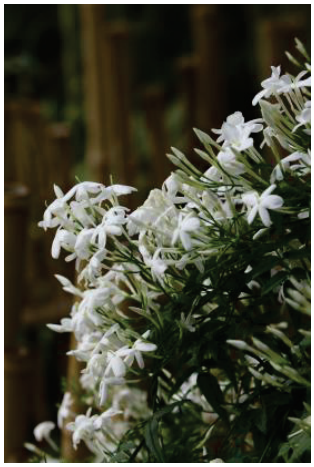


Figure 7. Jasmine flowers (Source: [31]).

The combination of jasmine flowers with exquisite lamps frequently resulted in the creation of jasmine lanterns. These lanterns determined widespread application in numerous settings. One source notes their versatility: "Flowers are also suitable for making lamps, carving jade and ice, exquisite and radiant in all directions, which can be utilized by tourists to guide cars and horses" [30]. In practice, individuals undertaking nighttime sightseeing would hang jasmine lanterns, with lights flashing inside, in front of their cars and horses. An intensified floral fragrance resulted from the candles' heat, hence cars and horses would spread this scent along their path. This observation demonstrates the intertwining of the artificial lightscape from jasmine lanterns with the smellscape. Collectively, they produced a flowing sensory picture. Another described use states, "When a HuoqingJiao festival is held in autumn and winter, myriad households hang jasmine lanterns shaped as dragons. These may also serve as tassels, with flowing ribbons luxuriant and hibiscus adorning the deity" [30]. Thousands of jasmine lanterns, varying in shape, were displayed under rows of eaves. In addition, jasmine lanterns adorned flower boats. For instance, "On the night of Qixi Festival in Guangzhou, numerous jasmine flower boats are employed to cruise through Haizhu, Xihao and Xiangpu" [30].

The demand for Jasminum flowers decreased towards the end of the Qing Dynasty (1644–1912) following the introduction of exotic flowers. Their gradual disappearance by the 1950s was further accelerated by the destruction of flower fields due to urban development. Efforts to reintroduce jasmine flowers have occurred since 2011. Haizhu District in Guangzhou has facilitated the introduction of fragmentary, self-supporting jasmine plants from Zhuangtou village residents into Zhuangtou Park.

2.2.2. Shop Lamps and Lanterns

During the Qing Dynasty (1644–1912), Guangzhou thrived as a commercial hub, where lamps and lanterns played a crucial role in enhancing the commercial lightscape atmosphere. A rich variety of lantern styles existed. For instance, foreign painting shops featured exquisite and unique glass lamps. In comparison, the "Xinsheng" lantern shop displayed an abundance of round and cylindrical lanterns (Figure 8).



(**a**) (**b**)

Figure 8. Lamps and lanterns: (**a**) the glass lamp of the foreign painting shop (redrawn from [32]); (**b**) lanterns in "Xinsheng" lantern shop (redrawn from [33]).

The work *Walks in the City of Canton* recorded how the profusion of lamps and lanterns in the Beijing Road's business center, along with their illumination, highlighted the prosperity of many shops. The text states: "major shops suspend numerous glass lamps from roof or ceiling, with grand lanterns at their gates, painted with splendid characters or patterns—birds, butterflies, temples, pavilions, gardens, mountains and waters; particularly along Shuangmendi street (today's Beijing road, named for the paired gates near Gongbei Tower) and before The Grand Buddha Monastery (West of today's Beijing road)" [34].

2.2.3. Night Market Lighting

A consistent feature of Beijing Road lies in its prosperous night markets. In *Zhuzhi ci Poems of Canton*, Jianhong He, a Qing Dynasty (1644–1912) native, described this vibrancy: "There is also a Shuangmendi night market, with lamps resembling those of Suzhou and Hangzhou throughout the night" [35]. This description indicates the prosperity of the night market. The lighting at that time generated a vibrant, fireworks-like atmosphere, reflecting commercial success. The West Lake illuminated night market, which evolved from these earlier markets after the reform and opening up period, gained further renown as the "Southern Pearl" [36]. West Lake consistently offered a bustling nocturnal scene each night (Figure 9). Thousands of stalls were arranged in lines. Above these stalls, hanging light tubes created a brilliant river of light. A broad array of commodities was illuminated by the interaction of light and shadow. Owing to this dynamic artificial lightscape, the West Lake Road illuminated night market became recognized as a beautiful scenic attraction in Guangzhou during that period. The operation of the West Lake Road illuminated night market ceased in 2001. This cessation resulted from a government initiative aimed at returning the road to public use.

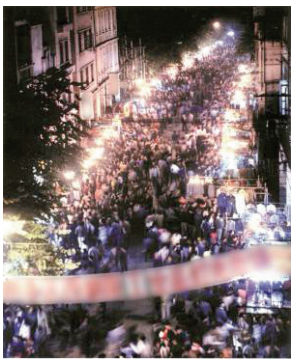


Figure 9. The West Lake Road illuminated night market (Source: [37]).

2.2.4. Lightscape of the Academy

Guangzhou housed a significant body of academies during the Qing Dynasty (1644–1912). The core area for these institutions was near Beijing Road, including Liushuijing, Damazhan, and Xiaomazhan. In an approximately three-square-kilometer area, hundreds of such academies were located. One such institution, the Lujiang Academy, is situated in Liushuijing (currently at No. 29, Liushuijing, West Lake Road). Its establishment dates back to the 13th year of Jiaqing in the Qing Dynasty (1808). The Guangzhou Municipal People's Government designated it as a municipal cultural relics protection unit in 1993 [38].

A couplet at the main ancestral hall gate of the Lujiang Academy offers insight into its past lightscape. The couplet reads: "The shadow of moon pursues the shadow of lamps, and the sound of books prevails over sounds of commerce". This verse suggests a scene where numerous students pursued their studies by lamplight, beneath the moonlight. An intermingling of book sounds and the fragrance of books and ink occurred with the ambient moonlight and lamplight. This combination produced a blend of soundscape, smellscape, and lightscape. Finally, this contributed to the unique and profound cultural atmosphere in the academy. Currently, the Lujiang Academy functions as the Lingnan Finance Museum.

2.2.5. Lightscape of Official Activities at Tianzi Wharf

During the Qing Dynasty (1644–1912), Tianzi Wharf functioned as an official wharf, representing the primary point for officials arriving in or departing from Guangzhou by water. A structure named the "Rijin Pavilion" (the term "Rijin" signifies "emperor", reflecting the officials' journey to the capital for imperial audiences) stood in front of this wharf. This pavilion, also commonly called the "Officials' Reception Pavilion", was specifically utilized for the reception and send-off of officials [39]. Export paintings from the Qing Dynasty (1644–1912) (Figure 10) depict two "frying pan handle" houses (characteristic of upper-class Lingnan traditional dwellings exclusively permitted for renowned official families during the Ming and Qing Dynasties (1368–1912)) situated adjacent to the "Rijin Pavilion". Traditional, patterned lanterns positioned before the doorways contributed to a solemn official atmosphere at the wharf. The arrival of new officials for their posts frequently occurred through Tianzi Wharf. Upon an official ship's docking, reflections from its twin mast flags and stern lanterns would appear on the water's surface (Figure 11), while local officials waited to extend their greetings. The scene became exceptionally lively with the unified sound of drum music, the roar of artillery salutes, and a dense formation of umbrellas and canopies resembling clouds [39]. A unique lightscape was formed from the relationship of ceremonial firelight from salutes and lantern light reflecting on the water, as further augmented by the accompanying smoke. Officials concluding their service would depart from Tianzi Wharf, following a formal "pay their formal respects to the Emperor" at the Officials' Reception Pavilion.

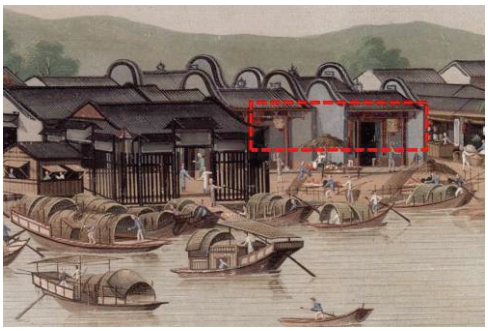


Figure 10. Tianzi Wharf and Rijin Pavilion (redrawn from [40]).

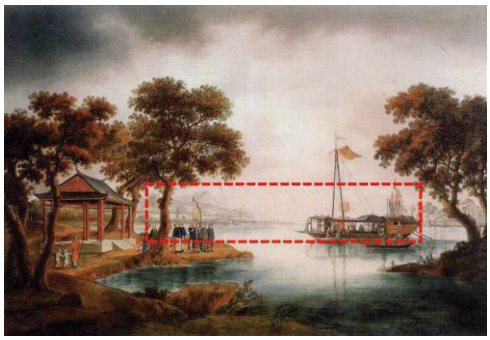


Figure 11. Greeting officials in oil painting (redrawn from [41]).

The exclusivity of Tianzi Wharf for government use reduced before and after the Tongzhi period of the Qing Dynasty (1862–1874), thus allowing civilian ships to berth there as well [42].

2.2.6. Summary of Artificial Lightscape

The artificial lightscapes of Beijing Road, mainly from the Ming and Qing Dynasties (1368–1912) to modern times, exhibit diverse characteristics and are closely intertwined with social activities (Table 2, Figure 12). They encompass various social activity scenes such as festivals, commerce, education, and official ceremonies, and also integrate with multi-dimensional sensory elements like soundscapes and smellscapes. Historical artificial lightscapes that have vanished with the passage of time also continue to exist through carriers such as poetry, literature, and export paintings.

Table 2. Artificial lightscape dynasty and location.

Dynasty	Artificial Lightscape	Location
From Ming Dynasty to Qing Dynasty (1368–1912)	Jasmine lantern: "Flowers are also suitable for making lamps, carving jade and ice, exquisite and radiant in all directions"	South Gate
	"Myriad households hang jasmine lanterns"	each and every family
	"On the night of Qixi Festival in Guangzhou, there are many jasmine flower boats"	the Pearl River
	"There is also a Shuangmendi night market, with lamps resembling those of Suzhou and Hangzhou throughout the night"	Shuangmendi (the former name of Beijing Road)
	The shop signs and lanterns are brightly colored and painted with vibrant text or patterns	Shuangmendi (the former name of Beijing Road), the Grand Buddha Monastery
	Lantern in front of the "frying pan handle" house, lightscape of official activities at Tianzi Wharf	Tianzi Wharf, Rijin Pavilion
	"The shadow of moon pursues the shadow of lamps, the sound of books prevails over sounds of commerce"	Lujiang Academy
After the reform and opening up (after 1978)	The West Lake Road illuminated night market	West Lake Road

2.3. Folk Lightscape

Folk light culture involves the traditions and phenomena related to light in folk culture and activities. The resulting landscapes formed by light and shadow is the folk lightscape. Folk lightscapes serve various functions, including nighttime illumination, economic activity, landscape appreciation, message conveyance, future prediction, and prayers for

blessings, protection from disaster, etc. These are realized through specific means such as the cultural content of the lightscape, the lighting instruments used, atmospheric creation, and spatial distribution [8].

The Guang Fu area is characterized by a wealth of folk activities. Lightscape, as an integral component of these folk customs, serves a dual purpose. It creates a festive atmosphere while inheriting the deep-rooted Lingnan culture.

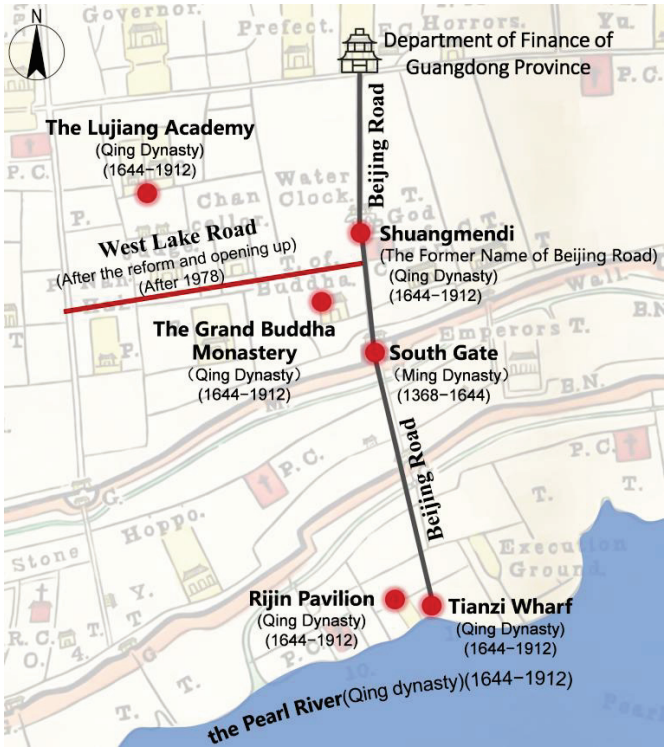


Figure 12. Locations of artificial lightscape (author's own work, base map from 1880 Guangzhou map.source [43]).

2.3.1. Dragon Boat Race

The Dragon Boat Festival, a folk custom displaying Han nationality characteristics, combines elements of history, belief, and competition. It's originated from the nature worship practices of ancient water towns. Then, the festival incorporated the legend commemorating Qu Yuan, thereby evolving into a Dragon Boat Festival custom. The extensive river network in Guangzhou offers a natural setting for this folk activity, a factor contributing to its long-term survival over time (Figure 13) [44].

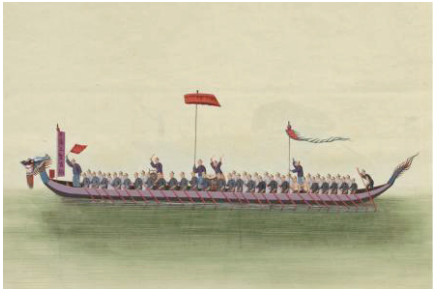


Figure 13. Dragon boat of the Festival of the Fifth Month. (Source: [45]).

In ancient times, the Dragon Boat Festival celebrations in the Guangfu region were renowned for their extraordinary vibrancy. Dragon Boat Race venues existed at Mingyue

Gorge and Yuye Lake (located near present-day West Lake Road) in West Lake from the Five Dynasties and Ten Kingdoms (907–979) period onward [46]. In the Song Dynasty (960–1276), Xinru Fang's *Nanhai Baiyong* recorded the Dragon Boat Festival palace race, stating: "Every Dragon Boat Festival, palace attendants were commanded to race upon it. The Mingyue Gorge bypassed Yuye Lake, and the colored boats competed to win out of the palace boudoir" [17]. Xu Zhang, recording in the Ming Dynasty (1368–1644), described *Yuye Lake* with the words: "On the fifth day of the fifth lunar month, colored teams emerge, and palace maidens vie for ornaments fine. Dragon boats race across Yuye Lake. Spring breezes gently stir the fragrant flowers and grass, while orioles newly sing and dance upon the walls. In those times the singing, dancing wanderers rejoiced…" Dragon boats raced across the sparkling Yuye Lake, set against the spectacle of the Dragon Boat Festival's grand parade and costumed concubines. This scene created a multisensory experience integrating light, sound, and fragrance, produced by the relationship of painted boat hulls with sunlight and water reflections, alongside the aroma of surrounding flowers and plants and the songs of orioles. Then, the tradition relocated to the Pearl River's waters due to silt deposition in Yuye Lake.

The Pearl River became a key venue for dragon boat race exhibitions during the Qing Dynasty (1644–1912) (Figure 14). Shizhen Wang, in *Zhuzhi ci Poems of Guangzhou*, portrayed the stunning lightscape of dragon boat race under the setting sun with the lines: "The willows on the Sea Pearl Rock grow dense and deep, while dragon boats surge through waves. A streak of setting sun illumines splendor bright, peacock and kingfisher plumes together form the boat canopies." Separately, Weisen Fu, in *Preface to the Poem of the Pearl River Race*, captured the intensity of this race, writing: "The Capricorn drum splits the waves asunder, and thousands of thunders roar as one. Oar blades flash beneath the waters like myriad swords in clash." Dragon boat races during this period evolved into major urban spectacles: daytime events featured sky-shaking drums and thousands of competing boats, while nighttime brought bright lights and numerous tourists [31]. Following the establishment of New China, dragon boat activities on Guangzhou's Pearl River not only persisted but also progressively expanded. Currently, the annual Guangzhou International Dragon Boat Invitational Race draws dozens of domestic and international teams, transforming into a city-wide event lasting 15 days [46].



Figure 14. Dragon Boat Race in the Pearl River in late Qing Dynasty (1840–1912) (Source: [47]).

2.3.2. Lantern Festival

In Guangzhou, night market experienced prosperity starting from the Song Dynasty (960–1276). During major festivals such as the Lantern Festival, the erection of lamp sheds and music sheds near Haishan Tower was a common practice. These lamp sheds featured an assortment of lights and were adorned with flowers, ribbons, and various other ornaments. Nightfall brought flickering colors from the lights, while the music sheds hosted activities such as flute playing, storytelling, and puppet performances [48]. Lantern

enjoyment was a universal activity on Lantern Festival days up through the Qing Dynasty (1644–1912), with households extensively decorated with lanterns. The Qing Dynasty (1644–1912) scholar Dajun Qu, in *Guangdong Xinyu*, offered a description of Guangzhou's Lantern Festival celebrations: "On Lantern Festival Eve, lanterns were hung and bonfires blazed, with roughly one in ten households setting off fireworks, and one in five igniting huatong. Merrymakers would carry ivory incense tubes tucked in their sleeves and delight in playing 'Eight Music Drum Cabinet'. Throughout the city, both inside and outside its walls, a hundred troupes performed lion, elephant, dragon, and phoenix dances, alongside another hundred troupes of men and women enacting the role of children." [30]. This historical record demonstrates that Lantern Festival activities of that era emphasized the creation of lightscapes and their integration with soundscapes and smellscapes.

The activity of guessing lantern riddles combined lightscapes with folk entertainment, thereby enhancing the festive atmosphere. Riddle enthusiasts (commonly known as riddlers) were present in the Guang Fu area during the Ming Dynasty (1368–1644). Dajun Qu, a prominent scholar from the Guang Fu area writing at the transition from the Ming to the Qing Dynasty (1368–1912), noted in *Guangdong Xinyu*: "During the Shangyuan Festival (Lantern Festival), on the streets of Guangzhou's lantern markets, riddles were displayed with prizes for those who could solve them, a custom termed 'Lantern Signal'" [30]. In his article tracing it back to the ancient and modern Guangzhou lantern riddles, Boyan Liang recorded "In the early years of the Republic of China, in areas such as Shuangmendi and Xiajiufu (present-day Xiajiu Road), and during every Shangyuan Festival, riddle stages were set up, always drawing vast crowds of onlookers". His records further detailed instances such as "Take, for example, the elderly teacher Zhan Juren. In anticipation of the Lantern Festival (around Yuanxiao), he would have a special decorative lantern custom-made. This lantern, hexagonal or octagonal in shape, had space on each face for two or three riddle slips, allowing for many riddles in total. An electric light bulb was fitted inside, making it luminous both inside and out, and it attracted a large gathering of riddle enthusiasts." The evidence thus indicates that lantern riddle activities on Beijing Road during the Qing Dynasty (1644–1912) were indeed plentiful. These events were significant not only for creating a lively lightscape but also for spreading Guangfu traditional folk culture.

2.3.3. Birthday of the Lord Huaguang

Celebrated annually in September, the "Birthday of the Lord Huaguang" stands as a unique folk festival in the Lingnan region ("Lord Huaguang" is recognized in Lingnan folklore as the "God of Fire" and is additionally considered the progenitor of the Cantonese Opera industry). Moreover, this event ranks among the most vibrant festivals celebrated in Shuangmendi. The embellishment and use of lights intensified the festive atmosphere of this folk event. Huiyan Chen's *Nanyue youji*, from the Qing Dynasty, offers a description: "Bamboo scaffolds were built along Xiongzhen street's thoroughfares. The structures stood several feet high, with open galleries painted in five colors. All depicted flowers, birds, and water sprites. Below hung fabric curtains, lamps were painted bright, with many colored glass pieces and foreign curiosities in. Colored pavilions stood at center, playing eight-tone music and singing grand opera, and passersby lingered to watch and listen. From the Domain Office to the south gate, lights blazed brilliant, and golden drums clamored loud." [49]. This passage clearly illustrates a rich lightscape atmosphere complemented by vivid soundscape scenes.

The folk custom of the "Birthday of the Lord Huaguang" began a gradual decline following a government notice issued in the final year of the Daoguang period (1850). This notice prohibited the activities aimed at rewarding gods [39].

2.3.4. Lightscape of Flower Market

The "flower market," a traditional folk custom observed in Guangzhou during the Spring Festival, originated from in the "flower ferry" of the late Ming Dynasty (1573–1644). A gradual evolution occurred in the middle of the Qing Dynasty (1662–1795), where the flower market began to emphasize nighttime leisure and viewing; this development led to the formation of two prominent night flower markets "before the Domain Office (currently before the Department of Finance of Guangdong Province building)" and "Shuangmendi". During the reign of Daoguang, the *Continuation of Local Records of Nanhai District* recorded the splendid atmosphere of the flower market situated before the vassal office, stating: "the flower market is in front of the Domain Office, the lights and the moon are shining, the fragrance of flowers is overwhelming, and the burning night is especially called beautiful scenery" [50]. This historical account details the intermingling of the flower market's lights with moonlight, the diffusion of floral fragrances, and the intertwined nature of lightscape and smellscape. The Lantern Festival flower market progressively formed during the Xianfeng Period, thus relocating to today's Beijing Road. Towards the end of the Qing Dynasty (1840–1912), an enhanced integration occurred between the lightscape of Guangzhou's night flower market and traditional festivals, such as the Spring Festival. Chengpu Xu, recording in his *Suimu Miscellaneous Poems* during the Tongzhi period, described the Shuangmendi flower market: "Through shuangmendi flower market lanterns flicker and flow, and baskets are filled with big trees." His words illustrate the lively scene represented by flickering lights, the movement of people and shadows, and the intersection of light and shadow in the New Year's Eve flower market. The flower market received its official formation in the Republic of China, at which point its timing was fixed from 28 December of the lunar calendar to the late night of New Year's Eve. The diverse array of lanterns present in the flower market at that time contributed to making the Spring Festival flower market's lightscape richer and more unique. Finally, Jiaoyu Road and West Lake Road, situated in the historic and cultural zone of Beijing Road, became the established location for the flower market, which is now recognized as Guangzhou's oldest. Visiting this market, a popular folk activity also known as "Flower Street," has continued as a grand occasion to this day [51].

2.3.5. Summary of Folk Lightscape

The lightscapes in the Guang Fu area, represented by Beijing Road, across different dynasties are closely related to folk activities (Table 3, Figure 15). Important festival scenes such as the Dragon Boat Festival dragon boat races, Lantern Festival, the Birthday of the Lord Huaguang, and the Spring Festival flower market not only create a strong visual atmosphere relying on natural and artificial light sources but also blend with soundscapes and smellscapes, forming a multi-sensory festival experience that showcases unique folk culture and regional characteristics.

Table 3. Folk lightscape dynasty and location.

Dynasty	Folk Lightscape	Location
Five Dynasties and Ten Kingdoms (907–979)	Dragon Boat Festival: "Every Dragon Boat Festival, palace attendants were commanded to race upon it and the colored boats competed to win out of the palace boudoir" People joyfully play with the shimmering waters and sunlight	West Lake
Song Dynasty (960–1276)	Lantern Festival: another major festival where colorful lights flicker inside the lamp shed	Haishan Tower

Table 3. *Cont.*

Dynasty	Folk Lightscape	Location
Qing Dynasty (1644–1912)	Birthday of the Lord Huaguang: "The lamps were painted with colors, the lights were brilliant" Flower Market: "The lamps and moon illuminate together, flower fragrance floods the air"	Shuangmendi (former name of Beijing Road)
	Dragon Boat Festival Dragon boat race: "The dragon boats surge through waves. A streak of setting sun illumines splendor bright"	the Pearl River
Republic of China (1912–1949)	Lantern Festival: riddle arenas combined with exquisitely crafted lanterns	Shuangmendi (former name of Beijing Road)

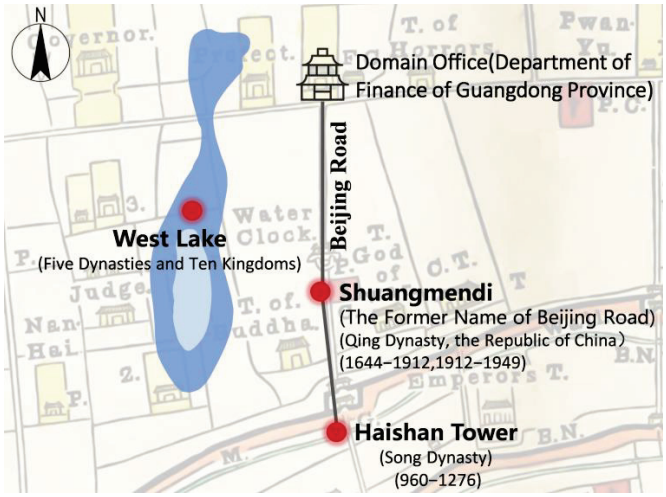


Figure 15. Locations of folk lightscape (author's own work, base map from 1880 Guangzhou map, source [43]).

3. Existing Lightscape and Construction Characteristics of the Beijing Road Historic and Cultural Zone

3.1. Natural Lightscape

Several components constitute the existing natural lightscape in the Beijing Road historic and cultural zone. These elements include skylight, sunset, sunset glow, moonlight, and starlight. Furthermore, the natural lightscape comprises light on the river, shadows from landscape sketches and people, and light and shadow patterns (light spots) created by tree branches and leaves. Further aspects involve the light and shadow on buildings and arcade colonnades, shadows cast by grills and other structures, light transmission and reflection from buildings and heritage glass, and the skyline formed by building outlines [52].

3.1.1. The Pearl River in the Area of Tianzi Wharf

Dynastic changes led to the gradual widening of the Beijing Road's south bank and shifts in Tianzi Wharf's location. Despite these transformations, the Pearl River's natural lightscape has persisted in this area. During daylight hours, sparkling water characterizes the river surface, which reflects both skylight and sunset glow.While the nighttime shows the moonlight resembling silver and stars scattered across the river, appearing to dance with its flow.

3.1.2. West Lake and Yaozhou Site

What was once the ancient West Lake has been transformed into land, and only the historic relic named "Nine Star Garden" remains (Figure 16). In the lake water, nine

"Jiuyao Stone," each unique in shape and color, have been placed, while a stone bridge and waterside pavilion sway in the blue waves. Sunlight causes the lake to sparkle. Under these conditions, the reflections of pavilions, stone bridges, and waterside pavilions sway in the lake, reflecting the actual scenery. Moreover, the whirling shadows of towering ancient trees are cast upon building facades, the lake surface, and the ground. These combined elements create a vivid natural lightscape [53].



Figure 16. Yaozhou site "Nine Star Garden" (images captured by the author).

3.1.3. Light and Shadow of Buildings and Structures

(1) Light and shadow on the Department of Finance of Guangdong Province Building

At the northern extremity of Beijing Road stands the Department of Finance of Guangdong Province Building. Construction of this building occurred in the fourth year of the Republic of China (1915). Currently, it holds the status of a provincial cultural relics protection unit in Guangdong. The building exhibits an architectural style characteristic of the European Renaissance with both solemnity and elegance. Imitating Western classical eclecticism, it ranks among the representative buildings of modern Guangzhou. Daytime sunlight causes the colossal Roman columns to accentuate changes in light and shadow. In front of the building, the whirling branches and leaves of three ancient trees cast mottled shadows onto its walls, while the glass in the arched and square windows reflects nearby buildings along with the blue sky and white clouds (Figure 17). The whole building is more solemn and elegant with the changes in light and shadow.



Figure 17. Department of Finance of Guangdong Province Building (images captured by the author).

(2) Light and shadow on arcade buildings in a street of time-honored shops

A street of time-honored shops occupies the northern part of Beijing Road (specifically from the Guangwei Road section to the Zhongshan 5th Road) as a hub for dozens of Guangzhou's time-honored brands. The entire section demonstrates an arcade building form that represents Lingnan architectural culture. A traditional "three-stage type" defines the facade of the arcade along the street; this type comprises a bottom, body, and roof [54]. Under sunlight during the day, the vivid displays of roof flower details become possible, and the layers of the building body appear more abundant. Meanwhile, colored glass on the windows, incorporating elements of Guangfu traditional residences, refracts colorful light spots. Meanwhile, a rhythm is formed by the projection of arcade columns at the

building's base. The combination of these elements results in a unique and adaptable light quality (Figure 18).



Figure 18. A street of time-honored shops (images captured by the author).

3.1.4. The Site of the Ruins of Time-Honored Beijing Road and Gongbei Tower

Five archaeological floors, dating from the Northern Song Dynasty to the Ming and Qing Dynasties (960–1912), are present at the site of the ruins of Gongbei Tower. Separately, excavations in the middle of Beijing Road unearthed 11 layers of pavement, which measure approximately 44 m in length and about 3.8 m in width, extending to a depth of 3.0 m below the ground surface. These layers, when viewed from top to bottom, correspond to the northern section of the site of the ruins of time-honored Beijing Road across five historical periods: the Republic of China, the Ming and Qing Dynasties (1368–1912), the Song and Yuan Dynasties (960–1368), the Southern Han Dynasty (917–971), and the Tang Dynasty (618–907) [55]. Following their excavation in 2002, a tempered glass structure was installed to cover and display both the site of the ruins of time-honored Beijing Road and Gongbei Tower. The site transformation of this site into a central city hot spot can be attributed to its unique landscape and historical and cultural significance. Daytime sunlight refracts through the glass and into the ruins, an effect that clearly indicates the details of the brick and stone floor. The glass surface also reflects its surroundings, including the blue sky, ancient trees, shops, red lanterns, and human figures. Moreover, leaves from ancient trees flanking the relics are scattered across the glass, creating a mottled light and shadow effect that contrast with the relics visible beneath the glass (Figure 19). This results in the formation of a rich natural lightscape.

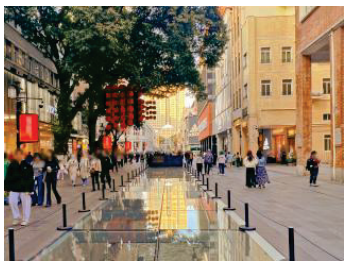


Figure 19. Daytime lightscape of the site of the ruins of time-honored Beijing Road (images captured by the author).

3.1.5. Summary of Natural Lightscape

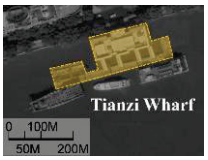
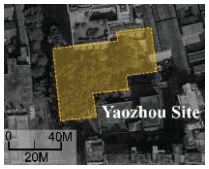
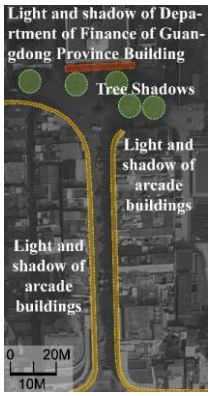
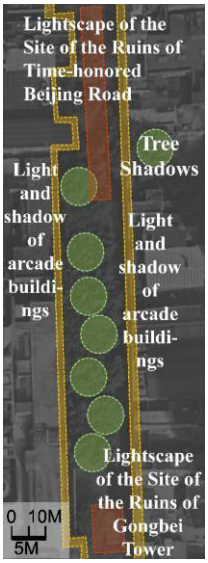
The existing main natural lightscapes along Beijing Road are formed by the combination of sunlight, tree shadows, and historical and cultural heritage sites (Table 4, Figure 20), fully demonstrating the historical heritage of Beijing Road.

3.2. Artificial Lightscape

Within the Beijing Road historic and cultural zone, the artificial lightscape comprises several categories: lamps and lanterns, architectural lighting, landscape lighting, and multimedia technology, among others. The category of lamps and lanterns comprises items

such as street lamps, special lanterns, lamp strips, and static or flashing billboard lights. Architectural lighting, accordingly, consists of decorative lighting for landmark or arcade buildings and light from architectural windows. Landscape lighting involves illumination or decorative lighting for landscape sketches or green landscapes, as well as ground lighting for pedestrian streets. Finally, multimedia technology includes elements such as animation, naked-eye 3D displays, holographic projections, and multimedia interactive devices, etc.

Table 4. Types of natural lightscape and environmental overview.

Lightscape Type	Space Type	Function of the Location	Lightscape Elements	Environmental Landscape Elements	Natural Lightscape Distribution Map	Picture
Lightscape of the Pearl River near Tianzi Wharf	Waterfront space	Viewing	Wave light, reflection	Waterscape		
Lightscape of West Lake and Yaozhou site	Waterfront space	Viewing	Lake light, tree shadow, lake reflection	Stone scenery, pavilions, stone bridges and waterside pavilions		
Light and shadow of arcade buildings	Street space	Traffic, leisure	Tree shadow, architectural light and shadow	Green plants, landscape sketch		 
Lightscape of the site of the ruins of time-honored Beijing Road and Gongbei Tower	Street space (pedestrian area	Viewing, leisure	Tree shadow, glass reflection, light and shadow of surrounding arcades	Old trees, landscape sketch		 

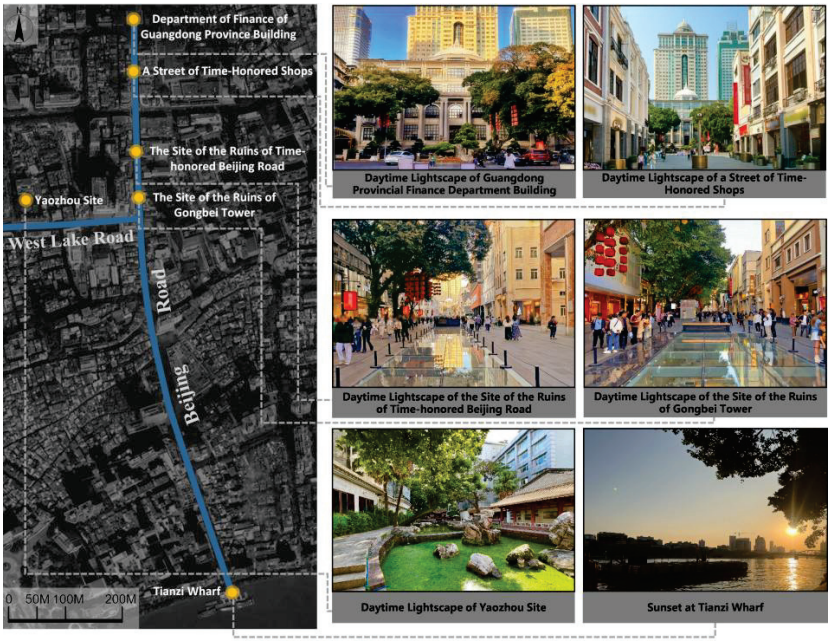


Figure 20. Distribution of existing natural lightscape locations on Beijing Road (author's own work, images captured by the author).

3.2.1. Lightscape of Lamps and Lanterns

Several typical types of lamps are identified in the area. Firstly, street lamps are installed to offer basic illumination. Secondly, various lanterns are utilized, a category that includes red and yellow lanterns suspended from the top of arcade colonnades, in addition to the red and colored lanterns adorning ancient trees. Thirdly, lamp strips and shaped lights can be observed wrapped around vertical components such as tree poles. Fourthly, static or dynamic lighting for shop billboards is also a common feature (Figure 21).



(**a**) (**b**) (**c**) (**d**) (**e**)

Figure 21. Lamps and lanterns: (**a**) lanterns hung on the top of the arcade colonnade (images captured by the author); (**b**) red lanterns hang on ancient trees (images captured by the author); (**c**) colorful lanterns hang on ancient trees (images captured by the author); (**d**) lamp strips and shape lights (images captured by the author); (**e**) shop billboard lighting (images captured by the author).

3.2.2. Lightscape of Building Lighting

(1) Lightscape of the Grand Buddha Monastery at night

The Grand Buddha Monastery, located south of the intersection between West Lake Road and Beijing Road, embodies a characteristic structure termed "temple hidden in the city, city and temple covered, city and temple combined, and temple and city dependent." Originally constructed during the Southern Han Dynasty (917–971), the monastery experienced abandonment in the Song Dynasty, followed by rebuilding in the Yuan Dynasty (960–1276), and its expansion into the Longzang Temple occurred in the Ming Dynasty

(1368–1644). The decline of Buddhism in the late Ming Dynasty (1573–1644) led to its governmental conversion into a public office. War resulted in the destruction of this government office in the seventh year of the Shunzhi reign of the Qing Dynasty (1644–1912). Reconstruction of the Grand Buddha Monastery took place in the second year of the Kangxi reign, establishing it as a Buddhist holy land south of the five ridges [56]. The Pujue building, representing a comprehensive Hongfa building, reached completion and opened towards the end of 2016. This seven-story structure features blue brick and nanmu, cornice brackets, and golden glazed tiles, presenting a magnificent monument. Its location across the street from Grandbuy Department Store has contributed to its status as a landmark building in the Beijing Road historic and cultural zone.

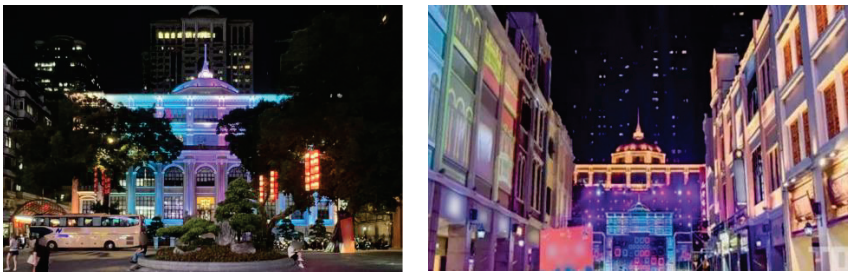
Daylight causes the golden glazed tiles of the Chinese-style building to shine brightly, while the changes in light and shadow accentuate its magnificence and solemnity. When night falls, bright lights appear, and orange illumination highlights architectural details including window frames, glass, brackets, and railings; it also outlines the overall architectural outline (Figure 22). A vivid reflection of the exquisite and spectacular charm of traditional buildings is offered by the Grand Buddha Monastery's lightscape, which attracts tourists to pause and observe.



Figure 22. Lightscape of the Grand Buddha Monastery at night (images captured by the author).

(2) Lightscape of Department of Finance of Guangdong Province Building at night

Dynamic colored floodlights illuminate the exterior wall of this building at night, thereby highlighting the elevation details of the roof, cornice, column, and window frame (Figure 23a). This approach also enhances the nighttime lightscape charm of the Department of Finance of Guangdong Province Building, injecting vitality into Beijing Road. The Department of Finance of Guangdong Province Building utilized its dynamic light show as a background for stage performances during the September 2020 opening ceremony that followed the renovation and upgrading of Beijing Road (Figure 23b). This combination became a landmark event showcasing the new appearance of this ancient city.



(**a**) (**b**)

Figure 23. Lightscape of Department of Finance of Guangdong Province Building: (**a**) the current night lightscape of Department of Finance of Guangdong Province Building (images captured by the author); (**b**) in September 2020, the light show of Department of Finance of Guangdong Province Building (Source [57]).

(3) Lightscape of arcade buildings in a street of time-honored shops at night

The north section of Beijing Road houses a street of time-honored shops, where the arcade remains well preserved. To create the arcade's nighttime lighting, numerous floodlights and spotlights are arranged at the bottom, body, and roof of the "three-stage-type" facade, forming a rich shadow.

On the arcade's ground floor, the colonnade, columns, and shop billboards effectively complement several lighting elements: streetlights on the ground floor's square columns, top lights on the colonnade, sign lights, and the shop's translucent interior. Building facades primarily feature window illumination, where LED lights emphasize window frame detail. These lights are interwoven with neon signs from shops that have transparent and changeable windows, a method that both strengthens the building wall's structural sense and increases the lighting's perceived extension along the street interface. Floodlighting is the method utilized for the roof's illumination, which highlights eave and parapet detail (Figure 24). This lighting approach strengthens the arcade's historical and cultural charm, thereby establishing it as a crucial display window for the Beijing Road historic and cultural zone.



(**a**) (**b**) (**c**)

Figure 24. Lightscape of arcade buildings: (**a**) lightscape of arcade buildings in the street of time-honored shops at night (images captured by the author); (**b**) shop entrance billboard (images captured by the author); (**c**) shop vertical billboard (images captured by the author).

3.2.3. Lightscape of Multimedia Technology

(1) Xin Da Xin Department Store naked-eye 3D curved screen

Positioned at the intersection of Beijing Road and Zhongshan 5th Road, Xin Da Xin Department Store sits in the core of Guangzhou's traditional, typically crowded and bustling, business zone.

Constructed in 1914, the building was subject to a facade renovation in 2020, after which China's largest outdoor naked-eye 3D curved screen was installed at the southeast facade's corner. This curved screen features a rounded corner radian that perfectly conforms to the structure of this building. Optimal viewing is achieved from an area 20–30 m south of Xin Da Xin Department Store, a location corresponding to the entrance of the Beijing Road commercial pedestrian street. Viewers are able to experience spatial and stereoscopic images without requiring 3D glasses or other auxiliary equipment, thus creating a strong visual impact [58]. A rich variety of content, including commercial advertisements, cultural publicity, and special art animations, is displayed on the 3D curved screen. Among the impressive displays was the naked-eye 3D video Dragon Soars Across the Four Seas, broadcast during the 2024 New Year, where a giant dragon appeared to cling vividly to the building [59]. Another notable animation featured a high-tech spaceship appearing stationary in front of the screen, from which astronauts extended a huge hand out towards the audience for interaction, an experience akin to watching 3D sci-fi blockbusters in a cinema (Figure 25).

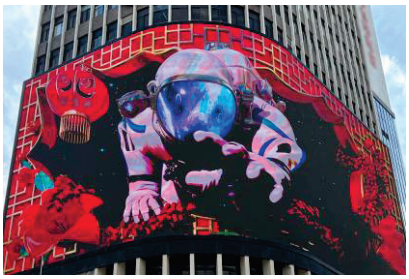
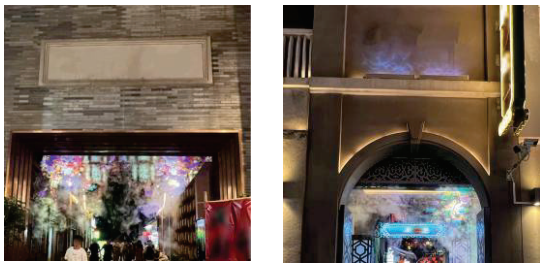


Figure 25. Xin Da Xin Department Store naked-eye 3D curved screen: Interaction between astronauts and tourists (images captured by the author).

(2) Holographic dynamic projection

The installations of 3D dynamic fog screen projections are set at the entrance of the Yuexiu Academy Street on the west side of Beijing Road and at Libai Lane on its east side (Figure 26). This technology uses water mist as the medium, and projects colorful dynamic flowers and other patterns onto the mist to create three-dimensional images. Travelers passing through the fog screen can shuttle amid changing light and shadow, thereby experiencing an interweaving of virtual and real elements. By decorating the ancient streets with a sense of science and technology, these dynamic fog screen projections attract tourists with an aura of mystery and enhance their lightscape experience.



(**a**) (**b**)

Figure 26. Three-dimensional dynamic fog screen projection: (**a**) 3D dynamic fog screen projection at the entrance of Yuexiu Academy Street (images captured by the author); (**b**) 3D dynamic fog screen projection at the entrance of Libai Lane (images captured by the author).

In addition, ground projection interactive devices have been introduced by the Beijing Road Pedestrian Street at multiple locations. These devices project a series of carefully designed patterns—including flowers, starry skies, and cartoon characters—onto the ground during nighttime (Figure 27), thereby enhancing the tour's fun and interactive qualities.



(**a**) (**b**) (**c**)

Figure 27. Ground projection interactive devices: (**a**) flowers patterns (images captured by the author); (**b**) starry skies patterns (images captured by the author); (**c**) cartoon characters patterns (images captured by the author).

(3) Facade projection of arcade building in the street of time-honored shops

Following an upgrade in 2020, the arcade building facade in the street of time-honored shops presents a new appearance. Special curtains installed on the facade windows act as a projection background, where, at specific times, the stage play *Encounter Beijing Road* is broadcast through projection (Figure 28). This play features the group portraits of Young Master Dongshan and Miss Xiguan as its protagonists, with their mutual love story as a narrative thread to demonstrate Guangfu's cultural characteristics. On the arcade's facade, modern technology demonstrates a dynamic, audio-visual multimedia lightscape effect, which injects new cultural vitality and scientific and technological meaning into the Beijing Road historic and cultural zone.



Figure 28. Facade projection of arcade building (source: [57]).

3.2.4. Lightscape of Landscape Lighting

(1) The site of the ruins of time-honored Beijing Road and Gongbei Tower

Professional display lights are installed at the site of the ruins of time-honored Beijing Road and Gongbei Tower, which also features an OLED transparent screen for displaying site information and 3D animation videos of the site. Through the screen glass, the ruins can be viewed when the screen is not active. The use of professional display lights renders the site details clearer during nighttime (Figure 29). A unique lightscape effect is conferred upon the site by modern technology, thereby enriching visitors' perception and comprehension of history and culture relating to Beijing Road.



Figure 29. Lightscape of the site of the ruins of time-honored Beijing Road and Gongbei Tower (images captured by the author).

(2) Copper Kettle Clepsydra

Xian Runyun and Du Zisheng forged the Copper Kettle Clepsydra timer (1316), in the third year of Yanyou (1316) of the Yuan Dynasty. This device stands as an important cultural relic of Guangzhou city. Its composition involves four copper kettles, with its timing function achieved through the sequential dropping of water. China's largest and best-preserved ancient timer is this particular clepsydra [60]. The National Museum of China now stores the original from the Gongbei Tower of Beijing Road, a piece once situated on the ancient traditional central axis of Guangzhou.

A copy of the "Copper Kettle Clepsydra" was produced in 2009. Then, in 2017, designers created and constructed the "Copper Kettle Clepsydra" landscape sketch at the original Gongbei Tower site on Beijing Road, integrating the Gongbei Tower's double door shape with the twelve Chinese zodiac signs and other elements (Figure 30). Copper pots

arranged in four steps dominate this landscape, where water is transmitted continuously in sequence, thereby reproducing the ancient timing principle. The decoration of the base includes bronze animal heads representing the Chinese zodiac, from whose mouths water flows into an annular pool. Engraved on the vertical brick square arch are the words "Beijing Road" and "from 214 BC." The nighttime lighting design is primarily aimed at highlighting the landscape's levels. Specifically, the warm light from LED circular spotlights emphasizes the blue brick texture of the square arch, while weak colored lights at the pool's bottom generate a sparkling effect through the water. Interwoven with the surrounding hustle and bustle of people and accompanied by the ticking sound of running water, the landscape lights at this location collaboratively create a unique historical and cultural block atmosphere with both lightscape and soundscape qualities [61].

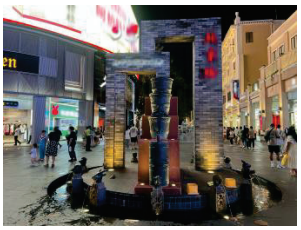


Figure 30. Landscape lighting of "Copper Kettle Clepsydra" (images captured by the author).

(3) New Flower Street

The "Huacheng Flower Street" is a new establishment situated in the south section of Beijing Road (an area extending from Wenming Road to Taikang Road). This street accommodates flower shops, flower art displays, cultural and creative arts stalls, as well as vendors offering special agricultural products. The regional cultural atmosphere of Huacheng Flower Street is effectively conveyed through various elements such as lights, signs, and glass windows. A central signboard, "Beijing Road Huacheng Flower Street," marks the entrance. Transparent display boxes flank this sign, showcasing dragon head and lion head artworks that embody Cantonese cultural characteristics. During nighttime, the bustling pedestrian street consistently emphasizes the traditional artistic image. In addition, flower street kiosks feature rich and diverse lighting solutions. These solutions consist of characteristic signboard lights, irregular light strips, and warm lights. In conjunction with the ring light strips on surrounding trees and colorful lanterns, they comprise a multi-level night lightscape for the flower street (Figure 31). This overall presentation has successfully attracted a considerable number of local residents and international tourists.



(**a**) (**b**) (**c**) (**d**)

Figure 31. Landscape of New Flower Street: (**a**) entrance signage (images captured by the author); (**b**) kiosk (images captured by the author); (**c**) flower stall (images captured by the author); (**d**) colorful lanterns hang on ancient trees (images captured by the author).

3.2.5. Summary of Artificial Lightscape

In the contemporary context, the artificial lightscapes of Beijing Road reflect the integration of new technologies with commerce, landscapes, and traditional culture (Table 5, Figure 32).

Table 5. Types of artificial lightscape and environmental overview.

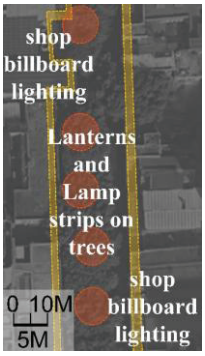
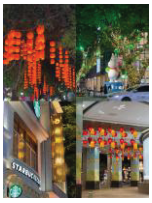
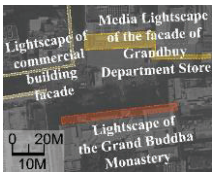
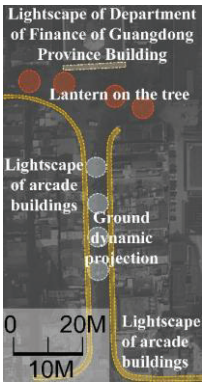
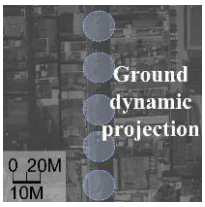
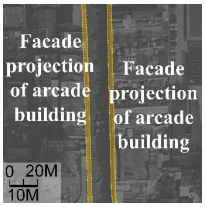
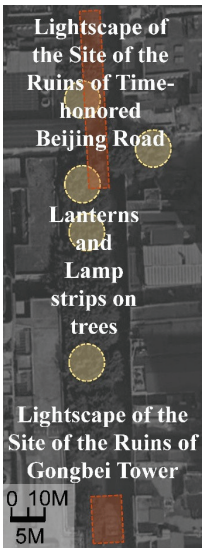
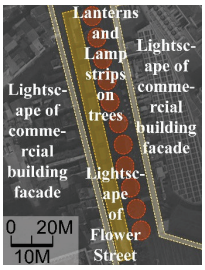
Lightscape Type		Space Type	Function of the Location	Lightscape Elements	Environmental Landscape Elements	Artificial Lightscape Distribution Map	Picture
Lamps and lanterns		Arcade ground floor colonnade, pedestrian street	Traffic, leisure	Street lamps, lanterns, lamp strips, billboard lights	Green plants, stalls, sculptures		
Building lighting	Lightscape of the Grand Buddha Monastery at night	Front square	Traffic, leisure and stay	Building facade lighting, Grandbuy facade media display, surrounding building lighting	Green plants, flower pools, pavilions, towers		
	Lightscape of Department of Finance of Guangdong Province Building at night	Front square	Traffic, leisure and stay	Building facade lighting, lanterns hanging from trees, and surrounding building lighting	Green plants, flower pool, landscape sketches		
	Lightscape of arcade facade at night	Pedestrian road	Traffic, leisure and stay, interaction	Holographic dynamic projection on the ground, building facade lighting, billboard lighting	Flower pool, landscape sketches		
Lightscape of multimedia technology	Xin Da Xin Department Store naked eye 3D curved screen	Outdoor plaza	Traffic, stay, guide	LED screen animation, billboard lighting, building facade lighting, building window lighting	Green plants, city model		
	Holographic dynamic projection on the ground	Pedestrian road	Traffic, stay, interaction	Dynamic projection	Flower pool, landscape sketches		
	Facade projection of arcade building	Pedestrian road	Traffic, leisure and stay, interaction	Facade projection	Flower pool, landscape sketches		

Table 5. *Cont.*

Lightscape Type		Space Type	Function of the Location	Lightscape Elements	Environmental Landscape Elements	Artificial Lightscape Distribution Map	Picture
Lights-cape of landscape lighting	Lightscape of the site of the ruins of time-honored Beijing Road and Gongbei Tower	Pedestrian road	Viewing, leisure and stay	Lights under the glass cover, reflective glass, lanterns on the surrounding ancient trees, lights of surrounding buildings	Ancient trees, landscape sketches		 
	Lightscape of Copper Kettle Clepsydra	Intersection	Viewing, leisure and stay, taking photos	Landscape sketch lighting, water lighting	Green plants, waterscape		
	Lightscape of new Flower Street	Pedestrian road	Leisure and stay, business	Landscape sketch lighting, shop lighting, tree lantern lighting	Green plants, flower pool, landscape sketches		 

3.3. Folk Lightscape

3.3.1. The Folk Custom of "Flower Street" and the Spring Festival Flower Market

Visiting the Spring Festival Flower Market, an event commonly known as "Flower Street," represents an important Spring Festival folk custom in the Guang Fu area. This event occurs annually, beginning on the 28th day of the twelfth lunar month and concluding on New Year's Eve. The tradition itself has continued since its origin during the Ming Dynasty (1368–1644) (see 2.3.4 summary). The lightscape as a critical element in establishing the atmosphere for these folk activities, consistently running through the entire event.

The lighting at the Spring Festival Flower Market is an indispensable folkloric symbol. The Spring Flower Market employs a modern lightscape design to evoke the historical lightscape of the traditional festivities. To illustrate, the 2024 Year of the Dragon Spring Festival Flower Market on West Lake Road offers a clear example (Figure 33): its temporary main archway, the "Gongbei Tower," was adorned with a light design integrating points, lines, and surface. The outline of the memorial archway was defined by warm yellow light, which also illuminated the archway's cornice, brackets, and carved decorations [62]. At the entrance side, the "Dragon Soaring Flower Sea" installation combined flowers with

the representations of flying dragons. Golden lights were used to accentuate the dragon's three-dimensional form. Flower stalls were arranged in close succession, and the lamps suspended from them, shining with star-like brightness, formed a magnificent corridor of light and shadow. The lighting decorations of the Spring Festival Flower Market effectively reproduce the historical lightscape described as "the lamps and moon illuminate together, while flower fragrance floods the air" in the *Continuation of Local Records of Nanhai District*.



Figure 32. Distribution of existing artificial lightscape locations on Beijing Road (author's own Work, images captured by the author).



(**a**) (**b**)

Figure 33. Spring Festival Flower Market: (**a**) main memorial archway "Gongbei Tower" lights up (images captured by the author); (**b**) West Lake Spring Festival Flower Market flower stalls (images captured by the author).

Building upon traditional lighting decoration, that year's Spring Festival Flower Market also incorporated the "Yuexiu West Lake Metaverse Flower Market" digital platform. Citizens, by scanning the landscape of the main archway or "Copper Kettle Clepsydra" with their mobile phones, could activate an AR interactive feature named "dragon flies into the sky." This offered a unique experience represented by the interweaving of virtual and actual reality. Modern scientific and technological means have infused new vitality

into the folk lightscape. Therefore, both the Spring Festival Flower Market and historical culture now demonstrate a unique appeal through this new form.

3.3.2. Guangfu Temple Fair

The Guangfu Temple Fair originated from the religious temple market activities that date back to the Han and Tang Dynasties (202 B.C.-907). Then, it developed into a cultural symbol of Guangfu following commercial expansion in the Song and Yuan Dynasties (960–1368). Its modern iteration commenced with the folk activities of the Lantern Festival, which were officially organized in 2011. The festival, inaugurated on the Lantern Festival, lasted for seven days. Spatially, the activities centered on the City God Temple and the Beijing Road historic and cultural zone, including forms such as deity processions, performances, and exhibitions [63]. Parade lanterns (Figure 34a) are a principal activity during the celebration. Furthermore, a lightscape atmosphere rich in Cantonese characteristics is cultivated through the display of Cantonese rosewood palace lanterns (Figure 34b). Traditional folk customs, including singing and dancing, dragon and lion dances, and Bayin Gong and drum performances, were interspersed throughout the activities, thereby fashioning a multi-level soundscape. A unique smellscape was formed from the aromas of mellow rice wine, salty preserved meat, and tangerine peel fragrance, which permeated the characteristic food street. Collectively, these varied landscapes establish a temple fair experience that integrates light, sound, and fragrance.



(**a**) (**b**)

Figure 34. Guangfu Temple Fair: (**a**) parade lanterns (source [64]); (**b**) Cantonese rosewood palace lantern market (source [65]).

In 2014, the unique Guangfu Water Temple Fair was introduced as an additional feature (Figure 35). The sailing ceremony for the water temple fair took place at Tianzi Wharf on the day of the Lantern Festival. The scene of folk sacrifice to the South Seas God, as practiced in the Sui and Tang Dynasties (581–907), was recreated through the traditional "Triple Offering Ritual" prayer ceremony. In this context, red lanterns and yellow canopies, under illumination, generated a warm lightscape atmosphere, while Cantonese folk music with a strong local style animated the festive environment of the wharf. The sailing ceremony, acting as the central ritual, cultivated a solemn soundscape atmosphere, composed of the underwater sounds from the washing ceremony, the voices of individuals reading congratulatory texts, and the accompaniment of ancient music. Throughout programs such as lantern riddle guessing, Guangcai course, Sichuan opera face changing and other programs, the catchwords of Cantonese explanation, the crisp sound of porcelain pen touch in the Guangcai course, and the sudden changes in gongs and drums of Sichuan opera face changing were all mingled with the laughter from the lantern riddle guessing on the open deck. During the Guangfu Water Temple Fair, the

Tianzi Wharf also launched a "South Seas God" and other antique cruise ships to join the "Pearl River Night Cruise." When these cruise ships navigated the sparkling waters of the Pearl River, the lights from both riverbanks and the vessels themselves created a complementary illumination, enabling people to experience the unique charm of the Pearl River, Guangzhou's mother river.

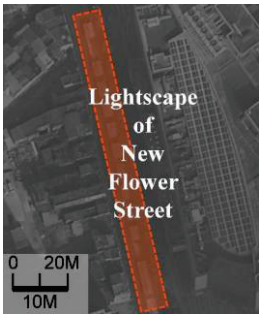
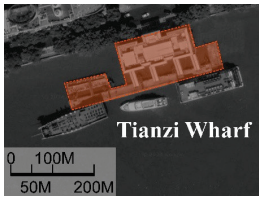
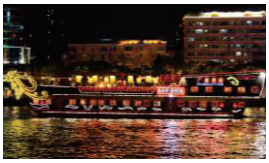


Figure 35. Guangfu Water Temple Fair (source [66]).

3.3.3. Summary of Folk Lightscape

The existing folk lightscapes along Beijing Road remain important showcases of Guangfu traditional culture. Folk lightscapes represented by "Flower Street" and "Guangfu Temple Fair" incorporate various elements such as soundscapes and smellscapes (Table 6, Figure 36), and enhance the visual expressiveness and immersion of folk festivals through modern technologies, revitalizing traditional folk customs in contemporary urban spaces.

Table 6. Types of folk lightscape and environmental overview.

Lightscape Type	Space Type	Function of the Location	Lightscape Elements	Environmental Landscape Elements	Folk Lightscape Distribution Map	Picture
Folk lightscape of "Flower Street"	Square, pedestrian road	Viewing, business, interaction	Lanterns, decorative lighting facade lighting of structures	Green plants, landscape sketches	 	
Guangfu Water Temple Fair	Wharf, waterfront space	Tour, traffic	Lanterns, decorative lighting	Waterscape, urban landscape		

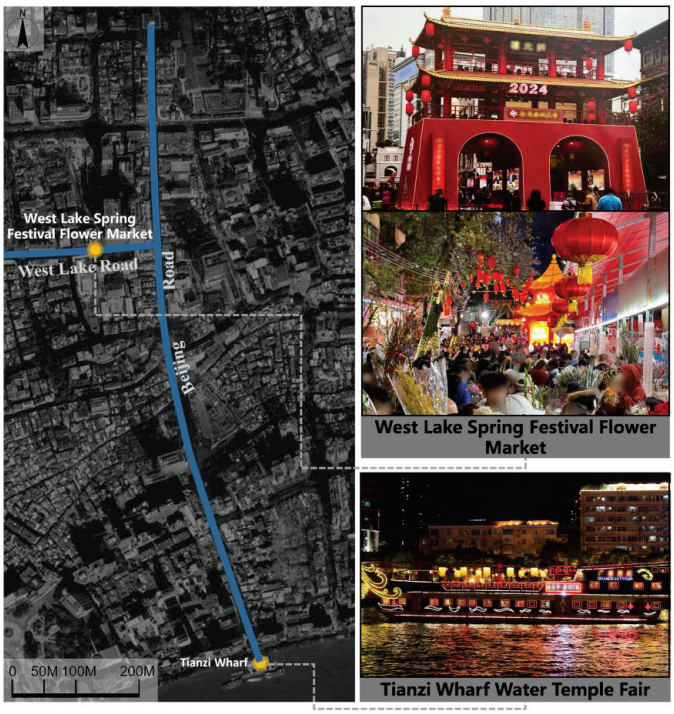


Figure 36. Distribution of existing folk lightscape locations on Beijing Road (author's own work, images source [66]).

4. Comparison of Ancient and Modern Lightscape

A comparison of the ancient (both vanished and preserved) and contemporary lightscapes in the Beijing Road historic and cultural zone indicates that urban development has changed the types of natural lightscape. Moreover, artificial lightscape has also been changed by the progress of science and technology. Folk lightscape continues to be an important approach for showcasing the traditional culture of Guangzhou. New technologies consistently facilitate the emergence of new forms of multimedia technology lightscape [67]. While some historical lightscapes have been preserved and persist to the present time, social changes have caused others to gradually disappear (Table 7, Figure 37).

Table 7. The main scenery of the Beijing Road historic and cultural zone from ancient to modern times.

Lightscape Type	Ancient and Modern Lightscape and Its Present Situation		Contemporary New Lightscape	The Vanished Historical Lightscape and the Reason for Disappearance	
Natural lightscape	The Pearl River near Tianzi Wharf: sunlight, moonlight, sunset glow, wave light, water light	The north bank of the Pearl River has moved southward, but its natural lightscape still exists	Lightscape of the site of the ruins of time-honored Beijing Road and Gongbei Tower	Enjoying "Hai Shan Xiao Ji" in Haishan Tower, watching the tide, reviewing the navy (Song Dynasty (960–1276)) sword and gun reflect the sun	Haishan Tower was destroyed by war in Yuan Dynasty (1271–1368)
	West Lake and Yaozhou site: Natural water light, water reflection, tree light and shadow	The area of West Lake and Yaozhou has been reduced, and now there is only the site of "Nine Star Garden"; Some natural lightscapes still exist		"Taiping Yanhu" is formed due to the hazy water vapor in sandbars	The north bank of the Pearl River moves southward, and sandbars merge into the north bank
	Light and shadow of arcade buildings	The arcade of the building is intact, and the light and shadow changes still exist		West Lake and Yaozhou: lotus shadow, dense Sea Island, cloud shadow in the water, mirage of pavilions, solitary smoke under the sunset and "The Spring Sunrise of Yaozhou"	The diversion of the water system led to the shrinkage of the lake. There is only one pond left after the Qing Dynasty (1644–1912), which is now the "Yaozhou site"

Table 7. *Cont.*

Lightscape Type	Ancient and Modern Lightscape and Its Present Situation		Contemporary New Lightscape	The Vanished Historical Lightscape and the Reason for Disappearance	
Artificial lightscape	All kinds of lanterns and lamps	The form and function have changed with the changes in the times	Lightscape of building lighting: Lights of the Grand Buddha Monastery at night, facade lighting and lighting show of Department of Finance of Guangdong Province Building, lighting of arcade facade at night	Jasmine lantern, lightscape of flower lights in the jasmine flower market at South Gate	Jasmine flowers are reduced due to the introduction of exotic flowers
			Multimedia technology: Xin Da Xin Department Store naked eye 3D curved screen, holographic dynamic projection on the ground, facade projection of arcade building	Glass lamps and lanterns shops in Shuangmendi and the Grand Buddha Monastery	Changes in products and business models due to changes in the times
	Lightscape of flower market	It has moved to the West Lake Road area and evolved into the current lightscape of the Spring Festival Flower Market	Lightscape of landscape lighting: lighting of the site of the ruins of time-honored Beijing Road and Gongbei Tower, lightscape of Copper Kettle Clepsydra, flower street lighting	Lightscape of night market on West Lake Road	Canceled
				Lightscape of Lujiang Academy	The academy is now used for other purposes
				Lightscape of official activities at Tianzi Wharf	Official activities no longer exist
Folk lightscape	Folk lightscape of "Flower Street"	The folk custom of "Flower Street" has been handed down to this day	Lightscape of the Guangfu Water Temple Fair at Tianzi Wharf	The light shed of Haishan Tower flickers	Haishan Tower was destroyed by war in Yuan Dynasty (1271–1368)
	The lightscape of dragon boat race in the Dragon Boat Festival	The location of the Dragon Boat Race has been transferred from West Lake to the Pearl River and has been handed down to this day		Birthday of the Lord Huaguang in Shuangmendi: the lamps were painted with colors, the lights were brilliant	It was banned by the government at the end of Daoguang. This folk custom has declined and disappeared
	Guangfu Temple Fair	It is now an official- led folk festival with a modern lantern festival			

4.1. The Type of Natural Lightscape Has Changed

Social and geographical transformations have led to changes in the types of natural lightscape in the region. Thus, some natural lightscapes that existed historically have vanished. For instance, "Hai Shan Xiao Ji," one of the Eight Ancient Scenic Spots of Yangcheng (Guangzhou) during the Song Dynasty (960–1276), disappeared following damage caused to the Haishan Tower in the Yuan Dynasty (1271–1368). The Song Dynasty (960–1276) scene depicting "swords and spears reflecting the sun" during naval division inspections is currently recorded only in literature. Preservation of some historical natural lightscapes remains possible. The natural lightscape of the Pearl River in the Tianzi Wharf area exemplifies this. While the wharf's location has changed, the core features of this lightscape have remained.

In the contemporary presentation of the ancient city, the natural lightscape is increasingly rich. Architectural space forms have become more diversified, and the composition of landscape elements in the urban environment is similarly varied. The glass materials utilized at the site of the ruins of the time-honored Beijing Road and the Gongbei Tower reflect surrounding scenes as well as light and shadow. This reflection creates a special atmosphere where historical and modern times overlap.

4.2. The Expression of Artificial Lightscape Has a New Form

Artificial lightscape exhibits more new forms in the contemporary context, primarily as it is more closely related to the technology of the times and prevailing social forms. Firstly, the decorative lighting of landmark buildings now represents an important part of the lightscape in the Beijing Road historic and cultural zone. Examples include the brilliant architectural lighting of the Grand Buddha Monastery, the dynamic transformation of

the colored floodlights on the external wall of the Department of Finance of Guangdong Province Building, and the "three-stage type" night lighting applied to the facades of arcade buildings in the street of time-honored shops. All these applications create a new lightscape atmosphere for the ancient city by means of modern lighting technology. Secondly, "night market" and "lantern" cultural expressions have become more diverse through the reliance on multimedia technology lightscapes. This diversification comprises the dynamic lightscape of naked-eye 3D curved screens, the immersive experience offered by holographic dynamic projections, and the theater night market featuring arcade facade projections, all of which are the innovative expressions of traditional culture. Thirdly, the site of the ruins of time-honored Beijing Road and the Gongbei Tower demonstrate the innovative application of artificial lightscape in the protection and display of cultural heritage. This is achieved through artificial lighting displays, the combination of the Copper Kettle Clepsydra with lightscape elements, and the ingenious collocation of flower street lanterns and lighting belts with ancient trees.

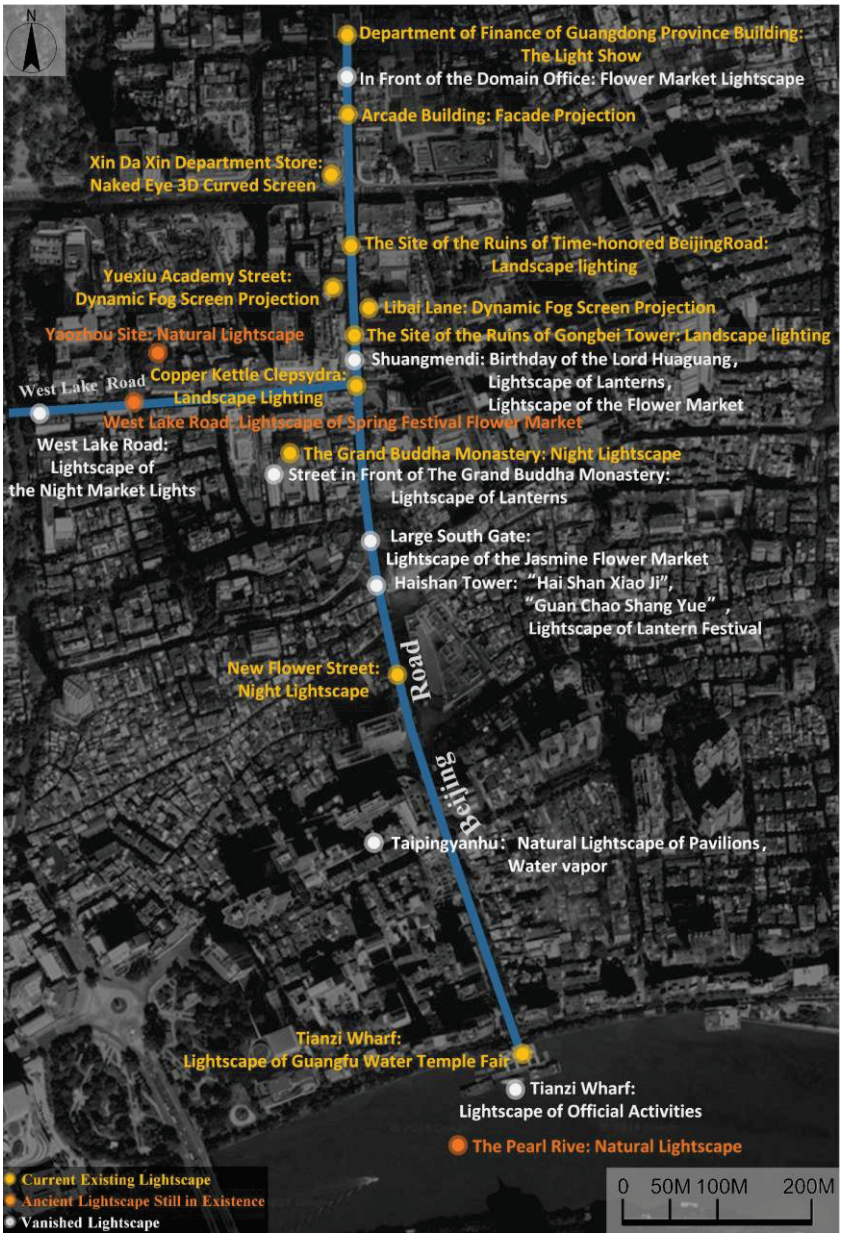


Figure 37. Distribution of major lightscape spots in ancient and modern times (author's own work).

4.3. Folk Lightscape Is Still an Important Part of Traditional Culture

With a history spanning over 2000 years, Guangzhou stands as a famous cultural city; its Beijing Road historic and cultural zone is situated in the earliest cultural and commercial center of the Lingnan area. Since ancient times, the display of Guangfu culture has uniquely benefited from the role of folk lightscape. Creating a festival atmosphere through the combination of lightscape and folk entertainment represents a mode inherited across generations. Existing folk activities, including guessing lantern riddles, flower streets, and temple fairs, continue to embody specific Guangfu cultural thoughts. These thoughts, "Seeking truth from entering the world" and "openness and compatibility," emphasize life rituals and are conveyed through unique entertainment and cultural meaning. The interaction between people and lightscape is evident during the Lantern Festival's lantern riddle guessing activity, where lanterns and riddles are combined. During the flower street activities of Spring Festival, a lively festival atmosphere is jointly constructed by elements such as colorful flowers, unique lanterns, New Year goods, and handicrafts. Through the visual display of colored lights and boats, alongside opera, dance, and other performances, the Guangfu Water Temple Fair effectively demonstrates its unique cultural heritage and regional customs.

5. Conclusions

This paper systematically examines the evolution of natural, artificial, and folk lightscapes in the Beijing Road historic and cultural zone. The key historical and current nodes for each category are summarized. Additionally, a comparison between ancient and modern lightscape is performed. It indicates how social development and geographical shifts have impacted the landscape of the Beijing Road historic and cultural zone. While certain historical lightscapes have vanished, many aspects of the Guangfu cultural spirit have survived. The region's contemporary urban landscape features a dominant lightscape transformed from traditional natural elements to new forms. They are represented by modern technologies such as 3D projection, multimedia interaction, and LED lighting. Regarding lightscape content, new technologies and methods are sometimes applied to convey the historical heritage of this Lingnan ancient city. However, other instances prioritize visual impact. Therefore, the city's profound cultural heritage is not effectively integrated into the landscape experience.

As an integral component of the urban landscape system in Guangzhou, the lightscape of the Beijing Road historic and cultural zone also functions as a crucial portal for displaying the city's culture. To create the overall image of this historic and cultural zone, it is necessary to make greater use of the special visual qualities of lightscape to highlight its characteristics and original historical and cultural meaning.

6. Future Work and Discussion

6.1. Recommendations and Strategies

Based on the historical and contemporary analyses of lightscapes, the following recommendations are proposed:

(1) For vanished lightscapes, digital reconstruction technologies, including multimedia restoration of historical photographs and paintings, provide viable revival solutions. This approach demonstrates a significant potential through the integration of 3D modeling techniques, which enable the transformation of historical lightscapes into dynamic visual representations. Such technological applications substantially enhance visitor engagement by delivering immersive experiences, particularly through

augmented reality (AR) systems that permit the overlay of virtual historical scenes onto physical environments via mobile devices. Compared to physical conservation methods (e.g., architectural reconstruction), digital restoration exhibits considerable advantages in terms of cost-effectiveness and unlimited reproducibility. Nevertheless, several limitations warrant consideration: the reconstruction quality is inherently dependent on source material integrity, while AI algorithms frequently produce aesthetically optimized outputs that may compromise historical accuracy. Furthermore, virtual reality (VR) implementations risk fostering misinterpretations among viewers who might perceive reconstructions as factual historical records, potentially leading to cognitive dissonance.

(2) For extant historical lightscapes, it is necessary to implement enhanced conservation and transmission measures. Regarding contemporary lightscape manifestations, innovative integration with Guangfu cultural elements can effectively showcase regional distinctiveness. Specifically, the interactive lightscape installations incorporating Guangfu cultural motifs could be developed, serving dual purposes of fostering public engagement and promoting cultural awareness.

(3) Regarding sustainable lighting design, the historical lightscapes of the Beijing Road historic and cultural zone represent a key cultural asset that can support sustainable development initiatives. When implementing illumination schemes, dual consideration must be given to visitor requirements in historic and cultural zones and ecological preservation [68]. Advanced solutions like motion-activated lighting systems can minimize light pollution while preserving distinctive nocturnal ambience and reducing energy expenditure. Particular attention should be devoted to preventing the urban nightscape homogenization caused by standardized lighting practices [69], with the prioritized conservation of regionally characteristic luminous heritage. These cultural assets not only embody the historical continuity of Guangzhou but also serve as crucial resources for urban sustainability, requiring innovative approaches that balance preservation with progressive development.

6.2. Future Work

Building upon established theoretical frameworks, subsequent investigations into Beijing Road's historic lightscapes will employ the following methodologies:

(1) A lightwalk methodology integrated with questionnaire surveys will be implemented to assess subjective perceptions. This approach, as a specialized form of sensory walk, involves a systematic pedestrian-based evaluation of luminous environments through predetermined routes [70]. Researchers will first identify critical spatial nodes—including high-density pedestrian areas and culturally significant landmarks—through preliminary field studies to establish optimized assessment paths. During implementation, trained facilitators will guide the participants along designated routes, with structured pauses at predetermined observation points for independent environmental evaluation. The participants will subsequently complete standardized questionnaires documenting their lightscape experiences both at observation nodes and along transit paths.

(2) Objective environmental measurements. A quantitative assessment of the photometric parameters in the lightscapes on Beijing Road will be conducted, including luminance distribution, correlated color temperature, and horizontal illuminance. High dynamic range (HDR) imaging technology will be systematically employed for comprehensive light environment analysis, following established protocols for urban lighting research.

(3) Laboratory simulation studies. On-site captured images will be replayed in the laboratory for participants to evaluate. This approach integrates eye-tracking, electrocardiogram (ECG), and galvanic skin response (GSR) measurements to analyze human perception of light environments.

As carriers of urban cultural memory, the lightscapes of urban historic and cultural zones constitute a vital component of diversified landscape systems. By investigating the lightscapes of Guangzhou's historic zones, examining people's perceptions of them, and analyzing their impacts can provide new perspectives for heritage conservation, urban renewal, and the preservation of nostalgic continuity in the historic zones across Lingnan.

Author Contributions: Conceptualization, J.Q.; methodology, J.Q.; software, W.C. and Y.L.; validation, J.Q., W.C. and H.Z.; formal analysis, W.C. and J.S.; investigation, W.C. and J.S.; resources, J.Q.; writing—original draft preparation, W.C. and J.S.; writing—review and editing, J.Q. and W.C.; visualization, W.C. and J.S.; supervision, J.Q. and H.Z.; project administration, J.Q.; funding acquisition, J.Q. All authors have read and agreed to the published version of the manuscript.

Funding: This research was funded by the Consultation Funding Project of the Chinese Academy of Sciences (2018-2W01-A-031); the Autonomous Research Project of the State Key Laboratory of Subtropical Building and Urban Science, South China University of Technology (2022KB06); the Project of China–Portugal Belt and Road Joint Laboratory on Cultural Heritage Conservation Science (SDYY2404); the National Natural Science Foundation of China (52578019).

Data Availability Statement: Data sharing not applicable to this article as no datasets were generated or analysed during the current study.

Acknowledgments: We appreciate the reviewers for their valuable comments.

Conflicts of Interest: The authors declare no conflicts of interest.

References

1. Wu, S. Main Points of Lightscape. *South Archit.* **2017**, *3*, 4–6. [CrossRef]
2. Qiu, J.; Wu, S. Lightscape and Architecture. *Archit. J.* **2017**, 115–118.
3. Qiu, J.; Li, J.; Li, Y.; Wei, T. Research Progress on Multi-Landscapes From Multi-Dimensional Perception Perspective. *J. Huaqiao Univ. Nat. Sci.* **2024**, *45*, 445–453. [CrossRef]
4. Wu, S.; Qiu, J. "Reading", "listening" and sound, light environment. *City Built Environ.* **2024**, *2*, 1. [CrossRef]
5. Lu, Y.; Su, X.; Wu, S.; Gao, W. Interpretation and Expansion of the 100 Smellscapes of Japan. *South Archit.* **2022**, 55–59.
6. Qiu, J.; Kang, J.; Wu, S. Progress of Soundscape Research and Practice in Europe. *Chin. Landsc. Archit.* **2022**, *38*, 58–63. [CrossRef]
7. Gazette of the People's Government of Guangzhou Municipality. *Notice of the General Office of the People's Government of Guangzhou Municipality on Issuing the "14th Five-Year Plan" for Ecological Environmental Protection in Guangzhou*; Gazette of the People's Government of Guangzhou Municipality: Guangzhou, China, 2022; pp. 1–56.
8. Yuan, X.; Qiu, J.; Chen, Y.; Wu, S. A Summary of the Academic Achievements of South China University of Tech. Team on "Trio-scape". *South Archit.* **2022**, 5–18.
9. Li, Y.; Wu, S.; Qiu, J.; Wei, T. Sustainable University Campuses: Temporal and Spatial Characteristics of Lightscapes in Outdoor Spaces. *Sustainability* **2024**, *16*, 7355. [CrossRef]
10. Xu, M. Beijing Road Historic and Cultural Zone in Guangzhou: Rejuvenating the Central Axis of the Millennium Commercial Capital. (19 October 2022). Available online: https://news.southcn.com/node_6a4048ba91/1a209a098a.shtml (accessed on 3 December 2024).
11. Li, Y.T.; Qiu, J.Z. Analysis of Moon Lightscape Configuration in Traditional Chinese Gardens. *Landsc. Archit.* **2023**, *30*, 130–136. [CrossRef]
12. Qiu, J.Z.; Li, Y. The Moonlight Thought in the Context of Lightscape. *Archit. Cult.* **2020**, 225–228.
13. Felice Beato.Treasury Street, Canton.Getty. Available online: https://www.getty.edu/art/collection/object/109BJE#full-artwork-details (accessed on 22 July 2025).
14. Zhu, Y.; Lu, Y.; Li, G. *Ping Zhou Ke Tan*; Shanghai Classics Publishing House: Shanghai, China, 2012.

15. Five and a Half Years Old Xiaobalagai. A Collection of Old Photos of Guangzhou III: 142 Masts Gathered in the Pearl River 2021. Available online: https://weibo.com/ttarticle/p/show?id=2309404681116237037661 (accessed on 13 June 2025).
16. Ganxinying. The Pearl River Scenery in the 19th Century. Available online: https://www.huitu.com/photo/show/20180713/101206142080.html (accessed on 13 July 2025).
17. Fang, X.; Zhang, Y.; Fan, F. *Nanhai Baiyong; Nanhai Zayong; Nanhai Baiyong Xubian*; Guangdong People's Publishing House: Guangzhou, China, 2010.
18. Wang, X. *Yu Di Ji Sheng*; Sichuan University Press: Chengdu, China, 2005.
19. Ye, S. *Guangzhou Biography*; Guangdong People's Publishing House: Guangzhou, China, 2020.
20. Chen, Z. *Canton Anecdotes: Selected Readings from Past & Present of Yangcheng*; Guangzhou Publishing House: Guangzhou, China, 2002.
21. Qiu, J. *Ancient Notes of the City of (Five) Goats. Chen Xianyou [19]*; Guangdong People's Publishing House: Guangzhou, China, 1993.
22. Zhang, S.; Shen, T. *Guangzhou Fu Zhi, Guangzhou Lidai Fangzhi Jicheng*; Lingnan Art Publishing House: Guangzhou, China, 2007.
23. Feng, J.; Li, R. Tide and Canton Gardens. *J. Archit. Hist.* **2023**, *4*, 147–161.
24. Art Museum of Beijing Fine Art Academy. Long Volume of Eight Ancient Scenic Spots of Yangcheng (Guangzhou) in the Past Dynasties-Song Dynasty Volume: Hai Shan Xiao Ji. Art Museum of Beijing Fine Art Academy. 2015. Available online: https://www.bjaa.com.cn/exhibit.html?hcs=11&clg=163&exhibit=223 (accessed on 18 October 2024).
25. Liang, M. *The Study of Lingnan Classical Garden Styles*; South China University of Technology: Guangzhou, China, 2013.
26. Huang, F. *Gazetteer of Guangzhou's City*; Guangdong People's Publishing House: Guangzhou, China, 1994.
27. Art Museum of Beijing Fine Art Academy. Long Volume of Eight Ancient Scenic Spots of Yangcheng (Guangzhou) in the Past Dynasties-Ming Dynasty Volume: The Spring Sunrise of Yaozhou.Art Museum of Beijing Fine Art Academy. 2015. Available online: https://www.bjaa.com.cn/exhibit.html?hcs=11&clg=163&exhibit=223 (accessed on 22 July 2025).
28. Huang, J. On the "jasmine complex" of the ancient Guangzhou people. *J. Xinyu Univ.* **2021**, *26*, 63–67. Available online: https://doi.org/CNKI:SUN:YGZX.0.2021-01-012 (accessed on 24 July 2025).
29. Ye, C. Flower Market and Flower Culture in Guangzhou. *J. Sun Yat-Sen Univ. Soc. Sci. Ed.* **1992**, 120–126.
30. Qu, D. *Guangdong Xinyu (New Narratives on Guangdong)*; Zhonghua Shuju: Beijing, China, 1997; reprint.
31. Litoulinao. Jasmine Flower. Photophoto 2019. Available online: https://www.photophoto.cn/sucai/32157847.html (accessed on 18 July 2025).
32. Anonymous. Hall of Quiet Study. THE MET 1959. Available online: https://www.metmuseum.org/art/collection/search/387080 (accessed on 22 July 2025).
33. Classic Visions, Close at Hand. Old Shopfronts in Their Glory Days: Watercolor Painting of Chinese Commodity Trade, 1825.zhihu 2021. Available online: https://zhuanlan.zhihu.com/p/63963115 (accessed on 23 July 2025).
34. Gray, J.H. *Walks in the City of Canton*; Guangdong People's Publishing House: Guangzhou, China, 2019.
35. Zhong, S.; Pan, C.; Sun, Z.Q. *Guangdong Zhuzhi Ci*; Guangdong Higher Education Press: Guangzhou, China, 2010.
36. Chen, M. *Beijing Road: The Iconic Pedestrian Street of Lingnan*; Guangdong People's Publishing House: Guangzhou, China, 2010.
37. Guangzhou Daily Digital Newspaper. In Guangzhou, the First Night Market Light Is Lit up. *Guangzhou Daily*, 2023. Available online: https://gzdaily.dayoo.com/pc/html/2023-12/18/content_631_844640.htm (accessed on 16 June 2025).
38. Huang, Y.; Chen, M. *Ancient Academies of Yuexiu, Guangzhou*; Guangdong People's Publishing House: Guangzhou, China, 2006.
39. Office of Local Chronicles of Yuexiu Distrct People's Government of Guangzhou; Committee of Learning Culture and History of Yuexiu District CPPCC (Eds.) *Historical Manuscripts of Yuexiu, Vol. 3: Qing Dynasty (Part 1)*; Guangdong Economy Publishing House: Guangzhou, China, 2015.
40. Han * He Bi. Scenes of Guangzhou City and the Pearl River Beach, etc. pan.baidu.2022. Available online: https://pan.baidu.com/s/1xiZC0MlnJJ3eouUOQwkLTA?pwd=6666#list/path=%2F (accessed on 14 July 2025).
41. Guangzhou Daily Digital Newspaper. A Road Through the Ancient and Modern, Three Axes Parallel to the City's Great Changes. *Guangzhou Daily*, 2022. Available online: https://gzdaily.dayoo.com/pc/html/2022-08/31/content_871_803037.htm (accessed on 22 July 2025).
42. The Palace Museum. *Panyu Xianzhi (Panyu County Gazetteer), 1872*; Hainan Publishing House: Haikou, China, 2001.
43. Historical Maps Network. 1880 Map of Guangzhou City. Historical Maps Network 2022. Available online: http://www.txlzp.com/ditu/3684.html (accessed on 22 July 2025).
44. Wang, J. Investigation and Research on Lingnan Dragon Boat Race. *Sports Cult. Guide* **2014**, 48–51.
45. Juzihui. Dragon Boat Race Illustration.huitu 2011. Available online: https://www.huitu.com/design/show/20220826/215118748033.html (accessed on 14 July 2025).

46. Zeng, Y. *Dragon Boat Racing: The Quintessential Duanwu Festival Tradition*; Guangdong Education Publishing House: Guangzhou, China, 2013.
47. Five and a Half Years Old Xiaobalagai. Guangzhou Old Photos: A.CHAN Photo Studio Work 3.weibo 2016. Available online: https://weibo.com/1273276401/3953299457497594?wm=3333_2001&from=10F5193010&sourcetype=weixin&s_trans=3838233261_3953299457497594&s_channel=4 (accessed on 13 July 2025).
48. Night Fair's Myriad Lamps Set Emerald Clouds Aglow, Guangzhou's Fiery Vivacity Outshines All Below. *Guangzhou Daily*, 8 November 2023. Available online: https://gzdaily.dayoo.com/pc/html/2023-11/08/content_871_841207.htm (accessed on 16 October 2024).
49. Chen, H. *A Record of Observations in Eastern Guangdong, Travel Accounts of Southern Yue*; Guangdong Higher Education Press: Guangzhou, China, 1990.
50. Huang, M. A Study on the Historical Evolution, Present Situation andReform of Guangzhou Flower Fair in Spring Festival. *J. Guangzhou City Polytech.* **2015**, *9*, 49–54.
51. Ma, Q.; Kuang, Y. The Historical and Cultural Connotation and Humanistic Care of Guangzhou Flower Market. *Lingnan Cult. Hist.* **2014**, 48–51.
52. Qiu, J.Z.; Wei, T.; Li, Y. A Preliminary Study on Comprehensive Evaluation of University Campus Lightscape A Case of South China University of Technology (Wushan Campus). *J. Light. Eng.* **2023**, *34*, 139–148.
53. Qiu, J.; Li, Y. Lightscape in Chinese Traditional Garden. *Chin. Landsc. Archit.* **2018**, *34*, 136–139.
54. Shi, J.; Guo, J. Analysis of Arcade Buildings in Guangzhou: Taking Beijing Road Arcade Street as an Example. *City House* **2021**, *28*, 148–149.
55. Beijing Road Cultural Tourism Zone. (9 June 2007). Available online: http://www.beijinglu.yuexiu.gov.cn/bjl/sj_bjl/lydl_bjl_sj/jd_bjl_sj/qnsy_bjl_sj/index.shtml (accessed on 27 September 2024).
56. Li, P.; Zhang, M.; Wang, H. Beijing Road Cultural Tourism Zone. (20 May 2023). Available online: http://www.beijinglu.yuexiu.gov.cn/bjl/sj_bjl/lydl_bjl_sj/jd_bjl_sj/lsjz_bjl_sj/index.shtml (accessed on 24 February 2025).
57. TOPFIRE. Guangzhou Beijing Road Building Facade Projection Show. TOPFIRE 2020. Available online: https://gztopfire.com/info.php?cid=2&id=41 (accessed on 13 July 2025).
58. Pei, L. *Research on the Expression and Evaluation of Night Lightscape of Media Architecture*; South China University of Technology: Guangzhou, China, 2022.
59. Nanfang Plus. Beijing Road Debuts '8K+3D+AI' Golden Dragon Display: Guangzhou's Cutting-Edge Ultra-HD Digital Innovation. Nanfang Plus 2024. Available online: https://static.nfapp.southcn.com/content/202402/06/c8582323.html (accessed on 27 September 2024).
60. Beijing Road Cultural Tourism Zone. (16 November 2018). Available online: http://www.beijinglu.yuexiu.gov.cn/bjl/pc_bjl/lydl_bjl/jd_bjl/qnsy_bjl/20181116/detail-208462.shtml (accessed on 27 September 2024).
61. Chen, R.; Qiu, J. Analysis of Lightscape Perception and Evaluation of Historic Area: A case Study of Yongqingfang Area in Guangzhou. *Archit. Cult.* **2022**, 175–179.
62. The Main Arch of West Lake Flower Market Replicates the Architectural Style of Gongbei Tower. *Information Times*, 18 December 2006. Available online: https://epaper.xxsb.com/html/content/2024-01/19/content_904956.html (accessed on 14 October 2024).
63. Liang, F. On the Cultural Value of New Folk Customs and the Role of Local Government from the Perspective of Guangfu Temple Fair. *J. Guangdong Inst. Public Adm.* **2017**, *29*, 92–96. [CrossRef]
64. Miss Kris. Guangfu Temple Fair Folk Parade Begins! Dragon and Lion Dance Celebrates Spring, Bringing Auspicious Blessings~. Xiaohongshu 2024. Available online: https://www.xiaohongshu.com/explore/65dc2aa2000000000b00fc26?app_platform=ios&app_version=8.89.2&share_from_user_hidden=true&xsec_source=app_share&type=normal&xsec_token=CBcqmOROPzPfGzHAf5gOE4GFRN65DMgIo-N_W4bAfWtqk=&author_share=1&xhsshare=WeixinSession&shareRedId=N0c7Qjs2SE9LP0ZFO0o1R0k1OT83OUdA&apptime=1753030248&share_id=8f18a8969cde4765bec75d1ba1dd1bbd&wechatWid=ccca32aac7cf3e090335a88fbd027e4f&wechatOrigin=menu (accessed on 14 July 2025).
65. Eva.Strolling Through the Guangfu Temple Fair.xiaohongshu 2025. Available online: https://www.xiaohongshu.com/explore/67b4619b000000002803da78?app_platform=ios&app_version=8.89.2&share_from_user_hidden=true&xsec_source=app_share&type=normal&xsec_token=CBrksV7PSY4KZLMu8ad5a5XnRE3BYfzludyqwoUPVUXFY=&author_share=1&xhsshare=WeixinSession&shareRedId=N0c7Qjs2SE9LP0ZFO0o1R0k1OT83OUdA&apptime=1753030495&share_id=318281cbec294ebc8d9355a1e4da72d8&wechatWid=ccca32aac7cf3e090335a88fbd027e4f&wechatOrigin=menu (accessed on 14 July 2025).
66. Meiyangyang's Meat Is So Delicious. Guangzhou Pearl River Cruise. Photophoto 2017. Available online: https://www.photophoto.cn/sucai/24103024.html (accessed on 20 July 2025).
67. Qiu, J.; Wu, S. New Technology Creates New Lightscape. In Proceedings of the 7th International Building Physics Conference, Syracuse, NY, USA, 23–26 September 2018.

68. Edensor, T. *From Light to Dark: Daylight, Illumination, and Gloom*; University of Minnesota Press: Minneapolis, MN, USA, 2017.
69. Jakle, J.A. *City Lights: Illuminating the American Night*; Johns Hopkins University Press: Baltimore, MD, USA, 2001.
70. Qiu, J.Z.; Li, Y.T.; Chen, J.Y. Soundwalk and Lightwalk: Special Methods for Exploring Environment. *J. Hum. Settl. West China* **2021**, *36*, 108–115.

Disclaimer/Publisher's Note: The statements, opinions and data contained in all publications are solely those of the individual author(s) and contributor(s) and not of MDPI and/or the editor(s). MDPI and/or the editor(s) disclaim responsibility for any injury to people or property resulting from any ideas, methods, instructions or products referred to in the content.

buildings

MDPI

Article

Research on the Optimization of Healthy Living Environments in Liyuan Block Empowered by CFD Technology: A Case Study of the Liyuan Block in Dabaodao, Qingdao

Huiying Zhang [1], Hui Feng [1], Xiaolin Zang [1,*] and Ang Sha [2]

[1] School of Architecture and Urban Planning, Qingdao University of Technology, Qingdao 266033, China; zhanghuiying@stu.qut.edu.cn (H.Z.); fenghui@stu.qut.edu.cn (H.F.)
[2] Innovation Institute for Sustainable Maritime Architecture Research and Technology, Qingdao University of Technology, Qingdao 266033, China; shaang@qut.edu.cn
* Correspondence: zangxiaolin@qut.edu.cn

Abstract: In the process of revitalizing historic districts, creating a healthy living environment requires a focus on the microclimate comfort of historic districts. Microclimate comfort refers to the comprehensive physiological perception and psychological satisfaction of climate elements such as heat, wind, and humidity under specific local environmental conditions, typically within a spatial range of horizontal scale < 100 m and vertical scale < 10 m. Among these, wind environment quality, as a key factor influencing pedestrian health experiences and cultural tourism appeal, holds particular research value. This study takes the Dabao Island Courtyard District in Qingdao as its subject, employing computational fluid dynamics (CFD) simulation methods from the artificial intelligence (AI) technology framework for modeling. CFD is a numerical method based on computer simulation, which solves fluid control equations (such as the Navier–Stokes equations) through iterative optimization to achieve high-fidelity simulation of physical environments such as airflow, turbulence, and heat transfer. A three-dimensional geometric model of the Dabao Island courtyard district was established, and boundary conditions were set based on local meteorological data. Numerical simulations were conducted to analyze the wind environment before and after the renovation of different layouts, functional spaces, and spatial scales (individual courtyards, clustered courtyards, and surrounding neighborhoods) of the courtyard district. The results indicate that factors such as building layout, street orientation, and renovation strategies significantly influence the wind environment of the Dabao Island neighborhood courtyards, thereby affecting residents' perceptions of wind comfort. For example, unreasonable building layouts can lead to excessive local wind speeds or vortex phenomena, reducing wind comfort, whereas reasonable renovation and update strategies can facilitate the introduction of wind corridors into the historical courtyard buildings, improving wind environment quality. This study contributes to better protection and utilization of traditional neighborhoods during urban renewal processes, creating a more comfortable wind environment for residents, providing scientific decision-making support for the renovation of historical neighborhoods under the Healthy China strategy, and offering methodological references for wind environment research in other similar traditional neighborhoods.

Keywords: wind comfort; CFD wind environment simulation; healthy living environment; Liyuan; heritage value; cultural gene; artificial intelligence systems

1. Introduction

Against the dual backdrop of the Healthy China Initiative and urban renewal initiatives, there has been a growing emphasis on the quality of historical district environments. The microclimate quality of historical districts has become a key indicator of the health performance of the human living environment [1]. As a crucial component of the microclimate, wind conditions directly influence pedestrian comfort [2–4], health outcomes, and the city's ecological environment [5]. A good wind environment accelerates the dissipation of sensible heat through efficient ventilation and enhances the potential for ventilation-induced cooling, which is crucial for mitigating the urban heat island effect in summer and promoting the dilution and transport of atmospheric pollutants [6,7]. This, in turn, is deeply intertwined with residents' respiratory health, the quality of outdoor activities [8], and the ecological sustainability of neighborhoods [9]. Optimizing the wind environment in outdoor gathering spaces has a positive impact on alleviating ventilation-dependent diseases such as asthma and allergic conditions [10]. A stable laminar flow in an ideal summer wind environment effectively prevents stagnant airflow and the accumulation of potential pathogens. Good design can ensure orderly airflow around the space, using natural ventilation to prevent the buildup of pollutants and reduce the concentration of allergens such as pollen, dust mites, viral aerosols, and PM2.5 in the air. This enhances the efficiency of directed pollutant removal, thereby mitigating the risk of respiratory diseases.

Numerous studies have confirmed that the morphological characteristics of traditional courtyard buildings significantly influence their outdoor wind environment. Courtyards, as enclosed or semi-enclosed spaces open to the sky and surrounded by buildings or walls (common forms include U-shaped, L-shaped, etc.), have key morphological parameters, including courtyard plan shape [11–13], building enclosure height [14–18], building orientation [19], key spatial proportions of the courtyard (such as aspect ratio) [20], location of door openings [21], application of shading facilities [22,23], and internal vegetation layout [24,25], directly shape internal airflow patterns (such as vortex structures and ventilation efficiency) and local wind speed distributions [26], thereby significantly influencing pedestrian wind comfort. The aforementioned wind environment characteristics at the courtyard scale form the microscopic foundation of the overall wind environment pattern in urban neighborhoods and are closely coupled with pollutant dispersion and sensible heat dissipation processes at the neighborhood and larger scales [27].

Previous studies have primarily been limited by the following shortcomings: they have overlooked the dynamic adjustments made to social and cultural strategies and climate adaptability, which have led to changes in wind environment comfort within the microclimate of historic districts. The Dabao Island Courtyard District in Qingdao serves as a typical example of traditional courtyard architecture in northern China [28]. Its nested, enclosed courtyard spaces serve as carriers of deep historical memories. For the Dabao Island Courtyard District, its unique architectural layout, scale, and spatial form differ significantly from modern buildings. The wind environment of the Dabao Island courtyard district is influenced by a combination of factors, including architectural layout [29,30], street orientation [31,32], renovation strategies [33], and surrounding topography [34,35]. These factors interact to form a complex wind field, which in turn affects residents' wind comfort. While these courtyards have persisted and evolved over the long course of history, they now face new challenges in terms of modern urban climate adaptability. Currently, although there is growing interest in healthy microclimate design, few studies have used advanced simulation tools to conduct quantitative and spatially detailed assessments of wind environments in historical urban settings. Based on this, this study employs computational fluid dynamics (CFD) technology, supported by artificial intelligence-driven

modeling tools, to simulate wind flow patterns at high spatial resolution. It constructs a wind environment simulation system for traditional neighborhoods, conducting in-depth research and comparisons of wind environments in courtyard neighborhoods before and after renovation strategies, as well as the coupled relationships between wind environments within courtyards and pollutant dispersion and sensible heat dissipation processes surrounding courtyard neighborhoods before and after renovation strategies, as well as the coupled relationship between wind environment within courtyards and pollutant dispersion and sensible heat dissipation processes. This research explores the intrinsic mechanisms linking historical spatial forms to healthy living environments, adapting to the architectural complexity of traditional areas. It provides empirical evidence for healthy living design based on historical wisdom and climate responsiveness. This not only enhances the microclimate quality of the Da Bao Island historical district and improves residents' quality of life, but also offers scientific planning strategies for optimizing microclimate quality and achieving sustainable protection and renewal of traditional districts.

2. Materials and Methods

2.1. Research Methods

CFD simulation software is widely used in the assessment of courtyard wind environments [36]. Research on wind environments in traditional historic districts typically evaluates the wind environment of a district based on two different wind directions in winter and summer. Generally, these studies combine airflow characteristics with wind comfort standards and local wind statistics to assess wind comfort. In this study, a CFD simulation approach is used to assess and study the wind environment of the Liyuan in the historical district of Dabaodao, Qingdao, employing LES (Large Eddy Simulation) to simulate the air flow field conditions. The corresponding control equations and a turbulence model were established based on fundamental physical laws such as mass conservation, momentum conservation, and energy conservation. The computational domain size was set to 100 m, with a boundary condition computational domain model range of 100 m, a calculation domain resolution of 0.3 m, an inlet turbulence intensity of 10%, and a reference height of 1.5 m, which determined the simulation's spatial range. Both wind direction and reference wind speed were based on local meteorological data from Qingdao. Based on the simulation trial calculation, the number of iterations was 255. The research framework of this study is depicted in Figure 1.

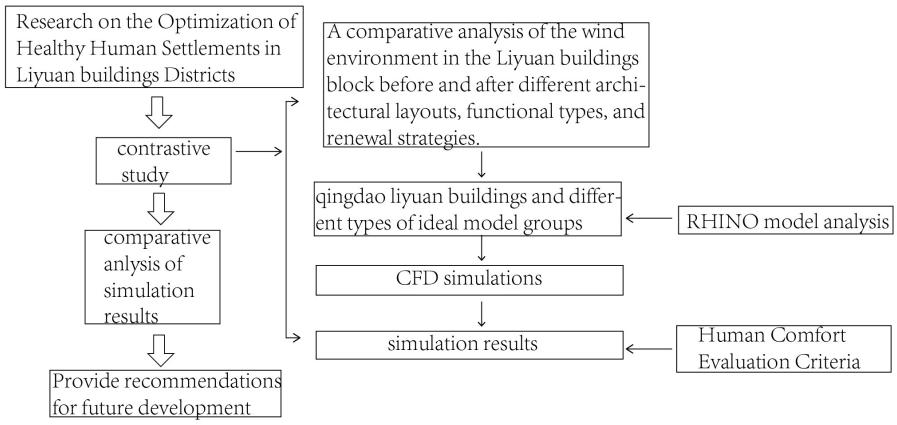


Figure 1. Research framework.

2.2. Ideal Model

The main characteristics of the Liyuan neighborhood are its wall-less urban community formed by the enclosure of primary and secondary urban roads, and the division of small and medium-sized streets into groups. The community has a high road network density, with narrow roads and a dense road network, and the seamless connection between community space and urban space is the main spatial characteristic of the Liyuan neighborhood. The organic combination of public spaces open to the outside and spaces for internal residential or commercial use is the main functional characteristic of the courtyard neighborhood.

The selected architectural models are representative of the spatial form and building layout observed in the courtyard district survey. A single courtyard is defined as a building that is separated by small and medium-sized streets and serves as the only enclosing structure separating the public space of the street from the private courtyard. A courtyard cluster is defined as a group of buildings separated by small and medium-sized streets. A courtyard neighborhood is defined as an area enclosed and separated by the city's main and secondary roads. According to the three different spatial scales—single courtyards, courtyard clusters, and surrounding neighborhoods—separate models were established for courtyard buildings and courtyard neighborhoods (Figure 2). For single-building structures, only the main building portion enclosed by the street and courtyard has been retained, as shown in the figure. The dimensions of the main building of the square-shaped structure are 60 m (length) × 45 m (width) × 8 m (height). Since the height of the decorative items and plants in the courtyard is less than 1.5 m, their impact on pedestrian height is negligible and can be ignored. The outdoor toilet is small, so its impact on wind speed is insignificant and can also be omitted. The models were converted to STL format for wind environment simulation, yielding wind environment simulation results at a height of 1.5 m above ground level for pedestrians [37].

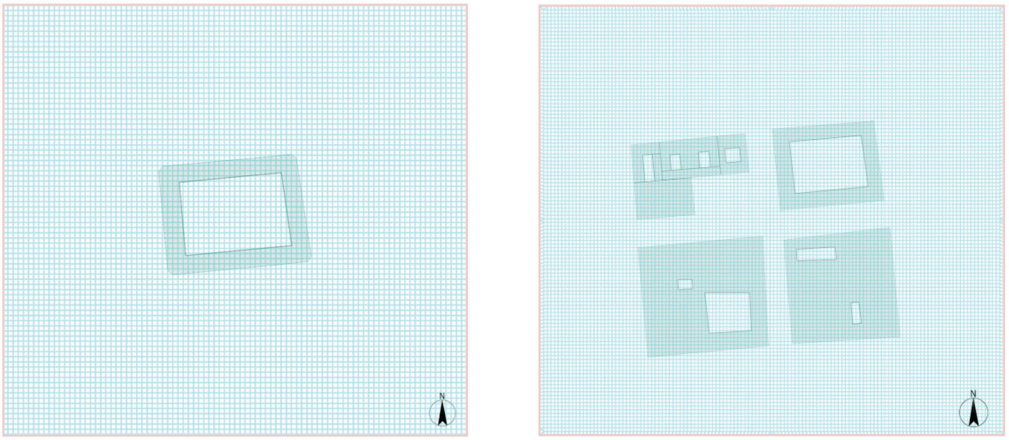


Figure 2. Grid arrangements.

2.3. Subjects of the Study

Qingdao is located in the southern part of the Shandong Peninsula, between 119°30′–121°00′ E longitude and 35°35′–37°09′ N latitude, surrounded by the sea on three sides and backed by mountains on one side (Figure 3). As a coastal hilly city, Qingdao features a terrain that is higher in the east and lower in the west, with undulations on both the northern and southern sides. Most of the traditional Liyuan in Qingdao are constructed in accordance with this terrain, generally parallel to the streets. Their external contours are determined by the direction of urban streets, typically square in shape, enclosed on all four sides, and forming a large courtyard in the center. These Liyuan are distributed

in an orderly manner according to the terrain, exhibiting diversity in size, height, and form. This study selects Liyuan buildings of different types in the Dabaodao block, including single courtyards and courtyard clusters, as research objects to conduct CFD wind environment simulations.



Figure 3. The location of Qingdao in China.

This study utilizes long-term local meteorological data. Based on the wind rose diagram of Qingdao, it is concluded that, as a typical coastal mountainous city, Qingdao has a north temperate monsoon climate with a relatively high annual average wind speed of 4.6 m/s. The prevailing wind in winter is the northeast wind, with an average speed of 3.67 m/s and a maximum speed of 5.2 m/s; the prevailing wind in summer is the south wind, with an average speed of 5.2 m/s and a maximum speed of 6.0 m/s. For the simulation in this study, the summer prevailing south wind with a speed of 5.2 m/s is adopted (Figure 4).

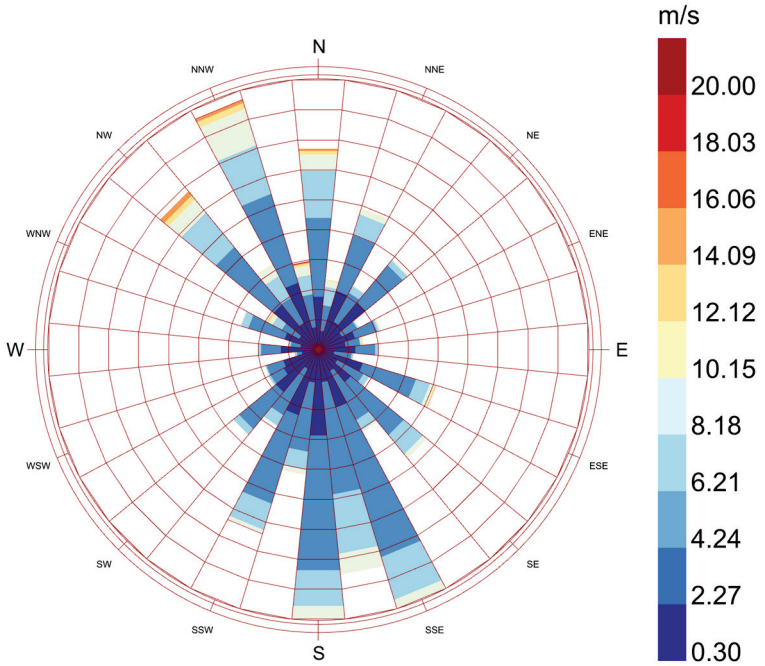


Figure 4. Statistics on wind direction frequency in Qingdao City.

2.4. Assessment Method

Wind comfort at the pedestrian level mainly focuses on the impact of wind force on the human body. To evaluate wind comfort in practical scenarios according to the Green Building Evaluation Standard (GB/T 50378-2019) [38], the division of wind comfort intervals has mainly been based on the mechanism of wind speed's impact on human activities and thermal comfort perception over the past few decades [39]. Previous relevant studies have shown that when only discussing the summer wind environment of courtyards, Murakami, Morikawa, and Zhang Hua [40,41] divided wind speed into three characteristic intervals in their research: low wind zone (0–0.7 m/s), comfortable wind zone (0.7–2.9 m/s), and strong wind zone (>2.9 m/s). In the field of wind environment assessment for traditional dwellings, Wang Zefa et al. proposed a wind environment comfort evaluation standard corresponding to the physical meaning of modern wind speed, along with the cultural cognition of ancient wind speed [42].

The wind environment evaluation standard adopted in this study is the dual-dimensional wind environment evaluation system proposed by Professor Yang Junyan from Southeast University, which integrates modern physical parameters and human perceptual cognition, based on Professor Ng's research on the thermal environment in Hong Kong (Table 1).

Table 1. Wind comfort assessment standard.

Wind Speed (m/s)	Characteristic	Human Comfort Label	Physical Perception
$V < 0.3$	No wind	stagnant and oppressive	poor thermal comfort
$0.3 \leq V < 0.6$	calm wind	barely perceptible or unnoticeable	relatively poor thermal comfort
$0.6 \leq V < 1.3$	light wind	slightly comfortable	relatively low thermal comfort, tolerable
$1.3 \leq V < 5.0$	gentle breeze	refreshed and comfortable	relatively good thermal comfort
$5 \leq V < 10$	strong wind	a feeling of being blown away	satisfactory thermal comfort
$10 \leq V < 15$	violent wind	too uncomfortable to move	uncomfortable thermal comfort

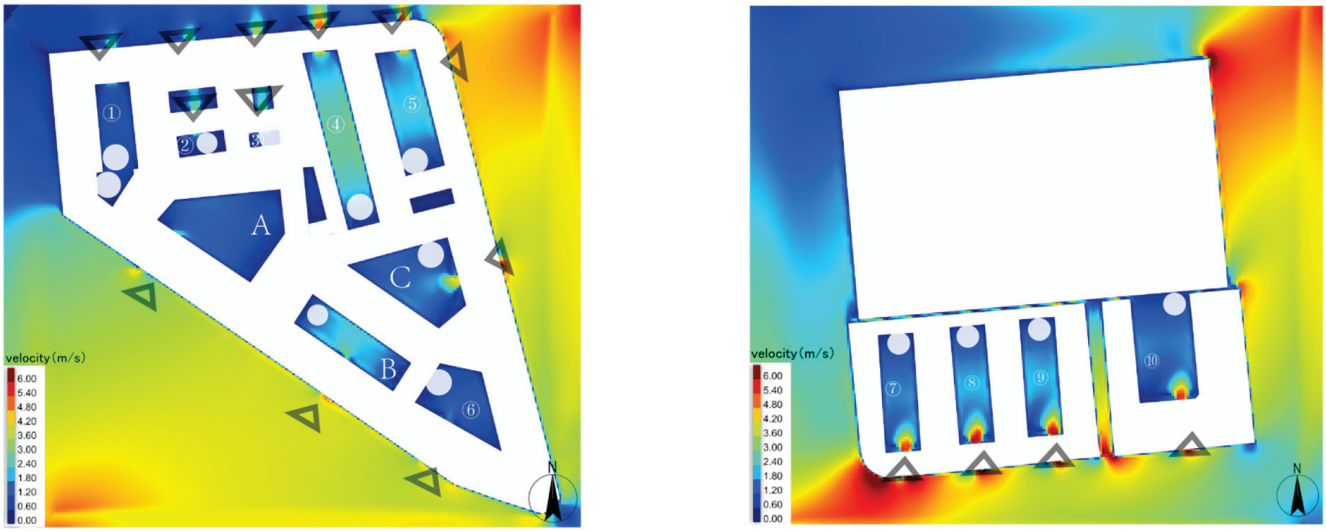
3. Results

3.1. Simulation Analysis of Natural Ventilation in Courtyard Buildings with Different Layouts of Sanitary Facilities

Against the backdrop of accelerating urbanization, it has been observed that the natural ventilation conditions of different sanitary facility layouts in courtyard buildings exhibit distinct characteristics. As shown in Figure 5, this study uses Junye Li and Yuxing Li as case studies to investigate how changes in toilet locations affect airflow and hygiene conditions in courtyard buildings. Taking Junyeli and Yuxingli as examples, based on the spatial positioning of toilets within the overall layout of the courtyard, two distinct forms of sanitary facility layout can be identified. The first involves toilets located on the opposite side of the courtyard entrance, while the second places toilets in the leeward area of the courtyard. Different toilet layout positions play distinct roles in airflow organization and spatial microclimate regulation, thereby exerting differentiated influences on the wind comfort of the courtyard.

Junyeli and Yuxingli are large courtyard clusters composed of multiple smaller inner courtyards. Taking the inner courtyards numbered ① to ⑥ in Junyeli as an example, the public toilets are located on the opposite side of the inner courtyard entrance, and this position is situated at the downwind end of the inner courtyard's airflow circulation system. Under the combined influence of factors such as airflow diffusion, friction, and spatial morphology, the wind speed significantly decreases as the airflow follows the predetermined path to the end of the courtyard. This layout aligns with the airflow circulation patterns of the courtyard. Additionally, since the wind speed is lower at the location of the sanitary facilities, it helps reduce the likelihood of pollutants spreading

extensively within the courtyard space through airflow circulation patterns. From a public health perspective, this effectively lowers the risk of disease transmission and has positive implications for creating a healthy living environment. Additionally, wind speed data in the figure shows that extremely low wind speeds are concentrated in the corners of spaces close to solid walls, while high-speed ventilation areas only appear near openings such as doors and vents. This indicates that the current design primarily relies on local strong winds to dilute the air and improve overall ventilation efficiency. Yuxingli consists of four connected inner courtyards, arranged from west to east as Courtyards ⑦ to ⑩, with public toilets located on the opposite side of the courtyard entrances. Further investigation revealed that, under the condition of equal courtyard lengths, there is a significant positive correlation between courtyard width and the area of low-wind-speed zones within the courtyard; that is, the wider the courtyard, the larger the area of low-wind-speed zones within it. This quantitative relationship provides a scientific basis for understanding the spatial morphology of courtyards and the characteristics of airflow distribution, offering important reference value for optimizing courtyard spatial layout and enhancing ventilation efficiency.



(**a**) (**b**)

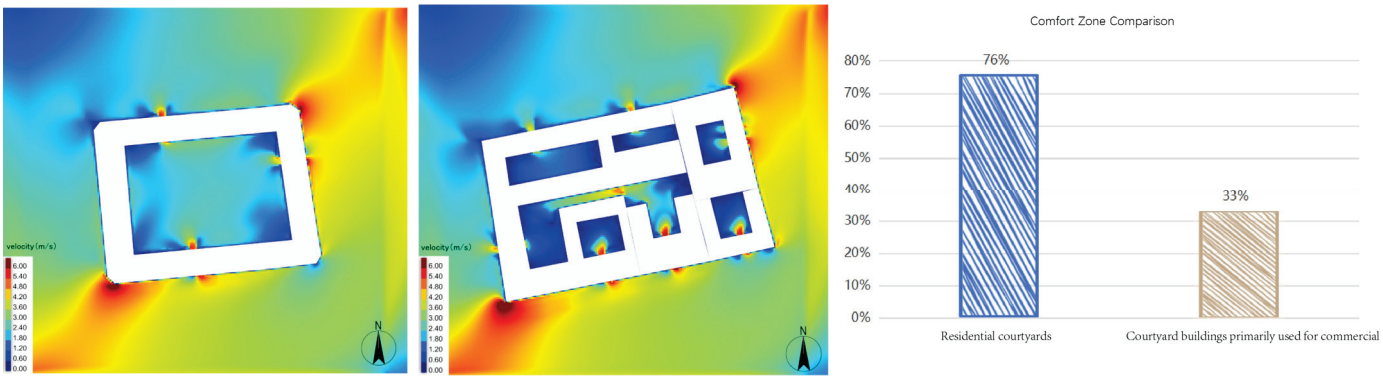
Figure 5. (**a**) Wind speed cloud map at 1.5 m above ground level in Junyeli. (**b**) Wind speed cloud map at 1.5 m above ground level in Yuxingli. (△ represents the entrance to the courtyard, ● represents the location of the toilet, A–C and ①–⑩ are the corresponding yard designations in the article).

Additionally, simulations conducted using professional airflow modeling software revealed that the A–C courtyards in Junyeli have restrooms located in the leeward area. During the summer monsoon season, this area cleverly avoids direct exposure to the wind direction at the entrance, remaining within the low-wind-speed leeward zone. From the perspective of aerodynamic principles and pollutant dispersion mechanisms, this layout effectively reduces the risk of pollutant airflow directly passing through the toilet area from the entrance and subsequently infiltrating the courtyard living area. It prevents polluted air from recirculating, effectively preventing the deposition or suspension of viral aerosols, mold spores, and other contaminants on wall surfaces, and reduces the time these pollutants linger in courtyards. Through comparisons of multiple simulation datasets and actual case studies, this layout significantly reduces pollutant dispersion in the courtyard living area, playing a positive role in creating a healthier and more hygienic courtyard living environment and providing robust spatial layout support for improving residents' quality of life.

3.2. Simulation Analysis of Wind Comfort in Different Functional Spaces of Courtyard Buildings

Given the significant differences in functional attributes among courtyard buildings, this study categorizes them into two main types based on their primary use: residential courtyard houses and commercial courtyard houses, both of which share comparable land area. This classification is significant because the two types exhibit markedly distinct characteristics in wind environment simulations.

Residential courtyards, as important spatial carriers for residents' daily lives, are typically composed of a large number of small courtyards clustered together to meet the functional requirements of privacy and compactness. The public areas within each small courtyard are relatively cramped, and the narrow spaces between courtyards make it easy for airflow to be obstructed by surrounding building facades, resulting in complex local wind speed variations. As observed and analyzed in Figure 6b, due to the highly dense spatial layout of residential courtyards, wind speeds primarily range between 0 and 2.4 m/s. From the perspective of pedestrian activity, this low-wind-speed environment creates a relatively suitable atmosphere for daily pedestrian activities. However, due to the relatively weak wind force within each courtyard, low-speed vortex zones are easily formed in the corner areas of the courtyards, which are often represented by dark blue areas in wind environment simulation diagrams. The presence of such low-velocity vortex zones makes it difficult for pollutants such as exhaust gases generated within the courtyard to disperse and be transported outward, resulting in poor air quality within the courtyard, necessitating targeted optimization strategies.



(**a**) (**b**) (**c**)

Figure 6. (**a**) Wind speed cloud map at a height of 1.5 m above ground level for courtyards primarily used for commercial purposes. (**b**) Wind speed cloud map at a height of 1.5 m above ground level for residential courtyards. (**c**) Comfort Zone Comparison.

From the perspective of overall architectural form and ventilation design, residential courtyard buildings typically only have doors on the street-facing facade, while the remaining three facades are closed off, lacking effective ventilation openings. This design pattern severely hinders airflow between the courtyard rooms and the courtyard, with wind speeds generally below 4.2 m/s. The limited number and improper placement of openings in the building envelope directly affect airflow paths and ventilation efficiency, as shown in the figure. Residential courtyard buildings typically have doors only on the street-facing facade, meaning that the intake and exhaust openings are on the same side. This can cause airflow to short-circuit, where fresh air is expelled immediately after entering, resulting in minimal airflow in areas far from the openings. The phenomenon of high-speed airflow concentrating around doorways also indicates that fresh air is expelled before it is fully mixed, reducing overall pollutant removal efficiency. Additionally, since door openings for ventilation are

often at the same elevation, this weakens the thermal pressure effect. When all openings are at the same height, natural ventilation cannot rely on thermal or wind pressure, and hot air cannot rise and exit, leading to more significant accumulation of contaminated air. During the hot summer months, such ventilation conditions hinder the rapid dissipation of indoor heat, making it difficult to effectively lower indoor temperatures and exacerbating feelings of stuffiness. Additionally, poor air circulation severely impedes the adequate exchange of indoor and outdoor air. This also leads to a decline in indoor air quality. The longer the air remains stagnant, the poorer the ventilation effect, which may result in the accumulation of pollutants, increased CO_2 concentrations, and moisture buildup, significantly impacting indoor air quality and adversely affecting residents' living comfort and health.

Courtyard buildings primarily used for commercial purposes typically feature a large courtyard surrounded by buildings, with a spacious and relatively open spatial layout that provides ample space for various commercial and social activities. Taking Guangxingli as a representative example, by the 1930s, Guangxingli had developed into a diverse and bustling area with a rich array of entertainment and cultural activities. The courtyard housed a variety of commercial establishments, including cinemas, photography studios, general stores, local product shops, dumpling shops, and children's clothing stores. Given the high requirements for environmental comfort in commercial activities, compared to residential courtyards of similar size, commercial courtyards place greater emphasis on ventilation and air circulation in their layout design.

In terms of spatial layout, commercial courtyards typically feature multiple openings. As shown in Figure 6a, the entrances to courtyards primarily used for commercial purposes are cleverly positioned on the southern, northern, and eastern sides. This multi-directional entrance layout facilitates the entry and circulation of airflow. Wind environment test results indicate that wind speeds within courtyards primarily used for commercial purposes can consistently reach 3.6 m/s. Under such wind speed conditions, it is conducive to the formation of strong and sustained through-drafts within the courtyard. Leveraging its powerful airflow driving force, air pollutants within the courtyard are rapidly expelled, effectively preventing their accumulation, thereby significantly improving the air quality of the courtyard. This creates a healthy and comfortable air environment for commercial activities, holding significant importance for enhancing commercial operational efficiency and consumer experience.

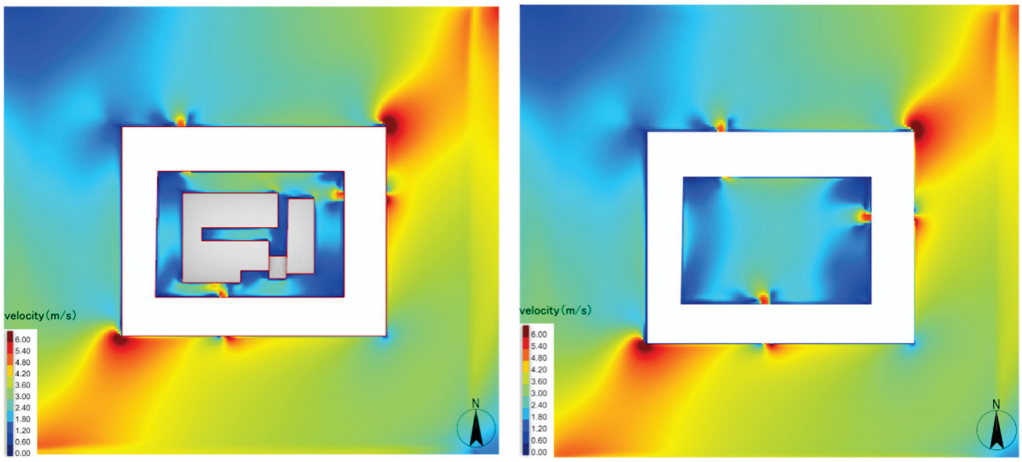
3.3. Sensitivity Analysis of Wind Comfort Before and After the Renovation of Traditional Courtyard Buildings

3.3.1. Simulation Analysis Comparing the Wind Environment in the Courtyard Before and After the Renovation of a Single Building in a Courtyard

In the 1920s and 1930s, as the population in courtyard neighborhoods continued to grow, residents' demand for usable space rose sharply. This practical need led to the gradual spread of illegal construction within courtyard areas. Such unauthorized construction activities have steadily eroded the originally open and public courtyard spaces, exerting a significant negative impact on the ventilation environment of courtyard areas. This has become a key factor constraining the improvement of wind environment quality in courtyard areas and their surrounding neighborhoods. This section examines the comparison of wind environment conditions in courtyards before and after the renovation of individual buildings in courtyard areas.

Taking Guangxingli as a typical case study, summer wind speed simulations using CFD software can visually analyze the comparison of ventilation conditions within single courtyards before and after renovation strategies. As shown in Simulation Figure 7a,

before the courtyard was renovated, i.e., when illegal structures were present within the courtyard, the wind speed in most areas of the courtyard was generally below 1.2 m/s. When the wind speed is below 1.2 m/s, poor thermal comfort occurs because low wind speeds lead to poor air ventilation and outdoor thermal comfort issues. This results in a significant decline in pedestrian wind comfort perception, with the overall wind speed environment in Guangxingli deteriorating. As shown in Figure 7b, after the renovation of the courtyard buildings, the summer wind speeds in most areas of Guangxingli are consistently maintained between 0 and 3.0 m/s, and the wind speeds across the entire area are below 4.2 m/s, meeting human comfort standards. This significant change clearly demonstrates that reasonable spatial clearance and planning can effectively improve the microclimate environment of courtyards, creating a more comfortable and healthy outdoor living space for residents. This highlights the importance and necessity of the renovation strategy of demolishing illegal structures in optimizing courtyard wind environments and enhancing spatial quality.



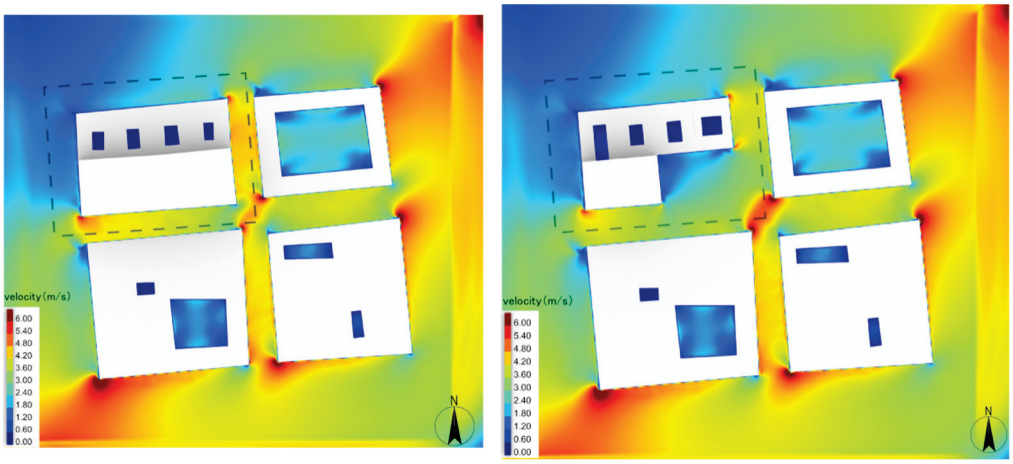
(**a**) (**b**)

Figure 7. (**a**) Wind speed cloud map of the courtyard building 1.5 m above ground level before the update. (**b**) Wind speed cloud map of the courtyard building 1.5 m above ground level after the update.

Upon further investigation of the underlying mechanisms, the illegally constructed buildings within the courtyard severely disrupt the natural formation process of through-drafts in the courtyard. The disorderly, illegal structures have made the originally smooth ventilation pathways complex and convoluted, causing severe airflow obstruction and completely destroying the original good ventilation environment. This ventilation obstruction leads to deteriorated ventilation conditions during high-temperature periods in summer, resulting in a significant increase in internal temperatures within the courtyard. The oppressive heat accumulates within the courtyard space, making it difficult to dissipate the residual heat from summer, thereby greatly reducing residents' living comfort. It should be noted that this study was conducted under simulated conditions with a single prevailing wind direction, which effectively reveals the core impact of the update strategy. However, the actual wind environment is subject to dynamic changes. At the same time, the simulation mainly focused on wind speed distribution and did not incorporate the comprehensive impact of real-time temperature changes during hot and humid periods in summer on thermal comfort, which may differ from the diversity found in reality.

3.3.2. Simulation Analysis Comparing Wind Conditions Before and After the Renovation of Clustered Courtyard Buildings

As shown in Figure 8a, for the clustered courtyard buildings (the building area within the black box in the figure), prior to renovation and upgrading, the majority of the accessible areas along the east and south streets of the clustered courtyard buildings experienced high wind speeds during the summer. In some sections of the east street, wind speeds exceeded the 5 m/s threshold for human comfort, while wind speeds along the east street ranged between 2.4 m/s and 6.0 m/s, creating stagnant wind conditions alternating with strong winds, resulting in an uncomfortable experience. As shown in Figure 8b, for the clustered courtyard buildings, after renovation and upgrading, wind speeds in the eastern street area of the square gradually decreased and stabilized within the range of 2.4 m/s to 4.2 m/s, falling within the comfortable wind speed range suitable for pedestrians to stand or rest for short periods. The open layout of the square facilitates rest and relaxation in this zone. The eastern edge of the square and the southern street area mostly have wind speeds within the comfortable range of 2.4 m/s to 4.2 m/s. Moving deeper into the newly opened square area, wind speeds decrease to the low wind speed range. Clearly, the wind environment quality of the clustered courtyard buildings improved after the renovation strategy was implemented, better aligning with human wind comfort requirements.



(**a**) (**b**)

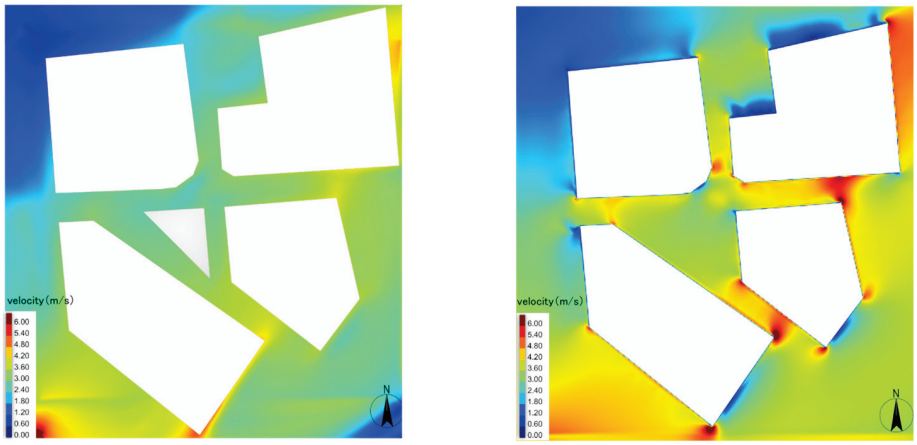
Figure 8. (**a**) Wind speed cloud map of the group courtyard 1.5 m above ground level before the update. (**b**) Wind speed cloud map of the group courtyard 1.5 m above ground level after the update.

Analyzing the summer simulation results of the courtyard buildings before and after renovation, comparative studies reveal that the wind speed variability in the eastern street area of the renovated courtyard buildings is reduced compared to the pre-renovation courtyard buildings, resulting in greater stability. The primary reason for these results is that after renovation, the high-rise buildings in the southeast direction of the courtyard buildings were demolished, and the square area was expanded, leading to more stable overall wind speeds within the courtyard buildings. This indicates that the design of airflow linkage between the square and the main activity street can enhance street wind speed stability, narrow the range of wind speed fluctuations, and significantly extend the duration of pedestrian comfort. This suggests that in the renovation of historic districts, the strategy of incorporating open spaces and constructing streamlined ventilation corridors can effectively improve the overall wind environment of historic districts.

3.3.3. Simulation Analysis Comparing the Wind Environment of the Surrounding Neighborhoods Before and After the Renovation of the Courtyard Buildings

In an in-depth study of the before-and-after updates of courtyard building districts, the four adjacent plots of land formed by the streets surrounding the courtyard district, as shown in the figure, were selected as the research subjects. By using CFD software to simulate summer wind speeds, it is possible to visually analyze the simulated comparison of pedestrian wind conditions in the courtyard building district before and after the update strategy.

As shown in Figure 9a, the summer simulation results for the courtyard building district indicate that, prior to renovation, the majority of the wind speed ranges in the courtyard district's active areas were approximately between 3.0 m/s and 4.2 m/s. The wind speeds around the triangular water supply building within the block remained at a relatively low level over the long term. As a result, the road space area exhibited a distinct low-wind zone characteristic, which was unfavorable for effective air circulation within the block. As shown in Figure 9b, the summer simulation results indicate that the removal of the triangular water supply building significantly improved the ventilation effect of the street. After demolition, wind speeds on the eastern side of the block increased significantly, with wind speeds in the newly created plaza area rising from 3.6 m/s to 4.8 m/s. Compared to the pre-renovation wind environment, this creates more favorable conditions for ventilation on the site. The demolition of the triangular water supply building creates an open space, restructuring the airflow pathways in this area. This effectively facilitated the smooth flow of air within the neighborhood. The series of wind environment changes triggered by the building demolition not only significantly optimized the neighborhood's microclimate but also, from the perspective of human thermal comfort theory, the strong airflow can quickly dissipate a large amount of heat within the neighborhood, thereby effectively lowering the overall temperature. It has a positive effect in alleviating the impact of high temperatures in summer and significantly improves the comfort of pedestrians walking in the neighborhood during hot summer periods. This provides an important wind environment foundation for creating a comfortable and healthy outdoor space.



(**a**) (**b**)

Figure 9. (**a**) Wind speed cloud map of the courtyard building district at a height of 1.5 m above ground level before the update. (**b**) Wind speed cloud map of the courtyard building district at a height of 1.5 m above ground level after the update.

This study demonstrates that the strategy of optimizing ventilation by removing redundant structures significantly improves the efficiency of air circulation in the neighborhood, a crucial step toward enhancing the thermal comfort experience in outdoor spaces. The

comfort of pedestrian wind environments requires an appropriate range of wind speeds, while also considering the combined effects of temperature, humidity, solar radiation, and other factors. Future research could further integrate field monitoring with thermal comfort models to conduct a comprehensive assessment of residents' thermal perceptions across different seasons and time periods, thereby providing more precise guidance for the renovation design of courtyard neighborhoods and ultimately achieving the core objective of enhancing the quality of residents' outdoor living.

4. Discussion

This study employs CFD simulation technology to systematically investigate the wind environment characteristics of the Qingdao Dabaodao District, focusing on analyzing and comparing the wind environment of courtyards with different layouts of sanitary facilities, different functional spaces, and different-scale spaces (individual courtyards, clustered courtyards, and surrounding courtyard districts) before and after renovation. The findings provide empirical evidence based on historical wisdom and climate responsiveness for healthy human habitation design. The research findings not only validate the intrinsic connection between traditional architectural forms and microclimate adaptability but also provide a scientific basis and practical pathways for optimizing healthy living environments in historical districts in the future.

The core arguments of this study resonate deeply with existing research in the field of courtyard microclimate. On the one hand, the research results confirm the mechanisms by which courtyard morphological parameters influence wind environments. Previous studies have demonstrated that elements such as courtyard plan shape, enclosure height, and opening locations directly impact ventilation efficiency by shaping airflow paths. This study further quantifies this relationship through CFD simulation: for example, in courtyards primarily used for commercial purposes, the large courtyard layout and multi-directional opening design (such as the three-sided entrances of Guangxingli) create efficient throughdrafts, maintaining a stable wind speed of 3.6 m/s in summer, which aligns closely with previous findings that courtyard openness is positively correlated with ventilation efficiency. However, residential courtyards with dense small courtyards and closed facades (street-facing openings only) result in low-speed vortices (0–2.4 m/s), confirming previous observations that narrow, enclosed spaces hinder airflow circulation. On the other hand, this study found that the low-speed vortex zones in residential courtyards not only reduce human wind comfort but also exacerbate heat accumulation and pollutant retention, providing a new perspective for the synergistic optimization of thermal and wind environments. By comparing the wind environment differences between courtyards primarily used for commercial purposes (publicly open) and residential courtyards (privately enclosed), this study reveals the pathways through which functional requirements (sociocultural attributes) indirectly regulate microclimate via spatial form, expanding the dimensions of traditional architectural climate adaptability research.

In terms of historical district preservation, illegally constructed buildings (such as the unrenovated additions in Guangxingli) disrupt the original ventilation pathways, resulting in very low wind speeds. However, after removing the illegal structures, wind speeds return to a comfortable range. This suggests that historical district renovations must prioritize form preservation to avoid blindly damaging microclimate adaptability. In terms of healthy living environment construction, the study reveals the mechanism by which wind environments function as implicit health infrastructure. The layout of sanitary facilities in downwind areas can utilize low wind speed environments to reduce pollutant dispersion, which aligns with the requirements of the Green Building Evaluation Standard

(GB/T 50378-2019) regarding the association between wind environments and public health safety. The stability of wind speeds improved after the renovation of cluster-style courtyard houses, meeting human comfort standards while reducing summer heat risks through enhanced ventilation. This provides further reference for assessing the health performance of historic districts under the Healthy China strategy. In terms of climate-responsive design, commercial courtyards maximize natural ventilation through large courtyards and multi-directional openings aligned with prevailing wind directions. This principle can be applied to modern urban design, for example, street canyons and building clusters should consider the guidance of dominant wind directions. The strategy of demolishing redundant buildings and creating squares in courtyard renovations provides an operational solution for optimizing wind environments in high-density cities through spatial restructuring. Looking ahead to future technological developments, to enhance the scientific management of densely populated historic urban areas, subsequent research could establish a CFD-GIS collaborative decision-making framework that integrates fluid dynamics simulation with spatial analysis techniques. This framework would support decision-making optimization for historic district conservation and renewal strategies, as well as improve the scientific rigor of decisions regarding sanitation facility layout and public health. GIS can serve as a spatial data hub, efficiently extracting and calculating building form parameters such as building density, wind-exposed area index, and sky view factor, to provide high-precision input for CFD simulations based on three-dimensional vector model analysis. This enables the construction of neighborhood-level ventilation potential assessments, identifying the minimum wind resistance paths between cold air sources and heat sink areas through morphological spatial pattern analysis, to guide the planning and design of urban ventilation corridors, thereby better assisting urban management and the creation of a favorable microclimate environment. Additionally, GIS-based accessibility analysis can be conducted to understand residents' travel patterns, precisely identify high-demand densely populated areas, and clarify service demand gaps. By coupling with CFD pollutant dispersion models, PM2.5 concentration fields and wind environment exposure risk indices can be generated to establish negative screening rules for facility site selection, imposing environmental health constraints. Finally, by comprehensively considering factors such as demand, environment, and cost, a scientific hierarchical classification and optimized site selection for sanitation facility layout are generated. In summary, this study utilized CFD technology to reveal the intrinsic connection between courtyard building forms and wind comfort. Its value lies not only in providing a scientific basis for the renewal of the Dabaodao district but also in establishing an analytical framework linking historical forms, microclimate performance, and healthy living environments. This framework can serve as a methodological reference for the sustainable renewal of other traditional districts.

This study has the following limitations, which require further refinement in future research: First, the limitations of the simulation scenarios. This study focuses on the dominant south wind in summer and does not account for the influence of the northeast wind in winter or extreme weather such as typhoons. As Qingdao is located in a monsoon climate zone, seasonal differences in wind fields may lead to dynamic changes in the courtyard wind environment, necessitating further comparative simulations across multiple seasons and wind speed scenarios. Second, the simplification of influencing factors. The study primarily analyzed the effects of building layout and functional types but did not delve into the influence of factors such as vegetation configuration and thermal performance of building materials on wind-heat coupling effects. These factors may indirectly regulate wind environments by altering surface roughness or thermal radiation characteristics and should be incorporated into a multi-physics coupling analysis framework.

To address these limitations, future research can be advanced in the following areas: First, dynamic monitoring and optimization. Combining IoT technology to establish a long-term monitoring network for courtyard wind environments, real-time capture of spatio-temporal changes in wind speed, temperature, and pollutant concentrations, and providing data support for the dynamic optimization of simulation models. Second, future analyses will integrate the thermal comfort index with the combined effects of wind, heat, and humidity in a multi-physics field to assess the impact of microclimate quality on shaping healthy living environments. The following aspects can be explored in depth: (1) The mechanism by which solar radiation affects ventilation efficiency: Solar radiation energy is primarily converted into sensible heat flux, heating the near-surface air to form a thermal pressure gradient, which drives local circulation. (2) The coupled effects of humidity and pollutants: In high-humidity environments, aerosol growth due to moisture absorption alters deposition rates. Under high-humidity conditions, low wind speeds exacerbate PM2.5 retention, while increased wind speeds promote wet deposition and reduce particulate matter concentrations. Additionally, PM2.5 concentrations are closely associated with respiratory diseases, and increased concentrations significantly elevate the risk of respiratory disease infections in populations. (3) Humidity constraints on thermal comfort regulation: In environments with relatively high humidity, the minimum wind speed required to maintain thermal comfort standards is significantly higher than in dry environments. Third, adaptive translation of cultural genes: extracting the wisdom of multi-directional ventilation designs in courtyard buildings primarily used for commercial purposes, and developing design guidelines for wind corridors suitable for modern high-density cities, thereby achieving the contemporary inheritance of traditional architectural wisdom.

5. Conclusions

This study takes the Liyuan neighborhood in Dabaodao, Qingdao, as its research subject. Based on computational fluid dynamics (CFD) numerical simulation technology, it has systematically investigated the coupling relationship between the architectural spatial form elements of the Liyuan neighborhood and wind field characteristics, providing a scientific basis and practical pathways for optimizing the healthy living environment of historical neighborhoods. By conducting numerical simulations of the wind environment of different layouts of sanitary facilities, different functional spaces, and spaces of different scales (individual courtyard buildings, clustered courtyard buildings, and surrounding neighborhoods) before and after the renovation, the study found that factors such as building layout, street orientation, renovation strategy distribution, and building height significantly influence the wind environment of the Dabaodao Liyuan district, thereby affecting residents' perceptions of wind comfort.

The main conclusions are as follows: First, the spatial layout of sanitary facilities has a significant impact on the wind environment and public health safety of courtyards. The study found that when toilets are located opposite the courtyard entrance or in the leeward area, the low wind speed environment can reduce the risk of pollutant dispersion with airflow, aligning with the spatial organization logic of healthy living environments. There is a positive correlation between the width of the inner courtyard and the area of the low wind speed zone, providing operational design references for future optimization of public facility layouts in courtyards.

Second, differentiated functional spatial forms create significant variations in wind environments. Residential courtyards, which prioritize privacy, feature dense small courtyard layouts that obstruct airflow and increase local vortex zones, resulting in wind speeds typically ranging from 0 to 2.4 m/s. While this meets basic activity requirements, it can

lead to pollutant stagnation. Commercial courtyards, designed with open spaces and large courtyards with multiple openings to meet openness requirements, achieve wind speeds of up to 3.6 m/s, facilitating through-drafts and improving air circulation efficiency, thereby providing a more comfortable wind environment for public activities. To optimize the health and livability of residential environments, it is necessary to balance ventilation efficiency with spatial privacy. Specific strategies include appropriately increasing the openness between buildings, such as by creating ventilation corridors, and offsetting adjacent buildings horizontally in a front-to-back or left-to-right configuration. This allows airflow to bypass building edges and enter interior spaces, enhancing ventilation efficiency and improving thermal comfort. Increasing openings or windows on the windward side of building facades at a certain angle to the prevailing wind direction. Additionally, optimizing vegetation layout can be achieved by installing windbreak forests on the periphery, planting evergreen trees on the north side of courtyards to reduce winter cold air penetration, and arranging sparse woodlands and grasslands on the south side to guide summer winds into the space. Meanwhile, low shrubs can be used internally to block views and enhance privacy. By ensuring healthy ventilation requirements while effectively maintaining residential privacy, the design achieves synergistic optimization of wind environment and spatial quality.

Furthermore, renovation strategies at different spatial scales significantly optimize the wind environment of courtyard building districts. At the individual courtyard level, removing illegal structures eliminates ventilation obstacles, stabilizing summer wind speeds at 0–3.0 m/s, which meets human comfort standards. At the courtyard cluster level, creating plazas and constructing ventilation corridors can effectively reduce wind speed fluctuations, maintaining street wind speeds within the comfortable range of 2.4–4.2 m/s. At the neighborhood level, removing redundant buildings that obstruct airflow (such as triangular water supply structures) can reconfigure ventilation pathways, increase regional wind speeds, and enhance heat dissipation and pollutant dispersion capabilities. This provides a methodology for the sustainable renewal of historic districts that combines scientific rigor with cultural sensitivity. Future research could further validate simulation results using field monitoring data and expand to multi-physics coupling analysis involving thermal-humid environments and pollutant dispersion, while exploring the synergistic effects of various factors to provide more comprehensive decision support for precise renewal of traditional districts and the creation of healthy living environments.

In summary, through CFD wind environment simulation technology, this study analyzed various factors affecting wind comfort in Liyuan of the Dabaodao district and clarified the specific mechanisms of each factor. Additionally, future research can be expanded to multi-physical field coupling analysis, such as thermal–humid environments and pollutant dispersion, to provide more precise decision-making support for creating healthy living environments. This technical approach provides a methodological framework that combines scientific rigor with cultural sensitivity for the sustainable renewal of traditional neighborhoods. These research findings not only guide the planning, design, and renovation of the Dabaodao neighborhood, improving its wind environment quality and residents' quality of life, but also lay the groundwork for future research. In the future, additional actual monitoring data can be integrated to validate and optimize simulation results, while further exploring the synergistic effects of different factors, thereby providing more precise support for the sustainable development of traditional neighborhoods.

Author Contributions: Data analysis and writing, H.Z. and H.F.; methodology, H.F.; software, A.S.; validation, X.Z.; formal analysis, H.Z.; investigation, H.F.; supervision, X.Z. All authors have read and agreed to the published version of the manuscript.

Funding: This work was supported by the Natural Science Foundation of Shandong Province (Grant No. ZR2023QD005).

Data Availability Statement: Data are contained within the article.

Conflicts of Interest: The authors declare no conflicts of interest.

References

1. Feng, W.; Ding, W.; Fei, M.; Yang, Y.; Zou, W.; Wang, L.; Zhen, M. Effects of traditional block morphology on wind environment at the pedestrian level in cold regions of Xi'an, China. *Environ. Dev. Sustain.* **2021**, *23*, 3218–3235. [CrossRef]
2. Littlefair, P.J. *Environmental Site Layout Planning: Solar Access, Microclimate and Passive Cooling in Urban Areas*; BRE Publications: London, UK, 2000.
3. Yang, L.; Liu, X.; Qian, F.; Niu, S. Research on the wind environment and air quality of parallel courtyards in a university campus. *Sustain. Cities Soc.* **2020**, *56*, 102019. [CrossRef]
4. Singh, M.; Laefer, D.F. Recent trends and remaining limitations in urban microclimate models. *Open Urban Stud. Demogr. J.* **2015**, *1*, 1–12. [CrossRef]
5. Dharmasastha, K.; Liang, H.; Lin, J.; Xie, Y.; Yu, Y.; Niu, J.-L. Evaluating thermal sensation in outdoor environments-Different methods of coupling CFD and radiation modelling with a human body thermoregulation model. *Build. Environ.* **2024**, *266*, 112081.
6. Ai, Z.T.; Mak, C.M. CFD simulation of flow in a long street canyon under a perpendicular wind direction: Evaluation of three computational settings. *Build. Environ.* **2017**, *114*, 293–306. [CrossRef]
7. Yu, Y.; Kwok, K.C.S.; Liu, X.P.; Zhang, Y. Air pollutant dispersion around high-rise buildings under different angles of wind incidence. *J. Wind Eng. Ind. Aerodyn.* **2017**, *167*, 51–61. [CrossRef]
8. Lin, Y.; Yuan, X.; Yang, W.; Hao, X.; Li, C. A Review on Research and Development of Healthy Building in China. *Buildings* **2022**, *12*, 376. [CrossRef]
9. Du, Y.; Mak, C.M. Improving pedestrian level low wind velocity environment in high-density cities: A general framework and case study. *Sustain. Cities Soc.* **2018**, *42*, 314–324. [CrossRef] [PubMed]
10. Guo, X.; Buccolieri, R.; Gao, Z.; Zhang, M.; Lyu, T.; Rui, L.; Shen, J. On the effects of urban-like intersections on ventilation and pollutant dispersion. *Build. Simul.* **2022**, *15*, 419–433. [CrossRef]
11. Rojas, J.M.; Galán-Marín, C.; Fernández-Nieto, E.D. Parametric Study of Thermodynamics in the Mediterranean Courtyard as a Tool for the Design of Eco-Efficient Buildings. *Energies* **2012**, *5*, 2381–2403. [CrossRef]
12. Yaşa, E.; Ok, V. Evaluation of the effects of courtyard building shapes on solar heat gains and energy efficiency according to different climatic regions. *Energy Build.* **2014**, *73*, 192–199. [CrossRef]
13. Moonen, P.; Dorer, V.; Carmeliet, J. Evaluation of the ventilation potential of courtyards and urban street canyons using RANS and LES. *J. Wind Eng. Ind. Aerodyn.* **2011**, *99*, 414–423. [CrossRef]
14. Al-Masri, N.; Abu-Hijleh, B. Courtyard housing in midrise buildings: An environmental assessment in hot-arid climate. *Renew. Sustain. Energy Rev.* **2012**, *16*, 1892–1898. [CrossRef]
15. Ghaffarianhoseini, A.; Berardi, U.; Ghaffarianhoseini, A. Thermal performance characteristics of unshaded courtyards in hot and humid climates. *Build. Environ.* **2015**, *87*, 154–168. [CrossRef]
16. Chen, K.; Mo, Z.; Hang, J. The recirculation flow after different cross-section shaped high-rise buildings with applications to ventilation assessment and drag parameterization. *Build. Simul.* **2024**, *17*, 509–524. [CrossRef]
17. Soflaei, F.; Shokouhian, M.; Shemirani, S.M.M. Traditional Iranian courtyards as microclimate modifiers by considering orientation, dimensions, and proportions. *Front. Archit. Res.* **2016**, *5*, 225–238. [CrossRef]
18. Soflaei, F.; Shokouhian, M.; Abraveshdar, H.; Alipour, A. The impact of courtyard design variants on shading performance in hot-arid climates of Iran. *Energy Build.* **2017**, *143*, 71–83. [CrossRef]
19. Guo, P.; Ding, C.; Guo, Z.; Liu, T.; Lyu, T. Coupling CFD simulation and field experiments in summer to prove Feng Shui optimizes courtyard wind environments: A case study of Prince Kung's mansion in Beijing. *Buildings* **2022**, *12*, 629. [CrossRef]
20. Manioğlu, G.; Oral, G.K. Effect of courtyard shape factor on heating and cooling energy loads in hot-dry climatic zone. *Energy Procedia* **2015**, *78*, 2100–2105. [CrossRef]
21. Jiang, Z.; Gao, W.; Yao, W. Research on the wind environment in an enclosed courtyard: Effect of the opening position, size and wind angle. *Urban Clim.* **2023**, *52*, 101737. [CrossRef]

22. López-Cabeza, V.P.; Galán-Marín, C.; Rivera-Gómez, C.; Roa-Fernández, J.; Borrego-Baena, J.M. Comparative Analysis of Thermal Performance between Courtyards in Mediterranean Climate. *Proceedings* **2018**, *2*, 1381. [CrossRef]
23. Cantón, M.A.; Ganem, C.; Barea, G.; Llano, J.F. Courtyards as a passive strategy in semi dry areas. Assessment of summer energy and thermal conditions in a refurbished school building. *Renew. Energy* **2014**, *69*, 437–446. [CrossRef]
24. Altunkasa, C.; Uslu, C. Use of outdoor microclimate simulation maps for a planting design to improve thermal comfort. *Sustain. Cities Soc.* **2020**, *57*, 102137. [CrossRef]
25. Del Rio, M.A.; Asawa, T.; Hirayama, Y.; Sato, R.; Ohta, I. Evaluation of passive cooling methods to improve microclimate for natural ventilation of a house during summer. *Build. Environ.* **2019**, *149*, 275–287. [CrossRef]
26. Asfour, O.S. Prediction of wind environment in different grouping patterns of housing blocks. *Energy Build.* **2010**, *42*, 2061–2069. [CrossRef]
27. Lizana, J.; López-Cabeza, V.P.; Renaldi, R.; Diz-Mellado, E.; Rivera-Gómez, C.; Galan-Marin, C. Integrating courtyard microclimate in building performance to mitigate extreme urban heat impacts. *Sustain. Cities Soc.* **2022**, *78*, 103590. [CrossRef]
28. Kairui, D.; Jiguang, X. Analysis on Qingdao Courtyard Architecture from a Cross-cultural Perspective. *Acad. J. Humanit. Soc. Sci.* **2023**, *6*, 93–97. [CrossRef]
29. Tang, L.; Nikolopoulou, M.; Zhao, F.-Y.; Zhang, N. CFD modeling of the built environment in Chinese historic settlements. *Energy Build.* **2012**, *55*, 601–606. [CrossRef]
30. Son, M.; Lee, J.-I.; Kim, J.-J.; Park, S.-J.; Kim, D.; Kim, D.-Y. Evaluation of the wind environment around multiple urban canyons using numerical modeling. *Atmosphere* **2022**, *13*, 834. [CrossRef]
31. Narimani, N.; Karimi, A.; Brown, R.D. Effects of street orientation and tree species thermal comfort within urban canyons in a hot, dry climate. *Ecol. Inform.* **2022**, *69*, 101671. [CrossRef]
32. Lyu, X.; He, Y.; Yin, S.; Wong, S.; Tse, T.K.; Ng, E. Evaluating urban design strategies for pedestrian-level ventilation improvement in a high-density urban living environment—A LiDAR and wind tunnel study. *Build. Environ.* **2025**, *269*, 112439. [CrossRef]
33. Zhang, Q.; Ma, X.; Xu, D.; Zhou, D.; Yang, Y.; Jiang, W. The Impact of Courtyard Spatial Characteristics Across Historical Periods on Summer Microclimates: A Case Study from China. *Buildings* **2025**, *15*, 224. [CrossRef]
34. Hayakawa, K.; Miyaoka, D. CFD (Computational Fluid Dynamics) on the Wind Environment of the Gassho-Style Houses in Shirakawa-mura Ogimachi. *Urban Hous. Sci.* **2012**, *14*, 14–19.
35. Wang, W.; Chen, H.; Wang, L.; Wang, S. Integrating multiple models into computational fluid dynamics for fine three-dimensional simulation of urban waterfront wind environments: A case study in Hangzhou, China. *Sustain. Cities Soc.* **2022**, *85*, 104088. [CrossRef]
36. Yao, X.B.; Han, S.; Dewancker, B. Wind Environment Simulation Accuracy in Traditional Villages with Complex Layouts Based on CFD. *Int. J. Environ. Res. Public Health* **2021**, *18*, 8644. [CrossRef]
37. Lee, D.S. Impacts of surrounding building layers in CFD wind simulations. *Energy Procedia* **2017**, *122*, 50–55. [CrossRef]
38. *GB/T 50378-2019*; Green Building Evaluation Standard. China Construction Industry Press: Beijing, China, 2019.
39. Chen, X.; Hu, H.; Xu, Z.; Wu, Z.; Ma, R.; Wang, X. Wind comfort criteria and numbers of wind directions: The dual impact mechanism on pedestrian wind comfort evaluation in Qingdao, China. *Build. Environ.* **2025**, *280*, 113103. [CrossRef]
40. Murakami, S.; Morikawa, Y. Creteria For Assessing Wind-Induced Discomfort Considering Temperature Effect. *J. Archit. Plan. Environ. Eng.* **1985**, *358*, 9–17.
41. Zhang, H. Research on Natural Ventilation Design of Rural Housing in Yangtze River Delta. Ph.D. Thesis, Southeast University, Nanjing, China, 2016.
42. Wang, Z.; Liu, T. Evaluation of the comfort of the wind environment in the historical sites of Quanzhou Haisi culture. *Chin. Gard.* **2020**, *36*, 89–94.

Disclaimer/Publisher's Note: The statements, opinions and data contained in all publications are solely those of the individual author(s) and contributor(s) and not of MDPI and/or the editor(s). MDPI and/or the editor(s) disclaim responsibility for any injury to people or property resulting from any ideas, methods, instructions or products referred to in the content.

buildings

MDPI

Article

Urban Form and Urban Energy Consumption at the Macro Scale in China

Yanxia Li [1,*], Tingkai Yan [1], Gang Yao [1], Wenjing Zhang [1], Chuwen Lai [1], Yuwei Wu [1], Binghui Si [2] and Xing Shi [3]

[1] School of Architecture and Design, China University of Mining and Technology, Xuzhou 221116, China; ytk@cumt.edu.cn (T.Y.); 4679@cumt.edu.cn (G.Y.); 15223548@cumt.edu.cn (W.Z.); 15224084@cumt.edu.cn (C.L.); 15234224@cumt.edu.cn (Y.W.)
[2] College of Architecture, Nanjing Tech University, Nanjing 211816, China; 202010006718@njtech.edu.cn
[3] College of Architecture and Urban Planning, Tongji University, Shanghai 200092, China; 20101@tongji.edu.cn
* Correspondence: 6636@cumt.edu.cn; Tel.: +86-178-5198-9189

Abstract: The research results show that urban form has a significant impact on urban building energy consumption. Therefore, it is of great significance to study the relationship between urban form and urban building energy consumption. This study selects 26 cities in China across four climate zones and studies the relationship on a macro scale. In terms of urban building energy consumption, this study summarizes a set of data collation methods for calculating the total energy consumption of residential buildings and public buildings. In terms of urban form, this study constructed three types of urban form indicators (basic indicators, two-dimensional indicators, and three-dimensional indicators) and proposes a set of methods for calculating the urban built-up area, the total urban building area, the urban residential building area, and the urban public building area. This research finds that in the four climate zones, total urban building energy consumption is extremely strongly correlated with indicators such as resident population, GDP, total building area, building base area, and built-up area, and urban building energy consumption per unit area is extremely strongly correlated with indicators such as clustering, building intensity, urban building orientation, shading factor, and shape coefficient of building, but the relevant indicators are not exactly the same in each climate zone.

Keywords: urban form method; urban energy consumption; urban form indicators

1. Introduction

Cities consume about three-quarters of the world's primary energy, with the building sector consuming about 40% of the world's energy [1–3]. Urban energy consumption is the main component of world energy consumption, and urban building energy consumption accounts for 60% of urban energy consumption.

Current research shows that urban form has a significant impact on building energy consumption [4–6]. The EBC Annex 51 project mentioned in the work report of the IEA aims to develop a municipal energy master plan and a neighborhood-scale energy action plan to help local governments develop and implement successful energy policies, providing detailed data sources and monitoring tools for both municipal and neighborhood scales. Urban morphology systematically introduces the basic theory, historical development, and application of urban morphology, combined with case studies and multidisciplinary perspectives, to provide readers with a comprehensive research framework. These studies investigated the correlation between energy consumption in urban buildings and a number

of variables, i.e., individual building configurations, relations between buildings, and coverage of water bodies, impervious surfaces, and greenery. However, little is known about the relationship between the macro urban form and urban energy consumption. Hence, this study is aimed at determining the correlation between urban form and urban energy consumption at the macro scale.

Current knowledge on the links between urban form and building energy consumption focuses on the following urban form variables:

- Greening rate, building density, and floor area ratio [7];
- Extent of water bodies [8–10];
- Extent of impervious surfaces [10];
- Sky view factor [11];
- Building perimeter [12,13];
- Street canyons [14,15].

However, due to the lack of large-scale measured urban energy consumption data, few studies have been conducted on the way urban form attributes affect building energy consumption in reality [16–20]. The study of the relationship between urban form and urban energy consumption at the macroscopic scale is extremely difficult to study, and its challenges are mainly reflected in three aspects.

Data need to be organized. The accuracy of urban form data currently obtained from various websites needs to be verified, and the collection and collation of validation data from different cities, the selection of validation criteria, and the unified collation of data formats will take a lot of time and effort. Moreover, these urban form data need to be further organized before they can be used for research and analysis [21–29]. Meanwhile, the obtained urban energy consumption data need to be analyzed for their statistical caliber and reliability and finally generate the required urban building energy consumption data.

Methodology needs to be explored. In the study of the correlation between urban form and urban energy consumption at the macroscopic scale, the method of collating quantitative data on urban form and urban energy consumption data needs to be explored [30–33]. A set of statistical methods for calculating the total energy consumption of residential buildings and the total energy consumption of public buildings in each city needs to be summarized from the relevant data of government departments; a set of methods for calculating the built-up area of cities, the total area of urban buildings, urban residential building area, and urban public building area is proposed; meanwhile, some urban morphology indicators at the macroscopic scale need to be constructed [34–36].

Correlation requires exploration. Urban form research is a popular topic in the field of urban planning. Many scholars have studied urban form at the macroscopic scale, but there are fewer studies that consider urban morphology and urban energy consumption at the same time at the macroscopic scale, and many studies summarize the relevant laws through statistical models but do not explain the deep internal mechanism [37–45].

Based on the analysis of the data from building energy consumption and urban form, this study provides a more comprehensive and detailed analysis of the correlation between urban form and urban energy consumption at the macroscopic scale and then analyzes the mechanism of the influence of urban morphology on urban building energy consumption.

This study investigates the relationship between urban building energy consumption indicators and urban form indicators using building energy consumption and urban form data from 26 cities in China as shown in Figure 1. The following are the exact definitions of severe cold areas, cold areas, hot-summer and cold-winter areas and hot-summer and warm-winter areas using Heating Degree Days (HDD) as a quantitative index (based on the Chinese national standard GB 50176-2017 and related studies). When HDD is greater

than 3000 and less than or equal to 5000, this area belongs to the severe cold area. When HDD is greater than 2000 and less than or equal to 3000, this area belongs to the cold areas. When HDD is greater than 1000 and less than or equal to 2000, this area belongs to the hot-summer and cold-winter areas, but it still needs to be heated in winter. When HDD is less than or equal to 1000, this area belongs to the hot-summer and warm-winter areas. Data are collected using a set of statistical methods for calculating total residential building energy consumption and total public building energy consumption for each city through the statistical yearbooks of each city in terms of urban building energy consumption. In terms of urban morphology, this study constructed three types of urban morphology indicators (basic indicators, 2D indicators, and 3D indicators), obtained and collated 3D urban morphology data, AOI data, POI data, and Landsat remote sensing data of the study cities, and proposed a set of methods to calculate urban built-up area, total urban building area, urban residential building area, and urban public building area. The paper is organized as follows. Section 1 provides the literature review and research questions. Section 2 gives the methodology. Section 3 provides the data analyses and discussion, and the final section concludes the paper.

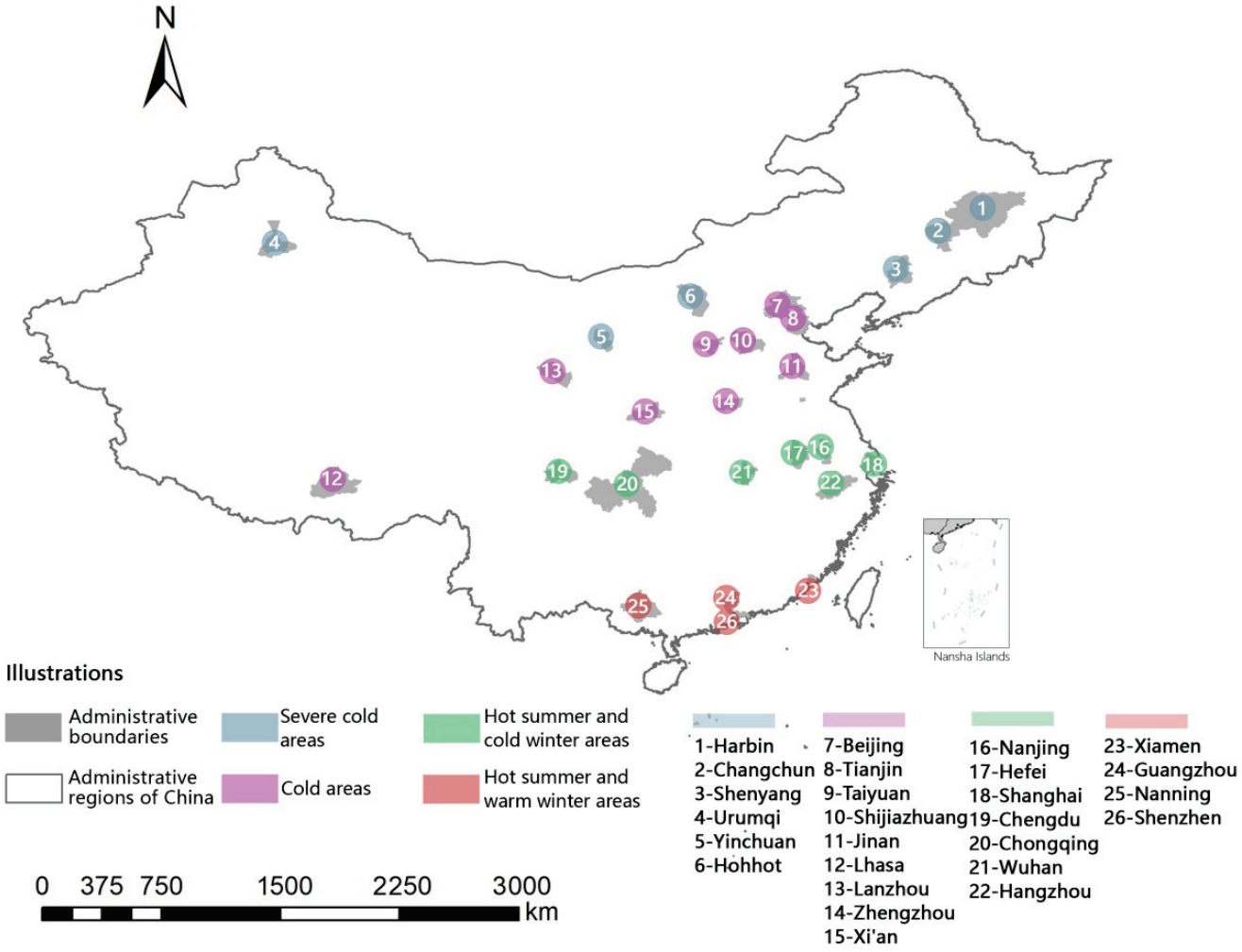


Figure 1. Study cities in four climate zones.

Although existing studies have confirmed that urban form has a significant impact on building energy consumption, due to the difficulty of extrapolating fine-scale data, the lack of measured energy consumption data at the macro-scale, and the lack of a unified methodological system, the existing results are mainly at the level of blocks or

individual buildings, and the systematic understanding of macro urban form and urban energy consumption is still a blank. Secondly, there is no recognized method for uniformly measuring the total energy consumption, total construction volume, and built-up area of urban residential and public buildings at the macro scale. Thirdly, most statistical models only describe the superficial correlation between morphology and energy consumption but fail to reveal its internal mechanism. In view of the above limitations, the core goal of this study is to establish a replicable macro scale analysis framework and reveal the mechanism of urban morphology on building energy consumption, and the innovation points are: (1) the multi-source big data (3D architecture, AOI/POI, Landsat remote sensing and statistical yearbook) of 26 Chinese cities are integrated, and a 2Dand 3D level index system is constructed, and a set of unified measurement methods for total urban buildings and total energy consumption is proposed; (2) Regional climate constraints (four types of areas divided by HDD: severe cold, cold, hot-summer and cold-winter, hot-summer and warm-winter) were introduced to test the moderating effect of climate on the morphology and energy consumption relationship. (3) Through the combination of statistics and mechanism models, the marginal contribution of macro morphological indicators to the energy consumption of residential and public buildings is quantified, and its influence path is analyzed. This research proposes the hypotheses that specific macro urban morphological indicators have a significant and stable impact on the energy consumption per unit area of urban residential and public buildings, and climate zoning strengthens or weakens the relationship between certain morphological indicators and building energy consumption.

2. Methodology

2.1. Statistical Method for Calculating the Total Energy Consumption of Residential Buildings and the Total Energy Consumption of Public Buildings in Each City

In this study, the residential building energy consumption is organized by climate zones, and the residential building energy consumption in severe-cold and cold regions includes three parts: urban residential electricity consumption and rural residential electricity consumption, household natural gas consumption and household liquefied petroleum gas consumption, and hot water heating and total steam heating (as in Equation (1)).

$$E_{r1} = E_e + E_g + E_h \tag{1}$$

In the formula, E_{r1} is the total energy consumption of residential buildings, E_e is the electricity consumption of urban residents and rural residents, E_g is the amount of household natural gas and household liquefied petroleum gas, and Eh is the total amount of hot water heating and steam heating.

The energy consumption of residential buildings in hot-summer and cold-winter areas and hot-summer and warm-winter areas includes the electricity consumption of urban residents and rural residents, the natural gas consumption of households, and the liquefied petroleum gas consumption of households in (as in Equation (2)).

$$E_{r2} = E_e + E_g \tag{2}$$

In the formula, E_{r2} is the total energy consumption of residential buildings, E_e is the electricity consumption of urban residents and rural residents, and E_g is the amount of household natural gas and household liquefied petroleum gas.

The electricity consumption of urban residents and rural residents is clearly counted in the statistical yearbooks of each city, but there are also some cities that provide the statistical caliber on electricity consumption for urban and rural residents, living consumption, and

living electricity. The electricity consumption of urban residents and rural residents in most cities is separated, and for cities where the two are not separated, this study decomposes the electricity consumption of residents of that city and rural residents by the ratio of urban to rural population. The heating data given in the statistical yearbook is the heat value, and this study converts the heat value into electricity uniformly for statistical needs. The conversion process is to convert the heat value in the statistical yearbook into standard coal and then convert the standard coal into electricity.

This study collates the energy consumption of public buildings by climate zones. The total electricity consumption of the whole society in the Chinese city statistical yearbook and the statistical yearbook of each city refers to the total electricity consumption of each industry and the electricity consumption of urban and rural residents' living. The total electricity consumption of the whole society is divided into the total electricity consumption of the whole industry (primary industry, secondary industry, and tertiary industry) and the statistics of urban and rural residents' living electricity consumption (urban residents and rural residents). Through the study of the comprehensive sectoral statistical reporting system, it is found that the industry-wide electricity consumption classification can be subdivided into eleven subcategories. The statistical caliber of electricity consumption in public buildings refers to the electricity consumption of each industry from five to eleven, as shown in Equation (3).

$$E_p = E_i + E_w + E_c + E_f + E_t + E_b + E_m \tag{3}$$

In the formula, E_p is the total energy consumption of public buildings, E_i is the electricity consumption of information transmission, software, and the information technology service industry, E_w is the electricity consumption of the wholesale and retail industry, E_c is the electricity consumption of the accommodation and catering industry, E_f is the electricity consumption of the financial industry, E_t is the electricity consumption of the real estate industry, E_b is the electricity consumption of the rental and business service industry, and E_m is the electricity consumption of the public service and management organization.

In all climate zones, most cities' electricity consumption statistics for public buildings refer to the electricity consumption of each industry above. The energy consumption of public buildings in individual cities is the difference between the total electricity consumption of the city and the electricity consumption of industry, transportation, urban and rural residents, agriculture, forestry, animal husbandry and fishery, and the construction industry. In some cities, the electricity consumption of transportation, construction and agriculture, forestry, animal husbandry, and fishery is derived by extrapolation. For example, in the cold region, Harbin city is used as the standard, and the electricity consumption of agriculture, forestry, animal husbandry, and fishery accounts for 0.023 of the city's total electricity consumption, 0.032 of the city's total electricity consumption in transportation, and 0.031 of the city's total electricity consumption in construction. In the unit conversion, 1 ton of standard coal is equal to 8130 kW·h. The final conversion results of building energy consumption indicators for each city are shown in Table 1.

Table 1. The final conversion results of building energy consumption indicators by climate zone.

Climate Zones	City Name	Urban Energy Consumption Indicators							
		Total Energy Consumption (10^8 kW·h)	Energy Consumption per Unit Area(kW·h/m^2)	Total Residential Energy Consumption (10^8 kW·h)	Residential Unit Energy Consumption (kW·h/m^2)	Total Energy Consumption of Public Buildings (10^8 kW·h)	Unit Energy Consumption of Public Building (kW·h/m^2)	Total Energy Consumption for Heating (10^8 kW·h)	Total Energy Consumption per Unit Area for Heating (kW·h/m^2)
Severe cold areas	Harbin	294.21	99.48	56.23	111.71	57.10	68.38	180.88	85.22
	Changchun	194.57	64.92	38.20	67.12	50.76	59.39	105.60	49.29
	Shenyang	310.51	66.41	61.58	62.55	86.58	69.79	162.35	45.35
	Xining	59.37	41.57	12.19	55.43	0.62	1.68	46.56	43.93
	Yinchuan	95.86	68.65	6.53	62.42	58.05	73.43	31.28	51.64
	Hohhot	120.02	66.49	23.71	68.75	24.60	58.95	71.70	51.66
	Urumqi	120.22	9.38	21.51	58.52	30.75	120.12	212.24	21.22
Cold areas	Beijing	569.46	50.55	145.65	52.25	155.75	46.50	267.93	33.85
	Tianjin	401.98	70.75	101.86	67.11	128.98	79.91	171.14	42.07
	Taiyuan	127.99	68.16	37.40	68.37	37.65	67.65	52.94	40.07
	Shijiazhuang	224.50	97.60	68.80	84.17	76.41	141.34	79.30	45.07
	Jinan	162.95	54.12	60.88	53.93	43.73	54.65	58.34	26.39
	Zhengzhou	221.77	56.66	95.53	45.36	104.55	78.59	21.69	8.39
	Lanzhou	46.47	44.92	21.28	33.47	25.10	63.40	0.09	0.14
	Lhasa	9.01	39.96	4.82	42.09	4.17	37.74	0.02	0.17
	Xi'an	301.72	70.35	107.16	64.63	96.66	86.66	97.91	30.86
Hot-summer and cold-winter areas	Shanghai	634.62	62.78	236.03	36.75	398.59	108.14	/	/
	Chongqing	302.77	39.04	172.38	30.65	130.39	61.23	/	/
	Chengdu	242.69	45.71	98.19	23.30	144.50	131.86	/	/
	Hangzhou	231.95	46.41	116.20	32.05	115.75	84.35	/	/
	Wuhan	220.81	31.81	98.96	20.94	121.85	54.97	/	/
	Nanjing	209.88	41.85	83.28	22.73	126.60	93.69	/	/
	Hefei	128.54	44.48	56.38	26.09	72.16	99.05	/	/
Hot-summer and warm-winter areas	Guangzhou	392.26	57.62	179.21	46.74	213.05	71.66	/	/
	Shenzhen	267.88	40.05	60.55	13.39	207.33	95.71	/	/
	Xiamen	115.59	49.10	60.48	42.08	55.11	60.13	/	/
	Nanning	102.55	44.47	53.96	32.83	48.59	73.39	/	/

2.2. Statistical Methods of Urban Built-Up Area, Urban Residential Building Area, and Urban Public Building Area

2.2.1. Calculation Methods

In this study, the built-up areas of the study cities were defined using the remote sensing technique. The satellite remote sensing data for each city were downloaded through the United States Geological Survey website, and the threshold of cloudiness was set at 10% for this study in the selection. The downloaded satellite remote sensing images needed to ensure that there were no clouds or only thin clouds in the study area. The application of Landsat remote sensing data in this study was in the separation of impervious surface. Firstly, it is necessary to collect remote sensing data of each view that can be assembled into a city, and then the remote sensing data of each view of a city will be supervised and classified separately. The supervised classified data are saved in Geotiff format and entered into GIS10.7 for processing, such as stitching, reclassification, and data statistics. In this study, the images were classified into impervious surface, green surface, water surface, and bare land. Finally, the images were classified into impervious surface (value 1) and non-impervious subsurface (value 0), as shown in Figure 2b. A 900 m × 900 m fishing network was established (Figure 2c), and the image element size of remote sensing data was 30 m × 30 m. The areas with impervious surface greater than 60% were counted in a table displaying zoning statistics. Landsat data with a resolution of 30 m has some limitations in supervised classification. For example, in the satellite remote sensing map in summer, some vegetation with higher height obscures a large area of the impervious surface, so there is an urban area classification error, and after supervised classification, the classification results need to be further corrected, and this study applies the high-definition satellite remote sensing data of LocaSpaceViewer, and the correction of the supervised classification results is performed by applying the urban building 3D data of LocaSpaceViewer, as shown in Figure 2d,e. The accuracy of the urban area can be greatly improved after the three-way cross-checking of Landsat data, building data, and high-definition data, as shown in Figure 2f. The supervision classification results and the results of urban built-up areas in the severe cold region, cold region, hot-summer and cold-winter region, and hot-summer and warm-winter region are shown in Figures 3 and 4.

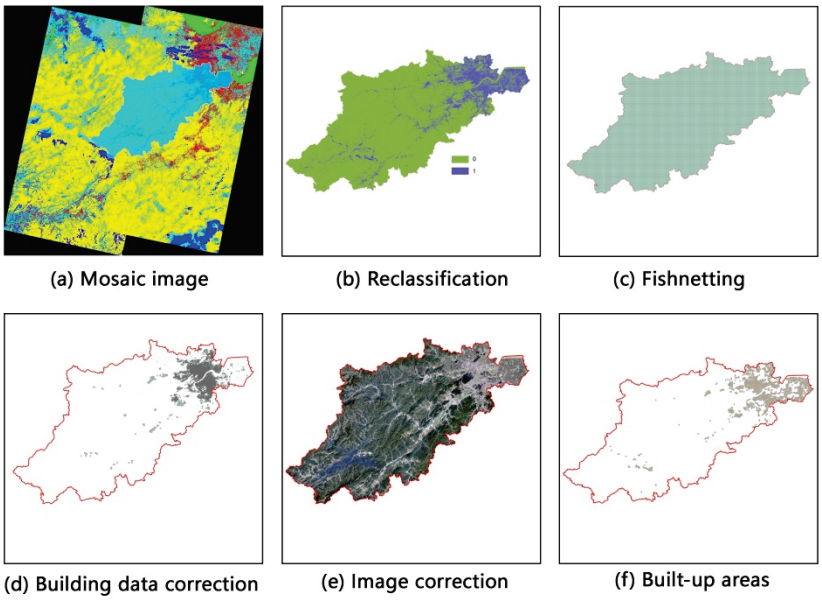


Figure 2. Calculation method of urban built-up area (taking Hangzhou city as an example) and of urban built-up area (taking Hangzhou city as an example).

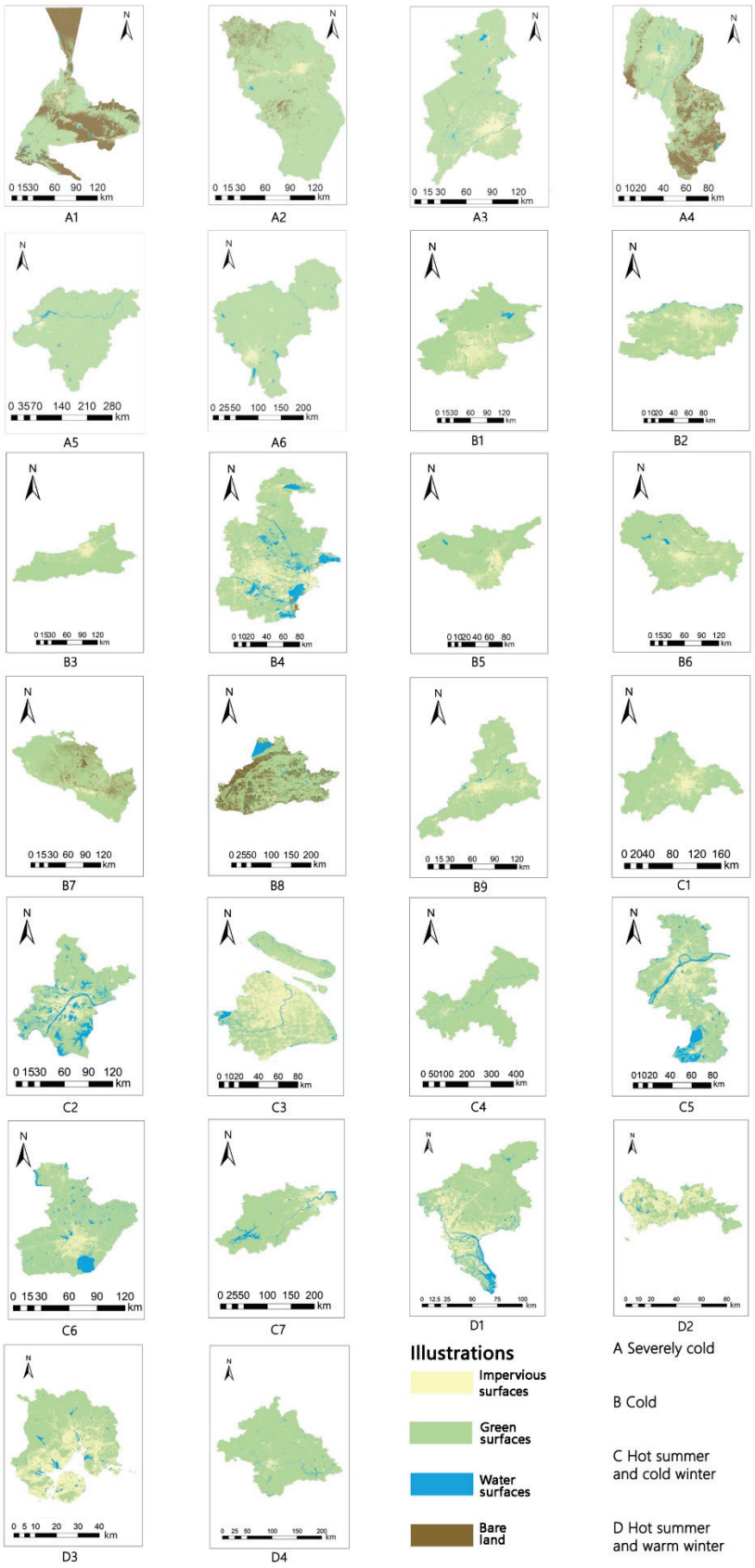


Figure 3. The supervision classification results: (**A1**–**A6**) Urumqi, Hohhot, Shenyang, Yinchuan, Harbin, Changchun; (**B1**–**B9**) Beijing, Tianjin, Zhengzhou, Shijiazhuang, Taiyuan, Xi'an, Jinan, Lanzhou, Lhasa; (**C1**–**C7**) Chengdu, Wuhan, Shanghai, Chongqing, Nanjing, Hefei, Hangzhou; (**D1**–**D4**) Guangzhou, Shenzhen, Xiamen, Nanning.

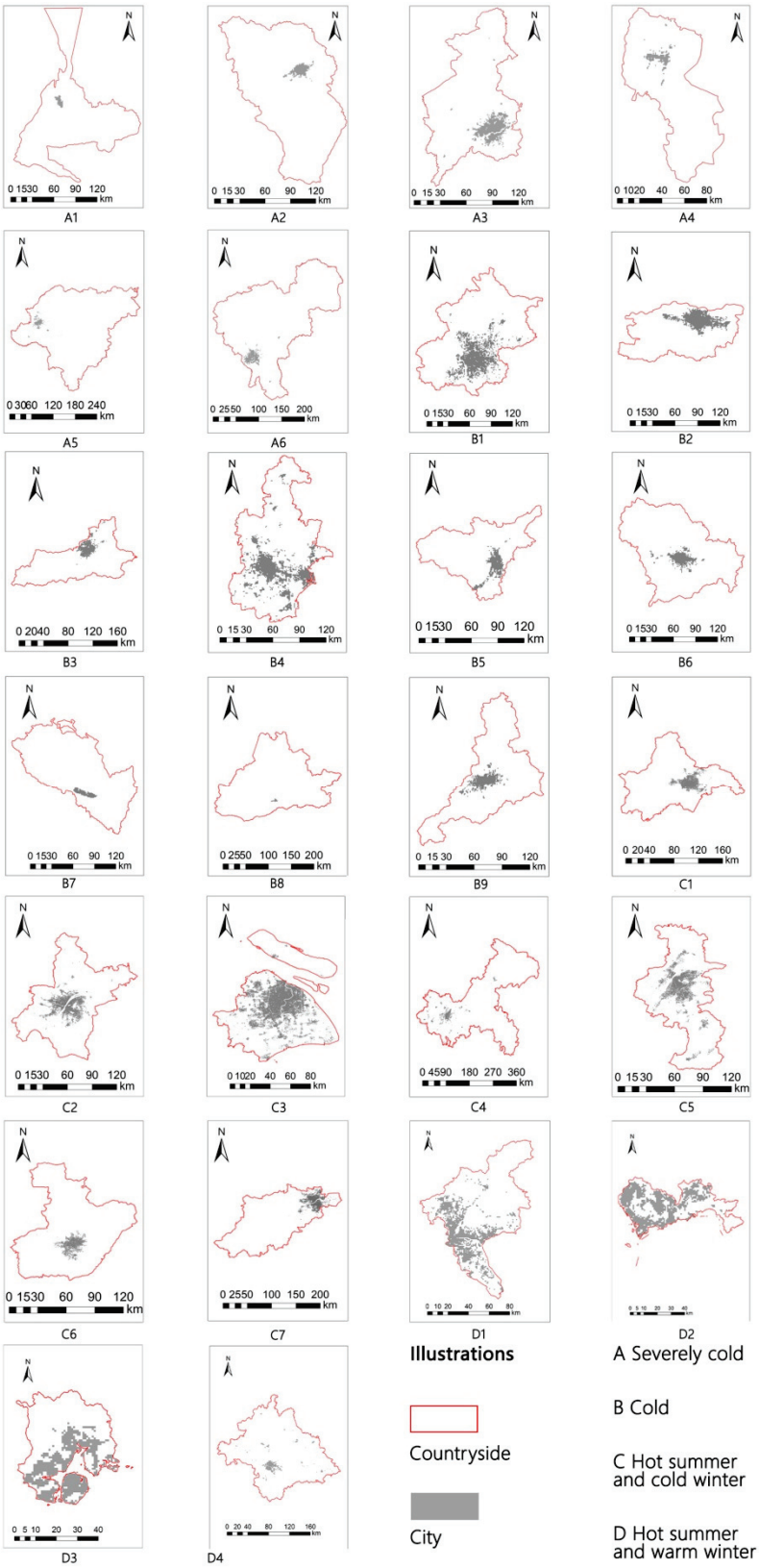


Figure 4. The results of urban built-up areas: (**A1**–**A6**) Urumqi, Hohhot, Shenyang, Yinchuan, Harbin, Changchun; (**B1**–**B9**) Beijing, Tianjin, Zhengzhou, Shijiazhuang, Taiyuan, Xi'an, Jinan, Lanzhou, Lhasa; (**C1**–**C7**) Chengdu, Wuhan, Shanghai, Chongqing, Nanjing, Hefei, Hangzhou; (**D1**–**D4**) Guangzhou, Shenzhen, Xiamen, Nanning.

In Shanghai's statistical yearbook, residential buildings are classified into six categories: garden houses, joint houses, apartments, new-style lanes, old-style lanes, and simple houses for statistics. However, it is not possible to find the residential building area in the statistical yearbooks of most cities in the past years. Therefore, a method for calculating residential building area needs to be explored. This study uses urban 3D building data, AOI data, and POI data to distinguish residential buildings from urban buildings and then calculates and counts the area of residential buildings in the whole city. The specific identification process is shown in Figure 5.

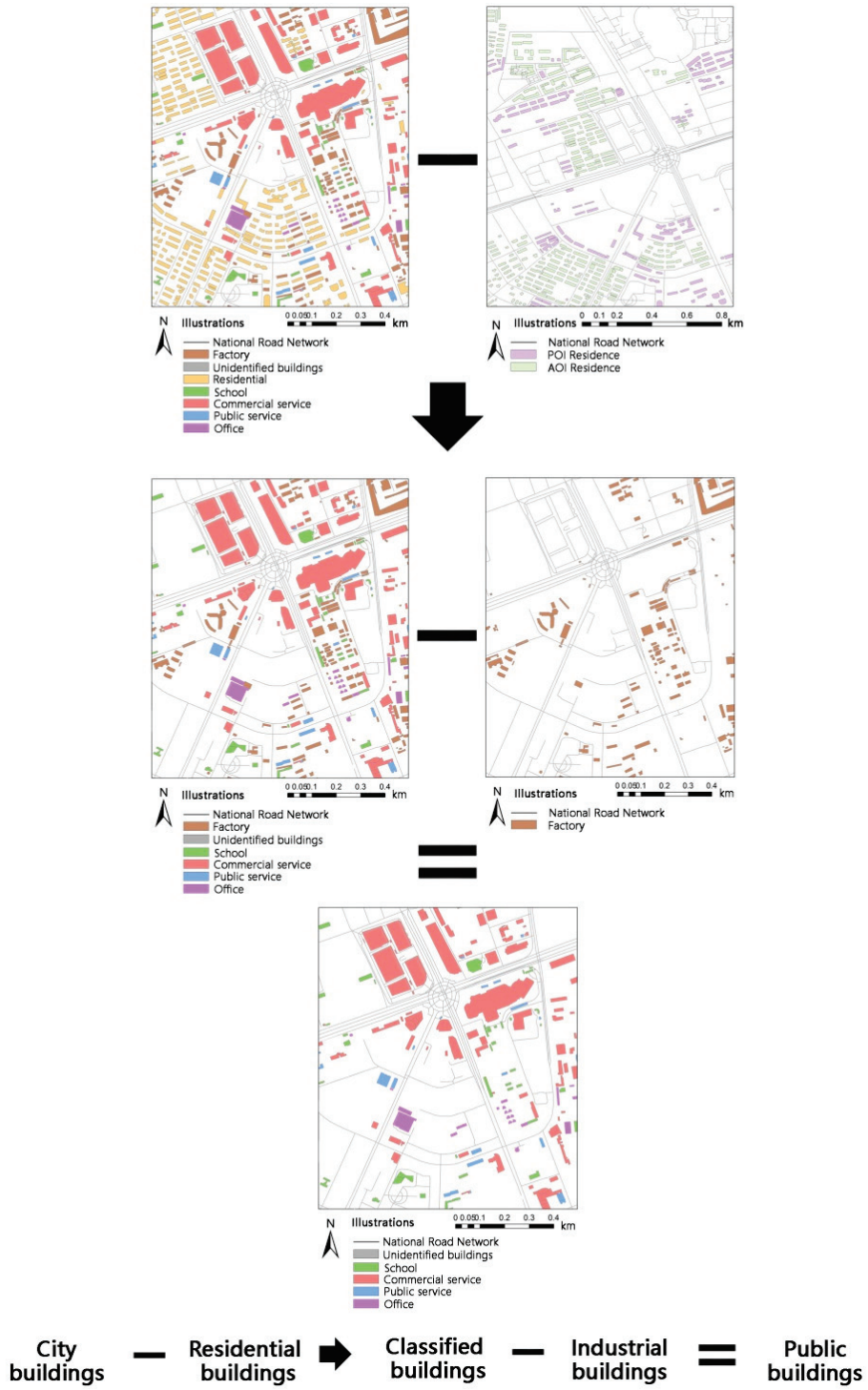


Figure 5. *Cont.*

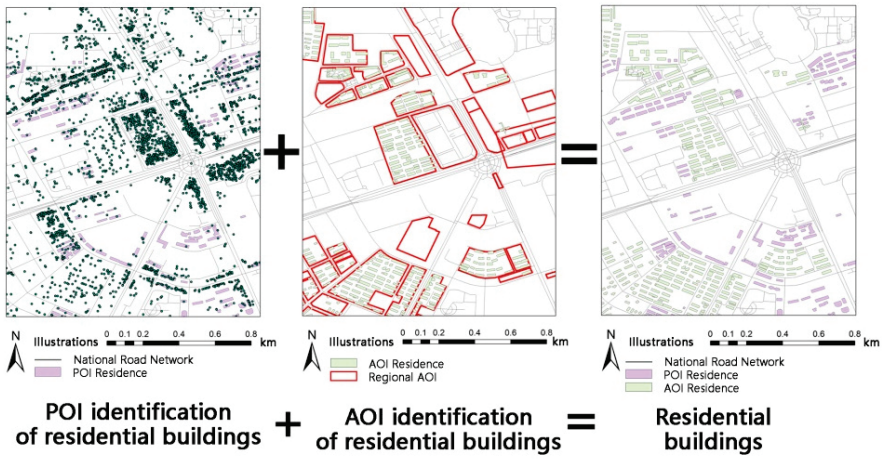


Figure 5. Residential and public building identification.

The 3D building data of this study includes information such as the building base outline and building height. This data needs to be first corrected for coordinate bias before use, and the data from Baidu coordinates are corrected to WGS1984 data. The data obtained from Baidu Map is then fused and projected after the correction. At the same time, buildings with a building area of less than 10 m^2 are deleted using the editing function. Building blocks smaller than 10 m^2 are mostly building components, and this study does not consider the area of this part of the building. In the study, the building height was divided by 3.2 m to get the number of floors of each building, and the number of floors was multiplied by the base area of each building to get the total building area of each building. The buildings that fall within the boundaries of the neighborhood were selected by location and identified as residential buildings, while other buildings were identified as non-residential buildings. From the perspective of the acquired data, this study divides the residential buildings into two categories: residential buildings in residential areas and business residential buildings. Residential buildings are distinguished from urban buildings by neighborhood boundary data (AOI data), and business residences are distinguished from urban buildings by POI data.

After distinguishing residential buildings from urban buildings, the remaining buildings in this study are divided into five categories: schools, office employment, public services, commercial services, and industrial buildings. This study mainly uses different types of POI data existing within and around a certain range of the building vector and spatially connects POI and building vector by ArcGIS10.7 and Excel2016 software using the principle of closest and a certain range and increases the functional type attribute with the highest weight value to the building vector by the weight coefficient method. However, all building functions at the urban scale cannot be fully identified by POI data alone, so this study continues to use AOI data to supplement the identification of the remaining unidentified buildings to achieve functional classification of urban buildings, as shown in Figure 5.

2.2.2. Validation Methods

This study takes Nanjing city as an example to verify the accuracy of the classification method by comparing and analyzing its research data with the actual measurement data. Firstly, the building data of Nanjing city are converted into point data, and the kernel density analysis is performed, and then the different building density zones of Nanjing city are measured. Two circular areas with a radius of 500 m are selected as samples, and

these two study areas are located in different building density zones, where sample 1 is located in the high-density zone, specifically near Xinjiekou in Xuanwu District, Nanjing, and sample 2 is located in the low-density zone, specifically near Yingtian Street in Jianye District, Nanjing, as shown in Figure 6.

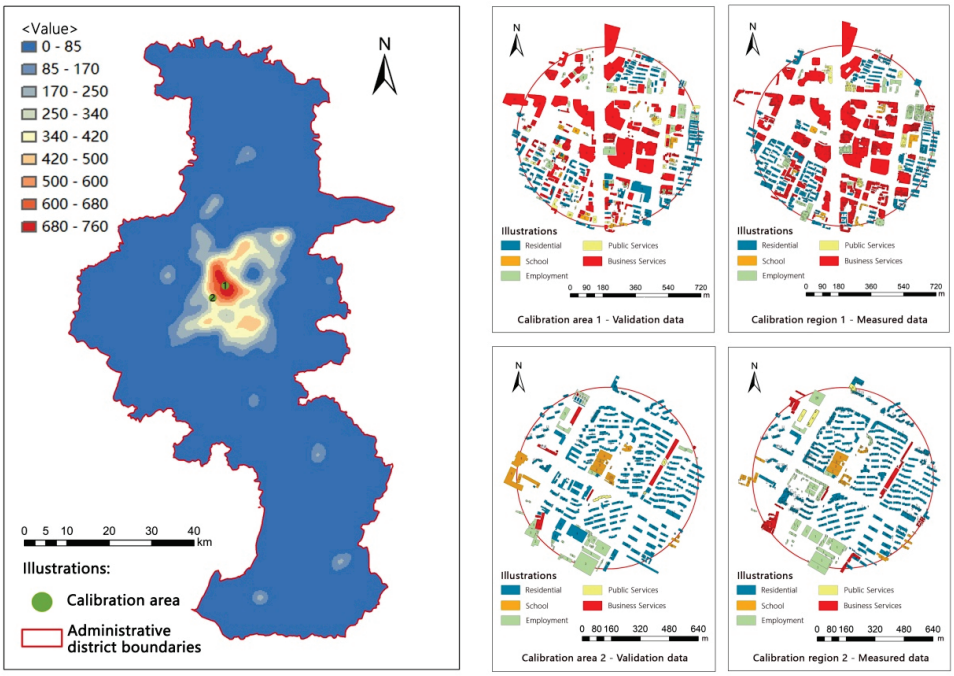


Figure 6. Comparison of validation and empirical data in Nanjing.

The building classification method of the empirical data is to check the buildings in the sample area with the usage status of the real buildings one by one and classify the building categories into one of the five categories: residential, school, commercial service, public service, and office employment. The detailed validation data and empirical data classification results are shown in Figure 5, and the validation statistics are shown in Table 2. It can be seen that the buildings are identified, and the accuracy of building data information is very high in both high-density and low-density building areas.

Table 2. Calibration area building information statistics of Nanjing.

Validate Area	Building Category	Building Area (m^2)			Number of Buildings		
		Verified Buildings	Measured Buildings	Accuracy	Verified Buildings	Measured Buildings	Accuracy
1	Residential Buildings	529,150.75	472,805.05	88.08%	150	168	89.29%
	Schools	76,187.61	545,36.95	60.30%	22	18	77.78%
	Commercial Buildings	1471353.68	2,046,872.43	71.88%	144	145	99.31%
	Buildings of Public Services	80,995.32	74,526.54	91.32%	23	15	46.67%
	Official Buildings	138,806.33	206,537.02	67.21%	44	40	90.00%
	Non-residential Buildings	1,767,342.93	2,382,472.94	74.18%	233	218	93.12%
	Total	2,296,493.68	2,855,277.99	80.43%	383	386	99.22%
2	Residential Buildings	1,054,009.73	1,085,333.14	97.11%	251	250	99.60%
	Schools	95,942.97	90,082.95	93.49%	19	24	79.17%
	Commercial Buildings	44,598.01	26,944.42	34.48%	12	20	60.00%
	Buildings of Public Services	11,461.822	20,528.43	55.83%	3	3	100.00%
	Official Buildings	128,335.04	137,094.72	93.61%	42	57	73.68%
	Non-residential Buildings	280,337.84	274,650.53	97.93%	76	104	73.08%
	Total	1,334,347.57	1,359,983.66	98.11%	327	354	92.37%

2.3. Methods of Calculating Three Types of Urban Morphology Indicators

2.3.1. Basic Morphological Index

(1) Building density

After defining the urban boundary, the building density in the urban patches is calculated. This building density is the building coverage, specifically the ratio of the building footprint in the urban boundary to the built-up area of the city. It reflects the open space rate and building density in the city. The building density is calculated as shown in the formula below.

$$AREA = AREA_f / AREA_b \quad (4)$$

AERA indicates building density; $AERA_f$ is the building footprint; and $AERA_b$ is the area of the built-up area of the city.

(2) Building intensity

The building intensity of this study refers to the concept of floor area ratio in architecture, and the building intensity refers to the ratio of the total building area within the city boundary to the area of the built-up area of the city. It should be noted that the total building area in this concept of building intensity does not include the unaccounted area, i.e., the area of underground garages, underground equipment rooms, and underground commercial.

$$\mathrm{I} = \mathrm{I}_a / \mathrm{I}_b \quad (5)$$

I denotes building intensity; I_a is the total building area; I_b is the built-up area of the city.

2.3.2. Two-Dimensional Morphological Indicators

(1) Clustering (mean distance)

This indicator describes the degree of agglomeration of buildings in a city, specifically the average distance between buildings in the city. The closer the distance between buildings, the stronger the clustering of buildings in the city.

$$\mathrm{ANN} = \overline{D}_O / \overline{D}_E \quad (6)$$

D_O is the observed average distance between each element and its nearest neighboring element.

$$\overline{D}_O = \frac{\sum_{i=1}^{n} d_i}{\mathrm{n}} \quad (7)$$

and D_E is the expected average distance between the specified elements in the random mode.

$$\overline{D}_E = \frac{0.5}{\sqrt{n/A}} \quad (8)$$

In the above equation, d_i equals the distance between an element and its closest neighbor, n corresponds to the total number of elements, and A is the area of the smallest outer rectangle that can include all elements, or a user-specified "area" value.

(2) Homogeneity

This index refers to dividing the whole city into several cells and calculating the building density in each cell grid. A 2 km × 2 km fishing grid is set up, the building vector data is rasterized according to the image element size of 40 m × 40 m, the building raster data is reclassified into 1 class, each raster data value is set to 1600, the sum of partition

statistics is calculated, the standard deviation of the sum is calculated, and the standard deviation is divided by 4×10^6.

$$H_a = \frac{\sqrt{\frac{\sum_{i=1}^{n}(a_n - a_i)^2}{n}}}{b} \tag{9}$$

where H_a refers to architectural equilibrium; a_n is the value of the nth fishing net statistic; a_i is the average of the sum of each net statistic; n is the number of nets, and b is equal to the area of each net, 4×10^6.

(3) Functional distribution

In this study, the buildings in the city are divided into two categories: residential buildings and non-residential buildings. The distribution characteristics of the two types of buildings in the city are analyzed, and the percentage of residential buildings and the percentage of non-residential buildings in the city are calculated.

$$F_u = F_a / F_b \tag{10}$$

F_u denotes functional distribution; F_a is the total residential building area; F_b is the total non-residential building area.

(4) Urban building orientation

The urban building orientation indicator referred to in this study mainly describes the extent to which a building deviates from its average orientation. Two identical buildings, one facing south and north and the other deflected by an angle, will receive different amounts of solar radiation, etc., and therefore have different energy consumption. The angle between each building in the city and due north is first found, then the average angle of one city building is found, and the degree of deflection between the angle of each building and the average angle is calculated and weighted by the building area.

$$D_\sigma = \sum_{i=1}^{n} \left| \frac{S_i}{S_{sum}} \times \left(D_i - D_{average} \right) \right| \tag{11}$$

D_σ is the deviation from the city direction; D_i is the angle of the i-th building, $D_{average}$ is the average angle of the building, n is the total number of buildings, and S_i is the area of the i-th.

2.3.3. Three-Dimensional Morphological Indicators

(1) High urban uniformity

There is no simple quantitative formula for this metric. Imagine that two cities have the same density and floor area ratio, but the buildings in one city are of varying heights and are tall and short, while in the other city, they are all the same height; then the two urban forms are clearly different and also have an impact on urban energy consumption. In this study, the height data of urban buildings are standard deviated to describe the uniformity of urban height.

$$H_\sigma = \sqrt{\frac{\sum_{i=1}^{n} \left(H_i - H_{average} \right)^2}{n}} \tag{12}$$

H_σ refers to the standard deviation of building heights (urban height uniformity); H_i is the height of the *i*-th building, $H_{average}$ is the average building height, and n is the total number of buildings.

(2) Urban sky view factor

The sky view factor calculated in this study is the ground sky view factor. The ground sky view factor (GSVF) reflects the sky view of each point on the ground, and the sky view factor of a city is the average of the GSVF values of each point in the city. The basic principle of calculating this index is to take a point on the ground as the center, form a hemisphere with a specific radius, and count the ratio of the projected area of buildings on the hemisphere to the entire surface area of the hemisphere, which is calculated by GIS10.7 software.

$$GSVF = 1 - \frac{\sum_{i=1}^{n} \sin a_i}{n} \tag{13}$$

$$\sin a_i = \frac{H}{\sqrt{R^2 + H^2}} \tag{14}$$

GSVF is the ground-level sky view factor; *H* is the height of the building, *R* is the buffer radius, which is 100 m in this study, and n is the total number of buildings intersecting the buffer.

(3) Shading factor

This index refers to the degree of mutual shading between buildings. In this study, the shading factor is calculated using the Hillshade tool (Hillshade), a tool provided by ArcGIS for shading hills, which simulates a sun-parallel line light source.

$$H_i = H_a / H_b \tag{15}$$

H_i is the shading factor, H_a is the area of the shaded building roof, and H_b is the total area of the building footprint.

(4) Shape coefficient of building

The shape coefficient of a building is an important indicator that affects building energy consumption at the individual building level, and the smaller the form factor, the more energy efficient the building. It is a comprehensive indicator of the overall building form factor in a city, which is closely related to energy consumption and directly affects the energy consumption of each individual building. The bulk factor of each building is weighted and summed by volume.

$$S_{average} = \frac{\sum_{i=1}^{n} \left(F_{i,roof} + F_{i,facades} \right)}{\sum_{i=1}^{n} V_i} \tag{16}$$

$S_{average}$ is the shape coefficient of the building; n is the total number of buildings; *i* is the *i*-th building; $F_{i,\,roof}$ is the roof surface area of the building; $F_{i,\,facades}$ is the surface area of the building envelope; and V_i is the volume of the *i*-th building.

3. Results

3.1. Correlation Between Total Urban Building Energy Consumption and Indicators of Urban Building Energy Consumption

- In severe cold regions, there is an overall trend that the larger the GDP, the number of resident population, the built-up area, and the building footprint area, the greater

the total urban building energy consumption, as shown in Figure 7(a1–a4). Total building energy consumption is significantly correlated with resident population, GDP, and building footprint area at the 0.05 level, as shown in Table 3. The correlation coefficient shows that the correlation between total building energy consumption and these factors is extremely strong, as shown in Table 3.

Table 3. Correlation between total building energy consumption and urban indicators by climate zone.

Climate Regions	Indicators	R	P
The severe cold regions	GDP (billion yuan)	0.866 *	0.026
	Resident population (10,000 people)	0.933 *	0.007
	Building footprint (million m^2)	0.870 *	0.024
	Total floor area (million m^2)	0.888 *	0.018
The cold regions	GDP (billion yuan)	0.957 **	0.000
	Resident population (10,000 people)	0.984 **	0.000
	Building footprint (million m^2)	0.974 **	0.000
	Total floor area (million m^2)	0.961 **	0.000
	Area of built-up area (square kilometers)	0.972 **	0.000
The hot-summer and cold-winter regions	GDP (billion yuan)	0.982 **	0.000
	Resident population (10,000 people)	0.929 **	0.003
	Building footprint (million m^2)	0.943 **	0.010
	Total floor area (million m^2)	0.908 **	0.005
	Area of built-up area (square kilometers)	0.875 **	0.010
In the hot-summer and warm-winter regions	Building footprint (million m^2)	0.964 *	0.036
	Total floor area (million m^2)	1.000 **	0.000
	Area of built-up area (square kilometers)	0.993 **	0.007
	Total floor area of public buildings (million m^2)	0.996 **	0.004

The significance at the 0.05, 0.01, and 0.001 levels is marked by * and **, respectively.

In cold regions, there is a general trend that the larger the GDP, the resident population, the built-up area, and the total building area, the greater the total energy consumption of urban buildings, as shown in Figure 7(b1–b4). Total building energy consumption is significantly correlated with total building area, resident population, GDP, and built-up area at the 0.01 level, as shown in Table 3. The correlation coefficient shows that the correlation between total building energy consumption and these factors is extremely strong.

- In hot-summer and cold-winter regions, there is a general trend that the larger the total building area, resident population, and built-up area, the larger the total energy consumption of urban buildings, as shown in Figure 7(c1–c4). Total building energy consumption is significantly correlated with building area, resident population, GDP, and built-up area at the 0.01 level, as shown in Table 3. The correlation coefficient shows that the correlation between total building energy consumption and these factors is extremely strong.
- In hot-summer and warm-winter regions, there is a general trend that the larger the resident population, GDP, and total building area, the larger the total energy consumption of urban buildings, as shown in Figure 7(d1–d4). The total energy consumption is significantly correlated with the built-up area at the level of 0.01. Total energy consumption is significantly correlated with resident population and GDP at the level of 0.05, as shown in Table 3. The correlation coefficient shows that the correlation between total energy consumption and these factors is extremely strong, as shown in Table 3.

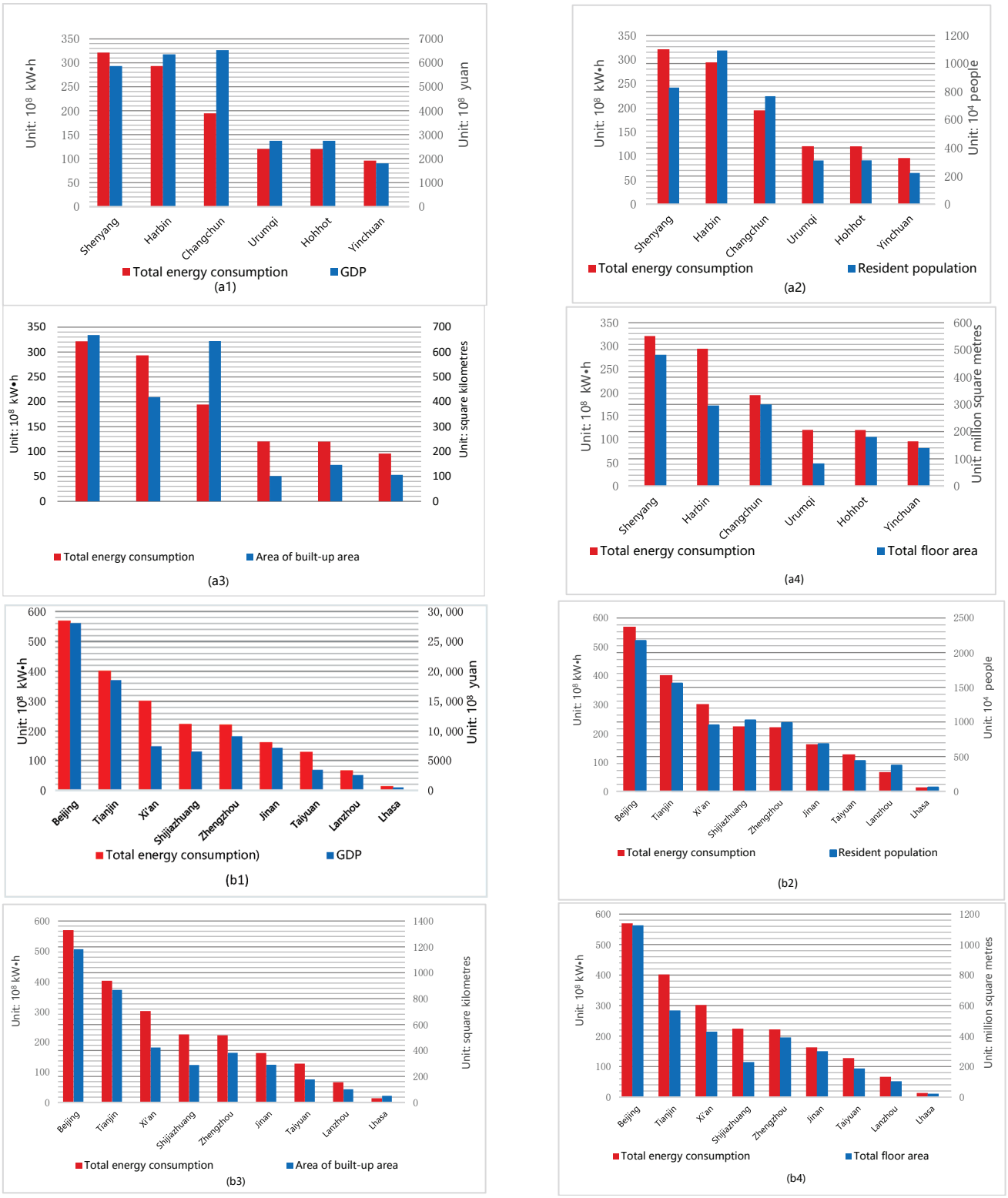


Figure 7. *Cont.*

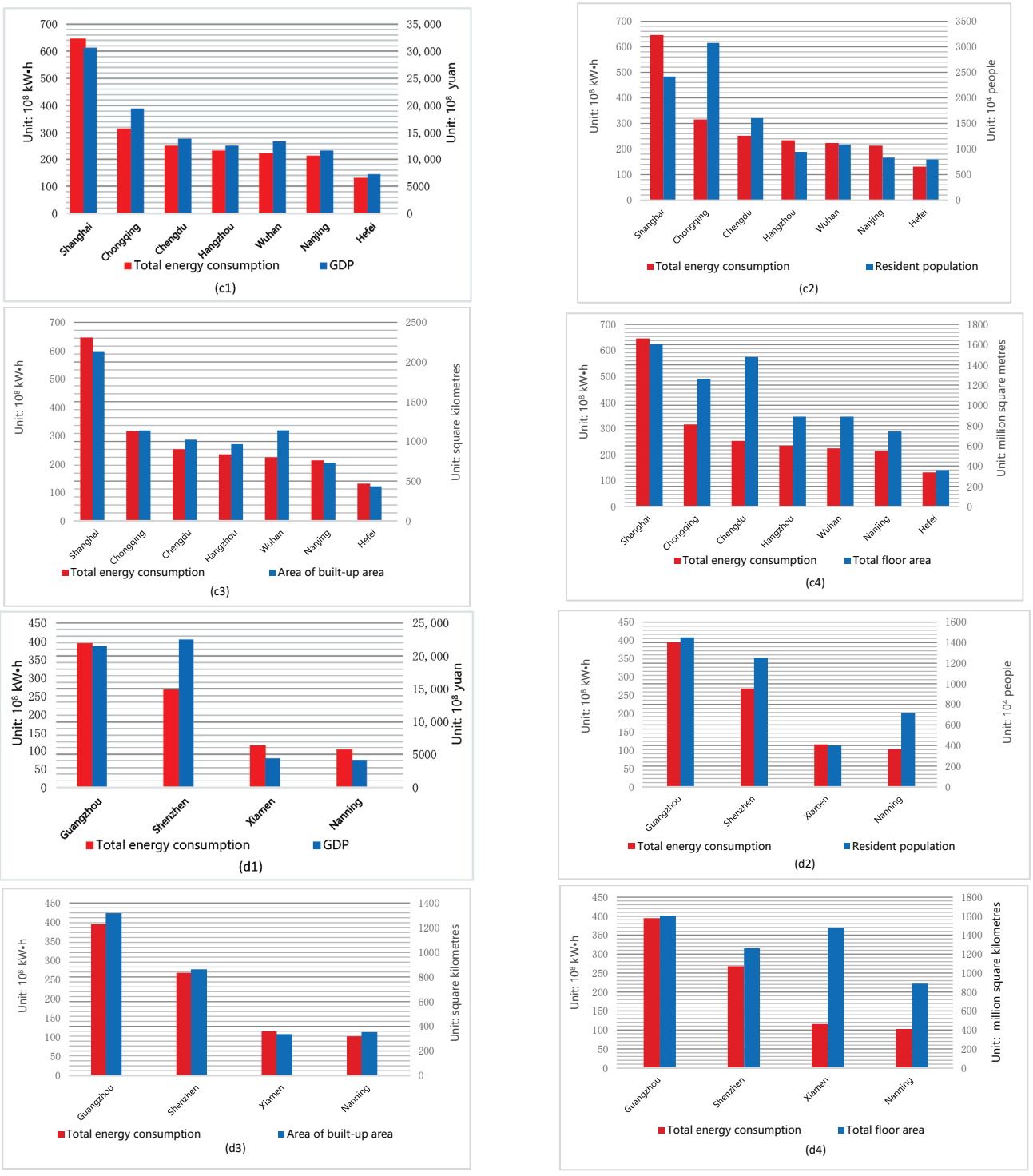


Figure 7. Relationship between total building energy consumption indicators and urban form indicators: the severe cold regions (**a1–a4**); cold regions (**b1–b4**); and hot-summer and cold-winter regions (**c1–c4**); hot-summer and warm-winter regions (**d1–d4**).

3.2. Correlation Between Energy Consumption of Urban Buildings and Urban Morphological Indicators Under Different Climate Zones

The average energy consumption per unit area in cities in severe cold regions is 67.59 kW·h/m^2, in cold regions 61.45 kW·h/m^2, and in hot-summer and cold-winter regions 43.26 kW·h/m^2. From the aspect of energy consumption per unit area, the severe cold

areas are higher than the cold areas, and the cold areas are higher than the hot-summer and cold-winter areas. From the data on total heating energy consumption and total residential energy consumption in northern cities, it can be seen that the heating energy consumption in cities in severe cold regions is 3–4 times the total residential energy consumption throughout the year, as shown in Figure 8. The total heating energy consumption of buildings in cities in cold regions is almost equal to the total energy consumption of residential buildings throughout the year. In terms of residential energy consumption per unit area, it can be seen that with the change of latitude, there is a trend of increasing residential energy consumption per unit area from low latitude to high latitude.

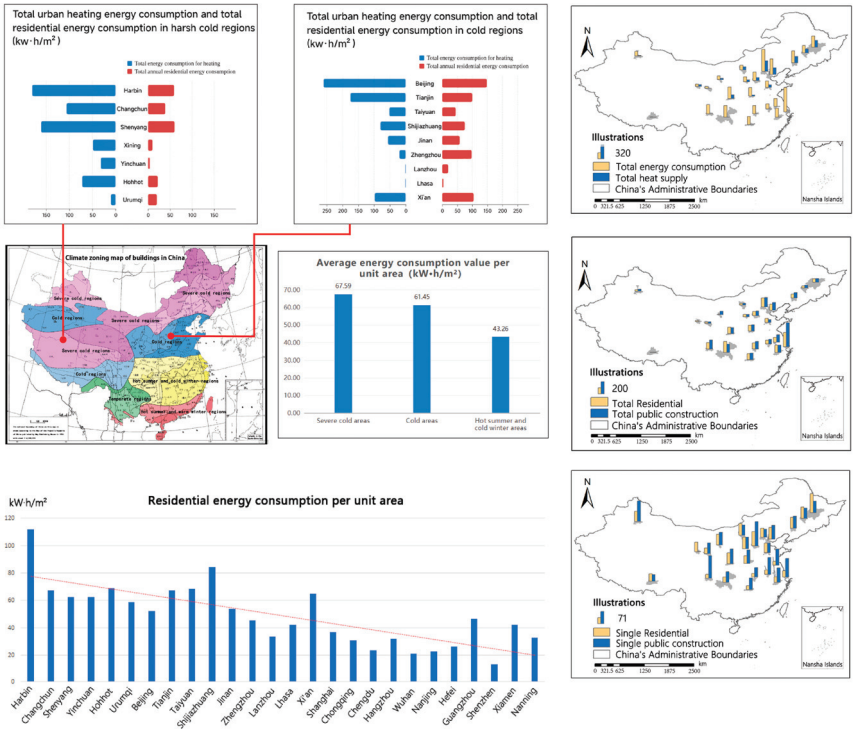


Figure 8. Relationship between total annual residential energy consumption and total heating energy consumption.

The correlation study in four climate zones found the following relationships between energy consumption per unit area of buildings and urban morphology indicators in severe cold regions, cold regions, hot-summer and cold-winter regions, and hot-summer and warm-winter cities.

The indicators of aggregation and energy consumption per unit area of urban buildings in severe cold regions are extremely strongly correlated, with a significant correlation at the 0.05 level and a negative correlation between the two. Therefore, the stronger the aggregation among buildings in severe cold regions, the lower the energy consumption per unit area of urban buildings. Therefore, urban design in the form of agglomeration is desirable in severe cold regions. Meanwhile, construction intensity and energy consumption per unit area of urban buildings show a very strong correlation, with a significant correlation at the 0.05 level and a positive correlation between the two. In severe cold regions, a certain building intensity should be maintained, which is conducive to reducing energy consumption per unit area at the urban scale. In cold regions, urban orientation is extremely strongly correlated with energy consumption per unit area of urban buildings, with a significant correlation at the 0.01 level and a negative correlation between the two. In other words, the greater the change in urban orientation, the lower the energy consumption

per unit area of urban buildings. Therefore, in cold regions, the enclosed building layout is conducive to urban energy efficiency.

- In hot-summer and cold-winter regions, shading coefficient, shape coefficient, and energy consumption per unit area of urban buildings are strongly correlated, with significant correlation at the 0.05 level, as shown in Table 4, and all of them are positively correlated. And it can be seen from the fitted equation that the shape coefficient has the greatest effect on urban building energy consumption per unit area. In hot-summer and cold-winter cities, the more complex the building's body shape is, the higher the energy consumption per unit area of urban buildings. Therefore, from the perspective of urban energy saving, in the design of building monoliths, complex building design solutions in terms of form should be avoided as much as possible. Meanwhile, the larger the shading factor, the higher the energy consumption per unit area of urban buildings. In hot-summer and cold-winter areas, the best orientation of urban buildings should be chosen as much as possible to avoid enclosure and ensure the circulation of buildings.
- In hot-summer and warm-winter regions, urban orientation is extremely strongly correlated with energy consumption per unit area of urban buildings, with a significant correlation at the 0.05 level and a negative correlation between the two, as shown in Table 5. In other words, the greater the change in urban orientation, the lower the energy consumption per unit area of urban buildings. Therefore, in hot-summer and warm-winter regions, the enclosed building layout is conducive to urban energy conservation.

3.3. The Mechanism of Urban Building Form Impacting Urban Building Energy Consumption

The correlation study of the four climate zones found that the urban morphological factors (basic morphological indicators, two-dimensional morphological indicators, and three-dimensional morphological indicators) influence the socio-economic behavior of the city and the urban microclimate through various factors, thus affecting the energy consumption of urban buildings, as shown in Figure 9. The indicator of aggregation is highly correlated with energy consumption per unit area of urban buildings in severe cold regions. Therefore, the stronger the aggregation among buildings in severe cold regions, the lower the energy consumption per unit area of urban buildings. When the aggregation of urban buildings is high, the density of urban buildings increases accordingly, which can minimize unnecessary building heat loss and gain, and the compact building layout can reduce the heating and cooling energy consumption of buildings, so cities with higher aggregation have lower energy consumption per unit area of urban buildings. Meanwhile, in severe cold regions, building intensity and energy consumption per unit area of urban buildings show an extremely strong correlation, with a significant correlation at the 0.05 level and a positive correlation between the two. In general, the construction intensity of a region is positively correlated with the degree of economic development of a city, and there is a direct correlation between the degree of economic development and building energy consumption, and as the population density increases and people's demand for quality of life improves, the city's energy consumption per area increases accordingly.

Table 4. Comparison table of analysis parameters of different regional climate types.

Climate Zones	City Name	Basic Indicator		2D Morphology Indicator				3D Morphology Indicator				Building Energy Consumption	
		Building Density	Floor Area Ratio	Aggregation	Equilibrium	Functional Mix	City Direction	Building Height Uniformity	Sky View Factor	Shading Coefficient	Weighted Shape Coefficient	Energy Consumption per Unit Area (kWh/m^2)	Total Energy Consumption (100 million kWh)
Severe cold regions	Harbin	0.14	0.65	0.16	0.09	1.11	73.49	19.07	0.84	0.38	0.22	99.48	294.21
	Changchun	0.11	0.44	0.22	0.09	1.23	62.56	14.90	0.85	0.55	0.24	64.92	194.57
	Shenyang	0.14	0.63	0.43	0.09	1.33	59.43	19.13	0.85	0.30	0.23	66.41	310.51
	Yinchuan	0.15	0.86	0.37	0.07	1.98	52.79	20.96	0.82	0.32	0.22	68.65	95.86
	Hohhot	0.14	0.60	0.53	0.09	0.43	64.52	19.65	0.85	0.36	0.22	66.49	120.02
	Urumqi	0.14	0.45	0.74	0.10	0.81	55.37	9.93	0.88	0.34	0.25	9.38	120.22
Cold regions	Beijing	0.13	0.55	0.24	0.08	1.25	64.55	15.26	0.87	0.07	0.24	50.55	569.46
	Tianjin	0.11	0.41	0.23	0.08	0.99	61.14	15.85	0.89	0.22	0.25	70.75	401.98
	Taiyuan	0.10	0.37	0.50	0.09	0.13	62.03	16.39	0.87	0.00	0.22	68.16	127.99
	Shijiazhuang	0.13	0.49	0.27	0.10	1.74	60.56	14.81	0.88	0.00	0.27	97.60	224.50
	Jinan	0.13	0.55	0.36	0.10	1.01	62.87	16.29	0.85	0.30	0.22	54.12	162.95
	Zhengzhou	0.10	0.45	0.44	0.10	1.24	62.03	15.86	0.85	0.25	0.25	56.66	221.77
	Lanzhou	0.13	0.50	0.67	0.09	0.61	52.44	16.93	0.88	0.18	0.22	44.92	46.47
	Lhasa	0.29	0.13	0.57	0.10	0.44	57.26	3.18	0.93	0.08	0.36	39.96	9.01
	Xi'an	0.17	0.84	0.32	0.09	0.43	58.60	18.90	0.87	0.21	0.21	70.35	301.72
Hot-summer and cold-winter regions	Shanghai	0.18	0.83	0.36	0.08	0.70	61.35	16.04	0.78	0.52	0.25	62.78	634.62
	Chongqing	0.12	0.75	0.07	0.05	0.62	55.57	24.12	0.72	0.22	0.22	39.04	302.77
	Chengdu	0.17	0.77	0.22	0.08	0.57	43.43	19.26	0.80	0.16	0.22	45.71	242.69
	Hangzhou	0.13	0.57	0.21	0.07	0.75	64.87	23.39	0.76	0.19	0.24	46.41	231.95
	Wuhan	0.13	0.60	0.28	0.08	0.90	51.78	17.05	0.76	0.20	0.21	31.81	220.81
	Nanjing	0.14	0.61	0.25	0.07	0.87	60.59	14.78	0.77	0.20	0.23	41.85	209.88
	Hefei	0.16	0.81	0.52	0.08	0.58	57.64	22.84	0.83	0.24	0.21	44.48	128.54
Hot-summer and warm-winter regions	Guangzhou	0.15	0.55	0.25	0.09	1.17	76.40	14.55	0.88	0.08	0.27	57.62	392.26
	Shenzhen	0.20	0.85	0.42	0.09	1.47	88.53	14.99	0.86	0.11	0.27	40.05	267.88
	Xiamen	0.14	0.75	0.35	0.08	1.38	79.34	20.10	0.86	0.11	0.21	49.10	115.59
	Nanning	0.16	0.70	0.19	0.08	2.08	83.69	14.31	0.89	0.08	0.26	44.47	102.55

Table 5. Correlation between energy consumption per unit area of urban buildings and urban form indicators by climate zone.

Climate Regions	Indicators	R	P
The severe cold regions	Building intensity	0.821 *	0.021
	Clustering	−0.867 *	0.023
The cold regions	City direction deviation	−0.883 **	0.024
The hot-summer and cold-winter regions	Shading factor	0.809 *	0.027
	Shape coefficient of building	0.797 *	0.032
In the hot-summer and warm-winter regions	City direction deviation	−0.962 *	0.038

The significance at the 0.05, 0.01, and 0.001 levels is marked by * and **, respectively.

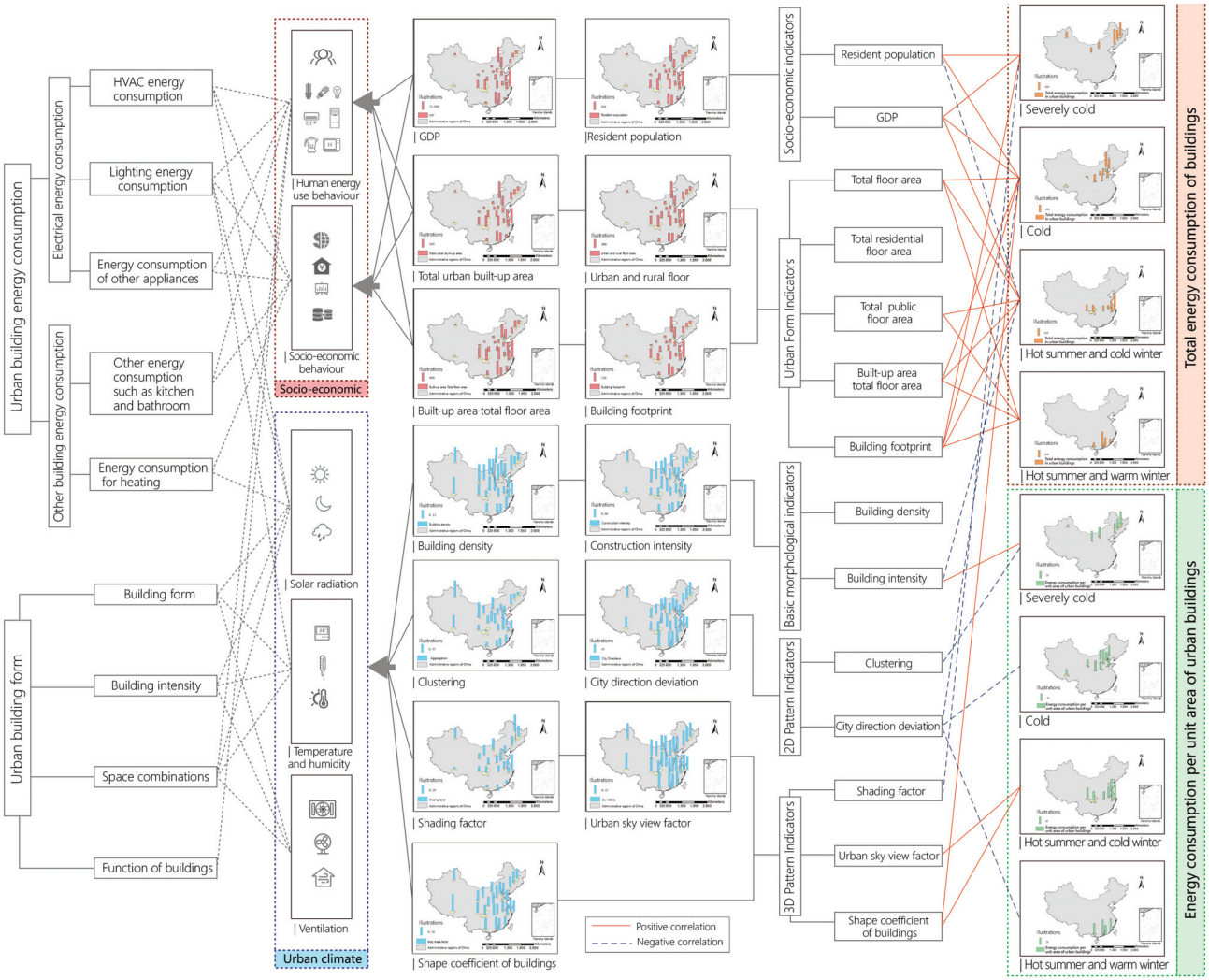


Figure 9. Analysis of the influence mechanism of urban morphological indicators on the energy consumption of buildings.

- In cold regions, urban orientation is extremely strongly correlated with energy consumption per unit area of urban buildings, with a negative correlation between the two. In other words, the greater the change in urban orientation, the lower the energy consumption per unit area of urban buildings. The organization of building groups, such as enclosed buildings, has an important impact on the heating, cooling, and ventilation energy consumption of buildings by affecting the intensity of the heat

island effect, the urban ventilation corridor effect, and the urban microclimate, and thus the heat dissipation rate of buildings.

- In hot-summer and cold-winter regions, the shape coefficients are strongly correlated with the energy consumption per unit area of urban buildings, both of which are positively correlated. In hot-summer and cold-winter cities, the more complex the building's shape is, the higher the energy consumption per unit area of urban buildings. The larger the building bulk factor is, the higher the demand for heating, cooling, and lighting energy consumption, thus making the energy consumption per unit area of the city higher. In hot-summer and cold-winter areas, the larger the shading coefficient, the higher the energy consumption per unit area of the building in the city. Avoiding enclosing buildings in hot-summer and cold-winter areas, building according to the best orientation of the city, and reducing mutual shading between buildings can obtain the maximum amount of solar radiation in winter, which has an impact on the building's energy consumption for heating and lighting; at the same time, it can ensure the circulation of the building, improve the ventilation performance, and have an impact on the microclimate of the city, thus reducing the energy consumption for building cooling.
- In hot-summer and warm-winter regions, urban orientation and energy consumption per unit area of urban buildings are extremely strongly correlated, with a negative correlation between the two. In other words, the greater the change in urban orientation, the lower the energy consumption per unit area of urban buildings. The organization of building groups, such as enclosed buildings, has an important impact on the heating, cooling, and ventilation energy consumption of buildings by influencing the intensity of the heat island effect, the urban ventilation corridor effect, and the urban microclimate, and thus the heat dissipation rate of buildings.

From the aspect of energy consumption per unit area, those in severe cold regions are higher than those in cold regions, and those in cold regions are higher than those in hot-summer and cold-winter regions, from which it can be seen that temperature is an important factor affecting energy consumption per unit area of urban buildings. As can be seen from the energy consumption per unit area of residential buildings, with the change of latitude, the energy consumption per unit area of residential buildings tends to increase from low latitude to high latitude. As the latitude increases, the temperature gradually decreases in winter, which creates higher requirements for the heating of buildings, and this is the most important reason for the increase in residential energy consumption per unit.

The total energy consumption of buildings in the four major climate zones increased significantly with population, GDP, land use, and building scale. The energy consumption per unit area increased from low latitude to high latitude, reaching 67.6 $kWh \cdot m^2$ in the cold area, which was about 1.5 times that of the hot-summer and cold-winter area, mainly due to the heating load in the high latitude winter. The coupling between urban form and energy consumption is significant, and high aggregation and low intensity in severe cold areas are conducive to energy saving; the enclosed and diversified orientation of cold- and hot-summer and warm-winter areas can reduce energy consumption; and the larger the body shape coefficient and shading in the hot-summer and cold-winter areas, the higher the energy consumption. The morphology determines the terminal energy consumption through microclimate regulation.

Comparison with existing studies shows that the findings of this paper are highly consistent with the conclusion of Su et al. that macro urban forms affect building energy consumption by regulating the urban thermal environment through the aggregation and dispersion dimension [42]. At the same time, the micro simulation results pointed out

by Li and Gou [44] in eight cities across climate zones that building height and body shape coefficient have a significant positive effect on photovoltaic potential and self-supply efficiency in cold cities are supplemented, and the negative energy consumption effect of aggregation in severe cold areas on reducing heating demand is quantified at the macro scale for the first time. In addition, Zhao et al. [43] demonstrated that the shading of surrounding buildings can reduce the heat load in severe cold areas by 3.1%, and this paper verifies and expands this effect in a large sample of 26 cities and gives an elastic threshold. However, the multi-index optimization study of Murathan and Manioğlu [45] in Istanbul lacks extrapolation, and this paper clarifies the differentiated weights of the three factors of orientation, shading, and body shape in different climate zones through climate zoning regression, making up for the limitations of single-city research. In view of the two major gaps pointed out by Zhao et al. [43], there is a lack of quantitative relationship between measured energy consumption and urban morphology at the macro scale. Su et al. [42] used statistical yearbooks and remote sensing data to provide the elasticity coefficient of morphological indicators for energy consumption for the first time and directly embedded the results into the energy-saving design guidelines for sub-climate zones, realizing a closed loop from macro identification to planning application.

4. Conclusions

Based on the core hypothesis that urban morphology indicators can explain the differences in building energy consumption per unit area in different climate zones, it was found in 26 sample cities that the energy consumption per unit area increased significantly from the low value of hot-summer and warm-winter areas to the high level of severe cold areas, and the energy consumption per unit area decreased by about 0.05 for every standard deviation increase in building aggregation degree in severe cold areas. For each increase in shading factor, the energy consumption increases significantly. This result confirms for the first time the dual moderating effect of the form and climate coupling effect on energy consumption on a large scale and fills the gap in the research on the quantitative relationship between urban form and building energy consumption in China. In practice, the energy consumption should be reduced through compact layout in severe cold areas, optimization of orientation layout in cold areas, and control of shape and shading in hot-summer and cold-winter areas, which provides a direct basis for the energy-saving design guidelines of zoning buildings.

In severe cold regions, there is an overall trend that the larger the GDP, the number of resident population, the built-up area, and the building footprint area, the greater the total urban building energy consumption. In cold regions, there is a general trend that the larger the GDP, the resident population, the built-up area, and the total building area, the greater the total energy consumption of urban buildings. In hot-summer and cold-winter regions, there is a general trend that the larger the total building area, resident population, and built-up area, the larger the total energy consumption of urban buildings. In hot-summer and warm-winter regions, there is a general trend that the larger the resident population, GDP, and total building area, the larger the total energy consumption of urban buildings.

From the aspect of energy consumption per unit area, those in severe cold areas are higher than those in cold areas, and those in cold areas are higher than those in hot-summer and cold-winter areas. From the aspect of residential energy consumption per unit area, it can be seen that with the change of latitude, from low latitude to high latitude, the residential energy consumption per unit area shows a tendency to increase.

The indicator of aggregation in severe cold regions shows a very strong correlation with energy consumption per unit area of urban buildings, with a significant correlation

at the 0.05 level and a negative correlation between the two. Meanwhile, the indicator of building intensity is strongly correlated with energy consumption per unit area of urban buildings, with a significant correlation at the 0.05 level and a positive correlation between the two. In cold regions, the indicator of urban orientation has a very strong correlation with energy consumption per urban building area, with a significant correlation at the 0.01 level and a negative correlation between the two. In hot-summer and cold-winter regions, the shading coefficient and shape coefficient of buildings are strongly correlated with energy consumption per unit area of urban buildings, and the correlation is significant at the 0.05 level, and both are positively correlated. In hot-summer and warm-winter regions, urban orientation and energy consumption per unit area of urban buildings showed a very strong correlation, and both were negatively correlated.

The stronger the aggregation among buildings in severe cold regions, the lower the energy consumption per unit area of urban buildings. In cold regions, urban orientation is extremely strongly correlated with energy consumption per unit area of urban buildings, with a negative correlation between the two. In hot-summer and cold-winter regions, the more complex the building's shape is, the higher the energy consumption per unit area of urban buildings. In hot-summer and warm-winter regions, the organization of building groups, such as enclosed buildings, has an important impact on the heating, cooling, and ventilation energy consumption of buildings by affecting the intensity of the heat island effect, the urban ventilation corridor effect, and the urban microclimate, thus affecting the heat dissipation rate of buildings.

From the aspect of energy consumption per unit area, the severe cold areas are higher than the cold areas, and the cold areas are higher than the hot-summer and cold-winter areas, from which it can be seen that temperature is an important factor affecting the energy consumption per unit area of urban buildings. As the latitude increases, the temperature gradually decreases in winter, which creates higher requirements for the heating of buildings.

Although this paper analyzes the correlation between building energy consumption and urban morphology indicators in 26 cities at a macroscopic scale, there are certain limitations, such as that the sample of cities is small and could be further increased, the urban building form data need to be further tested, and the correlation between urban morphology and urban building energy consumption needs to be further explored. This requires a more detailed cooperation system in future research and in-depth cooperation among different disciplines to enhance the accuracy of data and the validity of conclusions.

5. Limitations and Future Work

5.1. Scope of the Study and Methodological Limitations

In this study, there are certain research scopes and methodological limitations when discussing the impact of urban morphology on the energy consumption of urban buildings. First, the choice of study sample may have influenced the generalizability of the results. Due to resource and time constraints, the sample size may not be sufficient to fully represent the entire research field. Secondly, this study mainly relies on quantitative analysis, which provides data support but may lack an in-depth understanding of complex social phenomena. Additionally, some measurement tools and methods used in research can be subjective, which can affect the accuracy of the results.

The climate zone classification implies the assumption of topographic homogeneity, which does not discuss the impact that mountain cities may have on energy consumption through microclimate, building layouts, or energy infrastructure. The control of confounding variables mainly relies on the standardization and statistical decomposition of remote

sensing data, but no special correction method is designed for the terrain. Future studies need to clarify whether topographic variables can be used as independent factors for energy consumption prediction or stratified analysis.

5.2. Future Research Directions

Future studies may consider expanding sample size and sample diversity to improve the generalizability and reliability of research results. At the same time, it is recommended to employ qualitative research methods, such as in-depth interviews and case studies, to complement existing quantitative analysis for a more comprehensive understanding of the research topic. In addition, future studies can explore the impact of urban forms on urban building energy consumption under different cultural backgrounds to test the cross-cultural applicability of the results of this study. Finally, it is recommended to innovate research methods, such as the use of big data analysis or artificial intelligence technology, to improve research efficiency and depth. With these methods, future research will be able to provide deeper and more precise insights.

Author Contributions: Conceptualization, G.Y. and X.S.; methodology, G.Y., B.S. and X.S.; software, Y.L., T.Y., W.Z., C.L. and Y.W.; validation, Y.L.; formal analysis, B.S.; investigation, Y.L., W.Z., C.L. and Y.W.; resources, Y.L.; data curation, Y.L., T.Y. and W.Z.; writing—original draft preparation, Y.L., W.Z. and Y.W.; writing—review and editing, T.Y. and C.L.; visualization, Y.L.; supervision, G.Y., B.S. and X.S.; project administration, G.Y.; funding acquisition, Y.L. All authors have read and agreed to the published version of the manuscript.

Funding: This research is supported by the Fundamental Research Funds for the Central Universities (2025SK29), the National Natural Science Foundation of China (grant number 52308023), and the 16th Batch of the "Sailing Plan" for Young Teachers at China University of Mining and Technology (grant number 102524107).

Data Availability Statement: The original contributions presented in this study are included in the article. Further inquiries can be directed to the corresponding author.

Acknowledgments: Special thanks to the anonymous reviewers and the editor for their valuable comments to improve our manuscript.

Conflicts of Interest: The authors declare no conflict of interest.

Abbreviations

The following abbreviations are used in this manuscript:

GDP	Gross Domestic Product
EBC	Energy in Buildings and Communities
IEA	International Energy Agency
HDD	Heating Degree Days
AOI	Area of Interest
POI	Point of Interest
GIS	Geographic Information System
2D	Two-dimensional
3D	Three-dimensional

References

1. UN-Habitat. Energy. 2012. Available online: http://unhabitat.org/urban-themes/energy/ (accessed on 8 November 2016).
2. UNEP. Cities and Climate Change. 2015. Available online: https://www.ncei.noaa.gov/access/monitoring/monthly-report/global/201508 (accessed on 1 August 2015).

3. Chalal, M.L.; Benachir, M.; White, M.; Shrahily, R. Energy planning and forecasting approaches for supporting physical improvement strategies in the building sector: A review. *Renew. Sustain. Energy Rev.* **2016**, *64*, 761–776. [CrossRef]
4. Oliveria, V.; Silva, M. Urban form and energy. *Urban Morphol.* **2013**, *17*, 181–182. [CrossRef]
5. Oliveira, V. *Urban Morphology*; Springer International Publishing: Cham, Switzerland, 2016.
6. IEA ECBCS Annex 51-Subtask B, Case Studies on Energy Planning and Implementation Strategies for Neighborhoods, Quarters and Municipal Areas, 2012IEA SHC | | Task Publications. Available online: https://www.iea-shc.org/publications-tasks (accessed on 12 December 2016).
7. Zhou, Y.; Zhang, Z.; Yang, F.; Yu, Y.; Xie, X. Urban morphology on heat island and building energy consumption. *Procedia Eng.* **2017**, *205*, 2401–2406. [CrossRef]
8. Ewing, R.; Rong, F. The impact of urban form on US residential energy use. *Hous. Policy Debate* **2008**, *19*, 1–30. [CrossRef]
9. Colombert, M.; Diab, Y.; Salagnac, J.-L.; Morand, D. Sensitivity study of the energy balance to urban characteristics. *Sustain. Cities Soc.* **2011**, *1*, 125–134. [CrossRef]
10. Li, Y.; Zhang, X.; Zhu, S.; Wang, X.; Lu, Y.; Du, S.; Shi, X. Transformation of Urban Surfaces and Heat Islands in Nanjing during 1984–2018. *Sustainability* **2020**, *12*, 6521. [CrossRef]
11. Wong, N.H.; Jusuf, S.K.; Syafii, N.I.; Chen, Y.; Hajadi, N.; Sathyanarayanan, H.; Manickavasagam, Y.V. Evaluation of the impact of the surrounding urban morphology on building energy consumption. *Sol. Energy* **2011**, *85*, 57–71. [CrossRef]
12. Vartholomaios, A. A parametric sensitivity analysis of the influence of urban form on domestic energy consumption for heating and cooling in a Mediterranean city. *Sustain. Cities Soc.* **2017**, *28*, 135–145. [CrossRef]
13. Zhuang, D.; Zhang, X.; Lu, Y.; Wang, C.; Jin, X.; Zhou, X.; Shi, X. A performance data integrated BIM framework for building life-cycle energy efficiency and environmental optimization design. *Autom. Constr.* **2021**, *127*, 103712. [CrossRef]
14. Chatzipoulka, C.; Compagnon, R.; Nikolopoulou, M. Urban geometry and solar availability on façades and ground of real urban forms: Using London as a case study. *Sol. Energy* **2016**, *138*, 53–66. [CrossRef]
15. Ahn, Y.; Sohn, D.-W. The effect of neighbourhood-level urban form on residential building energy use: A GIS-based model using building energy benchmarking data in Seattle. *Energy Build.* **2019**, *196*, 124–133. [CrossRef]
16. Silva, M.; Oliveira, V.; Leal, V. Urban form and energy demand: A review of energy-relevant urban attributes. *J. Plan. Lit.* **2017**, *32*, 346–365. [CrossRef]
17. Salvati, A.; Monti, P.; Roura, H.C.; Cecere, C. Climatic performance of urban textures: Analysis tools for a Mediterranean urban context. *Energy Build.* **2019**, *185*, 162–179. [CrossRef]
18. Tereci, A.; Ozkan, S.T.E.; Eicker, U. Energy benchmarking for residential buildings. *Energy Build.* **2013**, *60*, 92–99. [CrossRef]
19. van Esch, M.M.E.; Looman, R.H.J.; de Bruin-Hordijk, G.J. The effects of urban and building design parameters on solar access to the urban canyon and the potential for direct passive solar heating strategies. *Energy Build.* **2012**, *47*, 189–200. [CrossRef]
20. Strømann-Andersen, J.; Sattrup, P.A. The urban canyon and building energy use: Urban density versus daylight and passive solar gains. *Energy Build.* **2011**, *43*, 2011–2020. [CrossRef]
21. Zhou, X.; Liu, T.; Yan, D.; Shi, X. An action-based Markov chain modeling approach for predicting the window operating behavior in office spaces. *Build. Simul.* **2021**, *14*, 301–315. [CrossRef]
22. Zhou, X.; Ren, J.; An, J.; Yan, D.; Shi, X.; Jin, X. Predicting open-plan office window operating behavior using the random forest algorithm. *J. Build. Eng.* **2021**, *42*, 102514. [CrossRef]
23. Asfour, O.S.; Alshawaf, E.S. Effect of housing density on energy efficiency of buildings located in hot climates. *Energy Build.* **2015**, *91*, 131–138. [CrossRef]
24. Ignatius, M.; Wong, N.H.; Jusuf, S.K. Urban microclimate analysis with consideration of local ambient temperature, external heat gain, urban ventilation, and outdoor thermal comfort in the tropics. *Sustain. Cities Soc.* **2015**, *19*, 121–135. [CrossRef]
25. Javanroodi, K.; Mahdavinejad, M.; Nik, V.M. Impacts of urban morphology on reducing cooling load and increasing ventilation potential in hot-arid climate. *Appl. Energy* **2018**, *231*, 714–746. [CrossRef]
26. Lima, I.; Scalco, V.; Lamberts, R. Estimating the impact of urban densification on high-rise office building cooling loads in a hot and humid climate. *Energy Build.* **2019**, *182*, 30–44. [CrossRef]
27. Santamouris, M.; Papanikolaou, N.; Livada, I.; Koronakis, I.; Georgakis, C.; Argiriou, A.; Assimakopoulos, D.N. On the impact of urban climate on the energy consumption of buildings. *Sol. Energy* **2001**, *70*, 201–216. [CrossRef]
28. Woo, Y.; Cho, G. Impact of the surrounding built environment on energy consumption in mixed-use buildings. *Sustainability* **2018**, *10*, 832. [CrossRef]
29. Steemers, K. Energy and the city: Density, buildings and transport. *Energy Build.* **2003**, *35*, 3–14. [CrossRef]
30. Kesten, D.; Tereci, A.; Strzalka, A.; Eicker, U. A method to quantify the energy performance in urban quarters. *HVACR&Res.* **2011**, *18*, 100–111.

31. Georgakis, C.; Santamouris, M. Experimental investigation of air flow and temperature distribution in deep urban canyons for natural ventilation purposes. *Energy Build.* **2006**, *38*, 367–376. [CrossRef]
32. Dawodu, A.; Cheshmehzangi, A. Passive cooling energy systems SWOT analyses for energy-use reductions at three spatial levels. *Energy Procedia* **2017**, *105*, 3411–3418. [CrossRef]
33. Cheng, V.; Steemers, K.; Montavon, M.; Compagnon, R. Urban form, density and solar potential. In Proceedings of the 23rd Conference on Passive and Low Energy Architecture, Geneva, Switzerland, 6–8 September 2006.
34. Chen, L.; Hang, J.; Sandberg, M.; Claesson, L.; Di Sabatino, S.; Wigo, H. The impacts of building height variations and building packing densities on flow adjustment and city breathability in idealized urban models. *Build. Environ.* **2017**, *118*, 344–361. [CrossRef]
35. Gu, Z.-L.; Zhang, Y.-W.; Cheng, Y.; Lee, S.-C. Effect of uneven building layout on air flow and pollutant dispersion in non-uniform street canyons. *Build. Environ.* **2011**, *46*, 2657–2665. [CrossRef]
36. Lee, Y.; Sohn, D. An analysis of the relationships between the characteristics of urban physical environment and air pollution in Seoul. *J. Urban Desi. Inst. Korea* **2015**, *16*, 5–19.
37. Ng, E. Policies and technical guidelines for urban planning of high-density cities—Air ventilation assessment (AVA) of Hong Kong. *Build. Environ.* **2009**, *44*, 1478–1488. [CrossRef] [PubMed]
38. Ma, J.; Cheng, J.C.P. Estimation of the building energy use intensity in the urban scale by integrating GIS and big data technology. *Appl. Energy* **2016**, *183*, 182–192. [CrossRef]
39. Zhao, H.-X.; Magoulès, F. A review on the prediction of building energy consumption. *Renew. Sustain. Energy Rev.* **2012**, *16*, 3586–3592. [CrossRef]
40. Shi, X.; Tian, Z.; Chen, W.; Si, B.; Jin, X. A review on building energy efficient design optimization from the perspective of architects. *Renew. Sustain. Energy Rev.* **2016**, *65*, 872–884. [CrossRef]
41. Zhang, Q. Climatic Zoning for the Thermal Design of Residences in China Based on Heating Degree-Days and Cooling Degree-Hours. *J. Asian Archit. Build. Eng.* **2005**, *4*, 533–539. [CrossRef]
42. Su, H.; Wang, Q.; Qi, Z. Macro-scale urban form and extreme heat events: Evidence from Monte Carlo simulation-based ensemble learning models. *Sustain. Cities Soc.* **2025**, *130*, 106582. [CrossRef]
43. Zhao, Y.; Ding, X.; Wu, Z.; Yin, S.; Fan, Y.; Ge, J. Impact of urban form on building energy consumption in different climate zones of China. *Energy Build.* **2024**, *320*, 114579. [CrossRef]
44. Li, X.; Gou, Z. Urban morphology and energy self-sufficiency: A comparative study of residential blocks in eight global cities. *Cities* **2025**, *166*, 106240. [CrossRef]
45. Murathan, E.K.; Manioğlu, G. Impact of urban form on energy performance, outdoor thermal comfort, and urban heat Island: A case study in Istanbul. *Energy Build.* **2025**, *345*, 116109. [CrossRef]

Disclaimer/Publisher's Note: The statements, opinions and data contained in all publications are solely those of the individual author(s) and contributor(s) and not of MDPI and/or the editor(s). MDPI and/or the editor(s) disclaim responsibility for any injury to people or property resulting from any ideas, methods, instructions or products referred to in the content.

buildings

MDPI

Article

Evolution Method of Built Environment Spatial Quality in Historic Districts Based on Spatiotemporal Street View: A Case Study of Tianjin Wudadao

Lujin Hu *, Yu Liu and Bing Yu

School of Surveying, Mapping and Urban Spatial Information, Beijing University of Civil Engineering and Architecture, Beijing 102616, China; 2108570023112@stu.bucea.edu.cn (Y.L.); 2108570023119@stu.bucea.edu.cn (B.Y.)

* Correspondence: hulujin@bucea.edu.cn; Tel.: +86-137-1646-3240

Abstract: With the accelerating pace of urbanization, historic districts are increasingly confronted with the dual challenge of coordinating heritage preservation and sustainable development. This study proposes an intelligent evaluation framework that integrates spatiotemporal street view imagery, affective perception modeling, and scene recognition to reveal the evolutionary dynamics of built environment spatial quality in historic districts. Empirical analysis based on multi-temporal data (2013–2020) from the Wudadao Historic District in Tianjin demonstrates that spatial quality is shaped by a complex interplay of factors, including planning and preservation policies, landscape greening, pedestrian-oriented design, infrastructure adequacy, and equitable resource allocation. These findings validate the framework's effectiveness as a tool for monitoring urban sustainability. Moreover, it provides actionable insights for the development of resilient, equitable, and culturally vibrant built environments, effectively bridging the gap between technological innovation and sustainable governance in the context of historic districts.

Keywords: built environment spatial quality; spatiotemporal street view imagery; historic districts; emotional perception; scene recognition

1. Introduction

With the acceleration of global urbanization, historic districts, as the core carriers of urban cultural identity and public spaces for residents, have become a key topic in urban planning [1]. The dynamic evolution mechanism of their spatial quality and its impact on urban sustainable development has attracted increasing attention. However, existing research primarily focuses on the evaluation of static spatial attributes (such as greenery coverage and building density) [2,3]. This limitation is particularly prominent in the study of historic districts, where the spatial quality not only involves the update of the built environment but also requires balancing the complex relationship between cultural heritage preservation, tourism development, and the needs of local residents [4].

Traditional spatial quality evaluation methods (such as surveys and field observations) have significant limitations in terms of coverage and temporal continuity [5]. In recent years, street view images have gradually become an important data source for urban spatial analysis due to their high resolution, spatiotemporal traceability, and potential for emotion perception. In the tradition of emotion perception, the term generally refers to the ability to recognize, distinguish, and interpret emotional information in the environment

through various cues such as facial expressions, body language, and contextual factors. With the advancement of research, the emotion perception of streetscapes has come to refer specifically to a method for assessing the emotional quality or the built environment quality of urban street spaces through street view imagery [6]. Existing studies have validated its effectiveness in areas such as vegetation monitoring and street safety assessment [7,8]. However, there are still three main shortcomings in the research on historic districts: (1) Lack of dynamism: Most studies are based on street view images from a single time point, lacking the long-term tracking of spatial quality evolution; (2) Limited emotional dimensions: Emotion perception models often focus on single dimensions such as safety and esthetics, neglecting the compound effects of negative emotions such as oppression and boredom on spatial quality; (3) Insufficient mechanism explanation: The separation between scene recognition and emotion analysis makes it difficult to interpret the driving factors behind changes in the built environment's spatial quality [9,10].

To address the aforementioned research gaps, this paper proposes a dynamic spatial quality evaluation framework that integrates spatiotemporal street view images, an emotion perception model, RSS-CNN (Ranking Streetscore Convolutional Neural Network), and scene recognition technology (Places365-ResNet) in the historic districts, and validates this framework with Tianjin's Five Avenues as a case study. By constructing a multi-stage street view dataset from 2013 to 2020, this study systematically explores the following scientific questions:

How can the spatiotemporal differentiation characteristics of spatial quality in historic districts be quantified?

What patterns emerge in the spatial quality evolution during different planning stages?

What are the key driving factors affecting the dynamic changes in spatial quality?

This study achieves three breakthroughs at the methodological level:

(1) It proposes a dynamic emotion perception model to evaluate the built environment spatial quality for historic districts based on temporal street view imagery.

(2) It constructs an "emotion–scene" coupling analysis framework to elucidate the evolutionary mechanisms of spatial quality in historic districts.

(3) It validates the differentiated intervention effects of policy texts on the spatial quality of historic districts.

This paper is divided into six chapters: Section 1 explains the research background and problems; Section 2 reviews the research progress in spatial quality evaluation and street view image analysis; Section 3 details the research methods and technical approach; Section 4 introduces the case study area and data sources; Section 5 presents the results of spatiotemporal evolution and driving factor analysis; Section 6 summarizes the research conclusions and proposes planning recommendations.

2. Related Work

2.1. Definition and Dynamic Evaluation of Built Environmental Framework Quality for Historic Districts

Spatial quality is a core indicator for measuring the functionality and humanity of urban environments. Its connotation has evolved from early static physical attributes (such as street width and greenery coverage) to more dynamic and multifaceted factors [11]. It has gradually expanded to include a multidimensional dynamic concept encompassing cultural atmosphere and emotional experience [12]. Kevin Lynch, in *The Image of the City*, pointed out that the essence of spatial quality lies in "the perception and interaction of people with their environment", emphasizing its subjectivity and time dependence [13]. In recent years, scholars have attempted to capture the evolutionary characteristics of

spatial quality through dynamic data (such as social media and mobile trajectories) [14]. For example, H. Zhou et al. used street view images and social media data to construct a dynamic evaluation model of urban visual perception equity [15]. However, existing studies primarily focus on modern commercial districts, lacking targeted research on historic districts, a special type of area [16]. The spatial quality of historic districts not only involves physical environment updates but also requires balancing the conflict between cultural heritage preservation and tourism development [17]. This gap urgently needs to be addressed.

2.2. The Potential and Limitations of Street View Images in Built Environment Spatial Quality

With its high resolution and spatiotemporal traceability, street view imagery has become an important data source for built environment spatial quality evaluation [18]. Biljecki, Filip, and Koichi Ito provided a systematic review of the applications of street view images in areas such as vegetation monitoring and traffic studies, demonstrating that they can effectively quantify the physical characteristics of street environments [6]. L. He et al. further used semantic segmentation models to reveal the correlation between street view elements (such as green visibility and building façade continuity) and socio-economic indicators (such as housing prices and crime rates) [19]. However, existing research has two main limitations:

Lack of temporal dimension: Most analyses are based on street view images from a single point in time, making it difficult to reveal the dynamic evolution patterns of urban spaces [20].

Single emotional dimension: Emotional perception models often focus on positive dimensions such as safety and esthetics, neglecting the complex impacts of negative emotions like oppression and boredom [21].

2.3. The Integration Progress of Deep Learning and Emotional Perception Models for Evaluation the Built Environment Spatial Quality

Deep learning technology provides powerful tools for the automated analysis of street view images [22]. Scene recognition models like Places365-ResNet, through training on massive datasets of images, can accurately classify street view functions (such as residential areas, commercial streets) [23]. Emotional perception models like Ranking Streetscore-CNN, through pairwise comparison learning, quantify the public's emotional feedback on the spatial environment (such as vitality and oppression) [24]. Recent studies have attempted to combine both types of models. For example, Liang et al., through time series street view images, tracked the ten-year evolution of visual clusters in Singapore's streets and found a trend of high-density visual experience zones spreading to emerging towns [9]. However, such studies mainly focus on modern cities and have not deeply analyzed the underlying mechanisms of emotional evolution in historic districts (such as the impact of cultural heritage preservation on the perception of beauty). Additionally, they lack a verification of the correlation between policy interventions and spatial quality [25].

2.4. The Built Environment Spatial Quality Research in Historic Districts

The evolution of spatial quality in historic districts has unique cultural and social attributes [26]. X. Zhu and S.-C. Chiou pointed out that the preservation of historic districts requires balancing "authenticity" and "functionality", with excessive commercialization, potentially weakening their cultural identity [27]. Baloch et al. proposed a framework for sustainable ecotourism development, using surveys and hierarchical regression analysis. They found that tourism development brought socio-economic benefits but also led to the

degradation of the natural environment and increased social environmental vulnerability. They proposed a framework for balancing commercial interests with environmental protection [28]. However, existing research still faces methodological limitations:

Insufficient data granularity: Relying on surveys or small sample street views makes it difficult to cover long-term, large-scale spatial changes [29];

Mechanistic explanation weakness: The separation between emotion perception and scene recognition models results in an inability to interpret the driving factors (e.g., how policy documents influence emotional scores through specific scene renovations).

In summary, this study uses the Tianjin Five Avenues Historic District as a case to develop a dynamic evaluation framework that integrates temporal street view imagery, emotion and scene recognition models, and policy text analysis. The research employs a multi-stage street view dataset (2013–2020) to uncover temporal changes in the spatial quality of historic districts, expands the evaluation by incorporating negative emotions such as oppression and boredom, and clarifies how planning interventions drive spatial quality evolution by combining scene recognition with policy analysis.

3. Experimental Area

3.1. Experimental Area Overview

Tianjin's Five Avenues, located in the Heping District, is an integral part of the city's historic and cultural heritage (Figure 1). Its origins date back to the late 19th and early 20th centuries, when it became a treaty port, attracting consular institutions and immigrants from multiple countries, including the UK, France, Italy, Germany, and Spain. This area developed a multicultural urban landscape [30]. The Five Avenues are famous for their diverse architectural styles, including British Victorian, French eclecticism, Italian Renaissance, German modernism, and Spanish Baroque, primarily composed of terraced houses and villas. The structures are solid and finely decorated, reflecting the blend of Western architectural techniques and Eastern lifestyles.

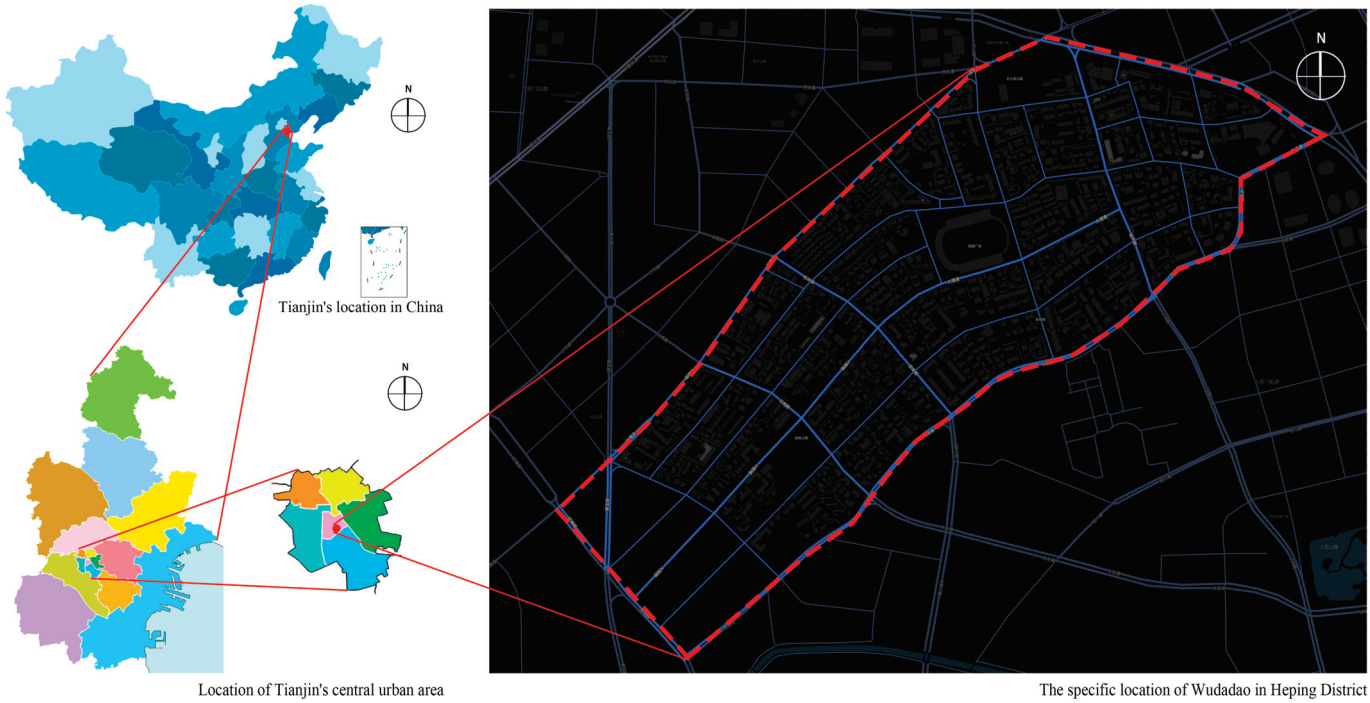


Figure 1. Study area location map.

The Five Avenues have not only been witness to the historical development of Tianjin but also serve as an important platform for Sino-foreign cultural exchange. It was once home to numerous foreign diplomats, merchants, and intellectuals, fostering rich cultural activities and social interactions. Today, it is a key tourist destination, attracting a large number of domestic and international visitors. Through the conversion of historical buildings into boutique hotels, cafes, and art galleries, the Five Avenues have achieved an organic integration of heritage protection and modern development. Government and related institutions ensure the preservation of its historical value, setting a benchmark for urban cultural heritage protection [31].

3.2. Data Collection Method

In this study, we initially obtained vector data of the Wudadao historic district from the OpenStreetMap platform and used QGIS software to extract road network data. Subsequently, we imported the data into ARCGIS software and performed coordinate projection transformation to ensure spatial consistency and accuracy. We then selected sampling points along the road network at 50 m intervals, which served as the locations for street view data collection (Figure 2).

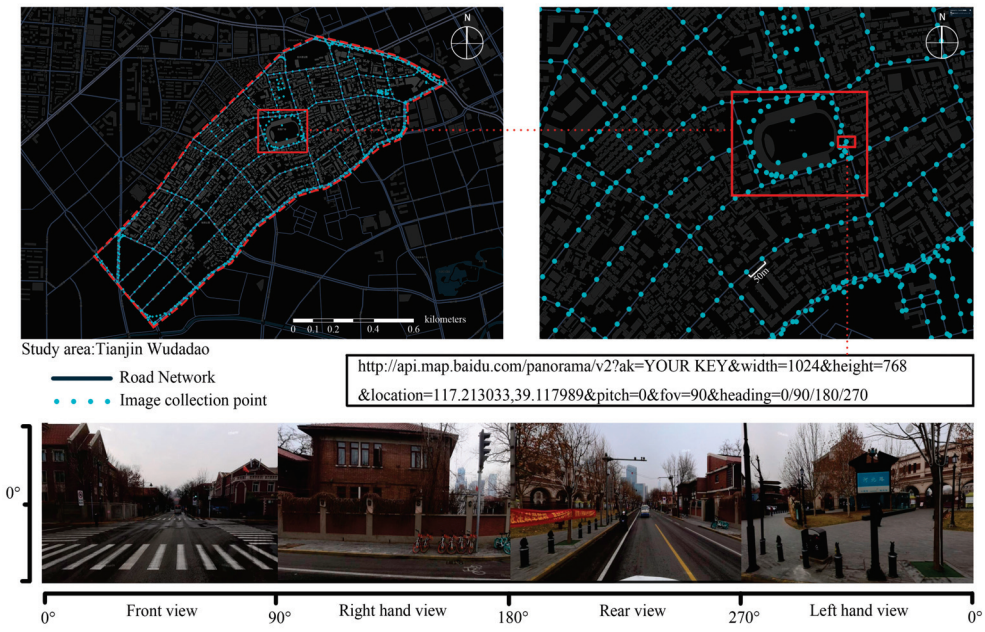


Figure 2. Schematic diagram of street view image collection.

Street view imagery was gathered using the Baidu Maps API from four distinct angles (0°, 90°, 180°, and 270°), with the pitch angle set to 0° to closely approximate the pedestrian's perspective. This adjustment minimizes experimental error and enhances the realism of the street view data collection [32]. This approach enabled the collection of street view images from the same set of coordinates within the study area across different years, facilitating the tracking of the spatial quality evolution of the Wudadao historic district over time.

However, due to the limitations in the frequency of street view image collection on Baidu Maps, the volume of street view data collected each year was not consistent. The specific data collection results for the Wudadao historic district are as follows: 2310 images in 2013, 30 images in 2014, 1397 images in 2015, 1162 images in 2016, 2393 images in 2017, 24 images in 2018, 1210 images in 2019, and 1254 images in 2020 (Figure 3).

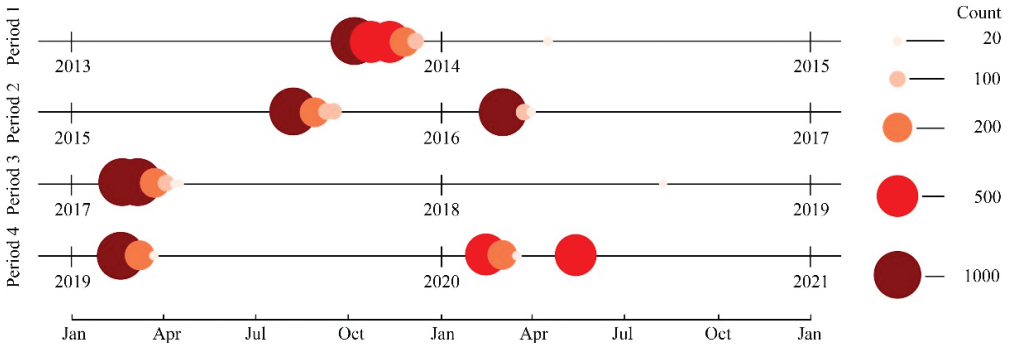


Figure 3. The number and temporal distribution of street view images utilized in this study (breakdown by the considered periods).

Given the variation in the number of street view images collected, we took into account the average distribution of data and the reasonableness of the annual intervals. Consequently, we divided the data into four phases: the first phase (2013–2014), the second phase (2015–2016), the third phase (2017–2018), and the fourth phase (2019–2020).

4. Evaluation Model for the Built Environment Spatial Quality in Historic Districts

4.1. Principle of the Method

Based on the street view images collected in Section 3.2, this study employs the affective perception model (Ranking SS-CNN) to quantitatively assess spatial quality within the research area. Leveraging the temporal characteristics of the street view images, the model identifies trends in spatial quality across different periods and highlights areas exhibiting significant feature changes. Furthermore, by integrating a scene recognition model (Places365-ResNet), we classify the scenes within these areas of pronounced change to pinpoint the specific factors influencing spatial quality evolution. The detailed experimental procedure is illustrated in Figure 4.

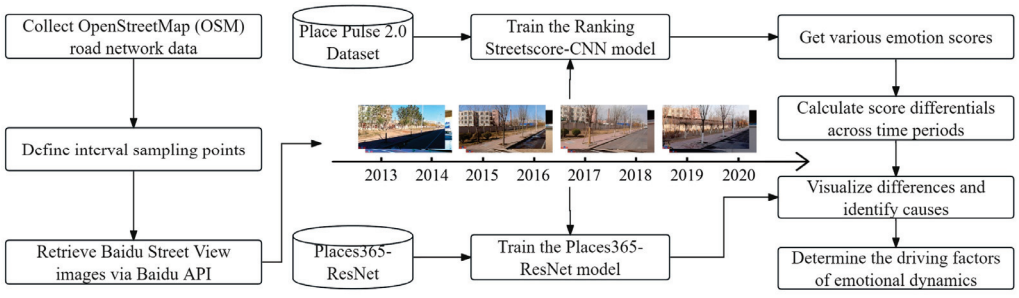


Figure 4. Evaluation framework diagram.

4.2. Emotion Perception Model for Evaluation the Built Environment Spatial Quality

We use the Ranking Streetscore-CNN (RSS-CNN) as the basic emotional perception model for evaluating the built environment spatial quality. The Ranking Streetscore-CNN (RSS-CNN) neural network model is derived from the Place Pulse 2.0 (PP 2.0) project developed by the MIT Media Lab. It evaluates six emotional dimensions of urban space quality through the comparison of city street images: safety, lively, boring, wealthy, depressing, and beautiful. The model does not explicitly define or standardize the physical characteristics corresponding to each perceptual attribute—such as safety, lively, boring, wealthy, depressing, and beautiful—in the study. The deep learning model (RSS-CNN) enables the

neural network to directly learn the underlying visual patterns behind human perception from comparative image data. During training, the network automatically extracts visual features associated with perceptual attributes, which may include (but are not limited to) the following: the appearance and maintenance of buildings, the cleanliness or clutter of streets, population density and street-level activity, greenery coverage and natural elements, and visual esthetics such as lighting brightness and color saturation. All these features were manually labeled through subjective evaluation as a pre-labeled training dataset, and then classified into emotional categories (e.g., beautiful, boring, depressing, lively, safety, wealthy) using the model of RSS-CNN (Ranking Streetscore Convolutional Neural Network). Data collection is achieved through a crowdsourced online game, wherein participants engage in pairwise comparisons of urban street view images. The dataset comprises 110,988 images from 56 cities and includes 1,170,000 paired comparisons provided by 81,630 online volunteers. Specifically, users are randomly presented with two Google Street View images and asked questions such as "Which place looks safer?" or "Which place looks more lively?". The strength of the model lies in its use of a large-scale, globally diverse dataset, which captures a wide range of visual contexts and enables the identification of patterns in universal human perception [24].

RSS-CNN consists of two main components: a dual feature extractor and a ranking subnetwork. The network learns image ranking through fully connected layers. The model training combines classification loss (for binary classification) and ranking loss (for sorting images within the entire dataset), which significantly enhances prediction accuracy. The function formulas for the classification loss (Lc) and ranking loss (Lr) are as follows (1) and (2).

$$L_c = \sum_{(i,j,y)\in P} \sum_{k}^{K} -1[y = k] \log\left(g_k\left(x_i, x_j\right)\right) \tag{1}$$

$$L_r = \sum_{(i,j,y)\in P} \left(\max\left(0, y \cdot \left(f_r\left(x_j\right) - f_r(x_i)\right)\right)\right)^2 \tag{2}$$

In this context, $\{x_i\}_{i=1}^{m}$ represents the image pixel space of m images, and $\{(i_k, j_k, y_k)\}_{k=1}^{N}$ denotes a series of N image comparison triplets, where $i, j \in \{1, \ldots, m\}, y \in \{+1, -1\}$. These triplets specify a pairwise comparison between image i and image j with y = +1 indicating that image i wins, and y = -1 indicating that image j wins. The model's objective is to learn a ranking function $f_r(x_i)$ based on the raw image pixels, as shown in Equation (3), that satisfies the maximum number of constraint conditions.

$$y \cdot \left(f_r(x_i) - f_r\left(x_j\right)\right) > 0 \; \forall (i, j, y) \in P \tag{3}$$

At the same time, the loss function L is minimized, which is a weighted combination of the classification (or softmax) loss (Lc) and the ranking loss (Lr) expressed as L = Lc(P) + λLr(P), $P = \{(i_{K,} j_{K,} y_{K,})\}_{k=1}^{N}$. P refers to the set of all comparison relations between image pairs in the training set. The hyperparameter λ is set through grid search on the validation set to maximize classification accuracy.

4.3. "Emotion–Scene" Coupling Analysis Framework

To construct an "Emotion–Scene"-coupled analytical framework, this study integrates an affective perception model (Ranking SS-CNN) with a scene recognition model (Places365-ResNet) to accurately assess urban spatial quality. The Places365-ResNet model is derived from the MIT Places database project, which comprises over 10 million images covering 98% of global scene types and annotated with 434 distinct scene categories. Based on the

residual network (ResNet) architecture, Places365-ResNet is specifically designed for scene classification tasks and trained on the Places365-Standard dataset, which contains more than 8 million images across 365 scene categories. This model exhibits outstanding classification performance, achieving over 54% Top-1 accuracy (the proportion of predictions where the model's top predicted category matches the true label) and exceeding 85% Top-5 accuracy (the proportion where the true label appears within the model's five highest-ranked predictions) on both validation and test datasets, demonstrating its robustness in large-scale scene classification tasks [23]. By leveraging the emotion ranking capability of the Ranking SS-CNN model and the scene classification strength of the Places365-ResNet model, the proposed "Emotion–Scene"-coupled analytical framework can simultaneously perform affective perception and scene categorization on urban street view images. This integration allows the framework to accurately characterize the spatial distribution of emotional attributes within urban areas and precisely identify the specific scene-related factors influencing these emotional perceptions. Consequently, this coupled approach enables a quantitative and refined assessment of urban spatial quality, effectively capturing perceptual characteristics across large urban areas, and providing more precise data support and evidence-based decision-making for urban design and planning.

5. Experimental Analysis

5.1. Results of Emotion Perception Model for the Study Area

The RSS-CNN model used in this study effectively predicts six key emotional perception indicators of the streets in the Wudadao historic district, including safety, vibrancy, esthetic appeal, wealth, oppression, and boredom. The model trained on this dataset demonstrates high accuracy, with a root mean square error (RMSE) below 10%. By applying the RSS-CNN model to the collected street view images, each image from various angles of a location is assigned a score, and the average perception score for each location is calculated. The average scores for all locations are then aggregated to create a temporal emotional perception distribution map of the spatial quality of the Wudadao historic district.

Additionally, to better observe the variations and their range, we subtract the scores of street view images from different stages and visualize the absolute values of the differences greater than five.

5.1.1. Beautiful Emotion Perception

Spatiotemporal Evolution of Beautiful Sentiment

Based on the sentiment scoring analysis using the RSS-CNN model, the perception of beauty in the Wudadao area has shown significant phase transitions between 2013 and 2020 (Figure 5). In the early stages (2013–2014), the overall beauty perception of the area was relatively low, with high-scoring regions sparsely distributed in the central areas, which may be attributed to insufficient greenery and the homogenization of architectural styles. As the related policies, such as the "Comprehensive Management Measures for the Wudadao Area in Heping District (Trial)" implemented in 2014, gradually took effect, the beauty perception significantly improved from 2015 to 2016, with the high-scoring areas expanding, especially along the main streets and key landscape nodes. However, between 2017 and 2018, the beauty perception experienced a decline, with the peripheral areas seeing a decrease in landscape quality due to delayed maintenance and construction impacts. By 2019–2020, although there was some recovery in the beauty perception, it did not return to the peak level, reflecting the diminishing marginal returns of resource investments.

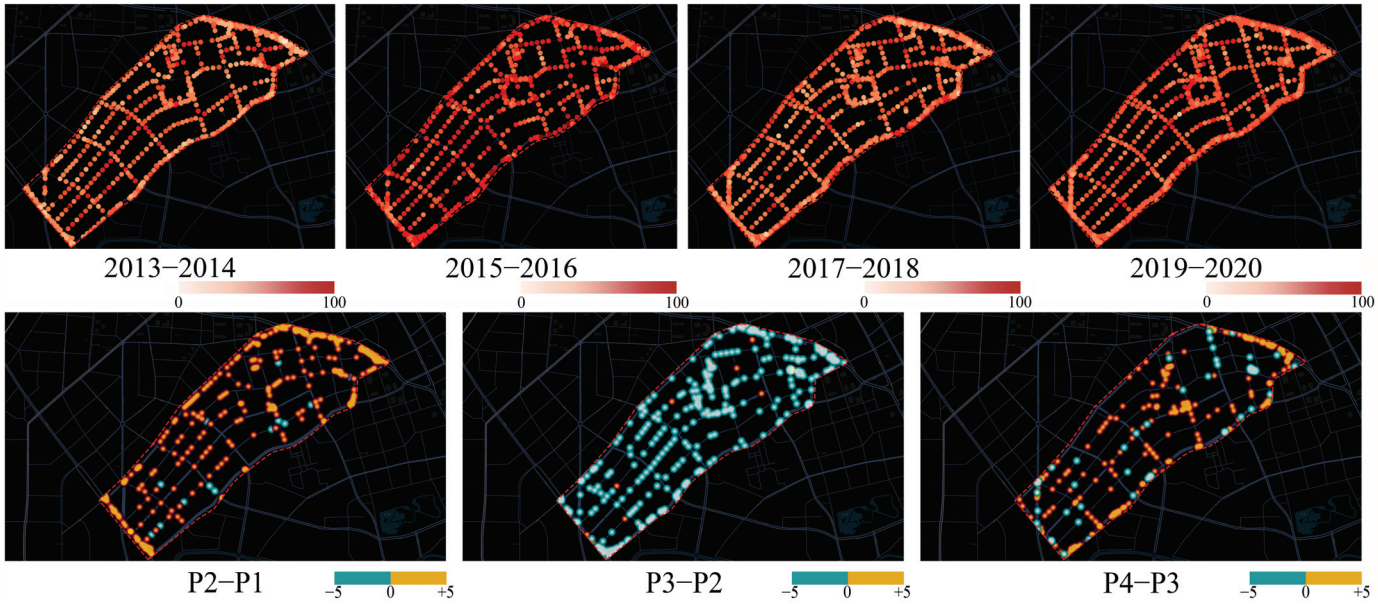


Figure 5. The changes in the beautiful emotional phase and the phase differences.

In terms of spatial differentiation, the analysis of stage-to-stage differences reveals that the improvement in beauty perception from 2015 to 2016 was concentrated in the central areas, while the decline from 2017 to 2018 was more significant in the peripheral areas. This differentiation is directly related to the uneven spatial distribution of policy resources—central areas were prioritized for greenery enhancements and architectural restoration, while the renovation of peripheral areas lagged for an extended period.

Driving Mechanisms

The fluctuations in beauty perception are mainly driven by two types of factors:

Positive Drivers: Protective restoration of historical buildings, enhancements in street greenery, and the optimization of pedestrian systems significantly improved visual attractiveness.

Negative Suppressors: Over-commercialization led to visual clutter, and insufficient resource investment in peripheral areas weakened the overall esthetic appeal.

5.1.2. Boring Emotion Perception

Spatiotemporal Evolution of Boring Sentiment

Based on sentiment scoring analysis, the perception of boredom in the Wudadao area exhibited phase fluctuations between 2013 and 2020 (Figure 6). In the early stages (2013–2014), the overall boredom perception of the area was relatively low, with the central region displaying strong spatial vitality due to the cultural appeal of historical buildings and frequent public activities. From 2015 to 2016, the implementation of policies such as the "Comprehensive Management Measures for the Wudadao Area in Heping District (Trial)" further optimized public spaces (e.g., the addition of walkways and small plazas), which helped reduce boredom. The peripheral areas, due to improvements in infrastructure, experienced a vitality boost for the first time. However, between 2017 and 2018, the central region saw a significant rise in boredom due to over-commercialization, which led to scene homogenization (e.g., the dense presence of chain stores). At the same time, the peripheral areas experienced a decline in vitality due to halted renovations. By 2019–2020, although some local areas alleviated boredom through the introduction of cultural activities (e.g., art markets), the overall perception of boredom did not return to its earlier levels.

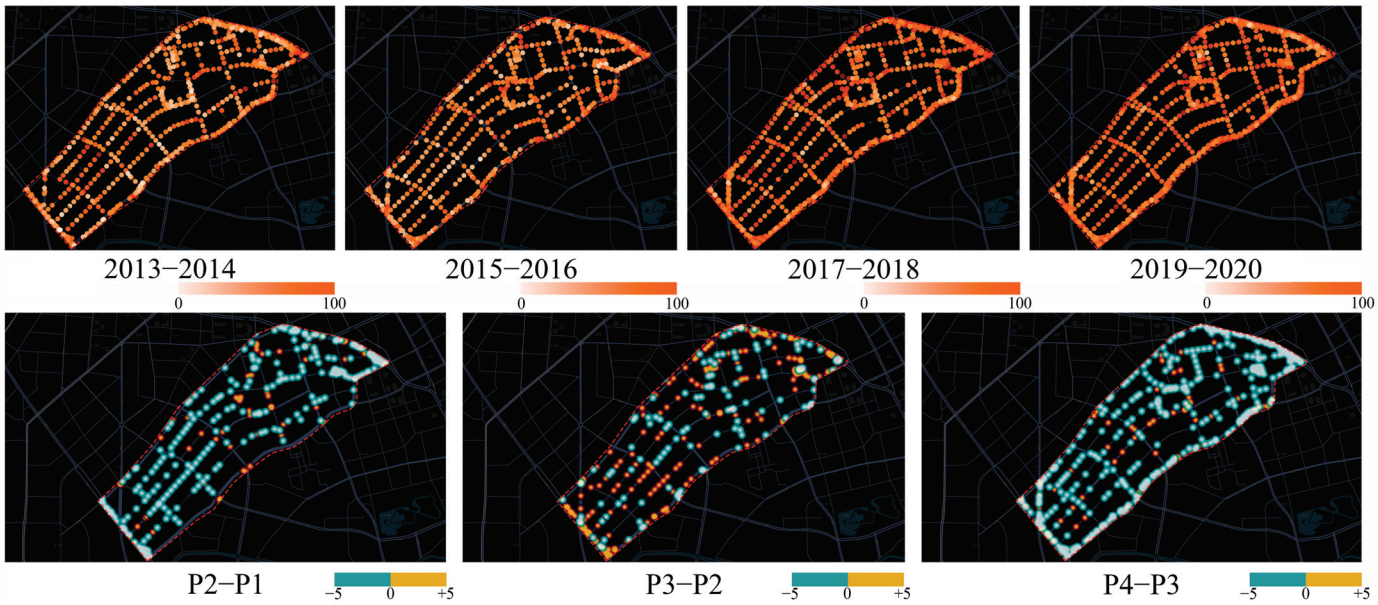


Figure 6. The changes in the boring emotional phase and the phase differences.

Spatial Differentiation: The difference analysis indicates that the intensification of boredom was concentrated in streets with a high degree of commercialization and single functionality, while areas dense with cultural facilities consistently maintained lower levels of boredom. This spatial differentiation reveals the suppressive effect of scene diversity and functional mix on boredom perception.

Driving Mechanisms

The evolution of boredom is primarily influenced by the following factors:

Negative Drivers: Scene Homogenization: Over-commercialization led to repetitive store types, weakening the appeal for exploration. Public Space Deactivation: The peripheral areas lacked continuous maintenance, causing some plazas and walkways to gradually fall into disuse.

Positive Suppressors: Cultural Activity Injection: Temporary markets and art exhibitions significantly enhanced interaction within the area. Mixed-Function Development: The transformation of historical buildings into "cultural + commercial" mixed-use spaces enriched the layers of the scene.

5.1.3. Depressing Emotion Perception

Spatiotemporal Evolution of Depressing Sentiment

Based on sentiment scoring analysis, the perception of depressing sentiment in the Wudadao area exhibited phase fluctuations between 2013 and 2020 (Figure 7). In the early stages (2013–2014), the overall depressing sentiment in the area was relatively low, with the open façades of historical buildings and continuous green belts creating a calming spatial atmosphere. From 2015 to 2016, as policies such as the "Comprehensive Management Measures for the Wudadao Area in Heping District (Trial)" promoted the optimization of the pedestrian system and green space, the perception of depressing sentiment further decreased, particularly in the central area, where street widening and the addition of public spaces led to significant improvements. However, between 2017 and 2018, certain areas saw a significant rise in depressing sentiment due to high-density commercial development (e.g., newly built high-rise hotels) and the prolonged presence of construction barriers, which enhanced spatial enclosure. By 2019–2020, the removal of temporary barri-

ers and the optimization of building setbacks alleviated some of the depressing sentiment, but certain narrow streets still maintained a high level of depressing sentiment due to delayed renovations.

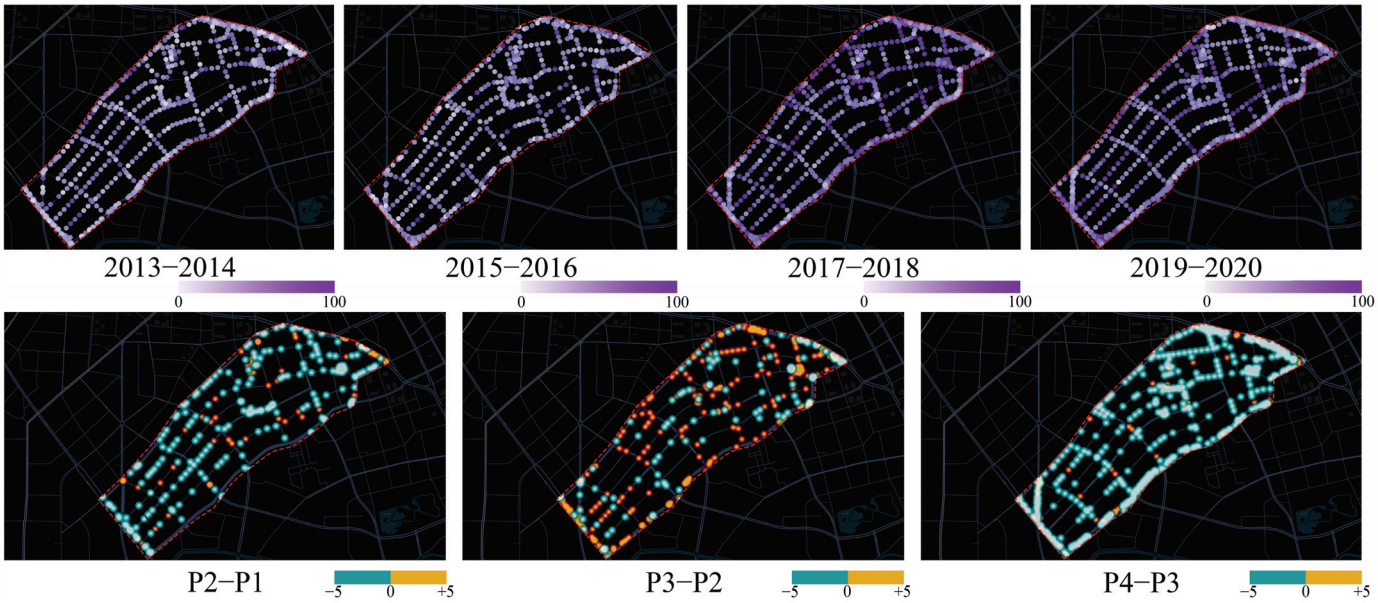


Figure 7. The changes in the depressing emotional phase and the phase differences.

Spatial Differentiation: The intensification of depressing sentiment was concentrated in streets with high building density and a lack of greenery, while open plazas and riverside areas consistently exhibited lower levels of depressing sentiment. This spatial differentiation reflects the role of spatial openness and visual permeability in alleviating depressing sentiment.

Driving Mechanisms

The evolution of depressing sentiment is primarily driven by the following factors:

Negative Drivers: Uncontrolled Building Density and Height: New high-rise buildings that surpassed the neighborhood's architectural guidelines intensified the street canyon effect. Temporary Construction Impact: Prolonged barriers and the accumulation of construction materials obstructed pedestrian sightlines and hindered movement, negatively affecting the experience.

Positive Suppressors: Improvement of Open Spaces: The removal of barriers and the addition of street greenery effectively enhanced spatial permeability. Optimization of Setback Design: The introduction of arcade-style colonnades and buffer zones in front of buildings alleviated the street's oppressive feeling.

5.1.4. Lively Emotion Perception

Spatiotemporal Evolution of Lively Sentiment

The perception of lively sentiment in the Wudadao area exhibited significant phase changes between 2013 and 2020 (Figure 8). In the early stages (2013–2014), the level of lively sentiment in the area was relatively low, with public activities concentrated around scattered historical building nodes, while the peripheral areas lacked vibrancy due to a single-function design. From 2015 to 2016, with the optimization of the pedestrian system and the introduction of cultural markets, lively sentiment significantly increased in the central area, enhancing street interaction and commercial activity. However, between

2017 and 2018, certain areas experienced a decline in lively sentiment due to excessive commercialization (e.g., the clustering of chain stores), leading to homogenized scenes. Additionally, the vitality in peripheral areas further decreased due to aging facilities. By 2019–2020, the introduction of seasonal art activities and community markets helped revive lively sentiment in some parts, but the overall level remained lower than the peak observed in the second stage.

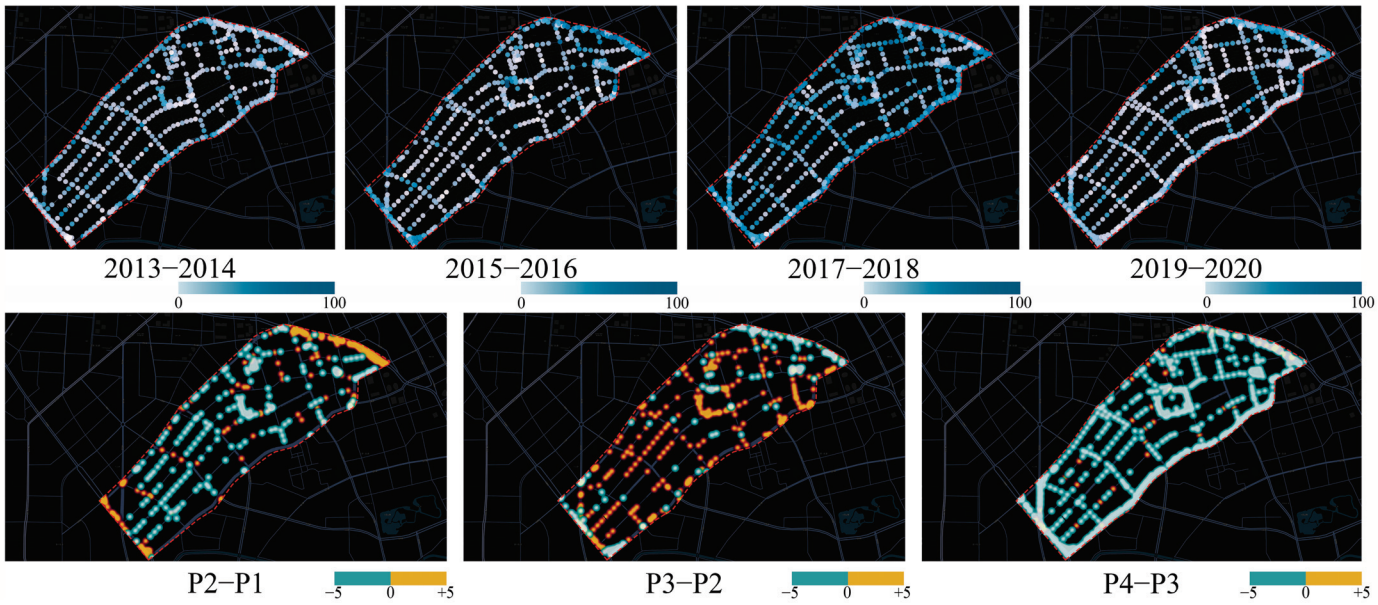


Figure 8. The changes in the lively emotional phase and the phase differences.

Spatial Differentiation: High-value lively sentiment areas were concentrated around cultural facilities and mixed-use districts (e.g., around Minyuan Square), while single-function streets (e.g., purely residential areas) consistently maintained low levels of lively sentiment. This differentiation reflects the key role that functional diversity and cultural activities play in fostering vibrancy.

Driving Mechanisms

The evolution of lively sentiment is influenced by the following factors:

Positive Drivers: Cultural markets, pedestrian-friendly design, and mixed-use development (e.g., "commercial + exhibition" spaces).

Negative Suppressors: Homogenization of business types, underutilization of public spaces, and the aging of peripheral area facilities.

5.1.5. Safety Emotion Perception

Spatiotemporal Evolution of Safety Sentiment

The perception of safety in the district showed a trend of "initial decline, followed by a rise and subsequent fluctuation" between 2013 and 2020 (Figure 9). In the early stage (2013–2014), the overall safety sentiment was high, as the low traffic flow in the historic district and the closed community management provided a stable environment. Between 2015 and 2016, a surge in tourist population and inadequate nighttime lighting led to a decrease in safety sentiment, especially in the peripheral backstreets and alleys. From 2017 to 2018, safety sentiment significantly improved due to the installation of surveillance equipment and the widening of sidewalks. However, between 2019 and 2020, safety

sentiment fluctuated again due to the excessive expansion of commercial activities in certain areas (e.g., street vendors occupying the streets).

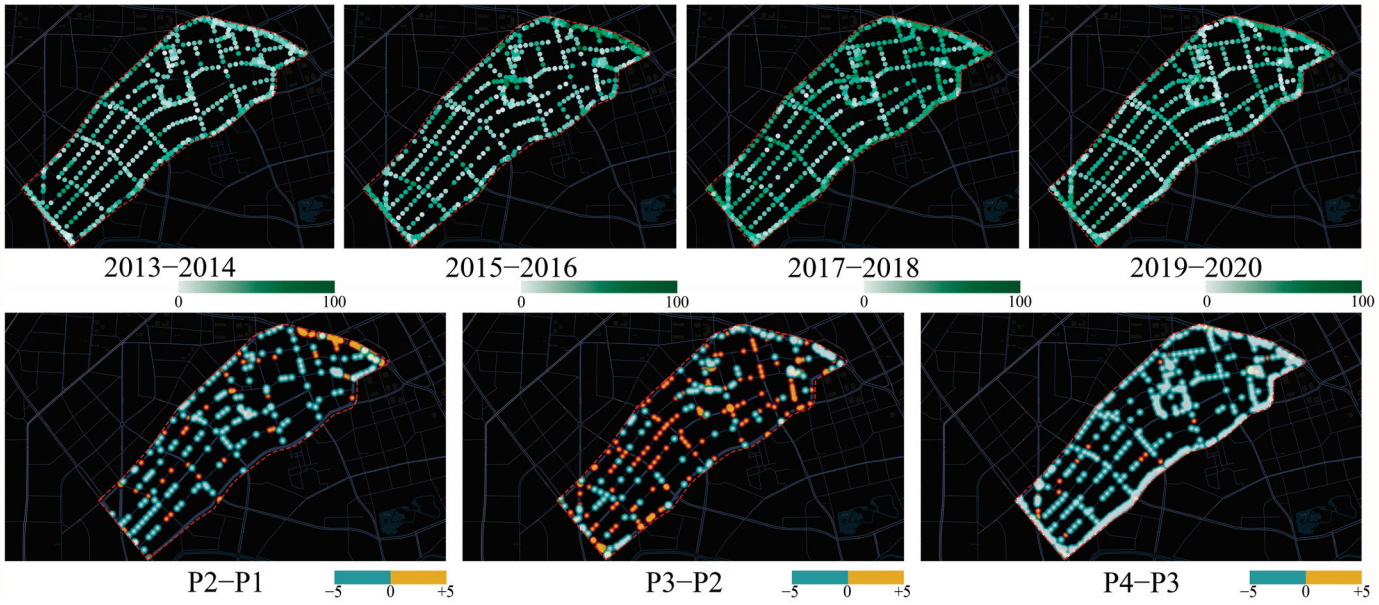


Figure 9. The changes in the safety emotional phase and the phase differences.

Spatial Differentiation: High-value safety areas were concentrated in strictly managed closed communities and main streets, while backstreets and temporary commercial zones consistently exhibited low safety values.

Driving Mechanisms

The fluctuation in safety sentiment is mainly influenced by the following factors:

Positive Drivers: Smart security systems, street lighting enhancements, and pedestrian–vehicle separation designs.

Negative Suppressors: Lack of management of street vendors and the single functionality of areas at night.

5.1.6. Wealthy Emotion Perception

Spatiotemporal Evolution of Wealthy Sentiment

The perception of wealth in the district exhibited characteristics of "central polarization and peripheral decline" between 2013 and 2020 (Figure 10). In the early stage (2013–2014), the distribution of wealthy sentiment was relatively balanced, with high-end residential areas mixed with ordinary communities. Between 2015 and 2016, the central area saw a sharp increase in wealthy sentiment due to the arrival of luxury stores and the high-end renovation of historical buildings, while the peripheral areas, lagging in facilities, began to show disparities. From 2017 to 2020, wealthy sentiment in the central area slowed down due to the over-concentration of commercial activities, leading to esthetic fatigue. In contrast, the peripheral areas saw a partial alleviation of the declining trend due to the introduction of a few boutique guesthouses.

Spatial Differentiation: High-value wealthy areas were concentrated around renovated colonial-style architectural complexes, while areas with ordinary residences remained consistently low in wealthy sentiment.

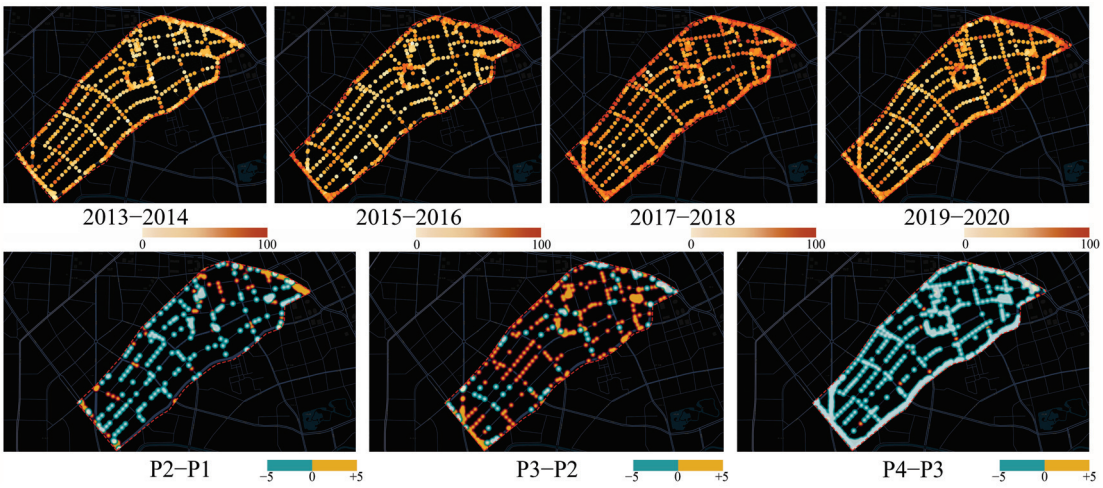


Figure 10. The changes in the wealth emotional phase and the phase differences.

Driving Mechanisms

The differentiation in wealthy sentiment was primarily driven by the following factors:

Positive Drivers: The introduction of high-end commercial spaces and the refined restoration of architectural features.

Negative Suppressors: Gentrification-induced community segregation and insufficient investment in peripheral areas.

5.1.7. Summary of Policy Documents

By analyzing the policy documents related to the Five Avenues area, it is evident that multiple policies have had a profound impact on the overall planning, urban management, environmental improvement, and the promotion of cultural tourism functions in the area. Notably, the "Comprehensive Management Measures for the Five Avenues Area in Heping District (Trial)" issued in 2014, as well as subsequent renovation mobilization and comprehensive improvement meetings, have provided a policy basis for the changes in the level of wealth in the Five Avenues district. The formation of the cultural historic district, the increase in commercial activities, and the optimization of infrastructure have all contributed to the enhancement of the wealthy sentiment in the central area. However, the economic stagnation in the peripheral areas reflects an ineffective allocation of resources. In terms of future policy design, based on the issues identified through the analysis of six emotional perceptions in Sections 5.1.1–5.1.6, we propose targeted optimization strategies for each emotion. The corresponding recommendations are summarized in Table 1.

Table 1. Policy recommendations.

Emotion	Corresponding Optimization Policy
Beautiful Emotion	Balance heritage preservation with equitable development; increase greenery; maintain pedestrian-friendly environments; minimize visual clutter; invest equitably in peripheral areas
Boring Emotion	Enhance functional diversity; activate peripheral micro-public spaces; regularly introduce diverse cultural activities and mixed-use developments
Depressing Emotion	Implement architectural controls on building density and height; manage construction dynamically (shorter barrier periods, transparent fencing); create open spaces and architectural setbacks; introduce small-scale spatial interventions (e.g., pocket parks, art installations)
Lively Emotion	Encourage community-driven initiatives; implement flexible zoning policies; support cultural markets and mixed-use spaces
Safety Emotion	Apply time-specific management strategies (e.g., pedestrian-only streets at night); enhance smart security and street lighting; introduce localized policing solutions (micro-police stations)
Wealthy Emotion	Promote inclusive development (retain affordable commercial options); establish equitable resource distribution and scenic compensation mechanisms for peripheral areas

5.1.8. Summary of Six Types of Sentiment

In the study of the six types of sentiment, we analyzed the distribution characteristics and evolution trends of different sentiments in different stages, conducted differential analysis, identified areas with significant changes, and analyzed the reasons behind those changes. It is clear that the introduction and implementation of planning policies play a crucial role in improving the spatial quality of historic districts. These policies have had a positive impact on beauty, liveliness, wealthy sentiment, and safety, while also inhibiting the emergence of depressing and boring sentiments. However, uneven planning resource allocation and unreasonable arrangements within the area have had negative effects on the spatial quality of certain regions. A search for the keyword "Five Avenues" in the Tianjin Municipal Planning and Natural Resources Bureau reveals that planning policies were concentrated around 2015, which also explains why significant fluctuations in the six types of sentiment occurred in 2015–2016, the second phase. However, subsequent spatial planning and detailed architectural planning did not keep pace. Between April 2015 and March 2020, no planning documents specifically addressing the Five Avenues district were issued, leading to a decline in the overall spatial quality of the area. Naturally, the impact of the COVID-19 pandemic also cannot be underestimated, as it negatively affected perceptions of liveliness and safety.

5.2. Results of the "Emotion–Scene" Coupling Analysis Framwork

The above content only analyzed the regions and reasons for changes but did not conduct a detailed analysis of the specific content of these changes. In the following section, we will use the Places365-ResNet model to perform scene recognition on street view images in the study area that exhibited significant changes in sentiment scores. We will extract the coordinates of street view images with noticeable changes (where the absolute value of the difference between two adjacent stages is greater than five), and perform scene recognition on the images from different stages in the four cardinal directions. Based on different sentiment types, the recognition results will be classified and summarized. The specific categories are shown in Table 2 below.

Table 2. Classification.

Classification	Scenario Factors
Transportation facilities	Bus station/indoor, Subway station/platform, Railway station/platform, Airport terminal, Highway, Runway, Race track, Parking lot, Parking lot/outdoor, Parking garage/outdoor, Garage/outdoor, Lane
Recreation	Park, Playground, Skating rink/outdoor, Skating rink/outdoor, Ski resort, Beer garden, Picnic area, Promenade, Terrace, Zen garden, Market/outdoor, Arcade
Residential area	Residential area, Apartment building/outdoor, Luxury house, Ordinary house, Courtyard, Roof garden, Balcony/outdoor, House, Inn/outdoor
Public facilities	Atrium/public, Hospital, Library/outdoor, Campus, Fire station, Fire exit, Prison, Prison cell, Embassy
Commercial area	Repair shop, Gas station, Fast food restaurant eatery/outdoor, Department store/outdoor, Storefront, Ticket booth, Restaurant/Outdoor restaurant terrace, Telephone booth
Industry and Infrastructure	Industrial area, Construction site, Building façade, Car factory, Car showroom, Motel, Dam, Canal/city, Server room, Lock, Lock chamber, Loading dock, Barn door, Drying room, Stable, Slum, Tree house, Hunting lodge/outdoors

Using the classification in the table above, the visualization and analysis of dynamic scene recognition results for different emotions within the study area are presented as follows.

5.2.1. Beautiful Driving Factors

Analysis of the Driving Scenes for the Emotion of Beauty

Based on the results of scene recognition (Figure 11), the dynamic changes in the sense of beauty in the Wudadao area are significantly associated with the adjustments in functional scenes. The study finds that the continuous expansion of public cultural facilities is the core driver of the enhancement of the sense of beauty. The addition of high-value scenes such as libraries and art galleries in historic districts, along with the collaborative design of building facade restoration and surrounding greening, has not only strengthened the cultural imagery but has also significantly increased visual appeal. For example, the renovation project of the art museum on the west side of Minyuan Square, which preserved the colonial-style arcade and added a glass curtain wall atrium, successfully integrated historical and modern esthetics, becoming a typical case of beauty enhancement.

The optimization of residential scenes is also crucial. The restoration of traditional courtyards and low-rise residences, combined with the moderate development of high-end apartments, injects modern living esthetics while retaining the continuity of historical styles. This type of renovation balances protection and renewal needs, alleviating the tendency for the district to become static. The improvement of transportation scenes has been achieved through the landscape design of infrastructure (such as green plant walls and artistic paving), reducing the visual abruptness of traditional facilities. However, the over-concentration of parking lots and highways has led to the homogenization of certain areas, with the eastern section of Chongqing Road consistently scoring lower than the average for its beauty due to the high proportion of parking lots.

The adjustments in commercial and leisure scenes show a dual impact on the sense of beauty. Initially, the functional positioning of commercial facilities gradually shifted toward esthetics and social value, with additions like small restaurants and restaurant terraces enriching the living atmosphere. However, excessive commercialization (such as clustering of chain brands) has led to the homogenization of scenes, weakening the appeal of exploration. In the leisure scenes, parks and promenades, as high-quality public spaces, have always been an important part of the sense of beauty, but insufficient subsequent maintenance has resulted in a decline in the continuity of ecological and cultural landscapes.

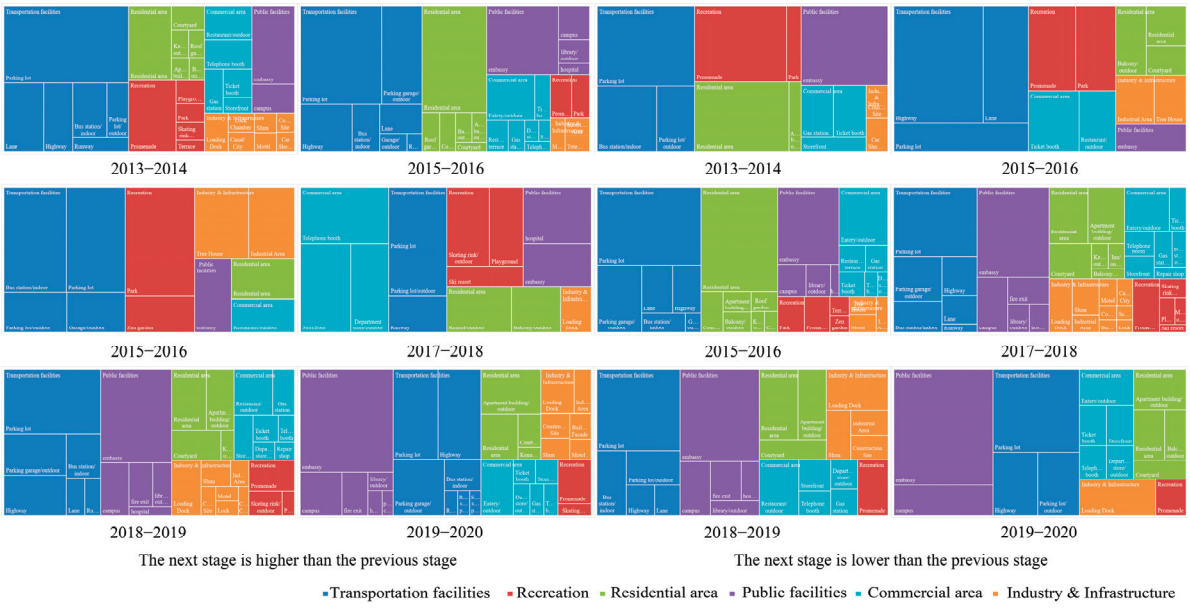


Figure 11. The dynamic recognition results of the beautiful emotion.

Planning Insights

Sustainable enhancement of the sense of beauty requires attention to the dynamic balance of scene functions:

Limit the single-function expansion: Control the proportion of transportation and industrial facilities through planning guidelines to avoid visual fragmentation.

Strengthen the cultural-leisure network: Embed small parks and exhibition galleries in the peripheral areas to address the "center-periphery" differentiation.

Conceal infrastructure: Employ underground parking lots and landscape shielding designs to balance functional and esthetic needs.

5.2.2. Boring Driving Factors

Analysis of the Driving Scenes for the Emotion of Boring

The spatial–temporal differentiation of the sense of boredom in the Wudadao area shows a significant association with the adjustments in functional scenes (Figure 12). The study finds that scene homogenization is the core factor contributing to the intensification of boredom. Between 2015 and 2016, the introduction of new walkways and small plazas briefly enhanced the vitality of the area, but later excessive commercialization led to the concentrated distribution of chain stores, which weakened the freshness of exploration. For example, the eastern section of Munan Road had a sustained higher boredom score than the district average from 2017 to 2020 due to the concentration of similar retail establishments, reflecting the negative impact of single-function spaces on spatial attraction.

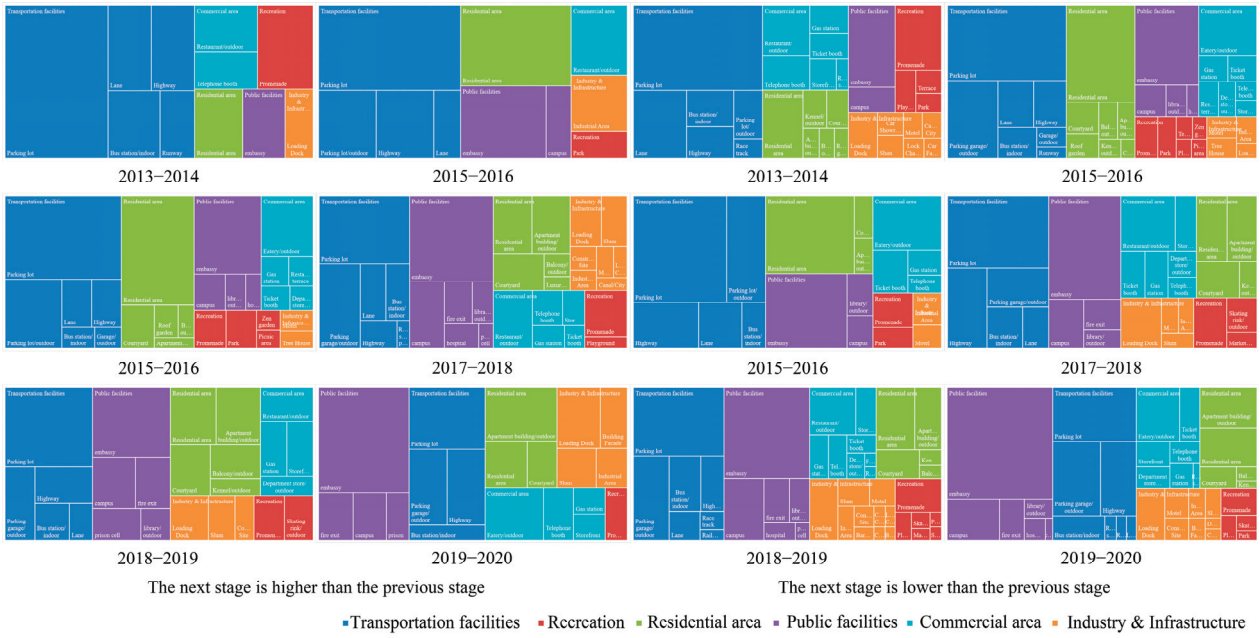


Figure 12. The dynamic recognition results of the boring emotion.

The inactivity of residential and public scenes further exacerbated the sense of boredom. Early courtyards and community squares maintained basic vitality through spontaneous activities (such as markets and tea gatherings), but as some squares became abandoned due to lack of maintenance, their social function significantly declined. At the same time, delayed residential renovations in peripheral areas failed to meet modern living demands, exacerbating the tendency for scenes to become static. In contrast, the introduction of temporary cultural markets and art exhibitions, through short-term scene activation,

provided partial relief to the boredom, but the lack of a long-term supply mechanism made the effects unsustainable.

The layout contradiction in transportation and industrial scenes is also crucial. Although the optimization of metro stations and walkways improved accessibility, the over-concentration of parking lots and loading docks led to functional stagnation in certain areas. For instance, the western section of Chongqing Road, due to frequent freight vehicle traffic and temporary storage piles, showed a significant positive correlation between scene disorder and boredom.

Planning Insights

To systematically reduce boredom, it is necessary to focus on scene diversity and functional mix:

Control of business type proportions: Limit the density of single-business types through district guidelines and encourage mixed functions such as "culture + commerce".

Activation of small spaces: Transform idle squares into community markets or open-air theaters, incorporating daily activities led by residents.

Dynamic scene supply: Establish a collaborative mechanism for seasonal art activities (such as the Autumn Creative Culture Week) and fixed cultural IPs (such as monthly intangible cultural heritage performances) to ensure sustained vitality.

5.2.3. Depressing Driving Factors

Analysis of the Driving Scenes for the Emotion of Depressing

He spatiotemporal differentiation of the depressing feeling in the Five Avenues District is closely related to adjustments in spatial form and scene functions (Figure 13). The study found that high-density development and enclosed scenes are the main driving factors for the intensification of the depressing feeling. From 2015 to 2016, the district briefly improved spatial permeability by removing walls and adding street green spaces. However, after 2017, newly constructed high-rise hotels broke the original esthetic control requirements, leading to a prominent street canyon effect with a significant reduction in visible sky coverage in some areas, thereby notably enhancing the visual sense of oppression.

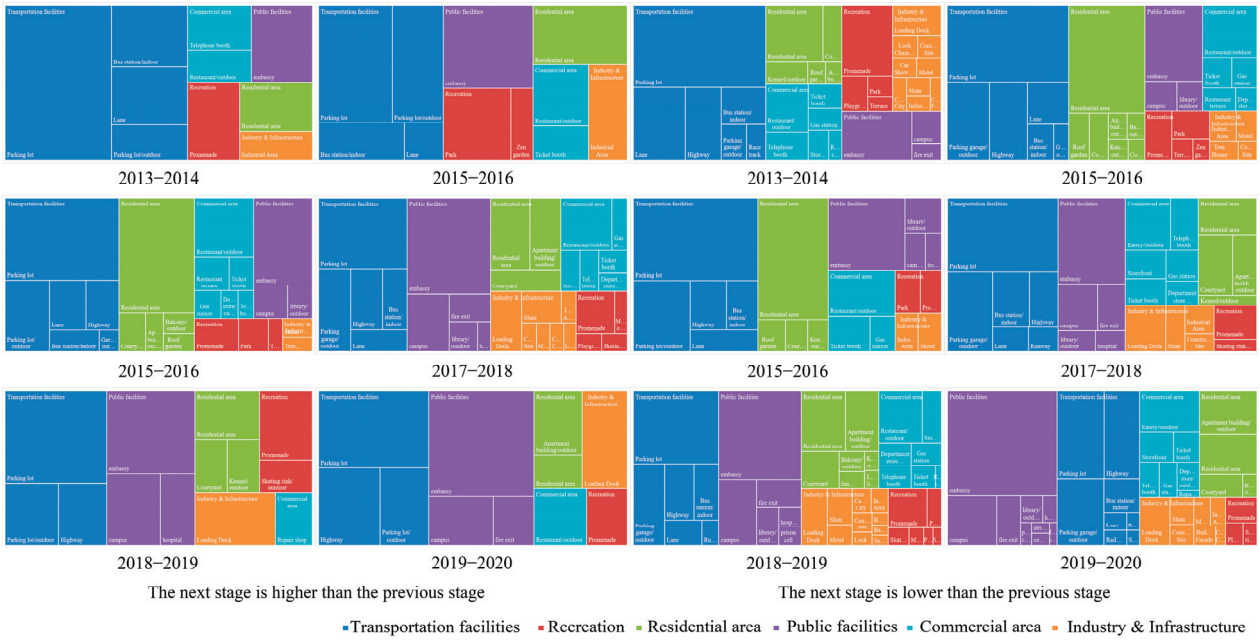


Figure 13. The dynamic recognition results of the depressing emotion.

The impact of temporary construction scenes cannot be ignored either. During the metro station construction period, long-term barriers blocked pedestrian flow and interrupted visual continuity, while the accumulation of construction materials further exacerbated the scene disorder. In contrast, improvements in open spaces and setback design optimizations alleviated the sense of depressing in certain areas by enhancing visual permeability.

The imbalanced distribution of green spaces amplifies spatial disparities. In the central areas, the integration of vertical greening and pocket parks has enhanced green coverage, while in the peripheral areas, the lack of maintenance and the degradation of vegetation have led to insufficient green coverage. Such spatial differentiation directly impacts psychological comfort.

Planning Insights

The systematic regulation of the depressing emotion requires three types of spatial interventions:

Rigid esthetic control: Strictly limit building height ($\leq$18 m) and floor-to-area ratio ($\leq$65%) to ensure the preservation of historic district scales.

Dynamic construction management: Use transparent barriers and phased construction strategies, reducing the enclosure period to less than three months.

Ecological compensation for peripheral areas: Ensure a green coverage rate of $\geq$25% through vertical greening and the transformation of abandoned land.

5.2.4. Lively Driving Factors

Analysis of the Driving Scenes for Lively Emotion

The spatiotemporal evolution of liveliness in the Wudadao area is significantly correlated with adjustments in functional scenes (Figure 14). The study reveals that the expansion and diversification of public facilities are the core drivers of liveliness. The continuous addition of high-value scenes such as libraries and art galleries, coupled with architectural esthetics and open spaces, has strengthened the cultural atmosphere and social vitality. For instance, the art gallery on the west side of Minyuan Square, through its integration of a glass curtain wall atrium and colonial-style arcades, has become a hotspot for interaction between residents and visitors.

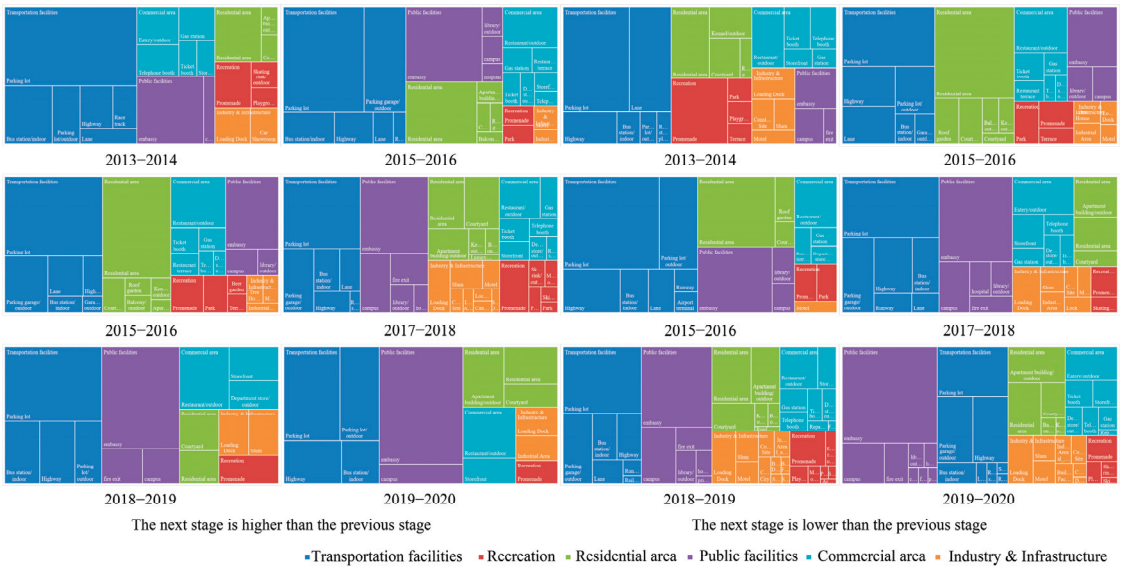


Figure 14. The dynamic recognition results of the lively emotion.

The optimization of residential scenes injects sustained momentum into liveliness. The combination of traditional courtyard restoration and high-end apartment development has enhanced the interactivity and visual appeal of the living environment while retaining the historical style. The incorporation of rooftop gardens and balcony landscapes balances static preservation with dynamic living needs, alleviating the tendency toward functional stagnation in the district.

The diversification of recreational and entertainment scenes plays a crucial role in enhancing liveliness. The corridor, as a fundamental social space, ensures continuity and daily vibrancy. Later additions, such as markets and open-air theaters, further enrich the dynamic experience. However, an overreliance on short-term activities leads to fluctuating vitality, and the absence of long-term cultural intellectual properties diminishes the sustained appeal.

Mechanisms Driving the Decline of Liveliness:

The weakening of transportation facilities significantly impacts liveliness. The reduction in parking lots and roadways has led to the loss of core dynamic scenes. Although the new subway stations have compensated for part of the functionality, their insufficient landscaping (such as a lack of green plant barriers) has failed to effectively maintain the original vitality. Although the commercial area has enhanced the living atmosphere through restaurant terraces, the excessive concentration of chain brands has led to homogeneity, reducing the interest in exploration.

The contraction of living-oriented scenes in residential areas further exacerbates the issue. The growth in the number of high-end apartments has not offset the reduction in traditional courtyards and community markets, thus compressing spaces for spontaneous resident activities. In the realm of public facilities, the increase in purely functional scenes such as fire escape routes, coupled with a lack of cultural and sports facilities, has created an imbalance in dynamism.

Planning Insights

Functionality and Mixed-Use Orientation: Guide regulations to limit the proportion of single-use business types (e.g., chain stores $\leq$ 20%) and encourage "culture + commerce" mixed scenes.

Activation of Small Micro-Spaces: Transform idle corner spaces into community gardens or street theaters, ensuring spaces for daily interaction.

Long-Term Vitality Supply: Establish a dynamic mechanism combining fixed cultural intellectual properties (e.g., seasonal themed markets) with flexible activities.

5.2.5. Safety Driving Factors

Analysis of Driving Scenes for Safety Perception

The safety perception in the Five Avenues District exhibited fluctuating evolution between 2013 and 2020 (Figure 15), with its changes closely related to adjustments in functional scenes and spatial management. The study found that the expansion of residential areas and the optimization of public facilities are the core driving forces behind the improvement of safety perception. From 2015 to 2016, the addition of fencing, improvements in community greening, and upgrades to nighttime lighting significantly increased residents' trust in their living environment. The maintenance and restoration of historic buildings further strengthened the continuity of the district's character, preserving its historical scale while improving emergency evacuation conditions.

The standardized management of public spaces played a key role in enhancing safety perception. From 2017 to 2020, through the optimization of pedestrian systems and en-

hanced public area surveillance, both the physical safety and psychological sense of safety in the district were improved simultaneously.

However, the decline in safety perception is mainly attributed to the degradation of two types of scenes:

Decline in Traffic Facilities: The reduction in parking lots and bus stops led to decreased convenience for residents' travel, and in some areas, the delayed management of alternative facilities exacerbated traffic chaos and safety anxiety.

Deactivation of Public Spaces: The reduction in cultural spaces such as libraries and corridors weakened social interaction frequencies, indirectly affecting community cohesion and safety perception.

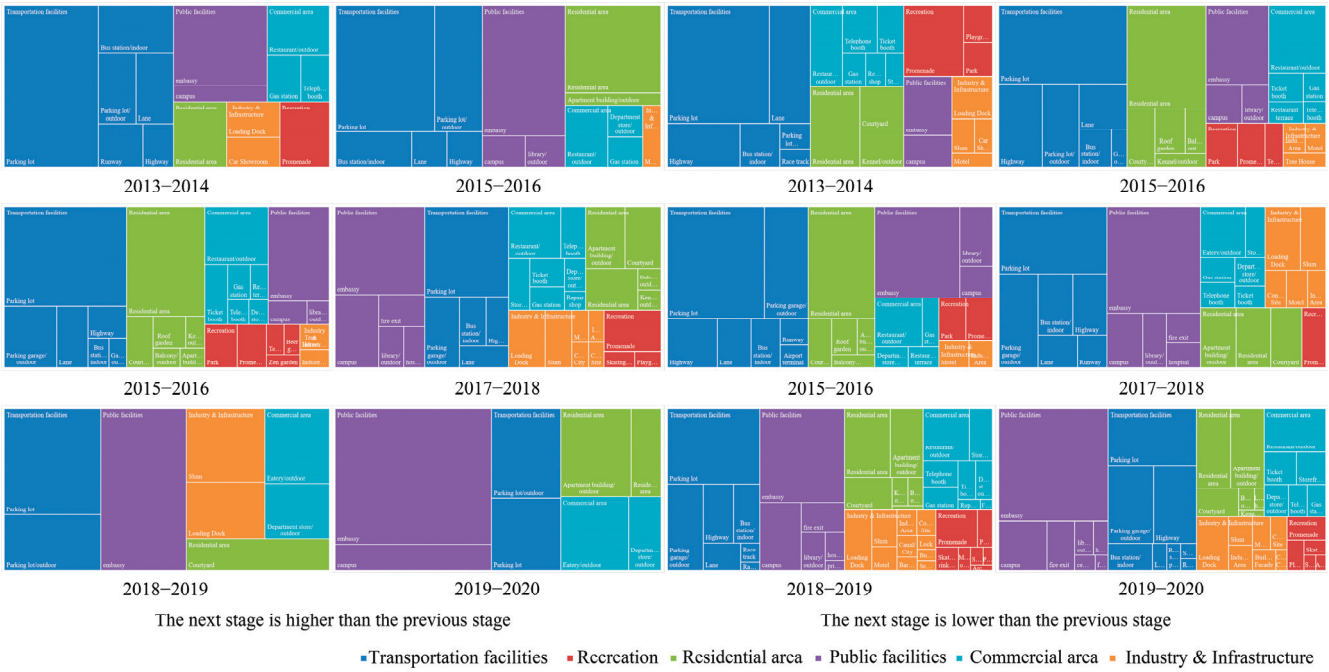


Figure 15. The dynamic recognition results of the safety emotion.

Planning Insights

Balanced Facility Distribution: Ensure comprehensive coverage of basic services (such as bus stops and police stations) through the "15 min living circle" planning.

Dynamic Safety Monitoring: Utilize intelligent security systems for real-time monitoring in high-density areas and optimize emergency response capabilities.

Community Participation in Governance: Enhance residents' sense of belonging by collaborating through community councils to manage small-scale spaces (e.g., alleyway greening, lighting maintenance).

5.2.6. Wealthy Driving Factors

Analysis of Driving Scenes for Wealthy Perception

The perception of wealth in the Five Avenues District exhibited an "urban core polarization and peripheral decline" evolution from 2013 to 2020 (Figure 16). The study found that the concentrated development of high-end scenes was the core driving force behind the enhancement of wealthy perception. From 2015 to 2016, the establishment of luxury stores and high-end renovations of historic buildings significantly improved the quality image of the central area. These renovations, through detailed facade restoration and functional upgrades, reinforced the district's rarity and cultural capital value.

The optimization of transportation facilities provided indirect support for the wealthy perception. The landscaped designs of parking lots and metro stations (e.g., plant-enclosed walls, artistic paving) enhanced the modern feel and convenience of the area, while the continuity of the pedestrian system (e.g., newly added tree-lined walkways) further improved the accessibility of high-end consumption scenes. The diversification of leisure and entertainment spaces (e.g., corridors, cafes) improved the quality of social spaces and conveyed a shift towards a more high-end lifestyle.

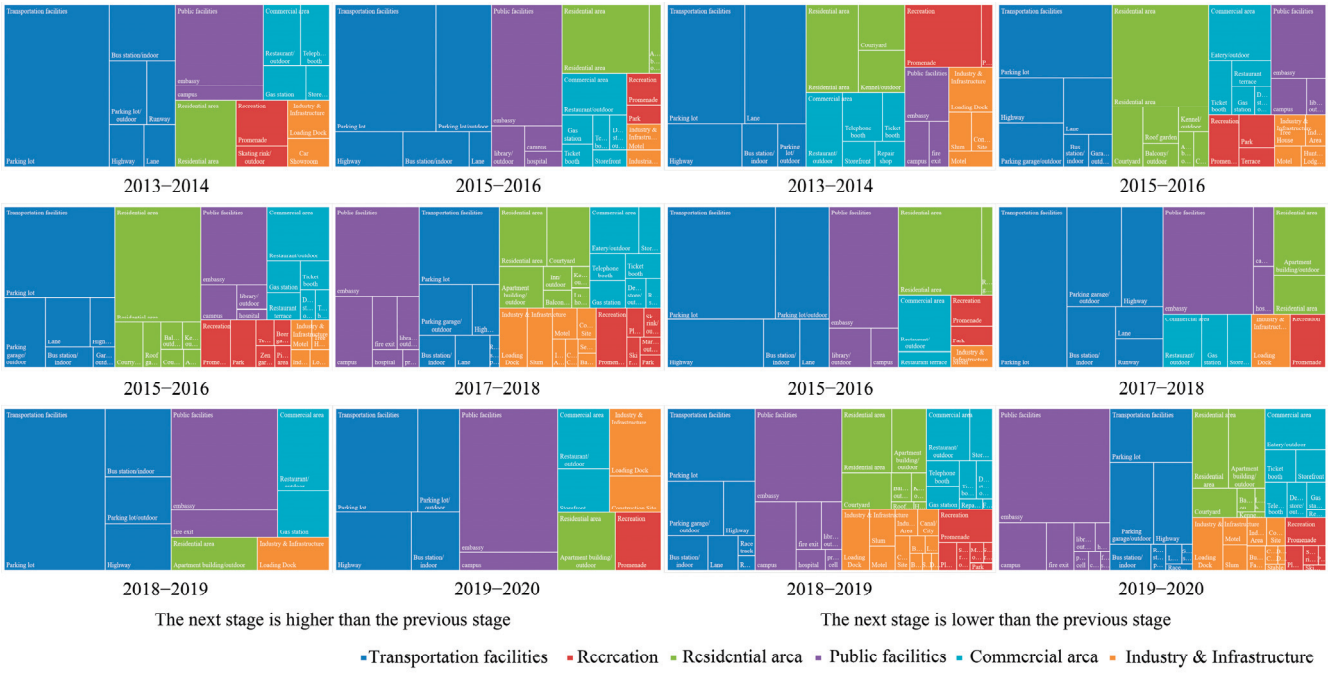


Figure 16. The dynamic recognition results of the wealth emotion.

Mechanisms Driving the Decline in Wealthy Perception:

The decline in the peripheral areas is the main cause of the differentiation in wealthy perception. After 2017, the central area suffered from esthetic fatigue due to excessive commercial concentration, with diminishing returns on resource investments. Meanwhile, the peripheral areas faced a reduction in transportation facilities (e.g., parking lots) and public services, exacerbating the decline in living convenience. The reduction in the number of residential areas further weakened community stability, especially with the disappearance of traditional courtyards, leading to the "gentrification" of living spaces, which reduced ordinary residents' sense of access to quality spaces.

Planning Insights

Balanced Development Strategy: Support small-scale updates in peripheral areas (e.g., historical residential renovation subsidies) through a "landscape compensation fund".

Mixed-use Control: Retain 20% affordable businesses in high-end commercial areas to ensure social inclusivity.

Long-term Quality Maintenance: Establish a system for regular facade maintenance and public space management to avoid short-term development trends.

6. Summary and Outlook

6.1. Main Findings of the Study

This research provides a systematic examination of the dynamic evolution mechanisms of spatial quality in historic districts through a case study of Tianjin's Five Avenues. The findings indicate that spatial quality evolves through complex interactions among policy interventions, scene modifications, and emotional perceptions. Specifically, the "Comprehensive Management Measures" policy implemented in 2014 significantly boosted spatial perceptions of beauty and safety by promoting infrastructure development and heritage conservation. However, the analysis also reveals persistent challenges. The depressing emotion and boring emotion are closely linked to factors such as monotonous commercial environments, underused public spaces, and construction-related disruptions. Peripheral areas continue to suffer from resource under-allocation and slower development, weakening emotional perceptions of beauty, safety, and prosperity in those zones. Importantly, the absence of new planning policies between 2015 and 2020, combined with the impact of the COVID-19 pandemic, contributed to a decline in overall spatial quality and emotional vitality, particularly in the second phase (2015–2016). These findings underscore the need for continuous, equitable, and fine-grained policy intervention to sustain emotional well-being and spatial quality in historic districts over time.

The study highlights three primary drivers influencing spatial quality evolution. First, the careful preservation and esthetic enhancement of historical architecture and public spaces foster emotional identity and improve visual quality. Second, scene diversity and mixed functionalities substantially enhance the vitality and liveliness of urban spaces. Conversely, excessive commercialization and repetitive scene elements negatively influence emotional experiences by increasing boredom and feelings of oppression. Lastly, reduced transportation infrastructure and the neglected maintenance of peripheral areas exacerbate spatial inequalities.

Methodologically, the proposed dynamic "spatiotemporal imagery–emotion–scene" evaluation framework effectively addresses limitations inherent in traditional static evaluations, providing a robust analytical tool for continuous urban space quality monitoring. This approach not only facilitates a deeper understanding of urban space dynamics but also supports evidence-based policymaking for sustainable tourism and heritage preservation initiatives.

6.2. Limitations of the Study

The conclusions of this study are primarily based on a single case of the Five Avenues area in Tianjin, and the generalizability of these conclusions should be approached with caution. Although this area holds research value as a typical representative of modern concession architecture, historic districts with different cultural backgrounds (e.g., ancient water towns in the Jiangnan region or industrial heritage districts) may exhibit distinct evolutionary paths due to differences in preservation policies and functional positioning. For instance, the quality evolution of traditional villages may rely more on community autonomy than planning interventions, while industrial heritage areas are driven by both technical restoration and the creative economy. This necessitates future research that validates the transferability of the theory through cross-regional comparisons.

While the emotional perception model can capture the public's intuitive response to streetscapes, its sensitivity to negative emotions (such as depressing or boring feelings) is insufficient, which may weaken the accuracy of analysis for complex social emotions. Additionally, the annotated data used to train the model still contains subjective biases—different cultural groups may have drastically different emotional responses to the same scene. More-

over, situational factors such as season, weather, and other environmental elements have not been incorporated into the evaluation framework, further limiting the stability of the results. Future research should combine physiological sensors (e.g., eye-tracking, heart rate monitoring) with semantic analysis technologies to construct a framework for emotional assessment that integrates both subjective and objective aspects.

The multidimensionality of spatial quality also presents an important limitation of this study. Although streetscape imagery can reflect visual and emotional dimensions, it is difficult to capture the composite impact of sensory experiences such as sound environments (e.g., traffic noise, market chatter) or odors (e.g., plant fragrance, cooking fumes) on spatial perception. For example, the visual appeal of Minyuan Square may be significantly diminished by the diffusion of cooking fumes from nearby restaurants. Such multisensory conflicts should be analyzed more deeply through interdisciplinary methods (e.g., wearable device monitoring).

On the technical front, the "black box" nature of deep learning models results in a lack of interpretability for the driving mechanisms. Although scene recognition technologies have revealed correlations between functional layout and emotional feedback, the causal pathways between the two (e.g., "why does increased greenery reduce feelings of depression") still need to be verified using traditional methods such as spatial syntax and behavioral annotations. Furthermore, the scale and quality of annotated data used for model training limit its generalizability to small-scale, highly heterogeneous districts, making the development of lightweight adaptive models an important direction for future breakthroughs.

6.3. Future Research Directions

The findings of this study provide a foundational framework for the dynamic analysis of built environment spatial quality in historic districts. However, further theoretical refinement and practical application still require multidimensional expansion. Firstly, cross-regional and cross-cultural comparative studies urgently need to be promoted. The diversity of historic districts in China (e.g., Jiangnan water towns, industrial heritage, and minority settlements) offers a natural laboratory to verify the universality of evolutionary mechanisms. For example, the spatial quality of ancient water towns in Jiangnan may rely more on water systems and community autonomy, while industrial heritage districts are driven by both technical restoration and the creative economy. By comparing the policy response patterns and emotional feedback differences, more adaptable planning theories can be distilled.

Secondly, the multisensory interaction mechanisms of spatial quality have not been fully revealed. While the visual analysis of streetscapes can capture explicit environmental features, the modulation effects of soundscapes (e.g., market noise, flowing water) and scentscapes (e.g., traditional food aromas, plant fragrances) on emotional experience cannot be ignored. Future research can combine wearable sensors with semantic segmentation technology to build a "visual–auditory–olfactory"-coupled evaluation model, analyzing the deeper impacts of multisensory conflicts (e.g., the offsetting effect of beautiful streetscapes and traffic noise) on spatial identity.

From a technical perspective, the transparency and adaptability of deep learning models need to be enhanced simultaneously. The development of dynamic quality simulation tools based on reinforcement learning can quantify the long-term effects of different planning scenarios (e.g., mixed-use, green space connectivity), providing a "policy testbed" for decision-makers. At the same time, the exploration of lightweight adaptive models will

enhance the analytical precision for small-scale, highly heterogeneous districts, advancing the methodology from "case validation" to "global simulation".

Lastly, spatial quality research needs to be deeply integrated into the sustainable development agenda. By linking with the United Nations Sustainable Development Goals (SDGs), a "quality enhancement—ecological resilience—social equity" synergistic pathway can be established. For example, embedding low-carbon materials and community co-governance elements in historic district renewal can ensure that spatial optimization simultaneously serves cultural heritage protection, carbon neutrality, and inclusive development, achieving the co-evolution of multidimensional values.

6.4. Conclusions

This study proposes an intelligent evaluation framework that integrates spatiotemporal street view imagery, affective perception modeling, and scene recognition to uncover the complex influences of policy interventions, environmental changes, and infrastructure conditions on spatial quality, and validates with Tianjin's Wudadao Historic District. The empirical findings indicate that targeted policy measures significantly enhance residents' emotional well-being, particularly in terms of esthetics, vibrancy, and perceived safety. However, they also reveal persistent disparities in spatial quality arising from uneven resource allocation.

Key insights suggest that the sustainable improvement of spatial quality in historic districts largely depends on the balanced preservation of cultural heritage, functional diversity, mixed-use recreational environments, and people-centered urban design principles. In contrast, excessive commercialization and spatial homogenization may undermine emotional resonance and lead to adverse outcomes, underscoring the necessity of refined scene management and equitable resource distribution.

Despite methodological innovations, this study acknowledges certain limitations, such as the cultural sensitivity of affective perception models and their adaptability across different socio-cultural contexts. Future research should incorporate multisensory environmental data and enhance model interpretability and adaptability to better accommodate the diverse historical settings of urban spaces.

Overall, the proposed intelligent evaluation framework not only advances the technological application of urban planning and design but also offers actionable insights for building resilient, equitable, and culturally vibrant built environments. It provides a practical means to bridge the gap between technological innovation and sustainable governance in the context of historical urban districts.

Author Contributions: Conceptualization, Y.L.; Methodology, Y.L.; Validation, B.Y.; Investigation, B.Y.; Resources, L.H.; Data curation, L.H.; Writing—original draft, Y.L.; Writing—review & editing, L.H.; Supervision, B.Y. All authors have read and agreed to the published version of the manuscript.

Funding: This research received no external funding.

Data Availability Statement: Due to the sensitive nature of certain data presented in this paper, the data are not being made publicly available for the time being. Researchers who are interested in accessing the experimental data may contact the corresponding author by email.

Conflicts of Interest: The authors declare no conflict of interest.

References

1. Go, H.; Kang, M. Metaverse tourism for sustainable tourism development: Tourism agenda 2030. *Tour. Rev.* **2023**, *78*, 381–394. [CrossRef]

2. Qianqian, Z.; Chengcai, T.; Ying, Z. Evaluation and Enhancement Model of the Development Potential of Green Tourism in Beijing's Ecological Conservation Area. *J. Resour. Ecol.* **2024**, *15*, 484–495. [CrossRef]
3. Encalada-Abarca, L.; Ferreira, C.C.; Rocha, J. Measuring tourism intensification in urban destinations: An approach based on fractal analysis. *J. Travel Res.* **2022**, *61*, 394–413. [CrossRef]
4. Ramkissoon, H. Perceived social impacts of tourism and quality-of-life: A new conceptual model. *J. Sustain. Tour.* **2023**, *31*, 442–459. [CrossRef]
5. Stessens, P.; Canters, F.; Huysmans, M.; Khan, A.Z. Urban green space qualities: An integrated approach towards GIS-based assessment reflecting user perception. *Land Use Policy* **2020**, *91*, 104319. [CrossRef]
6. Biljecki, F.; Ito, K. Street view imagery in urban analytics and GIS: A review. *Landsc. Urban Plan.* **2021**, *215*, 104217. [CrossRef]
7. Yu, X.; Her, Y.; Huo, W.; Chen, G.; Qi, W. Spatio-temporal monitoring of urban street-side vegetation greenery using Baidu Street View images. *Urban For. Urban Green.* **2022**, *73*, 127617. [CrossRef]
8. Hamim, O.F.; Ukkusuri, S.V. Towards safer streets: A framework for unveiling pedestrians' perceived road safety using street view imagery. *Accid. Anal. Prev.* **2024**, *195*, 107400. [CrossRef]
9. Liang, X.; Zhao, T.; Biljecki, F. Revealing spatio-temporal evolution of urban visual environments with street view imagery. *Landsc. Urban Plan.* **2023**, *237*, 104802. [CrossRef]
10. He, J.; Zhang, J.; Yao, Y.; Li, X. Extracting human perceptions from street view images for better assessing urban renewal potential. *Cities* **2023**, *134*, 104189. [CrossRef]
11. Nguyen, P.-Y.; Astell-Burt, T.; Rahimi-Ardabili, H.; Feng, X. Green space quality and health: A systematic review. *Int. J. Environ. Res. Public Health* **2021**, *18*, 11028. [CrossRef] [PubMed]
12. Amin, A. Collective culture and urban public space. *City* **2008**, *12*, 5–24. [CrossRef]
13. Lynch, K. *The Image of the City*; MIT Press: Cambridge, MA, USA, 1964.
14. Fleischmann, M.; Feliciotti, A.; Kerr, W. Evolution of urban patterns: Urban morphology as an open reproducible data science. *Geogr. Anal.* **2022**, *54*, 536–558. [CrossRef]
15. Zhou, H.; He, S.; Cai, Y.; Wang, M.; Su, S. Social inequalities in neighborhood visual walkability: Using street view imagery and deep learning technologies to facilitate healthy city planning. *Sustain. Cities Soc.* **2019**, *50*, 101605. [CrossRef]
16. Pike, A.; Béal, V.; Cauchi-Duval, N.; Franklin, R.; Kinossian, N.; Lang, T.; Leibert, T.; MacKinnon, D.; Rousseau, M.; Royer, J. 'Left behind places': A geographical etymology. *Reg. Stud.* **2024**, *58*, 1167–1179. [CrossRef]
17. Machicao, J.; Specht, A.; Vellenich, D.; Meneguzzi, L.; David, R.; Stall, S.; Ferraz, K.; Mabile, L.; O'brien, M.; Corrêa, P. A deep-learning method for the prediction of socio-economic indicators from street-view imagery using a case study from Brazil. *Data Sci. J.* **2022**, *21*, 6. [CrossRef]
18. Fan, Z.; Zhang, F.; Loo, B.P.; Ratti, C. Urban visual intelligence: Uncovering hidden city profiles with street view images. *Proc. Natl. Acad. Sci. USA* **2023**, *120*, e2220417120. [CrossRef] [PubMed]
19. He, L.; Páez, A.; Liu, D. Built environment and violent crime: An environmental audit approach using Google Street View. *Comput. Environ. Urban Syst.* **2017**, *66*, 83–95. [CrossRef]
20. Li, Y.; Peng, L.; Wu, C.; Zhang, J. Street View Imagery (SVI) in the built environment: A theoretical and systematic review. *Buildings* **2022**, *12*, 1167. [CrossRef]
21. Chen, C.; Li, H.; Luo, W.; Xie, J.; Yao, J.; Wu, L.; Xia, Y. Predicting the effect of street environment on residents' mood states in large urban areas using machine learning and street view images. *Sci. Total Environ.* **2022**, *816*, 151605. [CrossRef]
22. Sangers, R.; van Gemert, J.; van Cranenburgh, S. Explainability of Deep Learning models for Urban Space perception. *arXiv* **2022**, arXiv:2208.13555.
23. Zhou, B.; Lapedriza, A.; Khosla, A.; Oliva, A.; Torralba, A. Places: A 10 million image database for scene recognition. *IEEE Trans. Pattern Anal. Mach. Intell.* **2017**, *40*, 1452–1464. [CrossRef]
24. Dubey, A.; Naik, N.; Parikh, D.; Raskar, R.; Hidalgo, C.A. Deep learning the city: Quantifying urban perception at a global scale. In Proceedings of the Computer Vision–ECCV 2016: 14th European Conference, Amsterdam, The Netherlands, 11–14 October 2016; pp. 196–212.
25. Wei, H.; Zhou, M.; Kang, S.; Zhang, J. Sense of place of heritage conservation districts under the tourist gaze—Case of the Shichahai heritage conservation district. *Sustainability* **2022**, *14*, 10384. [CrossRef]
26. Zhang, Y.; Han, Y. Vitality evaluation of historical and cultural districts based on the values dimension: Districts in Beijing City, China. *Herit. Sci.* **2022**, *10*, 137. [CrossRef]
27. Zhu, X.; Chiou, S.-C. A study on the sustainable development of historic district landscapes based on place attachment among tourists: A case study of Taiping old street, Taiwan. *Sustainability* **2022**, *14*, 11755. [CrossRef]

28. Baloch, Q.B.; Shah, S.N.; Iqbal, N.; Sheeraz, M.; Asadullah, M.; Mahar, S.; Khan, A.U. Impact of tourism development upon environmental sustainability: A suggested framework for sustainable ecotourism. *Environ. Sci. Pollut. Res.* **2023**, *30*, 5917–5930. [CrossRef]
29. Wang, L.; Han, X.; He, J.; Jung, T. Measuring residents' perceptions of city streets to inform better street planning through deep learning and space syntax. *ISPRS J. Photogramm. Remote Sens.* **2022**, *190*, 215–230. [CrossRef]
30. Chen, Y.; Ren, X.; Xu, X.; Wang, R.; Xu, Y. Evaluation of Living Environment Quality in Urban Residential Areas under the Concept of Urban Renewal—A Case Study of Binjiang District, Hangzhou, China. *Sustainability* **2023**, *15*, 14104. [CrossRef]
31. Liu, X. The effects of commercialisation on urban heritage in Tianjin: A study of citizens' livelihood in the Five Avenues (Wudadao) historical district. *Built Herit.* **2024**, *8*, 42. [CrossRef]
32. Lu, Y. Using Google Street View to investigate the association between street greenery and physical activity. *Landsc. Urban Plan.* **2019**, *191*, 103435. [CrossRef]

Disclaimer/Publisher's Note: The statements, opinions and data contained in all publications are solely those of the individual author(s) and contributor(s) and not of MDPI and/or the editor(s). MDPI and/or the editor(s) disclaim responsibility for any injury to people or property resulting from any ideas, methods, instructions or products referred to in the content.

buildings

MDPI

Article

Analysis of Airflow Dynamics and Instability in Closed Spaces Ventilated by Opposed Jets Using Large Eddy Simulations

Congcong Wang [1], Yu Li [1], Pengchao Ding [1], Hongbing Chen [1,*], Yan Zhang [1] and Yongjie Xing [2]

[1] School of Environment and Energy Engineering, Beijing University of Civil Engineering and Architecture, Beijing 100044, China; wangcongcong@bucea.edu.cn (C.W.); liyx202411@163.com (Y.L.); dinpencho@163.com (P.D.); zhangyan01272023@163.com (Y.Z.)

[2] Institute of Resource and Environment, Beijing Academy of Science and Technology, Beijing 100044, China; xingyongjie@126.com

* Correspondence: chenhongbing@bucea.edu.cn

Abstract: This study quantitatively analyzes the effects of various ventilation parameters on airflow stability in confined spaces ventilated by opposed jets, a common configuration in high-density settings. Using large eddy simulations (LES), we evaluate how changes in supply velocity, airflow configuration, enclosure geometry, and thermal gradients influence airflow dynamics. Findings show that higher supply velocities, up to 1.92 m/s, lead to a measurable increase in oscillation period (from 7.7 s to 11.3 s) and reduce small-scale flow disturbances. The free jet configuration exhibits higher oscillation amplitude and a more disordered structure compared to the attached jet, resulting in uneven airflow distribution. Aspect ratio has a pronounced effect, with increased ratios extending oscillation periods from 10.6 s to 18.1 s and intensifying turbulence. Thermal gradients, with floor temperatures rising from 15 °C to 35 °C, and the oscillation period are increased, further dispersing airflow and reducing stability. Phase space reconstruction and power spectral analysis provide quantitative benchmarks for oscillation frequencies and patterns, correlating velocity time series with airflow structural changes. The findings from this study can serve as a foundation for future research on thermal comfort and air quality management in enclosed environments.

Keywords: enclosed space; large eddy simulation; opposed jets; airflow field structure; instability

1. Introduction

Respiratory infectious diseases such as influenza, severe acute respiratory syndrome (SARS), and coronavirus disease (COVID-19) have been threatening public health in the past two decades [1,2]. Relevant studies have shown that the virus is mainly spread through respiratory droplets and aerosols in closed spaces where humans live [3,4]. The transmission and distribution patterns of droplets and aerosols in enclosed indoor spaces are intricately determined by indoor airflow distribution and airflow field structure. Consequently, there has been a growing emphasis on the research of indoor airflow distribution and airflow field structure in relation to human habitation in enclosed spaces [5–7]. Enclosed indoor spaces primarily encompass residences, workplaces, and transportation vehicles, among others [8]. Airflow distribution and airflow field within these confined areas are fundamental prerequisites for ensuring the safety, health, and comfort of occupants. Enclosed spaces generally adopt mixing ventilation, displacement ventilation, or

personalized ventilation for airflow distribution, with mixed ventilation being the most widespread approach [9]. Mixing ventilation uses high-speed air supply to enhance air entrainment and mixing with indoor air, and utilizes the Coanda effect to achieve a good indoor thermal comfort environment [10,11]. In high thermal density enclosed spaces such as transportation vehicles, classrooms, and sports arenas, opposed jets are commonly used to create mixed ventilation. This method involves symmetric supply vents where jets of air are expelled. These symmetrical jets airflow attached to the ceiling, collide in the center region of the closed spaces, and then flow toward the exhaust vents. While this type of mixed ventilation has the advantage of high heat dissipation efficiency, making it widely used in large spaces and mobile transport enclosed environments. Related studies have reported that the structure of the flow field for this kind of mixing ventilation is unstable. The inherent instability of the airflow field structure in mixed ventilation brings about new challenges and issues for the transmission of infectious diseases, distribution of pollutants, and human thermal comfort [12].

The structural instability of the airflow field of opposed jets begins with the study of small-scale spaces. Many scholars use water and oil as research objects for analysis. Initially, Denshchikov et al. [13] observed the phenomenon of impingement surface deflection when two opposed jets collided in water, leading to the discovery of periodic oscillatory flow patterns in certain configurations. Drawing inspiration from these findings, Rolon et al. [14] employed laser Doppler measurements to investigate the flow field instability generated by opposed jets using oil as the medium. They observed the displacement of the stagnation point after the jet collision. Additionally, numerical simulation studies conducted by Champion and Libby [15] further confirmed these observations and sought to analyze the instability of the airflow field by considering factors such as turbulence integral scales and turbulence intensities. The above studies have shown that the unstable flow field structure of opposed impact jets is mainly reflected in the shift in the stagnation point after jet collision. However, they only qualitatively studied the instability phenomenon of opposed impact jets without in-depth study of the influencing factors leading to instability. In order to explore the influencing factors of the instability of opposed jets, Weersink et al. [16] conducted Particle Image Velocimetry (PIV) experiments to investigate the flow field structure of opposed jets. They found that when the collision angle of the jets was between 0° and 10°, the oscillation frequency was approximately 7 Hz. Furthermore, Li, W.F. et al. [17] the researchers observed a positive correlation between the exit velocity of the jets and the oscillation frequency of the flow field. Hassaballa et al. [18] studied the plane impact flow at high speed (150–250 m/s) and found that the plane impact flow still occurs deflection oscillation and has a high oscillation frequency. When the dimensionless nozzle spacing is 50 and the velocity at 200 m/s, deflection oscillation still exists at high speeds. Ansari et al. [19] determined the main influencing factors affecting the unstable flow field structure of opposed jets through experimental methods; these factors included the geometric structure, nozzle velocity distribution, and Reynolds number. The studies indicate that the main influencing factors affecting the instability of the opposed jet flow field include geometric structure, nozzle spacing, and Reynolds number. However, there is a lack of research on how these influencing factors mechanistically affect the instability of opposed jets.

The above research is only an analysis conducted in a completely free space, and some scholars have conducted research on closed spaces. Zhao and Brodky [20] investigated the airflow distribution structure of opposed jets in a closed mixer and discovered the occurrence of large-scale three-dimensional unstable motion. Johnson et al. [21] investigated the instability of free opposed jets in cylindrical cavities using laser Doppler velocimetry and

numerical simulations. Flow visualization indicated significant flow field asymmetry from regions away from the nozzle to the nozzle region. Both steady-state and unsteady-state numerical simulations confirmed the asymmetry of the flow field under these conditions. Pawlowski et al. [22] conducted a numerical simulation study on the flow structure and flow stability of isothermal opposed jets in both planar and axisymmetric configurations. They identified four flow regimes: symmetric steady flow, asymmetric steady flow, periodic deflected flow, and chaotic flow under different size ratios. Within a certain range of parameters (exit Reynolds number and nozzle spacing), the occurrence of skewed oscillations was also observed. Kind and Suthanthiran [23] conducted experimental research on the unstable flow field of two opposed jets near a wall in a closed space and observed the phenomenon of deflection after the collision and mixing of the jets. Wood et al. [24] conducted a study on airflow-opposed jets at low Reynolds numbers and observed oscillations in the airflow structure when the Reynolds number exceeded a critical value. Srisamran and Devahastin [25] studied the flow field structure of counterflow opposed jets in a T-shaped geometry and observed changes in the flow pattern as the Reynolds number increased. It can be seen from the research that there is instability in the airflow distribution of opposed jets in a closed space; however, they are all qualitative analyses of the phenomenon, and there is a lack of systematic and quantitative research on the influencing factors and the instability of the airflow distribution structure.

With further research, in residential closed spaces, some scholars have discovered that mixed ventilation formed by opposed jets has an unstable airflow distribution structure and have conducted certain studies. Wu et al. [26–29] employed numerical simulations to investigate the multiple flow regime phenomena in the airflow distribution structure of ventilated by opposed jets. They found that different flow regimes were influenced by geometric boundaries, the supply air velocity, and the supply outlet height. Liu et al. [30], in their study on opposed jet ventilation in enclosed chambers, identified three airflow distribution patterns and investigated the influence of the Reynolds number on these patterns, ranging from the steady state to the transitional state and then to the unsteady state. Zhao et al. [31] described the characteristics of the transition from laminar to chaotic mixed convection in the flow field structure of a two-dimensional opposed jets ventilation chamber. Additionally, they found that as the Richardson number (Ri) increases, the flow field structure may transition from a steady state to periodic oscillations and eventually into nonperiodic oscillations. Shishkina and Wagner [32] conducted direct numerical simulations to investigate the transient flow field characteristics in spaces ventilated by opposed jets. They discovered significant instabilities in the transient airflow distribution, which were found to be influenced by thermal plumes. Korner et al. [33], in their research on enclosed chambers ventilated by opposed jets, discovered that large-scale airflow distribution structures exhibit instability. Furthermore, they observed that the spatiotemporal characteristics of these structures are correlated with the Reynolds number and exhibit a certain oscillation frequency. Yang et al. [34] observed the phenomenon of airflow instability in cabin environments with mixed opposed jets through numerical simulations and attempted to explain this phenomenon using the theory of topology. Building upon this, Kandzia and Muller, among others [35–38], constructed simplified opposed jets ventilated chambers and reported that large-scale airflow distribution structures transition from stable to unstable as the supply Reynolds number increases by increasing the inlet velocity, the airflow structure becomes more stable. Thysen et al. [39] conducted relevant research on airflow structures in simplified cabin models, where the airflow distribution was characterized by mixed ventilation generated by opposed jets. They discovered that under this airflow distribution, the airflow distribution structure exhibited instability. The

aforementioned studies on mixed ventilation by airflow opposed jets have identified the characteristics of airflow distribution instability, but quantitative research on the influencing factors is lacking.

In existing research, the analysis of airflow instability in confined spaces with opposing jet ventilation has been limited to qualitative descriptions or single-parameter studies, lacking systematic quantitative investigations of the combined effects of multiple factors. The innovation of this study lies in the use of large eddy simulation (LES) to systematically reveal, for the first time, the synergistic effects of supply air velocity, jet configuration, space aspect ratio, and thermal gradient on the oscillation period, amplitude, and stability of airflow, and to propose quantitative evaluation criteria. Specific contributions, including a predictive model for the oscillation period under multi-parameter influences, were established, demonstrating that high supply air velocities (e.g., 1.92 m/s) can shorten the period (7.7 s) and suppress small-scale disturbances, significantly improving stability. The dynamic differences between free jets and attached jets were elucidated, revealing that the oscillation amplitude of free jets increases compared to attached jets, with the power spectrum period extending to 15.6 s, providing new guidelines for jet positioning in ventilation design. The amplifying effect of thermal gradient on airflow instability was quantified, showing that the oscillation period gradually increases as the ground temperature rises from 15 °C to 35 °C, revealing the complex interaction between thermal environment and mechanical ventilation. A novel integration of phase space reconstruction with power spectrum analysis was developed to validate the nonlinear chaotic characteristics of airflow oscillations in confined spaces, laying a theoretical foundation for dynamic ventilation control strategies. This research fills the gap in the existing literature regarding the combined effects of multiple parameters and the lack of a quantitative analysis framework. It provides direct scientific support for the optimization of ventilation and air quality management in high-density confined spaces, such as transportation cabins and sports venues.

In summary, there is instability in the airflow distribution formed by the opposed jets in the closed space of human settlements. These instability phenomena manifest as the deflection and oscillation of the airflow distribution, but their quantitative characteristics, the factors affecting its instability, and the formation mechanism are lacking.

Therefore, this study used the large eddy simulation (LES) method to simulate the airflow pattern of the opposed jets airflow distribution in a closed square cavity based on the experiments of. Blay D et al. [40]. The effects of different air supply velocities, different forms of air supply, different aspect ratios of closed spaces, and different ground source temperatures on the airflow distribution were studied. The periodicity and instability of the flow field structure were analyzed via the power spectrum and phase space reconstruction theory.

2. Experimental Setup

According to the experimental results of Blay D et al. [40], a closed space of 1.04 m × 1.04 m × 0.7 m was established. The model is shown in Figure 1. The closed space is equipped with an 18 mm high inlet and a 24 mm high outlet. The square cavity was constructed with a flat aluminum heat exchanger as its wall, where the air was subjected to heating or cooling through a water–air heat exchanger. The water temperature was regulated by a cryogenic thermostat with a precision level of 0.25 °C. In addition to the insulation wall, the wall between the square cavities was set to a fixed temperature of 15 °C, and the floor temperature was heated to 35.5 °C. To ensure a uniform air supply velocity at the air inlet, a honeycomb filter was installed at the air inlet. The air was supplied with a velocity of 0.57 m/s, the supply velocity was 0.85 m/s, the temperature

was 15 °C, and the turbulence intensity was 6%. At steady state, the original experiment employed two color laser Doppler velocimetry devices to measure the average velocity and turbulence fluctuation. The temperature measurements were performed with a 20 μm Cr-Al thermocouple.

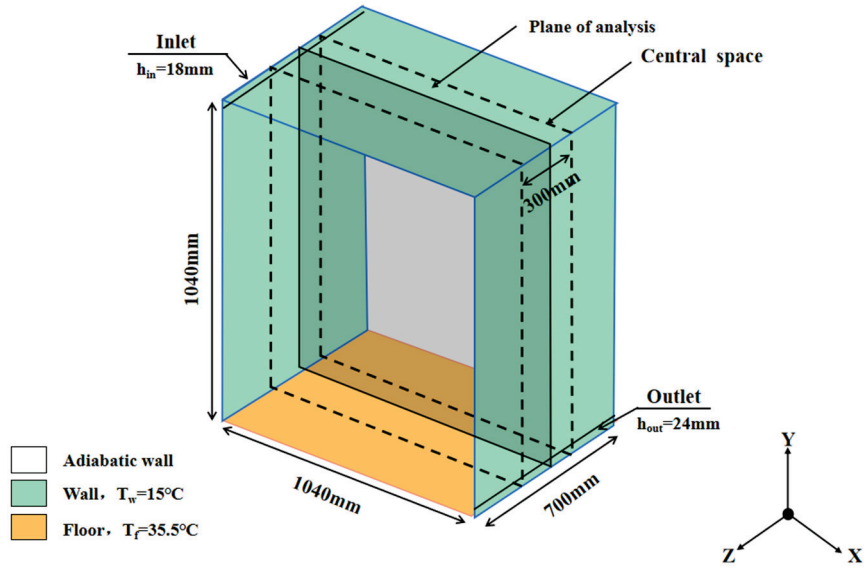


Figure 1. Experimental model.

3. Case Set

3.1. Geometric Model

The closed space was divided into three smaller spaces: one central working space where the measurements were performed and two guard spaces where the same flow as in the working cavity was simulated. The computational domain was created only for the central working space because it not only eliminates the thermal effect but also ensures good flow in the central working space. The air inlet in the closed central space was 300 mm long and 18 mm wide, and the air outlet was 300 mm long and 24 mm wide. The air supply vents, return air vents, and wall surface temperatures were configured to precisely match the experimental setup parameters. The model is shown in Figure 2.

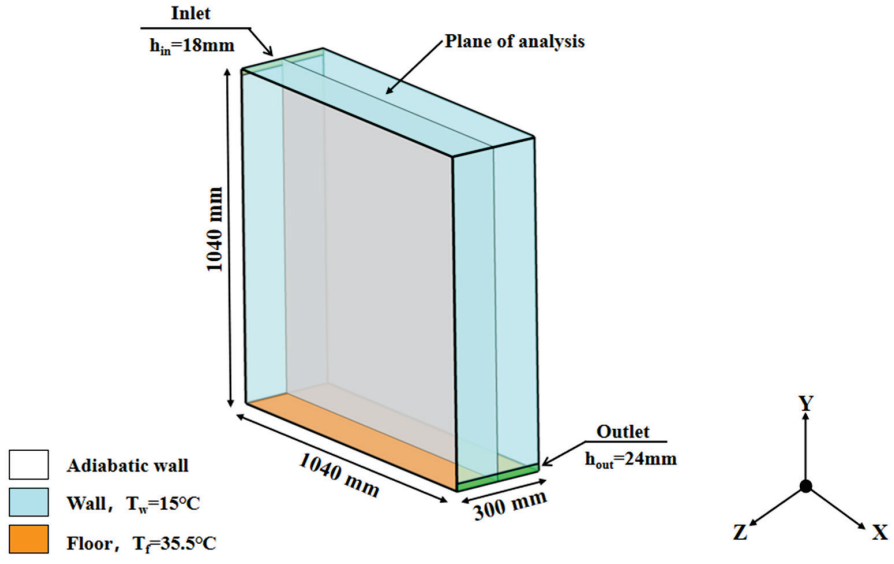


Figure 2. Three-dimensional diagram of the central square cavity for CFD simulation.

3.2. Boundary Conditions

The boundary conditions in the CFD simulation were set to be consistent with the boundary conditions used in the experiments. The inlet air temperature was T_{in} is 15 °C, and the outlet air was set to zero static pressure. The air supply vents, return air vents, and wall surface temperatures were configured to precisely match the experimental setup parameters. The two sidewalls were set as adiabatic walls, i.e., the heat flux was zero (zero heat flux condition). All the walls were set as nonslip smooth walls. An experiment was conducted to eliminate the radiation effects between walls, so the radiative heat transfer and conductive heat transfer between surfaces were not considered. The inlet velocity and turbulence intensity remained consistent with the experimental configuration. The corresponding hydraulic diameter (D_h) was specified as 0.0035 m. The specific parameter settings are shown in Table 1.

Table 1. All the change in parameters.

Case	Supply Air		Air Velocity (m/s)				Aspect Ratio of the Enclosed Space			Ground Temperature (°C)		
	Attached jet	Free jet	0.57	0.85	1.28	1.92	1:1	1:2	1:3	15	25	35
Case 1	√		√	√	√	√	√			√		
Case 2	√	√			√		√			√		
Case 3	√		√				√	√	√	√		
Case 4	√		√				√			√	√	√

3.3. Solver Settings

The fluid medium is air, and the turbulence model adopted is a large eddy simulation (LES). Due to the unknown sub grid-scale stresses generated by the filtering operation in LES models, the sub grid-scale model is set to the wall-adapting local eddy viscosity model. Due to the small diffusivity of the second-order discrete scheme, it was necessary to select a discretization scheme with at least second-order accuracy to overcome diffusion. This paper employs a second-order upwind scheme for the convection term, viscous term, and pressure interpolation term within the governing equations. The energy equation and momentum equation were both discretized using the bounded central differencing scheme. For the control equations governing fluid flow inside the cavity, the Boussinesq assumption was employed to handle the buoyancy force caused by temperature differences. When the residual values reached a steady state, the computations were considered to have converged. The residual convergence value for continuity, turbulent dissipation rate, turbulent kinetic energy, and velocity components were set at 10^{-5}, while that of the energy was set at 10^{-6}. In the case of reasonable grid accuracy, the PISO algorithm was found to have higher precision than the SIMPLE algorithm, because article chooses the PISO algorithm. The time step was set at 0.05 s. Numerical simulations were conducted by Ansys Fluent 19.0.

3.4. Grid

To reduce the number of grids and computational cost, the computational domain is set to the central working cavity. Because finer grids need to be used for large eddy simulations, this paper uses structured grids. To determine the independent solution of the grid, three grids were generated as shown in Figure 3, including 93,012, 122,771 and 330,423 elements, respectively. By adding the boundary layer grid and encrypting it, an accurate capture of the flow field is realized. Control y^+ within 5. Table 2 describes the maximum mesh size and Y+ corresponding to different mesh types.

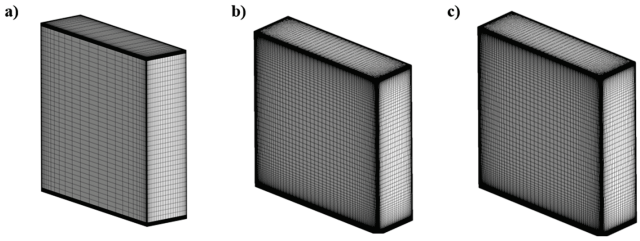


Figure 3. Number of different grid types used for grid-independent solutions: (**a**) coarse grid (93,012 cells); (**b**) basic grid (122,771 cells); and (**c**) fine grid (330,423 cells).

Table 2. The maximum grid size and Y+ corresponding to different grid types.

	Grid		
Y+	**Coarse**	**Basic**	**Fine**
Maximum	5.1	3.4	2.8
Average	1.6	1.0	0.6

The statistical average values of the unsteady calculation results after reaching stability were calculated and were compared with the experimental values. The numerical temperature and velocity on the horizontal centerline (Y is 0.52 m) and the vertical centerline (X is 0.52 m) were compared with experimental values. Figure 4a shows the dimensionless horizontal centerline velocities of the simulated and experimental values under grid elements 93,012, 122,771, and 330,423. The calculated mean deviations are 0.019, 0.005, and 0.009, respectively. Figure 4b shows the dimensionless vertical centerline velocity profile of three grid cells, and the average calculation deviations are 0.021, 0.007, and 0.035, respectively. Figure 4c shows the dimensionless vertical centerline temperature of the three grid units, and the average calculation deviations are 0.555, 0.003, and 0.807, respectively. Figure 4d shows the dimensionless vertical centerline temperature of the simulated and experimental values for grid numbers 93,012, 122,771, and 330,423, and the calculated mean deviations are 0.53, 0.05, and 1.34, respectively. When the grid number is 122,771, the simulation results are in good agreement with the experimental results. Through the above verification, the model is found to be suitable for large eddy simulation of 122,771 grid units. Therefore, in the following example, 122,771 is used for mesh CFD simulation analysis.

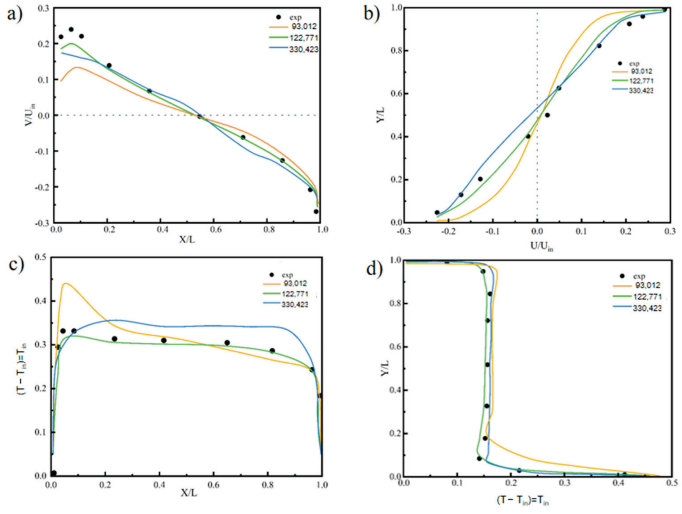


Figure 4. Comparison of CFD and literature experimental data: (**a**) V/U_{in} the horizontal centerline (**b**) U/U_{in} the vertical centerline. (**c**) $(T - T_{in})/T_{in}$, horizontal centerline; (**d**) $(T - T_{in})/T_{in}$, vertical centerline.

3.5. Numerical Case Setup

Based on the study of Blay et al. the air supply configuration was modified from a single inlet and single outlet to dual inlet and dual outlet as shown in Figure 5, while keeping the other boundary conditions constant. The LES method was used to simulate the opposed jets in the enclosed space. The instability of the airflow structure was analyzed by varying different parameters. The airflow influencing parameters included the air supply velocity, position of the air inlets, aspect ratio of the enclosed space, and thermal plume. The specific simulation variables are shown in Figure 5. The first case was the influence of different air supply velocities on the airflow structure under isothermal conditions, where the ground temperature is equal to the wall temperature, with a supply angle of φ is 0° and a constant air supply rate. Four velocities, 0.57 m/s, 0.85 m/s, 1.28 m/s, and 1.92 m/s, were selected for the simulation analysis. To maintain a constant airflow rate, the corresponding inlet heights for the four air supply velocities were set at 18 mm, 12 mm, 8 mm, and 5.3 mm, respectively. The second case simulates the airflow field at different locations of the air inlet under isothermal conditions and with a constant air supply velocity of U_{in} is 1.28 m/s and a supply angle of φ is 0°. Specifically, two air supply configurations were adopted: upwards supply and downwards return and central supply and downwards return (free jet). The third algorithm investigates the effect of different spatial aspect ratios on the flow field under isothermal conditions, with a fixed air supply velocity and supply angle. Three enclosed space aspect ratios, namely, 1:1, 1:2, and 1:3, were selected for instantaneous airflow field measurements. The fourth case investigates the effect of different ground temperatures on the flow field with an air supply velocity of 0.57 m/s and a supply angle of 0°. Ground temperatures of 15 °C, 25 °C, and 35 °C were selected as the respective boundary conditions for the simulation.

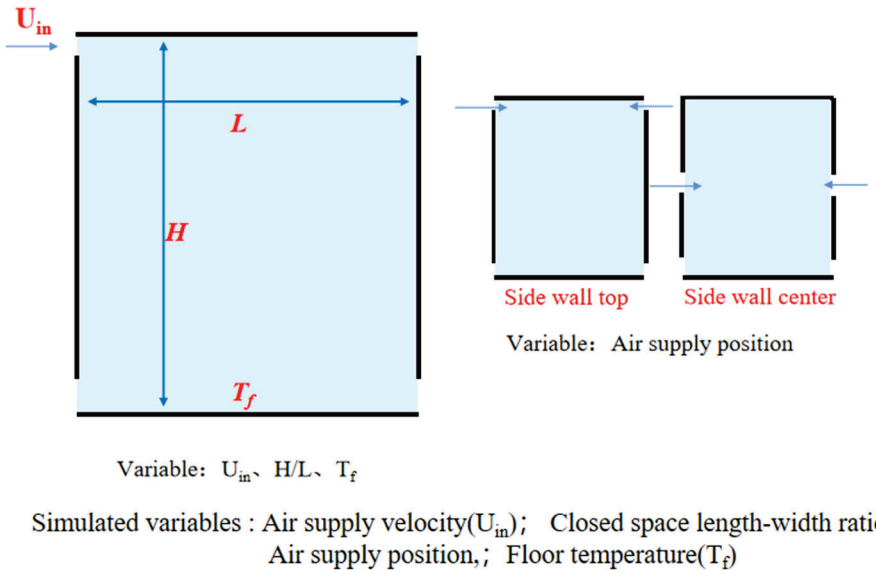


Figure 5. Schematic diagram of numerical simulation variables. Simulation variables: U_{in}, air supply position, H/L, and floor temperature.

Due to the temporal variation in the unsteady airflow structure within an enclosed cavity, this study investigates the velocity time series results of the unsteady airflow structure. A qualitative analysis of the velocity contour was conducted at the central section (Z is 0.15 m) of the enclosed cavity. Additionally, the velocity time series at the coordinates (0.52, 0.52, 0.15) in the center of the cavity were monitored.

To facilitate analysis, normalize the airflow velocity in the flow field:

$$u = \frac{U}{U_{in}}. \tag{1}$$

In the formula, U is the normalized velocity, u is the airflow speed in the flow field, m/s, and U_{in} is the air supply speed, m/s.

4. Result Analysis

4.1. Different Air Supply Velocities

The influence of the air supply velocity on the instantaneous airflow structure was studied under isothermal conditions with air supply angle was 0°. Figure 6 shows the transient flow field contour plot at the cross-section z is 0.15 m under different air supply velocities. A constant air supply rate was ensured by changing the height of the air inlet during this process. The two jets facing the opposite inlet collide in the cavity, and the air flow swings, showing an asymmetrical phenomenon. Figure 7 shows the monitoring curve of the 20 s~60 s velocity time series at the cavity center point (0.52, 0.52, 0.15) and the velocity probability density distribution at the center point. As the air supply velocity increases, the swing amplitude of the airflow structure decreases, and the small-scale airflow around the airflow decreases. It can be seen from Figure 7a that when the air supply velocity is 0.57 m/s, the speed range is distributed between 0.15 m/s–0.29 m/s.

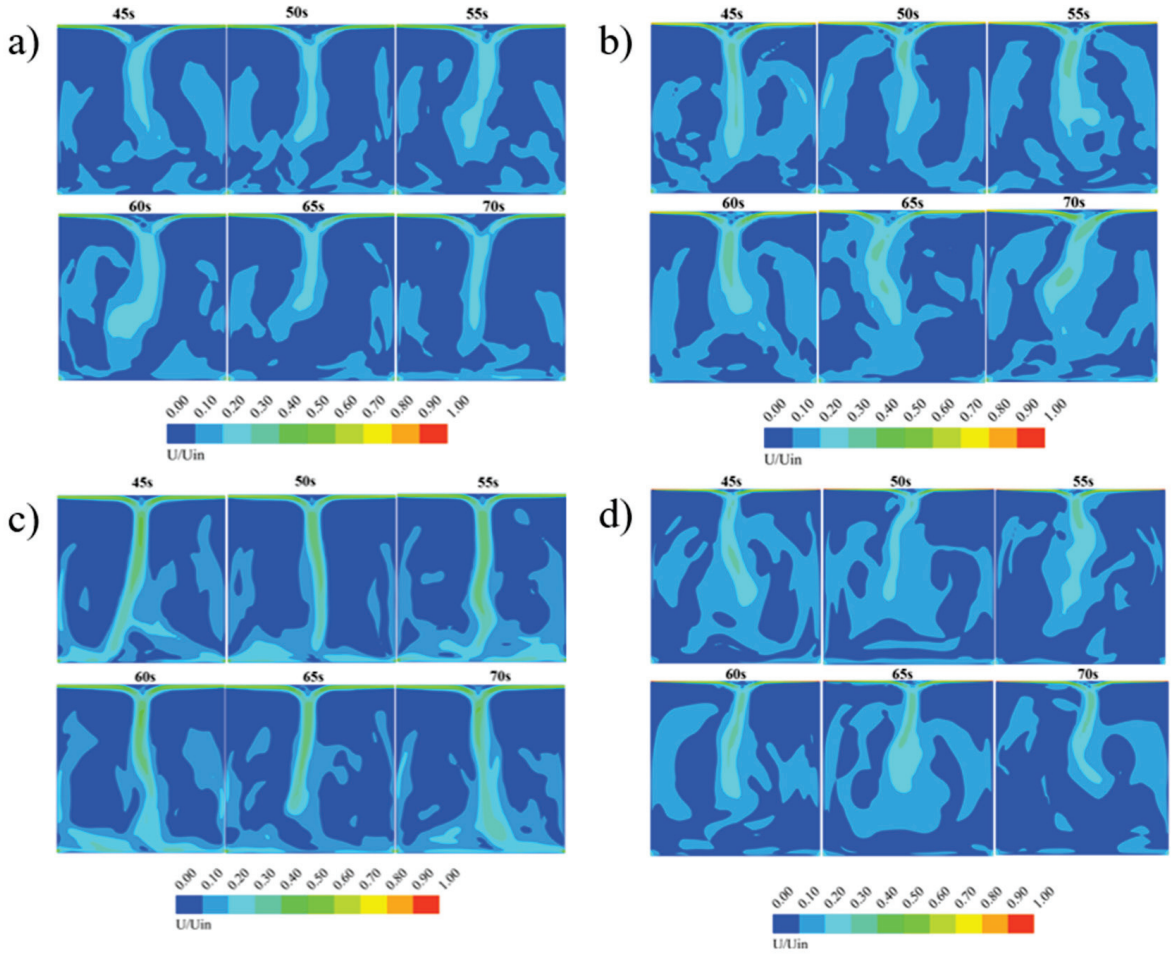


Figure 6. Velocity of the different airflow field distribution speeds at the analysis plane z = 0.15 are (**a**) U_{in} = 0.57 m/s, (**b**) U_{in} = 0.85 m/s, (**c**) U_{in} = 1.28 m/s, and (**d**) U_{in} = 1.92 m/s.

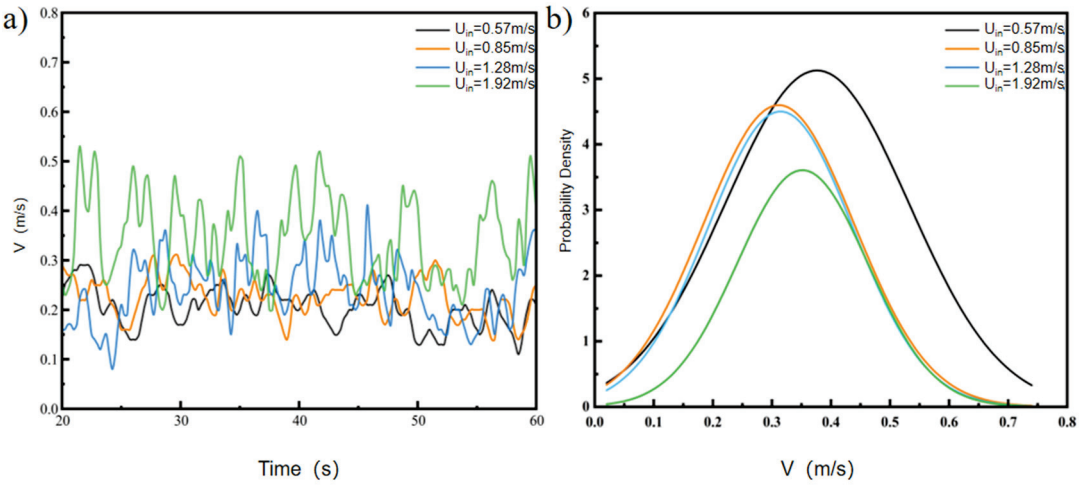


Figure 7. The four airflow velocities at the collision point (0.52, 0.52, 0.15). (**a**) Velocity time series monitoring curve and (**b**) velocity probability density distribution at the central point.

When the air supply velocity is 1.28 m/s, the velocity range is distributed between 0.10 m/s–0.35 m/s. When the velocity increases to 1.92 m/s, the velocity range is distributed between 0.15 m/s–0.51 m/s. The time interval between the maximum speed and the minimum velocity of air flow at the monitoring point is reduced from 8 s to 3 s. The data indicate that as the air supply velocity increases, the airflow swing frequency increases. It can be seen from Figure 7b that as the air supply velocity increases, the probability of the concentrated distribution range of air flow velocity at the monitoring point decreases, the amplitude of air flow swing decreases, and the air flow oscillation gradually stabilizes.

4.2. Impact of Air Supply Positions

The effect of different air supply positions on the transient airflow structure was studied when the isothermal air supply angle was 0° and the air supply velocity was 1.28 m/s. This paper studies the influence of the air supply position on the airflow structure of the enclosed space at the top of the cavity side wall and the middle of the side wall. The three-dimensional diagrams of the two air supply locations are shown in Figure 8. The model is meshed, and the number of mesh divisions is shown in Figure 9.

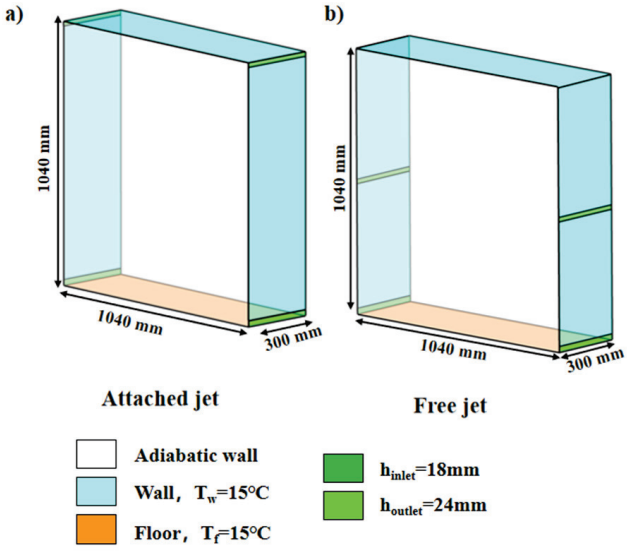


Figure 8. Different air supply models: (**a**) Attached jet; (**b**) Free jet.

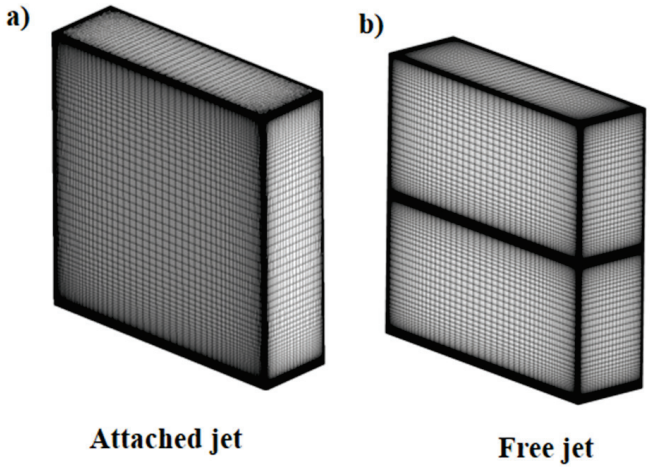


Figure 9. (**a**) Attached jet (330,423 cells); (**b**) Free jet (320,423 cells).

Figure 10 shows the transient flow field at different air supply positions with an air supply velocity of 1.28 m/s. When the air supply positions are located at the top of the side wall, the two jets collide in the cavity and the airflow swings, showing an asymmetrical phenomenon. When the air supply position is located at the center of the side wall, after the two jets collide, at different times, a jet deflects toward the ground, the deflection of another jet towards the top of the cavity. Moreover, during the jet deflection process, the surrounding small-scale airflow structure increases.

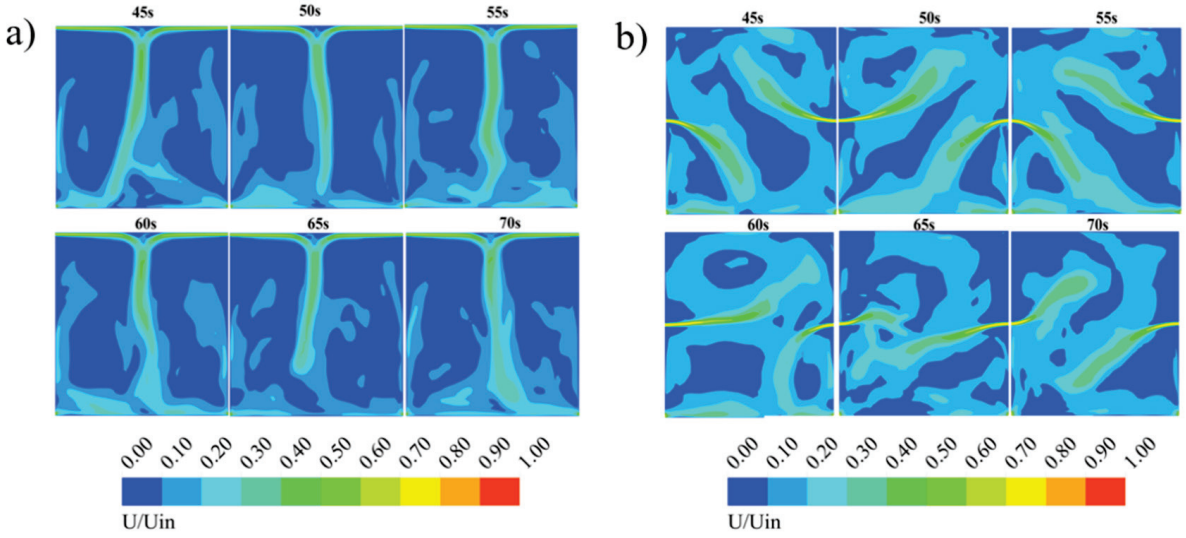


Figure 10. Velocities of the different air supply forms at the analysis plane z = 0.15. (**a**) Attached jet; (**b**) Free jet.

Figure 11 shows the monitoring curve of the 20 s~60 s velocity time series at the cavity center point (0.52, 0.52, 0.15) and the velocity probability density distribution at the center point. The air supply position is located at the top of the side wall, the velocity fluctuation at the monitoring point is small, and the velocity range is 0.15 m/s~0.37 m/s. The time interval between the maximum speed and the minimum speed of the airflow at the center point is 3 s. When the air supply position is located at the center of the side wall, the velocity at the center point fluctuates greatly, with the velocity concentrated at 0.05 m/s~0.7 m/s. The amplitude of the airflow swing is large, and the time interval between the maximum and minimum airflow speed at the center point is 7 s. It can be seen that when the air

supply position is located at the center of the side wall, the airflow oscillation amplitude at the center point increases and the airflow swing frequency decreases. When the air supply position is at the center of the side wall, it can be clearly seen that there is a large peak value in the instantaneous velocity of the center point at 65 s, with a velocity of 0.67 m/s. Combined with the velocity cloud chart at 65 s, the data indicate that when the center point velocity peaks, the airflow on both sides will re-enter a transition state. The airflow on the right side suppresses the airflow on the left side, gradually causing the airflow on the left side to deflect toward the top. When the left airflow is completely deflected, the center point velocity decreases again.

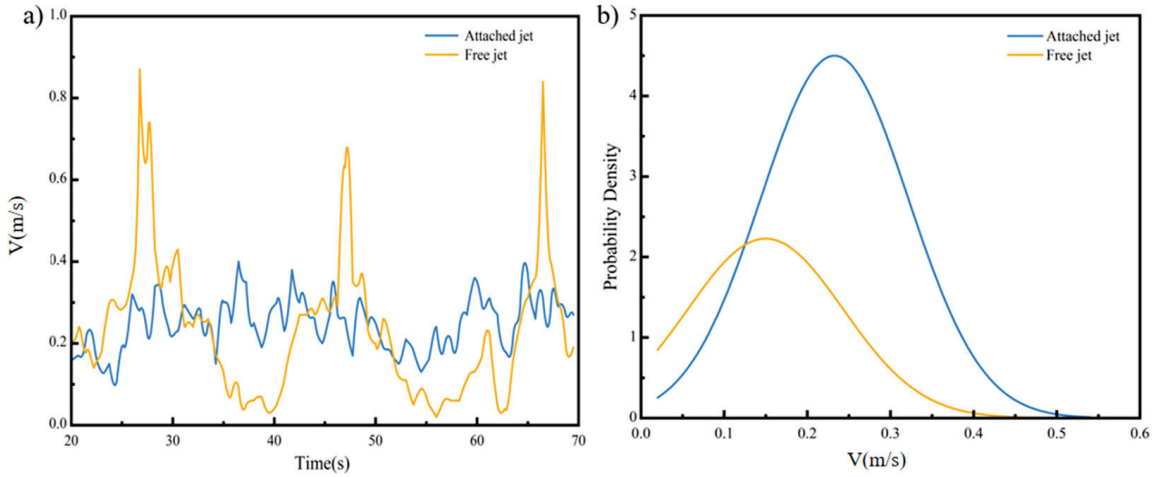


Figure 11. Velocity time series monitoring curves and probability density distributions of the different air supply forms at the collision points (0.52, 0.52, 0.15). (**a**) Velocity time series monitoring curves. (**b**) Probability density distributions.

4.3. Impact of the Aspect Ratio

The effect of different closed space aspect ratios on the transient airflow structure was studied when the isothermal air supply angle was 0° and the air supply speed was 1.28 m/s. Enclosed spaces with different aspect ratios are shown in Figure 12. The closed spaces with three aspect ratios are meshed, and the number of grid divisions is shown in Figure 13.

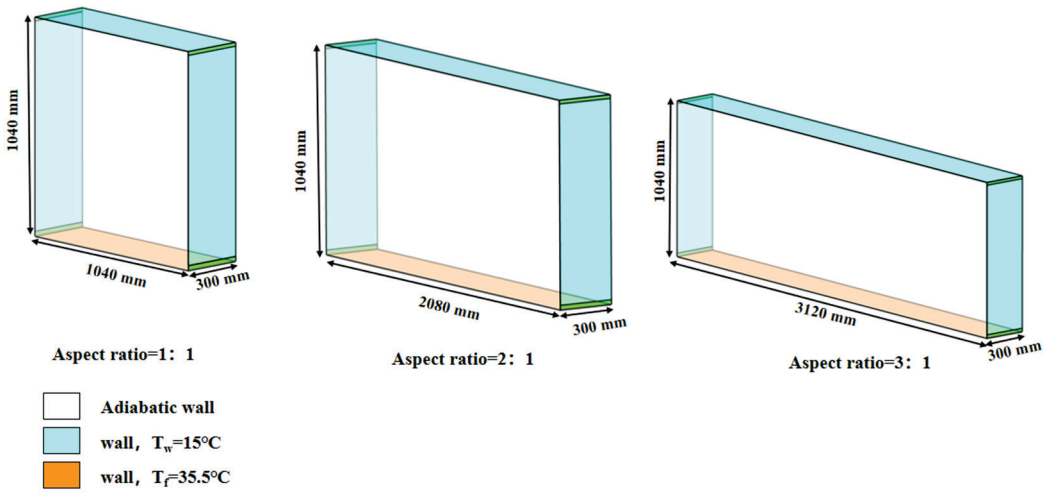


Figure 12. Different aspect ratio models: 1:1; 2:1; and 3:1.

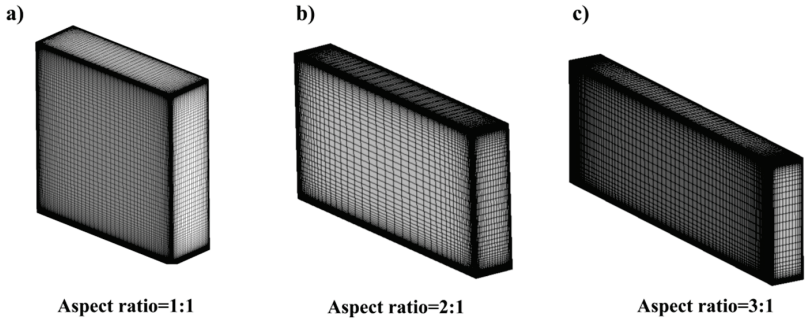


Figure 13. Grid generation: (**a**) 1:1 (31,251 cells); (**b**) 2:1 (320,851 cells); and (**c**) 3:1 (334,811 cells).

Figures 14–16 is a transient flow field diagram with different aspect ratios of 1:1, 1:2, and 1:3 at section z is 0.15. It can be seen from the figure that as the aspect ratio increases, the distance of the airflow jets on both sides increases. After the jets on both sides collide, one side of the airflow sweeps the surrounding small airflow structure and suppresses the other side of the airflow from flowing to the sidewall. For example, when the aspect ratio is 2:1 and when the airflow collides, the right airflow suppresses the left airflow, causing the airflow to move to the left and deflect. In the transition state, the airflow moves to the center of the closed cavity, and then the left airflow suppresses the right airflow from moving to the opposite sidewall. Moreover, an increase in the aspect ratio affects the distance of the air flow to the bottom of the closed cavity. This may be due to the increase in the small-scale air flow with the increase in the jet distance from the initial to the collision process of the air flow on both sides, which affects the deflection of the air flow, resulting in a shorter distance of the air flow to the bottom.

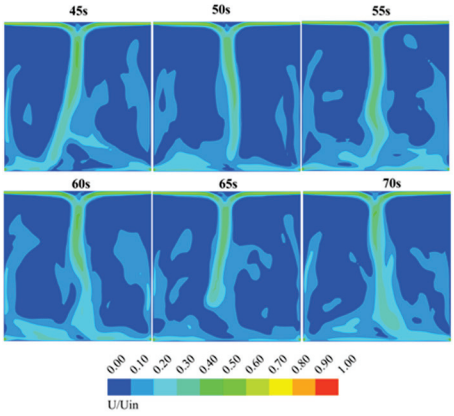


Figure 14. Velocity at the analysis plane z = 0.15 when the aspect ratio is 1:1.

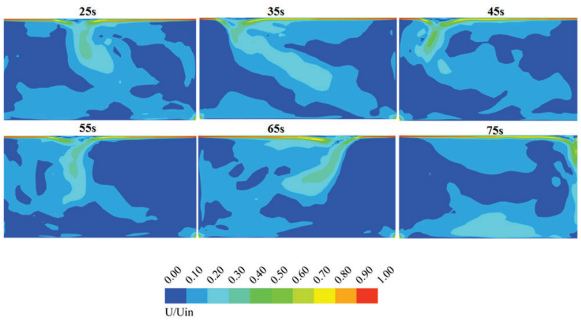


Figure 15. Velocity at the analysis plane z = 0.15 when the aspect ratio is 2:1.

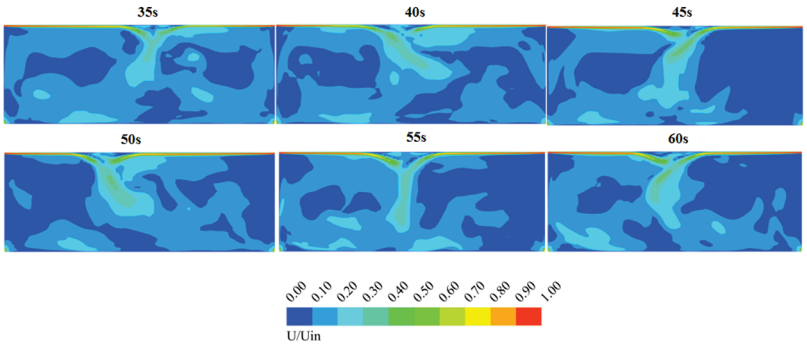


Figure 16. Velocity at the analysis plane z = 0.15 when the aspect ratio is 3:1.

Figure 17 shows the monitoring curve of the 20 s~60 s velocity time series at the cavity center point and the velocity probability density distribution at the center point. When the aspect ratio is 1:1, the speed is concentrated in the range of 0.28 m/s~0.8 m/s. When the aspect ratio is 3:1, the speed range is concentrated in the range of 0.1~0.4 m/s. With increasing length-to-width ratio, the velocity fluctuation amplitude decreases, which indicates that an increase in the length-to-width ratio leads to an increase in the airflow swing period. Combined with the above cloud images, when one side of the airflow suppresses the other side of the airflow to move to the sidewall, the fluctuation amplitude of the velocity at the collision point gradually decreases. Additionally, there is periodicity and instability in the airflow oscillation under different aspect ratios.

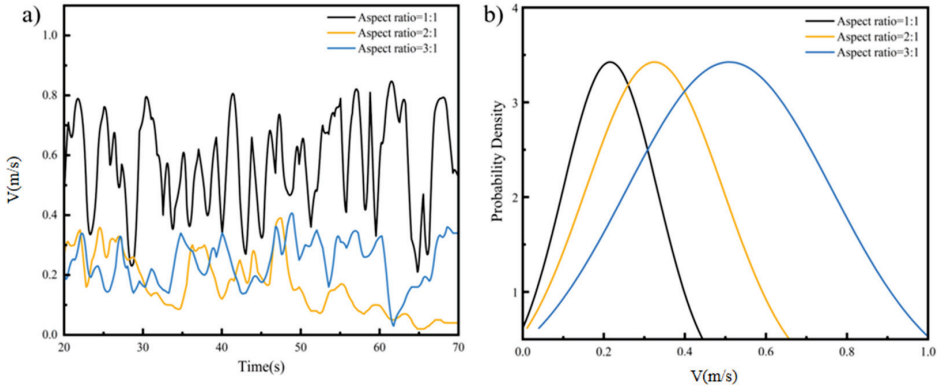


Figure 17. Velocity time series monitoring curve and probability density distribution of different aspect ratios at the collision point (0.52, 0.52, 0.15). (**a**) Velocity time series monitoring curve. (**b**) Probability density distribution.

4.4. Impact of Floor Temperature

The above studies were carried out under isothermal conditions. Previous research has shown that the heat source temperature also affects the deflection of airflow structures. Therefore, to ensure the same air supply speed and air supply angle, this paper studies the transient airflow structure when the floor temperature is heated to 15 °C, 25 °C and 35 °C. The airflow distribution is different from that under isothermal conditions. Under non-isothermal conditions, the airflow structure diffuses upwards due to the influence of the floor heat source temperature. As shown in Figure 18, the velocity cloud diagram at cross-section Z is 0.15 is analyzed. The diagram shows that the jet deflects after the collision. Under the action of the heat source temperature, the up- and down-oscillation of the airflow is suppressed. When the floor temperature increases from 15 °C to 35 °C, the dynamic airflow structure gradually becomes confused. The diffusion of the airflow to the surrounding area obviously drives the deflection of the jet after the collision to be

more obvious, and the airflow bifurcation is more refined. The dynamic airflow structure at different heat source temperatures shows periodic changes.

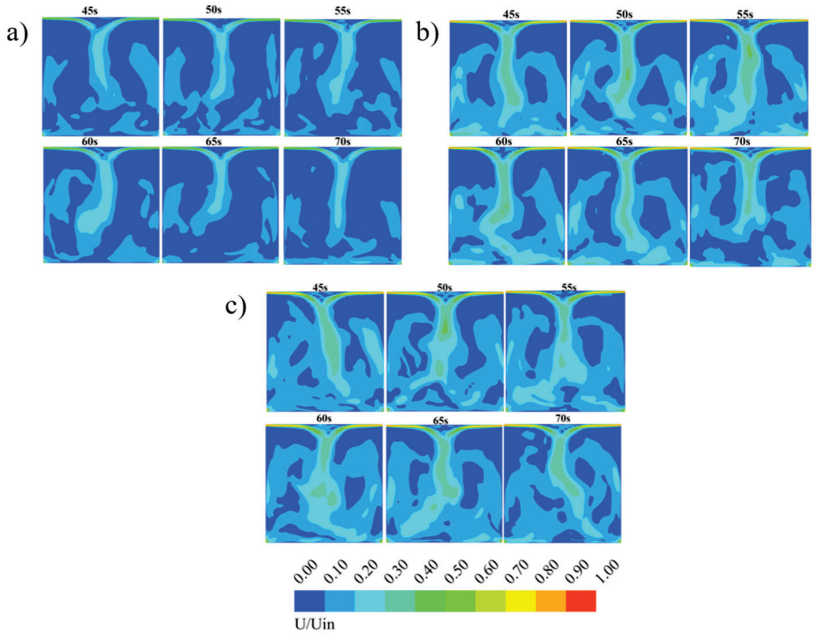


Figure 18. Velocities at different floor temperatures in the analysis plane at z = 0.15. (**a**) T_f is 15 °C; (**b**) T_f is 25 °C; (**c**) T_f is 35 °C.

It can be seen from Figure 19 that when the heat source temperature is the highest, the speed fluctuation range of the monitoring point is 0.14 m/s~0.28 m/s. Under isothermal conditions, the velocity fluctuation range of the monitoring points is 0.1 m/s~0.32 m/s. The larger the heat source temperature is, the smaller the velocity fluctuation at the monitoring point is. This is because when the heat source temperature exists, the airflow diffuses everywhere, forming a vortex airflow distribution, resulting in the airflow at the center point becoming a small airflow organization, and the velocity fluctuation changes more gradually. Figure 19 also shows that the airflow structure experiences a certain period. When the local plate temperature is heated to 35 °C, the period of the central monitoring point is clearly longer than that for a floor temperature of 15 °C.

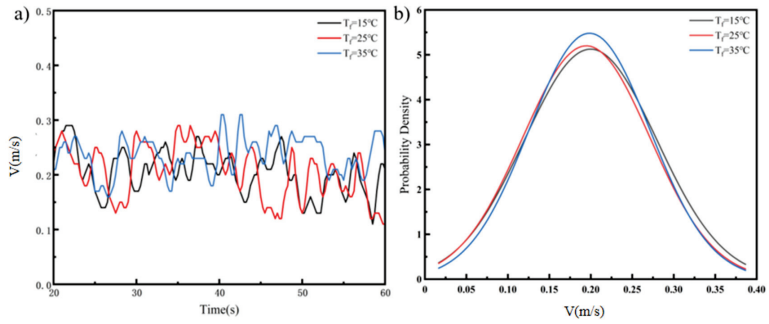


Figure 19. Velocity time series monitoring curve and probability density distribution of different floor temperatures at the collision point (0.52, 0.52, 0.15). (**a**) Velocity time series monitoring curve. (**b**) probability density distribution.

4.5. Periodicity Analysis

From the above analysis, it is obvious that the airflow oscillation in the central cavity is periodic under different parameter settings. However, the specific period cannot be

obtained from the velocity cloud diagram or velocity monitoring sequence. Therefore, to analyze the periodic characteristics of the velocity time series under an unsteady flow field, the energy spectrum is used for analysis. This paper uses the power spectrum method for analysis and calculation and deduces the calculation. Airflows oscillate during specific periods. The specific derivation calculation process is as follows:

Let $u(i)$ be a part of time series $u(i)$, i is 1, 2, . . ., I. For the fast Fourier transform of the velocity time series, the calculation formula can be based on (2):

$$F(k) = \sum_{i=1}^{I} u(i) e^{-\int 2\pi(k-1)\frac{i-1}{i}}. \quad (2)$$

After the velocity time series is transformed, the frequency is $f_i = 2\pi\frac{i-1}{I}$, where $i = 1, 2, \ldots$, is the maximum amplitude of the fast Fourier transform of the average period and the reciprocal of the corresponding frequency is the power. It is calculated using Formula (3):

$$P = \frac{1}{max[F(1), F(2), \ldots, F(I)]}. \quad (3)$$

The air supply velocities considered in the study are 0.57 m/s, 0.85 m/s, 1.28 m/s, and 1.92 m/s. The power spectrum distribution is depicted in Figure 20, where the horizontal axis represents time and the vertical axis represents power. Due to the periodicity of the small-scale airflow structure, multiple small peak powers can be observed in the graph. This suggests the presence of multiple periodicities in the small-scale airflow. Using the power spectrum method, the period of air flow oscillation in the cavity was calculated for a wind speed of 0.57 m/s. With an increase in the wind speed to 0.85 m/s, the period of air flow oscillation in the cavity was determined to be 11.3 s. Based on the power spectrum analysis, the air flow oscillation period was calculated to be 10.6 s for an inlet velocity of 1.28 m/s. Furthermore, as the air supply velocity increases to 1.92 m/s, the airflow oscillation period is shortened to 7.7 s. Figure 12 shows that with increasing inlet velocity, the period of air flow oscillation in the cavity becomes increasingly obvious, and the disturbance of small-scale air flow becomes increasingly less obvious. This is because when the air inlet velocity increases, the impact of the jet after the collision increases, and the airflow distribution is concentrated, so the small-scale airflow structure is less distributed.

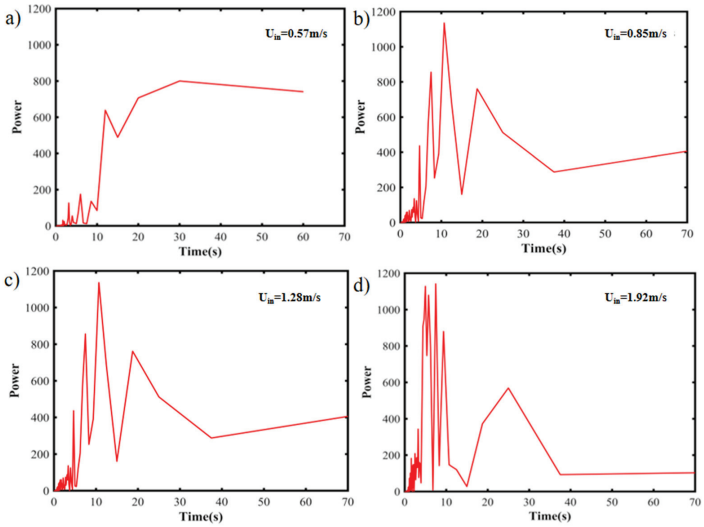


Figure 20. Periodic distribution of different supply air velocities: (**a**) U_{in} is 0.57 m/s, (**b**) U_{in} is 0.85 m/s, (**c**) U_{in} is 1.28 m/s, and (**d**) U_{in} is 1.92 m/s.

Figure 21 shows the power spectrum distributions under the different air supply modes. When the air supply is the upper supply and lower return, the airflow oscillation period in the closed cavity is 10.6 s. When the air supply is the middle supply and lower return, the airflow oscillation period is 15.6 s. The airflow oscillation period of the free jet formed by the middle feed and lower return is longer than that of the attached jet formed by the upper feed and lower return. This is because in the free jet, the collision and deflection of the two airflows lead to an increase in the surrounding small-scale airflow structure, and the small-scale airflow period is increased by 0~10 s, thus affecting the overall airflow oscillation period.

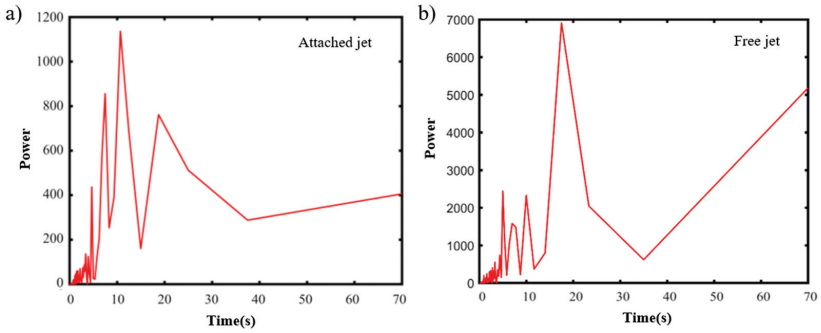


Figure 21. Periodic distributions of the different air supply forms: (**a**) Attached jet and (**b**) Free jet.

The power spectrum is used to analyze the airflow oscillation under different aspect ratios. The airflow oscillation with different aspect ratios in the closed space is periodic. When the aspect ratio is 1:1, the airflow oscillation period is 10.6 s. When the aspect ratio is 2:1, the oscillation period is 14.5 s. When the aspect ratio is 3:1, the period is 18.1 s. Periodic distribution of different aspect ratios as shown in Figure 22. As the aspect ratio increases, the airflow oscillation period increases. This is because in the process of jet collision, an increase in the length-to-width ratio leads to an increase in the jet distance, an increase in the surrounding small-scale airflow, and the continuous entrainment of the surrounding airflow to the collision center. The longer the jet distance is, the longer the movement time of the surrounding small airflow to the collision center, thus affecting the oscillation period of the airflow.

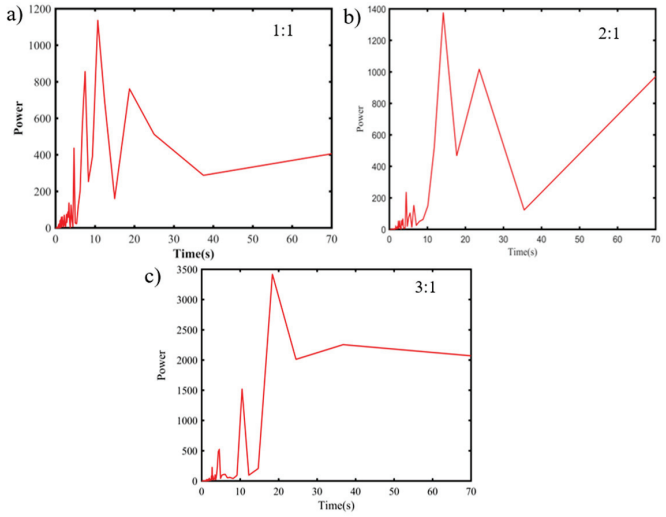


Figure 22. Periodic distribution of different aspect ratios: (**a**) 1:1, (**b**) 2:1, and (**c**) 3:1.

Figure 23 shows the power spectrum distributions at different heat source temperatures. The horizontal and vertical coordinates represent time and power, respectively, and the airflow oscillation period changes with the change in heat source temperature. When the heat source temperature is 15 °C (isothermal condition), the period of airflow oscillation is 11 s. When the temperature of the heat source increases to 25 °C, the period of airflow oscillation in the cavity becomes 13 s. When the heat source temperature is heated to 35 °C, the oscillation period of airflow in the cavity becomes 17 s. Figure 24 shows that when the heat source temperature increases from 15 °C to 35 °C, the period of airflow oscillation in the cavity becomes longer. This is due to the influence of the ground source temperature. After the two airflows collide with the jet, a small airflow structure is formed on both sides. These small airflow structures are continuously entrained on both sides, lengthening the airflow swing period and indicating that the heat source temperature has a significant effect on the airflow distribution.

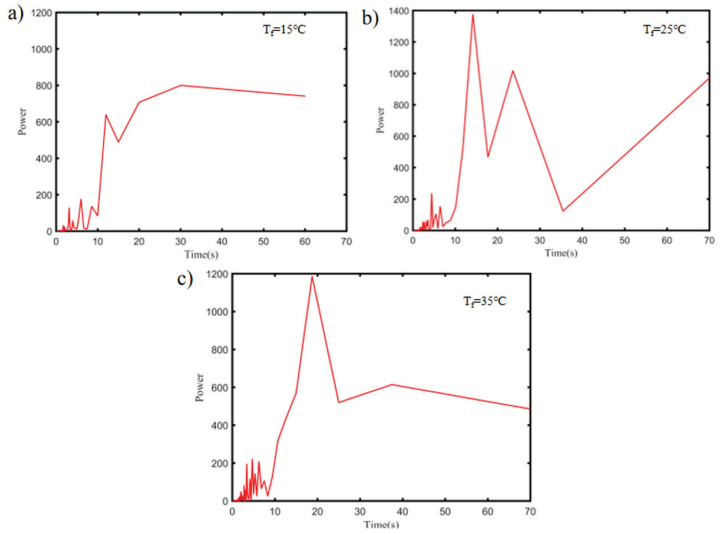


Figure 23. Periodic distribution of different floor temperatures: (**a**) T_f is 15 °C, (**b**) T_f is 25 °C, and (**c**) T_f is 35 °C.

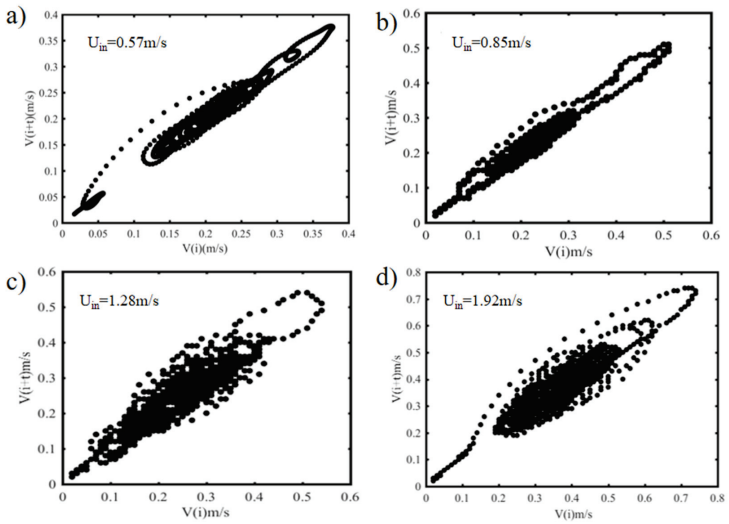


Figure 24. Two-dimensional phase space reconstruction diagram of different air supply velocity time series: (**a**) U_{in} = 0.57 m/s, (**b**) U_{in} = 0.85 m/s, (**c**) U_{in} = 1.28 m/s, and (**d**) U_{in} = 1.92 m/s.

4.6. Phase Space Reconstruction Analysis

To investigate the instabilities of flow field structures, this study employs a phase space reconstruction method to analyze the non-stationarity of time scales in flow field structures. By reconstructing the unsteady time series into low-order nonlinear sequences in phase space, the sequence is transformed into describable states, facilitating the discovery of its variation patterns.

According to the Takens F [41] mathematical theory, it is assumed that the one-dimensional univariate time series is shown as follows:

$$x_i = (x_1, x_2, \ldots, x_N).$$

The m-dimensional vector is formed by the time delay $X_i = \left[x_1, x_2, \ldots, x_{i+(m-1)\tau}\right]$, where X_i is the reconstructed vector, m is the embedding dimension, and τ is the delay time. If N is one-dimensional univariate data, then i = 1, 2, …, M; $m = N - (\mathrm{M} - 1)\ \tau$, the number of phase points of the phase space vector after M reconstruction. In phase space reconstruction, Takens' theorem states that for an ideal one-dimensional time series without noise, with arbitrary values for the embedding dimension m and delay time interval τ, there is a certain amount of noise in the actual measured time series. Therefore, the delay time interval and embedding dimension of the phase space reconstruction are taken into account.

In this study, two-dimensional phase space reconstruction is analyzed. According to the theory of phase space reconstruction, when the sampled signal is completely random white noise, its phase space reconstruction diagram fills the whole phase space. When the sampled signal is a chaotic signal, its phase space shows a certain shape, and different laws have different shapes [42], Research in the literature shows that two-dimensional phase space reconstruction diagrams of natural wind and mechanical wind are spindle-shaped and elliptical, respectively, which shows that natural wind has stronger autocorrelation than mechanical wind [43]. In this paper, two-dimensional phase space reconstructions at the collision points of air flow with different air supply forms and different aspect ratios of closed space are analyzed.

The figure shows the reconstruction of the two-dimensional phase space reconstruction of the velocity time series of the collision point. The abscissa and ordinate represent the original time series and the reconstructed time series, respectively. When the air supply speed is 0.57 m/s, the phase space reconstruction diagram of the collision point reveals that the aggregated spatial points exhibit a spindle shape, indicating that there is a strong correlation. Most of the velocity distributions are between 0.1 m/s and 0.25 m/s. With increasing air supply velocity, the velocity range at the collision point increases, and the correlation decreases. The shape of the phase space diagram increases with increasing air supply speed, the width of the spindle gradually increases, and the spindle-shaped tail speed gradually disperses. This phenomenon indicates that with the change in the air supply speed, the airflow fluctuation increases after the collision, and the surrounding small-scale airflow structure increases, revealing the phenomenon of unstable oscillation of the airflow after the collision.

Figure 25 shows a two-dimensional phase space reconstruction diagram of the velocity time series of the collision points selected for the different air supply forms. The phase space reconstruction diagram of the collision point reveals that the aggregation space points are spindle-shaped, indicating that there is a strong correlation between the velocity sequences of the two air supply forms. When the air supply is an attached jet, the velocity range is concentrated from 0.1 m/s to 0.4 m/s. When the air supply is a free jet, the

velocity is concentrated in the range of 0.1 m/s to 0.45 m/s. Compared with that of the attached jet, the speed of the spindle tail formed by the collision point of the free jet is more divergent after reconstruction, and these speed ranges are concentrated in the range of 0.6 m/s to 1 m/s. This phenomenon confirms that in the free jet, when the two airflows are deflected up and down, the velocity range of the collision point is small; however, when the two airflows are in the process of transition from collision to deflection, the velocity range of the collision point is large, reflecting the periodic deflection of the free jet airflow collision.

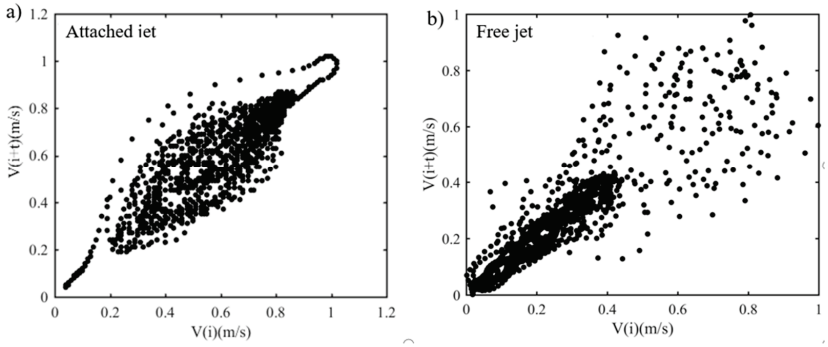


Figure 25. Two-dimensional phase space reconstruction diagram of the velocity time series of different air supply forms: (**a**) Attached jet and (**b**) Free jet.

Figure 26 shows the reconstructed image obtained by two-dimensional phase space reconstruction of the velocity time series of collision points at different aspect ratios. As the aspect ratio increases from 1:1 to 3:1, the velocity range of the collision point is maintained at 0.1 m/s to 1 m/s. The aggregated spatial points exhibit a spindle shape, indicating that there is a correlation between the velocity time series at the collision point.

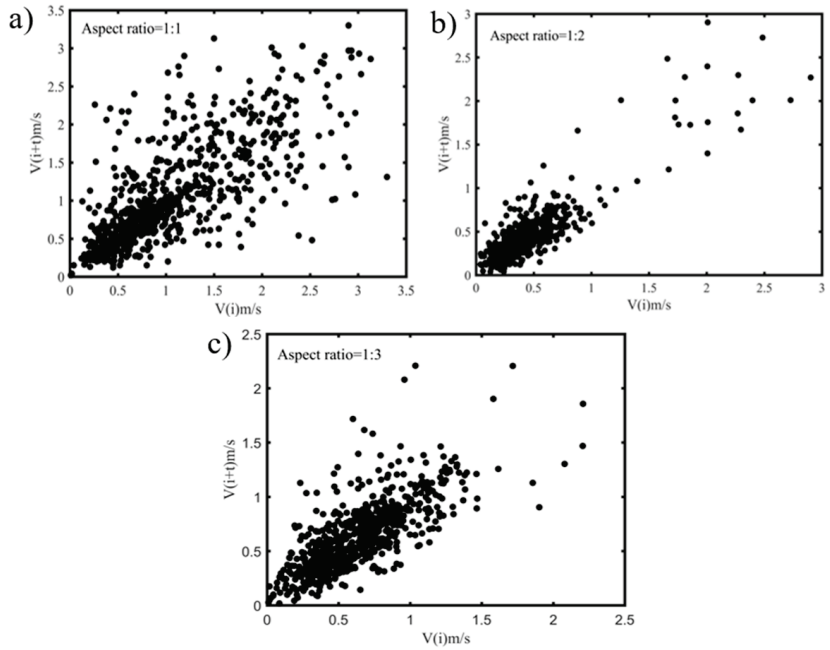


Figure 26. Two-dimensional phase space reconstruction of time series with different aspect ratios: (**a**) 1:1, (**b**) 1:2, and (**c**) 1:3.

Figure 27 shows the two-dimensional phase space reconstruction of the velocity time series at different temperatures The reconstructed image is obtained by reconstructing the

two-dimensional phase space of the collision point velocity time series at different ground source temperatures. The aggregated spatial points are spindle-shaped and exhibit obvious autocorrelation. With the increasing ground source temperature, the velocity increases from 0.1 m/s to 0.3 m/s. As the ground source temperature increases, the width of the spindle gradually becomes wider. This shows that an increase in temperature leads to an increase in small-scale airflow around the cavity, and the instability oscillation of airflow gradually becomes obvious. The effect of temperature on airflow instability in a closed cavity is revealed.

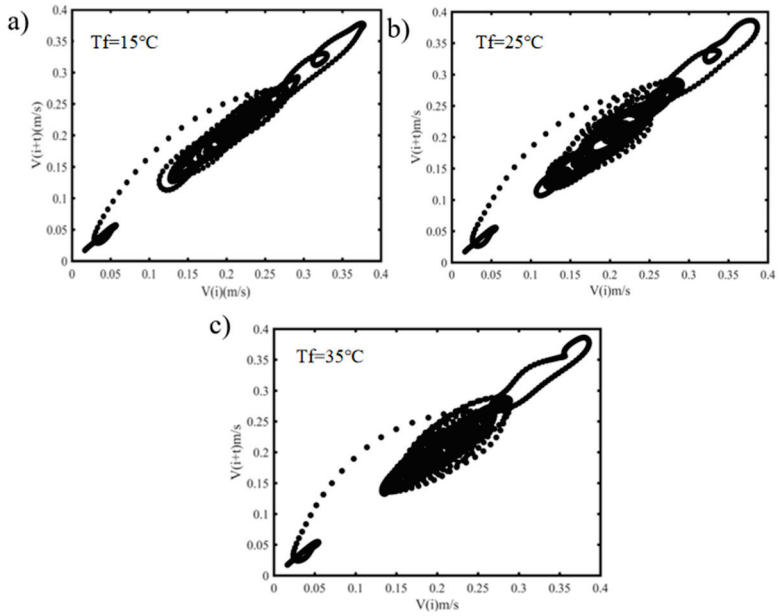


Figure 27. Two-dimensional phase space reconstruction of the velocity time series at different temperatures: (**a**) T_f is 15, (**b**) T_f is 25, and (**c**) T_f is 35 °C.

5. Discussion

Regarding the potential numerical errors and limitations of the adopted turbulence model, we have conducted the following discussion. Using the LES turbulence model, there are numerical errors in the prediction of anisotropic flows by the sub grid-scale (SGS) model. The model may fail to accurately capture the energy backscatter phenomenon from small to large scales. The LES turbulence model is limited by wall regions and high Reynolds numbers, and resolving the wall requires a significant increase in grid size, which in turn increases computational costs and loses the computational efficiency advantage.

Regarding the comparison between grid resolution and the established standard (e.g., Kolmogorov scale resolution), we have made the following specific discussion: In terms of grid resolution, the study ensured that $y < 5$ (average $y \approx 1$) of the near-wall grid, thereby fully resolving the viscous sublayer and meeting the best practice standards for LES in wall flows. Although it is challenging to fully resolve the Kolmogorov scale in high Reynolds number flows, the grid resolution ($\Delta x \approx 5$ mm) successfully captured more than 80% of the turbulent kinetic energy (TKE) spectrum, meeting the Pope criterion ($\Delta \leq \pi\eta$, where η is the Kolmogorov scale). This result was further verified by analyzing the energy spectrum attenuation in the inertial subregion. In addition, the power spectrum of the velocity fluctuations at the collision point exhibited the expected $-5/3$ slope in the inertial subregion, confirming the full resolution of the energy-containing vortices [44–46]. The study also acknowledged the limitations of the current method. For example, the WALE model assumes that the sub-grid turbulence is isotropic and may not fully capture the

anisotropic characteristics of the jet collision zone. In the future, it is planned to introduce a dynamic Smagorinsky model or compare it with DNS results to improve this. At the same time, although the current grid is able to resolve large-scale instabilities, local refinement of the collision zone may further improve the simulation accuracy of small-scale dynamics, which will be given priority in subsequent research.

Regarding the quantitative analysis of the transition from momentum-dominated to buoyancy-driven instabilities controlled by the dimensionless parameter Gr/Re^2, we have made the following specific discussion: at cross-section Z is 0.15 m, the Gr/Re^2 values corresponding to floor temperatures of 15 °C, 25 °C, and 35 °C are 0, 0.68, and 1.37, respectively. When the floor temperature is 15 °C, the flow exhibits pure forced convection without buoyancy effects, being entirely driven by external momentum with absolute dominance of inertial forces. At 25 °C, mixed convection occurs where buoyancy competes with inertia, resulting in flow direction co-influenced by both mechanisms and potential emergence of vortices or unstable stratification. The 35 °C condition represents buoyancy-dominated mixed convection, where buoyancy significantly outweighs inertial forces, establishing natural convection as the primary flow driver while forced convection plays a secondary role. These results demonstrate progressively enhanced buoyancy effects on flow patterns with increasing temperature.

Regarding humidity-driven stratification or pollutant transport (e.g., CO_2) and their interaction with flow field instability mechanisms, the following specific discussion is made: The humidity-driven stratification and flow field instabilities are dynamically coupled through density variations: increased humidity reduces air density, inducing buoyancy differentials that can either form stable stratification suppressing mixing (e.g., overlying humid air) or trigger convective instabilities due to density inversion (e.g., upward motion of low-density humid air near the surface). This mechanism governs pollutant (e.g., CO_2) diffusion modes (laminar diffusion vs. turbulent transport) by modulating turbulence intensity and vertical mixing efficiency. Simultaneously, latent heat release from phase transitions during humid air ascent further modifies the density field and amplifies flow instabilities, creating a positive feedback loop.

6. Conclusions

The study investigates the instability of airflow structures in enclosed spaces ventilated by opposed jets, focusing on factors such as air supply velocity, airflow configuration, spatial aspect ratio, and thermal gradients. Using large eddy simulations (LES), it was found that increasing air supply velocity enhances airflow stability by reducing oscillation amplitude and small-scale disturbances, while shortening the oscillation period. For instance, the period decreased from 11.3 s at 0.57 m/s to 7.7 s at 1.92 m/s. These findings highlight the role of supply velocity in stabilizing airflow structures and mitigating chaotic behavior.

Air supply configuration significantly influences airflow dynamics. Free jet configurations, where air is centrally supplied, generate more chaotic and less stable structures compared to attached jets with upper supply. This results in larger oscillation periods and amplitudes for free jets, demonstrating their less uniform airflow distribution. The positioning of air supply also affects oscillatory behavior, as centrally positioned supply streams create pronounced deflection patterns and increased turbulence compared to upper-positioned streams.

The aspect ratio of the enclosed space has a profound impact on airflow stability. Larger aspect ratios extend oscillation periods—from 10.6 s for a 1:1 ratio to 18.1 s for a 3:1 ratio—while reducing swing amplitudes. The increased distance between jets and

surrounding airflow entrainment at higher aspect ratios contributes to these effects, emphasizing the importance of spatial design in ventilation systems.

Thermal gradients further destabilize airflow structures. Higher floor temperatures increase oscillation periods and drive more dispersed and refined airflow patterns, highlighting the role of heat sources in enhancing instability. For instance, oscillation periods increased from 11 s at 15 °C to 17 s at 35 °C. These findings underscore the need to account for thermal effects in optimizing ventilation performance.

By employing power spectrum and phase space reconstruction analyses, the study demonstrates the periodic and unstable nature of airflow oscillations under different parameters. The results provide valuable insights for designing ventilation systems that ensure effective airflow distribution, improved air quality, and enhanced comfort in enclosed spaces. Future experimental validation using Particle Image Velocimetry (PIV) will strengthen the applicability of these findings.

Author Contributions: All authors contributed to the study conception and design. Material preparation and analysis were performed by Y.L., Y.Z. and P.D. The first draft of the manuscript was written by C.W. The manuscript was reviewed and revised. By Y.X. and H.C. All authors commented on previous versions of the manuscript. All authors have read and agreed to the published version of the manuscript.

Funding: This work was supported by the Beijing Municipal Science and Technology Project (Z231100006123014).

Data Availability Statement: The data are not publicly available due to their large size or specialized format, but subsets can be shared upon request.

Conflicts of Interest: The authors have no competing interests to declare that are relevant to the content of this article.

References

1. World Health Organization. *Modes of Transmission of Virus Causing COVID-19: Implications for IPC Precaution Recommendations: Scientific Brief 29 March 2020*; World Health Organization: Geneva, Switzerland, 2020.
2. Allan, M.; Lièvre, M.; Laurenson-Schafer, H.; De Barros, S.; Jinnai, Y.; Andrews, S.; Stricker, T.; Formigo, J.P.; Schultz, C.; Perrocheau, A.; et al. The world health organization COVID-19 surveillance database. *Int. J. Equity Health* **2022**, *21* (Suppl. S3), 167. [CrossRef] [PubMed]
3. National Health Commission. Novel Coronavirus Pneumonia Diagnosis and Treatment Plan (Trial Version 9). Available online: http://www.gov.cn/zhengce/zhengceku/2022-03/15/content_5679257 (accessed on 15 March 2022).
4. Tang, J.W.; Marr, L.C.; Li, Y.; Dancer, S.J. COVID-19 has redefined airborne transmission. *BMJ* **2021**, *373*, n913. [CrossRef] [PubMed]
5. Dai, H.; Zhao, B. Movement and transmission of human exhaled droplets/droplet nuclei. *Kexue Tongbao/Chin. Sci. Bull.* **2021**, *66*, 493–500. [CrossRef]
6. Cao, G.; Awbi, H.; Yao, R.; Fan, Y.; Sirén, K.; Kosonen, R.; Zhang, J.J. A review of the performance of different ventilation and airflow distribution systems in buildings. *Build. Environ.* **2014**, *73*, 171–186. [CrossRef]
7. Xu, C.; Yu, C.W.F. Prevention and control of COVID-19 transmission in the indoor environment. *Indoor Built Environ.* **2022**, *31*, 1159–1160. [CrossRef]
8. Nielsen, P.V.; Restivo, A.; Whitelaw, J.H. The velocity characteristics of ventilated rooms. *J. Fluids Eng.* **1978**, *100*, 291–298. [CrossRef]
9. Moureh, J.; Flick, D. Wall air–jet characteristics and airflow patterns within a slot ventilated enclosure. *Int. J. Therm. Sci.* **2003**, *42*, 703–711. [CrossRef]
10. Moureh, J.; Flick, D. Airflow characteristics within a slot-ventilated enclosure. *Int. J. Heat Fluid Flow* **2005**, *26*, 12–24. [CrossRef]
11. Li, W.F.; Huang, G.F.; Tu, G.Y.; Liu, H.F.; Wang, F.C. Experimental study of planar opposed jets with acoustic excitation. *Phys. Fluids* **2013**, *25*, 014108. [CrossRef]
12. Wang, C.; Zhang, J.; Chao, J.; Yang, C.; Chen, H. Evaluation of dynamic airflow structures in a single-aisle aircraft cabin mockup based on numerical simulation. *Indoor Built Environ.* **2022**, *31*, 398–413. [CrossRef]

13. Denshchikov, V.A.; Kondrat'Ev, V.N.; Romashov, A.N.; Chubarov, V.M. Auto-oscillations of planar colliding jets. *Fluid Dyn.* **1983**, *18*, 460–462. [CrossRef]
14. Rolon, J.C.; Veynante, D.; Martin, J.P.; Durst, F. Counter jet stagnation flows. *Exp. Fluids* **1991**, *11*, 313–324. [CrossRef]
15. Champion, M.; Libby, P.A. Reynolds stress description of opposed and impinging turbulent jets. Part I: Closely spaced opposed jets. *Phys. Fluids A Fluid Dyn.* **1993**, *5*, 203–216. [CrossRef]
16. Weersink, R. Experimental Study of the Oscillatory Interaction Between Two Free Opposed Turbulent Round Jets. Master's Thesis, University of Twente, Enschede, The Netherlands, 2010.
17. Li, W.F.; Yao, T.L.; Liu, H.F.; Wang, F.C. Experimental investigation of flow regimes of axisymmetric and planar opposed jets. *AIChE J.* **2011**, *57*, 1434–1445. [CrossRef]
18. Hassaballa, M.; Ziada, S. Self-excited oscillations of two opposing planar air jets. *Phys. Fluids* **2015**, *27*, 014109. [CrossRef]
19. Ansari, A.; Chen, K.K.; Burrell, R.R.; Egolfopoulos, F.N. Effects of confinement, geometry, inlet velocity profile, and Reynolds number on the asymmetry of opposed-jet flows. *Theor. Comput. Fluid Dyn.* **2018**, *32*, 349–369. [CrossRef]
20. Zhao, Y.; Brodkey, R.S. Averaged and time-resolved, full-field (three-dimensional), measurements of unsteady opposed jets. *Can. J. Chem. Eng.* **1998**, *76*, 536–545. [CrossRef]
21. Johnson, D.A. Experimental and numerical examination of confined laminar opposed jets part I. Momentum imbalance. *Int. Commun. Heat Mass Transf.* **2000**, *27*, 443–445. [CrossRef]
22. Pawlowski, R.P.; Salinger, A.G.; Shadid, J.N.; Mountziaris, T.J. Bifurcation and stability analysis of laminar isothermal counter-flowing jets. *J. Fluid Mech.* **2006**, *551*, 117–139. [CrossRef]
23. Kind, R.J.; Suthanthiran, K. The interaction of two opposing plane turbulent wall jets. *J. Fluid Mech.* **1973**, *58*, 389–402. [CrossRef]
24. Wood, P.; Hrymak, A.; Yeo, R.; Johnson, D.; Tyagi, A. Experimental and computational studies of the fluid mechanics in an opposed jet mixing head. *Phys. Fluids A Fluid Dyn.* **1991**, *3*, 1362–1368. [CrossRef]
25. Srisamran, C.; Devahastin, S. Numerical simulation of flow and mixing behavior of impinging streams of shear-thinning fluids. *Chem. Eng. Sci.* **2006**, *61*, 4884–4892. [CrossRef]
26. Wu, Q.G.; Liang, X.G.; Chen, Z.J.; Ren, J.X. Numerical study on the bifurcation phenomenon of convective heat transfer in square cavity oblique inlet. *J. Tsinghua Univ. Nat. Sci. Ed.* **2000**, *40*, 102–105.
27. Zou, K.; Yang, M.; Zhang, H.Y. Numerical study of mixed convection heat transfer in square space. *J. Eng. Thermophys.* **2001**, *22*, 207–210.
28. Zheng, Z.H.; Zhang, J.L. Characteristics and numerical simulation of ventilation and air conditioning in manned spacecraft cabin. *Build. Therm. Vent. Air Cond.* **2005**, *24*, 86–90.
29. Zhao, F.Y.; Liu, D.; Tang, G.F. Multiple steady fluid flows in a slot-ventilated enclosure. *Int. J. Heat Fluid Flow* **2008**, *29*, 1295–1308. [CrossRef]
30. Liu, D.; Zhao, F.Y.; Tang, G.F. Nonunique convection in a three-dimensional slot-vented cavity with opposed jets. *Int. J. Heat Mass Transf.* **2010**, *53*, 1044–1056. [CrossRef]
31. Zhao, M.; Yang, M.; Lu, M.; Zhang, Y. Evolution to chaotic mixed convection in a multiple ventilated cavity. *Int. J. Therm. Sci.* **2011**, *50*, 2464–2472. [CrossRef]
32. Shishkina, O.; Wagner, C. A numerical study of turbulent mixed convection in an enclosure with heated rectangular elements. *J. Turbul.* **2012**, *13*, N22. [CrossRef]
33. Körner, M.; Shishkina, O.; Wagner, C.; Thess, A. Properties of large-scale flow structures in an isothermal ventilated room. *Build. Environ.* **2013**, *59*, 563–574. [CrossRef]
34. Yang, C.; Zhang, X.; Cao, X.; Liu, J.; He, F. Numerical simulations of the instantaneous flow fields in a generic aircraft cabin with various categories turbulence models. *Procedia Eng.* **2015**, *121*, 1827–1835. [CrossRef]
35. Kandzia, C.; Mueller, D. Flow structures and Reynolds number effects in a simplified ventilated room experiment. *Int. J. Vent.* **2016**, *15*, 31–44. [CrossRef]
36. Kandzia, C.; Mueller, D. Stability of large room airflow structures in a ventilated room. *Int. J. Vent.* **2018**, *17*, 1–16. [CrossRef]
37. Thysen, J.H.; van Hooff, T.; Blocken, B.; Van Heijst, G.J.F. CFD simulations of two opposing plane wall jets in a generic empty airplane cabin: Comparison of RANS and LES. *Build. Environ.* **2021**, *205*, 108174. [CrossRef]
38. Thysen, J.H.; van Hooff, T.; Blocken, B.; van Heijst, G. PIV measurements of opposing-jet ventilation flow in a reduced-scale simplified empty airplane cabin. *Eur. J. Mech.-B/Fluids* **2022**, *94*, 212–227. [CrossRef]
39. Thysen, J.H.; van Hooff, T.; Blocken, B.; van Heijst, G.J.F. Instantaneous characteristics of interacting opposing plane jets in a generic enclosure measured with PIV. *Exp. Fluids* **2023**, *64*, 19. [CrossRef]
40. Blay, D. Confined turbulent mixed convection in the presence of horizontal buoyant wall jet. In *Fundamentals of Mixed Convection*; HTD-Vol. 213; ASME: New York, NY, USA, 1992.

41. Takens, F. Detecting strange attractors in turbulence. In *Dynamical Systems and Turbulence, Warwick 1980: Proceedings of a Symposium Held at the University of Warwick 1979/80*; Springer: Berlin/Heidelberg, Germany, 2006; pp. 366–381.
42. Packard, N.H.; Crutchfield, J.P.; Farmer, J.D.; Shaw, R.S. Geometry from a time series. *Phys. Rev. Lett.* **1980**, *45*, 712. [CrossRef]
43. Hara, T.; Shimizu, M.; Iguchi, K.; Odagiri, G. Chaotic fluctuation in natural wind and its application to thermal amenity. *Nonlinear Anal. Theory Methods Appl.* **1997**, *30*, 2803–2813. [CrossRef]
44. Davidson, L.; Nielsen, P.V. Large eddy simulations of the flow in a three-dimensional ventilated room. *Dep. Build. Technol. Struct. Eng. Indoor Environ. Technol.* **1996**, *R9651*, 59.
45. Ezzouhri, R.; Joubert, P.; Penot, F.; Mergui, S. Large Eddy simulation of turbulent mixed convection in a 3D ventilated cavity: Comparison with existing data. *Int. J. Therm. Sci.* **2009**, *48*, 2017–2024. [CrossRef]
46. Zhang, W.; Chen, Q. Large eddy simulation of natural and mixed convection airflow indoors with two simple filtered dynamic subgrid scale models. *Numer. Heat Transf. Part A Appl.* **2000**, *37*, 447–463.

Disclaimer/Publisher's Note: The statements, opinions and data contained in all publications are solely those of the individual author(s) and contributor(s) and not of MDPI and/or the editor(s). MDPI and/or the editor(s) disclaim responsibility for any injury to people or property resulting from any ideas, methods, instructions or products referred to in the content.

buildings

MDPI

Article

Impact of Streetscape Built Environment Characteristics on Human Perceptions Using Street View Imagery and Deep Learning: A Case Study of Changbai Island, Shenyang

Xu Lu [1], Qingyu Li [1], Xiang Ji [1], Dong Sun [1,*], Yumeng Meng [2], Yiqing Yu [2] and Mei Lyu [1]

[1] School of Architecture and Urban Planning, Shenyang Jianzhu University, Shenyang 110168, China
[2] Faculty of Environmental Engineering, The University of Kitakyushu, Kitakyushu 8080135, Japan
* Correspondence: sundong@sjzu.edu.cn

Abstract: Since the reform and opening-up policy, the accelerated urbanization rate has triggered extensive construction of new towns, leading to architectural homogenization and environmental quality degradation. As urban development transitions toward a "quality improvement" paradigm, there is an urgent need to synergistically enhance the health performance of human settlements through the optimization of public space environments. The purpose of this study is to explore the impact of the built environment of urban streets on residents' perceptions. In particular, in the context of rapid urbanization, how to improve the mental health and quality of life of residents by improving the street environment. Changbai Island Street in the Heping District of Shenyang City was selected for the study. Baidu Street View images combined with machine learning were employed to quantify physical characterizations like street plants and buildings. The 'Place Pulse 2.0' dataset was utilized to obtain data on residents' perceptions of streets as beautiful, safe, boring, and lively. Correlation and regression analyses were used to reveal the relationship between physical characteristics such as green visual index, openness, and pedestrians. It was discovered that the green visual index had a positive effect on perceptions of it being beautiful and safe, while openness and building enclosure factors influenced perceptions of it being lively or boring. This study provides empirical data support for urban planning, emphasizing the need to focus on integrating environmental greenery, a sense of spatial enclosure, and traffic mobility in street design. Optimization strategies such as increasing green coverage, controlling building density, optimizing pedestrian space, and enhancing the sense of street enclosure were proposed. The results of the study not only help to understand the relationship between the built environment of streets and residents' perceptions but also provide a theoretical basis and practical guidance for urban space design.

Keywords: city street; built environment; street view image; semantic segmentation; human perception

1. Introduction

Human perception plays an important role in public and environmental psychology [1]. Human perception has been shown in environmental psychology research to be a mediator between physical characteristics and human behavior [2]. Analyzing human perception in urban spaces is essential for researchers to uncover the intricate relationships between the built environment, psychological well-being, and spatial behavior [3,4]. Recent

investigations have significantly advanced our understanding of how human perception is shaped by environmental factors and its implications for urban sustainability [5]. Several studies have shown that visual space reflects much of the urban environment. The visual space of the built urban environment influences the psychological and health perceptions of its inhabitants [6,7].

Driven by the accelerated globalization process, urbanization has emerged as the most prominent spatial restructuring phenomenon in the 21st century. As the largest developing nation, China has seen its urbanization rate leap from 17.9% in 1978 to 66.16% in 2023. The initial pattern of urban expansion was a shift from the renewal of old urban areas to sprawl development dominated by new urban areas [8]. This initial rough construction has led to problems such as the decay of the environmental effectiveness of new urban areas [9]. The World Health Organization (2016) highlights that environmental pressures on new urban areas and lifestyle changes are exacerbating mental health risks for residents [10]. These challenges are prompting a shift in China's urban development paradigm from "extensive growth" to "quality-oriented improvement". China's State Council's 14th Five-Year Plan for Modern Urban Governance explicitly states that China should implement the "Urban Quality Enhancement Initiative" and lists the optimization of the public space environment as a core task of new urbanization. This requires urban planners and government personnel to realize a synergistic enhancement of the quality of the habitat and the well-being of the residents of new urban areas in the early stages of expansion within the context of people-centered planning [11,12]. Therefore, exploring how to solve the health and environmental problems brought about by urbanization in new towns and improving the quality of public space in roughly developed new towns plays a crucial role in modern urban development [13].

As a public space frequently engaged by urban residents in their daily activities, the street's spatial environment directly affects the residents' impression of the city [14], further influencing their behavior and mental health [15]. Streets connect different functional areas of the city [16,17], and at the same time, streets are defined for different functions such as commerce, transportation, and residence [18–20]. Moreover, emerging evidence highlights that the impacts of distinct street-scale built environments on human perception vary significantly. Empirical findings demonstrate divergent perceptual responses across zones with differing land-use compositions, where residential and commercial areas tend to evoke feelings of safety and vibrancy, whereas parklands and residential neighborhoods foster stronger aesthetic appreciation [1]. Several studies have found that negative perceptions are significantly related to poorer street built environments [21]. Therefore, improving the aesthetics and vibrancy of streets not only enhances the quality of urban streets but also reduces the psychological pressure on the public [22]. Several studies have shown that the creation of high-quality streets has a positive impact on residents [23], as well as enhancing their attachment to multiple places [24]. Several scholars in their research have proposed that the quality and spatial characteristics of streets affect public perceptions such as safety and stress [25]. Optimizing the spatial characteristics of streets as well as the quality of streets can alleviate human depression and anxiety [26].

Existing research at the street scale focuses on the preservation of historic districts [27], the analysis of residents' perceptions in old urban areas [28], and the assessment of the visual quality of campuses [29]. Over time, the problem of alienation of the built environment caused by the rough construction in the early stage of the expansion of new districts has become more and more obvious. The relationship between street form and human perception is more complex in new districts than in organically grown old districts. However, existing research has paid insufficient attention to the evaluation of visual quality

and perception of streets in the early stages of the expansion of new districts. A quantitative index system for street perception applicable to the expansion stage of new cities in China has not been established.

Based on previous research on urban quality, this study selected the Changbai Island area in Shenyang City as an empirical object, using streetscape big data and deep learning techniques to explore the integrated area in the early stages of urban rough construction. We developed evaluation indicators for the physical characteristics of street space and dimensions of human perception during the expansion of new districts and uncovered the mechanisms of spatial heterogeneity in how the physical environment shapes human perception. The methodological framework includes the following steps:

(1) Delineate the study area and determine the sample points in ArcGIS.
(2) Quantify physical street characteristics via semantic segmentation technology and extract key morphological indices, such as green visibility rate and interface continuity.
(3) Obtain residents' street perception data using the Place Pulse 2.0 dataset.
(4) Explore the relationship between physical street attributes and residents' emotional perceptions.

This study provides technical references for enhancing the quality of life and promoting the mental health of urban residents.

2. Literature Review

2.1. Theoretical Studies Related to Human Perception

Over the years, several disciplines and fields, such as environmental psychology, neuroscience, and urban planning, have been exploring the relationship between the environment and human perception [30,31]. Human perception of the city refers to the preference of urban residents for the urban environment and their cognitive judgment of specific scenes such as city streets, buildings, and parks [32]. In his book Space and Place: A Perspective on Experience, Tuan elaborated on the formation logic of space and place and analyzed how places influence human perceptions [33]. Based on environmental psychology, Rachel and Stephen Kaplan (1989) proposed that the natural environment influences human perception and mental health [30]. Ulrich's empirical research found that the natural environment influences people's aesthetic preferences [34]. In the 1990s, Ulrich proposed the Stress Reduction Theory (SRT) [35], and Kaplan proposed the Attention Restoration Theory (ART) [36]. Both theories emphasize the capacity of high-quality environments (natural and urban) to restore human attention and alleviate stress. Among the core elements in the Attention Restoration Theory are ease, fascination, coherence, and compatibility.

2.2. Human Perception Assessment of Urban Streets

Scholars have been scoring scenes in Chicago-area pictures based on visual attributes like safety, beauty, and landscape preference since 1967. Data on safety, beauty, and preference were used to analyze public perception studies of the visual appearance of neighborhoods. Building on this foundation, scholars have explored human perception and psychological well-being by examining factors such as socio-economic determinants, social dynamics, the physical environment [37], infrastructure configurations [38], and tourism-related attributes [39]. Humans' psychological perception of urban scenes stems from their perceptions [40] and satisfaction [41] after experiencing the place. It influences humans' emotions and, through perception, affects their willingness to engage in physical activities [42,43]. Human psychological perception after place experience mainly covers positive perceptions such as beauty and safety and negative perceptions such as boredom, insecurity, and depression [44–46].

In Maslow's Hierarchy of Needs Theory, safety and beauty are the main factors that fulfill people's basic needs [47]. Beauty is also the most basic aesthetic indicator and can be described as the "relatively aesthetic impeccability of a landscape" [48]. By setting rules for the design of urban aesthetics, it is possible to allow different areas to develop a unique style based on local culture and the needs of the inhabitants [49]. Scholars have employed visual aesthetic metrics to assess the visual quality of streets and parks [47,50]. Perceptions of safety are commonly desired and indicate that a person's presence in a place does not create feelings of embarrassment, foreboding, and danger [51]. Research has shown that the built environment, along with individual physiological and psychological factors, influences perceptions of crime risk [52]. Factors that primarily affect perceptions of safety include the quality of sidewalks as well as infrastructure in public places [53]. Street vitality, an external expression of social vitality in urban contexts, is a key indicator and important manifestation of urban livability [54]. Vitality is the interaction between a person being in that place and the environment. Empirical research has demonstrated that greenscapes significantly enhance street vitality. Conversely, the perception of boredom involves evaluating street aesthetics and represents a subjective experience of monotony during street use. There are significant differences in the perceptions formed by humans in built environments of different qualities [55,56].

2.3. Assessment of the Physical Characteristics of Urban Streets

Previous scholars have analyzed the urban built environment from the perspectives of geography, resource environment, land use, and infrastructure. Physical street characteristics, a key aspect of scholars' spatial quality assessments, accurately reflect the objective physical conditions of streets [57]. Scholars have focused on the physical elements of the street, such as buildings, sky openness, greenery, and sidewalks. Furthermore, the relationship between the street environment and human perception is analyzed based on these physical characteristics. Urban environmental factors such as population density, non-vegetated land cover, arterial road network, vehicular air pollution, tree canopy density, and Normalized Vegetation Index (NDVI) commonly affect human perception of urban space [55]. The richness of infrastructure and the context of different land use types can lead to differences in subjective perceptions [56].

Streets are entities of built space that have the role of linking public infrastructure to the physical characteristics of the built environment [58] and have a very important impact on public perception and mental health [59,60]. In previous studies, the physical characteristics of streets can represent the spatial quality of streets [61]. Scholars have found that the physical characteristics of street space, such as building scale [7], greenery [62], maintenance [3], walkability [63], and openness [60], influence human perception [64]. Among them, the area of vegetation cover affects the perception of beauty [48,65] and safety [66]. Conversely, streets with excessive building density and limited openness increase residents' stress and boredom [67]. Street scale, building density, and open space shape the perception of vitality [68].

2.4. Methods for Acquiring Human Perceptual Features

When studying the spatial quality of streets, traditional ways of investigating human perception include field surveys, interviews, and questionnaires [69,70], which use feedback to summarize the characteristics researchers need to form conclusions [71]. Traditional methods of collecting human perception data are time-consuming and resource-intensive, and they only facilitate the study of smaller areas [72]. The aesthetics evaluation method and the semantic differential method are traditional ways of evaluating visual quality [48]. Scholars often use a Likert scale to score the physical environment of a study area.

Through continuous research, methods to quantify human perception have gradually been rationalized. Cognitive maps, photography, and emoji-based emotion categorization approaches have become the main methods for studying human perception. Based on the development of neurological disciplines, scholars have advocated the use of physiological data to reflect the perceptual state of the public. Consequently, the acquisition of physiological metrics, including electrocardiogram (ECG), galvanic skin response (GSR), electroencephalogram (EEG), and blood pressure, has emerged as a valuable approach for capturing human perceptual responses in urban research [56]. Kacha et al. used EEG experiments to analyze the relationship between the physical characteristics of streetscape images and human perception [73]. However, physiological methods can be limited by small sample sizes, resulting in a failure to reflect true experimental results [74].

In recent years, advances have been made in visual perception research, with researchers transforming data collection and analysis methods through crowdsourcing methods and deep learning algorithms [55]. Crowdsourcing access to large-scale, diverse image data, combined with the powerful feature extraction capabilities of deep learning algorithms, has now become a new approach to studying the field of visual perception. Moreover, researchers are able to more accurately model and predict human perceptual responses to visual environments based on this approach [72].

Dubey et al. (2016) collected the MIT Place Pulse 2.0 dataset of 110,988 images from 56 cities and rated by 84,630 online volunteers, which led to the development of the FCN + RF deep learning visual model [15]. This deep learning model can more accurately predict perceptions of safety, wealth, vitality, beauty, boredom, and depression [75]. In the Place Pulse 1.0 study, it was found that the age, gender, or location of individual participants did not affect their preference for the appearance of the city [76], suggesting that there was no significant cultural bias in the dataset. Additionally, after an empirical study of multiple cities, it is clear that the deep learning visual model of the MIT Place Pulse 2.0 dataset is able to predict people's perceptions of safety, wealth, vitality, beauty, boredom, and depression more generally [75]. Such large-scale perceptual predictions enable automated audits of the urban appearance of cities around the world [29]. Currently, Zhang (2018) applied this large-scale perception model to analyze six dimensions of urban perception in Shanghai [72]. Ruifan Wang employed the FCN + RF model to assess urban perception in Wuhan, demonstrating its ability to efficiently recognize residents' perceptions [77]. This accuracy has enabled urban planners to integrate perceptual insights into planning practices.

2.5. Methods for Obtaining the Physical Spatial Characteristics of Streets

Scholars who studied the built environment of streets often used traditional quantitative methods such as field surveys [78], expert evaluations [79], and photography [80]. While these traditional research methods were more suitable for analyzing the problems of small-scale streets, they had difficulty analyzing the problems existing in large-scale street spaces in a refined way [81]. Over the past decade, advancements in artificial intelligence and big data analytics have driven crowdsourced mapping platforms and street-level imagery [82] to become key data resources for urban studies. Publicly available photos from Google Street View and Baidu Street View offer the advantages of broad accessibility, high resolution, and extensive spatial coverage [83].

In recent years, streetscape images have been used to examine the physical characteristics of the built environment of streets in terms of sky, buildings [84], water bodies [85], and greenery [86]. The results of several scholars' studies have shown that streetscape data can accurately depict the physical environment of a city, as well as show that streetscape images can analyze the visual perception of residents [85]. Streetscape imagery is currently widely used in

research on mental health [87], human perception [88], walkability [89], and the visual quality of streets [90]. With the development of computer vision technology, semantic segmentation has become the main method for processing massive data [91]. Scholars use datasets such as SegNet [92–94] and Cityscape for semantic segmentation. The boundaries of the landscape elements in the image are divided by automation. Researchers systematically analyze physical attributes in street-level imagery by quantifying the ratios of landscape components [91].

3. Materials and Methods

3.1. Study Site

The study site is Changbai Island in Heping District, Shenyang City, which is an integrated residential cluster (Figure 1). The area's residential, transportation, natural resources, educational resources, and commercial amenities have developed from 2008 to the present. Changbai Island is divided into an inner island and an outer island. The inner island covers an area of about 5 square kilometers, and the outer island is about 5.87 square kilometers. The inner and outer islands are separated by a circular water system of about 10 km in length. Forty-seven settlements have been built in the study area, with most completed between 2010 and 2019. These settlements are densely packed and feature a variety of architectural forms. At the same time, several large-scale comprehensive parks and recreational green squares have been constructed on the outer side of Changbai Island. Malls and several schools have also been built on the island. Overall, the Changbai Island area is a typical comprehensive residential area. This area demonstrates the diversity of physical characteristics of built space during urban expansion.

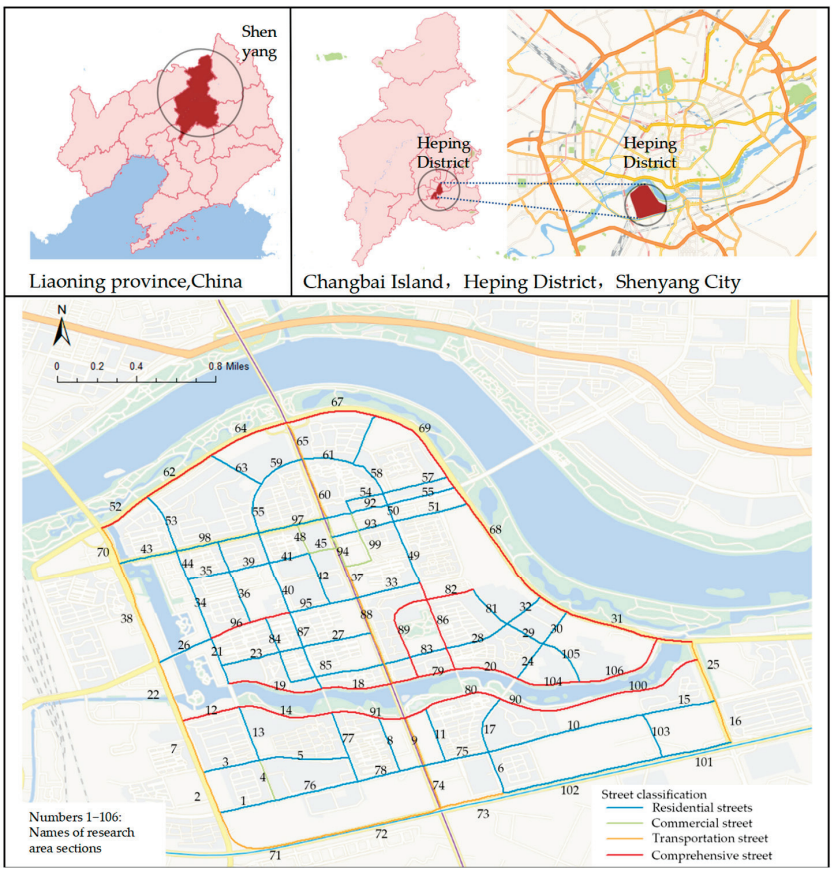


Figure 1. Study area and location of of Changbai Island.

In order to more clearly assess the spatial quality of streets in the study area, the streets have been categorized in various ways in previous studies. Based on the existing street design guidelines in China and the location, physical attributes, transportation, and functions of the study area, we classified the streets in the study area into four main street types: residential, commercial, transportation, and comprehensive streets (Table 1).

Table 1. Description of street classification.

Street Functional Type	Description	Typical Road Section
Transportation street	Transportation streets are characterized by continuous closed interfaces. These streets prioritize maximizing motor vehicle movement efficiency, focusing on facilities such as bus lanes.	Example: 2, 7, 22, 38, 70
Residential street	Residential streets serve as composite functional spaces dominated by residential use, where citizens' daily life and activities are concentrated. These streets constitute linear public space systems anchored by small- and medium-sized commercial services, cultural stations, and public facilities.	Example: 1, 3, 4, 5, 76, 78, 8, 9
Commercial street	Commercial streets are linear public spaces where commercial activities—such as retail, dining, and office uses—predominate, characterized by distinct service capacities or industrial clusters.	Example: 99, 94, 45, 48
Comprehensive street	Comprehensive streets exhibit diverse functions and activities along the roadway, integrating the characteristics of two or more street types (e.g., commercial, lifestyle services, transportation, and landscape–recreation).	Example: 52, 62, 64, 67, 69, 68, 31

A detailed overview of the data collection, processing, and analysis procedures is presented in Figure 2.

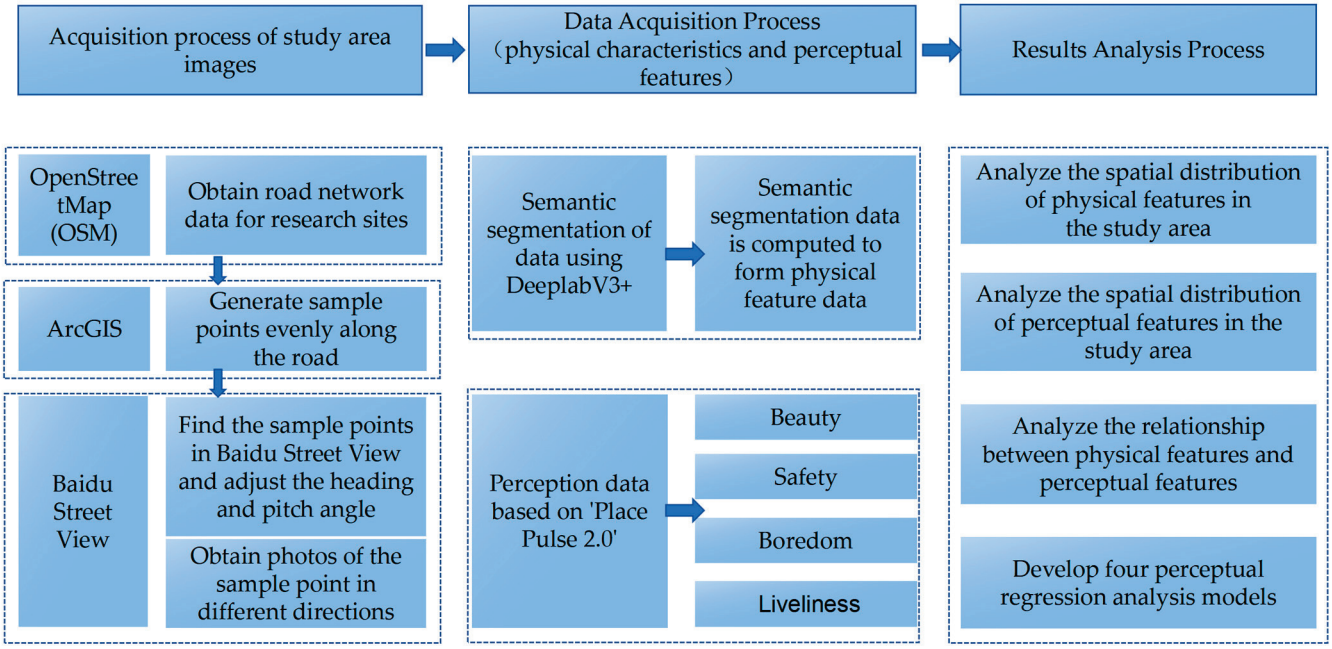


Figure 2. Experimental flow chart.

3.2. Baidu Street View Image Collection

Streetscape imagery is a method for obtaining data on the appearance of cities [95]. This method has been widely used to study the objective attributes of streets and subjective human perceptions [96]. Baidu Maps (https://map.baidu.com/ (accessed on 25 February 2023)) is the largest online map provider in China. Baidu Maps provides panoramic images similar to Google Street View (GSV) [67]. Baidu Street View images were captured by a team of collectors from 10 am to 4 pm on weekdays. To explore the relationship between visual perception and physical characteristics of streets, this study used OpenStreetMap (OSM) to obtain the road network data of the study area. The road network data were used to create road maps, which were then transferred into ArcGIS to simplify the network into single-lane streets [97]. ArcGIS10.2 software was used to delineate sampling points at 50-m intervals, creating a total of 955 sample points. To ensure that the street photos reflected the visual characteristics of pedestrians, the parameters of the street images were configured before capturing the images. Parameters were captured by presetting the street images to ensure the equivalence between the simulated visual field and the actual perception of pedestrians [98]. The heading angles were respectively set to 0, 90, 180, and 270 (Figure 3). Baidu Street View (BSV) images were then manually captured for all sample points in four horizontal directions.

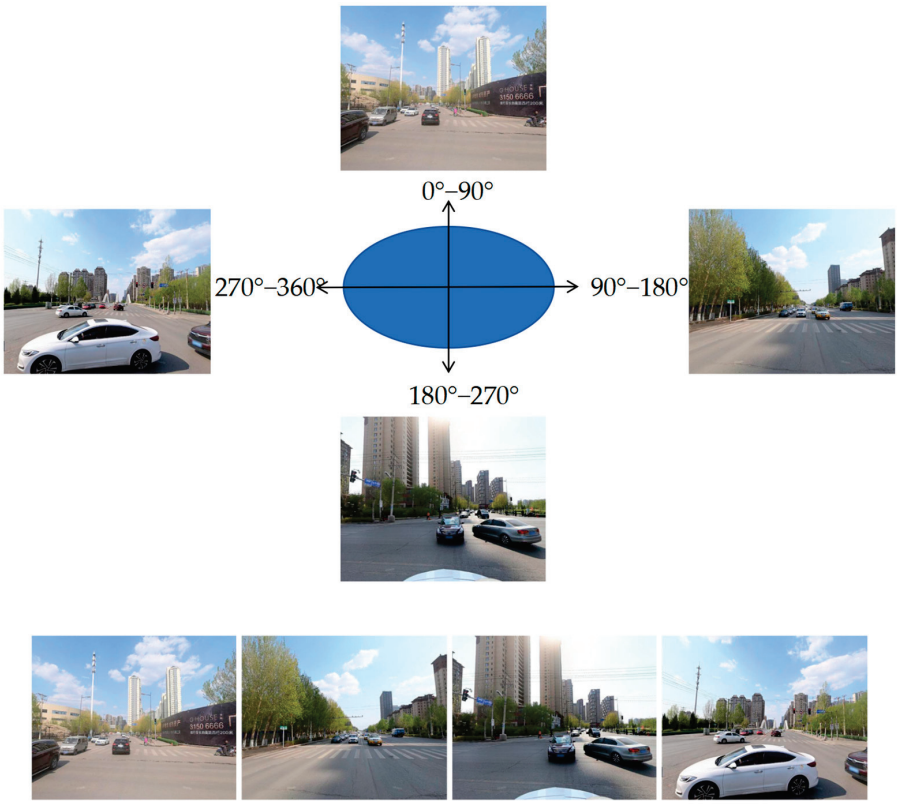


Figure 3. The sample point panoramic view and BSV image.

3.3. Street Space Environment Indicator Extraction

Semantic segmentation is an important part of computer vision technology. DeeplabV3+ is a convolutional neural network model for semantic segmentation algorithms, enabling more accurate information acquisition. In this study, the urban streetscape was classified by DeeplabV3+ into 19 categories, such as roads, sidewalks, and buildings, achieving an overall accuracy of 90% [99]. DeeplabV3+ is capable of handling high-

resolution streetscape analysis tasks and is suitable for micro-level assessment of urban areas [100–102] (Figure 4).

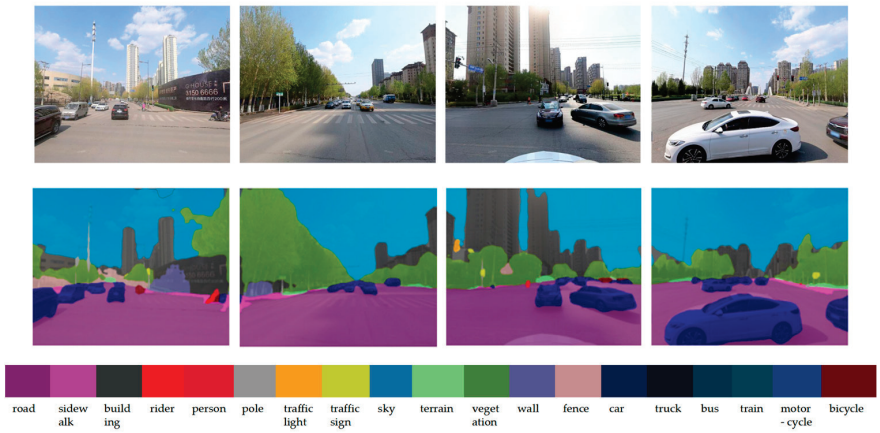


Figure 4. Examples of semantic segmentation.

We chose and identified seven important physical characteristics. It is important to note that all the physical characteristics can be calculated by semantic segmentation. The formulas for calculating the selected seven physical characteristics are shown in Table 2.

Table 2. Physical features of street space.

Physical Indicators	Formula	Interpretation	Definition
Green visual index	$GVI = \frac{1}{n}\sum_{i=1}^{n} T1_i + \frac{1}{n}\sum_{i=1}^{n} V1_i \{i \in (1,2,\cdots,n)\}$	$V1_i$ and $T1_i$ denote the proportions of vegetation and terrain pixels, respectively. n is the number of BSV images of a sample point.	It refers to the ratio of tree and grass pixels to the overall pixels.
Openness	$OP = \frac{1}{n}\sum_{i=1}^{n} S1_i \{i \in (1,2,\cdots,n)\}$	$S1_i$ denotes the proportion of sky pixels; the sum indicates the total number of sky pixels in each image.	It refers to the open degree in the coastal interface.
Walkable streets	$WS = \frac{1}{n}\sum_{i=1}^{n} P1_i + \frac{1}{n}\sum_{i=1}^{n} F1_i + \frac{1}{n}\sum_{i=1}^{n} R1_i \{i \in (1,2,\cdots,n)\}$	$P1_i$ denotes the proportion of pavement pixels; $F1_i$ denotes the proportion of fence pixels; $R1_i$ denotes the proportion of road pixels.	It refers to the ratio of walkable street pixels to the overall pixels.
Vehicle occurrence rate	$VOR = \frac{\frac{1}{n}\sum_{i=1}^{n} C1_i + \frac{1}{n}\sum_{i=1}^{n} T2_i + \frac{1}{n}\sum_{i=1}^{n} B1_i + \frac{1}{n}\sum_{i=1}^{n} T3_i}{\frac{1}{n}\sum_{i=1}^{n} R1_i} \{i \in (1,2,\cdots,n)\}$	$C1_i$ denotes the proportion of car pixels; $T2_i$ denotes the proportion of truck pixels; $B1_i$ denotes the proportion of bus pixels; $T3_i$ denotes the proportion of train pixels; $R1_i$ denotes the proportion of road pixels.	It refers to the proportion of vehicle attendance in the road space.
Natural to artificial ratio of the vertical interface	$VI = \frac{\frac{1}{n}\sum_{i=1}^{n} TI_i}{\frac{1}{n}\sum_{i=1}^{n} B2_i} \{i \in (1,2,\cdots,n)\}$	$T1_i$ denotes the proportion of tree pixels; $B2_i$ denotes the proportion of building pixels.	It refers to the ratio of natural pixels to artificial pixels in the vertical interface.
Pedestrians	$PR = \frac{1}{n}\sum_{i=1}^{n} P3_i \{i \in (1,2,\cdots,n)\}$	$P3_i$ denotes the proportion of pedestrian pixels; the sum indicates the total number of pedestrian pixelsin each image.	It refers to the ratio of pedestrian pixels to the overall street space pixels, including riders and standing or sitting pedestrians.
Building enclosure	$BE = \frac{1}{n}\sum_{i=1}^{n} B2_i \{i \in (1,2,\cdots,n)\}$	$B2_i$ denotes the proportion of building pixels.	It refers to the ratio of building pixels to the overall pixels.

3.4. Calculating Public Visual Perception Data

MIT's Place Pulse 2.0 was a crowdsourcing platform that aggregated data on human ratings of urban landscapes [100]. The platform employed a deep learning computer vision model developed by Dubey et al., capable of predicting human perceptions. Beauty and safety, as foundational dimensions of human perceptual needs [31], influence the attractiveness of urban spaces. In Kaplan's Attention Restoration Theory (ART), the element of

fascination reflects the degree to which a place engages attention, while boredom perception serves as an indicator of built environment unattractiveness. Liveliness perception, representing space-use efficiency, captures interactions and emotions between individuals and street environments, balancing human activities with urban contexts [103]. Although boredom is perceived as a negative emotion and safety, vitality, and beauty as positive ones, the four perceptions in this study are not opposites; each is independent and reflects distinct aspects of street visual quality. Thus, our focus in this study is to utilize this approach to obtain data on the four perceptions of beauty, safety, boredom, and liveliness in the study area.

3.5. Statistical Analysis

Correlation and regression analyses were performed in this study using SPSS 25.0. We treated four perceptual predictors of beauty, safety, boredom, and liveliness as dependent variables and seven physical characteristics, such as green visual index and openness, as independent variables. Regression analyses were conducted to explore the relationships between beauty, safety, boredom, and liveliness and physical characteristics, respectively. Four regression models were developed for beauty, safety, boredom, and liveliness.

4. Results

4.1. Physical Characteristics of the Study Area

In this study, DeeplabV3+ was used for semantic segmentation of sample point photographs, and elements from the built environment of the street were extracted. After the calculation, we obtained the information for the physical characteristics. Calculating the mean value for each physical characteristic, we obtained the following ranking of values: Natural to artificial ratio of the vertical interface (0.4433) > Walkable streets (0.3409) > Vehicle occurrence rate (0.3143) > Building (0.2423) > Green visual index (0.2085) > Openness (0.1589) > Pedestrians (0.0025). The information from the sample points was assigned to street segments, and the point information was homogenized to form street segment information. We analyzed the spatial distribution of physical characteristics based on the street segment information (Figure 5).

Plants were a key component of urban streets, and they affected people's emotional and mental health. We found differences in the degree of greening of different types of streets through the data on green visibility. Comprehensive streets (0.2143) and residential streets (0.2126) had a high GVI, while transportation streets (0.1995) had an average GVI, and commercial streets (0.1777) had the lowest GVI. Comprehensive streets were predominantly flanked by landscaped areas, residential neighborhoods, and schools, and these street segments had high levels of green visibility. For example, the 101st, 95th, and 106th Street segments had lush street trees, and the landscaped area was open on one side with a wide variety of plant species, creating a diverse vegetative landscape. Street segments in areas with mixed traffic and residential functions were bordered by tall and lush street trees and neatly trimmed bushes. Street segments in which schools were mixed with residential neighborhoods had well-aligned and well-grown street trees. The combination of plants on both sides of the road and on the campus effectively reduced street noise and created a quiet learning environment for students. The residential streets were adjoined by residential areas, the roads were narrow, and there was a concentration of green spaces on both sides, resulting in a high GVI. Commercial streets had elements that were primarily paved and amenities with relatively little plant cover, resulting in a low GVI.

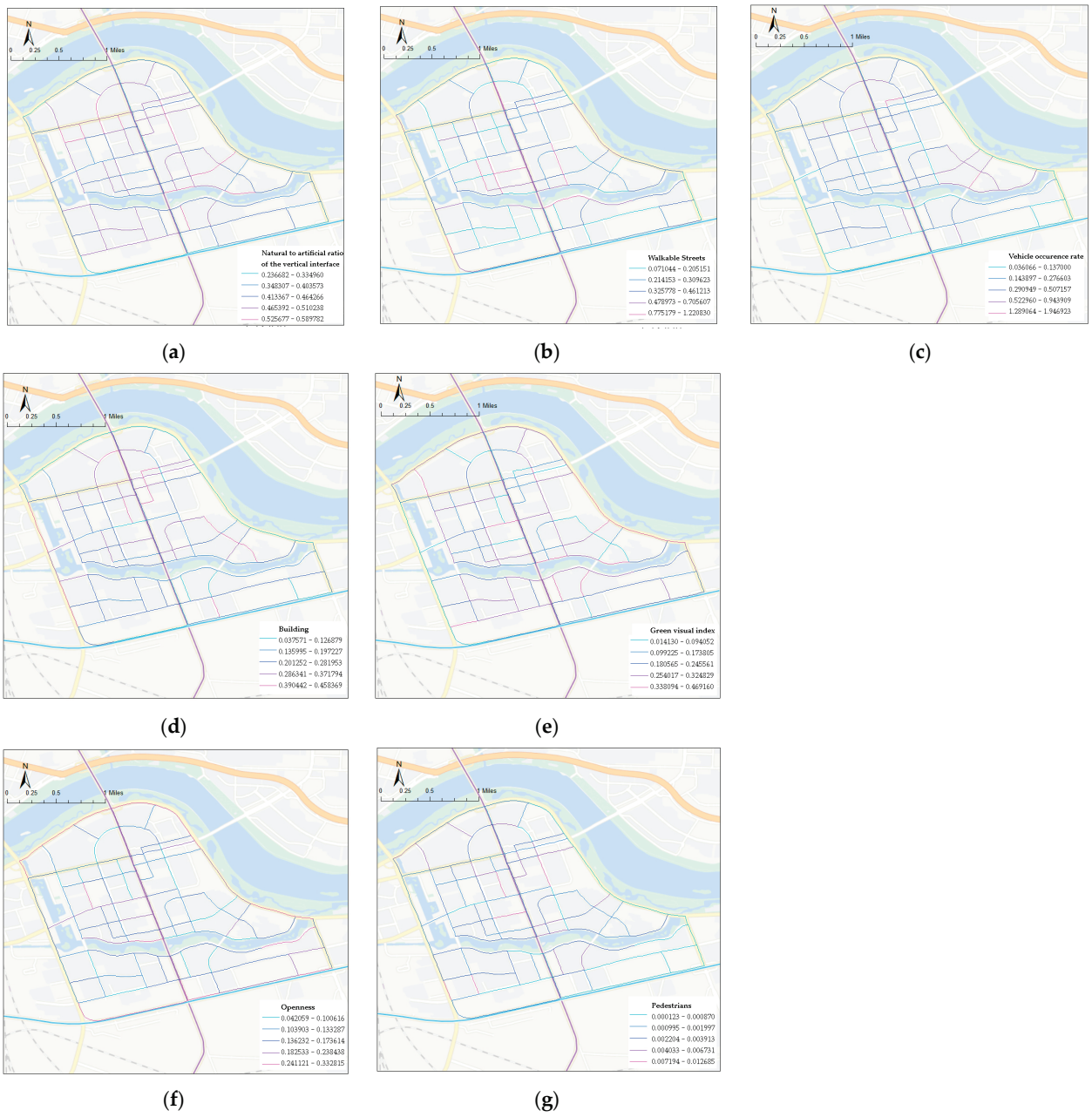


Figure 5. Spatial distribution maps of physical characteristics: (**a**) natural to artificial ratio of the vertical interface; (**b**) walkable streets; (**c**) vehicle occurrence rate; (**d**) building enclosure; (**e**) green visual index; (**f**) openness; (**g**) pedestrians. (Clear diagrams have been placed in Appendix A).

Commercial streets (0.3089) and residential streets (0.2701) exhibited higher BE values. There was less vegetation around the commercial streets, with buildings taking up a larger proportion of the area; residential streets were flanked by residential buildings. In addition to the street trees, a large percentage of the residential building facades were occupied. In contrast, comprehensive streets (0.2106) and transportation streets (0.2003) displayed a relatively low percentage of buildings. There was a large number of other elements in the composite street, hence the low Building Enclosure rating. Transportation streets had wide roadways, and buildings were set back from the roadway, so the percentage of buildings was lower. The results of the study indicated that factors such as street type, vegetation cover, and roadway width influenced the BE value in the built environment. Together,

these factors shaped the public's visual perception of the street. The results of the study showed that openness was highest on traffic streets. The wide roads of the traffic streets and the vegetation and buildings farther away from the traffic streets were the main factors that enhanced the openness. Residential street segments (0.1252) and commercial street areas (0.1242) had lower sky-view openness. Tall buildings and lush vegetation around the streets created shading and reduced the visual area of the sky.

The composite streets were composed of landscaped areas, residential neighborhoods, and schools. Residents and students mainly entered and exited the area on foot. Consequently, due to the high pedestrian traffic, the WS in this area had a higher value. Transportation and comprehensive streets were required to accommodate both pedestrian and vehicular traffic. To avoid congestion, the area of driveways on the portion of the composite street was increased, while the area of walkways was reduced. Transportation streets, generally regional main roads and expressways, were focused on transportation needs and consisted of wide motorized roads and pedestrian paths. Plantings were used to separate driveways and sidewalks, creating a sophisticated system for pedestrian–vehicle traffic separation. Commercial streets had a low average percentage of WS. Two main reasons contributed to this: first, commercial buildings were still under construction and not open to the public. Second, the presence of more automobiles outside these streets reduced the walkable street area.

Higher mean values of the VI were found on residential streets (0.4827) and commercial streets (0.4760). The high VI on residential streets was primarily due to street trees, residential building facades, and fences enclosing the neighborhood's outer layers. In contrast, commercial streets had a VI dominated by commercial buildings with a relatively small percentage of plantings. Traffic streets exhibited the lowest average VI values. The wide roads and open skies of traffic streets led to a diminished proportion of vegetation and buildings, which weakened their VI. Differences in VI were found to influence residents' spatial perception: high enclosure created a closed visual experience, while low enclosure fostered an open visual experience.

Residential and commercial streets had the highest average VOR values. This indicated that more vehicles were parked on both sides of these streets. Streets with standardized parking systems maintained orderly vehicle arrangements, while those lacking parking infrastructure exhibited disorderly vehicle placement, which negatively affected the overall street environment. Notably, a high number of non-motorized vehicles—primarily delivery and take-out worker vehicles—were parked in disorderly clusters in the rear areas of commercial streets. In contrast, composite and transportation streets had fewer parked vehicles, with traffic primarily consisting of moving roadway vehicles. Consequently, impacts on other areas of the roadway were limited.

PR values were the lowest across all streets, with a mean of only 0.0025. This can be attributed to the fact that street photography was conducted during weekday working hours, resulting in fewer pedestrians outdoors. Commercial streets (0.0034) had the highest average PR, which can be attributed to two main factors. First, commercial streets accommodate more workers and are primarily used for daily services such as commuting and food delivery; second, adjacent plazas and commercial facilities attract elderly individuals and children to linger and engage in activities in the area. In contrast, comprehensive streets (0.0019) exhibited the lowest pedestrian percentage.

4.2. Perceptual Characterization Data Results

We assigned the spatial perceptual prediction data to each street segment and calculated the average perceptual eigenvalue for each segment. The results of the four

perceptions of beauty, safety, boredom, and liveliness were visualized, and significant spatial heterogeneity in the perceptions of the study area was found (Figure 6). Overall, beauty and safety showed similar patterns in spatial distribution, while boredom and liveliness showed significantly different spatial distributions.

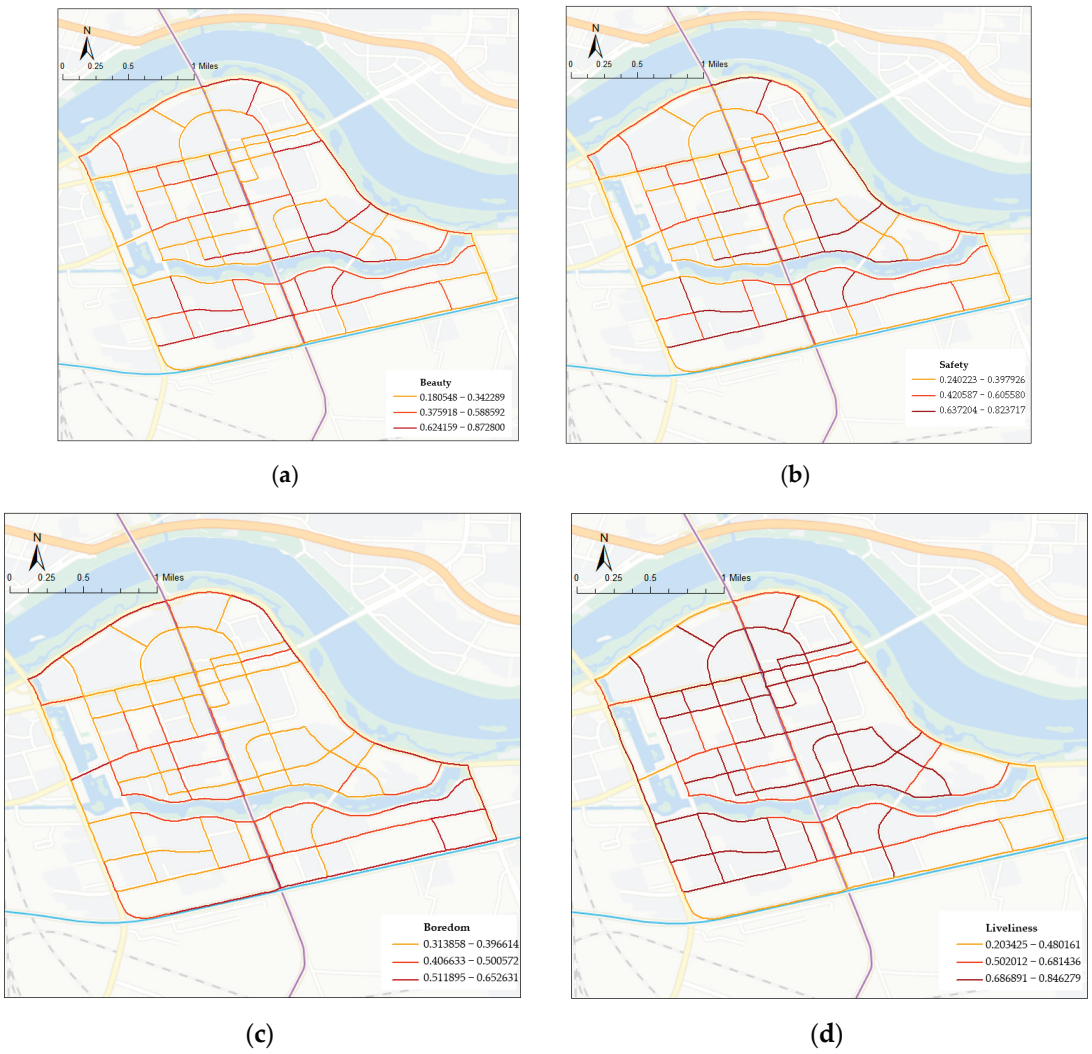


Figure 6. Spatial distribution maps of perception features: (**a**) beauty; (**b**) safety; (**c**) boredom; (**d**) liveliness. (Clear diagrams have been placed in Appendix B).

The average values of street perception were ranked as follows: Liveliness (0.661) > Safety (0.454) > Boredom (0.414) > Beauty (0.411) (Table 3). The ranking of the four perceptions revealed the public's overall tendency to perceive the street environment on Changbai Island. The results of the study showed that the average value of liveliness perception was the highest in the study area. The range of the data on liveliness perception was 0.253–0.846, and the standard deviation was 0.140, with a wide range of data variability. Most sections of Changbai Island streets were considered to have liveliness, and a few were considered to lack liveliness. We compared the average perceived values of different street types, which were ranked as follows: commercial streets (0.771) > residential streets (0.724) > comprehensive streets (0.641) > transportation streets (0.489) (Table 4). The study found that commercial and residential streets among the Changbai Island streets stood out in terms of perceived liveliness. Commercial streets (0.025) and residential streets (0.082) had smaller deviations. The deviation data suggested that commercial and residential

streets had more balanced perceptions of liveliness and that these two types of streets were also the primary high-liveliness-perceived streets on Changbai Island. Liveliness was closely related to the street's commercial activities, public space design, and public engagement, which together shaped the spatial vibrancy of the street.

Table 3. Perceptual feature profiles of Changbai Island Street.

Human Perception	Minimum	Minimum	Mean	Standard Deviation
Beauty	0.181	0.873	0.411	0.201
Boredom	0.314	0.626	0.414	0.073
Safety	0.240	0.824	0.454	0.172
Liveliness	0.253	0.846	0.661	0.140

Table 4. Perceptual feature profiles of different street types in Changbai Island.

Human Perception	Residential Streets		Transportation Streets		Commercial Streets		Comprehensive Streets	
	Mean	Standard Deviation	Mean	Standard Deviation	Mean	Standard Deviation	Mean	Standard Deviation
Beauty	0.429	0.224	0.395	0.1845	0.389	0.2219	0.396	0.175
Boredom	0.378	0.042	0.499	0.0842	0.359	0.026	0.431	0.063
Safety	0.470	0.195	0.424	0.151	0.443	0.181	0.450	0.150
Liveliness	0.724	0.082	0.489	0.160	0.771	0.025	0.641	0.123

The perceptions of safety data for streets ranged from 0.240 to 0.824, and the standard deviation of safety perceptions was 0.172. The data suggested that safety perceptions varied significantly between roadway segments. This implied that some sections of Changbai Island received positive ratings from the public in terms of perceived safety, while other sections received lower ratings. This situation may be related to factors such as traffic flow and the sharing of vehicles and pedestrians. The ranking of the mean values of perceived safety for different types of streets was residential streets (0.470) > comprehensive streets (0.450) > commercial streets (0.443) > transportation streets (0.424). This ranking revealed the differences in safety perception among different street types. The standard deviation of perceived safety was higher for residential streets and commercial streets. This showed that these two types of streets were unevenly distributed in terms of perceived safety. The standard deviation of safety perceptions was lower for transportation streets and comprehensive streets. It indicated that the distribution of safety perceptions for these two types of streets was balanced, and the public was more likely to perceive safety.

The boredom data for Changbai Island ranged between 0.314 and 0.626, with a mean value of 0.414, which was close to the neutral value. It indicated that the boredom of the streets of Changbai Island was at a moderate level. The standard deviation of boredom was 0.073, the smallest among the four perceptions. This result showed that the public was more consistent in their boredom perceptions of the streets of Changbai Island. The ranking of the mean boredom values for different types of streets was transportation streets (0.499) > comprehensive streets (0.431) > residential streets (0.378) > commercial streets (0.359). The standard deviation of boredom for all four types of streets was less than 0.100, while the standard deviation of residential and commercial streets was less than 0.05. This further confirmed that the distribution of boredom in the streets of Changbai Island was more balanced.

The beauty data for the streets in the study area fluctuated between 0.181 and 0.873, indicating significant differences between roadway segments. Overall, the average beauty of the streets of Changbai Island was 0.411. This indicated that the public gave a mod-

erately high rating to the perceived beauty of Changbai Island. The standard deviation of beauty was 0.201, showing the large variability and spatial dispersion of the public's evaluation of the perceived beauty of each road segment. It also suggested that the main factor influencing beauty perception was the subjective experience of the public, which was related to factors such as personal preference and cultural background. The uncertainty and subjectivity of beauty perception were emphasized. Specifically, for the different types of streets, the beauty data means were ranked as follows: residential streets (0.429) > mixed-use streets (0.396) > transportation streets (0.395) > commercial streets (0.389). The results showed that the public rated the beauty of residential streets as high. The highest standard deviation was found for residential streets, indicating that the distribution of beauty perceptions was uneven among residential streets. The standard deviation of beauty perceptions was lower for comprehensive and transit streets than for the other two types of streets. This indicated that the beauty distribution of comprehensive and transit streets was more balanced and that public perceptions of beauty were consistent. In summary, beauty showed significant differences across street types and was influenced by personal and cultural factors. This provides an important reference for urban planning and beautification.

4.3. The Effect of the Physical Characteristics of the Built Environment of Streets on Perceived Features

SPSS 25.0 was employed to conduct correlation and multiple regression analyses. The analysis aimed to explore the relationships between perceptual variables and physical characteristics and identify key physical factors influencing perceptual outcomes. We used correlation analysis to examine associations between the four perceptual dimensions and physical attributes. Regression analysis was performed with each perceptual feature as the dependent variable and the retained physical characteristics as independent variables. Stepwise model construction, a common statistical approach in regression analysis, involves selecting a subset of relevant predictor variables for model inclusion. In this study, forward selection was used for stepwise model building: physical indicators were retained based on a predefined significance level (p-value < 0.05), and four multiple regression models were constructed accordingly.

4.3.1. Correlation Analysis

The data of perceptual and physical characteristics were imported into SPSS software for correlation analysis. The results are shown in Table 5. Beauty perception was positively correlated with the GVI, VI, and OP and negatively correlated with BE. Perceived safety was positively correlated with the GVI and VI and negatively correlated with OP and BE. Perceived liveliness was positively correlated with the VOR, VI, PR, and BE and negatively correlated with OP. Boredom perception was positively correlated with OP and negatively correlated with the VOR, VI, PR, and BE.

Table 5. Correlation analysis.

Perceived Features	Beauty	Safety	Liveliness	Boredom
1. Green visual index (GVI)	0.804 **	0.793 **	0.024	−0.042
2. Vehicle occurrence rate (VOR)	0.011	−0.006	0.279 **	−0.326 **
3. Natural to artificial ratio of the vertical interface (VI)	0.345 **	0.362 **	0.701 **	−0.742 **
4. Walkable streets (WS)	0.003	−0.032	−0.024	−0.04
5. Openness (OP)	−0.285 **	−0.318 **	−0.763 **	0.783 **
6. Pedestrians (PR)	0.007	0.013	0.180 **	−0.196 **
7. Building enclosure (BE)	−0.550 **	−0.522 **	0.498 **	−0.508 **

** Significant correlation at the 0.01 level.

4.3.2. Regression Analysis

Perceived features were used as dependent variables, with physical characteristics retained after correlation analysis serving as independent variables. Stepwise regression analysis was performed using SPSS 25.0 to obtain regression models for beauty, safety, boredom, and liveliness perceptions.

(1) Multiple linear regression analysis of beauty perception

To model the relationship between beauty perception and physical street characteristics, we performed a stepwise regression analysis with beauty perception as the dependent variable and the four retained physical characteristics as independent variables (Figure 7). The standardized regression residuals exhibited a near-normal distribution, confirming that the data satisfied the model's normality assumption.

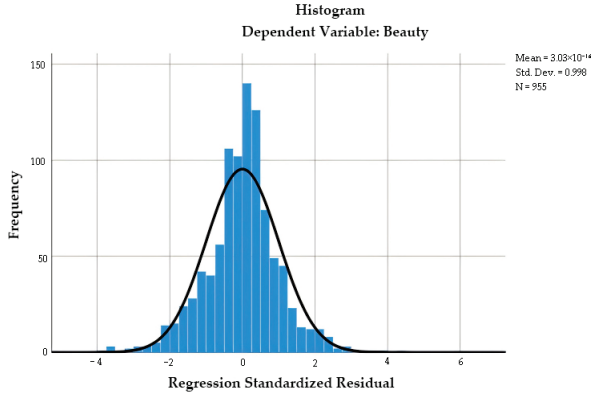


Figure 7. Regression standardized residuals for beauty perception.

As shown in Table 6, the R^2 value for the beauty perception regression analysis was 0.653, indicating the model effectively fits the data and can explain the perceptual outcomes. The F-test significance levels were all below 0.05, confirming the statistical significance of the multiple linear regression model and the validity of the overall regression relationship. The *p*-values of the t-tests were all less than 0.05, indicating significant regression coefficients. Additionally, the VIF values of the retained physical characteristics were all under 10, suggesting no multicollinearity among model factors.

Table 6. Regression analysis of beauty perception and physical characteristics.

Model		Unstandardized Coefficients		Standardized Coefficients	t	Sig.	VIF	Adjusted R Square	F-Sig.
		B	Std. Error	Beta					
3	(Constant)	−0.352	0.273		−1.292	0.197		0.653	0.000
	1. Green visual index (GVI)	4.738	0.414	0.641	11.452	0	8.605		
	5. Openness (OP)	−2.106	0.504	−0.177	−4.179	0	4.946		
	7. Building enclosure (BE)	−1.281	0.471	−0.16	−2.718	0.007	9.504		
Dependent Variable: Beauty									

In summary, the results of the regression model of beauty perception and physical characteristics of streets are valid.

The final regression equation for the beauty perception of Shenyang Changbai Island streets was as follows:

$$Y_1 = -0.352 + 4.738 \times GVI - 2.106 \times OP - 1.281 \times BE \quad (1)$$

where Y_1 was the beauty perception evaluation value.

The study shows that there are three physical features that affect the beauty perception of the streets of Changbai Island. The standardized beta coefficients indicate that the physical features of the street influence the beauty perception in the order of CVI, OP, and BE. The GVI was significantly positively correlated with beauty perception. The OP and BE ratings were significantly negatively correlated with beauty perception. Our analysis showed that lush vegetation along streets relaxed and delighted pedestrians, enhancing perceived street beauty. Conversely, high sky openness reflected street emptiness, reducing visual aesthetics, and excessive building dominance in the streetscape imposed psychological pressure on individuals, diminishing perceived beauty.

(2) Multiple linear regression analysis of safety perception

To model the relationship between safety perception and physical street characteristics, we performed a stepwise regression analysis with safety perception as the dependent variable and the four retained physical characteristics as independent variables (Figure 8). The standardized regression residuals exhibited a near-normal distribution, confirming that the data satisfied the model's normality assumption.

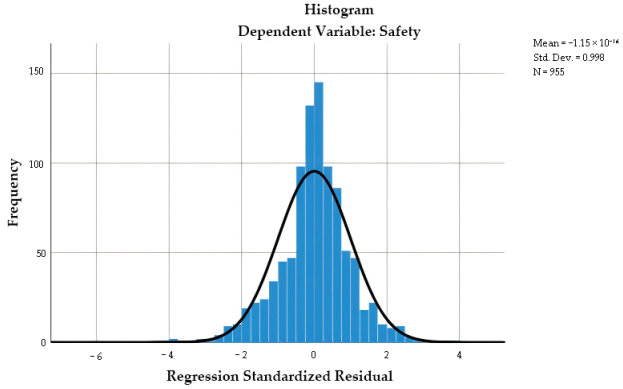


Figure 8. Regression standardized residuals for safety perception.

As shown in Table 7, the R^2 value for the safety perception regression analysis was 0.643, indicating the model effectively fits the data and can explain the perceptual outcomes. The F-test significance levels were all below 0.05, confirming the statistical significance of the multiple linear regression model and the validity of the overall regression relationship. The *p*-values of the t-tests were all less than 0.05, indicating significant regression coefficients. Additionally, the VIF values of the retained physical characteristics were all under 10, suggesting no multicollinearity among model factors.

Table 7. Regression analysis of safety perception and physical characteristics.

Model		Unstandardized Coefficients		Standardized Coefficients	t	Sig.	VIF	Adjusted R Square	F-Sig.
		B	Std. Error	Beta					
3	(Constant)	−0.105	0.277		−0.38	0.704			
	1. Green visual index (GVI)	4.382	0.419	0.593	10.447	0	8.605		
	5. Openness (OP)	−2.791	0.511	−0.235	−5.464	0	4.946	0.643	0.000
	3. Natural to artificial ratio of the vertical interface (VI)	−1.523	0.478	−0.19	−3.187	0.001	9.504		
Dependent Variable: Safety									

In summary, the results of the regression model of safety perception and physical characteristics of streets are valid.

The final regression equation for the safety perception of Shenyang Changbai Island streets was as follows:

$$Y_2 = 0.075 + 5.803 \times GVI - 3.223 \times OP - 1.754 \times VI \quad (2)$$

where Y_2 was the safety perception evaluation value.

The study showed that there are three physical features that affect the perception of safety on the streets of Changbai Island (2). Among them, the degree of influence of physical features of the street on the perception of safety is CVI, OP, and BE, in that order. The GVI was significantly positively correlated with safety perception ($p < 0.01$), while OP ($p < 0.05$) and VI ($p < 0.05$) were negatively correlated with safety perception. This suggested that abundant vegetation along streets could enhance pedestrian safety, whereas high sky openness or vertical interface closure reduced perceived safety.

(3) Multiple linear regression analysis of liveliness perception

To model the relationship between liveliness perception and physical street characteristics, we performed a stepwise regression analysis with liveliness perception as the dependent variable and the five retained physical characteristics as independent variables. The regression standardized residuals showed a slight left skew and extreme values (Figure 9); however, the main body of the data distribution (the middle region between −2 and 2) closely matched the normality curve. This distribution was considered to essentially satisfy the normality assumption, as indicated by the model diagnostics, confirming that the data met the regression model's requirements.

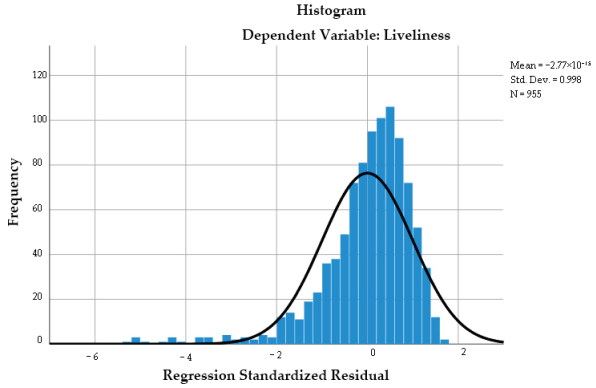


Figure 9. Regression standardized residuals for liveliness perception.

As shown in Table 8, the R^2 value for the liveliness perception regression analysis was 0.628, indicating the model effectively fits the data and can explain the perceptual outcomes. The F-test significance levels were all below 0.05, confirming the statistical significance of the multiple linear regression model and the validity of the overall regression relationship. The *p*-values of the t-tests were all less than 0.05, indicating significant regression coefficients. Additionally, the VIF values of the retained physical characteristics were all under 10, suggesting no multicollinearity among model factors.

Table 8. Regression analysis of liveliness perception and physical characteristics.

Model		Unstandardized Coefficients		Standardized Coefficients	t	Sig.	VIF	Adjusted R Square	F-Sig.
		B	Std. Error	Beta					
4	(Constant)	0.856	0.075		11.339	0			
	5. Openness (OP)	−7.805	0.261	−0.657	−29.944	0	1.236		
	7. Building enclosure (BE)	1.727	0.176	0.216	9.783	0	1.246	0.628	0.000
	2. Vehicle occurrence rate (VOR)	0.153	0.064	0.05	2.389	0.017	1.111		
	6. Pedestrians (PR)	10.746	5.361	0.04	2.004	0.045	1.035		
Dependent Variable: Liveliness									

In summary, the results of the regression model of liveliness perception and physical characteristics of streets are valid.

The final regression equation for the liveliness perception of Shenyang Changbai Island streets was as follows:

$$Y_3 = -0.856 - 7.805 \times OP + 1.727 \times BE + 0.153 \times VOR + 10.746 \times PR \quad (3)$$

where Y_3 was the liveliness perception evaluation value.

This shows that there are four physical features that affect the perception of the liveliness of the streets of Changbai Island. The standardized beta coefficients indicate that the degree of influence of physical features of the street on the perception of liveliness is OP, BE, VOR, and PR, in that order. OP had the greatest effect on liveliness perception and was notably negatively correlated with it. It indicated that the more open the sky is, the lower the perceived liveliness of the street. BE, VOR, and PR were significantly and positively correlated with the liveliness perception. This suggested that the higher the building, vehicle, and pedestrian occupancy of the street, the stronger the street's liveliness.

(4) Multiple linear regression analysis of boredom perception

To model the relationship between boredom perception and physical street characteristics, we performed a stepwise regression analysis with boredom perception as the dependent variable and the five retained physical characteristics as independent variables. The regression standardized residuals (Figure 10) showed that, although there was a slight left skew, the mean and median were close to 0, the standard deviation approximated 1, and the superimposed curves matched the data—especially in the middle region—indicating a near-normal distribution. These results confirmed that the data met the regression model's assumptions.

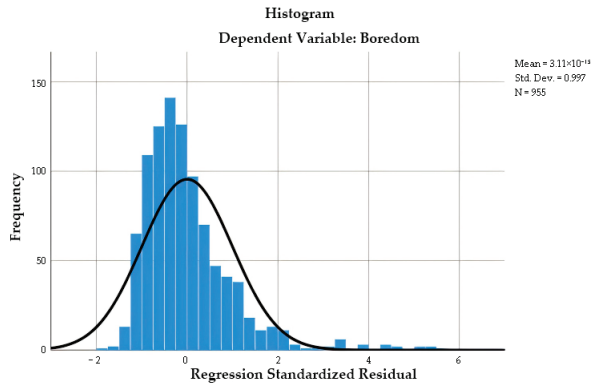


Figure 10. Regression standardized residuals for boredom perception.

As shown in Table 9, the R^2 value for the boredom perception regression analysis was 0.671, indicating the model effectively fits the data and can explain the perceptual outcomes. The F-test significance levels were all below 0.05, confirming the statistical significance of the multiple linear regression model and the validity of the overall regression relationship. The *p*-values of the t-tests were all less than 0.05, indicating significant regression coefficients. Additionally, the VIF values of the retained physical characteristics were all under 10, suggesting no multicollinearity among model factors.

Table 9. Regression analysis of boredom perception and physical characteristics.

Model		Unstandardized Coefficients		Standardized Coefficients	t	Sig.	VIF	Adjusted R Square	F-Sig.
		B	Std. Error	Beta					
5	(Constant)	0.129	0.308		0.418	0.676			
	5. Openness (OP)	6.185	0.59	0.521	10.489	0	7.155		
	7. Building enclosure (BE)	−1.677	0.166	−0.209	−10.101	0	1.247		
	2. Vehicle occurrence rate (VOR)	−0.3	0.06	−0.097	−4.968	0	1.112	0.671	0.000
	3. Natural to artificial ratio of the vertical interface (VI)	−1.553	0.479	−0.157	−3.241	0.001	6.811		
	6. Pedestrians (PR)	−14.225	5.042	−0.053	−2.821	0.005	1.035		
			Dependent Variable: Boredom						

The final regression equation for the boredom perception of Shenyang Changbai Island streets was as follows:

$$Y_4 = 0.129 + 5.803 \times OP - 1.677 \times BE - 0.3 \times VOR - 1.553 \times VI - 14.225 \times PR \quad (4)$$

where Y_4 was the boredom perception evaluation value.

This shows that there are five physical features that affect the perception of boredom of the streets of Changbai Island. The standardized beta coefficients indicate that the degree of influence of the physical features of the street on the perception of boredom is OP, BE, VI, VOR, and PR, in that order. OP was notably and positively correlated with street boredom perception. BE, VOR, VI, and PR were remarkably negatively correlated with street boredom perception. In summary, this suggested that streets with a high percentage of sky, which meant a low percentage of other landscape elements, were visually boring. The abundance of buildings, vehicles, pedestrians, and plants in the street reduced the perceived boredom of the street.

5. Discussion

5.1. Perceptual and Physical Characteristics of Urban Streets

Urban streets are not only a central component of the built environment but also a medium through which the urban environment is perceived, providing space for socialization, movement, and living [66]. To a large extent, the street also influences human perceptions and psychological responses [47]. Several studies have suggested that physical characteristics such as the green visual index, building openness, and sky openness of a street can directly affect residents' sensations of the street's beauty, vitality, and safety [75].

This study verified the significant impact of different physical characteristics on residents' sensations by analyzing the streets of Changbai Island. The results show that commercial and residential streets ranked highest in sensations of liveliness, which is closely related to the active social activities and adequate public space design of these streets. Commercial and residential streets have ample public spaces, and residents go out and participate in a wide range of social activities, thus enhancing the perceived vitality of the street [103]. Transportation streets showed a high sensation of boredom. Transportation streets are designed to ensure rapid vehicular movement [23], and the landscape elements of traffic streets are relatively simple in design, lacking a diversity of public spaces and pedestrian activity areas. Scholars such as Taylor have noted that transportation streets often lack visual variety and opportunities for interaction, easily leading to feelings of monotony and boredom [104], which is consistent with this study.

In addition, commercial streets had relatively low beauty perception scores, which were largely related to commercial building layout and functionality. Commercial streets

are dominated by dense commercial buildings, paving, and amenities, with fewer planting configurations. These factors contribute to the overall monotonous visual landscape of commercial streetscapes. Commercial streets lack natural elements and adequate open space, further reducing the perceived beauty of the street. The density and functional design of buildings directly affect the aesthetics of streets [71]. Wong scholars argue that overly dense buildings not only detract from aesthetics but also enhance dullness [105], which is consistent with this study. Residential and comprehensive streets demonstrated a high sensation of safety. The main reason for this is that these streetscapes are mostly flanked by residential or low-density buildings, creating a strong sense of spatial enclosure. At the same time, the streets are lined with lush street trees, reducing the sense of unease pedestrians feel about the outside space.

The beauty, safety, liveliness, and boredom perceptions of city streets can reflect residents' subjective evaluations of city streets. This study shows that the streets of Changbai Island have the highest mean value of liveliness perception and the lowest perception of boredom, indicating that the area has a high level of social vitality and spatial diversity. The green visual index, as a core physical feature, significantly influenced the public's perception of the beauty and safety of the street. This is consistent with the results of previous studies, emphasizing the role of greenery in enhancing the quality of urban environments [106,107]. Therefore, a deeper understanding of how the physical characteristics of urban streets affect human sensation is essential to guide future urban design.

5.2. Relationship Between Physical and Perceptual Characteristics

In this study, correlation and multiple regression analyses were used to reveal in detail the complex relationship between physical and perceived characteristics of streets. These physical characteristics were selected for their direct impact on residents' sensations. It was shown that these physical characteristics not only shape the visual and spatial qualities of the street but also influence the mood and behavior of the residents. The green visual index is significantly and positively correlated with emotion-related perceptions of beauty and safety. Studies have shown that the presence of verdant urban street vegetation significantly enhances people's visual beauty and safety sensations [7], while green space can play an important role in the public's mental health [46,108]. Lush green plants are an important part of urban streets, and the greater the complexity of their hierarchy and structure, the more they attract attention and stimulate positive emotional feedback [109,110].

Openness, which also refers to the degree of sky exposure, was negatively correlated with perceptions of beauty, liveliness, and safety, suggesting that overly open spaces may lead to negative emotions, which is consistent with existing research [23]. Too high or low sky exposure in the streetscape can negatively impact the public. When the sky visibility is overly high, the road appears more spacious, and buildings and plants seem farther away from the streetscape. This situation diminishes the beauty and liveliness of the streetscape and can induce a sense of emptiness. When the sky visibility is too low, buildings and plants in the streetscape are overly enclosed, often forming a more confined space, causing the public in the streetscape to feel depressed [7,72,111]. It has also been shown that large amounts of sky reduce the perceived safety of streets [112]. Therefore, urban planners should consider how to balance sky visibility in their designs to create an urban space that is neither empty nor oppressive, thereby enhancing the overall perception of residents.

The natural to artificial ratio of the vertical interface (VI) represents the percentage of natural and artificial elements in the street. A higher value of VI suggests that the street has more natural elements, and a lower value of VI indicates that the street has a higher percentage of artificial elements. This study found a negative correlation between

VI and safety perception, indicating that streets with more vegetation and fewer buildings are associated with lower safety perceptions. VI values are negatively correlated with boredom, indicating that when streets have a high proportion of architectural elements and a low proportion of vegetation, people feel bored and find the street unattractive. Relevant studies have shown that densely vegetated living spaces can be more enclosed and can increase residents' feelings of insecurity. Excessive built space, in turn, increases street homogeneity, which can induce boredom among residents [102]. In residential and commercial areas, mitigating greenery-induced enclosure can alleviate residents' negative perceptions [113,114]. Reducing the height of enclosed spaces created by high-rise buildings can enhance the attractiveness of streets and improve the quality of the street environment.

Vehicle occurrence rate (VOR) was positively correlated with liveliness perception and negatively correlated with boredom perception. Mahsa Farahani's study demonstrated that high traffic density induces congestion and slow-moving vehicles, fostering feelings of dullness and monotony in street experiences—findings consistent with this study [115]. The positive association between VOR and liveliness perception aligns with Jacobs' (1992) emphasis on urban vitality as a core livability criterion [116]. In urban spaces, crowded and chaotic transportation environments can create negative emotions [50]. Research has shown that motorized and non-motorized vehicles, as dynamic street elements, often evoke pedestrian insecurity [117]. However, some studies suggest that moderate vehicle presence enhances residents' safety perception, as road vehicles signal a harmonious and vibrant environment. Too many vehicles on the street can cause visual and physical discomfort [51]. These contradictory findings diverge from our results. Consequently, complex nonlinear relationships between VOR and safety in the study area may exist, warranting further in-depth investigation.

The pedestrian indicator is the percentage of people in the street. The streets we studied had a relatively small percentage of people on them. As images were captured during weekday working hours, there were fewer pedestrians and a lower pedestrian percentage in the streets. However, our analysis revealed a significant effect of pedestrian percentage on boredom perception. Pedestrian activity has also been shown in related studies to enhance the vitality and aesthetic appeal of streets by increasing social interaction and reducing boredom [118].

There was a negative correlation between building coverage ratio and perceptions of beauty and boredom, suggesting that increasing building coverage reduced street beauty and increased boredom. Dense building layouts and rundown structures detracted from street aesthetics, contributing to a monotonous and unappealing streetscape [100]. Therefore, a moderate reduction in floor area ratio, combined with increased open space and diverse greenery, could significantly enhance street visual aesthetics [119].

In our study, walkable streets were not significantly correlated with beauty, safety, liveliness, and boredom. The lack of correlation between walkable streets and perception indicators may be due to a combination of multidimensional drivers, variable interactions, and data limitations. First, the quantitative approach of the current study, which focuses on "percentage", fails to cover the core characteristics of the walking environment. Second, the percentage of walkable streets in the sample shows low variability, weakening the validity of the statistical test. Third, the effect of walkable streets on perceptions may be realized indirectly through mediating or moderating variables, but traditional linear regressions have difficulty capturing such nonlinear relationships. Despite insignificant macro-statistical associations, finely designed walking paths have been shown to be a central vehicle for enhancing social vitality [70].

This study revealed relationships between physical characteristics, including the GVI, BE, OP, and residents' perceptions of beauty, safety, liveliness, and boredom. These findings offer valuable references for urban planning while specifically highlighting the importance of integrating environmental greenery, spatial enclosure, and traffic mobility in street design. By improving physical street environments, urban planners can effectively elevate residents' quality of life and enhance the overall attractiveness of urban spaces. Therefore, balancing these factors is crucial to creating aesthetically pleasing, safe, vibrant, and non-monotonous urban environments.

5.3. Optimization Strategies Proposed by the Study

Based on these findings, we propose the following optimization strategies to improve the quality of urban streetscapes. First, enrich streetscapes with vegetation. Studies have shown that increasing vegetation on both sides of streetscapes significantly enhances the perceived beauty and safety of the street [120]. Planting more street trees and shrubs in residential and commercial streetscapes can boost the visual appeal of the streetscapes while enhancing the mental health and well-being of residents. Second, moderately control sky openness and the floor area ratio. Overly open street space and high-density building layouts can reduce residents' sense of safety and aesthetics. Rapoport (1990) suggested that moderate spatial enclosure can provide psychological comfort [121]. Therefore, urban planners should control building density during planning and retain a moderate amount of open space during the design process to ensure a sense of visual balance. At the same time, pedestrian space and transportation facilities need to be optimized. On commercial and residential streetscapes, the design of pedestrian areas should be enhanced by increasing the width and continuity of sidewalks and providing appropriate public facilities. Gehl (2010) emphasized that a pedestrian-friendly street design promotes social interaction and enhances the vitality of streetscapes [122]. Finally, enhance the sense of enclosure of the streetscapes. In commercial and residential streetscapes, enhancing the sense of enclosure by increasing the close connection between buildings and street greenery can effectively elevate the perception of street vitality.

5.4. Limitations of This Study

While our proposed framework aims to explore the relationship between street environments and human perception, integrating new data sources and methodologies would enable more nuanced investigations into this association. First, Baidu Street View, combined with semantic segmentation, can effectively quantify street features. However, Baidu Street View has time constraints, so it cannot completely replace field studies.

Second, regarding street environments, this study focuses on seven physical features. However, factors like street lighting, seating facility integrity, and pedestrian–vehicle separation should also be incorporated into such characteristics. Scholars of previous studies have also shown that visual data alone may not fully encapsulate the complexity of urban life [123]. Thus, future research should integrate POI data, nighttime light imaging, and acoustic measurement to capture variables like commercial activity, lighting quality, and noise levels. This would facilitate a more comprehensive analysis of built environment activities and cultural contexts.

Finally, regarding human perception, although previous studies have demonstrated that the dataset used in the current study is free of cultural and individual differences and is able to effectively quantify human perception, it cannot completely replace subjective perception. Human perception is shaped by the interaction between the physical environment, mental states, and social factors. Therefore, future research could consider

adding physiological monitoring techniques to further analyze the mechanisms of human perception and the influence of the built environment.

6. Conclusions

In this study, the streets of Changbai Island in Shenyang were used as the research object. We quantitatively analyzed the streetscape environment using streetscape images and machine learning. Meanwhile, we obtained data on four perceived features: safety, beauty, boredom, and liveliness. We analyzed the built environment of the streets in the study area from the perspectives of both physical traits and perceptual features. Moreover, we developed a regression model of perceptual and physical characteristics based on the four perceptual evaluations.

In terms of built environment physical characteristics, residential streets had low sky openness and walkability; commercial streets exhibited a high GVI; and transportation streets showed a low VI and high BE rating. Resident perception distributions indicated that residential streets elicited strong perceptions of liveliness, safety, and beauty, whereas transportation streets generated higher boredom and lower liveliness, beauty, and safety sensations. Comprehensive analysis revealed that the GVI influenced beauty and safety perceptions, addressing residents' fundamental needs, while OP, VOR, and BE shaped liveliness and boredom perceptions. Urban planners should integrate these factors to align urban environments with resident needs. This study explored relationships between street built environments and resident perceptions, identifying physical characteristics that impact subjective evaluations. The findings provide empirical data for urban planning and theoretical foundations for improving resident mental health and quality of life.

However, this study was constrained by temporal limitations in relying on Baidu Street View images for street characteristic quantification. Visually driven analytical frameworks, while effective, struggle to capture the multidimensional complexity of urban life. Although standardized perceptual datasets mitigate cultural biases, they cannot fully substitute for individual subjective experiences or dynamic mental processes.

Future research should integrate multi-source data, including POI, nighttime light imagery, and acoustic measurements, to construct a full-factor analysis system encompassing commercial activities and environmental quality. Additionally, incorporating physiological monitoring techniques alongside social and behavioral data will help uncover the mechanisms through which the physical environment influences perception via sensory experiences, bridging objective measurements and subjective human responses.

Author Contributions: Conceptualization, X.L., Q.L. and D.S.; Data curation, Q.L., X.J. and Y.M.; Formal analysis, Q.L. and D.S.; Funding acquisition, X.L. and Q.L.; Investigation, X.L., Q.L., D.S. and M.L.; Methodology, Q.L., X.J. and Y.M.; Project administration, X.L., D.S. and M.L.; Resources, X.L., D.S. and M.L.; Software, Q.L., X.J. and Y.Y.; Supervision, X.L. and D.S.; Validation, X.L., D.S. and M.L.; Visualization, Q.L.; Writing—original draft, X.L., Q.L., X.J., D.S. and Y.M.; Writing—review and editing, X.L., Q.L., Y.Y. and M.L. All authors have read and agreed to the published version of the manuscript.

Funding: This research was funded by the National Natural Science Foundation of China (grant number 52178045).

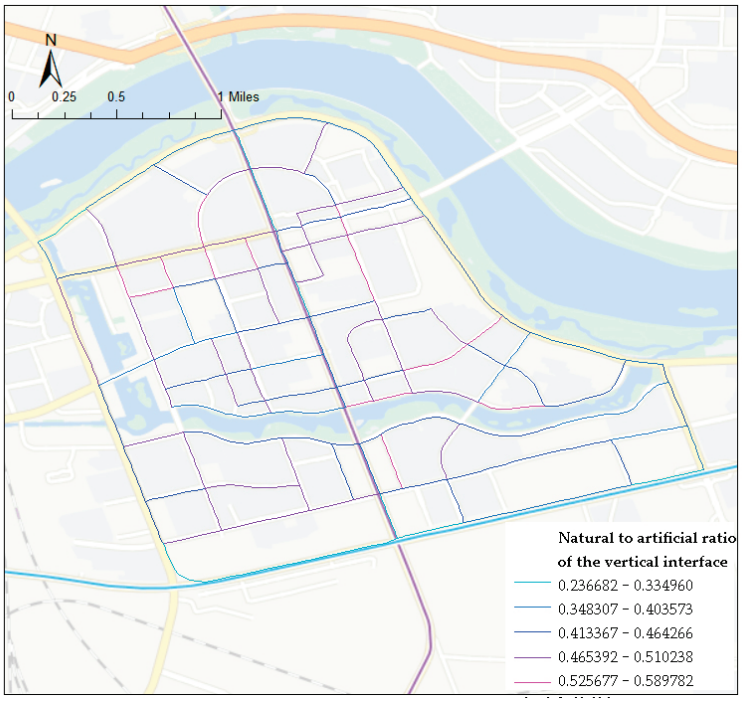
Data Availability Statement: Interview transcripts and interpreted statements supporting this study's findings and the smart contract codes are available from the corresponding author upon reasonable request.

Acknowledgments: We would like to thank the journal experts who edited this paper. We also appreciate the constructive suggestions and comments on the manuscript from the reviewers and editors.

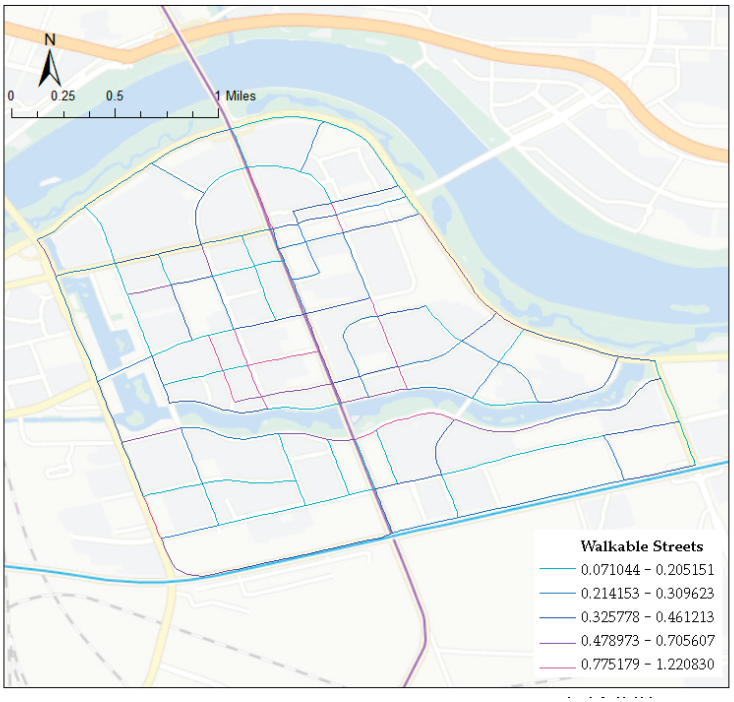
Conflicts of Interest: The authors declare no conflicts of interest.

Appendix A

The following are well-defined spatial distribution maps of street characteristics.

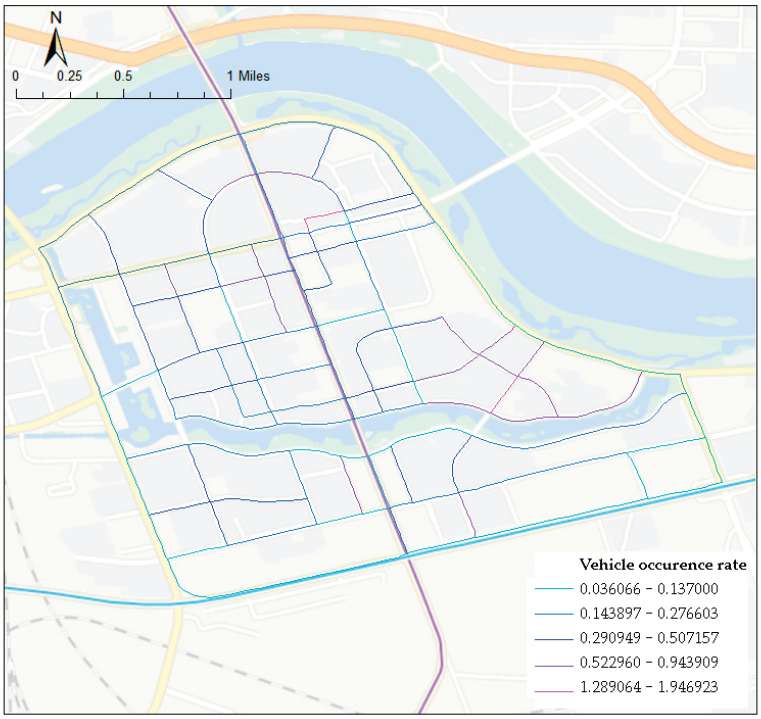


(**a**)

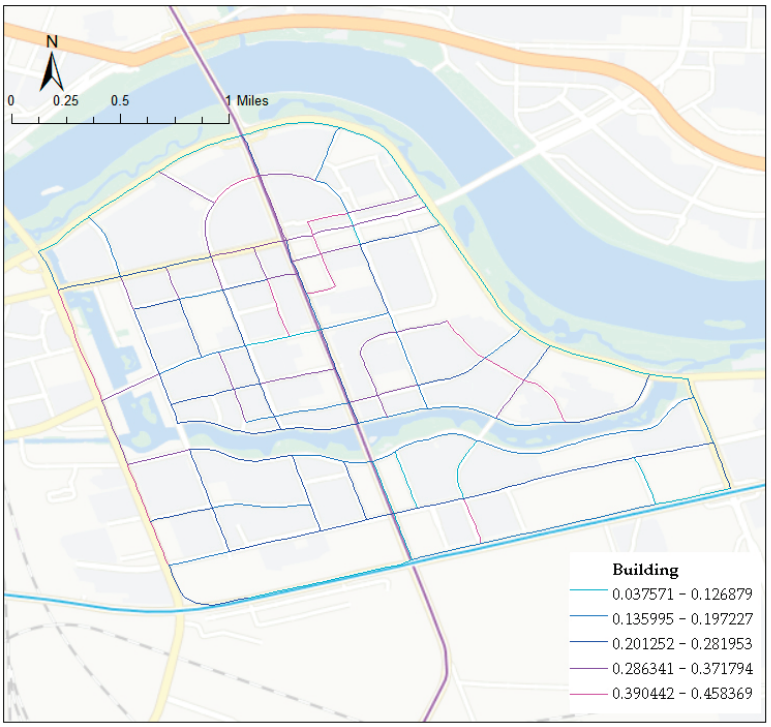


(**b**)

Figure A1. *Cont.*

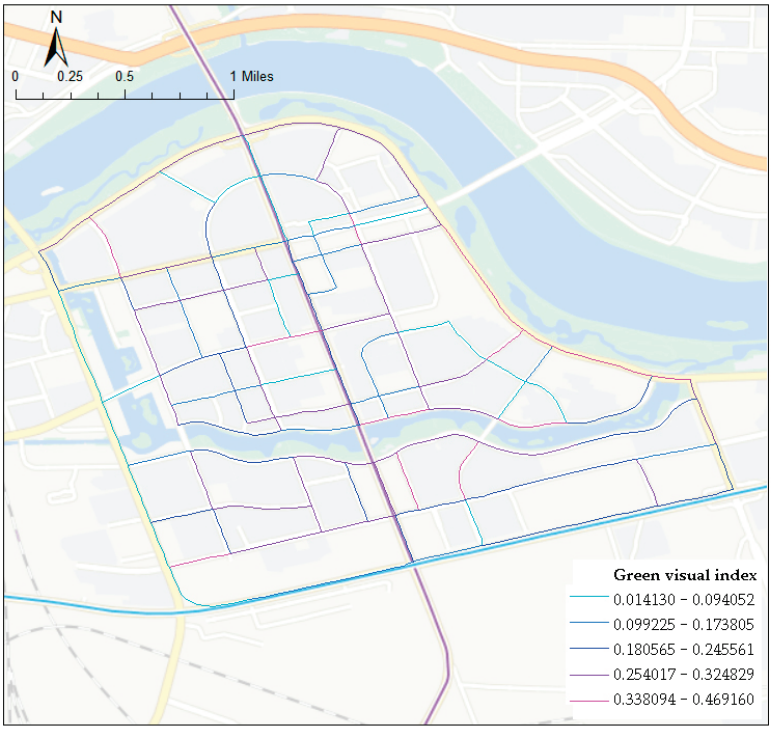


(**c**)

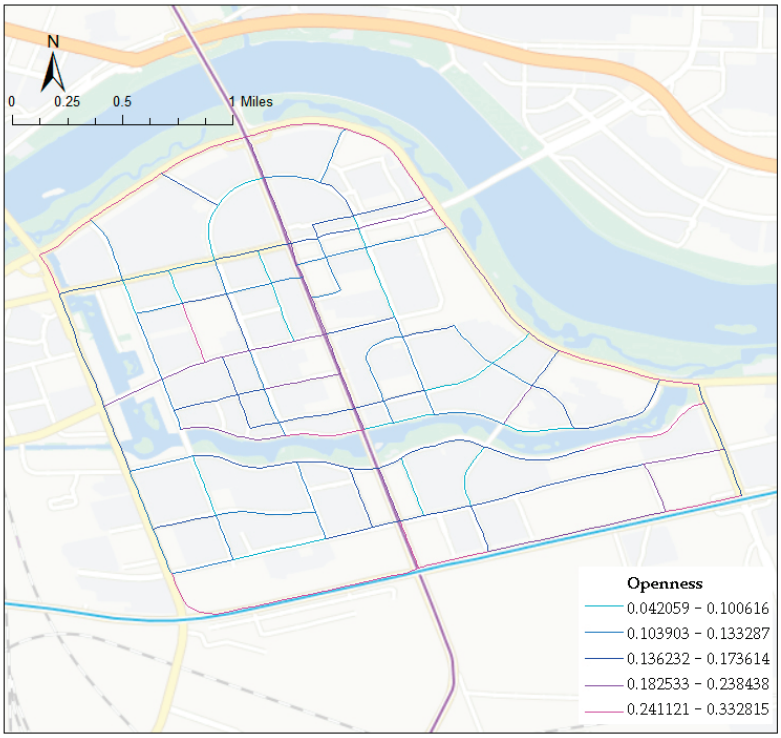


(**d**)

Figure A1. *Cont.*

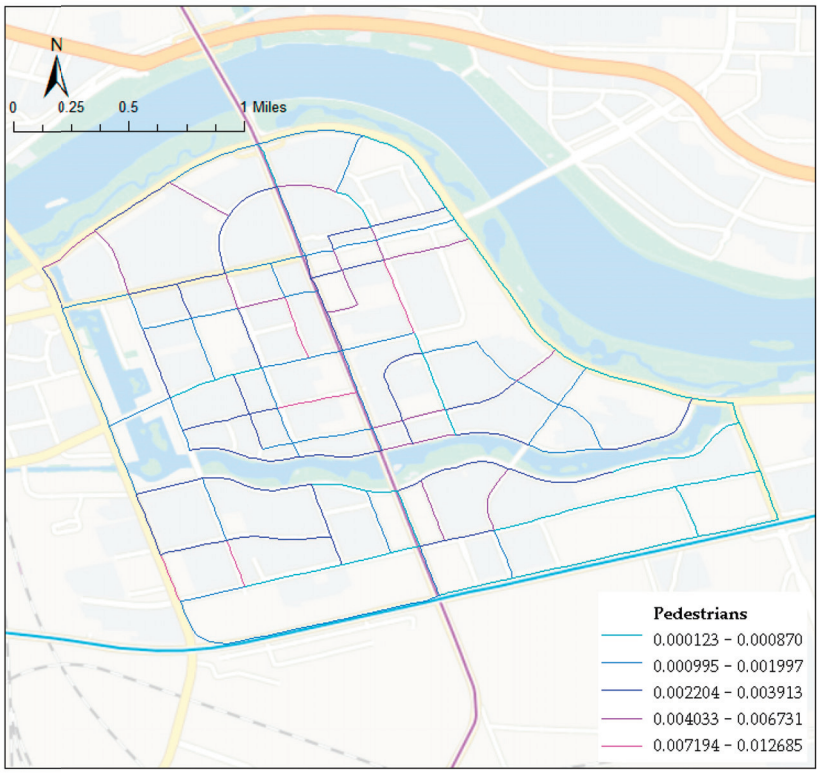


(**e**)



(**f**)

Figure A1. *Cont*.

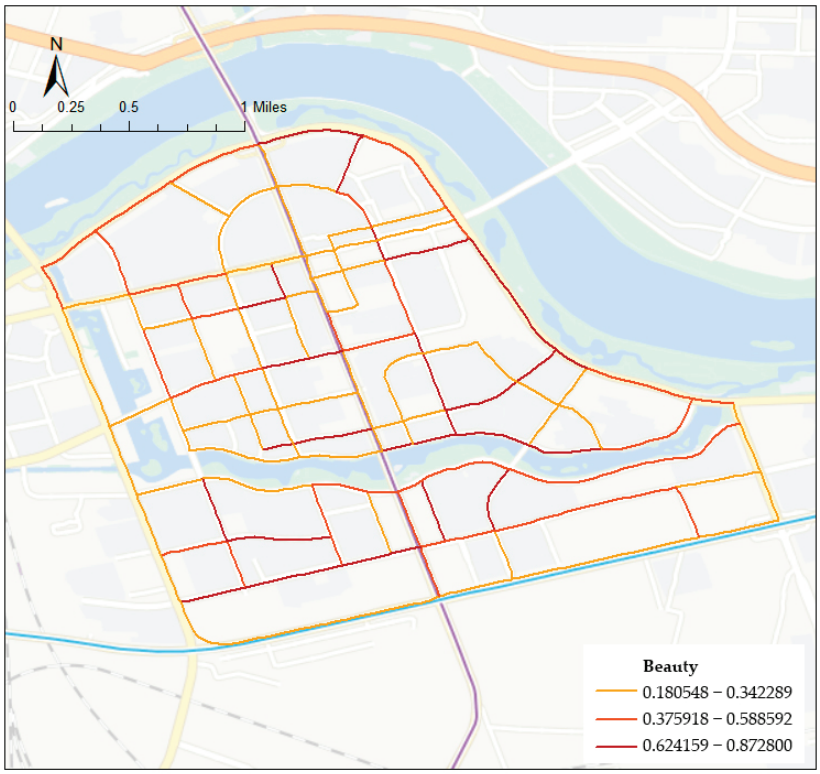


(**g**)

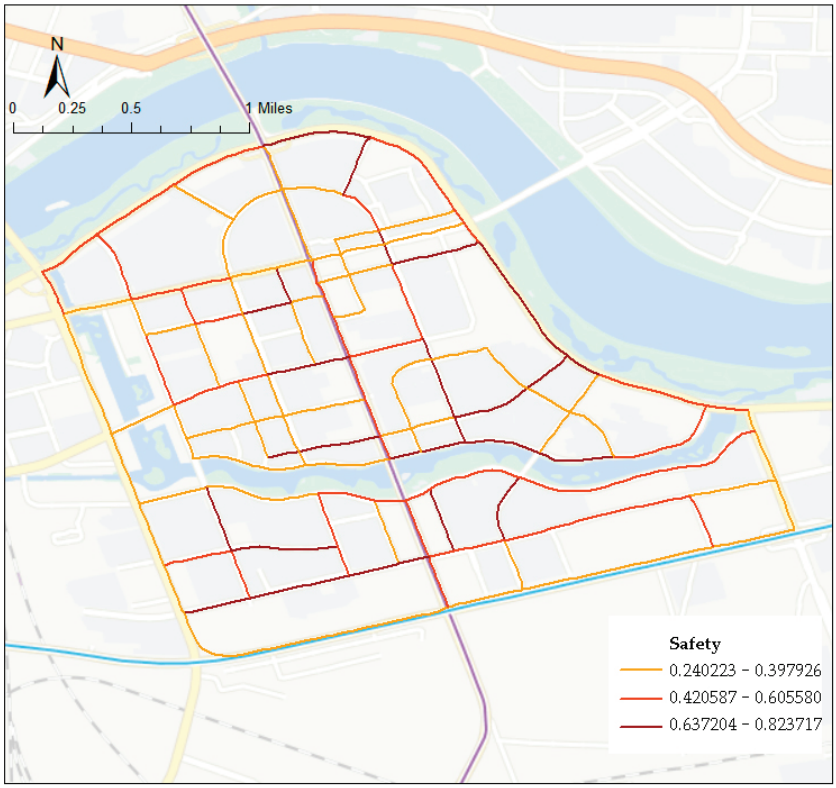
Figure A1. Spatial distribution maps of physical characteristics: (**a**) natural to artificial ratio of the vertical interface; (**b**) walkable streets; (**c**) vehicle occurrence rate; (**d**) building enclosure; (**e**) green visual index; (**f**) openness; (**g**) pedestrians.

Appendix B

The following are well-defined spatial distribution maps of perceptual characteristics.

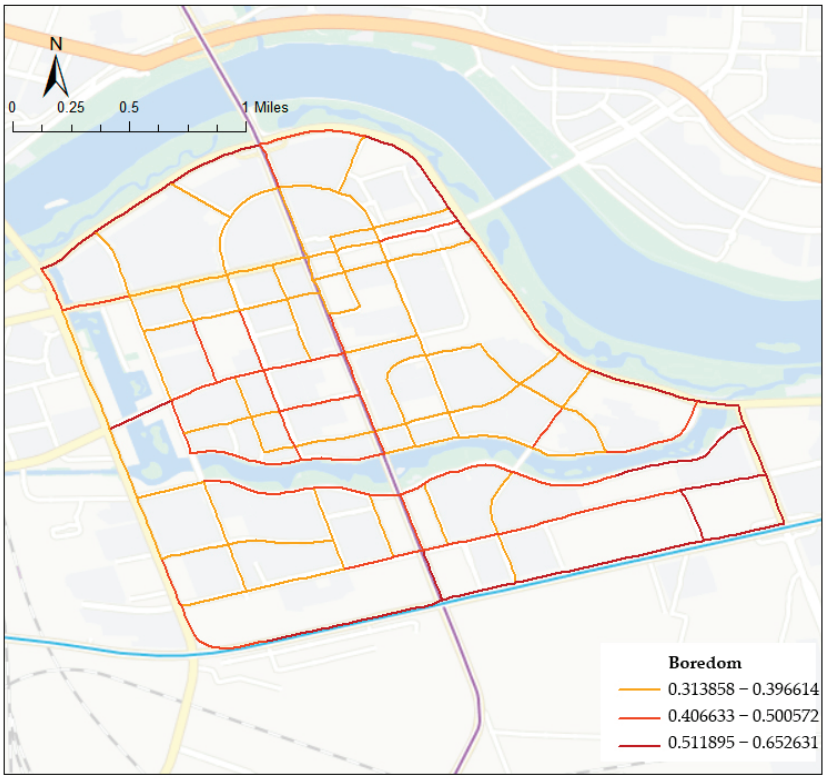


(**a**)

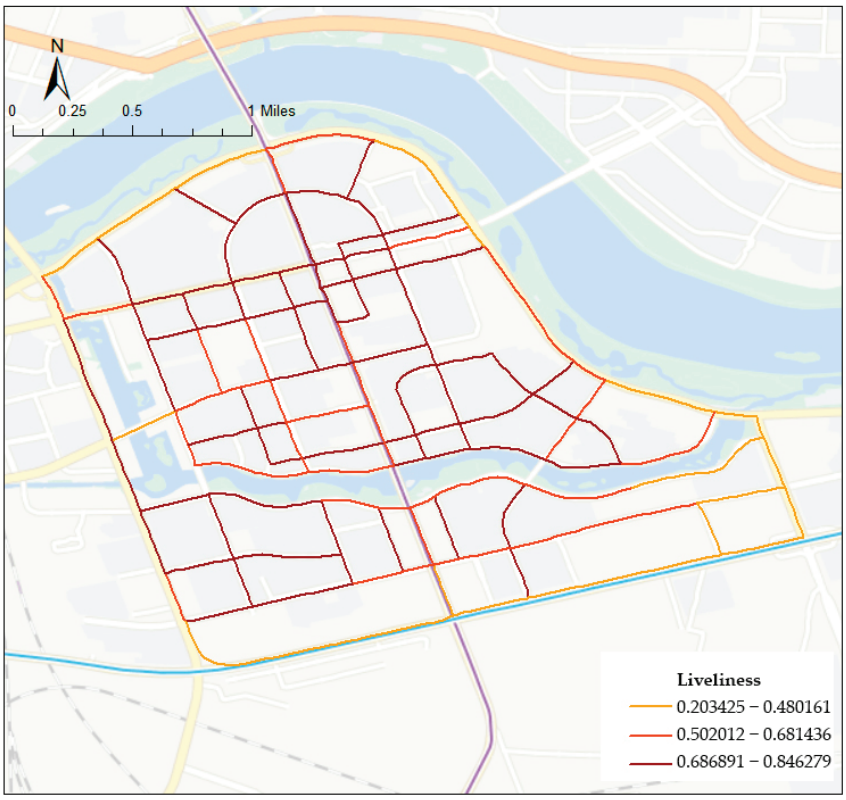


(**b**)

Figure A2. *Cont*.



(**c**)



(**d**)

Figure A2. Spatial distribution maps of perception features: (**a**) beauty; (**b**) safety; (**c**) boredom; (**d**) liveliness.

References

1. Wei, J.; Yue, W.; Li, M.; Gao, J. Mapping human perception of urban landscape from street-view images: A deep-learning approach. *Int. J. Appl. Earth Obs. Geoinf.* **2022**, *112*, 102886. [CrossRef]
2. Ewing, R.; Handy, S. Measuring the unmeasurable: Urban design qualities related to walkability. *J. Urban Des.* **2009**, *14*, 65–84. [CrossRef]
3. Wang, R.; Liu, Y.; Lu, Y.; Zhang, J.; Liu, P.; Yao, Y.; Grekousis, G. Perceptions of built environment and health outcomes for older Chinese in Beijing: A big data approach with street view images and deep learning technique. *Comput. Environ. Urban Syst.* **2019**, *78*, 101386. [CrossRef]
4. Nasar, J.L. Perception, Cognition, and Evaluation of Urban Places. *Public Places Spaces* **1989**, *10*, 31–56.
5. Wood, L.; Hooper, P.; Foster, S.; Bull, F. Public green spaces and positive mental health–investigating the relationship between access, quantityand types ofparks and mental wellbeing. *Health Place* **2017**, *48*, 63–71. [CrossRef]
6. Su, M.; Du, Y.K.; Liu, Q.M.; Ren, Y.J.; Kawachi, I.; Lv, J.; Li, L.M. Objective assessment of urban built environment related to physical activity—Development, reliability and validity of the China Urban Built Environment Scan Tool (CUBEST). *BMC Public Health* **2014**, *14*, 109. [CrossRef]
7. Dai, L.Y.; Zheng, C.L.; Dong, Z.K.; Yao, Y.; Wang, R.F.; Zhang, X.T.; Ren, S.L.; Zhang, J.Q.; Song, X.Q.; Guan, Q.F. Analyzing the correlation between visual space and residents' psychology in Wuhan, China using street-view images and deep-learning technique. *City Environ. Interact.* **2021**, *11*, 100069. [CrossRef]
8. Wang, X.X.; Shi, R.T.; Zhou, Y. Dynamics of urban sprawl and sustainable development in China. *Socio-Econ. Plan. Sci.* **2020**, *70*, 100736. [CrossRef]
9. Chen, C.; Li, H.; Luo, W.; Xie, J.; Yao, J.; Wu, L.; Xia, Y. Predicting the effect of street environment on residents' mood states in large urban areas using machine learning and street view images. *Sci. Total Environ.* **2022**, *816*, 151605. [CrossRef]
10. Li, X.Y.; Mou, Y.C.; Wang, H.Y.; Yin, C.H.; He, Q.S. How does polycentric urban form affect urban commuting? quantitative measurement using geographical big data of 100 cities in china. *Sustainability* **2018**, *10*, 4566. [CrossRef]
11. Musse, M.A.; Barona, D.A.; Santana Rodriguez, L.M. Urban environmental quality assessment using remote sensing and census data. *Int. J. Appl. Earth Obs. Geoinf.* **2018**, *71*, 95–108. [CrossRef]
12. Kaklauskas, A.; Bardauskiene, D.; Cerkauskiene, R.; Ubarte, I.; Raslanas, S.; Radvile, E.; Kaklauskaite, U.; Kaklauskiene, L. Emotions analysis in public spaces for urban planning. *Land Use Policy* **2021**, *107*, 105458. [CrossRef]
13. Barahmand, U.; Shahbazi, H.; Shahbazi, Z. Implications ofperceived physical and social aspects ofthe environment for self-reported physical and mental health. *Int. J. Environ. Health Res.* **2013**, *23*, 31–45. [CrossRef] [PubMed]
14. Li, X.; Zhang, C.; Li, W.; Ricard, R.; Meng, Q.; Zhang, W. Assessing street-level urban greenery using Google Street View and a modified green view index. *Urban For. Urban Green.* **2015**, *14*, 675–685. [CrossRef]
15. Dubey, A.; Naik, N.; Parikh, D.; Raskar, R.; Hidalgo, C.A. Deep Learning the City: Quantifying Urban Perception at a Global Scale. In Proceedings of the European Conference on Computer Vision, Amsterdam, The Netherlands, 11–14 October 2016.
16. Karndacharuk, A.; Wilson, D.J.; Dunn, R. A review of the evolution of shared (street) space concepts in urban environments. *Transp. Rev.* **2014**, *34*, 190–220. [CrossRef]
17. Liu, M.; Han, L.; Xiong, S.; Qing, L.; Ji, H.; Peng, Y. Large-scale street space quality evaluation based on deep learning over street view image. In Proceedings of the International Conference on Image and Graphics, Beijing, China, 23–25 August 2019.
18. Zhu, D.; Wang, N.; Wu, L.; Liu, Y. Street as a big geo-data assembly and analysis unit in urban studies: A case study using Beijing taxi data. *Appl. Geogr.* **2017**, *86*, 152–164. [CrossRef]
19. Xing, H.; Meng, Y. Measuring urban landscapes for urban function classification using spatial metrics. *Ecol. Indic.* **2020**, *108*, 105722. [CrossRef]
20. Ma, F.; Ren, F.; Yuen, K.F.; Guo, Y.; Zhao, C.; Guo, D. The Spatial Coupling Effect between Urban Public Transport and Commercial Complexes: A Network Centrality Perspective. *Sustain. Cities Soc.* **2019**, *50*, 101645. [CrossRef]
21. Galea, S.; Ahern, J.; Rudenstine, S.; Wallace, Z.; Vlahov, D. Urban built environment and depression: A multilevel analysis. *J. Epidemiol. Community Health* **2005**, *59*, 822–827. [CrossRef]
22. Carmona, M.; Gabrieli, T.; Hickman, R.; Laopoulou, T.; Livingstone, N. Street appeal: The value of street improvements. *Prog. Plan.* **2018**, *126*, 1–51. [CrossRef]
23. Lei, Y.L.; Zhou, H.T.; Xue, L.; Yuan, L.B.; Liu, Y.G.; Wang, M.; Wang, C. Evaluating and comparing human perceptions of streets in two megacities by integrating street-view images, deep learning, and space syntax. *Buildings* **2024**, *14*, 1847. [CrossRef]
24. Han, X.; Wang, L.; He, J.; Jung, T. Restorative perception of urban streets: Interpretation using deep learning and MGWR models. *Front. Public Health* **2023**, *11*, 1141630. [CrossRef]
25. Jiang, Y.; Han, Y.; Liu, M.; Ye, Y. Street vitality and built environment features: A data-informed approach from fourteen Chinese cities. *Sustain. Cities Soc.* **2022**, *79*, 103724. [CrossRef]

26. Moore, T.H.M.; Kesten, J.M.; López-López, J.A.; Ijaz, S.; McAleenan, A.; Richards, A.; Gray, S.; Savovic, J.; Audrey, S. The effects of changes to the built environment on the mental health and well-being of adults: Systematic review. *Health Place* **2018**, *53*, 237–257. [CrossRef]
27. Luo, S.; Shang, W.; Yan, Z.; Bi, S. Research on factors influencing the style of Chinese historic districts based on the mask R-CNN deep learning model. *Buildings* **2024**, *14*, 420. [CrossRef]
28. Ma, D.F.; Zhang, S.J.; Xiao, T.Q.; Shui, T.T. Aspects of new and old urban parks most valued by residents on social media: A case study in Hefei. *Sustainability* **2023**, *15*, 13771. [CrossRef]
29. Meng, Y.M.; Li, Q.Y.; Yu, Y.Q.; Yue, D.; Gan, M.Q.; Wang, S.Y.; Niu, J.N.; Fukuda, H. Research on campus space features and visual quality based on street view images: A case study on the Chongshan Campus of Liaoning University. *Buildings* **2023**, *13*, 51332. [CrossRef]
30. Kaplan, R.; Kaplan, S. *The Experience of Nature: A Psychological Perspective*; Cambridge University Press: Cambridge, UK, 1989.
31. Lynch, K. *The Image of the City*; MIT Press: Cambridge, MA, USA, 1960; Volume 11.
32. Porzi, L.; Rota Bul'o, S.; Lepri, B.; Ricci, E. Predicting and understanding urban perception with convolutional neural networks. In Proceedings of the 23rd ACM International Conference on Multimedia, Brisbane, Australia, 26–30 October 2015.
33. Tuan, Y.F. *Space and Place: The Perspective of Experience*; University of Minnesota Press: Minneapolis, MN, USA, 1977.
34. Ulrich, R. *Aesthetic and Affective Response to Natural Environment*; Plenum Press: New York, NY, USA, 1983; Volume 6, pp. 85–125.
35. Ulrich, R. Stress recovery during exposure to natural and urban environments. *J. Environ. Psychol.* **1991**, *11*, 201–230. [CrossRef]
36. Kaplan, S. The restorative benefits of nature: Toward an integrative framework. *J. Environ. Psychol. Green Psychol.* **1995**, *15*, 169–182. [CrossRef]
37. Rui, J.; Li, X. Decoding vibrant neighborhoods: Disparities between formal neighborhoods and urban villages in eye-level perceptions and physical environment. *Sustain. Cities Soc.* **2024**, *101*, 105122. [CrossRef]
38. Sayers, J.M.; Cleary, M.; Hunt, G.E.; Burmeister, O.K. Service and infrastructure needs to support recovery programmes for Indigenous community mental health consumers. *Int. J. Ment. Health Nurs.* **2017**, *26*, 142–150. [CrossRef] [PubMed]
39. Silva, M.G.E.; Remoaldo, P.; Peluso, M.L. Human values and tourism perception: A new approach in residents' perceptions. *Curr. Issues Tour.* **2024**, *28*, 353–358. [CrossRef]
40. Cresswell, T. *Place: An Introduction*, 2nd ed.; Wiley: Chichester, UK, 2014; pp. 165–190.
41. Jeon, J.Y.; Jo, H.I. Effects of audio-visual interactions on soundscape and landscape perception and their influence on satisfaction with the urban environment. *Build. Environ.* **2020**, *169*, 106544. [CrossRef]
42. Farias, J.C.; Lopes, A.D.; Mota, J.; Santos, M.P.; Ribeiro, J.C.; Hallal, P.C. Perception of the social and built environment and physical activity among Northeastern Brazil adolescents. *Prev. Med.* **2011**, *52*, 114–119.
43. Jack, E.; McCormack, G.R. The associations between objectively-determined and self-reported urban form characteristics and neighborhood-based walking in adults. *Int. J. Behav. Nutr. Phys. Act.* **2014**, *11*, 71. [CrossRef]
44. Polat, A.T.; Akay, A. Relationships between the visual preferences of urban recreation area users and various landscape design elements. *Urban For. Urban Green.* **2015**, *14*, 573–582. [CrossRef]
45. Wu, Z.F.; Ren, Y. The influence of greenspace characteristics and building configuration on depression in the elderly. *Build. Environ.* **2021**, *188*, 107477.
46. Gascon, M.; Sánchez-Benavides, G.; Dadvand, P.; Martínez, D.; Gramunt, N.; Gotsens, X.; Cirach, M.; Vert, C.; Molinuevo, J.L.; Crous-Bou, M.; et al. Long-term exposure to residential green and blue spaces and anxiety and depression in adults: A cross-sectional study. *Environ. Res.* **2018**, *162*, 231–239. [CrossRef]
47. Song, L.Y.; Zhang, A.; Hu, Z.W. Greenspace exposure is conducive to the resilience of public sentiment during the COVID-19. *Health Place* **2023**, *83*, 103096. [CrossRef]
48. Sun, D.; Li, Q.Y.; Gao, W.J.; Huang, G.H.; Tang, N.; Lyu, M.; Yu, Y.Q. On the relation between visual quality and landscape characteristics: A case study application to the waterfront linear parks in Shenyang, China. *Environ. Res. Commun.* **2021**, *3*, 115013. [CrossRef]
49. Nasar, J.L. Urban design aesthetics: The evaluative qualities of building exteriors. *Environ. Behav.* **1994**, *26*, 377. [CrossRef]
50. Huang, G.H.; Yu, Y.Q.; Lyu, M.; Sun, D.; Zeng, Q.; Bart, D. Using google street view panoramas to investigate the influence of urban coastal street environment on visual walkability. *Environ. Res. Commun.* **2023**, *5*, 065017. [CrossRef]
51. Kawshalya, L.W.G.; Weerasinghe, U.G.D.; Chandrasekara, D.P. The impact of visual complexity on perceived safety and comfort of the users: A study on urban streetscape of Sri Lanka. *PLoS ONE* **2022**, *17*, e0272074. [CrossRef] [PubMed]
52. Dillon, R. Designing urban space for psychological comfort: The Kentish Town Road project. *J. Public Ment. Health* **2005**, *4*, 10–20. [CrossRef]
53. Park, Y.; Garcia, M. Pedestrian safety perception and urban street settings. *Int. J. Sustain. Transp.* **2020**, *14*, 860–871. [CrossRef]

54. Liu, M.; Jiang, Y.; He, J.L. Quantitative evaluation on street vitality: A case study of Zhoujiadu Community in Shanghai. *Sustainability* **2021**, *13*, 3027. [CrossRef]
55. Larkin, A.; Gu, X.; Chen, L.Z.; Hystad, P. Predicting perceptions of the built environment using GIS, satellite and street view image approaches. *Landsc. Urban Plan.* **2021**, *216*, 104257. [CrossRef]
56. Zhang, J.X.; Yu, Z.L.; Li, Y.Q.; Wang, X.Q. Uncovering Bias in Objective Mapping and Subjective Perception of Urban Building Functionality: A Machine Learning Approach to Urban Spatial Perception. *Land* **2023**, *12*, 1322. [CrossRef]
57. Lee, J.; Kim, D.; Park, J. A machine learning and computer vision study of the environmental characteristics of streetscapes that affect pedestrian satisfaction. *Sustainability* **2022**, *14*, 5730. [CrossRef]
58. Ma, X.Y.; Ma, C.Y.; Wu, C.; Xi, Y.L.; Yang, R.F.; Peng, N.Y.Z.; Zhang, C.; Ren, F. Measuring human perceptions of streetscapes to better inform urban renewal: A perspective of scene semantic parsing. *Cities* **2021**, *110*, 103086. [CrossRef]
59. Li, X.J.; Ratti, C.; Seiferling, I. Quantifying the shade provision of street trees in urban landscape: A case study in Boston, USA, using Google Street View. *Landsc. Urban Plan.* **2018**, *169*, 81–91. [CrossRef]
60. Lu, Y. Using Google Street View to investigate the association between street greenery and physical activity. *Landsc. Urban Plan.* **2019**, *191*, 103435. [CrossRef]
61. Harvey, C.; Aultman-Hall, L.; Hurley, S.E.; Troy, A. Effects of skeletal streetscape design on perceived safety. *Landsc. Urban Plan.* **2015**, *142*, 18–28. [CrossRef]
62. Li, X.J.; Cai, B.; Ratti, C. Using Street-level Images and Deep Learning for Urban Landscape Studies. *Landsc. Archit. Front.* **2018**, *6*, 20. [CrossRef]
63. Zhou, H.; He, S.; Cai, Y.; Wang, M.; Su, S. Social inequalities in neighborhood visual walk ability: Using street view imagery and deep learning technologies to facilitate healthy city planning. *Sustain. Cities Soc.* **2019**, *50*, 101605. [CrossRef]
64. Wu, B.; Yu, B.; Shu, S.; Liang, H.; Zhao, Y.; Wu, J. Mapping fine-scale visual quality distribution inside urban streets using mobile LiDAR data. *Build. Environ.* **2021**, *206*, 108323. [CrossRef]
65. Orzechowska-Szajda, I. Classification model ofurban riverside landscape using the oder river as an example. *Pol. J. Environ. Stud.* **2019**, *29*, 205–215. [CrossRef]
66. Wang, L.; Han, X.; He, J.; Jung, T. Measuring residents' perceptions of city streets to inform better street planning through deep learning and space syntax. *ISPRS J. Photogramm. Remote Sens.* **2022**, *190*, 215–230. [CrossRef]
67. Tang, Y.W.; Zhang, J.X.; Liu, R.J.; Li, Y.Q. Exploring the impact of built environment attributes on social followings using social media data and deep learning. *ISPRS Int. J. Geo-Inf.* **2022**, *11*, 325. [CrossRef]
68. Ames, D.L. The new urbanism: Toward an architecture of community. *J. Urban Aff.* **2002**, *24*, 118–122.
69. Miller, B. In place out of place: Geography, ideology, and transgression. *Ann. Assoc. Am. Geogr.* **1998**, *88*, 737–739.
70. Montello, D.R.; Goodchild, M.F.; Gottsegen, J.; Fohl, P. Where's downtown?: Behavioral methods for determining referents of vague spatial queries. *Spat. Cogn. Comput.* **2003**, *3*, 185–204.
71. Santosa, H.; Ernawati, J.; Wulandari, L.D. Visual quality evaluation of urban commercial streetscape for the development of landscape visual planning system in provincial street corridors in Malang, Indonesia. *IOP Conf. Ser. Earth Environ. Sci.* **2018**, *126*, 012202. [CrossRef]
72. Zhang, F.; Zhou, B.L.; Liu, L.; Liu, Y.; Fung, H.H.; Lin, H.; Ratti, C. Measuring human perceptions of a large-scale urban region using machine learning. *Landsc. Urban Plan.* **2018**, *180*, 148–160. [CrossRef]
73. Kacha, L.; Matsumoto, N.; Mansouri, A. Electrophysiological evaluation of perceived complexity in streetscapes. *J. Asian Archit. Build. Eng.* **2015**, *14*, 585–592. [CrossRef]
74. Sun, D.; Zhou, F.J.; Lin, J.J.; Yang, Q.R.; Lyu, M. A study on landscape feature and emotional perception evaluation of waterfront greenway. *Environ. Res. Commun.* **2024**, *6*, 095023. [CrossRef]
75. Yao, Y.; Liang, Z.T.; Yuan, Z.H.; Liu, P.H.; Bie, Y.P.; Zhang, J.B.; Wang, R.Y.; Wang, J.L.; Guan, Q.F. A human-machine adversarial scoring framework for urban perception assessment using street-view images. *Int. J. Geogr. Inf. Sci.* **2019**, *33*, 2363–2384. [CrossRef]
76. Mouratidis, K. Urban planning and quality of life: A review of pathways linking the built environment to subjective well-being. *Cities* **2021**, *115*, 103229. [CrossRef]
77. Wang, R.; Ren, S.; Zhang, J.; Yao, Y.; Wang, Y.; Guan, Q. A comparison of two deep-learning-based urban perception models: Which one is better? *Comput. Urban Sci.* **2021**, *1*, 3. [CrossRef]
78. Tang, L.; Ding, W.W. Linking the signs on street façades to the characteristics of street space. *Archit. J.* **2015**, *2*, 18–22.
79. Ewing, R.; Cervero, R. Travel and the built environment: A synthesis (with discussion). *Transp. Res. Rec.* **2001**, *1780*, 87–114. [CrossRef]
80. Zhao, J.W.; Luo, P.J.; Wang, R.H.; Cai, Y.L. Correlations between aesthetic preferences ofriver and landscape characters. *J. Environ. Eng. Landsc. Manag.* **2013**, *21*, 123–132. [CrossRef]

81. Ye, Y.; Zhang, Z.X.; Zhang, X.H.; Zeng, W. Human-scale quality on streets: A large-scale and efficient analytical approach based on street view images and new urban analytical tools. *Urban Plan. Int.* **2019**, *34*, 18–27. [CrossRef]
82. Liu, Y.; Liu, X.; Gao, S.; Gong, L.; Kang, C.G.; Zhi, Y.; Chi, G.H.; Shi, L. Social sensing: A new approach to understanding our socioeconomic environments. *Ann. Assoc. Am. Geogr.* **2015**, *105*, 512–530. [CrossRef]
83. Lyu, M.; Meng, Y.M.; Gao, W.J.; Yu, Y.Q.; Ji, X.; Li, Q.Y.; Huang, G.H.; Sun, D. Measuring the perceptual features of coastal streets: A case study in Qingdao, China. *Environ. Res. Commun.* **2022**, *4*, 115002. [CrossRef]
84. Gong, F.Y.; Zeng, Z.C.; Zhang, F.; Li, X.J.; Ng, E.; Norford, L.K. Mapping sky, tree, and building view factors of street canyons in a high-density urban environment. *Build. Environ.* **2018**, *134*, 155–167. [CrossRef]
85. Helbich, M.; Yao, Y.; Liu, Y.; Zhang, J.B.; Liu, P.H.; Wang, R.Y. Using deep learning to examine street view green and blue spaces and their associations with geriatric depression in Beijing, China. *Environ. Int.* **2019**, *126*, 107–117. [CrossRef]
86. Meng, Y.M.; Shi, J.X.; Lyu, M.; Sun, D.; Fukuda, H. Research into the Influence Mechanisms of Visual-Comfort and Landscape Indicators of Urban Green Spaces. *Land* **2024**, *13*, 1688. [CrossRef]
87. Sun, D.; Ji, X.; Gao, W.J.; Zhou, F.J.; Yu, Y.Q.; Meng, Y.M.; Yang, M.Q.; Lin, J.J.; Lyu, M. The Relation between Green Visual Index and Visual Comfort in Qingdao Coastal Streets. *Buildings* **2023**, *13*, 457. [CrossRef]
88. Yao, Y.; Wang, J.L.; Hong, Y.; Qian, C.; Guan, Q.F.; Liang, X.; Dai, L.Y.; Zhang, J.B. Discovering the homogeneous geographic domain of human perceptions from street view images. *Landsc. Urban Plan.* **2021**, *212*, 104125. [CrossRef]
89. Sun, D.; Ji, X.; Lyu, M.; Fu, Y.; Gao, W.J. Evaluation and diagnosis for the pedestrian quality of service in urban riverfront streets. *J. Clean. Prod.* **2024**, *452*, 142090. [CrossRef]
90. Lyu, M.; Lin, J.J.; Zhou, F.J.; Niu, J.N.; Sun, D.; Meng, Y.M.; Ji, X. A method for evaluating the visual quality of wetland park landscapes: A case study of qianlu lake wetland park in Wuping, China. *Environ. Res. Commun.* **2024**, *6*, 105024. [CrossRef]
91. Kido, D.; Fukuda, T.; Yabuki, N. Assessing future landscapes using enhanced mixed reality with semantic segmentation by deep learning. *Adv. Eng. Inform.* **2021**, *48*, 101281. [CrossRef]
92. Tang, J.X.; Long, Y. Measuring visual quality of street space and its temporal variation: Methodology and its application in the Hutong area in Beijing. *Landsc. Urban Plan.* **2019**, *191*, 103436. [CrossRef]
93. Shen, Q.; Zeng, W.; Ye, Y.; Arisona, S.M.; Schubiger, S.; Burkhard, R.; Qu, H. StreetVizor: Visual Exploration of Human-Scale Urban Forms Based on Street Views. In Proceedings of the IEEE Transactions on Visualization and Computer Graphics, Phoenix, AZ, USA, 1–6 October 2017.
94. Zhang, Y.L.; Dong, R.C. Iimpacts of street-visible greenery on housing prices: Evidence from a hedonic price model and a massive street view image dataset in Beijing. *ISPRS Int. J. Geo-Inf.* **2018**, *7*, 104. [CrossRef]
95. He, J.L.Y.; Zhang, J.B.; Yao, Y.; Li, X. Extracting human perceptions from street view images for better assessing urban renewal potential. *Cities* **2023**, *134*, 104189. [CrossRef]
96. Li, Y.Q.; Yabuki, N.; Fukuda, T. Measuring visual walkability perception using panoramic street view images, virtual reality, and deep learning. *Sustain. Cities Soc.* **2022**, *86*, 104140. [CrossRef]
97. Li, Y.Q.; Yabuki, N.; Fukuda, T.; Zhang, J.X. A big data evaluation of urban street walkability using deep learning and environmental sensors a case study around Osaka University Suita campus. In Proceedings of the International Conference on Education and Research in Computer Aided Architectural Design in Europe, Berlin, Germany, 6 November 2024.
98. Li, X.; Zhang, C.R.; Li, W.D.; Kuzovkina, Y.A.; Weiner, D. Who lives in greener neighborhoods? The distribution of street greenery and its association with residents' socioeconomic conditions in Hartford, Connecticut, USA. *Urban For. Urban Green.* **2015**, *14*, 751–759. [CrossRef]
99. Rahman, A.K.M.M.; Zaber, M.; Cheng, Q.W.; Nayem, A.B.S.; Sarker, A.; Paul, O.; Shibasaki, R. Applying State-of-the-Art Deep-Learning Methods to Classify Urban Cities of the Developing World. *Sensors* **2021**, *21*, 7469. [CrossRef]
100. Chen, Y.X.; Zhang, Q.L.; Deng, Z.; Fan, X.R.; Xu, Z.M.; Kang, X.D.; Pan, K.L.; Guo, Z.H. Research on green view index of urban roads based on street view image recognition: A case study of changsha downtown areas. *Sustainability* **2022**, *14*, 16063. [CrossRef]
101. Meng, Y.M.; Sun, D.; Lyu, M.; Niu, J.N.; Fukuda, H. Measuring human perception of residential built environment through street view image and deep learning. *Environ. Res. Commun.* **2024**, *6*, 055020. [CrossRef]
102. Wu, C.; Peng, N.; Ma, X.; Li, S.; Rao, J. Assessing multiscale visual appearance characteristics of neighbourhoods using geographically weighted principal component analysis in Shenzhen, China. *Comput. Environ. Urban Syst.* **2020**, *84*, 101547. [CrossRef]
103. Yang, J.Y.; Li, X.M.; Du, J.; Cheng, C.H. Exploring the relationship between urban street spatial patterns and street vitality: A case study of Guiyang, China. *Int. J. Environ. Res. Public Health* **2023**, *20*, 1646. [CrossRef] [PubMed]
104. Taylor, N. The aesthetic experience of traffic in the modern city. *Urban Stud.* **2003**, *40*, 1609–1625. [CrossRef]

105. Wong, M.S.; Nichol, J.; Ng, E. A study of the "wall effect" caused by proliferation of high-rise buildings using GIS techniques. *Landsc. Urban Plan* **2011**, *102*, 245–253. [CrossRef]
106. Fleming, C.M.; Manning, M.; Ambrey, C.L. Crime, greenspace and life satisfaction: An evaluation of the New Zealand experience. *Landsc. Urban Plan.* **2016**, *149*, 1–10. [CrossRef]
107. Zhang, Y.; Van den Berg, A.E.; Van Dijk, T.; Weitkamp, G. Quality over quantity: Contribution of urban green space to neighborhood satisfaction. *Int. J. Environ. Res. Public Health* **2017**, *14*, 535. [CrossRef]
108. Vries, S.D.; Verheij, R.A.; Groenewegen, P.P.; Spreeuwenberg, P. Natural environments: Healthy environments? An exploratory analysis of the relationship between greenspace and health. *Environ. Plan. A Econ. Space* **2003**, *35*, 1717–1731. [CrossRef]
109. Wang, R.; Lu, Y.; Zhang, J.; Liu, P.; Yao, Y.; Liu, Y. The relationship between visual enclosure for neighbourhood street walkability and elders' mental health in China. *J. Transp. Health* **2019**, *13*, 90–102. [CrossRef]
110. Wolf, K.L. Business district streetscapes, trees, and consumer response. *J. For.* **2005**, *103*, 396–400. [CrossRef]
111. Duan, J.P.; Liao, J.J.; Liu, J.; Gao, X.X.; Shang, A.L.; Huang, Z.H. Evaluating the spatial quality of urban living streets: A case study of Hengyang city in central south China. *Sustainability* **2023**, *15*, 10623. [CrossRef]
112. Hamim, O.F.; Ukkusuri, S.V. Towards safer streets: A framework for unveiling pedestrians' perceived road safety using street view imagery. *Accid. Anal. Prev.* **2024**, *195*, 107400. [CrossRef] [PubMed]
113. Nordbø, E.C.A.; Nordh, H.; Raanaas, R.K.; Aamodt, G. GIS-derived measures of the built environment determinants of mental health and activity participation in childhood and adolescence: A systematic review. *Landsc. Urban Plan.* **2018**, *177*, 19–37. [CrossRef]
114. Ji, Q.; Yin, M.; Li, Y.; Zhou, X. Exploring the influence path of high-rise residential environment on the mental health of the elderly. *Sustain. Cities Soc.* **2023**, *98*, 104808. [CrossRef]
115. Farahani, M.; Razavi-Termeh, S.V.; Sadeghi-Niaraki, A.; Choi, S.M. A hybridization of spatial modeling and deep learning for people's visual perception of urban landscapes. *Sustainability* **2023**, *15*, 10403. [CrossRef]
116. Jacobs, J. *The Death and Life of Great American Cities*; Vintage: New York, NY, USA, 1992.
117. Xu, L.; Jiang, W.; Chen, Z. Study on perceived safety in public spaces: Take perception of stree view in shanghai as an example research on the sense of security in public space. *Landsc. Archit.* **2018**, *25*, 23–29.
118. Si, R.; Lin, Y.; Xiao, Z.; Ye, Y. Spatio-temporal analysis of built environment and street vitality relationship based on street-level imagery: A case study of Futian District, Shenzhen. *Sci. Geogr. Sin.* **2021**, *41*, 1536–1545.
119. Wang, L.; Zhou, Y.; Wang, F.; Ding, L.; Love, P.E.; Li, S. The influence of the built environment on people's mental health: An empirical classification of causal factors. *Sustain. Cities Soc.* **2021**, *74*, 103185. [CrossRef]
120. Li, Y.C.; Peng, L.; Wu, C.W.; Zhang, J.Z. Street view imagery (SVI) in the built environment: A theoretical and systematic review. *Buildings* **2022**, *12*, 1167. [CrossRef]
121. Rapoport, A. *The Meaning of the Built Environment: A Nonverbal Communication Approach*; University of Arizona Press: Tucson, AZ, USA, 1990.
122. Gehl, J. *Cities for People*; Island Press: Washington, DC, USA, 2010.
123. Zhang, F.; Salazar-Miranda, A.; Duarte, F.; Vale, L.; Hack, G.; Chen, M. Urban visual intelligence: Studying cities with artificial intelligence and street-level imagery. *J. Plan. Lit.* **2024**, *39*, 453. [CrossRef]

Disclaimer/Publisher's Note: The statements, opinions and data contained in all publications are solely those of the individual author(s) and contributor(s) and not of MDPI and/or the editor(s). MDPI and/or the editor(s) disclaim responsibility for any injury to people or property resulting from any ideas, methods, instructions or products referred to in the content.

buildings

MDPI

Article

Evaluating and Diagnosing Urban Function and Perceived Quality Based on Multi-Source Data and Deep Learning Using Dalian as an Example

Yumeng Meng [1], Mei Lyu [2], Dong Sun [3,*], Jiaxuan Shi [1] and Hiroatsu Fukuda [1]

[1] Faculty of Environmental Engineering, The University of Kitakyushu, Kitakyushu 808-0135, Japan
[2] School of Design and Art, Shenyang Jianzhu University, Shenyang 110168, China
[3] School of Architecture and Urban Planning, Shenyang Jianzhu University, Shenyang 110168, China
* Correspondence: sundong@sjzu.edu.cn

Abstract: Currently, coordinated development in terms of perceived urban quality and function has become a key problem. However, there is an imbalance between the street environment and urban amenities. It is necessary to explore the current status and propose optimization strategies to promote the coordinated development of urban spaces. Dalian, China, was selected as the study area. Based on space syntax, high-accessibility and low-accessibility streets were selected as study sites. An evaluation system was constructed as part of the study. It included the urban function and perceived street quality. Data on the density and diversity of urban amenities were obtained by establishing points of interest (POIs). The subjective and psychological perception of quality was calculated using street view images (SVIs). Then, a coupling analysis based on the urban function and perceived quality was conducted as part of the study. The results indicated that there were differences in the development levels of urban amenities and in regard to spatial quality in Dalian. Specifically, high-accessibility streets and urban amenities were mainly concentrated in the central urban area. The perceived quality of high-accessibility streets was higher than low-accessibility streets. The coupling analysis found that high-accessibility and low-accessibility streets had the highest proportions of advantage streets and opportunity streets. The urban amenities and subjective perception of quality were the highest in regard to advantage streets. The perception of beauty was the lowest in regard to maintenance streets. The psychological perception was the highest among improvement streets. Openness was the highest in regard to opportunity streets. As a result of the coupling analysis, this study not only helps to optimize the layout of urban amenities and improve the quality of the street environment, but also provides practical guidance for future urban design. Additionally, the results of this study will help to promote the coordinated development of street environments and urban amenities and enhance the overall livability and spatial quality of the urban environment.

Keywords: urban function; perceived quality; accessibility; deep learning; multi-source data

1. Introduction

Urban amenities and perceived quality represent urban vitality and environmental quality, respectively [1]. Urban amenities play an important role in determining the quality of life, experiences, livability, and well-being of residents [2,3]. The availability and accessibility of urban amenities are helpful for enhancing the quality of urban life [4].

However, due to the differences in urban development, the accessibility of urban amenities is limited in certain areas [5,6]. Improving the uneven distribution of urban functions is an essential strategy to construct healthier and more livable urban development [7]. The perceived quality of streets directly affects the accessibility and attractiveness of amenities [8]. A comfortable, beautiful, and safe street environment could attract more pedestrian and commercial activities, promoting economic development [9].

Coastal cities have rich natural environments and economic conditions, leading to a high population density and high levels of urbanization [10]. Therefore, these cities attract large numbers of tourists. Urban amenities are required that have a high density and diversity, such as entertainment, education, transportation, and shopping facilities [11,12]. The provision of comprehensive urban amenities and a high level of perceived quality in terms of those amenities could meet the needs of tourists and residents. They are helpful for enhancing the livability and attractiveness of the city [13,14].

Currently, cities are facing some problems as follows: (1) the distribution of urban amenities is uneven; (2) the existing density of transportation and public services is insufficient to meet the needs of tourists and residents; and (3) there are some perceived quality problems in terms of streets, including a lack of aesthetic qualities and uniqueness, poorly designed sidewalks, and low levels of greening.

Scholars initially quantified street accessibility in terms of street connectivity. Street space quality was quantified according to objective perceptions, such as road density, greening, and building density. Space quality could influence human psychological perceptions of the street environment. Then, some scholars quantified psychological perceptions such as safety, comfort, imageability, complexity, and transparency. Meanwhile, they explored the influence of the mechanisms between objective perception and psychological perception. A high-quality street environment not only affects residents' daily walking experiences, but also enhances social interactions and contributes to the urban image. Urban amenities serve as the core support for urban functions. Their density and diversity affect residents' living convenience and space utilization efficiency. In regard to urban planning and spatial optimization, it is hard to reveal the complexity of the urban environment using single-dimensional analysis. Therefore, this study conducted a coupled analysis of perceived quality, urban amenities, and accessibility. It helps to enable a more scientific and systematic assessment of the rationality of urban planning. Additionally, the results of this study could help to develop optimization strategies for urban governance and planning.

Urban amenities provide urban functions for residents, such as residential, educational, office, commercial, leisure, entertainment, and health services [15,16]. They are essential parts of daily life [17]. The density and diversity of urban amenities play a crucial role in enhancing the livability and attractiveness of cities. Previous studies have shown that multifunctional facilities can attract residents, thereby stimulating demand for services and, thus, attracting more residents [18,19]. Meanwhile, they enhance unban vitality [20]. Some street environment factors encourage people to travel and take part in social activities, such as mixed land use [21], parks [22], and sports services [23]. These factors are helpful for promoting human physical and mental well-being [24,25]. In previous studies, scholars have explored urban amenities from different perspectives, such as in regard to spatial distribution, equity [26,27], accessibility effects [28,29], and economic impacts [30].

Furthermore, the urban function and perceived street quality can together promote public travel [31]. Some design qualities can influence the walking environment and human perception, such as street design, safety, and land use [32,33]. Previous studies have shown that visual is crucial for spatial perception [34]. It plays an important role in street space quality. Some landscape elements are associated with the perceived quality of streets, such

as buildings, walls, greening, and walking spaces [35–37]. Additionally, a street's spatial features, like greenery and openness, can promote positive spatial perceptions [38,39]. For example, Ewing evaluated street design quality using five perceptual features, imageability, enclosure, transparency, human scale, and complexity [40,41].

Accessibility is the most common measure used to evaluate the equity of urban amenities [42]. Street accessibility affects people's access to convenient facilities [17]. In previous studies, space syntax theory has been widely used to measure street accessibility [43]. Spatial syntax is an important theory in regard to urban morphology for describing and analyzing the urban space and human activities [44,45]. In the 1970s, it was introduced by Bill Hillier. Since then, this theory has been widely applied in some fields, such as architecture [46], the urban environment [47], and spatial planning [48]. Some scholars have used this theory to research street accessibility [49,50], spatial structures [51], space syntax, and big data [52,53]. For example, based on space syntax and points of interest (POIs), Wang et al. explored the relationship between street accessibility and urban amenities, from the city scale to the street scale [54]. Furthermore, spatial syntax and Geographic Information Systems (GIS) could enhance the expressive capability of spatial syntax analysis [55].

The core urban area in Dalian, China, is selected as the study site. The POIs are used to quantify the density and diversity of the urban amenities. Then, an evaluation system is established to assess street perception quality from both psychological and objective perspectives. The streets are divided into four types according to their urban function and perceived quality. This study analyzes urban function and perceived quality according to different levels of accessibility and proposes corresponding optimization strategies. The Section 2 in this paper introduces the review of urban function and perceived quality in the literature, and the relevant quantitative methods. Section 3, the research framework is introduced, as well as the evaluation systems, data sources, and analysis methods. Sections 4 and 5 present the results and discussion. This study analyzes the spatial distribution of urban amenities and perceived quality. Meanwhile, the study diagnoses problems with different types of streets and proposes optimization strategies. Finally, the study concludes with a presentation of the findings and its contributions.

2. Literature Review

2.1. Study of Urban Function and Perceived Quality

Previous studies have shown that the spatial distribution of urban amenities has a significant impact on residents' quality of life, accessibility, and travel patterns [56]. Urban amenities include green public space [57], shopping services [58], transportation services [59,60], and cultural services [61]. Transportation services are one of the built environment factors that can encourage walking and reduce automobile use [62,63]. Shopping services are essential to support the sustainability of daily life [64]. Public services mainly refer to green spaces and open spaces in the city. Green public spaces are fundamental elements of the built environment and are essential public services [65,66]. They provide daily leisure activities for residents. They enhance the aesthetics of the urban landscape [67,68], improving the environmental function [69], and climate regulation [70,71]. Additionally, cities offer educational opportunities. The diversity and accessibility of education can influence public well-being. Public services enhance the positive evaluation of a neighborhood's social quality [72]. The diversity of POIs reflects the richness of the surrounding urban amenities [73]. Communities with high diversity in terms of land use have easier access to various facilities and services [25,74,75].

Perceived quality is a key factor in quantifying the spatial experience of streets. It is divided into objective perception and psychological perception [76–78].

Objective perception refers to the physical features of street quality that can be measured and observed [79]. Physical features were used to establish an objective framework. They were extracted from SVIs to evaluate streetscape perceptions [80,81]. As key landscape elements of the built environment, greenness can improve spatial quality and alleviate urban heat island effects. Additionally, they can promote human physical and mental health, and enhance people's sense of well-being [82,83]. Imageability refers to the environmental quality that strongly impresses observers [84]. The proportion of buildings and traffic signs can reflect the memorability of street spaces [85]. The literature on visual evaluations indicated that the level of enclosure is one of the significant features influencing human responses to the environment [86]. It is formed by horizontal interfaces and vertical landscape elements [87]. Openness refers to the visibility of the sky. Previous studies have shown that openness not only promotes mental health, but also enhances the attractiveness of streetscapes and increases spatial comfort [38,88]. Street design can influence the walking environment and pedestrian perceptions [87,89]. The amount of paved sidewalks can be used to measure pedestrian safety and comfort [84,90]. Walkability is a fundamental aspect of accessibility. It can provide pedestrians with more accessible movement, thereby creating a better walking environment [91]. These studies indicate that objective features of the street space influence the quality of the street space, such as openness, greenness, enclosure, and walkability.

Psychological perception refers to personal experiences and feelings in regard to the quality of streets [92]. Human perception directly reflects the quality of the street environments [93]. Positive perceived street quality can promote positive perceptions [94,95]. Previous studies have shown that street space design influences certain perceptions, such as whether the environment is safe, beautiful, or depressing [56]. Safe and beautiful are two fundamental human perceptions [96]. Boring and lively represent the attractiveness of the public in the street space [56]. The "Place Pulse 2.0" dataset was produced by Massachusetts Institute of Technology (MIT). It evaluated human perceptions in regard to six aspects: beautiful, lively, boring, depressing, wealthy, and safe. These perceptions related to residents' lives [81,97]. Zhang et al. validated the effectiveness of this dataset in capturing human perceptions [98]. These studies indicate that psychological perception is influenced by physical features, such as spatial design, greening, and social activities. Additionally, psychological perception was closely related to residents' mental health.

In summary, the research indicates that the density and diversity of urban amenities could represent urban functions, such as transportation, shopping, green public spaces, public services, and science/culture and education services. A high-quality street environment could enhance the utilization efficiency of the facilities. The spatial features of streets and human psychological perceptions were measured in order to evaluate the perceived street quality. Therefore, this study conducted a coupling analysis in regard to three dimensions, namely street accessibility, urban function, and perceived quality.

2.2. Methods of Measuring Urban Function and Perceived Quality

In previous studies, the data collection methods used mainly included questionnaire surveys [99], interviews [100], photography [101], and field surveys [102]. Due to time and cost restrictions, these methods are often limited to small-scale studies. However, with the development of data collection technology, multiple-source datasets are gradually being applied in urban research. Data collection technologies include street view images (SVIs) [103], social media data [104], Location-Based Services (LBSs) [105], and point of interest (POI) data [106]. These datasets include the objective features of street environments and human perceptions on a large scale [107]. For example, SVIs can directly show real

spatial environments of streets [108]. By using SVIs, some studies have carried out the extraction of landscape elements for street quality evaluations on a large scale [109]. On the other hand, POIs provide spatial and attribute information in terms of geography. This information is relevant to people's daily life. So, POIs are widely used in identifying urban functions and evaluating street vitality [110,111].

Currently, new computer technologies include Geographic Information Systems (GIS) and deep learning. These technologies have been used to process data. These technologies are helpful for enhancing our understanding of urban morphology on a large scale [112]. For example, deep learning integrates the advantages of convolutional neural networks, recurrent neural networks, and generative adversarial networks. Deep learning increases the efficiency of such networks by reducing the need for interventions [113]. Some scholars have combined street view images with deep learning to carry out research [114,115]. The relevant research includes assessing building facade quality, walkability, aesthetics, and human perceptions across micro, meso, and macro scales [116,117]. As a geographic spatial system for analyzing, managing, and visualizing all types of geographic spatial data, GIS have been widely applied in some studies related to urban planning and land resource management [118,119].

3. Materials and Methods

3.1. Research Framework

Firstly, the study obtained the data on the original road network in Dalian, China, from OpenStreetMap (OSM) and simplified the road network. Based on spatial syntax, a street accessibility analysis was conducted as part of the study, with high-accessibility streets and low-accessibility streets selected as study sites.

Secondly, in this study, street view images and points of interest (POIs) data were obtained for high-accessibility and low-accessibility streets. Using street view images and deep learning, the perceived street quality was obtained, including psychological and objective perceptions. Using semantic segmentation, six objectives perceptions were quantified, namely openness, greenness, paved sidewalks, walkability, imageability, and enclosure. Using the "Place Pulse 2.0" dataset, six psychological perceptions were obtained, namely beautiful, lively, boring, wealthy, depressing, and safe. Additionally, based on POIs data and the ArcGIS software, this study calculated the POI diversity and five types of facility densities (green public space, shopping facility, transportation facility, cultural facility, and public facility). The Delphi method was used to obtain weights for the psychological and objective perception features. Then, in this study, the heterogeneity of the perceived quality and urban function for high-accessibility streets and low-accessibility streets were analyzed.

Finally, this study established a coordinate system with regard to perceived quality, urban function, and street accessibility. The streets were divided into four types (advantage street, maintained street, improvement street, and opportunity street). The study conducted a heterogeneity analysis of the perceived quality and urban functions of different types of streets. This analysis is helpful for the development of urban amenities and urban planning (Figure 1).

3.2. Study Site

As a coastal industrial city, Dalian has undergone rapid urbanization in recent years. The city is gradually transitioning from a traditional industrial city to an eco-tourism city. Meanwhile, the land use and functional layout of Dalian have undergone significant changes. The core areas in Dalian (121.6147° E, 38.9140° N) were chosen as the study area.

These are the Zhongshan District, Xigang District, Shahekou District, and Ganjingzi District (Figure 2). These areas are the center of polity, the economy, and culture in Dalian. The core area is located at the south of the Liaodong Peninsula, which borders the Yellow Sea to the east and the Bohai Sea to the west. In addition, it has excellent port conditions and abundant marine resources. With a total area of approximately 573 square kilometers and a dense population, the core urban area has various urban functions, such as shopping, administration, cultural, industry, and transportation facilities for residents. It includes the main residential areas and commercial areas in Dalian.

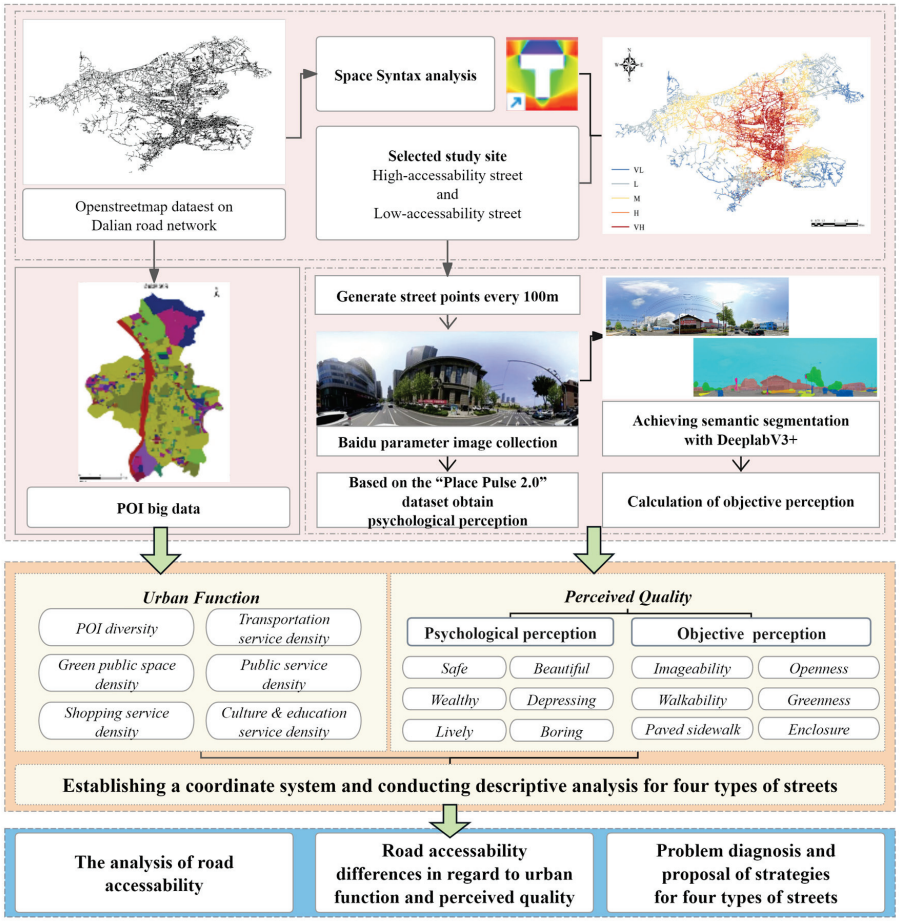


Figure 1. Research framework.

3.3. Evaluation and Analysis Methods

3.3.1. Data Collection

This study utilizes three types of data: road network data in Dalian, street view images, and POIs data.

The original road network data from Dalian were provided by OpenStreetMap (OSM). Space syntax theory was used to conduct topological analysis of the spatial features [120]. This theory pointed out that higher integration values indicate greater accessibility [121]. So, this study selected the angle patterns in the segment model to evaluate street accessibility. A radius of 500 m (R = 500) was set as the accessibility radius [122,123]. The study obtained the local integration in regard to the core urban area in Dalian. Then, the results of the street accessibility assessment were classified into five classes using the natural breaks classification method. Finally, we selected streets with very high accessibility (VH) and streets with very low accessibility (VL) as the study sites.

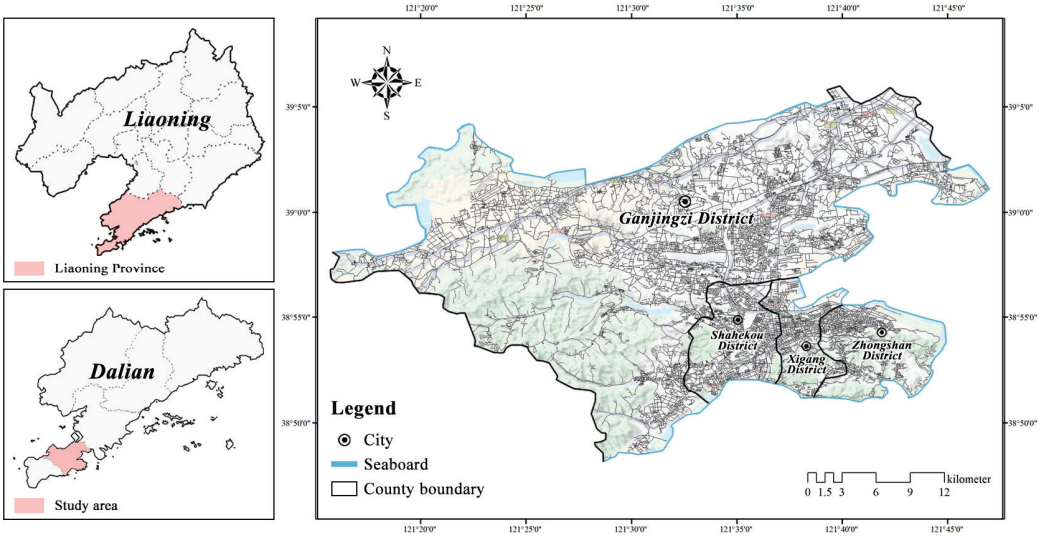


Figure 2. Study site and location of the core urban area in Dalian.

The Baidu map was selected as a data source for the street view images. Using the ArcGIS10.8 software, we generated sample points every 100 m, based on the simplified road network, and obtained their latitude and longitude coordinates [95]. Next, the image dimensions were set to 2048 × 624 pixels, the heading and pitch were set at 0°, and the images were selected from April to October. A total of 6273 images were obtained for high-accessibility streets, and 3295 images for low-accessibility streets. The DeepLabV3+ semantic segmentation architecture was used to partition the landscape elements using the ADE20K dataset, such as trees, buildings, fences, roads, and sidewalks [124,125]. The proportions of the landscape elements in the study area were used to calculate the objective perception values using the formulas listed in Table 1. In addition, six psychological perceptions were measured using a deep learning model and the "Place Pulse 2.0" dataset [126]. The method has been widely used to quantify human perception on a large scale [127]. It can be used to explore the relationship between the urban built environment and public sentiment [128].

Table 1. The formulas used in the study.

Features	Formula	Expression	Features
Urban function	POI diversity	$PDI = -\frac{1}{n}\sum_{i=1}^{n}(P_i * \ln P_i)$	P_i is the proportion in terms of the number of class I facilities in regard to the total number of facilities.
	Shopping service density	$SH = \text{Num (N)}/\text{Area } (\text{m}^2)$	Num (N) is the number of shopping services in the buffer area in terms of the N th sample point.
	Science/culture and education service density	$CE = \text{Num (N)}/\text{Area } (\text{m}^2)$	Num (N) is the number of science/culture and education services in the buffer area in terms of the N th sample point.
	Public facility density	$PF = \text{Num (N)}/\text{Area } (\text{m}^2)$	Num (N) is the number of public facilities in the buffer area in terms of the N th sample point.
	Transportation service density	$TS = \text{Num (N)}/\text{Area } (\text{m}^2)$	Num (N) is the number of transportation services in the buffer area in terms of the N th sample point.
	Green public space density	$GPS = \text{Num (N)}/\text{Area } (\text{m}^2)$	Num (N) is the number of green public spaces in the buffer area in terms of the N th sample point.

Table 1. *Cont.*

Features	Formula	Expression	Features
Objective perception	Imageability	$I_i = \frac{1}{n}\sum_{i=1}^{n} B_i + \frac{1}{n}\sum_{i=1}^{n} S1_i$ $\{i \in (1, 2, \ldots, n)\}$	B_i denotes the proportion of building pixels, $S1_i$ denotes the proportion of signboard pixels.
	Openness	$O_i = \frac{1}{n}\sum_{i=1}^{n} S2_i$ $\{i \in (1, 2, \ldots, n)\}$	$S2_i$ denotes the proportion of sky pixels.
	Enclosure	$E_i = \frac{\frac{1}{n}\sum_{i=1}^{n} B_i + \frac{1}{n}\sum_{i=1}^{n} T_i + \frac{1}{n}\sum_{i=1}^{n} W_i}{\frac{1}{n}\sum_{i=1}^{n} P1_i + \frac{1}{n}\sum_{i=1}^{n} F_i + \frac{1}{n}\sum_{i=1}^{n} R_i}$ $\{i \in (1, 2, \ldots, n)\}$	B_i is the percentage of building pixels; T_i is the percentage of tree pixels; W_i is the percentage of wall pixels; $P1_i$ is the percentage of pavement pixels; F_i is the percentage of fence pixels; R_i is the percentage of road pixels.
	Greenness	$G_i = \frac{1}{n}\sum_{i=1}^{n} T_i + \frac{1}{n}\sum_{i=1}^{n} G1_i$ $\{i \in (1, 2, \ldots, n)\}$	T_i denotes the proportion of tree pixels, $G1_i$ denotes the proportion of grass pixels.
	Walkability	$E_i = \frac{\frac{1}{n}\sum_{i=1}^{n} S3_i + \frac{1}{n}\sum_{i=1}^{n} F_i}{\frac{1}{n}\sum_{i=1}^{n} R_i}$ $\{i \in (1, 2, \ldots, n)\}$	$S3_i$ is the percentage of sidewalk pixels; F_i is the percentage of fence pixels; R_i is the percentage of road pixels.
	Paved sidewalk	$P2_i = \frac{\frac{1}{n}\sum_{i=1}^{n} S3_i}{\frac{1}{n}\sum_{i=1}^{n} S3_i + \frac{1}{n}\sum_{i=1}^{n} R_i}$ $\{i \in (1, 2, \ldots, n)\}$	$S3_i$ is the percentage of sidewalk pixels; R_i is the percentage of road pixels.
Psychological perception	Beautiful		Human perception of the locals as beautiful.
	Lively		Human perception of the locals as lively.
	Boring		Human perception of the locals as boring.
	Depressing		Human perception of the locals as depressing.
	Safe		Human perception of the local area as safe.
	Wealthy		Human perception of locals as wealthy.

As a form of geographic big data, POIs have advantages in terms of extensive coverage, ease of access, and high positional accuracy [129,130]. The Gaode open platform was selected as the data resource. A total of 122,314 POIs data were obtained in the core urban area in Dalian. These data include attribute information, such as name, address, type, coordinates, and administrative region. Then, the POIs data were divided into five types: green public space, shopping service, transportation service, public service, and science/culture and education service.

3.3.2. The Establishment of the Evaluation System

In previous studies, perceived street quality was divided into psychological perception and objective perception. Psychological perception quality is represented by the terms beautiful, lively, wealthy, safe, depressing, and boring, while objective perception includes greenness, openness, imageability, walkability, paved sidewalk, and enclosure. In addition, POI diversity was used to represent urban function. Shannon's index was used to calculate it. In this study, the densities of the five types of facilities were calculated, according to a 500 m × 500 m grid [131] (Table 1).

The Delphi method is used to determine the weights of evaluation indicators. It is an iterative questionnaire that collects opinions from multiple experts on the same indicators. The experts answer questionnaires during two or more rounds. Finally, we obtained the weights of the indicator. The Delphi method has been widely applied in previous studies for establishing various evaluation indicator systems [132,133]. In this study, 20 experts

from three majors (architecture, urban planning, and landscape design) were invited to evaluate the importance of three groups of indicators, using a 1–5 scale. A total of 20 complete questionnaires were obtained. Finally, we obtained weight values for objective perception quality, psychological perception quality, and urban function (Table 2). In addition, the overall perceived quality of the streets was obtained by averaging the weights of the objective and psychological perceptions.

Table 2. The evaluation system for urban function and perceived quality.

First Indicators	Secondary Indicators	Weight
Objective perception	Imageability	0.136
	Openness	0.209
	Enclosure	0.100
	Greenness	0.200
	Walkability	0.200
	Paved sidewalk	0.155
Psychological perception	Beautiful	0.242
	Lively	0.211
	Boring	0.074
	Depressing	0.063
	Safe	0.232
	Wealthy	0.179

3.4. Spatial Diagnosis

This study involved the carrying out of a couple of analyses of street accessibility, urban function, and perceived quality. A three-dimensional coordinate system was established in this study, with the perceived quality as the X axis, the urban function as the Y axis, and the street accessibility as the Z axis. The streets in the core urban area were divided into four types of street spaces, including advantage streets, maintenance streets, improvement streets, and opportunity streets (Figure 3).

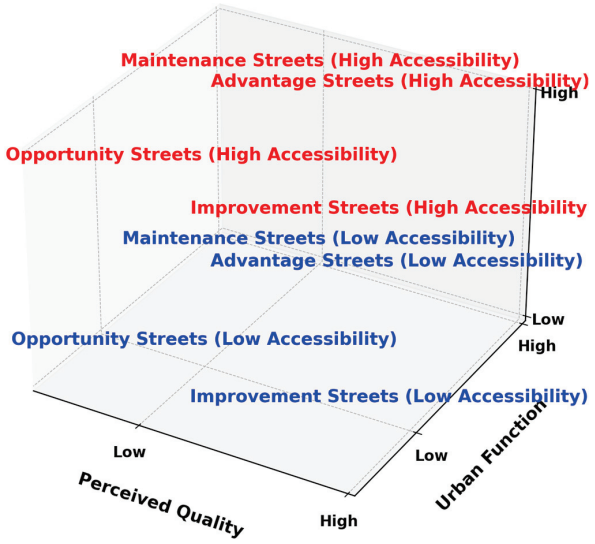


Figure 3. Establishment of the coordinate system.

4. Results

4.1. Analysis of Street Accessibility

Figure 4 illustrates the street accessibility in the core urban area of Dalian, based on a 500 m radius. High-accessibility streets and low-accessibility streets were separately

marked in blue and red. In the core urban area in Dalian, the street accessibility showed a trend of decreasing from the center towards the suburbs. High-accessibility streets were mainly located in the central areas of the core urban area. These streets were mainly major urban expressways and main streets. Low-accessibility streets were mainly located in suburban areas. These streets were mainly located in the suburbs of the Ganjingzi District and the mountains in the Zhongshan District.

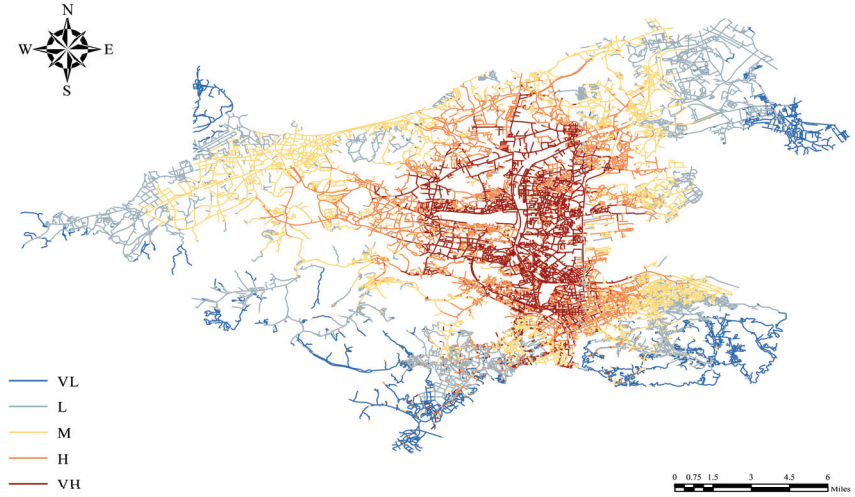
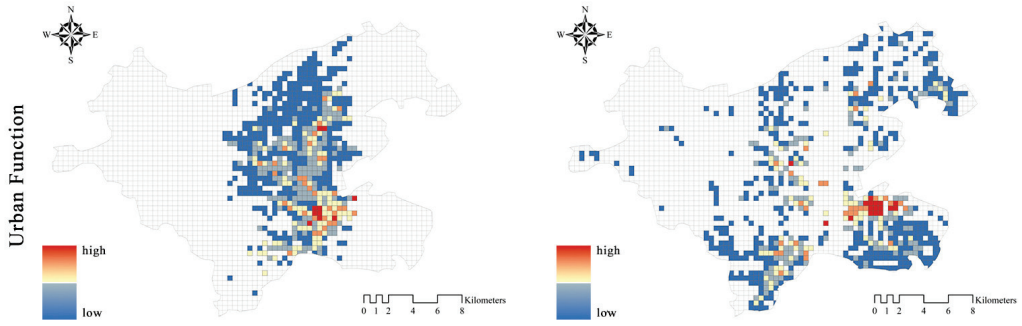


Figure 4. Space syntax model analysis result.

4.2. The Analysis of Urban Functions

To further explore the regional differences in the distribution and density of various urban amenities, spatial distribution, density, and diversity analyses of the urban amenities in terms of high and low accessibility were conducted in this study.

There was a clear clustering pattern in the core area of Dalian (Figure 5). The high-accessibility streets had a higher density of urban amenities than low-accessibility streets. In addition, high-value areas in high-accessibility streets accounted for 5.87% of the total area. High-value areas in low-accessibility streets accounted for 5.52% of the total area. The results showed that the distribution of urban amenities is more balanced in regard to low-accessibility streets (Table 3). In regard to different types of urban amenities, only the density of green public spaces was lower than low-accessibility streets. The results indicated that the central areas could provide residences with a higher density of urban functions and urban amenities than suburban areas. However, there were more green public spaces in low-accessibility streets.



(a) High amount of urban amenities (b) Low amount of urban amenities

Figure 5. The overall distribution of urban functions in the core urban area of Dalian.

Table 3. Comparison of urban function in streets with different levels of accessibility.

		High-Accessibility Streets	Low-Accessibility Streets
Green public space	Density	0.364	0.482
	The proportion of high-value amenities	0.98%	1.02%
Shopping service	Density	47.4	32.209
	The proportion of high-value amenities	4.89%	3.48%
Transportation service	Density	12.018	9.269
	The proportion of high-value amenities	6.20%	4.35%
Public facility	Density	2.439	1.903
	The proportion of high-value amenities	1.79%	1.45%
Science/culture and education service	Density	5.866	4.331
	The proportion of high-value amenities	5.71%	3.19%
POI diversity	Density	1.679	1.449
	The proportion of high-value amenities	66.39%	50.65%

In high-accessibility streets, five types of urban amenities clustered together to form the core area of the city. These were mainly located in the north of the Xigang District and the central part of the Ganjingzi District (Figure 6). In addition, the mean value of the facility density ranked as follows: shopping service > transportation service > science/culture and education service > public facility > green public facility (Table 3). This indicated that shopping malls and commercial districts were mainly clustered in high-accessibility streets. They provide residents with more commercial services. However, the density of green public spaces was the lowest, which suggested a lack of large green spaces in high-accessibility streets. Furthermore, the high-value areas in terms of POI diversity accounted for 66.39% of high-accessibility streets. This result indicated that the urban functions with a very high density included residential, shopping, leisure, transportation, medical, and cultural services. This finding reflects the high level of urbanization, high convenience, and high vitality in high-accessibility streets. These facilities could meet the basic needs of pedestrians (Figure 6f).

In low-accessibility streets, the distribution of urban amenities exhibited a scattered pattern (Figure 7). The results showed two minor peaks in the density distribution. These facilities were mainly located in the north of the Zhongshan District and the south of the scenic coastal area in the Ganjingzi District. The north of the Zhongshan District included several major urban functions, such as Dalian Railway Station and Roosevelt Plaza. There was lower pedestrian accessibility in the south of the Ganjingzi District. However, some scenic areas were located there, such as Xinghai Square. Transportation services, shopping services, and cultural facilities were densely concentrated within the area. Table 3 shows the mean value of the facility densities, which ranked as follows: shopping service > transportation service > science/culture and education service > public facility > green public facility. This result indicated that in terms of land use, shopping services and transportation services took priority and were responsible for the major urban functions in the area. However, green public spaces were constrained. High-value areas in terms of POI

diversity accounted for 50.65% of low-accessibility streets. This result indicated that most streets in these areas had a single functional diversity, resulting in lower urban vitality.

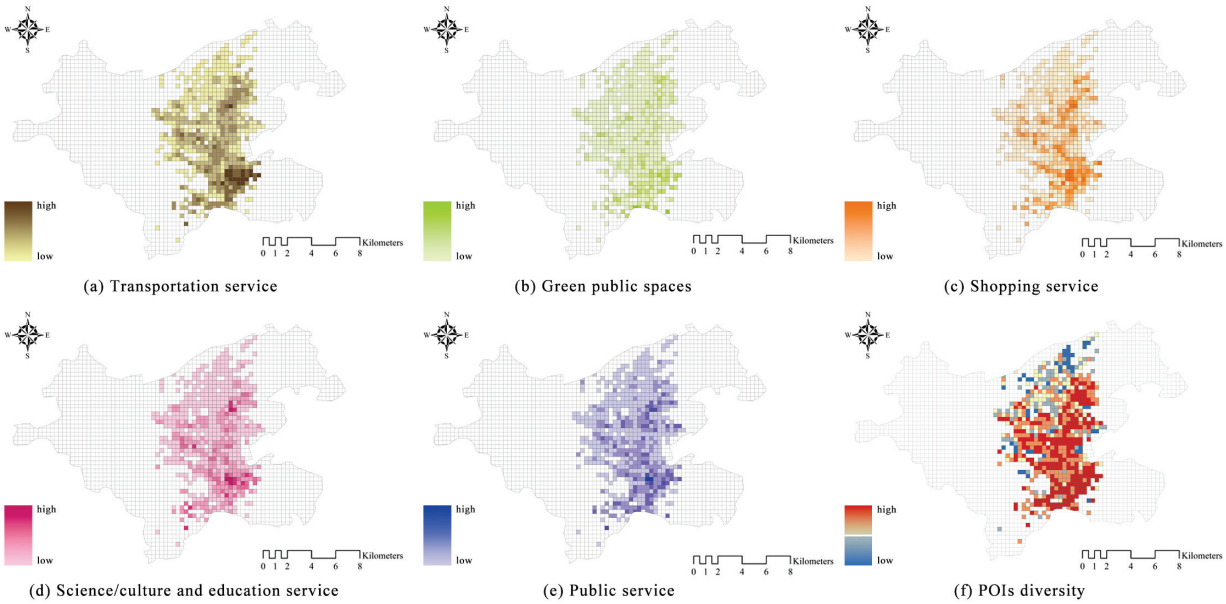


Figure 6. The spatial distribution of urban functions in high-accessibility streets.

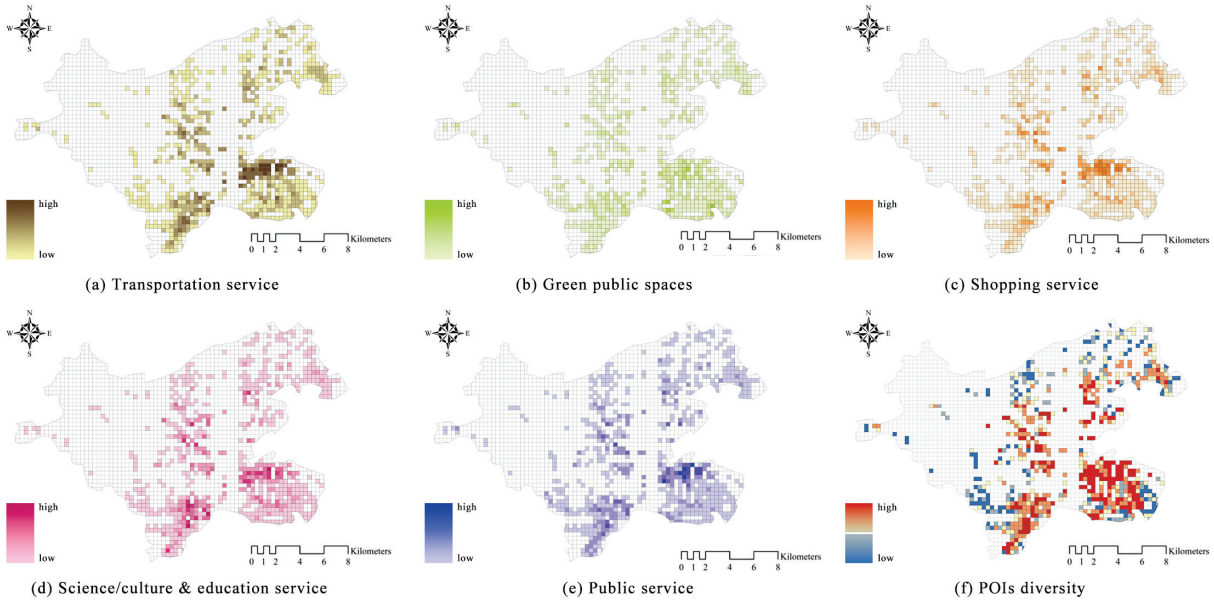


Figure 7. The spatial distribution of urban functions in low-accessibility streets.

4.3. The Analysis of Perceived Quality

The perceptual quality of streets showed minimal differences between the different levels of accessibility. Figure 8 illustrates that high-accessibility streets exhibit a higher overall level of perceptual quality compared to those with low accessibility. In terms of objective perception, low-accessibility streets rated higher than those with high accessibility. However, in terms of subjective perception, high-accessibility streets scored higher than those with low accessibility.

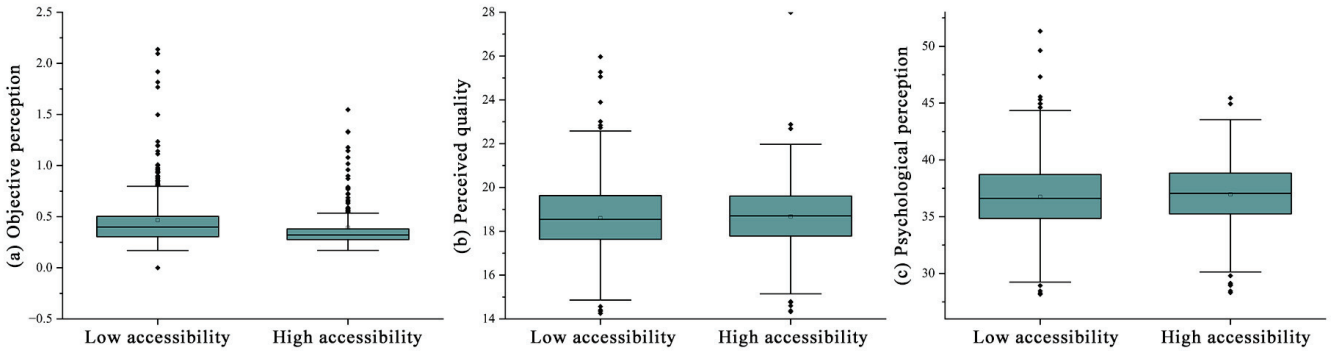


Figure 8. The overall perceived quality of the streets with different levels of accessibility in the core urban area of Dalian.

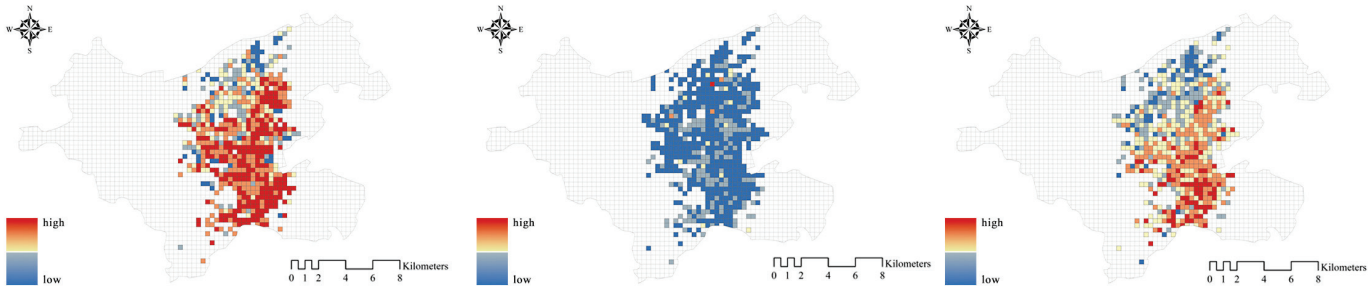
Table 4 presents subjective and objective perception quality evaluations of the streets with different levels of accessibility. In terms of objective perception, high-accessibility streets exhibited a higher level of openness and lower enclosure compared to those with low accessibility, albeit slightly lower levels of green coverage, intentionality, and pedestrian convenience. Regarding subjective perception, high-accessibility streets scored higher in regard to perceived vibrancy, safety, and affluence compared to their low-accessibility counterparts. They also rated lower in terms of perceived beauty, depressiveness, and boredom, indicating that high-accessibility streets tend to evoke more positive psychological responses among the public.

Table 4. The results on perceived quality.

Indicators	High-Accessibility Streets		Low-Accessibility Streets	
	Mean Value	Standard Deviation	Mean Value	Standard Deviation
Perceived quality	18.63	1.329	18.542	1.437
Objective perception	0.363	0.275	0.45	0.399
Openness	0.569	0.076	0.55	0.084
Greenness	0.06	0.048	0.078	0.070
Paved sidewalk	0.085	0.073	0.097	0.092
Walkability	0.237	0.549	0.318	2.258
Imageability	0.14	0.097	0.132	0.099
Enclosure	1.527	2.431	1.748	2.869
Psychological perception	36.898	2.649	36.635	2.833
Beautiful	34.375	5.815	34.676	6.913
Boring	59.159	3.624	60.353	4.663
Depressing	50.825	3.436	51.226	3.880
Lively	32.426	5.186	31.06	6.625
Safe	33.764	2.786	33.457	3.614
Wealthy	35.545	3.921	35.042	4.759

In high-accessibility streets, those with a higher perceived quality are predominantly located in the Xigang District (Figure 9a). The distribution of the objective quality perceptions is more dispersed (Figure 9b), with Table 3 showing the average ranking of the objective perceptions, as follows: enclosure > openness > walkability > imageability > paved sidewalk > greenness. This result indicates that most streets have the highest enclosure and lowest greenness. The strong sense of enclosure in these streets is influenced by the large proportion of sky coverage and significant presence of motorways, minimal pedestrian pavements, and poor walkability, thus offering inadequate walking conditions for residents. Moreover, these street spaces lack distinctive buildings and landscapes, making it difficult for the public to form lasting impressions of the street environment

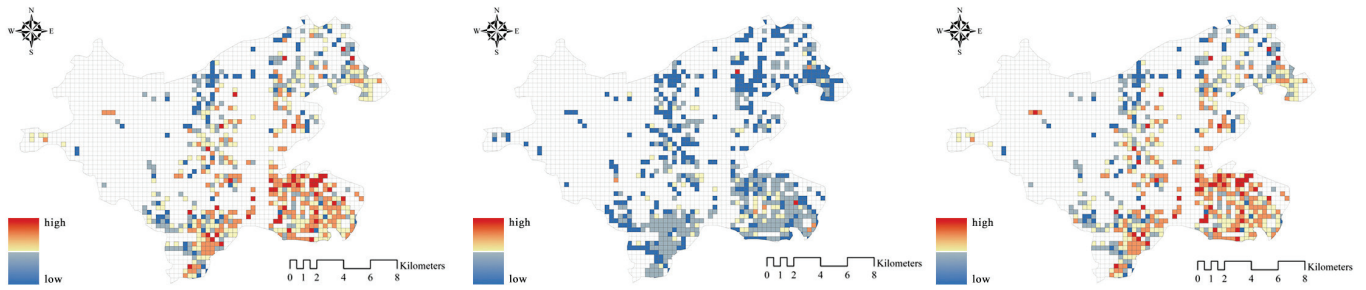
(Appendix A.1). Streets with a higher subjective perception quality are mainly concentrated in the central areas of Xigang and Ganjingzi districts (Figure 9c). The ranking of the subjective perceptions are as follows: boredom > depressing > affluence > beauty > safety > vibrancy. This indicates that in high-accessibility street spaces, the public experiences more negative psychological perceptions of boredom and depression, with a lack of vibrancy. The poor environmental conditions and deteriorating buildings diminish the overall aesthetic appeal of the streets and reduce public perceptions of safety, leading to anxiety.



(a) Perceived quality (b) Objective perception (c) Psychological perception

Figure 9. The spatial distribution of perceived quality in high-accessibility streets.

In low-accessibility streets, those with a higher perceived quality exhibit a dispersed pattern, mainly distributed in the southern part of the central area of Dalian City (Figure 10a). Streets with higher objective quality perceptions also show a scattered distribution, with weak clustering tendencies (Figure 10b). The overall green coverage in these street spaces is relatively low. Table 3 displays the average ranking of the objective perceptions, as follows: enclosure > openness > walkability > imageability > paved sidewalks > greenness. The low green coverage ratio and high level of enclosure indicate that buildings constitute the primary component of low-accessibility streets. Due to the relatively high openness of these street spaces, it suggests that most buildings are low-rise structures. While the streets exhibit good walkability, the low intentionality suggests a scarcity of iconic streetscape elements, such as traffic signs and billboards (Appendix A.2). Subjectively, perceptions are also dispersed (Figure 10c). The ranking of the subjective perceptions are as follows: boring > depressing > wealthy > beautiful > safe > lively. Low-accessibility streets score lowest in terms of vibrancy and highest in regard to depression and boredom, indicating that such perceptions have an impact on public social behavior. Streets with low perceptions in terms of safety accompany higher crime rates. Low perceptions of beauty and affluence suggest that the built street environment has a lower maintenance level.



(a) Perceived quality (b) Objective perception (c) Psychological perception

Figure 10. The spatial distribution of perceived quality in low-accessibility streets.

4.4. Spatial Diagnostics

Based on high accessibility and low accessibility, this study established two coordinate systems. Perceived quality was used as the horizontal axis. Urban function was used as the vertical axis (Figure 11).

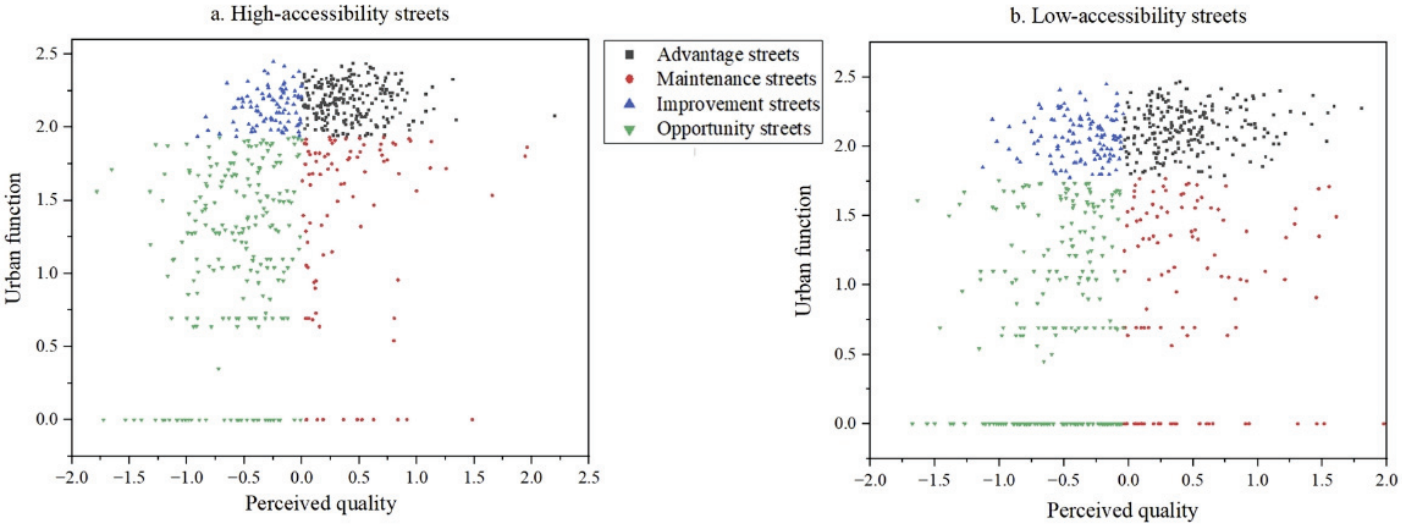


Figure 11. Establishment of the coordinate system.

4.4.1. The Spatial Diagnosis in Terms of High-Accessibility Streets

Table 5 shows the distribution of four types of streets in terms of high-accessibility streets. Advantage streets and opportunity streets are the most common, accounting for 35.23% and 34.91%. Table 6 shows the subjective and objective qualities and urban facility results for the four types of high-accessibility street spaces. From Table 6, it can be seen that compared to other streets, advantage streets provide residents with sufficient density and variety in terms of urban infrastructure. These streets also rank the highest in terms of certain psychological perceptions, including boring, depressing, lively, safe, and wealthy. In terms of objectives perception, advantage streets exhibit the highest values for paved sidewalks and imageability. However, their greenness and openness are the lowest among the four street types. Maintenance streets have a relatively high amount of urban infrastructure, primarily consisting of public and commercial facilities. However, their perceived quality is lower due to poor levels of paved sidewalks, walkability, and imageability. In terms of psychological perceptions, attributes such as beautiful, depressing, lively, and wealthy were ranked lower. Improvement streets exhibited an overall high level of perceived quality, with the highest objective perception value. Enclosure and walkability were the highest ranked among the four street types. However, these streets have a lower quantity and variety of urban facilities, making it difficult for all residents to fully benefit from these urban functions. Transportation service is the lowest ranked type, while only the commercial facility density is relatively high in regard to this street type, meeting residents' basic living needs. Increasing other types of facilities would help enhance the quality of life and overall livability in this regard. Opportunity streets have the lowest urban functions and perceived quality, showing significant potential for improvement among high-accessibility streets. However, openness is the highest ranked among the four types.

Table 5. Distribution density of four street types in regard to streets with different levels of accessibility.

Diagnosed Streets	High-Accessibility Streets		Low-Accessibility Streets	
	Number	Proportions	Number	Proportions
Advantage Streets	216	35.23%	230	33.42%
Maintenance Streets	92	15.01%	115	16.72%
Improvement Streets	91	14.85%	115	16.72%
Opportunity Streets	214	34.91%	228	33.14%

Table 6. Comparative analysis of three types of indicators in regard to high-accessibility streets.

	POIs Diversity	Public Facility	Shopping Service	Transportation Service	Sports Service	Science/Culture and Education Service		
Advantage Streets	2.18	20.70	75.76	0.51	4.39	11.12		
Maintenance Streets	2.14	14.76	42.97	0.6	2.93	6.91		
Improvement Streets	1.35	7.98	64.32	0.36	2.13	4.21		
Opportunity Streets	1.12	3.83	13.39	0.11	0.39	0.84		
	Perceived Quality	**Openness**	**Greenness**	**Paved Sidewalk**	**Walkability**	**Imageability**	**Enclosure**	**Objective Perception**
Advantage Streets	0.43	−0.77	−0.04	0.66	0.04	0.68	0.04	0.07
Maintenance Streets	−0.28	0.09	0.09	−0.02	−0.1	−0.14	−0.15	−0.17
Improvement Streets	0.60	−0.20	0.06	0.03	0.37	0.15	0.47	0.66
Opportunity Streets	−0.58	0.82	−0.02	−0.67	−0.16	−0.69	−0.18	−0.28
		Beautiful	**Boring**	**Depressing**	**Lively**	**Safe**	**Wealthy**	**Psychological Perception**
Advantage Streets		0.27	0.33	0.37	0.72	0.54	0.64	0.80
Maintenance Streets		−0.22	0.00	−0.20	−0.33	−0.24	−0.21	−0.38
Improvement Streets		0.47	0.02	0.02	0.43	0.15	0.27	0.54
Opportunity Streets		−0.38	−0.34	−0.30	−0.77	−0.51	−0.67	−0.88

4.4.2. The Spatial Diagnosis in Terms of Low-Accessibility Streets

Table 5 shows the distribution of four types of streets in low-accessibility areas of the main urban area in Dalian. Among them, advantage streets and opportunity streets are the most common, accounting for 33.42% and 33.14%. From Table 7, it can be seen that compared to other street types, advantage streets have the highest quality and variety of urban facilities, allowing them to carry out most public urban functions. In terms of psychological perceptions, advantage streets have the highest score among the four street types, particularly for the terms depressing, lively, safe, and wealthy. In regard to objective perceptions, paved sidewalks and imageability are the highest ranked among the four street types, while openness is the lowest. Maintenance streets have a relatively high level of urban functionality, but lower perceived quality. In terms of psychological perceptions, beautiful has the lowest score among the four street types. In terms of objective perceptions, greenness and enclosure are the lowest ranked types, indicating a lack of aesthetic attractiveness. Enhancing greenness by planting a diverse range of vegetation to improve both the aesthetics and overall environmental quality would be beneficial. Improvement streets have a relatively low density and variety of urban facilities, showing that increasing the density and variety of facilities on these streets would help enhance their attractiveness and enrich the urban functions. The perceived quality of improvement streets was the highest among the four street types. In terms of objective perceptions, improvement streets have the highest score for greenness, walkability, and enclosure. In terms of psychological perceptions, beautiful has the highest score among the four street types. Opportunity streets have the lowest amount of urban facilities and level of quality

among the four street types. However, openness has the highest, indicating significant potential for improvements to enhance the accessibility of these street.

Table 7. Comparative analysis of three types of indicators in regard to low-accessibility streets.

	POIs Diversity	Public Facility	Shopping Service	Transportation Service	Sports Service	Science/Culture and Education Service		
Advantage Streets	2.13	0.88	64.79	17.83	3.92	8.81		
Maintenance Streets	2.06	0.44	41.80	13.09	2.72	6.31		
Improvement Streets	0.91	0.5	8.33	3.04	0.28	1.39		
Opportunity Streets	0.73	0.10	6.66	1.88	0.28	0.31		
	Perceived Quality	**Openness**	**Greenness**	**Paved Sidewalk**	**Walkability**	**Imageability**	**Enclosure**	**Objective Perception**
Advantage Streets	0.47	−0.47	−0.08	0.33	−0.01	0.56	0.03	0.17
Maintenance Streets	−0.38	0.06	−0.29	0.00	−0.04	0.10	−0.14	−0.18
Improvement Streets	0.56	−0.2	0.49	0.17	0.19	−0.18	0.16	0.48
Opportunity Streets	−0.57	0.54	−0.02	−0.42	−0.07	−0.52	−0.05	−0.32
		Beautiful	**Boring**	**Depressing**	**Lively**	**Safe**	**Wealthy**	**Psychological Perception**
Advantage Streets		0.08	0.14	0.37	0.74	0.46	0.60	0.77
Maintenance Streets		−0.36	−0.11	−0.19	−0.27	−0.24	−0.41	−0.57
Improvement Streets		0.68	0.14	−0.06	0.2	0.23	0.22	0.65
Opportunity Streets		−0.24	−0.16	−0.25	−0.70	−0.46	−0.50	−0.81

5. Discussion

5.1. The Analysis of the Coupling Between Street Accessibility and Urban Functions

Streets are the basic framework of the urban space. They connect different functional areas, such as shopping, transportation, culture, and public services [17]. The street network in Dalian was evaluated using accessibility analysis and space syntax. Then, we quantified the urban amenities using POI data. The study found that the functional distribution of urban functions showed strong centripetal characteristics, gradually decreasing from the center to the outer area. High-accessibility streets have a higher density and diversity of urban functions than low-accessibility streets, particularly in regard to shopping services, transportation services, science/culture and education services, and public services. The spatial concentration of facilities reflects urbanization development model in Dalian. Urban functions are mainly located in streets with higher accessibility, which is consistent with the findings by Yin and Hajrasouliha [134].

Additionally, this study found that high-accessibility streets have higher perceived quality than low-accessibility streets. In terms of psychological perceptions, high-accessibility streets provide the public with a sense of liveliness, safety, and wealth. The results showed that rich facilities and social opportunities helped to decrease public stress. Thus, these benefits offer advantages in terms of mental health [135]. At the same time, the high amount of urban functions on offer reduces car travel. These functions provide the public with more opportunities for walking and cycling [136]. Therefore, residents find it easier to take part in daily physical activities, such as walking to the shops, visiting attractions, or going to parks. These activities are helpful for reducing the risk of obesity and cardiovascular diseases [137].

In the context of urban renewal, high-accessibility streets are often located in core areas where urban functions and facilities are concentrated. Living in core areas means it is easier to access urban amenities than living in suburban areas [138,139].

Furthermore, this difference reflected the land use strategies and priorities adopted in the city center. In Dalian, the commercial, transportation, cultural, and public facilities

were constructed first. Based on spatial syntax theory, some research has shown that high-accessibility streets foster high street vitality [140]. These streets with convenient walking environments typically promote higher pedestrian flows and urban economic activities. A high density of shopping services indicated that economic activities were concentrated in certain areas. These facilities could meet the needs of consumers and businesses and promote economic growth. A high density of transportation services was helpful for enhancing spatial vitality, because a high density of transportation services could increase public mobility and social interactions [141]. Transportation services could also promote the integration of urban amenities, enhancing urban livability and sustainability [142]. A high density of education and medical facilities could meet residents' basic needs [143]. Meanwhile, public services provided diverse leisure activities. Sports services were helpful for physical health. The reasonable planning of public facilities could enable residents to enjoy convenient and efficient services. It could enhance public life-related satisfaction and well-being [144]. However, the total area of green spaces in the central district was limited by other land uses. It is hard to increase the amount of green spaces.

On the other hand, a high-quality street environment could enhance the facility utilization efficiency. It could offer more convenience to residents and tourists. A good walking environment could improve street accessibility. It was found that some urban amenities were easier to use, such as commercial and public facilities. For example, high levels of greenness and openness provide the public with high-quality resting spaces. These subjective features were helpful for decreasing the pressure due to high-density streets. Therefore, they could enhance street comfort and safety, thus increasing the public's willingness to stay in the area.

Low-accessibility streets were mainly located in suburban areas. Some streets with a high density of urban amenities and a high level of perceived quality need to improve their accessibility. These streets were helpful for enhancing residents' walking experiences and easier to gain access to urban functions. Increasing transportation facilities is one way to improve convenience for non-motorized vehicles and pedestrians. For example, constructing dedicated pedestrian and bicycle lanes was helpful for creating safe and convenient walking and cycling environments. Studies have indicated that well-designed pedestrian and cycling facilities not only reduced traffic congestion, but also promoted healthy lifestyles [145]. Furthermore, some methods could be used to improve street accessibility, such as enhancing street quality, optimizing street layout, or enhancing landscape design. In addition, increasing the number of green spaces and sidewalk widths were helpful for optimizing street layouts. This could enhance comfort and safety for pedestrians and cyclists and promote vitality in these areas [146]. Integrating art installations and urban culture into street spaces was helpful for enhancing the perceived quality of the area by residents and visitors, enhancing social interactions and vitality in the area [147].

5.2. Identify the Priority Roads in the Location

This study established a coordinate system based on urban function, street accessibility, and perceived quality. Then, spatial diagnostics were conducted for every type of street.

Advantage streets had high-density and high-diversity urban amenities. These streets could provide diverse services and amenities. They were helpful for meeting the needs of residents and tourists. In addition, these streets showed a high level of perceived quality, with well-designed public spaces. In regard to objective perceptions, paved sidewalks and imageability were the highest ranked of the four street types. This indicates that advantage streets have advantages in terms of the walking environment and landscape ionizability. But greenness and openness were the lowest ranked types, because high-density buildings

reduce green spaces and open spaces. In terms of psychological perceptions, depressing, lively, safe, and wealthy types were the lowest ranked in terms of the four street types. This indicated that these streets are generally considered to be more prosperous, safe, and economically developed areas.

In regard to maintenance streets, the distribution of urban amenities was clustered together. These facilities could meet residents' basic needs. Moreover, enhancing the perceived quality could improve the environment in regard to these streets. In regard to objective perceptions, paved sidewalks, walkability, and imageability were the lowest ranked in regard to the four street types. This indicates that creating a pleasant walking and leisure environment is key to enhancing objective perceptions in regard to maintenance streets [148]. In terms of psychological perceptions, beautiful was ranked lower in regard to maintenance streets in regard to high- and low-accessibility streets. Reinforcing infrastructure maintenance could enhance street aesthetics [149].

Improvement streets have high potential. These streets need to increase infrastructure investment, while preserving and enhancing existing the environmental quality. Urban functions could be enhanced by adding commercial, education, and medical services. Street vitality could be improved by improving transportation services [150]. In terms of perceived quality, improvement streets had a high level of greenness, but the street interface was closed and it was stressful for pedestrians. Increasing vertical greening not only enhanced the level of greenness, but also improved sky visibility [151,152].

Opportunity streets had significant potential for development in regard to both urban amenities and spatial aspects. Investing in infrastructure construction could enhance the region's basic service levels. Increasing the level of openness could enhance the comfort of public activities, positive emotions, and psychological well-being [80]. Furthermore, constructing unique architecture, installing landscape features, and planting diverse vegetation could enhance the aesthetics and attractiveness of streetscapes [153]. Thereby, enhancing the overall perceptual quality of opportunity streets.

5.3. Limitations

This study has certain limitations that need to be discussed.

It focuses on the city level. But this study does not include a functional classification for commercial, residential, shopping, and cultural services. Classification research is beneficial for formulating more targeted policies and measures based on the specific needs and characteristics of different functional areas. This method could promote coordinated development among different zones and enhance the urban functions in the city.

This study conducts spatial analysis based on street accessibility. In future research, urban heat maps could be used to learn about pedestrian and traffic flows at different times. Analyzing urban functional vitality at various times could help identify deficiencies in living facilities and services, thereby improving residents' quality of life and satisfaction.

Furthermore, deep learning and street view images were used to quantify public perceptions in this study. In future research, neurobiological methods could be applied to more precisely measure and evaluate residents' real-time experiential environment while walking and sitting. This approach could explore the impact of street density and the distribution of various urban amenities on human perceptions [106].

6. Conclusions

Based on space syntax theory, this study analyzed street accessibility. Then, high- and low-accessibility streets were identified for the study. Points of interest (POIs) data were used to measure the density of urban amenities. Perceived quality was quantified using

deep learning and SVIs. In addition, this study involved carring out a coupling analysis from three dimensions: street accessibility, urban amenities, and perceived street quality. Then, the spatial distribution differences in terms of urban amenities and perceived quality were analyzed in this study in regard to streets with different levels of accessibility. Then, the streets were divided into four types. Problems with the layout of facilities and spatial quality were explored in terms of the different street types. Meanwhile, the study proposed targeted optimization strategies. This study is helpful for ensuring residents can equitably enjoy urban amenities and high-quality streets.

This study's findings are as follows:

(1) In the core area of Dalian, high-accessibility streets were mainly located in the central region, while low-accessibility streets mainly located in the urban periphery;
(2) High-accessibility streets have a higher perceived quality than low-accessibility streets. Specifically, in terms of psychological perceptions, lively, safe, and depressing perceptions scored higher in regard to high-accessibility streets than low-accessibility streets. In terms of objective perceptions, high-accessibility streets ranked lower than low-accessibility streets. Greenness, the amount of paved sidewalks, and walkability in high-accessibility streets need to be improved;
(3) By comparing the density of urban amenities, shopping services were ranked the highest in regard to high-accessibility streets and low-accessibility streets. However, public services were ranked the lowest;
(4) Through carrying out coupling analysis, this study found that high-accessibility streets and low-accessibility streets share similar advantages and problems in regard to the four street types. The proportion of advantage streets and opportunity streets were high in regard to the four types of streets. The density and diversity of urban amenities were the highest in regard to advantage streets. In terms of psychological perceptions, depressing, lively, safe, and wealthy were ranked the highest in regard to the four street types. In terms of objective perceptions, paved sidewalks and imageability were ranked the highest in terms of the four types of streets. In regard to the maintenance streets, beautiful was ranked the lowest of the four street types. In regard to the improvement streets, the objective perception was ranked the highest in terms of the four types of streets. However, beautiful was ranked the highest. In regard to opportunity streets, openness was the highest ranked of the four types of streets.

Optimizing the function and quality of different street types not only enhances the overall environmental quality, but also promotes social equity and economic development. It is helpful for sustainable urban development. Meanwhile, this study provides scientific data analysis and a comprehensive evaluation of the area for urban planning and management departments. It is helpful for creating more urban development strategies that enhance overall urban livability and attractiveness.

Author Contributions: Conceptualization, Y.M., J.S., H.F. and M.L.; methodology, Y.M., J.S. and H.F.; software, Y.M., J.S. and D.S.; validation, J.S., M.L. and H.F.; formal analysis, J.S., M.L. and H.F.; investigation, Y.M., J.S. and D.S.; resources, Y.M., J.S., M.L. and H.F.; data curation, Y.M. and J.S.; writing—original draft preparation, Y.M., J.S. and M.L.; writing—review and editing, Y.M., J.S., M.L. and D.S.; visualization, Y.M. and D.S.; supervision, Y.M., H.F. and M.L.; project administration, H.F. and M.L.; funding acquisition, M.L. All authors have read and agreed to the published version of the manuscript.

Funding: This research was funded by a Project of Liaoning Provincial Department of Education, grant numbers, JYTMS20231583.

Data Availability Statement: Interview transcripts and interpreted statements supporting this study's findings and the smart contract codes are available from the corresponding author upon reasonable request.

Acknowledgments: We would like to thank the journal experts who edited this paper. We also appreciate the constructive suggestions and comments on the manuscript from the reviewers and editors.

Conflicts of Interest: The authors declare that there are no conflicts of interest.

Appendix A

Appendix A.1

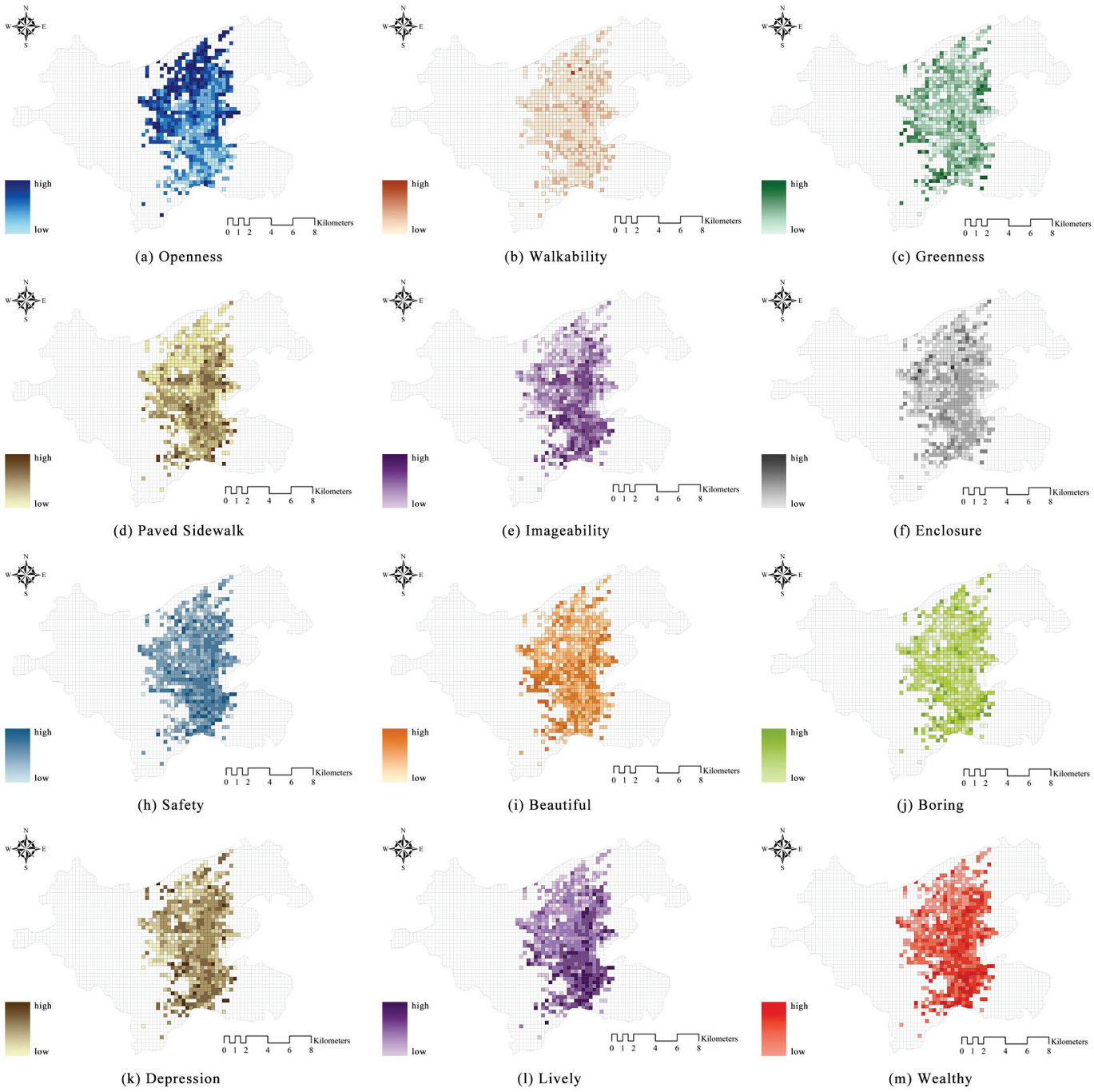


Figure A1. The spatial distribution of perceptual features in high-accessibility streets.

Appendix A.2

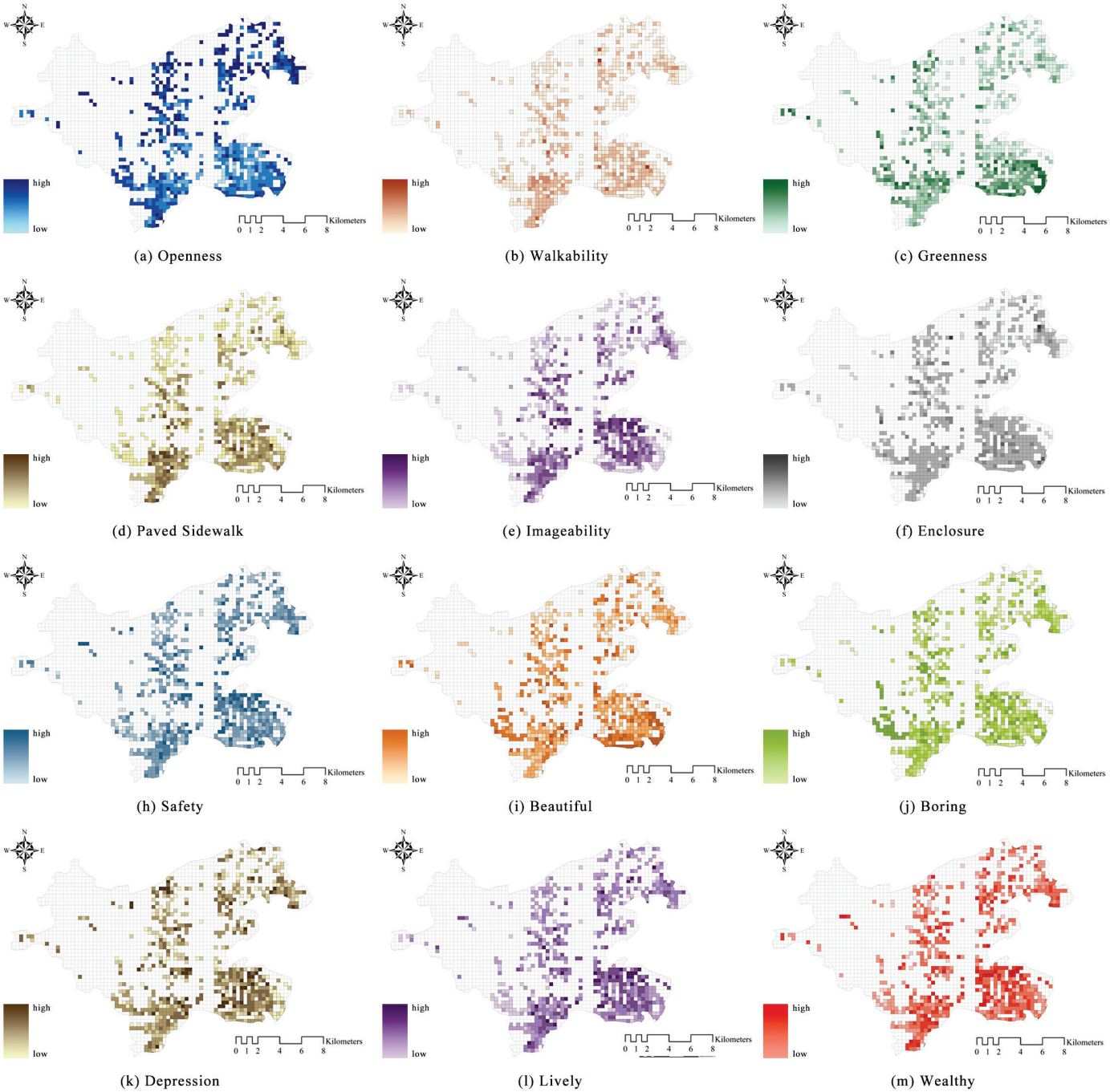


Figure A2. The spatial distribution of perceptual features in low-accessibility streets.

References

1. Gehl, J. *Cities for People*; Island Press: Washington, DC, USA, 2010.
2. Cai, Z.; Kwak, Y.; Cvetkovic, V.; Deal, B.; Mörtberg, U. Urban spatial dynamic modeling based on urban amenity data to inform smart city planning. *Anthropocene* **2023**, *42*, 100387. [CrossRef]
3. Smith, B.A. Measuring the value of urban amenities. *J. Urban Econ.* **1978**, *5*, 370–387. [CrossRef]
4. Larsson, A.; Elldér, E.; Vafeiadis, E.; Curtis, C.; Steiner, A. Exploring the potential for sustainable accessibility across settlement types. A Swedish case. *Transp. Res. Part D: Transp. Environ.* **2022**, *107*, 103297. [CrossRef]
5. Olsen, J.R.; Thornton, L.; Tregonning, G.; Mitchell, R. Nationwide equity assessment of the 20-min neighbourhood in the scottish context: A socio-spatial proximity analysis of residential locations. *Soc. Sci. Med.* **2022**, *315*, 115502. [CrossRef] [PubMed]

6. Olsen, J.R.; Nicholls, N.; Whitley, E.; Mitchell, R. Association between local amenities, travel behaviours and urban planning: A spatial analysis of a nationwide UK household panel study. *J. Transp. Health* **2024**, *36*, 101784. [CrossRef]
7. Xiao, Y.; Wang, Z.; Li, Z.; Tang, Z. An assessment of urban park access in Shanghai—Implications for the social equity in urban China. *Landsc. Urban Plan.* **2017**, *157*, 383–393. [CrossRef]
8. Jane, J. *The Death and Life of Great American Cities*; Random House: New York, NY, USA, 1961.
9. Carmona, M. *Public Places Urban Spaces: The Dimensions of Urban Design*, 3rd ed.; Routledge: London, UK, 2021.
10. Zhang, G.; Xing, L. Research on tourism economic effect under the threshold of new-type urbanization in coastal cities of China: From the perspective of development economics. *Ocean. Coast. Manag.* **2023**, *239*, 106587. [CrossRef]
11. Özer, M.; Küçüksakarya, S.; Maiti, M. Nexus of tourism demand, economic growth, and external competitiveness in leading tourist destination countries. *Tour. Manag. Perspect.* **2022**, *42*, 100965. [CrossRef]
12. Santamaria, D.; Filis, G. Tourism demand and economic growth in Spain: New insights based on the yield curve. *Tour. Manag.* **2019**, *75*, 447–459. [CrossRef]
13. Montgomery, J. Making a city: Urbanity, vitality and urban design. *J. Urban Des.* **2007**, *3*, 93–116. [CrossRef]
14. Gehl, J. *Life Between Buildings: Using Public Space*; Island Press: Washington, DC, USA, 2011.
15. Liu, J.; Meng, B.; Shi, C. A multi-activity view of intra-urban travel networks: A case study of Beijing. *Cities* **2023**, *143*, 104634. [CrossRef]
16. Burger, M.J.; van der Knaap, B.; Wall, R.S. Polycentricity and the Multiplexity of Urban Networks. *Eur. Plan. Stud.* **2013**, *22*, 816–840. [CrossRef]
17. Yang, X.; Zheng, X.; Cao, Y.; Chen, H.; Tang, L.; Yang, H. Connectivity analysis in pedestrian networks: A case study in Wuhan, China. *Appl. Geogr.* **2023**, *151*, 102843. [CrossRef]
18. Li, H.; Wei, Y.D.; Wu, Y. Urban amenity, human capital and employment distribution in Shanghai. *Habitat Int.* **2019**, *91*, 102025. [CrossRef]
19. Glaeser, E.L.; Kominers, S.D.; Luca, M.; Naik, N. Big Data and Big Cities: The Promises and Limitations of Improved Measures of Urban Life. *Econ. Inq.* **2016**, *56*, 114–137. [CrossRef]
20. Mulligan, G.F.; Carruthers, J.I. Amenities, Quality of Life, and Regional Development. In *Investigating Quality of Urban Life*; Marans, R., Stimson, R., Eds.; Springer: Dordrecht, The Netherlands, 2011.
21. Mobley, L.R.; Root, E.D.; Finkelstein, E.A.; Khavjou, O.; Farris, R.P.; Will, J.C. Environment, obesity, and cardiovascular disease risk in low-income women. *Am. J. Prev. Med.* **2006**, *30*, 327–332. [CrossRef] [PubMed]
22. Kaczynski, A.T.; Besenyi, G.M.; Stanis, S.A.; Koohsari, M.J.; Oestman, K.B.; Bergstrom, R.; Potwarka, L.R.; Reis, R.S. Are park proximity and park features related to park use and park-based physical activity among adults? Variations by multiple socio-demographic characteristics. *Int. J. Behav. Nutr. Phys. Act.* **2014**, *11*, 146. [CrossRef]
23. Halonen, J.I.; Stenholm, S.; Kivimaki, M.; Pentti, J.; Subramanian, S.V.; Kawachi, I.; Vahtera, J. Is change in availability of sports facilities associated with change in physical activity? A prospective cohort study. *Prev. Med.* **2015**, *73*, 10–14. [CrossRef]
24. Sarkar, C.; Webster, C. Urban environments and human health: Current trends and future directions. *Curr. Opin. Environ. Sustain.* **2017**, *25*, 33–44. [CrossRef]
25. Ewing, R.; Cervero, R. Travel and the Built Environment. *J. Am. Plan. Assoc.* **2010**, *76*, 265–294. [CrossRef]
26. Tahmasbi, B.; Mansourianfar, M.H.; Haghshenas, H.; Kim, I. Multimodal accessibility-based equity assessment of urban public facilities distribution. *Sustain. Cities Soc.* **2019**, *49*, 101633. [CrossRef]
27. Ashik, F.R.; Mim, S.A.; Neema, M.N. Towards vertical spatial equity of urban facilities: An integration of spatial and aspatial accessibility. *J. Urban Manag.* **2020**, *9*, 77–92. [CrossRef]
28. Xu, Y.; Zhang, Q.; Zheng, S. The rising demand for subway after private driving restriction: Evidence from Beijing's housing market. *Reg. Sci. Urban Econ.* **2015**, *54*, 28–37. [CrossRef]
29. Zhang, Y.; Dong, R. Impacts of Street-Visible Greenery on Housing Prices: Evidence from a Hedonic Price Model and a Massive Street View Image Dataset in Beijing. *ISPRS Int. J. Geo-Inf.* **2018**, *7*, 104. [CrossRef]
30. Aschauer, D.A. Is Public Expenditure Productive? *J. Monet. Econ.* **1989**, *23*, 177–200. [CrossRef]
31. Næss, P.; Strand, A.; Wolday, F.; Stefansdottir, H. Residential location, commuting and non-work travel in two urban areas of different size and with different center structures. *Prog. Plan.* **2019**, *128*, 1–36. [CrossRef]
32. Naess, P. Urban form and travel behavior: Experience from a Nordic context. *J. Transp. Land Use* **2012**, *5*, 21–45. [CrossRef]
33. Newman, P.W.G.; Kenworthy, J.R. *Cities and Automobile Dependence: A Sourcebook*; Gower Technical: Farnham, UK, 1989.
34. Cafuta, M.R. Open Space Evaluation Methodology and Three Dimensional Evaluation Model as a Base for Sustainable Development Tracking. *Sustainability* **2015**, *7*, 13690–13712. [CrossRef]
35. Lee, J.; Kim, D.; Park, J. A Machine Learning and Computer Vision Study of the Environmental Characteristics of Streetscapes That Affect Pedestrian Satisfaction. *Sustainability* **2022**, *14*, 5730. [CrossRef]

36. Proshansky, H.M. The City and Self-Identity. *Environ. Behav.* **2016**, *10*, 147–169. [CrossRef]
37. Ye, Y.; Zeng, W.; Shen, Q.; Zhang, X.; Lu, Y. The visual quality of streets: A human-centred continuous measurement based on machine learning algorithms and street view images. *Environ. Plan. B Urban Anal. City Sci.* **2019**, *46*, 1439–1457. [CrossRef]
38. Tang, J.; Long, Y. Measuring visual quality of street space and its temporal variation: Methodology and its application in the Hutong area in Beijing. *Landsc. Urban Plan.* **2019**, *191*, 103436. [CrossRef]
39. Johansson, M.; Sternudd, C.; Kärrholm, M. Perceived urban design qualities and affective experiences of walking. *J. Urban Des.* **2016**, *21*, 256–275. [CrossRef]
40. Cheng, L.; Chu, S.; Zong, W.; Li, S.; Wu, J.; Li, M. Use of Tencent Street View Imagery for Visual Perception of Streets. *ISPRS Int. J. Geo-Inf.* **2017**, *6*, 265. [CrossRef]
41. Ewing, R.; Cervero, R. Travel and the Built Environment: A Synthesis. *Transp. Res. Rec.* **2001**, *1780*, 87–114. [CrossRef]
42. Lee, J.; Miller, H.J. Measuring the impacts of new public transit services on space-time accessibility: An analysis of transit system redesign and new bus rapid transit in Columbus, Ohio, USA. *Appl. Geogr.* **2018**, *93*, 47–63. [CrossRef]
43. Ye, Y.; Richards, D.; Lu, Y.; Song, X.; Zhuang, Y.; Zeng, W.; Zhong, T. Measuring daily accessed street greenery: A human-scale approach for informing better urban planning practices. *Landsc. Urban Plan.* **2019**, *191*, 103434. [CrossRef]
44. Hillier, B. The Hidden Geometry of Deformed Grids: Or, Why Space Syntax Works, When it Looks as Though it Shouldn't. *Environ. Plan. B Plan. Des.* **1999**, *26*, 169–191. [CrossRef]
45. Hillier, B.; Hanson, J. *The Social Logic of Space*; Cambridge University Press: London, UK, 1984.
46. Zhang, T.; Lian, Z.; Xu, Y. Combining GPS and space syntax analysis to improve understanding of visitor temporal–spatial behaviour: A case study of the Lion Grove in China. *Landsc. Res.* **2020**, *45*, 534–546. [CrossRef]
47. Hacar, Ö.; Gülgen, F.; Bilgi, S. Evaluation of the Space Syntax Measures Affecting Pedestrian Density through Ordinal Logistic Regression Analysis. *ISPRS Int. J. Geo-Inf.* **2020**, *9*, 589. [CrossRef]
48. Bafna, S. Space Syntax. *Environ. Behav.* **2016**, *35*, 17–29. [CrossRef]
49. Li, Q.; Liu, X.; Lian, X.; Lin, S.; Li, J. Research on Park Green Space Accessibility of Nantai Island in Fuzhou City, China, Based on Space Syntax. *J. Guangxi Norm. Univ. Nat. Sci. Ed.* **2021**, *39*, 181–195. [CrossRef]
50. Tan, W.; Liu, L.; Chen, T.; Lv, L.; Pan, H. Accessibility of Comprehensive Parks of Fuzhou City Based on Spatial Syntax. *J. Chin. Urban For.* **2019**, *18*, 52–56.
51. Tao, W.; Lin, K.; Gu, H.; Liao, C.; Liu, S.; Ou, Q. Spatio-Temporal Evolution of Shawan Ancient Town in Guangzhou from the Perspective of Spatial Syntax. *Trop. Geogr.* **2020**, *40*, 970–980. [CrossRef]
52. Fu, Y.; Yang, F.; Bao, Z. Research on Accessibility of Hangzhou Comprehensive Parks Based on Spatial Syntax and LBS Big Data. *Landsc. Archit.* **2021**, *28*, 69–75. [CrossRef]
53. Gu, H.; Huang, D.; Shen, T.; Qin, X. Space Syntax Model Verification and Application in Urban Design with Multi-source Data. *Planners* **2019**, *35*, 67–73.
54. Wang, C.; Li, Y. Study on the Space Utilization Optimization of Urban Historic Districts Based on Space Syntax and POI Analysis: A Case of Shichahai District in Beijing. *Urban. Archit.* **2023**, *20*, 69–87. [CrossRef]
55. Jiang, B.; Claramunt, C.; Klarqvist, B. Integration of space syntax into GIS for modelling urban spaces. *Int. J. Appl. Earth Obs. Geoinf.* **2000**, *2*, 161–171. [CrossRef]
56. Jia, J.; Zhang, X.; Huang, C.; Luan, H. Multiscale analysis of human social sensing of urban appearance and its effects on house price appreciation in Wuhan, China. *Sustain. Cities Soc.* **2022**, *81*, 103844. [CrossRef]
57. Chang, H.-S.; Liao, C.-H. Exploring an integrated method for measuring the relative spatial equity in public facilities in the context of urban parks. *Cities* **2011**, *28*, 361–371. [CrossRef]
58. Tsou, K.-W.; Hung, Y.-T.; Chang, Y.-L. An accessibility-based integrated measure of relative spatial equity in urban public facilities. *Cities* **2005**, *22*, 424–435. [CrossRef]
59. Welch, T.F.; Mishra, S. A measure of equity for public transit connectivity. *J. Transp. Geogr.* **2013**, *33*, 29–41. [CrossRef]
60. Sahitya, K.S.; Prasad, C.S.R.K. Evaluation of opportunity based urban road network accessibility using GIS. *Spat. Inf. Res.* **2020**, *28*, 487–493. [CrossRef]
61. Witten, K.; Exeter, D.; Field, A. The Quality of Urban Environments: Mapping Variation in Access to Community Resources. *Urban Stud.* **2016**, *40*, 161–177. [CrossRef]
62. Sun, D.; Ji, X.; Lyu, M.; Fu, Y.; Gao, W. Evaluation and diagnosis for the pedestrian quality of service in urban riverfront streets. *J. Clean Prod.* **2024**, *452*, 142090. [CrossRef]
63. Cerbero, R.; Kockelman, A.K. Travel demand and the 3Ds Density, diversity, and design. *Transp. Res. Part D Transp. Environ.* **1997**, *2*, 199–219.
64. Hwang, J.; Joh, K.; Woo, A. Social inequalities in child pedestrian traffic injuries: Differences in neighborhood built environments near schools in Austin, TX, USA. *J. Transp. Health* **2017**, *6*, 40–49. [CrossRef]

65. Woo, A.; Yu, C.-Y.; Lee, S. Neighborhood walkability for subsidized households: Revisiting neighborhood environments of Housing Choice Voucher and Low-Income Housing Tax Credit households. *Cities* **2019**, *89*, 243–251. [CrossRef]
66. Dumbaugh, E.; Li, W.; Joh, K. The built environment and the incidence of pedestrian and cyclist crashes. *Urban Des. Int.* **2013**, *18*, 217–228. [CrossRef]
67. Smith, M.; Hosking, J.; Woodward, A.; Witten, K.; MacMillan, A.; Field, A.; Baas, P.; Mackie, H. Systematic literature review of built environment effects on physical activity and active transport—An update and new findings on health equity. *Int. J. Behav. Nutr. Phys. Act.* **2017**, *14*, 158. [CrossRef]
68. Besenyi, G.M.; Kaczynski, A.T.; Stanis, S.A.; Bergstrom, R.D.; Lightner, J.S.; Hipp, J.A. Planning for health: A community-based spatial analysis of park availability and chronic disease across the lifespan. *Health Place* **2014**, *27*, 102–105. [CrossRef] [PubMed]
69. Xiao, Y.; Li, Z.; Webster, C. Estimating the mediating effect of privately-supplied green space on the relationship between urban public green space and property value: Evidence from Shanghai, China. *Land Use Policy* **2016**, *54*, 439–447. [CrossRef]
70. Kong, F.; Sun, C.; Liu, F.; Yin, H.; Jiang, F.; Pu, Y.; Cavan, G.; Skelhorn, C.; Middel, A.; Dronova, I. Energy saving potential of fragmented green spaces due to their temperature regulating ecosystem services in the summer. *Appl. Energy* **2016**, *183*, 1428–1440. [CrossRef]
71. Yang, J.; Guan, Y.; Xia, J.C.; Jin, C.; Li, X. Spatiotemporal variation characteristics of green space ecosystem service value at urban fringes: A case study on Ganjingzi District in Dalian, China. *Sci. Total Environ.* **2018**, *639*, 1453–1461. [CrossRef] [PubMed]
72. Costanza, R.; Chichakly, K.; Dale, V.; Farber, S.; Finnigan, D.; Grigg, K.; Heckbert, S.; Kubiszewski, I.; Lee, H.; Liu, S.; et al. Simulation games that integrate research, entertainment, and learning around ecosystem services. *Ecosyst. Serv.* **2014**, *10*, 195–201. [CrossRef]
73. Knoke, T.; Paul, C.; Hildebrandt, P.; Calvas, B.; Castro, L.M.; Hartl, F.; Dollerer, M.; Hamer, U.; Windhorst, D.; Wiersma, Y.F.; et al. Compositional diversity of rehabilitated tropical lands supports multiple ecosystem services and buffers uncertainties. *Nat. Commun.* **2016**, *7*, 11877. [CrossRef]
74. Pelorosso, R.; Gobattoni, F.; Geri, F.; Leone, A. PANDORA 3.0 plugin: A new biodiversity ecosystem service assessment tool for urban green infrastructure connectivity planning. *Ecosyst. Serv.* **2017**, *26*, 476–482. [CrossRef]
75. Mouratidis, K.; Yiannakou, A. What makes cities livable? Determinants of neighborhood satisfaction and neighborhood happiness in different contexts. *Land Use Policy* **2022**, *112*, 105855. [CrossRef]
76. Wu, L.; Kim, S.K. Exploring the equality of accessing urban green spaces: A comparative study of 341 Chinese cities. *Ecol. Indic.* **2021**, *121*, 107080. [CrossRef]
77. Pan, Z.; Liu, Y.; Liu, Y.; Huo, Z.; Han, W. Age-friendly neighbourhood environment, functional abilities and life satisfaction: A longitudinal analysis of older adults in urban China. *Soc. Sci. Med.* **2024**, *340*, 116403. [CrossRef]
78. Biswas, B.; Sultana, Z.; Priovashini, C.; Ahsan, M.N.; Mallick, B. The emergence of residential satisfaction studies in social research: A bibliometric analysis. *Habitat Int.* **2021**, *109*, 102336. [CrossRef]
79. Lyu, M.; Meng, Y.; Gao, W.; Yu, Y.; Ji, X.; Li, Q.; Huang, G.; Sun, D. Measuring the perceptual features of coastal streets: A case study in Qingdao, China. *Environ. Res. Commun.* **2022**, *4*, 115002. [CrossRef]
80. Ma, X.Y.; Ma, C.Y.; Wu, C.; Xi, Y.L.; Yang, R.F.; Peng, N.Y.Z.; Zhang, C.; Ren, F. Measuring human perceptions of streetscapes to better inform urban renewal: A perspective of scene semantic parsing. *Cities* **2021**, *110*, 26. [CrossRef]
81. Qiu, W.S.; Zhang, Z.Y.; Liu, X.; Li, W.J.; Li, X.J.; Xu, X.; Huang, X.K. Subjective or objective measures of street environment, which are more effective in explaining housing prices? *Landsc. Urban Plan.* **2022**, *221*, 24. [CrossRef]
82. Lee, S.; Ye, X.; Nam, J.W.; Zhang, K. The association between tree canopy cover over streets and elderly pedestrian falls: A health disparity study in urban areas. *Soc. Sci. Med.* **2022**, *306*, 115169. [CrossRef] [PubMed]
83. Hughey, S.M.; Walsemann, K.M.; Child, S.; Powers, A.; Reed, J.A.; Kaczynski, A.T. Using an environmental justice approach to examine the relationships between park availability and quality indicators, neighborhood disadvantage, and racial/ethnic composition. *Landsc. Urban Plan.* **2016**, *148*, 159–169. [CrossRef]
84. Shin, H.-S.; Woo, A. Analyzing the effects of walkable environments on nearby commercial property values based on deep learning approaches. *Cities* **2024**, *144*, 104628. [CrossRef]
85. Park, K.; Ewing, R.; Sabouri, S.; Larsen, J. Street life and the built environment in an auto-oriented US region. *Cities* **2019**, *88*, 243–251. [CrossRef]
86. Wang, R.; Lu, Y.; Zhang, J.; Liu, P.; Yao, Y.; Liu, Y. The relationship between visual enclosure for neighbourhood street walkability and elders' mental health in China: Using street view images. *J. Transp. Health* **2019**, *13*, 90–102. [CrossRef]
87. Ewing, R.; Handy, S. Measuring the Unmeasurable: Urban Design Qualities Related to Walkability. *J. Urban Des.* **2009**, *14*, 65–84. [CrossRef]

88. Dai, L.; Zheng, C.; Dong, Z.; Yao, Y.; Wang, R.; Zhang, X.; Ren, S.; Zhang, J.; Song, X.; Guan, Q. Analyzing the correlation between visual space and residents' psychology in Wuhan, China using street-view images and deep-learning technique. *City Environ. Interact.* **2021**, *11*, 100069. [CrossRef]
89. Mouratidis, K. Urban planning and quality of life: A review of pathways linking the built environment to subjective well-being. *Cities* **2021**, *115*, 12. [CrossRef]
90. Zang, P.; Lu, Y.; Ma, J.; Xie, B.; Wang, R.; Liu, Y. Disentangling residential self-selection from impacts of built environment characteristics on travel behaviors for older adults. *Soc. Sci. Med.* **2019**, *238*, 112515. [CrossRef]
91. Wei, Z.; Cao, K.; Kwan, M.-P.; Jiang, Y.; Feng, Q. Measuring the age-friendliness of streets' walking environment using multi-source big data: A case study in Shanghai, China. *Cities* **2024**, *148*, 104829. [CrossRef]
92. Zhou, X.; Chen, S.; Chen, L.; Li, L. Social Class Identity, Public Service Satisfaction, and Happiness of Residents: The Mediating Role of Social Trust. *Front. Psychol.* **2021**, *12*, 659657. [CrossRef]
93. Quercia, D.; Schifanella, R.; Aiello, L.M. The shortest path to happiness. In Proceedings of the 25th ACM conference on Hypertext and Social Media, Santiago, Chile, 1–4 September 2014; pp. 116–125.
94. Meng, Y.; Li, Q.; Ji, X.; Yu, Y.; Yue, D.; Gan, M.; Wang, S.; Niu, J.; Fukuda, H. Research on Campus Space Features and Visual Quality Based on Street View Images: A Case Study on the Chongshan Campus of Liaoning University. *Buildings* **2023**, *13*, 1332. [CrossRef]
95. Wu, Y.; Liu, Q.; Hang, T.; Yang, Y.; Wang, Y.; Cao, L. Integrating restorative perception into urban street planning: A framework using street view images, deep learning, and space syntax. *Cities* **2024**, *147*, 104791. [CrossRef]
96. McLeod, S. Maslow's hierarchy of needs. *Simply Psychol.* **2007**, *1*, 1–18.
97. Meng, Y.; Sun, D.; Lyu, M.; Niu, J.; Fukuda, H. Measuring human perception of residential built environment through street view image and deep learning. *Environ. Res. Commun.* **2024**, *6*, 055020. [CrossRef]
98. Zhang, F.; Zhou, B.; Liu, L.; Liu, Y.; Fung, H.H.; Lin, H.; Ratti, C. Measuring human perceptions of a large-scale urban region using machine learning. *Landsc. Urban Plan.* **2018**, *180*, 148–160. [CrossRef]
99. Wang, Z.; Zhu, Z.; Xu, M.; Qureshi, S. Fine-grained assessment of greenspace satisfaction at regional scale using content analysis of social media and machine learning. *Sci. Total Environ.* **2021**, *776*, 145908. [CrossRef] [PubMed]
100. Susaki, J.; Kubota, S. Automatic Assessment of Green Space Ratio in Urban Areas from Mobile Scanning Data. *Remote Sens.* **2017**, *9*, 215. [CrossRef]
101. Sun, D.; Li, Q.; Gao, W.; Huang, G.; Tang, N.; Lyu, M.; Yu, Y. On the relation between visual quality and landscape characteristics: A case study application to the waterfront linear parks in Shenyang, China. *Environ. Res. Commun.* **2021**, *3*, 115013. [CrossRef]
102. Xu, L.Q.; Kang, Q. The relationship between pedestrian behaviors and the spatial features along the ground-floor commercial street: The case of West Nanjing road in Shanghai. *Urban Plan. Forum* **2014**, *3*, 103–111.
103. He, J.; Zhang, J.; Yao, Y.; Li, X. Extracting human perceptions from street view images for better assessing urban renewal potential. *Cities* **2023**, *134*, 104189. [CrossRef]
104. Li, J.; Ahn, H.-J. Sensitivity of Chinese stock markets to individual investor sentiment: An analysis of Sina Weibo mood related to COVID-19. *J. Behav. Exp. Financ.* **2024**, *41*, 100860. [CrossRef]
105. Wangbao, L. Spatial impact of the built environment on street vitality: A case study of the Tianhe District, Guangzhou. *Front. Environ. Sci.* **2022**, *10*, 966562. [CrossRef]
106. Pan, C.; Wu, S.; Li, E.; Li, H.; Liu, X. Identification of urban functional zones in Macau Peninsula based on POI data and remote information sensors technology for sustainable development. *Phys. Chem. Earth Parts A/B/C* **2023**, *131*, 103447. [CrossRef]
107. Liu, L.; Silva, E.A.; Wu, C.; Wang, H. A machine learning-based method for the large-scale evaluation of the qualities of the urban environment. *Comput. Environ. Urban Syst.* **2017**, *65*, 113–125. [CrossRef]
108. Carmona, M.; Gabrieli, T.; Hickman, R.; Laopoulou, T.; Livingstone, N. Street appeal: The value of street improvements. *Prog. Plan.* **2018**, *126*, 1–51. [CrossRef]
109. Nagata, S.; Nakaya, T.; Hanibuchi, T.; Amagasa, S.; Kikuchi, H.; Inoue, S. Objective scoring of streetscape walkability related to leisure walking: Statistical modeling approach with semantic segmentation of Google Street View images. *Health Place* **2020**, *66*, 102428. [CrossRef] [PubMed]
110. Hu, Y.; Han, Y. Identification of Urban Functional Areas Based on POI Data: A Case Study of the Guangzhou Economic and Technological Development Zone. *Sustainability* **2019**, *11*, 1385. [CrossRef]
111. Jin, X.; Long, Y.; Sun, W.; Lu, Y.; Yang, X.; Tang, J. Evaluating cities' vitality and identifying ghost cities in China with emerging geographical data. *Cities* **2017**, *63*, 98–109. [CrossRef]
112. He, S.; Zhang, Z.; Yu, S.; Xia, C.; Tung, C.-L. Investigating the effects of urban morphology on vitality of community life circles using machine learning and geospatial approaches. *Appl. Geogr.* **2024**, *167*, 103287. [CrossRef]

113. Pouyanfar, S.; Sadiq, S.; Yan, Y.; Tian, H.; Tao, Y.; Reyes, M.P.; Shyu, M.-L.; Chen, S.-C.; Iyengar, S.S. A Survey on Deep Learning. *ACM Comput. Surv.* **2018**, *51*, 1–36. [CrossRef]
114. Huang, G.; Yu, Y.; Lyu, M.; Sun, D.; Zeng, Q.; Bart, D. Using google street view panoramas to investigate the influence of urban coastal street environment on visual walkability. *Environ. Res. Commun.* **2023**, *5*, 065017. [CrossRef]
115. Zeng, Q.; Bao, X.; Dewancker, B.J. Association between built environment on transport and recreational walking in Japan: The case of Kitakyushu. *City Built Environ.* **2023**, *1*, 10. [CrossRef]
116. Lu, Y.; Sarkar, C.; Xiao, Y. The effect of street-level greenery on walking behavior: Evidence from Hong Kong. *Soc. Sci. Med.* **2018**, *208*, 41–49. [CrossRef]
117. Middel, A.; Lukasczyk, J.; Zakrzewski, S.; Arnold, M.; Maciejewski, R. Urban form and composition of street canyons: A human-centric big data and deep learning approach. *Landsc. Urban Plan.* **2019**, *183*, 122–132. [CrossRef]
118. Chen, Y.; Liu, X.; Li, X.; Liu, X.; Yao, Y.; Hu, G.; Xu, X.; Pei, F. Delineating urban functional areas with building-level social media data: A dynamic time warping (DTW) distance based k -medoids method. *Landsc. Urban Plan.* **2017**, *160*, 48–60. [CrossRef]
119. Liu, X.; Niu, N.; Liu, X.; Jin, H.; Ou, J.; Jiao, L.; Liu, Y. Characterizing mixed-use buildings based on multi-source big data. *Int. J. Geogr. Inf. Sci.* **2018**, *32*, 738–756. [CrossRef]
120. Hillier, B. Spatial sustainability in cities: Organic patterns and sustainable forms. In Proceedings of the 7th International Space Syntax Symposium, Stockholm, Sweden, 8–11 June 2009; Royal Institute of Technology: Stockholm, Sweden, 2009.
121. Lyu, Y.; Abd Malek, M.I.; Jaàfar, N.H.; Sima, Y.; Han, Z.; Liu, Z. Unveiling the potential of space syntax approach for revitalizing historic urban areas: A case study of Yushan Historic District, China. *Front. Archit. Res.* **2023**, *12*, 1144–1156. [CrossRef]
122. Chan, E.T.H.; Schwanen, T.; Banister, D. The role of perceived environment, neighbourhood characteristics, and attitudes in walking behaviour: Evidence from a rapidly developing city in China. *Transportation* **2019**, *48*, 431–454. [CrossRef]
123. Lyu, Y.; Forsyth, A. Attitudes, perceptions, and walking behavior in a Chinese city. *J. Transp. Health* **2021**, *21*, 101047. [CrossRef]
124. Sun, D.; Ji, X.; Gao, W.; Zhou, F.; Yu, Y.; Meng, Y.; Yang, M.; Lin, J.; Lyu, M. The Relation between Green Visual Index and Visual Comfort in Qingdao Coastal Streets. *Buildings* **2023**, *13*, 457. [CrossRef]
125. Rui, J. Exploring the association between the settlement environment and residents' positive sentiments in urban villages and formal settlements in Shenzhen. *Sustain. Cities Soc.* **2023**, *98*, 104851. [CrossRef]
126. Leibe, B.; Matas, J.; Sebe, N.; Welling, M. Computer Vision–ECCV 2016. In Proceedings of the 14th European Conference, Amsterdam, The Netherlands, 11–14 October 2016.
127. Zhang, F.; Zu, J.; Hu, M.; Zhu, D.; Kang, Y.; Gao, S.; Zhang, Y.; Huang, Z. Uncovering inconspicuous places using social media check-ins and street view images. *Comput. Environ. Urban Syst.* **2020**, *81*, 101478. [CrossRef]
128. Larkin, A.; Gu, X.; Chen, L.; Hystad, P. Predicting Perceptions of the Built Environment using GIS, Satellite and Street View Image Approaches. *Landsc. Urban Plan* **2021**, *216*, 104257. [CrossRef] [PubMed]
129. Wang, M.; Liu, J.; Zhang, S.; Zhu, H.; Zhang, X. Spatial pattern and micro-location rules of tourism businesses in historic towns: A case study of Pingyao, China. *J. Destin. Mark. Manag.* **2022**, *25*, 100721. [CrossRef]
130. Jiang, S.; Alves, A.; Rodrigues, F.; Ferreira, J.; Pereira, F.C. Mining point-of-interest data from social networks for urban land use classification and disaggregation. *Comput. Environ. Urban Syst.* **2015**, *53*, 36–46. [CrossRef]
131. Saleh, A.Y.; Abdu, S.A.; Ali, H.N. Evaluating the connectivity level of Fayoum city roads network: A new method using GIS. *Pr. Kom. Geogr. Komun. PTG* **2018**, *21*, 44–56. [CrossRef]
132. Liu, L.; Zhu, J.; Wu, J.; Sun, F. Application on Expert Scoring Method in L/HIRF Evaluation Factors. *Aviat. Maint. Eng.* **2017**, *7*, 41–43. [CrossRef]
133. Wang, G.; Zhang, B.; Tang, C.; Yan, G. Application of Delphi Experts Grading Method Based on The Computer Simulation in Visual Parameter Analysis of Bridge Landscape. *J. Hunan Inst. Sci. Technol. Nat. Sci.* **2014**, *27*, 76–81.
134. Hajrasouliha, A.; Yin, L. The impact of street network connectivity on pedestrian volume. *Urban Stud.* **2014**, *52*, 2483–2497. [CrossRef]
135. Sugiyama, T.; Leslie, E.; Giles-Corti, B.; Owen, N. Associations of neighbourhood greenness with physical and mental health: Do walking, social coherence and local social interaction explain the relationships? *J. Epidemiol. Community Health* **2008**, *62*, e9. [CrossRef]
136. Frank, L.D.; Schmid, T.L.; Sallis, J.F.; Chapman, J.; Saelens, B.E. Linking objectively measured physical activity with objectively measured urban form: Findings from SMARTRAQ. *Am. J. Prev. Med.* **2005**, *28*, 117–125. [CrossRef]
137. Saelens, B.E.; Sallis, J.F.; Frank, L.D. Environmental correlates of walking and cycling: Findings from the transportation, urban design, and planning literatures. *Ann. Behav. Med.* **2003**, *25*, 80–91. [PubMed]
138. Dang, Y.; Yu, J.; Zhang, W.; Li, Y.; Chen, L.; Zhan, D. Satisfaction evaluation of living environment and influencing factors in the Bohai Rim area. *Prog. Geogr.* **2016**, *35*, 184–194.

139. Guang, R.; Xi, J.; Cheng, Y. Social support measurement and influencing factors for community-living elderly in Beijing. *J. Beijing Norm. Univ. Nat. Sci.* **2020**, *56*, 102–109. [CrossRef]
140. Yang, D.; Wang, X.; Han, R. Nonlinear and Synergistic Effects of the Built environment on Street Vitality: The Case of Shenyang. *Urban Plan. Forum* **2023**, *5*, 93–102. [CrossRef]
141. Melis, G.; Gelormino, E.; Marra, G.; Ferracin, E.; Costa, G. The Effects of the Urban Built Environment on Mental Health: A Cohort Study in a Large Northern Italian City. *Int. J. Environ. Res. Public Health* **2015**, *12*, 14898–14915. [CrossRef]
142. Tuli, S. Beyond Mobility: Planning Cities for People and Places. *Urban Policy Res.* **2019**, *37*, 271–273. [CrossRef]
143. Mouratidis, K. Built environment and social well-being: How does urban form affect social life and personal relationships? *Cities* **2018**, *74*, 7–20. [CrossRef]
144. Pan, H.; Luo, W. The Role of Public Spaces in Promoting Social Interaction: A Case Study of Urban Parks in Beijing. *J. Urban Des.* **2022**, *27*, 309–325.
145. Pucher, J.; Dijkstra, L. Promoting Safe Walking and Cycling to Improve Public Health: Lessons From The Netherlands and Germany. *J. Public Health-Heidelb.* **2010**, *100*, 1986–1987. [CrossRef] [PubMed]
146. Zhang, Y.; Zou, Y.; Zhu, Z.; Guo, X.; Feng, X. Evaluating Pedestrian Environment Using DeepLab Models Based on Street Walkability in Small and Medium-Sized Cities: Case Study in Gaoping, China. *Sustainability* **2022**, *14*, 15472. [CrossRef]
147. Carr, S.; Francis, M.; Rivlin, L.G.; Stone, A.M. *Public Space*; Cambridge University Press: Cambridge, UK, 2010.
148. Dempsey, N.; Brown, C.; Bramley, G. The key to sustainable urban development in UK cities? The influence of density on social sustainability. *Prog. Plan.* **2012**, *77*, 89–141. [CrossRef]
149. Lavy, S.; Garcia, J.A.; Dixit, M.K. Establishment of KPIs for facility performance measurement: Review of literature. *Facilities* **2010**, *28*, 440–464. [CrossRef]
150. Cheshmehzangi, A.; Butters, C.; Xie, L.; Dawodu, A. Green infrastructures for urban sustainability: Issues, implications, and solutions for underdeveloped areas. *Urban For. Urban Green.* **2021**, *59*, 127028. [CrossRef]
151. Wu, W.; Guo, J.; Ma, Z.; Zhao, K. Data-Driven Approach to Assess Street Safe: Large-Scale Analysis of the Microscopic Design. *ISPRS Int. J. Geo-Inf.* **2022**, *11*, 537. [CrossRef]
152. Wu, H.; Zhang, Z.; Chen, Y.; Jiao, J. The impact of street characteristics on older pedestrians' perceived safe in Shanghai, China. *J. Transp. Land Use* **2020**, *13*, 469–490. [CrossRef]
153. Wang, L.; Han, X.; He, J.; Jung, T. Measuring residents' perceptions of city streets to inform better street planning through deep learning and space syntax. *ISPRS J. Photogramm. Remote Sens.* **2022**, *190*, 215–230. [CrossRef]

Disclaimer/Publisher's Note: The statements, opinions and data contained in all publications are solely those of the individual author(s) and contributor(s) and not of MDPI and/or the editor(s). MDPI and/or the editor(s) disclaim responsibility for any injury to people or property resulting from any ideas, methods, instructions or products referred to in the content.

buildings

MDPI

Article

Impact of Physical Features on Visual Walkability Perception in Urban Commercial Streets by Using Street-View Images and Deep Learning

Gonghu Huang [1,*], Yiqing Yu [1,*], Mei Lyu [2], Dong Sun [3], Bart Dewancker [1] and Weijun Gao [1]

[1] Faculty of Environmental Engineering, The University of Kitakyushu, Kitakyushu 808-0135, Japan; bart@kitakyu-u.ac.jp (B.D.); gaoweijun@me.com (W.G.)
[2] School of Art and Design, Shenyang Jianzhu University, Shenyang 110168, China; lynmei@sjzu.edu.cn
[3] School of Architecture and Urban Planning, Shenyang Jianzhu University, Shenyang 110168, China; sundong@sjzu.edu.cn
* Correspondence: d2dbb404@eng.kitakyu-u.ac.jp (G.H.); e3dbb402@eng.kitakyu-u.ac.jp (Y.Y.); Tel.: +81-070-1180-9523 (G.H.)

Abstract: Urban commercial streets are a crucial component of urban life, serving as the central hubs of commercial activity and providing vital spaces for both residents and visitors to engage in various activities. Walkability is commonly used as a key indicator of environmental quality, playing a significant role in improving residents' health, community interaction, and environmental quality of life. Therefore, promoting the development of a high-quality walking environment in commercial districts is crucial for fostering urban economic growth and the creation of livable cities. However, existing studies predominantly focus on the impact of the built environment on walkability at the urban scale, with limited attention given to commercial streets, particularly the influence of their physical features on walking-need perceptions. In this study, we utilized Google Street-View Panorama (GSVP) images of the Tenjin commercial district and applied the Semantic Differential (SD) method to assess four walking-need perceptions of visual walkability perception, including usefulness, comfort, safety, and attractiveness. Additionally, deep-learning-based semantic segmentation was employed to extract and calculate the physical features of the Tenjin commercial district. Correlation and regression analysis were used to investigate the impact of these physical features on the four walking-need perceptions. The results showed that the different walking-need perceptions in the Tenjin commercial district are attractiveness > safety > comfort > usefulness. Furthermore, the results show that there are significant spatial distribution differences in walking-need perceptions in the Tenjin commercial district. Safety perception is more prominent on primary roads, all four walking-need perceptions in the secondary roads at a high level, and the tertiary roads have generally lower scores for all walking-need perceptions. The regression analysis indicates that walkable space and the landmark visibility index have a significant impact on usefulness, street cleanliness emerges as the most influential factor affecting safety, greenness is identified as the primary determinant of comfort, while the landmark visibility index exerts the greatest influence on attractiveness. This study expands the existing perspectives on urban street walkability by focusing on street-level analysis and proposes strategies to enhance the visual walkability perception of commercial streets. These findings aim to better meet pedestrian needs and provide valuable insights for future urban planning efforts.

Keywords: commercial streets; physical features; visual walkability perception; street-view images; deep learning

1. Introduction

Commercial districts are one of the most frequently utilized spaces for social interactions and public life among urban residents [1]. These areas play a key role in economic activity by creating job opportunities through the concentration of commercial facilities [2]. In addition to fulfilling daily shopping, leisure, and consumption needs, commercial streets provide urban residents with ideal spaces for relaxation and entertainment activities [3]. Furthermore, commercial streets play a vital role in fostering local community vitality by encouraging face-to-face interactions among customers and pedestrians [4]. High-quality urban street environments also contribute significantly to enhancing residents' well-being [5], life satisfaction [6], and community cohesion [7]. Thus, building a high-quality urban commercial street environment is not only the key to urban image building and economic development but also an important way to improve residents' quality of life and achieve sustainable development.

The concept of walkability was first introduced in the late 1990s in transportation studies in the United States. Walkability covers all aspects of the built environment related to pedestrian transportation [8]. Better service facilities, higher landscape environment quality, diversified land use, and convenient travel paths all improve street walkability [9]. Many studies have shown that walkable street environments benefit both public health and environmental sustainability [10]. An environment with high walkability can reduce the sedentary behaviors of residents, increase physical activity levels, and improve health status. Relevant studies point out that walkable communities help reduce motor vehicle speeds, traffic volumes, and unsafe behaviors [11,12]. Violent crime and burglary are generally less likely to occur in neighborhoods with good walking conditions [13]. Additionally, walkable streets can promote economic prosperity in communities and society [14]. As hubs of economic activity, commercial districts attract people who may consume or need services. Therefore, a walkable environment in commercial areas may increase visitor numbers and spending [15]. It has important implications for enhancing the attractiveness of neighborhoods, extending customer dwell times and consumption willingness, and promoting the development of the urban economy. Studies confirm that greater satisfaction with pedestrian environments correlates with longer stays in commercial areas, which increases the likelihood of purchasing decisions [16]. Furthermore, features of a walkable environment have a positive impact on the per-capita sales of individual businesses [17]. Given this background, planners and scholars increasingly emphasize that the quality of pedestrian environments in commercial areas significantly affects their stability and sustainability. While walkability offers numerous benefits, it is also important to consider potential challenges for residents arising from increased street or neighborhood attractiveness. For instance, the higher walkability of commercial districts may lead to an increase in the likelihood of conflicts between pedestrians and vehicles, therefore raising the risk of pedestrian collisions [18]. Over-commercialization may also diminish the cultural identity and sense of belonging of locals [19]. Furthermore, as more visitors are drawn to these neighborhoods, the competition for shared public resources, such as parking spaces, parks, and public transit, may intensify, impacting residents' access to these amenities. Acknowledging and addressing these potential drawbacks is essential for planners and policymakers to ensure that the benefits of walkable environments are equitably distributed while minimizing unintended consequences for local communities.

In early studies, Gehl [18] described the quality of outdoor spaces needed for walking. Based on this study, related scholars have assessed walkability by designing vocabularies related to walkability and constructing evaluation systems [20,21], such as the Pedestrian Environment Review System, the Neighborhood Environment Walkability Scale, and Pedestrian Level of Service [22] methodology. Rosenberg et al. [23] used NEWS-Y to study the relationship between U.S. neighborhood environments and adolescents' perceptions of walkability, finding that traffic safety, aesthetics, pedestrian or bike facilities, land-use mix, and the overall environment were positively associated with perceived walkability. In China, Cerin et al. [24,25] used NEWS and NEWS-A to study the impact of the built environment on perceived walkability among older adults in Hong Kong, identifying service accessibility and pedestrian and vehicular traffic as significantly related factors. However, these methods rely heavily on individual perceptual variables, resulting in one-sided assessments of the walking environment. Due to the high cost of this evaluation method, researchers can only conduct case studies on limited neighborhood areas. In recent years, related studies have utilized computer-assisted audits based on urban big data, such as Geographic Information System (GIS), to measure macro-level walkability in the city, country, or state. Researchers attempt to combine these objective attributes into a single walkability index to evaluate the degree to which a built environment supports walking. These macro-level attributes include intersection density, population density, and land-use diversity [26–28]. Walk Score, as a commonly used tool, is applied to analyze street walkability in various countries and regions [29]. These computer-assisted audits, which are based on urban big data, overcome the limitations of small sample sizes in manual assessments, providing opportunities for large-scale walkability evaluation. However, walkability as a complex concept is influenced by both objective environmental factors and subjective perceptions [30]. The physical features of a street can influence people's perception of the environment, therefore affecting their actual walking behavior and willingness to walk. The walkability index that relies heavily on macro-environmental features often overlooks the impact of street-level characteristics on walkability perception. Relevant scholars have suggested that walkability can be broadly perceived through four aspects: usefulness, safety, comfort, and attractiveness [31,32]. Usefulness reflects the motivating factors for walking, which may be influenced by factors such as destination accessibility and land-use diversity [33]. In addition, perceived walking barriers, such as physical obstacles, impassable land uses (gated communities), psychological barriers (overly wide roads), and environmental colors can affect pedestrians' perception of usefulness. Lynch et al. pointed out that color plays an important role in the recognition of spatial elements such as paths, landmarks, and edges in The Image of the City [34]. Safety refers to whether the street environment appears free from crime and traffic accidents, which is often associated with visual elements such as graffiti, litter, and abandoned buildings. A study shows that obstructed sightlines can increase fear of crime [35]. Wu et al. measured pedestrian safety perceptions using walkability, spatial enclosure, visual permeability, and vitality [36]. Traffic factors, such as motor vehicles and bicycles on the streets, also affect pedestrians' sense of safety in the street environment [37]. Comfort refers to whether the street environment enhances pedestrians' walking experience, which is closely related to factors such as street furniture, sidewalk conditions, urban design amenities, and accessibility features. Some scholars have explored the relationship between comfort and built environment factors such as street greening [38,39], street openness [40], and street facilities [41]. Attractiveness refers to the sensory and psychological enjoyment that pedestrians experience while walking in a particular environment [32]. with the aesthetic appeal, interest, and activity level of the street environment influencing pedestrians' perception of attractiveness. Some factors

that may contribute to an attractive environment include street greening, historical or unique architecture, pedestrian traffic, and mixed land use. Moreover, due to differences in regional economic development and social-cultural backgrounds, pedestrians' perceptions of walking needs vary significantly across different areas [42,43]. A study comparing the perceptions of walking needs between pedestrians in Bangkok and Nagoya found that safety was regarded as a higher priority in Bangkok. This could be attributed to the poorer street conditions in Bangkok, where narrow sidewalks and lower cleanliness levels create greater concerns [44].

With the development of computer technology and crowdsourced mapping services, fully accessible Street-View Image (SVI) data provides high-resolution, real-world, and street-level image data for studying urban street built environments [45]. Compared to on-site surveys, SVI offers a cost-effective and time-saving method for large-scale assessment [46]. Consequently, SVI is widely applied in community environment evaluations [47–50] and has become a primary data source in urban studies, providing an opportunity to evaluate the built environment at a micro level on a large scale, for example, identifying the structural components of the landscape [51], evaluating sky openness [52], and measuring street greenery and physical activity levels [53]. Some scholars have utilized SVI data to explore the impact of streetscape elements on public perception [54,55]. Visuals are the primary way for people to perceive their surroundings. Zhou et al. introduced the concept of visual walkability based on street-view images and proposed the visual walkability index as a quantitative measure for evaluating visual walkability [56]. Li et al., based on the hierarchy of walking needs, introduced the concept of visual walkability perception to represent whether the built environment visually encourages walking. They explored the influence of visual elements on walking-need perceptions by using street-view images, virtual reality, and deep-learning techniques [34,57].

In summary, the foundation for constructing high-quality urban commercial streets is the use of an effective approach to measuring visual walkability perception and the physical features of these streets. In addition, exploring the impact of commercial street physical features on visual walkability perception based on the public's walking needs has great significance in both theoretical and practical terms. As shown in Figure 1, this study applies semantic segmentation and Semantic Differential (SD) methods based on Google Street-View Panorama (GSVP) images to measure the built environment features and human visual walkability perception on commercial streets, revealing how physical features impact public visual walkability perception. Specifically, we collected street images from the Tenjin commercial district in Fukuoka, Japan, using web crawlers. Four walking needs of visual walkability perception—usefulness, safety, comfort, and attractiveness—were measured using the SD method. Meanwhile, using semantic segmentation technology based on deep learning, we identified the proportions of landscape elements in the images, calculating 12 physical features representative of the commercial street environment. Finally, correlation and regression analysis were applied to investigate the influence of the street's physical features on public visual walkability perception. The key questions of this study are as follows: (1) applying an efficient, accurate method to measure visual walkability perception and physical features of commercial streets; (2) analyzing the spatial distribution differences of visual walkability perception in the Tenjin commercial district; (3) exploring the impact mechanisms of physical features on public visual walkability perception, thus providing suggestions for planners to create walkable commercial street environments.

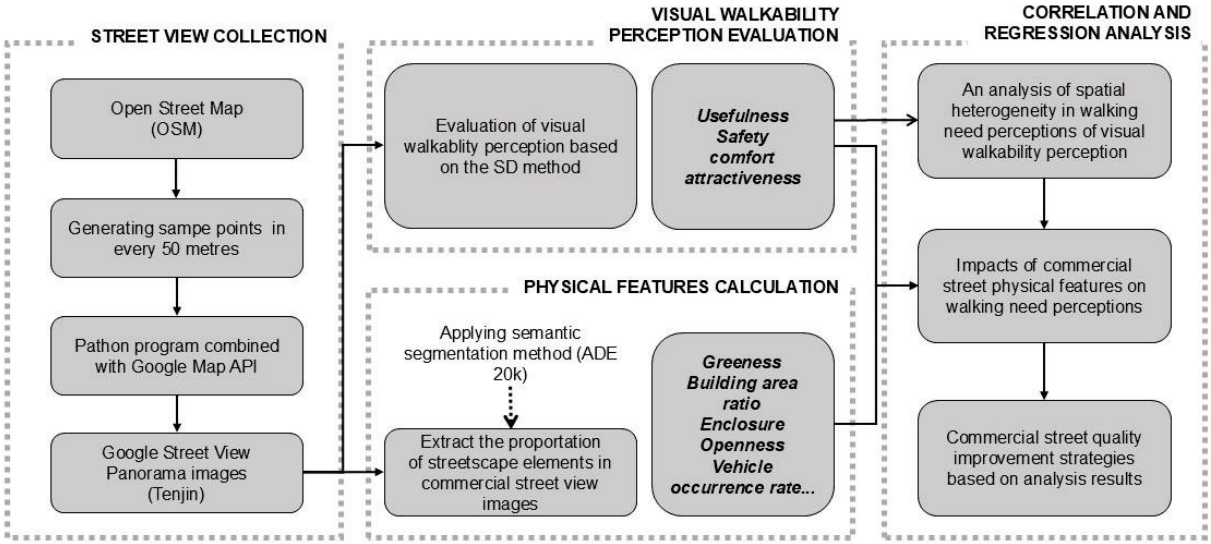


Figure 1. Research framework.

2. Materials and Methods

2.1. Study Area

The research area for this study is the Tenjin area, located in Chuo-ku, Fukuoka City, Japan (Figure 2). The Tenjin area is also a primary commercial center, which is Kyushu. The research area spans approximately 1.8 square kilometers, with average weekday foot traffic ranging from 500,000 to 600,000 people. The Tenjin area is not only the economic center of Fukuoka City but also a significant shopping and entertainment hub in western Japan, attracting a high volume of tourists and residents. The total length of the study streets is approximately 16.2 km, and its road system consists of primary, secondary, and tertiary roads that support pedestrian walking and vehicular traffic, as well as commercial activities. In addition, the Tenjin area contains a number of large department stores, recreational parks, and tourist attractions. The streetscape is varied and rich. As an important commercial area in Kyushu, Japan, the Tenjin area plays an important role in promoting the city's commercial development and showcasing the city's image.

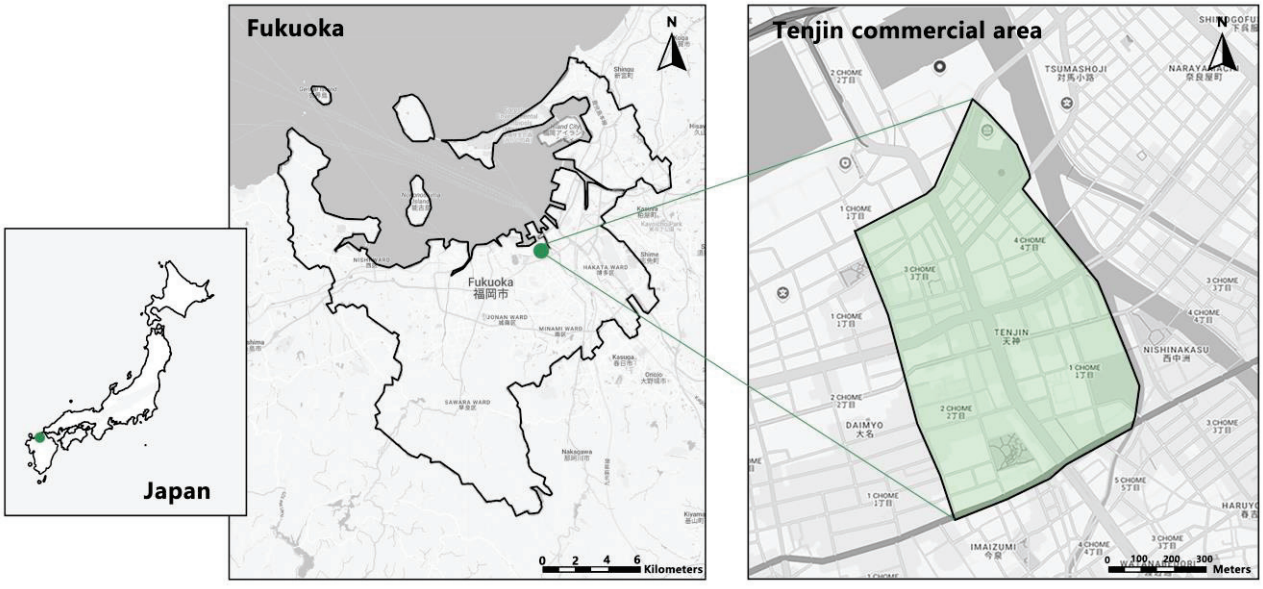


Figure 2. Location of the study area.

2.2. Street-View Image Collection

Street-view images have a wide range of applications in urban research due to their ability to capture real-world scenes in urban environments and provide rich visual data [58,59]. In this study, we obtained the road network data of the Tenjin area in Fukuoka City using Open Street Map (OSM). The study used Arc GIS10.2 to set Google Street-View Panoramic (GSVP) sample collection points every 50 m along the road network and obtained the latitude and longitude information of each sample collection point. A total of 481 sample collection points were generated in the Tenjin area, including 97 on primary roads, 136 on secondary roads, and 248 on tertiary roads. The study collected GSVP images of each sample point by web crawlers that were integrated with the Google Street-View Map Application Programming Interface (Figure 3). The pixels of the GSVP image were set to 2048 × 624, and the pitch angle of the image was set to 0° to achieve a more realistic pedestrian view. To minimize the impact of seasonal variations on greenery in streetscapes, we examined the capture dates of the images to ensure that all streetscape images were taken in April 2023. Additionally, indoor scenes were excluded to maintain consistency. In total, 475 GSVP images were collected for this study.

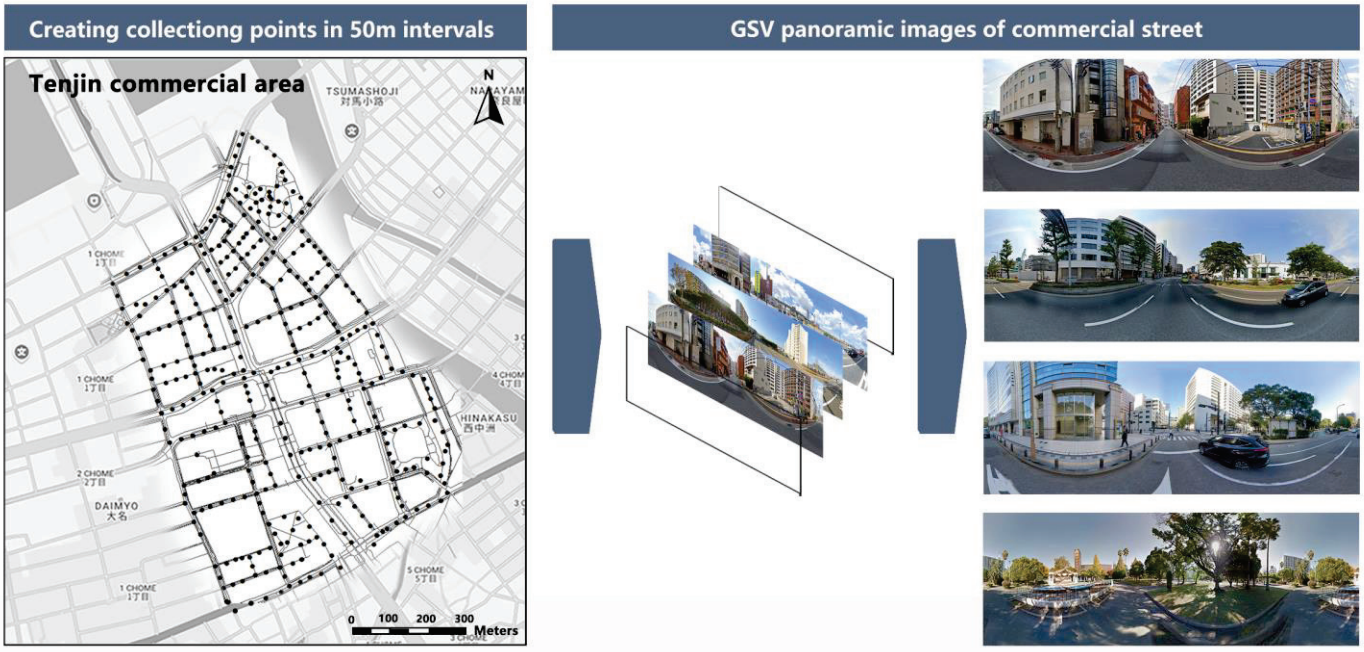


Figure 3. Google Street-View Panorama images collection.

2.3. Visual Walkability Perception Evaluation

In previous studies, Virtual Reality (VR) technology has been used to provide immersive environments, allowing participants to experience motion and other dynamic effects, offering significant advantages in simulating real-world scenarios and improving the accuracy of perceptual assessments [60]. However, VR-based evaluations are characterized by a high level of detail and resource intensity, which often limits the sample size and scalability of such studies. Therefore, in this study, we used the Semantic Difference (SD) method to evaluate the visual walkability perception of GSVPs in the Tenjin commercial district, which includes the four walking-need perceptions (usefulness, safety, comfort, and attractiveness). The Semantic Difference (SD) method was introduced by Charles E. Osgood in 1957 [61] and has been widely used in environmental assessment studies due to its applicability [62,63]. The selection of adjective pairs is particularly important in the

evaluation process of the SD method. According to previous studies [32,64], we selected four walking-need perceptions of usefulness, safety, comfort, and attractiveness as the evaluation indexes (Table 1). The evaluation process of the SD method usually involves 20 to 50 observers. Many studies have shown that students' and the public's perceptions of the environment are highly correlated [65], so students are often used as observers in street environment evaluation [66,67]. In this study, we recruited 35 students (14 graduate students and 21 undergraduate students) as observers to evaluate four walking-need perceptions in 475 samples. Considering the large number of samples to be evaluated in this study (n = 475), the 475 samples were divided into 3 groups and organized into 3 slide presentations (the first slide included 159 images, while the second and third slides each contained 158 images). These slides were projected in a multimedia classroom using an ultra-high-resolution projector to ensure a clear and consistent visual presentation. Before the slide presentations, we provided all observers with an explanation of the definitions for the four walking-need perceptions. Additionally, they were given an overview of all the samples to develop a general understanding of the scoring criteria. During the evaluation process, each street-view image was displayed for 40 s. Observers were instructed to observe the images statically (no interaction was allowed) and evaluate the four walking-need perceptions for each street-view image. To prevent visual fatigue from prolonged observation, a 30-minute break was provided between each group of slides during the evaluation process. The evaluations were based on a five-point scale (1–5), with positive and negative adjectives being compared to the walking-need perception. In this context, higher scores were associated with meanings closer to the adjectives on the right side of the scale. A total of 35 questionnaires were returned. We conducted an intraclass correlation coefficient (ICC) test, and all 35 questionnaires were valid.

Table 1. Characteristics of visual walkability perception.

Evaluated Item	Adjectives in Pair
Usefulness	Useless (1)—Useful (5)
Safety	Unsafe (1)—Safe (5)
Comfort	Uncomfortable (1)—Comfortable (5)
Attractiveness	Unattractive (1)—Attractive (5)

2.4. Street Physical Features Calculation

The semantic segmentation method based on deep learning was used to extract the proportions of streetscape elements from GSVP images and to quantify the physical features of commercial streets in this study. Semantic segmentation, as a computer-vision technique, can classify images at the pixel level (roads, buildings, sky, pedestrians, vehicles, etc.). This method has been widely used in studies for analyzing urban street environments [68–71]. The study employed the semantic segmentation model PSPNet [72] to extract the proportions of streetscape elements from GSVP images. Compared to other semantic segmentation models, such as FCN, SegNet, and DeepLab, PSPNet effectively handles multi-scale objects within scenes and achieves high accuracy, demonstrating superior performance across multiple datasets, including COCO and ADE20K. Additionally, the ADE20K dataset was used as the training dataset. This dataset contains annotations for 150 categories that encompass indoor, outdoor, street, natural landscape, and architectural scenes. This extensive coverage makes ADE20K well-suited for fine-grained segmentation tasks [73]. The PSPNet semantic segmentation model demonstrated advanced performance on the ADE20K dataset, achieving an accuracy exceeding 80%. The collected GSVP images were processed through PSPNet, where the PSPNet decoder categorizes the streetscape elements and calculates

the proportions of each element in the GSVP image. As shown in Figure 4, key streetscape elements can be clearly extracted from GSVP images.

Example of semantic segmentation results



The top 15 streetscape elements proportion

Streetscape elements	Mean value	Standard deviation
road	0.318	0.132
building	0.298	0.131
sky	0.175	0.073
sidewalk	0.082	0.105
tree	0.058	0.082
car	0.016	0.026
grass	0.012	0.051
car	0.011	0.022
plant	0.008	0.016
fence	0.005	0.013
wall	0.005	0.014
signboard	0.005	0.008
truck	0.004	0.014
earth	0.003	0.026
pedestrians	0.002	0.003

Figure 4. Example of semantic segmentation and percentage of each tag.

Ewing and Handy (2009) proposed the influential concept of urban design quality, which includes five dimensions: imageability, enclosure, human scale, transparency, and complexity [20]. Subsequent researchers have conducted studies on urban street quality based on these indicators [20,74,75]. Through a review of this literature, we selected 12 physical features that could be counted (Table 2). These physical features have often been used in previous studies to reflect the street built environment [76–80]. Additionally, we incorporated a commercial signage index to reflect the ambiance of commercial streets. Previous studies have highlighted that the atmosphere of commercial streets can significantly influence visitors' willingness to walk and shop, suggesting its potential impact on pedestrian engagement and consumer behavior [81,82].

2.5. Statistical Analysis

In this study, we conducted correlation analysis and regression analysis on the commercial street physical features and visual walkability perception using SPSS 26.0 software. Specifically, the four walking-need perceptions (usefulness, safety, comfort, and attractiveness) were used as dependent variables. The street physical features were used as independent variables in multiple linear regression analyses to explore the specific impact of the built environment on walking-need perception in commercial streets.

Table 2. Commercial street physical features selection and definition.

Physical Feature	Formula	Expression	Definition
Greenness	$G_i = \frac{1}{n}\sum_{i=1}^{n} V1_i\{i \in (1,2,\cdots,n)\}(1)$	$V1_i$ denotes the proportion of trees, grass, and plant pixels. The sum indicates the total number of vegetation pixels in each image.	It refers to the ratio of trees, plants, and grasses pixels to the overall pixels.
Openness	$O_i = \frac{1}{n}\sum_{i=1}^{n} S1_i\{i \in (1,2,\cdots,n)\}(2)$	$S1_i$ denotes the proportion of sky pixels. The sum indicates the total number of sky pixels in each image.	It refers to the open degree in the street space.
Enclosure	$E_i = \frac{\frac{1}{n}\sum_{i=1}^{n} V2_i}{\frac{1}{n}\sum_{i=1}^{n} H1_i}\{i \in (1,2,\cdots,n)\}(3)$	$V2_i$ is the percentage of wall, building, and tree pixels. $H1_i$ is the percentage of road, sidewalk, fence, and earth pixels.	It reflects the degree of enclosure of the street canyon.
Walkable space	$WS_i = \frac{1}{n}\sum_{i=1}^{n} S2_i\{i \in (1,2,\cdots,n)\}(4)$	$S2_i$ denotes the proportion of sidewalk pixels. The sum indicates the total number of sidewalk pixels in each image.	It refers to the ratio of sidewalk pixels to the overall pixels.
Pedestrian occurrence rate	$POR_i = \frac{1}{n}\sum_{i=1}^{n} P1_i\{i \in (1,2,\cdots,n)\}(5)$	$P1_i$ denotes the proportion of pedestrian pixels. The sum indicates the total number of pedestrian pixels in each image.	It reflects the proportion of pedestrians appearing in the street space.
Vehicle occurrence rate	$VOR_i = \frac{1}{n}\sum_{i=1}^{n} V3_i\{i \in (1,2,\cdots,n)\}(6)$	$V3_i$ denotes the proportion of car, bus, and truck pixels. The sum indicates the total number of vehicle pixels in each image.	It refers to the proportion of vehicles appearing in the street space.
Street cleanliness	$SC_i = 1 - \frac{1}{n}\sum_{i=1}^{n} G_i\{i \in (1,2,\cdots,n)\}(7)$	$G1_i$ denotes the proportion of garbage, scrawl, bits, and bobs pixels, 1—Represents the cleanliness of the street.	It reflects the degree of tidiness in the street space.
Landmark visibility index	$LVI_i = \frac{1}{n}\sum_{i=1}^{n} L1_i\{i \in (1,2,\cdots,n)\}(8)$	$L1_i$ denotes the proportion of landmark pixels. The sum indicates the total number of landmark pixels in each image.	It reflects the proportion of iconic landscapes or buildings in the overall pixel.

Table 2. *Cont.*

Physical Feature	Formula	Expression	Definition
Transparency index	$TI_i = \frac{1}{n}\sum_{i=1}^{n} GL_i + \frac{1}{n}\sum_{i=1}^{n} WI_i\{i \in (1,2,\cdots,n)\}(9)$	GL_i denotes the proportion of glass pixels. WI_i denotes the proportion of window pixels.	It reflects the degree of transparency in the street space.
Commercial signage index	$CSI_i = \frac{1}{n}\sum_{i=1}^{n} S3_i\{i \in (1,2,\cdots,n)\}(10)$	$S3_i$ denotes the proportion of commercial sign board pixels. The sum indicates the total number of commercial sign board pixels in each image.	It reflects the proportion of commercial sign board in the overall pixel.
landscape diversity index	$SHDI = -\sum_{i=1}^{n}(P_i * InP_i)(11)$	In denotes the landscape log, P_i denotes the proportion of the entire community made up of landscape elements i.	It refers to the richness degree of the landscape elements that can be observed in the street.
Environment color diversity	$ECi = 1 - \frac{1}{n}\sum_{i=1}^{n}\left(\frac{P_{ij}}{\sum_{i=1}^{j} P_{ij}}\right)^2 (12)$	P_{ij} denotes the number of j color pixels in i-image, and J indicates the total number of the environment colors in i-image.	It refers to the richness degree of environmental colors that can be observed in the streets.

3. Results

3.1. Visual Walkability Perception Analysis of Tenjin Commercial District

This study explored the current distribution of visual walkability perceptions in the Tenjin commercial district based on four walking-need perceptions: usefulness, safety, comfort, and attractiveness. A comparison of the results for these four walking-need perceptions (Table 3) revealed the following ranking: attractiveness > safety > comfort > usefulness. In the Tenjin commercial district, attractiveness and safety were both high walking-need perceptions. The standard deviation for safety was moderate, indicating a strong sense of safety across the streets with little variation between segments. However, the standard deviation for attractiveness was relatively high (1.089), suggesting an uneven distribution with some sections showing perceptual fluctuations. Usefulness and comfort were medium walking-need perceptions overall, with moderate standard deviations, reflecting clear but stable characteristics across the streets without significant fluctuations.

Table 3. The walking-need perceptions of Tenjin commercial district.

Walking-Need Perception	Mean Value	Standard Deviation	Number
Usefulness	2.931	0.963	475
Safety	3.018	0.922	475
Comfort	2.968	0.985	475
Attractiveness	3.254	1.089	475

By comparing the high and low samples for different walking-need perceptions (Figure 5), the study identified distinct patterns in their manifestation. In the samples with high usefulness, the presence of small-scale landscape elements such as fountains or sculptures enhanced the recognizability and appeal of public spaces, offering places for walking and group activities. Conversely, in the low-usefulness samples, construction barriers and fences diminished the openness of the streets, restricting pedestrian flow. The lack of vegetation made the visual environment monotonous, while the fences obstructed street connectivity, reducing visual permeability and walking comfort.

In the high-safety samples, the street environments were spacious and clean, with designs emphasizing pedestrian-vehicle separation. Clear road zoning effectively reduced conflicts between vehicles and pedestrians. The open street design provided good visibility, allowing pedestrians to easily observe surrounding traffic and the environment. Light-colored streets and buildings were harmonized with the green of natural plants, contributing to a fresh and bright atmosphere. In contrast, low-safety samples had narrow street canyons formed by tall buildings, further restricted by construction areas at some nodes, limiting sky visibility. These spaces with low safety contained obstacles, graffiti, and street litter, causing a cluttered visual experience. The lack of prominent landmarks and relatively monotonous streetscapes diminished the sense of safety.

As shown in Figure 6, in the high-comfort samples, the street trees on both sides of the road were in good condition, providing natural shading. Additionally, high-comfort streets have a large green area and a wide view of the sky above the streets. The sidewalks were spacious and clearly separated from the vehicle lanes. Although the pavement lacked excessive decorations or distinctive landscapes, its design was simple, clean, and orderly, contributing to an orderly street environment. In the low-comfort samples, they exhibit a significant lack of greenery, resulting in an environment devoid of natural elements. The pedestrian streets were narrow and lacked functionality, with some walking spaces even cut off by building corners, preventing pedestrians from walking freely and safely.

Low-comfort streets also tended to have dense buildings on both sides, creating a sense of oppression. Even in areas with slightly open skies, urban infrastructure such as buildings and utility poles fragmented the view, failing to provide sufficient spatial openness. Moreover, the outdated and deteriorated building facades gave pedestrians an impression of poor maintenance and aesthetics.

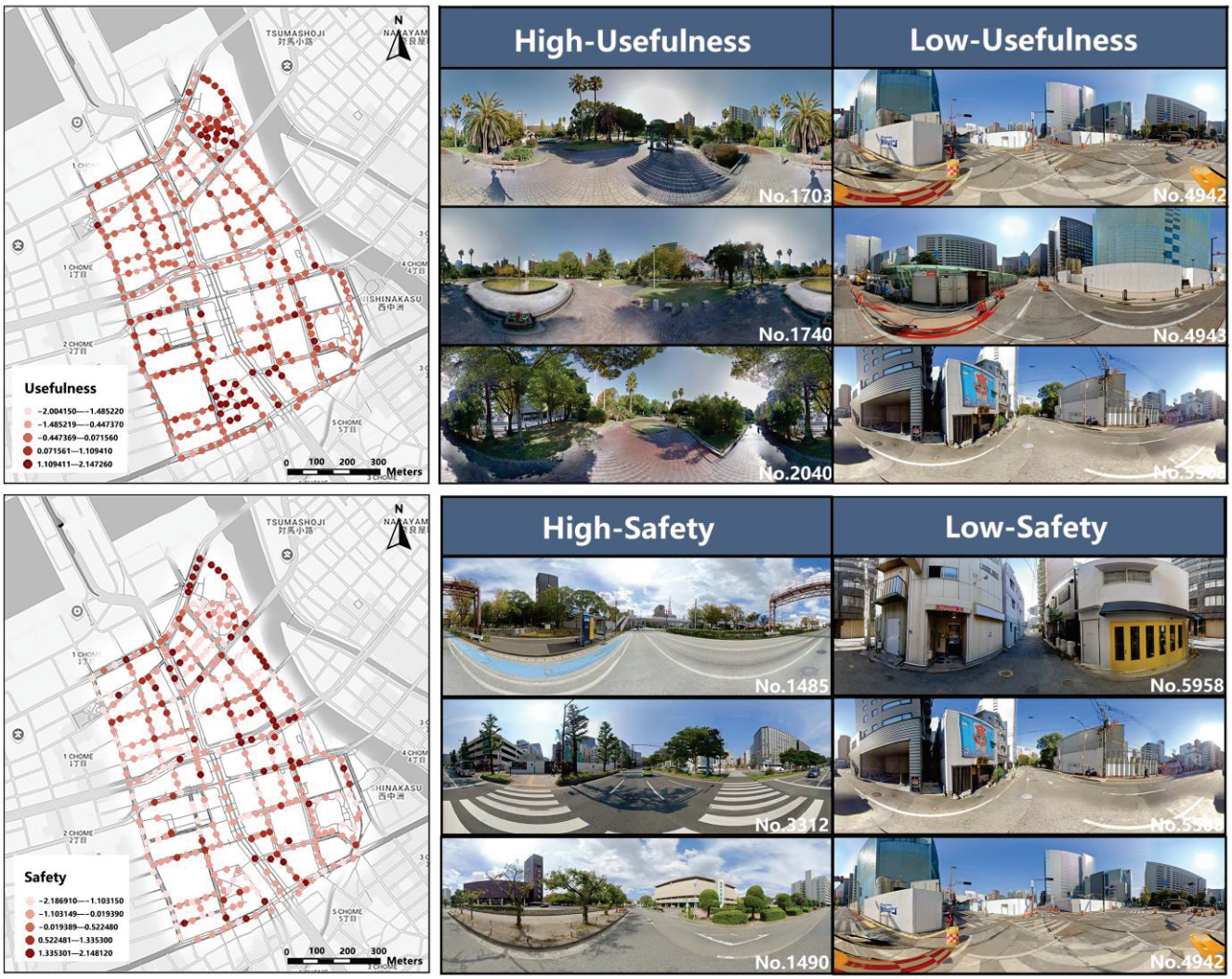


Figure 5. Sample examples of usefulness and safety with high and low values.

Street spaces in high-attractiveness samples had dense and diverse vegetation with vibrant colors. The open streets, combined with a variety of natural landscapes, enhanced the sense of spatiality. The pedestrian paths were wide, flat, and clean. Streets with high attractiveness often featured modern large-scale buildings or unique landmarks, which not only promoted visual appeal but also provided spaces for rest and social interaction. However, in the low-attractiveness samples, the streets lacked greenery and diverse landscape elements, resulting in a cluttered and unappealing environment. The surrounding buildings were tall, and pedestrian paths were obstructed by fences or barriers, restricting walking spaces and negatively impacting the pedestrian experience.

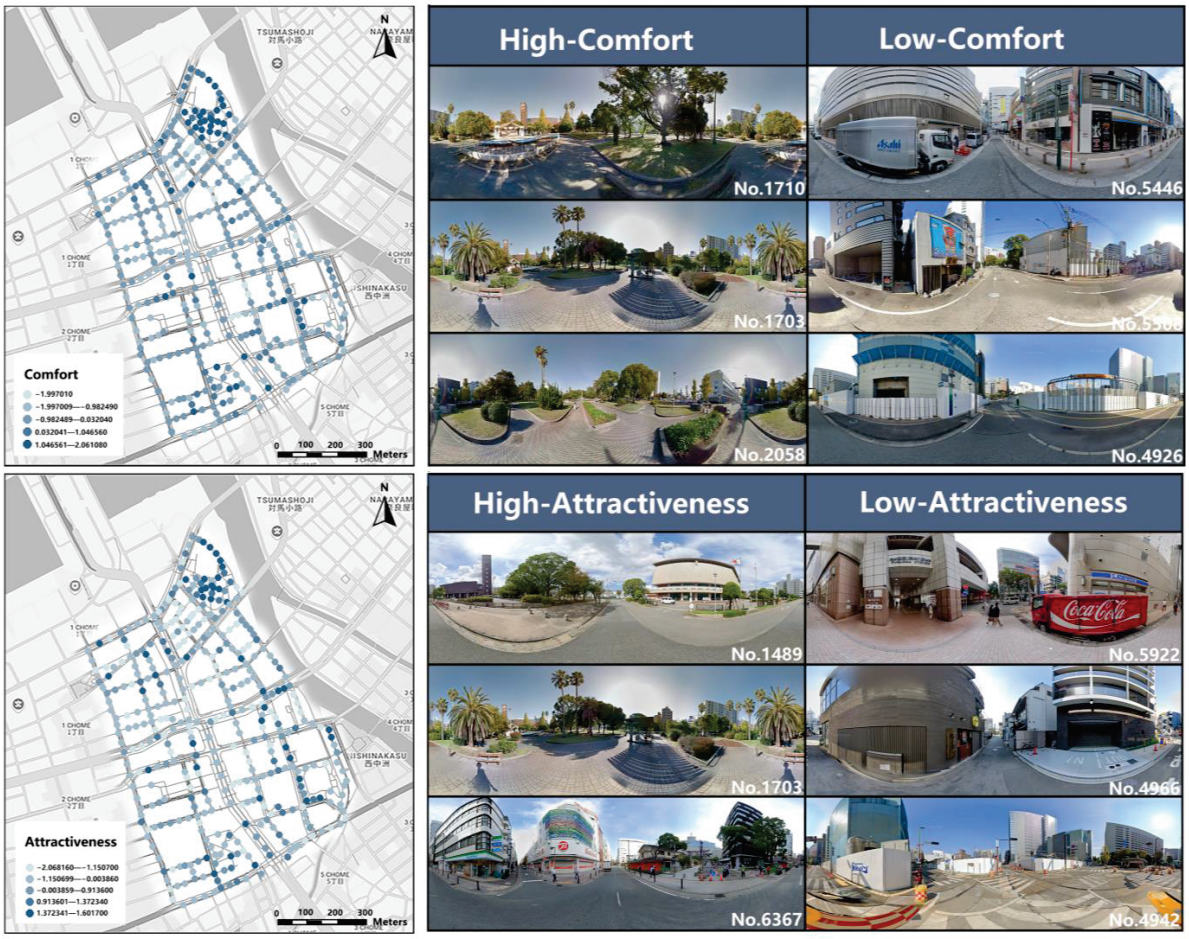


Figure 6. Sample examples of comfort and attractiveness with high and low values.

3.2. Spatial Distribution of Walking-Need Perceptions

To further investigate the spatial distribution of walking-need perceptions, this study analyzed four walking-need perceptions across primary roads, secondary roads, and tertiary roads in the Tenjin commercial district.

As shown in Table 4, primary roads exhibited a high perception of safety and attractiveness, with moderate standard deviations. However, usefulness and comfort were low walking-need perception with smaller standard deviations. This indicated that the perception of safety and attractiveness was particularly prominent on primary roads, whereas their overall usefulness and comfort were relatively low. The design of primary roads in the Tenjin commercial district emphasized safety. These roads were wide with multiple lanes, providing clear and designated spaces for motor vehicles, reducing traffic conflicts and minimizing the risk of accidents. Additionally, primary roads were mostly located on flat terrain, and the wide and simple road design offered unobstructed views, enabling both pedestrians and drivers to navigate easily and effectively. Buildings along primary roads were predominantly high-rise commercial or office structures, characterized by robust construction and orderly arrangement, forming clear street boundaries. The tall and stable walls not only enhanced the sense of boundary but also provided pedestrians with a degree of visual safety, fostering impressions of order and stability. Furthermore, the modern architectural style and uniform appearance of these buildings promoted the visual appeal of the roads. However, as major traffic arteries, primary roads also negatively impacted pedestrian experiences. The mixed use by pedestrians and vehicles resulted in noise and air pollution, diminishing overall comfort. In addition, the tall and enclosed facades of

buildings along these roads lacked transparency in some sections, restricting pedestrian views and hindering navigation for both walkers and cyclists.

Table 4. The result of walking-need perceptions for different roads.

	Primary Road (N = 97)		Secondary Road (N = 136)		Tertiary Road (N = 248)	
	Mean Value	Standard Deviation	Mean Value	Standard Deviation	Mean Value	Standard Deviation
Usefulness	2.727	0.75	3.106	0.953	2.916	1.024
Safety	3.152	1.013	3.022	0.878	2.962	0.902
Comfort	2.845	0.854	3.097	0.945	2.947	1.045
Attractiveness	3.245	0.999	3.378	0.993	3.19	1.165

The secondary roads demonstrated high perception levels across safety, usefulness, comfort, and attractiveness, with standard deviations for all four walking-need perceptions being moderate or low. This suggested that secondary roads provided a balanced and favorable walking experience. As roads that connected various urban areas and served as feeders for traffic distribution, secondary roads generally experienced lower traffic volumes than primary roads, resulting in slower vehicle speeds. This created a safer interaction environment for pedestrians and non-motorized vehicles, reducing accident risks and encouraging activities in these areas. The moderate width of secondary roads, often accompanied by green belts and trees, provided visual buffers that protected pedestrians from external traffic disruptions, fostering a relaxed and secure psychological environment. Spatially, the diverse layout of secondary roads, incorporating green spaces, parks, and commercial zones, offered a variety of activity spaces to meet diverse needs. This diversity also promoted social interactions, enhancing the overall attractiveness and comfort of the area.

In tertiary roads, attractiveness was a prominent walking-need perception, but its high standard deviation indicated an uneven distribution, with some segments lacking appeal. Safety and comfort showed moderate perception levels; however, comfort showed significant variability, reflecting inconsistent distribution. The usefulness was evaluated as a low walking-need perception, indicating poor performance in this aspect. The design of tertiary roads tended towards pedestrian-friendly spaces such as footpaths and parks, with open areas providing gathering and socializing opportunities. These streets often included significant green spaces, parks, and public seating, creating areas for relaxation, leisure, and daily activities while supporting social interactions. Clean roads and well-arranged vegetation reduced visual clutter, offering an enhanced aesthetic experience. However, some segments of tertiary roads suffered from reduced attractiveness. Monotonous building facades lacking visual appeal and the absence of natural elements or greenery in some areas diminished the desire for people to stay. The overall usefulness of tertiary roads was poor, as they were often narrower than primary roads, with limited openness and a lack of well-developed pedestrian infrastructure, restricting walking spaces. Moreover, barriers such as fences, buildings, or construction sites obstructed some routes, further limiting accessibility and convenience for pedestrians.

3.3. Correlation and Regression Analysis

This study conducted a correlation analysis between four walking-need perceptions and 12 physical features using SPSS software, revealing the relationships between different walking-need perceptions and street physical features. The results are shown in Figure 7.

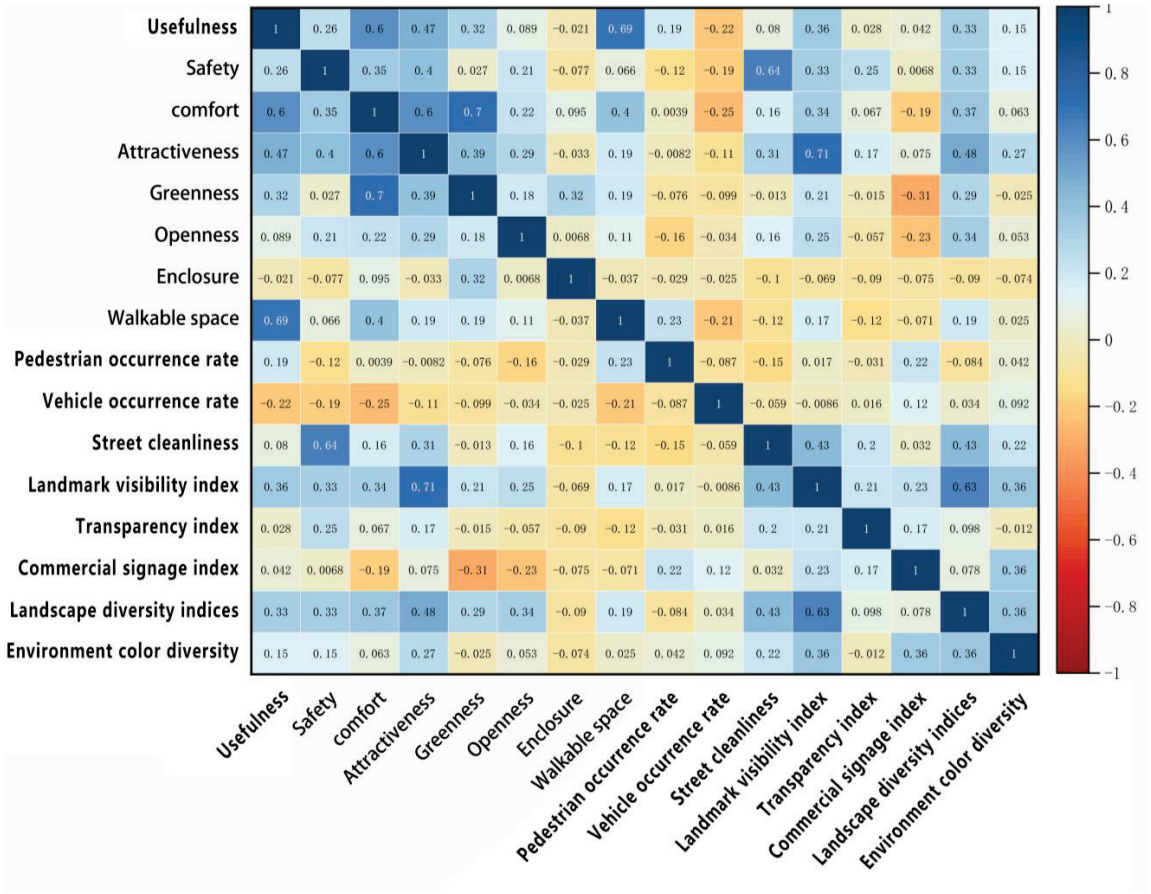


Figure 7. Correlation analysis between walking-need perceptions and physical features.

The correlation analysis for usefulness indicated that usefulness was positively correlated with greenness, walkable space, pedestrian occurrence rate, landmark visibility index, landscape diversity index, and environmental color diversity while negatively correlated with vehicle occurrence rate. For safety, the results showed positive correlations with openness, street cleanliness, landmark visibility index, transparency index, landscape diversity index, and environmental color diversity, and negative correlations with pedestrian occurrence rate and vehicle occurrence rate. Comfort was significantly positively correlated with greenness, openness, walkable space, street cleanliness, landmark visibility index, and landscape diversity index, with a weaker positive correlation with enclosure. However, it was negatively correlated with vehicle occurrence rate and commercial signage index. Attractiveness was positively correlated with greenness, openness, walkable space, street cleanliness, landmark visibility index, transparency index, landscape diversity index, and environmental color diversity and showed a weaker negative correlation with vehicle occurrence rate.

In this study, the street physical features identified through correlation analysis were used as independent variables, while the four walking-need perceptions—usefulness, safety, comfort, and attractiveness—were treated as dependent variables in stepwise regression analyses. By gradually excluding insignificant physical features, regression models for the four walking-need perceptions were developed.

As shown in Figure 8, the standardized residuals from the regression closely follow a normal distribution, indicating that the residuals meet the assumption of normality. These results provide further support for the validity of the model assumptions.

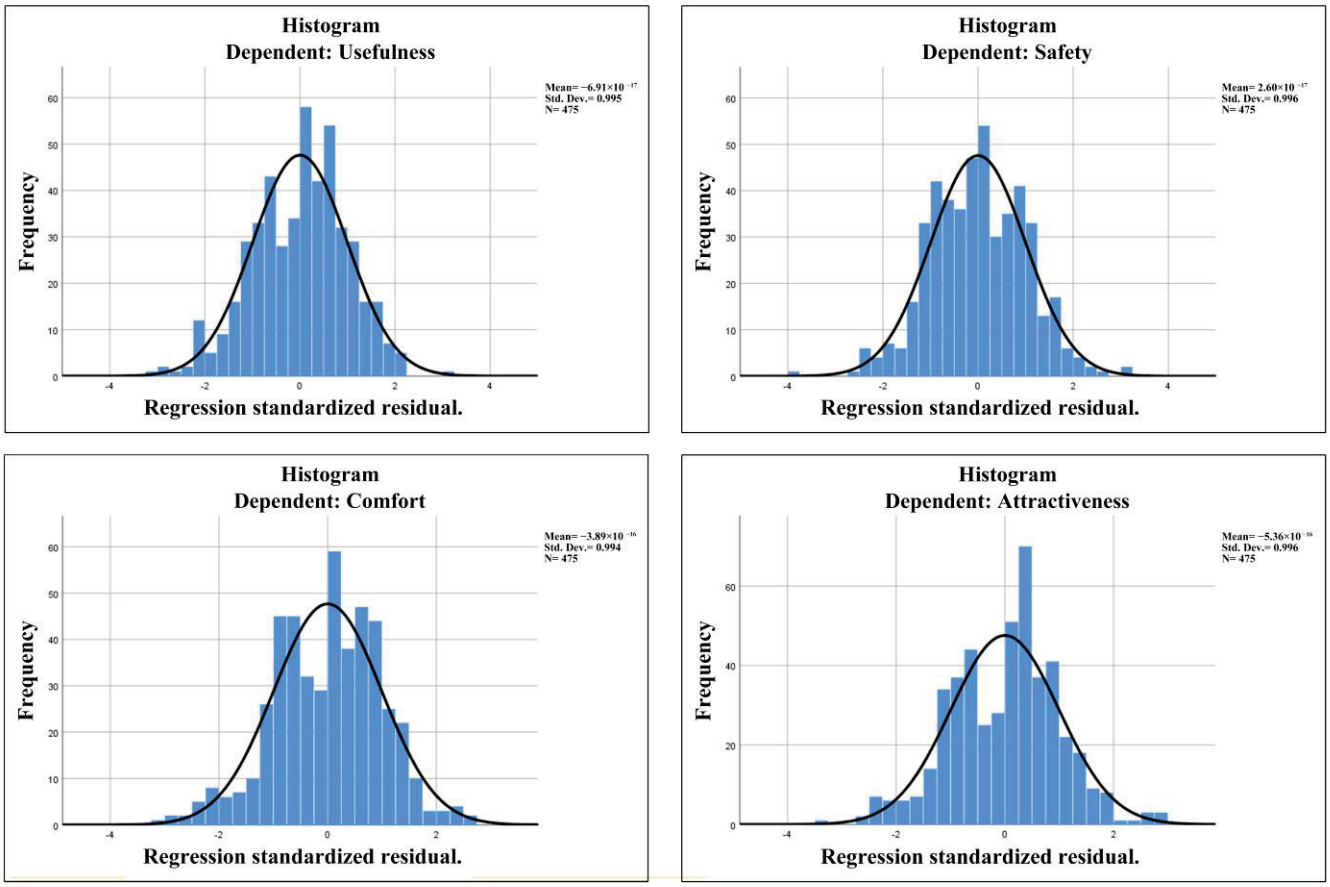


Figure 8. Regression standardized residual of four walking-need perceptions.

As can be seen from Table 5, the regression analysis for usefulness revealed that walkable space, landmark visibility index, and greenness had significant positive effects on usefulness, with walkable space having the most pronounced influence. Environmental color diversity also showed a positive effect (Beta = 0.075), though weaker. In contrast, a higher vehicle occurrence rate was found to decrease usefulness. All variables had low VIF values, indicating no multicollinearity issues. Overall, optimizing walkable space, enhancing landmark landscapes and greenery, and reducing traffic conflicts can effectively improve feasibility perception in waterfront spaces. For safety, the regression results demonstrated that street cleanliness had the most substantial positive impact, followed by transparency index and openness, with Beta values of 0.137 and 0.123, respectively. Conversely, the vehicle occurrence rate negatively affected safety, indicating that reducing traffic conflicts enhances safety perception. All variables had VIF values below 1.1, suggesting no multicollinearity. In summary, improving street cleanliness, increasing street interface transparency, enhancing openness, and alleviating traffic pressure can significantly enhance safety perception. The regression analysis for comfort indicated that greenness had the strongest positive effect on comfort, followed by walkable space and street cleanliness, with Beta values of 0.243 and 0.143, respectively. Conversely, vehicle occurrence rate and enclosure had negative effects on comfort, while the landmark visibility index had a minor positive effect (Beta = 0.085). All variables showed low VIF values, confirming no multicollinearity. Overall, increasing greenery, improving pedestrian environments, and enhancing street cleanliness are effective strategies to improve comfort in commercial street spaces. For attractiveness, the results showed that the landmark visibility index had the most significant positive impact, followed by greenness and openness, with Beta values

of 0.235 and 0.080, respectively. In contrast, vehicle occurrence rate negatively impacted attractiveness, suggesting that reducing vehicle occurrence rate could enhance it. All variables had VIF values below 1.1, indicating no multicollinearity. In conclusion, increasing landmark landscapes and greenery, increasing sky openness, and reducing vehicle flow rate can significantly improve attractiveness.

Table 5. Regression analysis results of Usefulness, Safety, Comfort, and Attractiveness.

	Model	Unstandardized Coefficients		Standardized Coefficients		Sig.	VIF	R^2	F.Sig
		B	Std. Error	Beta	t				
Usefulness	(Constant)	-2.788×10^{-15}	0.030		0.000	1.000		0.561	0
	Walkable space	0.610	0.032	0.610	19.090	0.000	1.102		
	Landmark visibility index	0.191	0.034	0.191	5.644	0.000	1.241		
	Greenness	0.153	0.032	0.153	4.834	0.000	1.088		
	Vehicle occurrence rate	−0.079	0.031	−0.079	−2.518	0.012	1.061		
	Environment color diversity	0.075	0.033	0.075	2.287	0.023	1.177		
Safety	(Constant)	-1.293×10^{-15}	0.034		0.000	1.000		0.457	0.000
	Street cleanliness	0.584	0.035	0.584	16.638	0.000	1.077		
	Vehicle occurrence rate	−0.150	0.034	−0.150	−4.436	0.000	1.005		
	Transparency index	0.137	0.035	0.137	3.957	0.000	1.051		
	Openness	0.123	0.034	0.123	3.565	0.000	1.034		
Comfort	(Constant)	1.455×10^{-15}	0.028		0.000	1.000		0.626	0.000
	Greenness	0.657	0.031	0.657	21.057	0.000	1.232		
	Walkable space	0.243	0.030	0.243	7.980	0.000	1.171		
	Street cleanliness	0.143	0.032	0.143	4.431	0.000	1.319		
	Vehicle occurrence rate	−0.126	0.029	−0.126	−4.328	0.000	1.068		
	Enclosure	−0.090	0.030	−0.090	−2.972	0.003	1.151		
	Landmark visibility index	0.085	0.033	0.085	2.569	0.011	1.380		
Attractiveness	(Constant)	2.177×10^{-16}	0.030		0.000	1.000		0.577	0
	Landmark visibility index	0.642	0.031	0.642	20.499	0.000	1.100		
	Greenness	0.235	0.031	0.235	7.593	0.000	1.07 5		
	Vehicle occurrence rate	−0.080	0.030	−0.080	−2.681	0.008	1.010		
	Openness	0.080	0.031	0.080	2.554	0.011	1.090		

** It is significant at the 0.01 level. * It is significant at the 0.05 level.

4. Discussion

This study aims to investigate the mechanisms by which physical features of commercial streets impact visual walkability perception. Measuring the relationship between them is important for understanding how to optimize walking experiences in urban neighborhoods and improve the quality of public spaces. In this study, GSVP images were automatically collected using Python, and the deep-learning-based semantic segmentation method was applied to analyze street physical features. This approach enabled efficient and precise extraction of various landscape elements in the street-view images, ensuring systematic and consistent data. Meanwhile, the SD method was used to assess four walking-need perceptions of visual walkability perception, and a comprehensive dataset of 475 samples enhanced the representativeness and accuracy of the findings. The combination of these methods provides a scientific and innovative approach to reveal the relationship between physical features and four walking-need perceptions in commercial streets.

Through the correlation and regression analysis of the physical features and walking-need perceptions in Tenjin commercial streets, this study found that a spacious walking area, abundant street greenery, and the presence of iconic landmarks significantly enhance public walking perception and experience. The study showed that walkable streets positively

impact usefulness, supporting prior research on objective walkability and perceptions of walkable streets [68,83]. Wide walkable streets not only provide convenient passage for pedestrians but also encourage more people to walk rather than drive into commercial areas, it is consistent with Southworth's [84] findings on the importance of pedestrian space width for walkability. Additionally, increased vegetation significantly extended residents' walking time; plants enrich the street environment by creating a sense of nature and attractiveness, fostering a more pleasant walking atmosphere [85]. Zhang et al. (2024) indicate that iconic landmarks on streets significantly improve the walking experience for residents by enhancing visual appeal and landmark effects [86]. Moreover, color plays a critical role in shaping uniqueness and identifying features. Studies have shown that distinctive colors and appearances contribute to enhancing spatial memory and emotional connections [87]. Related research indicates that color-rich public spaces can foster an open and inclusive atmosphere, encouraging social interactions among people [88]. The study further validates the positive impact of street cleanliness on safety, consistent with previous research findings [89,90]. A clean environment can reduce anxiety caused by a "sense of disorder". Ghossoub found in a study of New York City streets that disordered elements such as litter and damaged infrastructure significantly decrease pedestrians' sense of safety [91], while a clean street environment enhances their safety perception, making them more willing to use public spaces. The effect of greenness on comfort was found to be the most significant, followed by walkable space and street cleanliness. The study suggests that greenness not only provides shade and reduces temperature but also improves air quality and microclimate, promoting thermal comfort for pedestrians [92–94]. In addition, street vegetation can reduce traffic noise, which can enhance acoustic comfort [95]. This effect makes pedestrians feel more relaxed and pleased in greenery-rich street environments, making walking and staying more comfortable [47]. Wider walkable spaces increase street walkability, making pedestrians pass more comfortably, consistent with the conclusions of Frackelton et al. [96]. On the other hand, a clean and organized walking environment not only improves residents' psychological comfort but also extends their stay, enhancing the walking experience [97]. However, high levels of enclosure will reduce street comfort. High enclosure in street spaces can easily trigger feelings of anxiety and oppression in pedestrians [98,99]. As pointed out by some scholars, open spaces are generally more comfortable for people than enclosed spaces [100]. Additionally, an increased landmark visibility index can significantly enhance street appeal, therefore strengthening place identity. Kevin Lynch, in The Image of the City [101], proposed that landmark landscapes add visual character to streets, helping people recognize specific areas and enhancing distinctiveness. This visual appeal not only strengthens residents' sense of belonging but can also attract tourists and potential investors, promoting neighborhood image and economic value [86]. The positive effects of greenness are also supported by other studies on the benefits of urban greenery for commercial streets [102]. In studies by A.T. Row and J. Jacobs, urban greenery, such as trees and lawns, was shown to significantly improve the urban aesthetic, particularly their visual attractiveness [103]. Finally, the vehicle occurrence rate negatively affects usefulness, safety, comfort, and attractiveness. Streets with high vehicle occurrence rates are more prone to accidents, heightening pedestrians' sense of insecurity. This negative perception of safety also discourages walking, especially among children and elderly individuals [104]. Frequent accidents psychologically increase pedestrian tension, decreasing comfort. Such incidents often lead to street disorder, leaving negative visual elements which in turn reduces the attractiveness of the street.

The analysis of the spatial distribution of walking needs perception in Tenjin's commercial district revealed that primary roads exhibit poor usefulness and comfort, while

tertiary roads showed shortcomings in usefulness. To enhance the overall pedestrian environment of urban streets, it is recommended that future street renovations prioritize improvements in usefulness on both primary roads and tertiary roads. Specifically, increasing the number of pedestrian pathways and widening pedestrian spaces can enhance pedestrian flow [105]. Additionally, rational planning of traffic routes effectively facilitates a connection between transit lines, service facilities, and recreational walking paths, thus optimizing the walking experience [106]. Improving the natural environment on primary roads is also a key strategy, which can be achieved by adding more greenery along the streets to boost environmental appeal [107]. For instance, implementing vertical greening along streets [108] not only beautifies the streetscape but also significantly enhances street comfort. To minimize vehicular interference with pedestrian activity, various speed control measures should be implemented into street design, such as shortening intersection distances and reducing turning radii. These modifications can lower vehicle speeds and improve pedestrian safety [109].

This study has several limitations that need to be considered. First, the accuracy of using objective environmental factors to predict perception is typically limited. The study primarily investigates the influence of commercial street environmental features on visual walkability perception from four walking-need perceptions. Second, GSVP images capture only a specific moment in time, which may not comprehensively reflect variations in pedestrian and vehicle appearance rates throughout the day or week. Previous studies have shown that pedestrian and traffic flow exhibit significant temporal variations [110,111]. In future research, we will collect and compare street images from the same locations at multiple time intervals to explore how built environment characteristics influence human activity patterns. Third, this study was conducted in Tenjin, Fukuoka, a central commercial district characterized by its unique geographical location, cultural context, and high-density commercial activities. These factors may differ from those in other commercial areas, and therefore, the findings may not be entirely applicable to all types of commercial districts. Finally, previous research on environmental perception suggests that using students as a substitute for the public is feasible. Our study primarily selected university students as respondents for evaluating walking-need perceptions; however, the users of commercial street environments may include tourists from various cultural backgrounds. This study did not incorporate individual demographic factors such as age, gender, or socioeconomic status into the analysis. Previous research has shown that these socio-demographic characteristics significantly influence perceptions of walking needs. Future research should explore the intersection of socio-demographic factors and walking-need perceptions by integrating these variables into the analytical framework. This approach could provide a more comprehensive understanding of how urban street design impacts diverse population groups and help inform more inclusive urban planning and design practices.

5. Conclusions

In this study, we evaluated the visual walkability perception and quantified the physical features of urban commercial streets based on street-view images using the SD method and deep-learning-based semantic segmentation method. Additionally, correlation and regression analyses were applied to explore the impact of physical features on walking-need perception. The application of these methods to quantitatively assess the objective environment of commercial streets on a large scale and to capture public walking-need perception with minimal cost is significant for urban planning and environmental design.

The results of the study show that the overall walking-need perceptions of the Tenjin commercial district are ranked as follows: attractiveness > safety > comfort > usefulness.

In addition, the results show that there are significant spatial distribution differences in walking-need perceptions in the Tenjin commercial district. Safety perception is more prominent on primary roads, all four walking-need perceptions in the secondary roads at a high level, and the tertiary roads have generally lower scores for all walking-need perceptions. The regression analysis indicates that walkable space and the landmark visibility index have a significant impact on usefulness, street cleanliness emerges as the most influential factor affecting safety, greenness is identified as the primary determinant of comfort, while the landmark visibility index exerts the greatest influence on attractiveness. Based on the differences in the spatial distribution of walking-need perceptions, targeted adjustments and optimization of the physical features of different commercial streets can effectively enhance public visual walkability perception. These strategies can promote residents' health, foster community interaction, and improve overall quality of life. The findings provide practical insights for future urban planning, contributing to the development of pedestrian-friendly urban environments.

Author Contributions: Conceptualization, G.H., Y.Y., B.D. and W.G.; Data curation, G.H. and Y.Y.; Formal analysis, G.H. and Y.Y.; Investigation, G.H., Y.Y. and M.L.; Methodology, G.H., Y.Y., M.L. and D.S.; Project administration, Y.Y., M.L. and W.G.; Resources, G.H., Y.Y. and D.S.; Software, G.H. and Y.Y.; Supervision, G.H., M.L., B.D. and W.G.; Validation, G.H., Y.Y. and M.L.; Visualization, G.H.; Writing—original draft, G.H. and Y.Y.; Writing—review and editing, G.H., Y.Y., M.L., D.S. and B.D. All authors have read and agreed to the published version of the manuscript.

Funding: This research received no external funding.

Data Availability Statement: Interview transcripts and interpreted statements supporting this study's findings and the smart contract codes are available from the corresponding author upon reasonable request.

Acknowledgments: We would like to thank the journal experts who edited this paper. We also appreciate the constructive suggestions and comments on the manuscript from the reviewers and editors.

Conflicts of Interest: The authors declare no conflicts of interest.

References

1. Huff, D.L. Defining and estimating a trading area. *J. Mark.* **1964**, *28*, 34–38. [CrossRef]
2. Park, S.J. The Roles of Shop Owners in Boosting Conventional Markets. *J. Distrib. Sci.* **2011**, *9*, 93–102.
3. Fouad, M.A. Towards sustainable commercial streets. *J. Al-Azhar Univ. Eng. Sect.* **2019**, *14*, 1004–1023. [CrossRef]
4. Zhang, J.; Zhou, W.; Lian, H.; Hu, R. Research on Optimization Strategy of Commercial Street Spatial Vitality Based on Pedestrian Trajectories. *Buildings* **2024**, *14*, 1240. [CrossRef]
5. Ma, S.; Wang, B.; Liu, W.; Zhou, H.; Wang, Y.; Li, S. Assessment of street space quality and subjective well-being mismatch and its impact, using multi-source big data. *Cities* **2024**, *147*, 104797. [CrossRef]
6. Subramanian, G.H.; Verma, M.; Verma, A. Measuring Motivation and Satisfaction Level of Visitors of a Pedestrianized Urban Street in India for an Improved Quality of Life. *J. Urban Plan. Dev.* **2023**, *149*, 05023026. [CrossRef]
7. Dempsey, N. Are good-quality environments socially cohesive? Measuring quality and cohesion in urban neighbourhoods. *Town Plan. Rev.* **2009**, *80*, 315–345. [CrossRef]
8. Ubiali, A.; Gori, D.; Rochira, A.; Raguzzoni, G.; Fantini, M.P. Measures of walkability in the pediatric population: A qualitative review of the literature. *Ann. Ig. Med. Prev. Comunità* **2021**, *33*, 67–85.
9. Abley, S.; Hill, E. *Designing Living Streets-a Guide to Creating Lively, Walkable Neighbourhoods*; Living Streets: London, UK, 2005.
10. Bull, F.C.; Al-Ansari, S.S.; Biddle, S.; Borodulin, K.; Buman, M.P.; Cardon, G.; Carty, C.; Chaput, J.-P.; Chastin, S.; Chou, R.; et al. World Health Organization 2020 guidelines on physical activity and sedentary behaviour. *Br. J. Sports Med.* **2020**, *54*, 1451–1462. [CrossRef]
11. Ewing, R.; Dumbaugh, E. The built environment and traffic safety: A review of empirical evidence. *J. Plan. Lit.* **2009**, *23*, 347–367. [CrossRef]

12. Stoker, P.; Garfinkel-Castro, A.; Khayesi, M.; Odero, W.; Mwangi, M.N.; Peden, M.; Ewing, R. Pedestrian safety and the built environment: A review of the risk factors. *J. Plan. Lit.* **2015**, *30*, 377–392. [CrossRef]
13. Rees-Punia, E.; Hathaway, E.D.; Gay, J.L. Crime, perceived safety, and physical activity: A meta-analysis. *Prev. Med.* **2018**, *111*, 307–313. [CrossRef] [PubMed]
14. Duncan, D.T.; Aldstadt, J.; Whalen, J.; White, K.; Castro, M.C.; Williams, D.R. Space, race, and poverty: Spatial inequalities in walkable neighborhood amenities? *Demogr. Res.* **2012**, *26*, 409. [CrossRef]
15. Choi, M.J.; Shin, S.M. An empirical analysis of the effect of pedestrian volume on retail sales. *J. Korea Plan. Assoc.* **2001**, *36*, 75–83.
16. Hong, S.J.; Lee, K.H.; Ahn, K.H. The effect of street environment on pedestrians' purchase in commercial street-Focused on Insa-dong and Munjeong-dong commercial street. *J. Archit. Inst. Korea* **2010**, *26*, 229–236.
17. Credit, K.; Mack, E. Place-making and performance: The impact of walkable built environments on business performance in Phoenix and Boston. *Environ. Plan. B Urban Anal. City Sci.* **2019**, *46*, 264–285. [CrossRef]
18. Gehl, J. *Life Between Buildings:Using Public Space*; Island Press: Washington, DC, USA, 2011.
19. Montgomery, J. Making a city: Urbanity, vitality and urban design. *J. Urban Des.* **1998**, *3*, 93–116. [CrossRef]
20. Ewing, R.; Handy, S. Measuring the unmeasurable: Urban design qualities related to walkability. *J. Urban Des.* **2009**, *14*, 65–84. [CrossRef]
21. Blečić, I.; Cecchini, A.; Trunfio, G.A. Towards automatic assessment of perceived walkability. In *Computational Science and Its Applications, Proceedings of the ICCSA 2018, Melbourne, VIC, Australia, 2–5 July 2018*; Lecture Notes in Computer Science; Springer: Cham, Switzerland, 2018; Volume 10962. [CrossRef]
22. Talavera-Garcia, R.; Soria-Lara, J.A. Q-PLOS, developing an alternative walking index. A method based on urban design quality. *Cities* **2015**, *45*, 7–17. [CrossRef]
23. Rosenberg, D.; Ding, D.; Sallis, J.F.; Kerr, J.; Norman, G.J.; Durant, N.; Harris, S.K.; Saelens, B.E. Neighborhood Environment Walkability Scale for Youth (NEWS-Y): Reliability and relationship with physical activity. *Prev. Med.* **2009**, *49*, 213–218. [CrossRef] [PubMed]
24. Cerin, E.; Sit, C.H.P.; Cheung, M.; Ho, S.; Lee, L.; Chan, W. Reliable and valid NEWS for Chinese seniors: Measuring perceived neighborhood attributes related to walking. *Int. J. Behav. Nutr. Phys. Act.* **2010**, *7*, 84. [CrossRef]
25. Cerin, E.; Conway, T.L.; Cain, K.L.; Kerr, J.; De Bourdeaudhuij, I.; Owen, N.; Reis, R.S.; Sarmiento, O.L.; Hinckson, E.A.; Salvo, D.; et al. Sharing good NEWS across the world: Developing comparable scores across 12 countries for the Neighborhood Environment Walkability Scale (NEWS). *BMC Public Health* **2013**, *13*, 309. [CrossRef] [PubMed]
26. Shashank, A.; Schuurman, N. Unpacking walkability indices and their inherent assumptions. *Health Place* **2019**, *55*, 145–154. [CrossRef]
27. Duncan, D.T.; Aldstadt, J.; Whalen, J.; Melly, S.J. Validation of Walk Scores and Transit Scores for estimating neighborhood walkability and transit availability: A small-area analysis. *GeoJournal* **2013**, *78*, 407–416. [CrossRef]
28. Yoshida, T.; Tanaka, K. Land-use diversity index: A new means of detecting diversity at landscape level. *Landsc. Ecol. Eng.* **2005**, *1*, 201–206. [CrossRef]
29. Kim, E.J.; Kim, H. Neighborhood walkability and housing prices: A correlation study. *Sustainability* **2020**, *12*, 593. [CrossRef]
30. Forsyth, A. What is a walkable place? The walkability debate in urban design. *Urban Des. Int.* **2015**, *20*, 274–292. [CrossRef]
31. Alfonzo, M.A. To walk or not to walk? The hierarchy of walking needs. *Environ. Behav.* **2005**, *37*, 808–836. [CrossRef]
32. Marquet, O. Speck, Jeff (2012). Walkable City: How Downtown Can Save America, One Step at a Time. ISBN 978-0865477728. *Doc. D'anàl. Geogr.* **2015**, *61*, 436–437.
33. Handy, S.L. Understanding the link between urban form and nonwork travel behavior. *J. Plan. Educ. Res.* **1996**, *15*, 183–198. [CrossRef]
34. Lynch, K. The image of the environment. *Image City* **1960**, *11*, 1–13.
35. Kuo, F.E.; Bacaicoa, M.; Sullivan, W.C. Transforming inner-city landscapes: Trees, sense of safety, and preference. *Environ. Behav.* **1998**, *30*, 28–59. [CrossRef]
36. Wu, W.; Guo, J.; Ma, Z.; Zhao, K. Data-driven approach to assess street safety: Large-scale analysis of the microscopic design. *ISPRS Int. J. Geo-Inf.* **2022**, *11*, 537. [CrossRef]
37. Li, Y.; Yabuki, N.; Fukuda, T. Integrating GIS, deep learning, and environmental sensors for multicriteria evaluation of urban street walkability. *Landsc. Urban Plan.* **2023**, *230*, 104603. [CrossRef]
38. Santosa, H.; Ernawati, J.; Wulandari, L.D. Visual quality evaluation of urban commercial streetscape for the development of landscape visual planning system in provincial street corridors in Malang, Indonesia. *IOP Conf. Ser. Earth Environ. Sci.* **2018**, *126*, 012202. [CrossRef]
39. Sun, D.; Ji, X.; Gao, W.; Zhou, F.; Yu, Y.; Meng, Y.; Yang, M.; Lin, J.; Lyu, M. The relation between green visual index and visual comfort in Qingdao coastal streets. *Buildings* **2023**, *13*, 457. [CrossRef]

40. Oliveira, V. *Urban Morphology: An Introduction to the Study of the Physical Form of Cities*; Springer: Berlin/Heidelberg, Germany, 2016.
41. Moura, F.; Cambra, P.; Gonçalves, A.B. Measuring walkability for distinct pedestrian groups with a participatory assessment method: A case study in Lisbon. *Landsc. Urban Plan.* **2017**, *157*, 282–296. [CrossRef]
42. Qazimirsaeed, A.; Khosravi, H.; Rafieian, M.; Mirzahossein, H.; Forciniti, C. Walkability policies in developing countries: What do people need and prefer in Iran? *Sustainability* **2022**, *14*, 10808. [CrossRef]
43. Lamour, Q.; Morelli, A.M.; Marins, K.R.C. Improving walkability in a TOD context: Spatial strategies that enhance walking in the Belém neighbourhood, in São Paulo, Brazil. *Case Stud. Transp. Policy* **2019**, *7*, 280–292. [CrossRef]
44. Vichiensan, V.; Nakamura, K. Walkability perception in Asian cities: A comparative study in Bangkok and Nagoya. *Sustainability* **2021**, *13*, 6825. [CrossRef]
45. Gaw, L.Y.; Chen, S.; Chow, Y.S.; Lee, K.; Biljecki, F. Comparing street view imagery and aerial perspectives in the built environment. ISPRS Annals of the Photogrammetry. *Remote Sens. Spat. Inf. Sci.* **2022**, *10*, 49–56. [CrossRef]
46. Farahani, M.; Razavi-Termeh, S.V.; Sadeghi-Niaraki, A.; Choi, S. A Hybridization of Spatial Modeling and Deep Learning for People's Visual Perception of Urban Landscapes. *Sustainability* **2023**, *15*, 10403. [CrossRef]
47. Ki, D.; Lee, S. Analyzing the effects of Green View Index of neighborhood streets on walking time using Google Street View and deep learning. *Landsc. Urban Plan.* **2021**, *205*, 103920. [CrossRef]
48. Koo, B.W.; Guhathakurta, S.; Botchwey, N. How are neighborhood and street-level walkability factors associated with walking behaviors? A big data approach using street view images. *Environ. Behav.* **2022**, *54*, 211–241. [CrossRef]
49. Lu, Y.; Sarkar, C.; Xiao, Y. The effect of street-level greenery on walking behavior: Evidence from Hong Kong. *Soc. Sci. Med.* **2018**, *208*, 41–49. [CrossRef] [PubMed]
50. Li, X.; Zhang, C.; Li, W.; Ricard, R.; Meng, Q.; Zhang, W. Assessing street-level urban greenery using Google Street View and a modified green view index. *Urban For. Urban Green.* **2015**, *14*, 675–685. [CrossRef]
51. Tang, J.; Long, Y. Measuring visual quality of street space and its temporal variation: Methodology and its application in the Hutong area in Beijing. *Landsc. Urban Plan.* **2019**, *191*, 103436. [CrossRef]
52. Zeng, L.; Lu, J.; Li, W.; Li, Y. A fast approach for large-scale Sky View Factor estimation using street view images. *Build. Environ.* **2018**, *135*, 74–84. [CrossRef]
53. Ye, Y.; Richards, D.; Lu, Y.; Song, X.; Zhuang, Y.; Zeng, W.; Zhong, T. Measuring daily accessed street greenery: A human-scale approach for informing better urban planning practices. *Landsc. Urban Plan.* **2019**, *191*, 103434. [CrossRef]
54. Salesses, P.; Schechtner, K.; Hidalgo, C.A. The collaborative image of the city: Mapping the inequality of urban perception. *PLoS ONE* **2013**, *8*, e68400. [CrossRef]
55. Zhang, F.; Zhou, B.; Liu, L.; Fung, H.H.; Lin, H.; Ratti, C. Measuring human perceptions of a large-scale urban region using machine learning. *Landsc. Urban Plan.* **2018**, *180*, 148–160. [CrossRef]
56. Zhou, H.; He, S.; Cai, Y.; Wang, M.; Su, S. Social inequalities in neighborhood visual walkability: Using street view imagery and deep learning technologies to facilitate healthy city planning. *Sustain. Cities Soc.* **2019**, *50*, 101605. [CrossRef]
57. Li, Y.; Yabuki, N.; Fukuda, T. Measuring visual walkability perception using panoramic street view images, virtual reality, and deep learning. *Sustain. Cities Soc.* **2022**, *86*, 104140. [CrossRef]
58. Muller, E.; Gemmell, E.; Choudhury, I.; Nathvani, R.; Metzler, A.B.; Bennett, J.; Denton, E.; Flaxman, S.; Ezzati, M. City-Wide Perceptions of Neighbourhood Quality using Street View Images. *arXiv* **2022**, arXiv:2211.12139.
59. Naik, N.; Kominers, S.D.; Raskar, R.; Hidalgo, C.A. Computer vision uncovers predictors of physical urban change. *Proc. Natl. Acad. Sci. USA* **2017**, *114*, 7571–7576. [CrossRef] [PubMed]
60. Bellazzi, A.; Bellia, L.; Chinazzo, G.; Corbisiero, F.; Agostino, P.A.; Devitofrancesco, A.; Fragliasso, F.; Ghellere, M.; Megale, V.; Salamone, F. Virtual reality for assessing visual quality and lighting perception: A systematic review. *Build. Environ.* **2022**, *209*, 108674. [CrossRef]
61. Osgood, C.E. *The Measurement of Meaning*; University of Illinois Press: Urbana, IL, USA, 1957.
62. Lyu, M.; Lin, J.; Zhou, F.; Niu, J.; Sun, D.; Meng, Y.; Ji, X. A method for evaluating the visual quality of wetland park landscapes: A case study of qianlu lake wetland park in Wuping, China. *Environ. Res. Commun.* **2024**, *6*, 105024. [CrossRef]
63. Sun, D.; Li, Q.; Gao, W.; Huang, G.; Tang, N.; Lyu, M.; Yu, Y. On the relation between visual quality and landscape characteristics: A case study application to the waterfront linear parks in Shenyang, China. *Environ. Res. Commun.* **2021**, *3*, 115013. [CrossRef]
64. Mireles de Villafranca, A.E.; Connors, R.D.; Wilson, R.E. Static traffic assignment on ensembles of synthetic road networks. In *Traffic and Granular Flow'17, Proceedings of the TGF: International Conference on Traffic and Granular Flow 2017*; Springer International Publishing: Berlin/Heidelberg, Germany, 2019; pp. 29–36. [CrossRef]
65. Yao, Y.; Zhu, X.; Xu, Y.; Yang, H.; Wu, X.; Li, Y.; Zhang, Y. Assessing the visual quality of green landscaping in rural residential areas: The case of Changzhou, China. *Environ. Monit. Assess.* **2012**, *184*, 951–967. [CrossRef] [PubMed]

66. Park, Y.; Garcia, M. Pedestrian safety perception and urban street settings. *Int. J. Sustain. Transp.* **2020**, *14*, 860–871. [CrossRef]
67. Takizawa, A.; Kinugawa, H. Deep learning model to reconstruct 3D cityscapes by generating depth maps from omnidirectional images and its application to visual preference prediction. *Des. Sci.* **2020**, *6*, e28. [CrossRef]
68. Nagata, S.; Nakaya, T.; Hanibuchi, T.; Amagasa, S.; Kikuchi, H.; Inoue, S. Objective scoring of streetscape walkability related to leisure walking: Statistical modeling approach with semantic segmentation of Google Street View images. *Health Place* **2020**, *66*, 102428. [CrossRef] [PubMed]
69. Lumnitz, S.; Devisscher, T.; Mayaud, J.R.; Radic, V.; Coops, N.C.; Griess, V.C. Mapping trees along urban street networks with deep learning and street-level imagery. *ISPRS J. Photogramm. Remote Sens.* **2021**, *175*, 144–157. [CrossRef]
70. Chen, L.; Lu, Y.; Ye, Y.; Xiao, Y.; Yang, L. Examining the association between the built environment and pedestrian volume using street view images. *Cities* **2022**, *127*, 103734. [CrossRef]
71. Gonzalez, D.; Rueda-Plata, D.; Acevedo, A.B.; Duque, J.C.; Ramos- Pollán, R.; Betancourt, A.; Garcia, S. Automatic detection of building typology using deep learning methods on street level images. *Build. Environ.* **2020**, *177*, 106805. [CrossRef]
72. Zhao, H.; Shi, J.; Qi, X.; Wang, X.; Jia, J. Pyramid scene parsing network. In Proceedings of the IEEE Conference on Computer Vision and Pattern Recognition, Honolulu, HI, USA, 21–26 July 2017; pp. 2881–2890.
73. Zhou, B.; Zhao, H.; Puig, X.; Fidler, S.; Barriuso, A.; Torraiba, A. Scene parsing through ade20k dataset. In Proceedings of the IEEE Conference on Computer Vision and Pattern Recognition, Honolulu, HI, USA, 21–26 July 2017; pp. 633–641.
74. Dai, L.; Zheng, C.; Dong, Z.; Yao, Y.; Wang, R.; Zhang, X.; Ren, S.; Zhang, J.; Song, X.; Guan, Q. Analyzing the correlation between visual space and residents' psychology in Wuhan, China using street-view images and deep-learning technique. *City Environ. Interact.* **2021**, *11*, 100069. [CrossRef]
75. Lyu, M.; Meng, Y.; Gao, W.; Yu, Y.; Ji, X.; Li, Q.; Huang, G.; Sun, D. Measuring the perceptual features of coastal streets: A case study in Qingdao, China. *Environ. Res. Commun.* **2022**, *4*, 115002. [CrossRef]
76. Zhou, L.; Hsieh, C.M. A multiscale walkability assessment approach creating walkable streets: A case study of high-density city, Macau. *Res. Transp. Bus. Manag.* **2024**, *57*, 101217. [CrossRef]
77. Chen, Y.; Huang, X.; White, M. A study on street walkability for older adults with different mobility abilities combining street view image recognition and deep learning-The case of Chengxianjie Community in Nanjing (China). *Comput. Environ. Urban Syst.* **2024**, *112*, 102151. [CrossRef]
78. Zhou, H.; Liu, L.; Lan, M.; Zhu, W.; Song, G.; Jing, F.; Zhong, Y.; Su, Z.; Gu, X. Using Google Street View imagery to capture micro built environment characteristics in drug places, compared with street robbery. *Comput. Environ. Urban Syst.* **2021**, *88*, 101631. [CrossRef]
79. Keralis, J.M.; Javanmardi, M.; Khanna, S.; Dwivedi, P.; Huang, D.; Tasdizen, T.; Nguyen, Q.C. Health and the built environment in United States cities: Measuring associations using Google Street View-derived indicators of the built environment. *BMC Public Health* **2020**, *20*, 215. [CrossRef] [PubMed]
80. Wang, R.; Lu, Y.; Zhang, J.; Liu, P.; Yao, Y.; Liu, Y. The relationship between visual enclosure for neighbourhood street walkability and elders' mental health in China: Using street view images. *J. Transp. Health* **2019**, *13*, 90–102. [CrossRef]
81. Mu, X.; Mu, L.; Zhang, J. The Impact of Street Elements on Pedestrian Stopping Behavior in Commercial Pedestrian Streets from the Perspective of Commercial Vitality. *Sustainability* **2024**, *16*, 7727. [CrossRef]
82. Singh, P.; Katiyar, N.; Verma, G. Retail shoppability: The impact of store atmospherics & store layout on consumer buying patterns. *Int. J. Sci. Technol. Res.* **2014**, *3*, 15–23.
83. Blečić, I.; Canu, D.; Cecchini, A.; Congiu, T.; Fancello, G. Factors of perceived walkability: A pilot empirical study. In *Computational Science and Its Applications, Proceedings of theICCSA 2016: 16th International Conference, Beijing, China, 4–7 July 2016*; Proceedings, Part IV 16; Springer International Publishing: Berlin/Heidelberg, Germany, 2016; pp. 125–137. [CrossRef]
84. Southworth, M. Designing the walkable city. *J. Urban Plan. Dev.* **2005**, *131*, 246–257. [CrossRef]
85. Held, D. *Urban Landscape Entomology*; Academic Press: Cambridge, MA, USA, 2019.
86. Zhang, F.; Sun, X.; Liu, C.; Qiu, B. Effects of Urban Landmark Landscapes on Residents' Place Identity: The Moderating Role of Residence Duration. *Sustainability* **2024**, *16*, 761. [CrossRef]
87. Nasar, J.L. Urban design aesthetics: The evaluative qualities of building exteriors. *Environ. Behav.* **1994**, *26*, 377–401. [CrossRef]
88. Carr, S. *Public Space*; Cambridge University Press: Cambridge, UK, 1992.
89. Herrmann-Lunecke, M.G.; Mora, R.; Sagaris, L. Persistence of walking in Chile: Lessons for urban sustainability. *Transp. Rev.* **2020**, *40*, 135–159. [CrossRef]
90. Kim, Y.; Choi, B.; Choi, M.; Ahn, S.; Hwang, S. Enhancing pedestrian perceived safety through walking environment modification considering traffic and walking infrastructure. *Front. Public Health* **2024**, *11*, 1326468. [CrossRef] [PubMed]
91. Ghossoub, C. Associations of 'Eyes on the Street' with the Perception of Safety in New York City. Master's Thesis, Columbia University, New York, NY, USA, 2020. [CrossRef]

92. Liu, Y.; Yu, Z.; Song, Y.; Yu, X.; Zhang, J.; Song, D. Psychological influence of sky view factor and green view index on daytime thermal comfort of pedestrians in Shanghai. *Urban Clim.* **2024**, *56*, 102014. [CrossRef]
93. Zhu, H.; Nan, X.; Kang, N.; Li, S. How much visual greenery can street trees generate from a humanistic perspective? An attempt to quantify the canopy green view index based on tree morphology. *Forests* **2024**, *15*, 88. [CrossRef]
94. Sakamoto, S.; Kogure, M.; Hanibuchi, T.; Nakaya, N.; Hozawa, A.; Nakaya, T. Effects of greenery at different heights in neighbourhood streetscapes on leisure walking: A cross-sectional study using machine learning of streetscape images in Sendai City, Japan. *Int. J. Health Geogr.* **2023**, *22*, 29. [CrossRef] [PubMed]
95. Ren, X.; Li, Q.; Yuan, M.; Shao, S. How visible street greenery moderates traffic noise to improve acoustic comfort in pedestrian environments. *Landsc. Urban Plan.* **2023**, *238*, 104839. [CrossRef]
96. Frackelton, A.; Grossman, A.; Palinginis, E.; Castrillon, F.; Elango, V.; Guensler, R. Measuring walkability: Development of an automated sidewalk quality assessment tool. *Suburb. Sustain.* **2013**, *1*, 4. [CrossRef]
97. Distefano, N.; Leonardi, S. Fostering urban walking: Strategies focused on pedestrian satisfaction. *Sustainability* **2023**, *15*, 16649. [CrossRef]
98. Asgarzadeh, M.; Koga, T.; Hirate, K.; Farvid, M.; Lusk, A. Investigating oppressiveness and spaciousness in relation to building, trees, sky and ground surface: A study in Tokyo. *Landsc. Urban Plan.* **2014**, *131*, 36–41. [CrossRef]
99. Chung, W.K.; Chau, C.K.; Masullo, M.; Pascale, A. Modelling perceived oppressiveness and noise annoyance responses to window views of densely packed residential high-rise environments. *Build. Environ.* **2019**, *157*, 127–138. [CrossRef]
100. Xia, Y.; Yabuki, N.; Fukuda, T. Sky view factor estimation from street view images based on semantic segmentation. *Urban Clim.* **2021**, *40*, 100999. [CrossRef]
101. Lynch, K. *The Image of the City*; MIT Press: Cambridge, MA, USA, 1964.
102. Joye, Y.; Willems, K.; Brengman, M.; Wolf, K. The effects of urban retail greenery on consumer experience: Reviewing the evidence from a restorative perspective. *Urban For. Urban Green.* **2010**, *9*, 57–64. [CrossRef]
103. Rowe, A. *Jacobs: The Death and Life of Great American Cities*; Random House: New York, NY, USA, 1962.
104. Baobeid, A.; Koç, M.; Al-Ghamdi, S.G. Walkability and its relationships with health, sustainability, and livability: Elements of physical environment and evaluation frameworks. *Front. Built Environ.* **2021**, *7*, 721218. [CrossRef]
105. Bunds, K.S.; Casper, J.M.; Hipp, J.A.; Koenigstorfer, J. Recreational walking decisions in urban away-from-home environments: The relevance of air quality, noise, traffic, and the natural environment. *Transp. Res. Part F Traffic Psychol. Behav.* **2019**, *65*, 363–375. [CrossRef]
106. Tang, Z.; Ye, Y.; Jiang, Z.; Fu, C.; Huang, R.; Yao, D. A data-informed analytical approach to human-scale greenway planning: Integrating multi-sourced urban data with machine learning algorithms. *Urban For. Urban Green.* **2020**, *56*, 126871. [CrossRef]
107. Wang, L.; Han, X.; He, J.; Jung, T. Measuring residents' perceptions of city streets to inform better street planning through deep learning and space syntax. *ISPRS J. Photogramm. Remote Sens.* **2022**, *190*, 215–230. [CrossRef]
108. Perini, K.; Ottelé, M. Vertical greening systems: Contribution to thermal behaviour on the building envelope and environmental sustainability. *WIT Trans. Ecol. Environ.* **2012**, *165*, 239–250.
109. Ma, X.; Ma, C.; Wu, C.; Xi, Y.; Yang, R.; Peng, N.; Zhang, C.; Ren, F. Measuring human perceptions of streetscapes to better inform urban renewal: A perspective of scene semantic parsing. *Cities* **2021**, *110*, 103086. [CrossRef]
110. Garrido-Valenzuela, F.; Cats, O.; van Cranenburgh, S. Where are the people? Counting people in millions of street-level images to explore associations between people's urban density and urban characteristics. *Comput. Environ. Urban Syst.* **2023**, *102*, 101971. [CrossRef]
111. Olszewski, P.; Szagała, P.; Wolański, M.; Zielińska, A. Pedestrian fatality risk in accidents at unsignalized zebra crosswalks in Poland. *Accid. Anal. Prev.* **2015**, *84*, 83–91. [CrossRef] [PubMed]

Disclaimer/Publisher's Note: The statements, opinions and data contained in all publications are solely those of the individual author(s) and contributor(s) and not of MDPI and/or the editor(s). MDPI and/or the editor(s) disclaim responsibility for any injury to people or property resulting from any ideas, methods, instructions or products referred to in the content.

buildings

MDPI

Review

Exploring Carbon Emissions in the Construction Industry: A Review of Accounting Scales, Boundaries, Trends, and Gaps

Qinfeng Zhao [1,2,3,4], Zhirui Wu [4,5], Yi Yu [4], Tian Wang [4] and Shan Huang [1,2,3,*]

[1] The Architectural Design and Research Institute of Zhejiang University Co., Ltd., Hangzhou 310027, China; zhaoqinfeng0122@163.com
[2] The Center for Balance Architecture, Zhejiang University, Hangzhou 310028, China
[3] College of Civil Engineering and Architecture, Zhejiang University, Hangzhou 310027, China
[4] Faculty of Environmental Engineering, The University of Kitakyushu, Kitakyushu 8080135, Japan; f4dbb401@eng.kitakyu-u.ac.jp (Z.W.); e3dbb419@eng.kitakyu-u.ac.jp (Y.Y.); dawang_703122@163.com (T.W.)
[5] School of Civil Engineering and Architecture, Guizhou Minzu University, Guiyang 550025, China
* Correspondence: huangshanzju@gmail.com

Abstract: The construction industry, characterized by high energy consumption and carbon emissions, plays a pivotal role in climate change mitigation. This paper employs bibliometric analysis, based on 282 articles from the SCIE and SSCI in the Web of Science spanning 1992–2022, to explore research trends and themes in Carbon Emissions of Construction Industry (CECI). A manual review was conducted to identify challenges and possibilities concerning accounting scales, objects, boundaries, and methods in CECI research. Key findings include (1) temporal and thematic evolution, with a notable increase in research activity since 2015, primarily focusing on energy efficiency, sustainable development, green building technologies, and policy evaluation; (2) scale-specific gaps, as 80.7% of studies are conducted at macro (national/regional) or micro (building/material) levels, while city-scale analyses are significantly underrepresented, with only 13 articles identified; (3) object granularity deficiencies, with 74.8% of studies not distinguishing between building types, resulting in rural residential, educational, and office buildings being significantly underrepresented; (4) system boundary limitations, as few studies account for emissions from building demolition or the disposal and recycling of construction waste, indicating a substantial gap in life-cycle carbon assessments. Furthermore, the predominant reliance on the carbon emission factor method, along with embedded assumptions in accounting processes, presents challenges for improving carbon accounting accuracy. This review synthesizes insights into prevailing research scales, object classifications, system boundaries, and methodological practices, and highlights the urgent need for more granular, lifecycle-based, and methodologically diverse approaches. These findings provide a foundation for advancing CECI research toward more comprehensive, accurate, and context-sensitive carbon assessments in the construction sector.

Keywords: carbon emissions of construction industry; carbon neutrality goals; accounting boundary; research scale

1. Introduction

Since the industrial revolution, the emission of various types of greenhouse gases, especially CO_2, from human production and life has led to significant changes in the concentration of greenhouse gases in the atmosphere. Climate change caused by the greenhouse effect poses a great challenge to environmental protection and even human survival

and development [1]. Construction activities are characterized by high energy consumption [2], and the production of building materials [3], construction processes [4], building operations [5], and the disposal of waste from demolition [6] all contribute significantly to energy use and carbon emissions. The construction industry consumes one-third of the world's energy demand, and the entire building sector accounts for 39% of CO_2 emissions from energy use [7].

According to the World Cities Report 2022, the urban population accounted for 56% of the total global population in 2021 and is expected to grow to 68% by 2050. The increase in population will inevitably increase the construction of cities, and high construction demand will drive more Carbon Emissions from the Construction Industry (CECI) [8,9]. Against this backdrop, the decarbonization of the construction industry has garnered widespread attention. The methods of literature review, systematically summarizing the research findings of predecessors, deeply reflecting on the current state of carbon emission growth in the construction industry, and exploring effective strategies to curb further increases in its carbon emissions have become hot research directions.

Many scholars have summarized the development of construction technology and proposed a range of carbon emission management measures, from building materials and construction processes to operational energy efficiency, to curb the growth of CECI [10]. In terms of building materials, the use of low-embodied-energy materials has become a common solution [11]. Some scholars, through summarizing material properties, have found that replacing high-carbon components such as cement and aggregates in traditional concrete can effectively reduce material carbon emissions without compromising performance [12]. The continuous progress of alternative binders, new adhesives, and energy-saving production technologies has driven the research and application of zero-carbon concrete [13]. Meanwhile, as an emerging technology, bio-concrete can sequester CO_2 through carbonation, reducing carbon emissions while enhancing concrete strength [14].

Some scholars have focused on construction processes and pointed out that employing BIM technology for decision-making in the initial stage of a project can significantly promote the sustainability of buildings [15]. The use of prefabricated components can reduce embodied carbon emissions by 15.6% and operational carbon emissions by 3.2% [16]. More scholars have focused on building operational efficiency. Chastas reviewed the correlation between energy efficiency levels and carbon emissions in residential buildings [17], while Atmaca assessed the carbon footprint of residential buildings, finding that residents' daily energy use is a major contributor and needs to be closely managed [18]. Gao reviewed studies on carbon emissions in public buildings, finding that building characteristics, structure, and the application of digital technologies are key focuses in current carbon emission management [19].

The aforementioned studies are mostly centered on carbon reduction strategies and focus on specific subjects. Few studies have systematically reviewed and comprehensively summarized the development of CECI accounting research from the carbon source definition. In fact, the source definition is the foundation for the quantification and assessment of CECI. Some scholars have summarized the research progress in this field through bibliometric analysis or meta-analysis. Lai reviewed the quantification process of CECI and outlined the definition of carbon sources in existing studies from a stage perspective [20]. Wang divided the definition of carbon sources in existing studies of the construction industry into two aspects: stage and scope through bibliometric analysis [21]. To ensure the accuracy of CECI accounting results, it is essential to select appropriate research objects, determine the proper scale, and clarify the accounting boundaries [22].

Although some existing studies have recognized the importance of carbon source definition in CECI research, none have yet provided a comprehensive summary within an integrated framework. This review innovatively categorizes the carbon source definition into three dimensions: research object, scale, and boundary. It systematically reviews the development, current gaps, and limitations of CECI accounting studies. Specifically, Section 2 introduces the data sources and the methods used in the bibliometric and manual reviews. Section 3 presents the results of the bibliometric analysis. Section 4 summarizes the evolution of carbon source definition in CECI accounting based on manual evaluation. Section 5 provides an outlook on potential future research directions in the field. Finally, Section 6 presents the conclusions.

The main contributions of this study are fourfold. (1) It outlines the core research themes and development trends in CECI accounting. (2) It identifies the lack of attention to cities as medium-scale accounting units and emphasizes the importance of urban-scale studies for regional carbon mitigation goals. (3) It highlights the current neglect of end-of-life processes such as demolition and material recycling, underscoring the need to extend accounting boundaries to the full building lifecycle. (4) It points out the methodological limitations of relying solely on emission factor-based approaches and stresses the need for data transparency and diversified accounting methods to advance future research.

2. Literature Searching and Review Method

2.1. The Literature Retrieved

The data sources and retrieval strategies in this study are based on Science Citation Index Expanded (SCIE) and Social Sciences Citation Index (SSCI) in the WOS Core collection. These two indices are regarded as important data sources for bibliometric research.

Figure 1 shows the process of literature retrieval. Firstly, define the search terms and criteria to be used for retrieving the relevant publications, including the keywords, author names, publication years, and publication types. The publication period of the search literature is set to be 1992–2022, as research on carbon emissions has developed since 1992, when the United Nations Framework Convention on Climate Change was adopted.

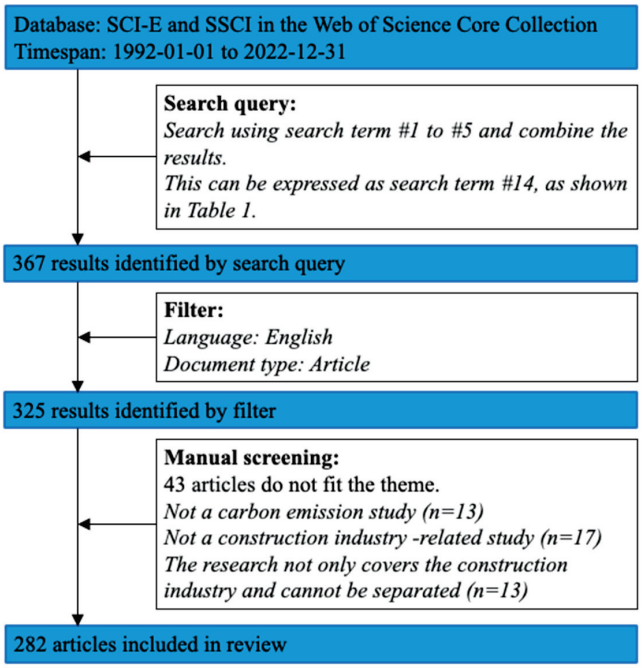


Figure 1. Literature retrieval process.

To ensure a comprehensive and thematically relevant dataset, a structured search strategy is applied. The search query combined carbon-related terms ("carbon emission*", "carbon peak", "carbon neutral*", "carbon footprint", "CO_2 emission*", etc.) with construction-related terms ("building sector", "construction sector", "building industry", "construction industry"). Here, the use of the asterisk (*) serves as a wildcard, allowing for the retrieval of various word forms and derivatives. The search was conducted using the Topic (TS) field, which retrieves records based on matches in the title, abstract, author keywords, and Keywords Plus. In addition, combinations with Title (TI) and Keywords Plus (KP) fields were used to improve specificity and ensure inclusion of high-relevance articles.

Five search terms were constructed according to different related phrases, and, by combining these search terms to simplify the search results, 367 publications were recorded. The search terms are shown in Table 1, and the final expressions for #6–#14 are shown in Appendix A, Table A1. Research articles are selected for analysis, as they generally provide higher-quality and more detailed information than other types of publications. Review papers, non-research articles, and non-English literature are excluded. A total of 325 research articles are retrieved from the WOS database, each including metadata such as authors, affiliations, country/region, publication year, source journal, title, abstract, and keywords.

Table 1. Search term used in WOS Core collection.

No.	Search Term	Publication	Article	Reviews	Other
#1	TS = ("carbon emission*" OR "carbon peak" OR "carbon neutral*" OR "carbon footprint")	40,944	36,878	3115	951
#2	TS = ("CO_2 emission*" OR "CO_2 peak" OR "CO_2 neutral*" OR "CO_2 footprint")	48,390	45,058	2794	538
#3	TS = ("building sector" OR "construction sector" OR "building industry" OR "construction industry")	17,842	16,051	1448	343
#4	TI = ("building sector" OR "construction sector" OR "building industry" OR "construction industry")	2815	2339	217	259
#5	KP = ("building sector" OR "construction sector" OR "building industry" OR "construction industry")	718	633	83	2
#6	#1 AND #3	977	856	117	4
#7	#2 AND #3	934	821	109	4
#8	#1 AND #4	189	170	17	2
#9	#1 AND #5	89	77	12	0
#10	#2 AND #4	181	162	18	1
#11	#2 AND #5	86	80	6	0
#12	#8 OR #9	265	235	28	2
#13	#10 OR #11	255	230	24	1
#14	#12 OR #13	367	325	39	3

To ensure the relevance of the selected literature, titles and abstracts are manually screened. Articles are excluded based on the following criteria: (1) the study is unrelated to carbon emissions; (2) the study is unrelated to the construction sector; and (3) the study involves multiple sectors without clearly distinguishable data for the construction industry. The screening is conducted sequentially according to these criteria. As a result, 43 articles are excluded, and 282 research articles are included for further analysis.

2.2. Bibliometric Tool

With the development of bibliometrics, many different types of knowledge mapping tools have been developed. VOSviewer, Publish or Perish, CiteSpace, HistCite, etc., are commonly used analysis tools, which have different characteristics and limitations.

Many literature databases have developed their own literature statistics systems relying on the huge literature foundation, such as Scopus, Google Scholar, and WOS. Users can obtain analysis results through simple operations while sub-searching the literature, which is convenient and fast. These web tools can only provide some simple bibliometric analysis, often only classifying the literature by publication date, publication, author, or type. The development of AI technology has also brought convenience to bibliometrics. Several AI technology-based web platforms have developed bibliometric tools. Such as "AMiner" and "wisdom.ai", which can automatically search the literature and generate analysis charts by simply entering keywords. However, these tools suffer from small literature databases and unclear data sources. There are also platforms that are similar to traditional bibliometric software and use records from literature databases to analyze the literature, such as "bibliometric.com".

Compared to emerging bibliometric platforms, traditional bibliometric software is complex to operate but has more powerful features. VOSview 1.6.20, which was developed at Leiden University in the Netherlands, has been selected for analyzing the contributions and collaborations of institutions and authors. It performs well in visualizing contributions and collaborations. The CiteSpace software (6.3.R1 Basic), invented by Prof. Chaomei Chen, is characterized by co-occurrence and co-citation analysis, which is advantageous in trend detection. Therefore, this software is used in this chapter for the co-occurrence of keywords and topics and the co-citation analysis of journals and authors.

2.3. The Process of Manual Review

The focus of this paper is on identifying key gaps in CECI research. Therefore, a more detailed manual review is conducted on the retrieved literature. To ensure the accuracy and relevance of the dataset, a manual review is conducted on all retrieved articles. In addition to reviewing titles, abstracts, and keywords, the main text is also examined, when necessary, to determine the study's primary focus. This process allows for more precise identification and classification of research themes.

To facilitate structured analysis, each article is manually coded along four thematic dimensions: research scale, research object, accounting boundary, and accounting method. These dimensions are selected based on commonly used classifications in the existing CECI literature and are refined through iterative reading of the main text.

The research scale is closely related to the object. The changes in the scale and object of research on CECI can well reflect the development of research in this field. For research scale, studies are classified into national, regional, city, or building levels. Articles without a clearly defined scale are marked as "undefined". For research objectives, studies are categorized into four types: the whole construction industry (WCI), multiple types of civil buildings (MTCB), a single type of civil building (STCB), and materials and others. STCB includes studies focused on a specific building type, such as residential, educational, or office buildings. If different types of civil buildings are included in the study objectives, they will be classified as MTCB.

The determination of the accounting boundary is the most important part of carbon emission research. Different accounting boundaries for the same research objectives will produce different accounting results. The accounting boundaries of previous studies are reviewed, and the accounting methods are discussed based on them. The accounting boundary is categorized into eight types: Construction (C), Materials (M), Operation (O), Waste (W), Construction & Materials (C&M), Materials & Waste (M&W), Construction, Materials & Operation (C, M&O), and Whole Life Cycle. Ambiguous cases are marked as "Other" or "Not Mentioned". For accounting methods, studies are classified into

four groups: emission factor methods, carbon intensity methods, hybrid methods, and input-output models, depending on how carbon emissions are quantified.

Each article is assigned to one or more categories within these dimensions through a consistent manual coding process. The frequency distributions of these classifications are analyzed statistically to identify dominant themes and research gaps, which are discussed in the subsequent results section.

3. Results of Bibliometric Analysis

3.1. Trends in Publishing

The distribution of publication dates for research articles on CECI provides insights into the pace of development and knowledge accumulation in this field. Based on the retrieved literature, the research on CECI began in 1998 and showed an increasing trend after 2006. Related publications grew rapidly after the Paris Climate Conference in 2015. The Paris Agreement has a huge impact on the energy policies of all countries, and the CECI has gradually become a hot topic.

Figure 2 displays publishing trends in 12 countries that have published more than five papers on the topic. China leads the way with 168 published papers, which is over half of the total. The annual number of published papers in China has been steadily increasing, reflecting the Chinese government's policy direction. The 13th Five-Year Plan for Controlling Greenhouse Gas Emissions in 2016 and the "Dual Carbon" Target in 2020 have been the driving forces behind this rapid growth. England, the United States, and Australia are also major contributors, with an increasing number of publications. These indicate that CECI research has entered a rapid development phase, particularly driven by major international climate agreements and corresponding policy influence.

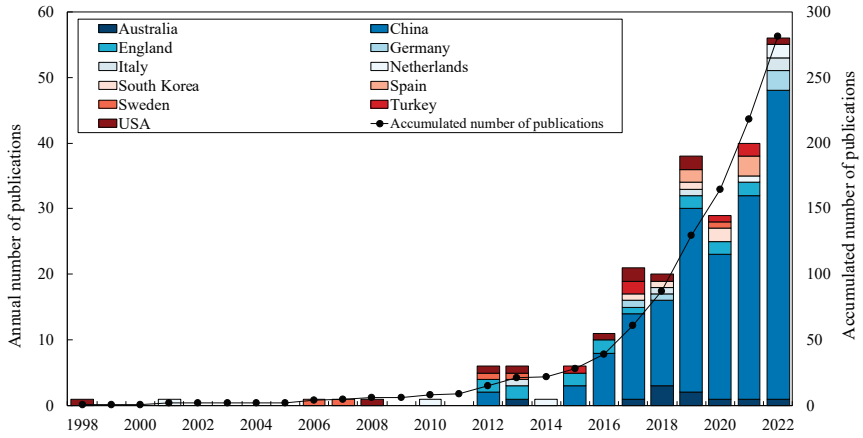


Figure 2. Annual trend of CECI research papers published.

3.2. Contribution and Collaboration

The analysis of the author's contribution and collaboration in CECI research can show the author's influence, which is conducive to quickly understanding the research situation of CECI. There are 884 authors who contributed to the study of CECI. A total of 13 authors have more than five papers; Table 2 lists these authors who made major contributions. Cai Weiguang, a professor at Chongqing University in China, has published 22 articles with a total of 1239 citations. Prof. Cai has not only conducted in-depth research on the CECI but also has a great influence in this field. Prof. Ma Minda, from Lawrence Berkeley National Laboratory, has a high average number of citations, indicating that his research is widely

recognized. Prof. Du Qiang from Chang'an University has published 10 articles and made great contributions to the research and development of CECI.

Table 2. The top authors with the most published articles in the field of CECI.

Rank	Author	Article	Citations	TLS
1	Cai Weiguang	22	1239	75
2	Ma Minda	12	890	30
3	Du Qiang	10	184	44
4	Chen Jindao	8	387	27
5	Hong Jingke	8	268	33
6	Ren Hong	8	284	33
7	Shen Liyin	8	603	30
8	Huo Tengfei	7	291	33
9	Shi Qian	6	354	19
10	Bai Libiao	5	53	22
11	Feng Wei	5	216	20
12	Lu Yujie	5	237	12
13	Wu Min	5	114	21

Figure 3 visualizes the total link strength, showing eight large clusters derived from the analysis of 110 authors who published more than two articles, as imported into VOSviewer. The connection between Cluster 1 and Cluster 5 indicates that extensive collaboration already exists in the CECI research area. The largest cluster is led by Prof. Cai Weiguang, and influential scholars, such as Prof. Huo Tengfei, Prof. Ren Hong, and Prof. Feng Wei, are members of the cluster. Ma Minda, another well-published professor, works closely with Prof. Cai and is the core of Cluster 2. Cluster 6, Cluster 7, and Cluster 8 exist independently, with less collaboration with scholars outside the cluster; this means that their research may have some uniqueness.

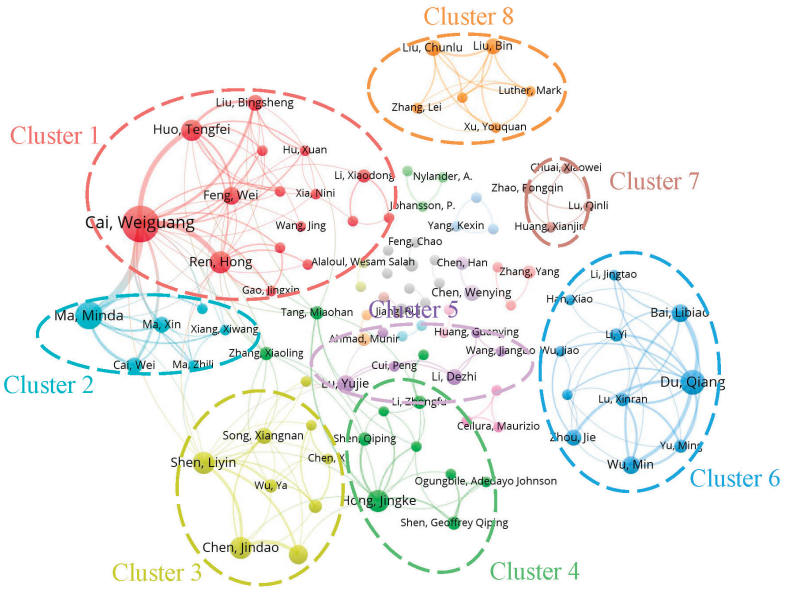


Figure 3. Collaboration between authors.

As shown in Figure 4, Chongqing University, as the core of the largest cluster, ranks first in both the total number of publications and total citations. They have contributed to a total of 43 published papers, accounting for 15.2% of the overall publications, which indicates their outstanding contributions to the field of CECI. Moreover, Chongqing University has established

close collaborative relationships with other institutions in the CECI field, as evidenced by a total link strength of 86. Thirteen research institutions have published more than six research papers related to CECI, as shown in Table 3. Hong Kong Polytech University, Tsinghua University, and Lawrence Berkeley National Laboratory ranked 2–4. They all belong to Cluster 1 and come from different countries or regions, indicating that cooperation in the field of CECI has been widely carried out in different regions. The four institutions ranked 5–8 are the cores of the other four clusters. The four clusters are not closely connected, and the inter-agency cooperation is mainly carried out within the clusters.

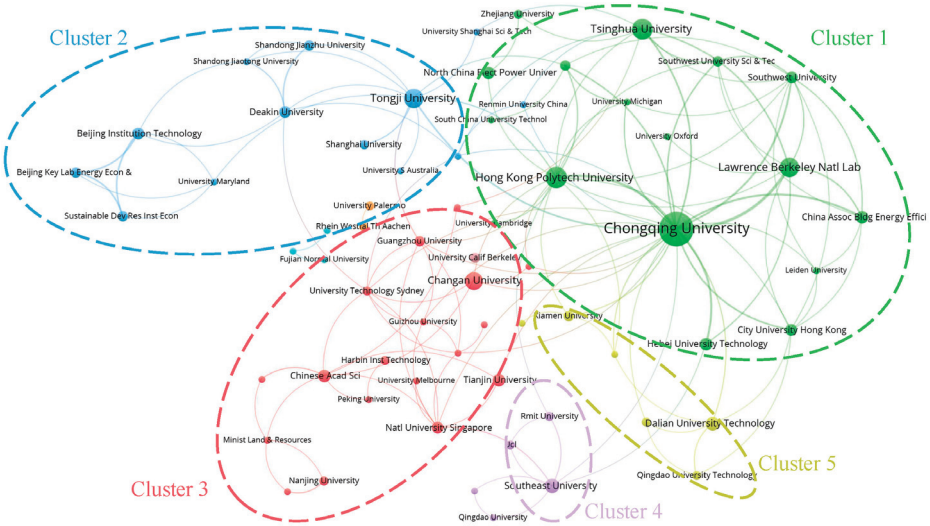


Figure 4. Collaboration between organizations.

Table 3. The top organizations with the most published articles in the field of CECI.

Rank	Organization	Country/Region	Article	Citations	TLS
1	Chongqing University	China	43	2041	86
2	Hong Kong Polytech University	Hong Kong, China	17	684	35
3	Tsinghua University	China	16	484	23
4	Lawrence Berkeley National Laboratory	USA	14	789	27
5	Tongji University	China	14	598	22
6	Chang'an University	China	12	195	9
7	Southeast University	China	8	253	15
8	Dalian University of Technology	China	7	77	10
9	China Association of Building Energy Efficiency	China	6	553	14
10	Chinese Academy of Sciences	China	6	159	12
11	Hebei University of Technology	China	6	152	10
12	North China Electric Power University	China	6	192	3
13	Tianjin University	China	6	134	7

The author and institution network analysis highlights a small number of highly influential researchers and organizations dominating the field. While certain clusters exhibit strong internal collaboration, overall global collaboration remains fragmented. Future research would benefit from more cross-institutional and international cooperation to enhance the diversity of perspectives and broaden methodological development.

3.3. Research Trend and Frontier

The use of keywords to understand research key points and frontiers is considered feasible and credible [23]. Co-occurrence analysis was performed using CiteSpace, with

keywords proposed by the authors and "Keyword plus" provided by the journals as sources of keywords. Using one year as a slice, the top 10% of keywords appearing in each slice were selected for analysis. A total of 150 keywords were analyzed. As shown in Figure 5, these keywords were divided into 10 clusters, covering areas such as energy policy, life cycle assessment, structural path analysis, building energy consumption, sustainability, energy efficiency, decoupling analysis, supply chain, and the application of artificial intelligence. The larger the keyword node, the higher its burst intensity. Topics such as "performance", "decomposition analysis", "life cycle assessment", "CO_2 emission", "energy savings", "emissions mitigation", and "scenario analysis" have been extensively studied.

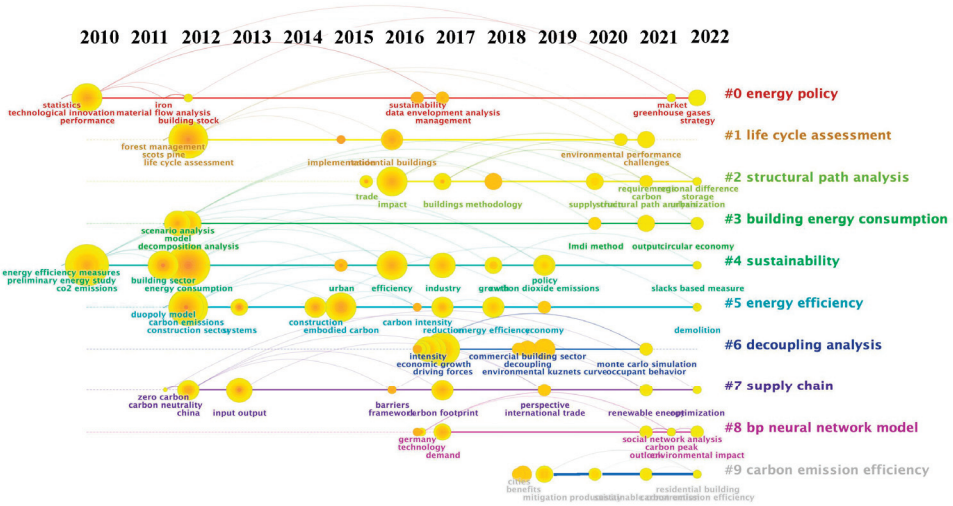


Figure 5. The keyword outbreak timeline.

Research on carbon accounting in the construction industry has witnessed a growing number of keywords since 2010, falling into four categories: carbon accounting methods, research objects, research purposes, and analysis methods. The methods include "input-output" and "life cycle assessment", while the research objects encompass "China" and the "construction sector". The research purposes involve "climate change mitigation" and "sustainability", and analysis methods encompass "decoupling analysis", "bp neural network model", and "decomposition analysis". These categories reflect the wide interest in carbon accounting research within the construction industry.

From the evolution of keywords over time, carbon accounting research in the construction industry is experiencing a phase of rapid development, with research content gradually shifting from a single-dimensional to a multi-dimensional analysis and an increasingly diverse range of exploration angles. Since 2015, the research focus on energy efficiency, sustainable development, green buildings, and policy evaluation has intensified, reflecting global and national efforts to mitigate carbon emissions in the construction sector. Below is a detailed analysis of these emerging trends:

Energy Efficiency: Hydrogen fuel cell combined heat and power (CHP) systems and smart technologies (such as BIM and digital twins) have become essential tools for enhancing building energy efficiency, optimizing energy use, and reducing carbon footprints.

Sustainable Development: The rise of climate-positive and circular buildings is driving architectural design towards low emissions, material reuse, and waste reduction, helping to minimize the environmental impact of construction.

Green Buildings: The adoption of zero-energy and zero-water technologies, green roofs, and degradable or recyclable materials is further advancing the green building movement, lowering resource consumption and carbon emissions.

Policy Evaluation: Policy supports and interdisciplinary research play a crucial role in optimizing green building policies, offering effective incentives and guidance to steer the construction industry towards a low-carbon future.

Scenario Analysis: Scenario analysis and predictive modeling enable researchers to simulate future carbon emission trends, providing scientific support for policy development.

The keyword analysis further reveals a growing diversification in research themes, with an evolution from single-dimensional to multi-dimensional analytical frameworks. However, there is still a need to deepen methodological integration, especially in the application of artificial intelligence, decoupling analysis, and predictive modeling. In addition, the overlap and segmentation among thematic clusters suggest untapped opportunities for more interdisciplinary synthesis and cross-sectoral dialogue in future CECI research.

These emerging trends illustrate a shift in the construction industry towards integrating advanced technologies and adopting a holistic approach to reduce carbon emissions. Notably, keywords such as "BIM", "prefabrication", "renewable energy", and "low-carbon materials" have surged in frequency since 2015, frequently co-occurring with research themes like "LCA", "energy efficiency", and "scenario analysis". This pattern suggests that technological advancements are not only being studied as research subjects but also enabling new methodological approaches and driving the evolution of CECI research. In parallel, industrial policies such as China's Dual Carbon strategy, the 14th Five-Year Plan for Building Energy Efficiency, and green building evaluation standards have actively promoted the adoption of these technologies, further reinforcing their presence in academic discourse. A feedback mechanism has thus emerged, wherein policy drives technological deployment, which in turn shapes academic focus, and research outcomes feed back into policy refinement. Recognizing this interplay is essential for understanding how CECI research has evolved into a more integrated, data-informed, and practice-oriented field.

3.4. Research Hotspot

In the academic literature, citations are used to demonstrate the connection between the cited literature and the citing literature, while co-citations show the relationship between citing literatures. The frequency of co-citation not only reflects the relevance of the study but also highlights emerging hot topics. Table 4 displays the top 10 co-cited papers in research on CECI, including the time of the co-citation outbreak. Total citations for these papers were obtained from the WOS database, and all 10 papers were published after 2015.

Table 4. Top 10 most co-cited references.

No.	Cited References	Co-Citation Times	Burst, Strength, Begin-End	Citation Times
1	Lu et al., 2016 [24]	33	2.12, 2018–2022	131
2	Shi et al., 2017 [25]	30	-	122
3	Huang et al., 2018 [26]	30	3.09, 2019–2022	263
4	Tan et al., 2018 [27]	27	-	106
5	Zhou et al., 2018 [28]	26	2.73, 2020–2022	169
6	Lin & Liu, 2015 [29]	25	6.00, 2017–2020	91
7	J. Chen et al., 2017 [30]	24	-	96
8	Hong et al., 2016 [31]	24	1.64, 2016–2017	129
9	Y. Wu et al., 2018 [32]	22	-	134
10	P. Wu et al., 2019 [33]	21	3.91, 2020–2022	66

How to find the drivers of CECI is the hottest topic. Lu applied the LMDI method in CECI research, identifying the fact that construction materials were the largest contributor to increased emissions, while energy intensity reduced emissions [24]. Lu's research

provides a valuable reference for future studies and initiates a co-citation burst in 2018. Based on this research, P. Wu introduced the concept of the whole life cycle, suggesting high development density and improved energy efficiency as ways to reduce operational emissions [33]; Y. Zhang et al. incorporated non-combustion processes into LCA and proposed controlling unnecessary construction activities and improving material production efficiency as means to reduce China's CECI [34]; Li et al. decomposed CECI drivers in different provinces, and strategies for achieving peak CECI in China were proposed [35]. The structural decomposition analysis is another way to find drivers of carbon emissions that has also attracted a lot of attention. By using this method, Shi found that final demand is the largest contributor to CECI growth, and that the high reliance on the construction sector in the Chinese economy is driving the growth of CECI [25]. Building on Shi's method, Chen argued that the energy sector and the building materials sector are the main contributors to China's CECI [30], which is also recognized and ranked seventh in Table 4.

How to account for CECI is another hot topic. The use of regional input–output analysis to examine the carbon footprint has attracted wide attention. Huang [26] and Hong [31] accounted for global and China CECI by this method, discovered that China emerges as the largest contributor to CECI, and the cross-regional importation of building materials has led to the central regions of China assuming the carbon emissions for the eastern coastal regions. The use of predictive models to account for carbon emissions from building operations has also gained acceptance. Tan's bottom-up model considered important variables, such as population, urbanization rate, and building size, and suggested that cross-sectoral synergies are more effective than single-sectoral reductions [27]. Zhou, utilizing the Berkeley Lab's China 2050 Demand Resource Energy Analysis Model to project building growth rates and building envelope efficiency in China, acknowledges the potential of building energy efficiency technologies, systems, or practices to reduce carbon emissions [28]. However, Zhou also emphasizes that strict policies are essential to address the multiple barriers hindering the implementation of these technologies.

In addition, the decoupling analysis of CECI from economic development [32] and the policy-based carbon reduction potential assessment are also hot topics [29].

Co-citation analysis identifies the most influential studies and research themes in the field. These studies have established methodological foundations for carbon accounting and driver identification. However, the dominance of studies from China and the limited representation of policy-focused comparative studies indicate a need for broader geographical inclusion and more policy-oriented analyses to guide practical decarbonization strategies.

4. Manual Review

According to bibliometric analysis, research on CECI is a vast and complex topic that has led to many related studies. Due to the diverse research objectives, scales, and objects, as well as differences in accounting and analytical methods, a manual review is necessary to explore further and determine the research status, identify gaps, and uncover future research direction in the area of CECI.

4.1. Research Scales and Objects

Carbon emission studies rely on the calculation of energy and emission-related data, and the lack of basic data is an important factor limiting the development of comprehensive and accurate carbon emission accounting. As shown in Figures 6 and 7, the collected literature is categorized separately by research scale and research object; residential, public, commercial, educational, and office buildings are widely studied civil buildings.

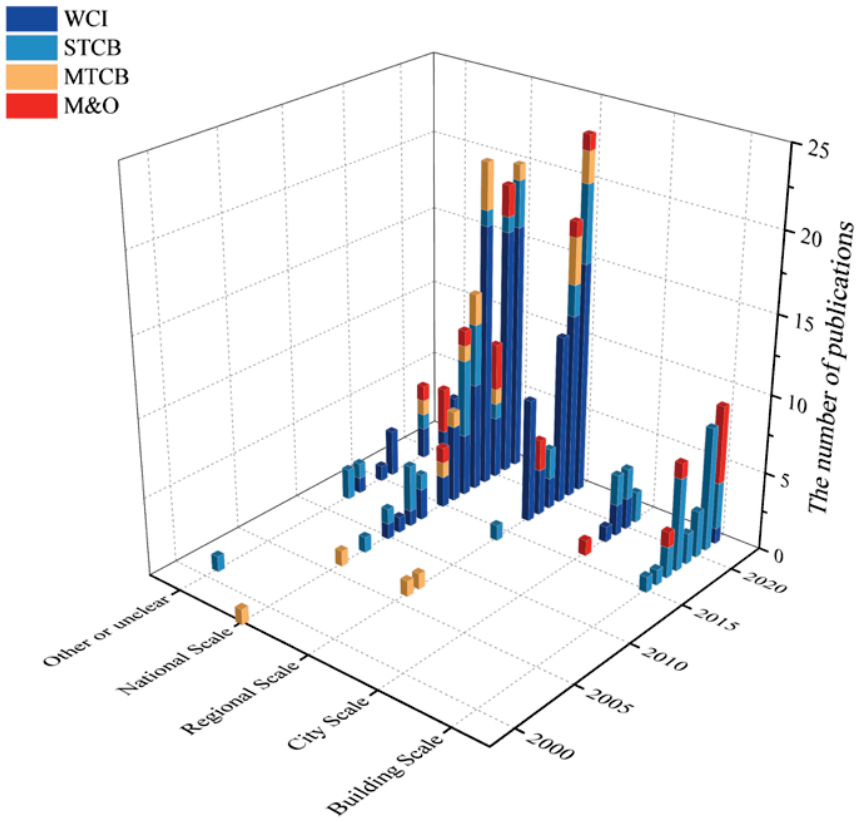


Figure 6. Research scale and object of publication.

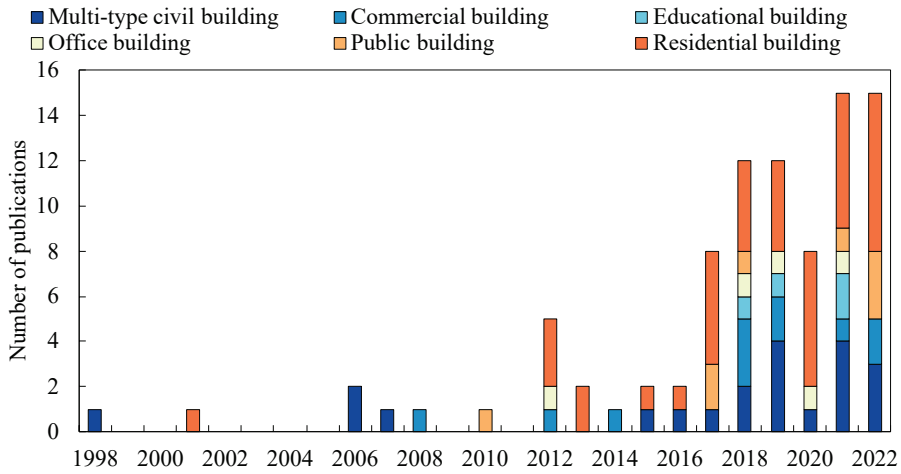


Figure 7. Publication of research on civil buildings.

(1) National scale

Exploring the carbon emissions of civil buildings on a national scale is the earliest study. In 1998, Koomey conducted an operational carbon emissions projection for U.S. residential buildings based on U.S. Department of Energy report data for commercial and residential buildings throughout the United States [36]. Up to now, civil buildings are still the mainstream research object, and residential building is the hot spot [37]. Calculating CECI for residential buildings at the national scale to explore the costs and strategies for carbon reduction has long been a focus [38,39]. In recent years, what strategy to adopt and how to develop a reasonable carbon reduction roadmap have become hot topics [40].

With the focus on climate issues, other types of civil buildings have also been studied at a national scale, with a focus on energy efficiency and improvement strategies [5,41]. Ma's team focused on the drivers of carbon emissions from the operation of public buildings [42], commercial buildings [43,44] in China based on the CMBECSS 2.0 database, and compared the differences between China and the USA [45].

The WCI is the main object of national-scale research. In the early days, researchers were focused on the impact of patents, policies, behaviors, standards, and materials on the construction industry [46,47], without accounting for the energy consumption or carbon emissions of the WCI. After Kucukvar and Tatari introduced input–output models to assess the sustainability of the construction industry [48], major carbon-emitting countries and even the globe's CECI were widely carried out [49,50]. To date, the exploration of emission reduction pathways at the national scale [49,51] and carbon transfer between countries [52] remains a hot topic.

(2) Regional scale

Research at the regional scale began in 2006, and its development history is similar to that of the national scale. Initially focusing on MTCB, Johansson conducted a study of carbon emissions from electricity and primary energy demand for heating residential and office buildings in southern Sweden [53,54]. As research progressed and data became publicly available, STCB studies were conducted. Kahn examined commercial building electricity carbon emissions in the western United States [55], and Ma studied the carbon intensity and operational carbon transition of commercial buildings in the top five city clusters in China [56,57]. The regional scale WCI carbon emissions study started in 2017. Hu compared the CECI performance by states in Australia [58]. Li accounted for China's provincial CECI and predicted carbon peaking [59]. Accounting for and comparing carbon emissions and influencing factors across Chinese provinces has been widely explored [60].

Compared with the national scale, the study of civil buildings at the regional scale is carried out later. The reason for this is the non-disclosure and lack of data. Kahn's research was made possible by a partnership with the power company [55]. Regional scale CECI research in China began to break out after 2016, thanks to the publication of China Building Energy Consumption Study Report, which proposed a series of data processing methods to remedy the problems of changing caliber, missing indicators, and incomplete data of statistical yearbooks [61]. Since then, research on energy consumption and carbon emissions of civil buildings at the regional scale has been better carried out [62].

(3) City scale

Only a few studies have examined CECI at the city scale. Hung quantifies WCI carbon emissions in Hong Kong, China [63]. Kamei assesses and predicts city transformations in Tokyo, Japan, where carbon emissions from buildings are an important indicator [64]. Balali assesses passive measures to reduce energy consumption in buildings using Shiraz, Iran, as an example [65]. Residential buildings and commercial buildings are popular research objects. Ma et al. evaluated the CECI of commercial buildings in four Chinese municipalities, Beijing, Shanghai, Chongqing, and Tianjin [56]. Esch-sur-alzette is the second most populous city in Luxembourg, and Mastrucci assessed the potential environmental impact of the renovation of residential buildings in this city [66].

These studies have been conducted for large cities or cities with special status, and few studies have investigated ordinary cities. City-scale CECI has not yet been in-depth. This is caused by the difficulty of obtaining municipal-level data, for which Shan proposed a method to estimate the city-level through provincial-level data [67]. Zhao applied this method to accounting for CECI in Hangzhou, China [22]. Some scholars attempted to

address the problem using a downscaling approach, estimating city-scale carbon emissions from provincial energy data and gridded socioeconomic parameters [68].

(4) Building scale

The study of building scale has been a hot topic of research [69]. Compared to other scales, building scale research has been widely studied due to the single object and the fact that complete data can often be obtained directly from the builder, user, etc.

These studies have usually focused on the building itself, without extending the results to the construction sector and without using "construction sector" as a keyword. In the literature retrieved in this paper, such studies are conducted from the perspective of an STCB, using a bottom-up approach to carbon accounting by analyzing the energy, material demand, and C&D waste output of a specific building. Atmaca conducted a carbon emission assessment of two residential buildings in Turkey based on construction drawings, energy consumption data, etc., provided by the construction company [70]. Huang used a life-cycle assessment of Fuzhou University's dormitory buildings based on tender information, utility bills, and maintenance reports provided by the university, with carbon emissions as one of the indicators [71].

It is now the mainstream to conduct studies on the carbon emissions of the WCI at a large scale, like national or regional. Micro-scale carbon emission accounting with case buildings as the research object has also received extensive attention. In contrast, city-scale studies at the meso-level are limited, and limited to a few cities, leaving a lack of basis for assessing the development of the city-scale construction industry and formulating policies. As an important implementation unit for the carbon target, it has become imperative for cities to strengthen the accounting of CECI at the city scale.

4.2. Accounting Boundaries and Methods

Accounting boundaries and methods for carbon emissions from the construction industry often determine each other. As shown in Figure 8, the accounting boundaries of previous studies are reviewed, and the accounting methods are discussed based on them. Among the single-phase boundaries, building operation was the most frequently used, followed by construction and materials, accounting for 29.6%, 9.1%, and 9.5% of the total publications, respectively. Only four studies focused on the demolition phase, indicating a research gap in carbon emissions from building demolition and waste reuse. In addition, some studies accounted for carbon emissions in multiple phases, with C&M and whole life cycle being the most common, accounting for 28.9% and 6.3% of the total publications, respectively.

Building operations serve as the largest contributor to carbon emissions throughout the entire lifecycle of a building [59], and are a key focus for carbon reduction efforts. Carbon emissions during this stage primarily originate from daily energy consumption by users to maintain a comfortable living environment and support household and work-related activities. In studies with detailed energy consumption data, the carbon emission factor method is the most commonly used accounting method [72], as shown in Formula (1). Secondary energy sources, such as electricity and heating, as well as primary energy sources, like natural gas and liquefied petroleum gas, are the primary forms of energy consumed. The carbon emission factors for secondary energy are typically sourced from energy supply sectors or government data [73], while the emission factors for primary energy are calculated using Formula (2).

$$CE = \sum_1^n Q_q \cdot EF_q \quad (1)$$

$$EF = V_c \cdot V_u \cdot R_c \cdot 44/12 \quad (2)$$

where CE denotes carbon emission, Q_q denotes the energy q consumption, EF_q denotes the carbon emission factor of energy q, V_c denotes low heating values, V_u denotes carbon content per unit of heating value, R_c denotes the rate of carbon oxidation, and 44/12 denotes the transformation coefficient from carbon to CO_2.

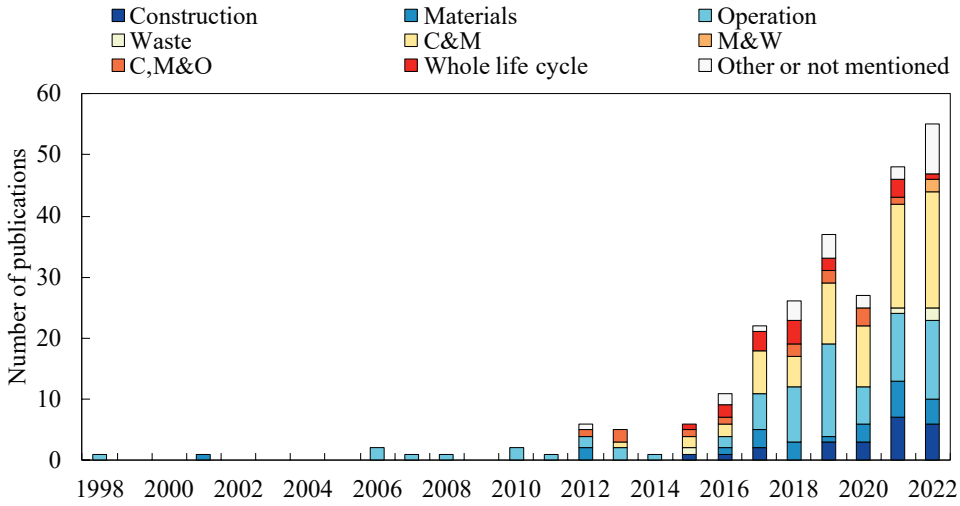


Figure 8. Carbon emission accounting boundaries for publications.

When energy consumption data for building operations are missing or when carbon emissions need to be predicted for a yet-to-be-built structure, the carbon emission intensity method is often employed. As shown in Formula (3), this method uses floor area and carbon emission intensity to estimate the CECI of building operations [74]. Carbon emission intensity is typically obtained from historical data or similar studies. Tan used the heating energy consumption data in the statistical yearbook to measure carbon emission intensity, and to account for carbon emissions and reduction potential [27]. Ma uses the Kaya equation and LMDI method to measure the carbon intensity of buildings to account for the operational carbon emissions of commercial buildings in China [43].

$$CE = FA \cdot CI_{area} \quad (3)$$

where FA denotes floor area and CI_{area} denotes the carbon emission intensity.

Using software or models to predict operational carbon emissions is another common approach. The incorporation of these tools allows for the consideration of more variables in the accounting process, thereby obtaining carbon emission data with higher resolution. Cellura uses TRNSYS to model buildings and simulate the impact of climate change on building operating energy [69]. Satre-Meloy uses Scout, an open-source software program developed by the U.S. Department of Energy, to estimate carbon emissions [75]. This program provides hourly data and is widely used. In addition, the C^3IAM/NET-Building mode [76], AIM/Enduse model [77], etc., are also applied to operational carbon accounting.

The production process of building materials is considered the most carbon-intensive stage in the whole lifecycle of buildings, due to the significant emissions released during raw material extraction, manufacturing, transportation, and other related processes. Carbon emission accounting with building materials as the boundary often relies on the carbon emission intensity method. As shown in Formula (4), the total carbon emissions of building materials are calculated by material consumption and material carbon intensity. Material

carbon intensity data are often obtained from manufacturers or previous studies. The life cycle assessment method, which splits the carbon emission process of materials into production, transportation, and installation processes, is a common method in studies that use materials as the accounting boundary [78]. Relying on this method, prediction models for building materials carbon emission have also been developed and applied. These models predict the carbon emissions of building materials by calculating the demand for those materials [46].

$$CE = \sum_1^n M_i \cdot CI_i \tag{4}$$

where M_i denotes demand for building materials i and CI_i denotes the carbon emission intensity of building materials i.

The construction of buildings is an extremely broad activity, encompassing a series of engineering tasks ranging from site preparation, foundation construction, main structure construction, to interior decoration and equipment installation [74]. During these activities, carbon emissions primarily originate from the consumption of fossil fuels such as diesel and gasoline by heavy machinery and transport vehicles, as well as from the electricity consumption of some smaller equipment [79]. For the purpose of construction cost accounting, the construction party will meticulously record energy consumption [80]. Consequently, the process of carbon emission accounting with construction as the boundary is straightforward, often directly adopting the carbon emission factor method. The accounting results are often used to analyze the relationship between the construction industry and social and economic development [81].

The relationship between building materials and construction is closely intertwined, as the process of material use is essentially the process of building construction. Some scholars combine these two boundaries and calculate carbon emissions from both materials and construction together, calling it carbon emissions of the building materialization process, or C&M boundary carbon emissions. As shown in Formula (5), some studies calculate construction and materials boundary emissions separately, then sum them to obtain C&M boundary emissions.

Based on this approach, some studies have considered the material reuse, as in Formula (6). Some scholars refer to this approach as the simplified LCA method [32], stating it includes the carbon emissions of C, M&W boundaries. However, this paper classifies these calculations as C&M, since this method only deducts carbon emissions from reused materials and does not consider emissions from waste treatment and material recycling.

$$CE = \sum_1^n Q_q \cdot EF_q + \sum_1^n M_i \cdot CI_i \tag{5}$$

$$CE = \sum_1^n Q_q \cdot EF_q + \sum_1^n M_i \cdot CI_i \cdot (1 - \varepsilon_i) \tag{6}$$

where ε_i denotes the reuse rate of material i.

In recent years, input–output models have increasingly been applied in the field of carbon emissions. As shown in Formula (7), this method establishes the relationship between demand in the construction industry and the supply from related sectors, calculating the carbon emissions from material, energy, and other sectors driven by construction demand [22]. These emissions are typically referred to as indirect CECI. Adding the fossil energy carbon emissions from the construction site results in the C&M boundary carbon emissions [82]. Some studies further include operational carbon emissions on top of the C&M boundary [33], forming the C, M&O boundary analysis.

$$CE_I = \sum_1^n (C_{a,b} / X_{a,b}) \cdot (X \cdot k_{a,b}) \tag{7}$$

where C_I denotes indirect carbon emission, $C_{a,b}$ denotes the direct carbon emissions of sector a in region b, $X_{a,b}$ denotes the total output of sector a in region b, $C_{a,b}/X_{a,b}$ represents carbon emission factor, X denotes the total output of the construction sector, and $k_{a,b}$ denotes the construction industry's complete consumption coefficient to sector a in region b.

While input–output models provide a macro-level understanding of indirect carbon emissions, they are limited by low data granularity and sectoral aggregation. The IO tables used are often based on national or regional economic statistics, which lack the spatial, temporal, and technological detail required for building-level analysis. In addition, the use of averaged emission factors across sectors introduces uncertainties and may lead to biased results, particularly when comparing different project types or locations.

Studies that use the whole life cycle of buildings as the accounting boundary are the most typical. These studies usually use LCA combined with carbon emission factor method to divide the whole life cycle of a building from "cradle to death" into several stages and obtain the whole life cycle carbon emissions of a building by accounting for carbon emissions in each stage and summing them up, such as Formula (8). This approach is often referred to as a process-based method. Evangelista divided the whole building life cycle into pre-operational phase, operational phase, and post-operational phase, to account for the carbon performance of a typical residential building in Brazil [83]. Huang evaluated the environmental costs of campus buildings in China by accounting for five phases [71]. Based on process-based LCA methods, several CECI accounting tools have been developed, and it has become a popular method to quickly calculate CECI with the help of accounting tools [84].

$$CE = \sum_1^m CE^s = \sum_1^m \sum_1^n Q_q \cdot EF_q \tag{8}$$

where CE^s denotes carbon emission from stages.

Hybrid LCA methods that combine different approaches to accounting for carbon emissions have also been used in some studies [85]. Zhang employed the input–output method to account for carbon emissions in the construction and demolition phases, and the carbon emission factor method to account for carbon emissions in the operation phase [86]. This hybrid approach is sometimes referred to as input–output LCA. Although hybrid LCA attempts to balance the detail of process-based LCA with the comprehensiveness of input-output models, it still faces critical challenges. The integration of data from heterogeneous sources can result in inconsistencies in emission boundaries, units, or system assumptions. Moreover, hybrid methods partially inherit the data quality limitations of IO models, including coarse sector classifications and outdated statistical inputs. These issues reduce the comparability and reliability of hybrid LCA outcomes, especially in cross-regional or cross-sector analyses.

However, as studies use Waste as the accounting boundary, which is still in the emerging stage [87], accounting for carbon emissions in the construction industry over the whole life cycle has some limitations. Some studies exclude the disposal of C&D waste from the boundary, calculating only the carbon emissions from the demolition activity [88]. Others assume all C&D waste is disposed of in landfills, overlooking the carbon reduction potential of material reuse [89]. This is largely due to the lack of a well-developed accounting framework. In the limited research available, process-based LCA methods are often used, calculating carbon emissions by dividing waste generation, recycling, and final disposal into separate stages to assess energy consumption. The disposal of concrete and metals is a key focus [90]. Some studies also consider both materials and C&D waste, using an emission factor approach to calculate carbon emissions from production, transportation, disposal, and recycling of materials based on material recycling concepts [91].

The determination of accounting boundaries is the basis of carbon emission studies, and the standardization of the boundary is particularly important. In single-phase boundary studies, the calculation process and methods are simple, with carbon emission factor methods and carbon intensity methods being commonly used. For multiple phase boundary studies, the accounting boundary is complicated, and the carbon emission accounting is usually performed by mixing multiple methods or summing up after accounting in phases.

Research on CECI is still in its early stages, and several issues have been highlighted by previous studies. First, there is a degree of ambiguity in boundary definitions, as building demolition, waste disposal, and recycling are often left out [92]. Accounting methods are also still uncertain; different accounting methods for the same boundary often yield different results [93]. Moreover, accounting methods are highly dependent on carbon emission factors or carbon intensity factors. These data are typically sourced from suppliers or from previous studies based on individual building or project measurements. Using data from different sources will likely lead to biased accounting results, making it difficult to compare data between different regions, organizations, and projects.

Although national- and building-scale studies dominate current CECI research, our analysis reveals a significant lack of studies at the city scale. This gap is critical because cities are often the key operational units for implementing carbon reduction targets, such as urban carbon peaking and low-carbon planning initiatives. Without reliable city-scale emission accounting models and data, urban policymakers may face difficulties in designing evidence-based interventions. Similarly, the limited research on specific building types may hinder the development of targeted policies for schools, offices, or rural residential buildings. These findings suggest a misalignment between academic research and policy needs, highlighting the importance of future studies that more directly support the formulation and evaluation of low-carbon policies.

5. Future Research in CECI

This study reviews the literature on CECI from 1992 to 2022, summarizing it from the perspectives of study subjects, scales, accounting methods, and boundaries, with a view to providing directions for CECI research. The literature search was conducted through WOS and does not cover all studies completed.

While current research primarily focuses on macro and micro scales, there is a significant gap at the city scale. Cities are the main spaces of population concentration [94,95] and production activities [96], and they are also areas of concentrated resource consumption [97] and environmental load [98,99]. Studies have demonstrated the inequity in carbon emissions between cities due to transboundary CO_2 flows [100]. With environmental policies tightening in more developed cities, high-emission industries often relocate to neighboring cities. Differences in energy technology and industrial standards in these areas may further increase overall emissions [22]. Policymakers should consider city-scale perspectives when developing policies, identifying emission sources and locations, revealing intercity carbon flows, and uncovering the driving forces of carbon emissions to prevent undesirable carbon leakage.

In contrast, there are positive examples, such as Tianjin Eco-City, which integrated various boundary-based carbon reduction strategies from its initial planning stages. These strategies include the use of energy-efficient building materials, prefabrication techniques during construction, and a smart energy management network during operation [101]. In particular, the complementary relationship between intercity energy supply and carbon reduction has enabled an annual reduction of 100,000 tons of CO_2 emissions solely through green electricity trading with surrounding areas [102].

Residential buildings have been fully explored from the perspective of carbon reduction cost [38], technology application [103], and regional differences [104], and the accounting boundary has covered all stages of the whole life cycle [84]. However, these studies do not distinguish between urban and rural areas or take urban dwellings as the subject of study [105]. Rural housing and urban housing have differences in structure, materials, thermal performance, etc., and there is a large stock of rural housing [106]. Research on commercial buildings has also been carried out in depth [107]. Ma has conducted carbon accounting, driving force analysis, carbon emission reduction prediction, and economic decoupling analysis for commercial buildings at national, regional, and city scales, respectively [57]. This research demonstrated that China's series of building energy-saving efforts have made substantial contributions to carbon reduction in commercial buildings, suggesting that these efforts should be further implemented [43,44].

Fewer studies have been conducted for office buildings and educational buildings. With the development of urbanization, the demand for office buildings will increase. Educational buildings are different from other civil buildings in terms of indoor environment demand and usage behavior due to their special characteristics [108]. With the strengthening of carbon emission control and energy conservation needs [109], further segmentation of civil building types in research will help stimulate technological innovation and promote technological development. Future research within CECI should focus on the carbon emissions of rural residential buildings, educational buildings, and office buildings, using modeling to analyze carbon characteristics by building type. This approach would support the development of more tailored carbon reduction strategies.

In terms of accounting boundaries for carbon emissions, the material, construction, and operational boundaries have been extensively studied, while studies of the demolition phase are often conducted through assumptions. One study estimates that energy consumption during demolition accounts for only 9% of the construction phase [86], another estimates approximately 90% [110], and yet another suggests that demolition represents just 0.2% of a building's total lifecycle primary energy consumption [70]. The substantial disparity between the estimated percentages of energy consumption during the demolition phase of a building among various studies greatly exacerbates the level of ambiguity in carbon accounting. The carbon emissions from waste disposal and material recycling are often neglected [111]. This reveals a gap in the research on carbon emissions from building demolition and waste disposal processes. However, a study from Kitakyushu, Japan, demonstrated that comprehensive recycling of construction waste could provide up to 6.8% carbon reduction potential for the entire construction industry [87]. Given the large number of old buildings currently facing demolition or renovation, and the negative environmental impact of solid waste landfills [7,112], there is an urgent need to supplement recycling of building demolition and construction waste within the CECI study's accounting boundary.

In addition, the research on CECI also suffers from a deficiency of accounting methods. The standardization of carbon emission research methods in the construction industry is low, and a set of reliable and scientific assessment methods and index systems cannot be formed to comprehensively assess CECI. Current accounting methods rely heavily on the carbon emission factor method, the LCA method, the input–output method, and the carbon intensity method, all of which are accounting methods based on the carbon emission factor method. Accounting often uses previously measured carbon emission factors, which do not accurately evaluate the status of carbon emissions and demonstrate the differences between building projects. It will be a major issue to introduce methods such as the monitoring method [113] and mass balance method [114,115], which have been fully applied in other disciplines, into the carbon accounting of the construction

industry and to establish a standard and reliable carbon accounting system. At the same time, local policy assessment, knowledge sharing, and data standardization should be strengthened, municipal policies should be assessed, regional best practices should be adopted, and an open and standardized database of emission factors should be created in order to improve the accuracy of carbon accounting and to enhance cooperation on carbon emission reduction.

Given the identified gaps, future research should focus on expanding the scope of city-scale studies to better represent the complex carbon dynamics across cities. This could involve using spatial downscaling techniques or multi-source data integration to account for municipal-level emissions more accurately. For underrepresented building types, such as educational and office buildings, further investigation can leverage BIM to analyze specific energy use patterns and materials. Addressing the demolition phase in the lifecycle requires process-based LCA methods combined with waste recycling assessments to capture carbon flows in construction waste management effectively. Integrating these methodologies can enrich the current CECI framework and enhance accounting accuracy across diverse building categories and stages.

6. Conclusions

The study of CECI is a complex process. As one of the main contributors to carbon emissions, reducing carbon emissions throughout the whole lifecycle of buildings has become an urgent and practical issue. In this study, we conducted a bibliometric analysis and manual review of 282 previous studies on CECI. The aim was to understand the challenges and possibilities in this field. The focus on carbon emission accounting objects, scales, and boundaries is the innovation point of this paper.

The bibliometric analysis revealed that the research system on CECI is in a stage of vigorous development. Core keywords were identified, including “performance”, “decomposition analysis”, “life cycle assessment”, “driving forces”, “embodied carbon”, and so on, which can be classified into the following categories: carbon accounting methods or systems, research objects or accounting boundaries, research purposes, and carbon emissions analysis methods.

Through manual review, it was found that (1) large and small scales of research objects, such as nations or buildings, have been emphasized in carbon emission research, while medium-scale research, represented by cities, has been neglected. Cities are important units for implementing carbon caps and carbon neutrality. Conducting carbon emission accounting at the city scale will be a key focus of future research. (2) Civil buildings have been widely studied. Different types of civil buildings have significant differences in carbon emissions. One future research direction for CECI is to investigate how to specifically conduct carbon emissions research on rural residential, office, and educational buildings. (3) The material production, construction, and operation of buildings are currently the main accounting boundaries used in carbon emission research. Processes such as building demolition and waste recycling have not been considered by most studies and represent research gaps that need to be urgently addressed. (4) The carbon accounting methods used in current research are single and highly dependent on carbon emission factor methods. Developing or introducing other methods will be a major challenge in the future.

It is worth noting that data are an important factor limiting the development of research on CECI. The relevant data sources are relatively limited, and the evaluation standards are not uniform, which makes it difficult to assess the level of CECI comprehensively and accurately. The publicization and standardization of carbon emission and energy data will greatly promote the development of research on CECI.

This study also has some limitations. The search strategy was designed to focus on carbon emissions accounting, using keywords such as "carbon emission", "carbon footprint", and "CO_2 emission". While this ensures thematic consistency, it may exclude relevant literature using broader terms, like "NetZero", "decarbonization", or "low carbon", which could reflect related but more conceptual or policy-driven perspectives. Future research may consider expanding the keyword scope or incorporating multi-level search strategies to include a wider range of carbon reduction studies while maintaining methodological focus.

Research on CECI is an important and complex field that requires interdisciplinary and comprehensive research approaches and methods. This review helps to deepen our understanding of the status and future directions of research on CECI, providing a reference and guidance for CECI research.

Author Contributions: Conceptualization, Q.Z. and Z.W.; methodology, Q.Z. and T.W.; software, Z.W. and T.W.; validation, Q.Z.; data curation, Q.Z.; writing—original draft preparation, Q.Z. and Z.W.; writing—review and editing, Q.Z. and Y.Y.; visualization, Y.Y. and T.W.; supervision, S.H.; funding acquisition, Q.Z. and S.H. All authors have read and agreed to the published version of the manuscript.

Funding: This research was funded by the Zhejiang Province Construction Research Project (Grant Number: 2024K299 and 2023K245); this research was also funded by the Construction and Scientific Research Projects of the Center for Balance Architecture, Zhejiang University (Grant Number K-20212791, K-20203314, and K-20242715).

Data Availability Statement: No new data were created or analyzed in this study. Data sharing is not applicable to this article.

Conflicts of Interest: Authors Qinfeng Zhao and Shan Huang were employed by the company The Architectural Design and Research Institute of Zhejiang University Co., Ltd. The remaining authors declare that the research was conducted in the absence of any commercial or financial relationships that could be construed as a potential conflict of interest.

Abbreviations

The following abbreviations are used in this manuscript:

C	Construction
CECI	Carbon Emissions from the Construction Industry
C&M	Construction & Materials
C, M&O	Construction, Materials & Operation
M	Materials
MTCB	Multiple Types of Civil Buildings
M&W	Materials & Waste
O	Operation
SCI-E	Science Citation Index Expanded
SSCI	Social Sciences Citation Index
STCB	Single Type of Civil Buildings
W	Waste
WCI	the whole construction industry

Appendix A

Table A1. Final expressions of search terms used in the WOS core collection.

No.	Search Term
#1	TS = (“carbon emission*” OR “carbon peak” OR “carbon neutral*” OR “carbon footprint”)
#2	TS = (“CO_2 emission*” OR “CO_2 peak” OR “CO_2 neutral*” OR “CO_2 footprint”)
#3	TS = (“building sector” OR “construction sector” OR “building industry” OR “construction industry”)
#4	TI = (“building sector” OR “construction sector” OR “building industry” OR “construction industry”)
#5	KP = (“building sector” OR “construction sector” OR “building industry” OR “construction industry”)
#6	TS = ((“carbon emission*” OR “carbon peak” OR “carbon neutral*” OR “carbon footprint”) AND (“building sector” OR “construction sector” OR “building industry” OR “construction industry”))
#7	TS = ((“CO_2 emission*” OR “CO_2 peak” OR “CO_2 neutral*” OR “CO_2 footprint”) AND (“building sector” OR “construction sector” OR “building industry” OR “construction industry”))
#8	TS = (“carbon emission*” OR “carbon peak” OR “carbon neutral*” OR “carbon footprint”) AND TI = (“building sector” OR “construction sector” OR “building industry” OR “construction industry”)
#9	TS = (“carbon emission*” OR “carbon peak” OR “carbon neutral*” OR “carbon footprint”) AND KP = (“building sector” OR “construction sector” OR “building industry” OR “construction industry”)
#10	TS = (“CO_2 emission*” OR “CO_2 peak” OR “CO_2 neutral*” OR “CO_2 footprint”) AND TI = (“building sector” OR “construction sector” OR “building industry” OR “construction industry”)
#11	TS = (“CO_2 emission*” OR “CO_2 peak” OR “CO_2 neutral*” OR “CO_2 footprint”) AND KP = (“building sector” OR “construction sector” OR “building industry” OR “construction industry”)
#12	((TS = (“carbon emission*” OR “carbon peak” OR “carbon neutral*” OR “carbon footprint”) AND TI = (“building sector” OR “construction sector” OR “building industry” OR “construction industry”)) OR (TS = (“carbon emission*” OR “carbon peak” OR “carbon neutral*” OR “carbon footprint”) AND KP = (“building sector” OR “construction sector” OR “building industry” OR “construction industry”)))
#13	((TS = (“CO_2 emission*” OR “CO_2 peak” OR “CO_2 neutral*” OR “CO_2 footprint”) AND TI = (“building sector” OR “construction sector” OR “building industry” OR “construction industry”)) OR (TS = (“CO_2 emission*” OR “CO_2 peak” OR “CO_2 neutral*” OR “CO_2 footprint”) AND KP = (“building sector” OR “construction sector” OR “building industry” OR “construction industry”)))
#14	(((TS = (“carbon emission*” OR “carbon peak” OR “carbon neutral*” OR “carbon footprint”) AND TI = (“building sector” OR “construction sector” OR “building industry” OR “construction industry”)) OR (TS = (“carbon emission*” OR “carbon peak” OR “carbon neutral*” OR “carbon footprint”) AND KP = (“building sector” OR “construction sector” OR “building industry” OR “construction industry”))) OR ((TS = (“CO_2 emission*” OR “CO_2 peak” OR “CO_2 neutral*” OR “CO_2 footprint”) AND TI = (“building sector” OR “construction sector” OR “building industry” OR “construction industry”)) OR (TS = (“CO_2 emission*” OR “CO_2 peak” OR “CO_2 neutral*” OR “CO_2 footprint”) AND KP = (“building sector” OR “construction sector” OR “building industry” OR “construction industry”))))

References

1. Fetanat, A. Water-energy-carbon nexus and sustainability-oriented prioritization of negative emissions technologies for the oil & gas industry: A decision support system under Fermatean fuzzy environment. *Process Saf. Environ. Prot.* **2023**, *179*, 462–483.
2. United Nations Environment Programme. *2023 Global Status Report for Buildings and Construction: Beyond Foundations—Mainstreaming* Sustainable Solutions to Cut Emissions from the Buildings Sector; United Nations Environment Programme: Nairobi, Kenya, 2024; ISBN 978-92-807-4131-5.
3. Sahoo, N.; Kumar, A. Samsher Potential of solar thermal calciner technology for cement production in India and consequent carbon mitigation. *Process Saf. Environ. Prot.* **2023**, *179*, 667–676. [CrossRef]
4. Hu, J.; Yao, W.; Cai, G.; Zhao, Q.; Wang, C.; Xu, T.; Shi, C.; Gao, W. Metropolitan construction carbon emission efficiency: An integrative static-dynamic analytical framework. *Environ. Res. Commun.* **2025**, *7*, 011002. [CrossRef]

5. Teamah, H.M. Potential retrofits in office buildings located in harsh Northern climate for better energy efficiency, cost effectiveness, and environmental impact. *Process Saf. Environ. Prot.* **2022**, *3*, 100126. [CrossRef]
6. Yuan, L.; Yang, B.; Lu, W.; Peng, Z. Carbon footprint accounting across the construction waste lifecycle: A critical review of research. *Environ. Impact Assess. Rev.* **2024**, *107*, 107551. [CrossRef]
7. Mostafaei, H.; Rostampour, M.A.; Chamasemani, N.F.; Wu, C. An In-depth Exploration of Carbon Footprint Analysis in the Construction Sector with Emphasis on the Dam Industry. In *Carbon Footprint Assessments: Case Studies & Best Practices*; Muthu, S.S., Ed.; Springer Nature Switzerland: Cham, Switzerland, 2024; pp. 45–80, ISBN 978-3-031-70262-4.
8. Wang, T.; Zhao, Q.; Gao, W.; He, X. Research on Energy Consumption in Household Sector: A Comprehensive Review based on Bibliometric Analysis. *Front. Energy Res.* **2024**, *11*, 1209290. [CrossRef]
9. Liu, M.; Yang, X.; Wen, J.; Wang, H.; Feng, Y.; Lu, J.; Chen, H.; Wu, J.; Wang, J. Drivers of China's carbon dioxide emissions: Based on the combination model of structural decomposition analysis and input-output subsystem method. *Environ. Impact Assess. Rev.* **2023**, *100*, 107043. [CrossRef]
10. Zhao, Y.; Li, C.Z.; Shen, G.Q.; Teng, Y.; Wu, H.; Liu, R. Managing carbon emissions in construction: Current status and emerging trends. *Renew. Sustain. Energy Rev.* **2025**, *211*, 115237. [CrossRef]
11. Dakwale, V.A.; Ralegaonkar, R.V. Review of carbon emission through buildings: Threats, causes and solution: Table 1. *Int. J. Low-Carbon Technol.* **2012**, *7*, 143–148. [CrossRef]
12. Felipe Arbeláez Pérez, O.; Senior Arrieta, V.; Hernán Gómez Ospina, J.; Herrera Herrera, S.; Ferney Rodríguez Rojas, C.; María Santis Navarro, A. Carbon dioxide emissions from traditional and modified concrete. A review. *Environ. Dev.* **2024**, *52*, 101036. [CrossRef]
13. Al Khaffaf, I.; Hawileh, R.A.; Sahoo, S.; Abdalla, J.A.; Kim, J.H. Toward carbon- neutral construction: A review of zero-carbon concrete. *J. Build. Eng.* **2025**, *99*, 111578. [CrossRef]
14. Hussain, A.; Ali, D.; Koner, S.; Hseu, Z.-Y.; Hsu, B.-M. Microbial induce carbonate precipitation derive bio-concrete formation: A sustainable solution for carbon sequestration and eco-friendly construction. *Environ. Res.* **2025**, *270*, 121006. [CrossRef] [PubMed]
15. Liu, Z.; Li, P.; Wang, F.; Osmani, M.; Demian, P. Building Information Modeling (BIM) Driven Carbon Emission Reduction Research: A 14-Year Bibliometric Analysis. *Int. J. Environ. Res. Public Health* **2022**, *19*, 12820. [CrossRef] [PubMed]
16. Teng, Y.; Li, K.; Pan, W.; Ng, T. Reducing building life cycle carbon emissions through prefabrication: Evidence from and gaps in empirical studies. *Build. Environ.* **2018**, *132*, 125–136. [CrossRef]
17. Chastas, P.; Theodosiou, T.; Kontoleon, K.J.; Bikas, D. Normalising and assessing carbon emissions in the building sector: A review on the embodied CO_2 emissions of residential buildings. *Build. Environ.* **2018**, *130*, 212–226. [CrossRef]
18. Atmaca, A.; Atmaca, N. Carbon footprint assessment of residential buildings, a review and a case study in Turkey. *J. Clean. Prod.* **2022**, *340*, 130691. [CrossRef]
19. Gao, Z.; Liu, H.; Xu, X.; Xiahou, X.; Cui, P.; Mao, P. Research Progress on Carbon Emissions of Public Buildings: A Visual Analysis and Review. *Buildings* **2023**, *13*, 677. [CrossRef]
20. Lai, K.E.; Abdul Rahiman, N.; Othman, N.; Ali, K.N.; Lim, Y.W.; Moayedi, F.; Mat Dzahir, M.A. Quantification process of carbon emissions in the construction industry. *Energy Build.* **2023**, *289*, 113025. [CrossRef]
21. Wang, Y.; Jiang, Z.; Li, L.; Qi, Y.; Sun, J.; Jiang, Z. A Bibliometric and Content Review of Carbon Emission Analysis for Building Construction. *Buildings* **2023**, *13*, 205. [CrossRef]
22. Zhao, Q.; Gao, W.; Su, Y.; Wang, T. Carbon emissions trajectory and driving force from the construction industry with a city-scale: A case study of Hangzhou, China. *Sustain. Cities Soc.* **2023**, *88*, 104283. [CrossRef]
23. Luo, T.; Tan, Y.; Langston, C.; Xue, X. Mapping the knowledge roadmap of low carbon building: A scientometric analysis. *Energy Build.* **2019**, *194*, 163–176. [CrossRef]
24. Lu, Y.; Cui, P.; Li, D. Carbon emissions and policies in China's building and construction industry: Evidence from 1994 to 2012. *Build. Environ.* **2016**, *95*, 94–103. [CrossRef]
25. Shi, Q.; Chen, J.; Shen, L. Driving factors of the changes in the carbon emissions in the Chinese construction industry. *J. Clean. Prod.* **2017**, *166*, 615–627. [CrossRef]
26. Huang, L.; Krigsvoll, G.; Johansen, F.; Liu, Y.; Zhang, X. Carbon emission of global construction sector. *Renew. Sustain. Energy Rev.* **2018**, *81*, 1906–1916. [CrossRef]
27. Tan, X.; Lai, H.; Gu, B.; Zeng, Y.; Li, H. Carbon emission and abatement potential outlook in China's building sector through 2050. *Energy Policy* **2018**, *118*, 429–439. [CrossRef]
28. Zhou, N.; Khanna, N.; Feng, W.; Ke, J.; Levine, M. Scenarios of energy efficiency and CO_2 emissions reduction potential in the buildings sector in China to year 2050. *Nat. Energy* **2018**, *3*, 978–984. [CrossRef]
29. Lin, B.; Liu, H. CO_2 mitigation potential in China's building construction industry: A comparison of energy performance. *Build. Environ.* **2015**, *94*, 239–251. [CrossRef]

30. Chen, J.; Shen, L.; Song, X.; Shi, Q.; Li, S. An empirical study on the CO_2 emissions in the Chinese construction industry. *J. Clean. Prod.* **2017**, *168*, 645–654. [CrossRef]
31. Hong, J.; Shen, G.Q.; Guo, S.; Xue, F.; Zheng, W. Energy use embodied in China's construction industry: A multi-regional input-output analysis. *Renew. Sustain. ENERGY Rev.* **2016**, *53*, 1303–1312. [CrossRef]
32. Wu, Y.; Chau, K.W.; Lu, W.; Shen, L.; Shuai, C.; Chen, J. Decoupling relationship between economic output and carbon emission in the Chinese construction industry. *Environ. IMPACT Assess. Rev.* **2018**, *71*, 60–69. [CrossRef]
33. Wu, P.; Song, Y.; Zhu, J.; Chang, R. Analyzing the influence factors of the carbon emissions from China's building and construction industry from 2000 to 2015. *J. Clean. Prod.* **2019**, *221*, 552–566. [CrossRef]
34. Zhang, Y.; Yan, D.; Hu, S.; Guo, S. Modelling of energy consumption and carbon emission from the building construction sector in China, a process-based LCA approach. *Energy Policy* **2019**, *134*, 110949. [CrossRef]
35. Li, R.; Yu, Y.; Cai, W.; Liu, Q.; Liu, Y.; Zhou, H. Interprovincial differences in the historical peak situation of building carbon emissions in China: Causes and enlightenments. *J. Environ. Manag.* **2023**, *332*, 117347. [CrossRef]
36. Koomey, J.; Martin, N.; Brown, M.; Price, L.; Levine, M. Costs of reducing carbon emissions: US building sector scenarios. *Energy Policy* **1998**, *26*, 433–440. [CrossRef]
37. Sun, L. Energy scheduling of a fuel cell based residential cogeneration system using stochastic dynamic programming. *Process Saf. Environ. Prot.* **2023**, *175*, 272–279. [CrossRef]
38. Kesicki, F. Costs and potentials of reducing CO_2 emissions in the UK domestic stock from a systems perspective. *Energy Build.* **2012**, *51*, 203–211. [CrossRef]
39. Oberheitmann, A. CO_2-emission reduction in China's residential building sector and contribution to the national climate change mitigation targets in 2020. *Mitig. Adapt. Strateg. Glob. Change* **2012**, *17*, 769–791. [CrossRef]
40. Ma, M.; Ma, X.; Cai, W.; Cai, W. Low carbon roadmap of residential building sector in China: Historical mitigation and prospective peak. *Appl. Energy* **2020**, *273*. [CrossRef]
41. Pavkovic, B.; Zanki, V.; Cacic, G. Energy Efficiency in Building Sector in Croatia—Preliminary Energy Studies. *Strojarstvo* **2010**, *52*, 681–694.
42. Ma, M.; Yan, R.; Cai, W. An extended STIRPAT model-based methodology for evaluating the driving forces affecting carbon emissions in existing public building sector: Evidence from China in 2000–2015. *Nat. Hazards* **2017**, *89*, 741–756. [CrossRef]
43. Ma, M.; Cai, W.; Cai, W. Carbon abatement in China's commercial building sector: A bottom-up measurement model based on Kaya-LMDI methods. *Energy* **2018**, *165*, 350–368. [CrossRef]
44. Ma, M.; Cai, W. What drives the carbon mitigation in Chinese commercial building sector? Evidence from decomposing an extended Kaya identity. *Sci. Total Environ.* **2018**, *634*, 884–899. [CrossRef] [PubMed]
45. Xiang, X.; Ma, X.; Ma, Z.; Ma, M.; Cai, W. Python-LMDI: A Tool for Index Decomposition Analysis of Building Carbon Emissions. *Buildings* **2022**, *12*, 83. [CrossRef]
46. Eriksson, L.O.; Gustavsson, L.; Hanninen, R.; Kallio, M.; Lyhykainen, H.; Pingoud, K.; Pohjola, J.; Sathre, R.; Solberg, B.; Svanaes, J.; et al. Climate change mitigation through increased wood use in the European construction sector-towards an integrated modelling framework. *Eur. J. For. Res.* **2012**, *131*, 131–144. [CrossRef]
47. Noailly, J.; Batrakova, S. Stimulating energy-efficient innovations in the Dutch building sector: Empirical evidence from patent counts and policy lessons. *Energy Policy* **2010**, *38*, 7803–7817. [CrossRef]
48. Kucukvar, M.; Tatari, O. Towards a triple bottom-line sustainability assessment of the U.S. construction industry. *Int. J. Life Cycle Assess.* **2013**, *18*, 958–972. [CrossRef]
49. Cheng, M.; Lu, Y.; Zhu, H.; Xiao, J. Measuring CO_2 emissions performance of China's construction industry: A global Malmquist index analysis. *Environ. Impact Assess. Rev.* **2022**, *92*, 106673. [CrossRef]
50. Gholipour, H.F.; Arjomandi, A.; Yam, S. Green property finance and CO_2 emissions in the building industry. *Glob. Finance J.* **2022**, *51*. [CrossRef]
51. Alcantara, V.; Padilla, E. CO_2 emissions of the construction sector in Spain during the real estate boom: Input-output subsystem analysis and decomposition. *J. Ind. Ecol.* **2021**, *25*, 1272–1283. [CrossRef]
52. Zhang, L.; Liu, B.; Du, J.; Liu, C.; Li, H.; Wang, S. Internationalization trends of carbon emission linkages: A case study on the construction sector. *J. Clean. Prod.* **2020**, *270*, 122433. [CrossRef]
53. Johansson, P.; Nylander, A.; Johnsson, F. Electricity dependency and CO_2 emissions from heating in the Swedish building sector—Current trends in conflict with governmental policy? *Energy Policy* **2006**, *34*, 3049–3064. [CrossRef]
54. Johansson, P.; Nylander, A.; Johnsson, F. Primary energy use for heating in the Swedish building sector—Current trends and proposed target. *Energy Policy* **2007**, *35*, 1386–1404. [CrossRef]
55. Kahn, M.E.; Kok, N.; Quigley, J.M. Carbon emissions from the commercial building sector: The role of climate, quality, and incentives. *J. Public Econ.* **2014**, *113*, 1–12. [CrossRef]

56. Ma, M.; Cai, W.; Cai, W.; Dong, L. Whether carbon intensity in the commercial building sector decouples from economic development in the service industry? Empirical evidence from the top five urban agglomerations in China. *J. Clean. Prod.* **2019**, *222*, 193–205. [CrossRef]
57. Ma, M.; Feng, W.; Huo, J.; Xiang, X. Operational carbon transition in the megalopolises' commercial buildings. *Build. Environ.* **2022**, *226*, 109705. [CrossRef]
58. Hu, X.; Si, T.; Liu, C. Total factor carbon emission performance measurement and development. *J. Clean. Prod.* **2017**, *142*, 2804–2815. [CrossRef]
59. Li, D.; Huang, G.; Zhu, S.; Chen, L.; Wang, J. How to peak carbon emissions of provincial construction industry? Scenario analysis of Jiangsu Province. *Renew. Sustain. Energy Rev.* **2021**, *144*, 110953. [CrossRef]
60. Wen, Q.; Chen, Y.; Hong, J.; Chen, Y.; Ni, D.; Shen, Q. Spillover effect of technological innovation on CO_2 emissions in China's construction industry. *Build. Environ.* **2020**, *171*, 106653. [CrossRef]
61. Cai, W. (Ed.) *Chinese Building Energy Consumption Report*; CABEE: Beijing, China, 2016.
62. Wang, T.; Zhao, Q.; Gao, W.; He, X. Subdividing end-use energy consumption based on household characteristics and climate conditions: Insights from urban China. *Front. Energy Res.* **2023**, *11*, 1267975. [CrossRef]
63. Hung, C.C.W.; Hsu, S.-C.; Cheng, K.-L. Quantifying city-scale carbon emissions of the construction sector based on multi-regional input-output analysis. *Resour. Conserv. Recycl.* **2019**, *149*, 75–85. [CrossRef]
64. Kamei, M.; Kurisu, K.; Hanaki, K. Evaluation of long-term urban transitions in a megacity's building sector based on alternative socioeconomic pathways. *Sustain. Cities Soc.* **2019**, *47*, 101366. [CrossRef]
65. Balali, A.; Hakimelahi, A.; Valipour, A. Identification and prioritization of passive energy consumption optimization measures in the building industry: An Iranian case study. *J. Build. Eng.* **2020**, *30*, 101239. [CrossRef]
66. Mastrucci, A.; Marvuglia, A.; Benetto, E.; Leopold, U. A spatio-temporal life cycle assessment framework for building renovation scenarios at the urban scale. *Renew. Sustain. Energy Rev.* **2020**, *126*, 109834. [CrossRef]
67. Shan, Y.; Guan, D.; Liu, J.; Mi, Z.; Liu, Z.; Liu, J.; Schroeder, H.; Cai, B.; Chen, Y.; Shao, S.; et al. Methodology and applications of city level CO_2 emission accounts in China. *J. Clean. Prod.* **2017**, *161*, 1215–1225. [CrossRef]
68. Chen, H.; Chen, W. Carbon mitigation of China's building sector on city-level: Pathway and policy implications by a low-carbon province case study. *J. Clean. Prod.* **2019**, *224*, 207–217. [CrossRef]
69. Cellura, M.; Guarino, F.; Longo, S.; Tumminia, G. Climate change and the building sector: Modelling and energy implications to an office building in southern Europe. *Energy Sustain. Dev.* **2018**, *45*, 46–65. [CrossRef]
70. Atmaca, N. Life-cycle assessment of post-disaster temporary housing. *Build. Res. Inf.* **2017**, *45*, 524–538. [CrossRef]
71. Huang, L.; Liu, Y.; Krigsvoll, G.; Johansen, F. Life cycle assessment and life cycle cost of university dormitories in the southeast China: Case study of the university town of Fuzhou. *J. Clean. Prod.* **2018**, *173*, 151–159. [CrossRef]
72. Yu, D.; Zhou, X.; Qi, H.; Qian, F. Low-carbon city planning based on collaborative analysis of supply and demand scenarios. *City Built Environ.* **2023**, *1*, 7. [CrossRef]
73. Zhou, H.; Tian, X.; Zhao, Y.; Chang, C.; Lin, B. Investigation of policy tools for energy efficiency improvement in public buildings in China—Current situation, obstacles, and solutions. *City Built Environ.* **2024**, *2*, 2. [CrossRef]
74. Wang, G.; Luo, T.; Luo, H.; Liu, R.; Liu, Y.; Liu, Z. A comprehensive review of building lifecycle carbon emissions and reduction approaches. *City Built Environ.* **2024**, *2*, 12. [CrossRef]
75. Satre-Meloy, A.; Langevin, J. Assessing the time-sensitive impacts of energy efficiency and flexibility in the US building sector. *Environ. Res. Lett.* **2019**, *14*, 124012. [CrossRef]
76. Tang, B.; Zou, Y.; Yu, B.; Guo, Y.; Zhao, G. Clean heating transition in the building sector: The case of Northern China. *J. Clean. Prod.* **2021**, *307*, 127206. [CrossRef]
77. Xing, R.; Hanaoka, T.; Masui, T. Deep decarbonization pathways in the building sector: China's NDC and the Paris agreement. *Environ. Res. Lett.* **2021**, *16*, 44054. [CrossRef]
78. Heravi, G.; Rostami, M.; Kebria, M.F. Energy consumption and carbon emissions assessment of integrated production and erection of buildings' pre-fabricated steel frames using lean techniques. *J. Clean. Prod.* **2020**, *253*, 120045. [CrossRef]
79. Li, L.; Chen, K. Quantitative assessment of carbon dioxide emissions in construction projects: A case study in Shenzhen. *J. Clean. Prod.* **2017**, *141*, 394–408. [CrossRef]
80. Zhu, C.; Li, X.; Zhu, W.; Gong, W. Embodied carbon emissions and mitigation potential in China's building sector: An outlook to 2060. *Energy Policy* **2022**, *170*, 113222. [CrossRef]
81. Yan, S.; Chen, W. Analysis of the decoupling state and driving forces of China's construction industry under the carbon neutrality target. *Environ. Sci. Pollut. Res.* **2022**, *29*, 78457–78471. [CrossRef]
82. Du, Q.; Zhou, J.; Pan, T.; Sun, Q.; Wu, M. Relationship of carbon emissions and economic growth in China's construction industry. *J. Clean. Prod.* **2019**, *220*, 99–109. [CrossRef]

83. Evangelista, P.P.A.; Kiperstok, A.; Torres, E.A.; Goncalves, J.P. Environmental performance analysis of residential buildings in Brazil using life cycle assessment (LCA). *Constr. Build. Mater.* **2018**, *169*, 748–761. [CrossRef]
84. Dong, Y.; Liu, P.; Hossain, M.U.; Fang, Y.; He, Y.; Li, H. An Index of Completeness (IoC) of life cycle assessment: Implementation in the building sector. *J. Clean. Prod.* **2021**, *283*, 124672. [CrossRef]
85. Shui, B.; Luo, X.; Huang, G. Greenhouse gas emissions benefits of the lightweight vehicle fleet in China: A dynamic fleet perspective. *Resour. Conserv. Recycl.* **2024**, *205*, 107544. [CrossRef]
86. Zhang, X.; Wang, F. Hybrid input-output analysis for life-cycle energy consumption and carbon emissions of China's building sector. *Build. Environ.* **2016**, *104*, 188–197. [CrossRef]
87. Zhao, Q.; Gao, W.; Su, Y.; Wang, T.; Wang, J. How can C&D waste recycling do a carbon emission contribution for construction industry in Japan city? *Energy Build.* **2023**, *298*, 113538. [CrossRef]
88. Wang, J.; Wu, H.; Duan, H.; Zillante, G.; Zuo, J.; Yuan, H. Combining life cycle assessment and Building Information Modelling to account for carbon emission of building demolition waste: A case study. *J. Clean. Prod.* **2018**, *172*, 3154–3166. [CrossRef]
89. Coelho, A.; de Brito, J. Influence of construction and demolition waste management on the environmental impact of buildings. *Waste Manag.* **2012**, *32*, 532–541. [CrossRef]
90. Bertin, I.; Saade, M.; Le Roy, R.; Jaeger, J.-M.; Feraille, A. Environmental impacts of Design for Reuse practices in the building sector. *J. Clean. Prod.* **2022**, *349*, 131228. [CrossRef]
91. Yang, X.; Hu, M.; Zhang, C.; Steubing, B. Urban mining potential to reduce primary material use and carbon emissions in the Dutch residential building sector. *Resour. Conserv. Recycl.* **2022**, *180*, 106215. [CrossRef]
92. Ahmad, M.; Jabeen, G.; Hayat, M.K.; Khan, R.E.A.; Qamar, S. Revealing heterogeneous causal links among financial development, construction industry, energy use, and environmental quality across development levels. *Environ. Sci. Pollut. Res.* **2020**, *27*, 4976–4996. [CrossRef]
93. Saynajoki, A.; Heinonen, J.; Junnila, S.; Horvath, A. Can life-cycle assessment produce reliable policy guidelines in the building sector? *Environ. Res. Lett.* **2017**, *12*, 013001. [CrossRef]
94. UN Department of Economic and Social Affairs. World Population Projected to Reach 9.8 Billion in 2050, and 11.2 Billion in 2100. 21 June 2017. Available online: https://www.un.org/development/desa/en/news/population/world-population-prospects-2017.html (accessed on 25 May 2025).
95. Li, D.; Shang, X.; Huang, G.; Zhou, S.; Zhang, M.; Feng, H. Can Smart City Construction Enhance Citizens' Perception of Safety? A Case Study of Nanjing, China. *Soc. Indic. Res.* **2024**, *171*, 937–965. [CrossRef]
96. Huang, G.; Li, D.; Yu, L.; Yang, D.; Wang, Y. Factors affecting sustainability of smart city services in China: From the perspective of citizens' sense of gain. *Habitat Int.* **2022**, *128*, 102645. [CrossRef]
97. Huang, G.; Li, D.; Zhu, X.; Zhu, J. Influencing factors and their influencing mechanisms on urban resilience in China. *Sustain. Cities Soc.* **2021**, *74*, 103210. [CrossRef]
98. Huang, G.; Li, D.; Ng, S.T.; Wang, L.; Wang, T. A methodology for assessing supply-demand matching of smart government services from citizens' perspective: A case study in Nanjing, China. *Habitat Int.* **2023**, *138*, 102880. [CrossRef]
99. United Nations. Cities and Pollution. [Online]. Available online: https://www.un.org/en/climatechange/climate-solutions/cities-pollution (accessed on 25 May 2025).
100. Xing, Z.; Jiao, Z.; Wang, H. Carbon footprint and embodied carbon transfer at city level: A nested MRIO analysis of Central Plain urban agglomeration in China. *Sustain. Cities Soc.* **2022**, *83*, 103977. [CrossRef]
101. NDRC. Implementation Plan for the China-Singapore Tianjin Eco-City National Green Development Demonstration Zone (2024–2035). August 2024. Available online: https://www.gov.cn/zhengce/zhengceku/202408/content_6971015.htm (accessed on 25 May 2025).
102. China News Network. The Annual Emission Reduction of About 100,000 tons of Carbon Dioxide in the Sino-Singapore Tianjin Eco-City Has Further Increased the Proportion of Green Electricity. Available online: https://www.tj.chinanews.com.cn/bhxq/2024-10-11/detail-ihehwccy6197462.shtml (accessed on 25 May 2025).
103. Nassen, J.; Holmberg, J. On the potential trade-offs between energy supply and end-use technologies for residential heating. *Energy Policy* **2013**, *59*, 470–480. [CrossRef]
104. Liang, Y.; Cai, W.; Ma, M. Carbon dioxide intensity and income level in the Chinese megacities' residential building sector: Decomposition and decoupling analyses. *Sci. Total Environ.* **2019**, *677*, 315–327. [CrossRef]
105. Huo, T.; Xu, L.; Feng, W.; Cai, W.; Liu, B. Dynamic scenario simulations of carbon emission peak in China's city-scale urban residential building sector through 2050. *Energy Policy* **2021**, *159*, 112612. [CrossRef]
106. Sun, Z.; Ma, Z.; Ma, M.; Cai, W.; Xiang, X.; Zhang, S.; Chen, M.; Chen, L. Carbon Peak and Carbon Neutrality in the Building Sector: A Bibliometric Review. *Buildings* **2022**, *12*, 128. [CrossRef]

107. Su, Y.; Miao, Z.; Wang, L.; Wang, L. Energy consumption and indoor environment evaluation of large irregular commercial green building in Dalian, China. *Energy Build.* **2022**, *276*, 112506. [CrossRef]
108. Hu, J.; He, Y.; Hao, X.; Li, N.; Su, Y.; Qu, H. Optimal temperature ranges considering gender differences in thermal comfort, work performance, and sick building syndrome: A winter field study in university classrooms. *Energy Build.* **2022**, *254*, 111554. [CrossRef]
109. Zhang, C.; Lin, B. Assessing and interpreting carbon market efficiency based on an interpretable machine learning. *Process Saf. Environ. Prot.* **2023**, *179*, 822–834. [CrossRef]
110. Zhang, Z.; Wang, B. Research on the life-cycle CO_2 emission of China's construction sector. *Energy Build.* **2016**, *112*, 244–255. [CrossRef]
111. Can, C.; Zhen, W.; Guoshu, B. Life-cycle CO_2 Emissions and Their Driving Factors in Construction Sector in China. *Chin. Geogr. Sci.* **2019**, *29*, 293–305. [CrossRef]
112. Mor, S. Municipal solid waste landfills in lower- and middle-income countries: Environmental impacts, challenges and sustainable management practices. *Process Saf. Environ. Prot.* **2023**, *174*, 510–530. [CrossRef]
113. Kalogerakis, G.C.; Boparai, H.K.; Sleep, B.E. The journey of toluene to complete mineralization via heat-activated peroxydisulfate in water: Intermediates analyses, CO_2 monitoring, and carbon mass balance. *J. Hazard. Mater.* **2022**, *440*, 129739. [CrossRef]
114. Bareha, Y.; Affes, R.; Moinard, V.; Buffet, J.; Girault, R. A simple mass balance tool to predict carbon and nitrogen fluxes in anaerobic digestion systems. *Waste Manag.* **2021**, *135*, 47–59. [CrossRef]
115. Kim, J.; Seo, B.; Lee, T.; Kim, J.; Kim, S.; Bae, G.-N.; Lee, G. Airborne estimation of SO_2 emissions rates from a coal-fired power plant using two top-down methods: A mass balance model and Gaussian footprint approach. *Sci. Total Environ.* **2023**, *855*, 158826. [CrossRef]

Disclaimer/Publisher's Note: The statements, opinions and data contained in all publications are solely those of the individual author(s) and contributor(s) and not of MDPI and/or the editor(s). MDPI and/or the editor(s) disclaim responsibility for any injury to people or property resulting from any ideas, methods, instructions or products referred to in the content.

MDPI AG
Grosspeteranlage 5
4052 Basel
Switzerland
Tel.: +41 61 683 77 34

Buildings Editorial Office
E-mail: buildings@mdpi.com
www.mdpi.com/journal/buildings



Disclaimer/Publisher's Note: The title and front matter of this reprint are at the discretion of the Guest Editors. The publisher is not responsible for their content or any associated concerns. The statements, opinions and data contained in all individual articles are solely those of the individual Editors and contributors and not of MDPI. MDPI disclaims responsibility for any injury to people or property resulting from any ideas, methods, instructions or products referred to in the content.





Academic Open
Access Publishing

mdpi.com

ISBN 978-3-7258-8874-0